CMBBE 2021

7 – 9 September 2021, Bonn, Germany

17th International Symposium on Computer Methods in Biomechanics and Biomedical Engineering
and 5th Conference on Imaging and Visualization

ABSTRACT BOOK

www.cmbbe-symposium.com

Peter Augat

Towards a clinical pathway for computational planning of operative stabilization of fractured bones

Operative treatment of broken bones involves their mechanical stabilization using a metallic implant. The primary goal of operative stabilization (i.e. osteosynthesis) is to provide the bone with sufficient mechanical stability to allow functional rehabilitation of the patient. The art of operative fracture care involves choosing the adequate implant and applying the appropriate techniques to reach the goal of sufficient mechanical stabilization. However, an accurate estimation of the implant's load-bearing capacity is often challenging because of complex loading scenarios and difficult to predict the interaction between bone and metallic implant. Modern computer technology, including finite element analysis, has shown to be capable of accurately calculating the mechanical performance of a fractured bone stabilized with a metallic implant. Yet, clinical reality has not yet seen the use of this technique. This presentation will demonstrate how the mechanical performance of fracture stabilization can be computed and how the existing barriers to translate this technology into the clinical application can be overcome.

Biography

Peter Augat is a Professor of Biomechanics at Paracelsus Medical University in Salzburg, Austria and the Director of the Institute of Biomechanics at Berufsgenossenschaftliche Unfallklinik Murnau, Germany. He received his MSc in physics from the University of Ulm in 1990 and obtained his Ph.D. in biology in 1995. His previous positions include Head of the Osteoporosis and Fracture Healing Research Group at the Institute of Orthopaedic Research at the University of Ulm and Assistant Adjunct Professor in the Department of Radiology at the University of California, San Francisco. Peter is Past President of the International Society for Fracture Repair (ISFR), Past President of the German Society of Biomechanics (DGfB), and Member of several societies in the area of musculoskeletal research including ESB, ORS and IBMS. He is on the editorial board of several orthopaedic journals including Biomedical Engineering, AOTS, JOT, EJTS and also reviewer for most major musculoskeletal journals. Peter's research is focused on biomechanics of fracture repair and on the clinical translation of orthopaedic research. He published more than 200 scientific articles and supervised more than 80 doctoral theses.

Merryn Tawhai

Linking imaging-based lung structure to patient respiratory system function using biophysically-based models

There are currently very few methods for quantitative assessment of the lung to assist with planning surgical or other interventions. Current tools focus on image analysis, usually based on densitometry or texture analysis. No tools are currently available for patient-specific prediction of respiratory system function post-treatment. We are developing an imaging-, statistical-, and biophysically-based lung model to predict patient-specific response to various interventions and treatments. This digital lung spans from the nasal and oral airways to the deepest smallest parts of the lung, and connects to sophisticated models of the pulmonary circulation, respiratory and other gas exchange, and interacts with models of respiratory control. The model incorporates imaging and lung function data from healthy subjects aged 20-90 years of age to appropriately represent structure-function relationships over the full adult lifespan. The ultimate goal is to provide a comprehensive tool that can be used to predictively test interventional approaches and therapies (both well in advance and at the bedside), provide mechanistic insight into imaging-based biomarkers, and to develop and optimise new and current treatments to the individual patient.

Biography

Professor Merryn Tawhai is the Director of New Zealand's national Medical Technologies Centre of Research Excellence and Deputy Director of the Auckland Bioengineering Institute at the University of Auckland. She has led efforts to develop a quantitative description of lung anatomy and accompanying multi-scale models that bring together cell function, tissue mechanics, and transport and exchange processes in anatomically-detailed models of the lung. Her research links patient-specific lung structure to function for simulation of ventilation distribution, perfusion distribution, and gas exchange; as well as simulation of a range of pulmonary function tests. Professor Tawhai is a Fellow of the Royal Society of New Zealand Te Apārangi (RSNZ), the American Institute for Medical and Biological Engineering, the International Academy of Medical and Biological Engineering. She was awarded the 2016 MacDiarmid Medal by the RSNZ for the potential impact of her research on human health.

Ellen Kuhl

Data-driven modelling of neurodegeneration

Neurodegeneration will undoubtedly become a major challenge in medicine and public health because of demographic changes worldwide. More than 45 million people are living with dementia today and this number is expected to triple by 2050. Recent studies have reinforced the hypothesis that the prion paradigm, the templated growth and spreading of misfolded proteins, could help explain the progression of a variety of neurodegenerative disorders. However, our current understanding of prion-like growth and spreading is rather empirical and the precise propagation dynamics of misfolded protein within the living brain remain poorly understood. Here we show that a physics-based reaction-diffusion model can explain the growth and spreading of misfolded protein in a variety of neurodegenerative disorders. We integrate the classical Fisher-Kolmogorov equation for population dynamics into a brain network model, which we represent through a connectivity-weighted Laplacian graph created from 418 human brain images. To test the hypothesis that misfolded proteins propagate preferably along neuronal connections, we follow 46 subjects for three years and compare their positron emission tomography scans against brain network models of intracellular and extracellular spreading. For each subject, we identify a personalized set of model parameters that characterizes the individual progression of misfolded tau protein. We show that intracellular spreading along neuronal connections explains the propagation dynamics of Alzheimer's disease better than extracellular spreading. Our results suggest that misfolded proteins in neurodegenerative disorders grow and spread according to a universal law that follows the basic physical principles of nonlinear reaction and anisotropic diffusion. A more quantitative understanding of the timeline of neurodegeneration could help detect non-clinical symptoms at an earlier stage and make informed predictions about the timeline of neurodegeneration on an individual personalized basis.

Biography
Ellen Kuhl is the Robert Bosch Chair of Mechanical Engineering at Stanford University. She received her PhD from the University of Stuttgart and her Habilitation from the University of Kaiserslautern. Her area of expertise is Living Matter Physics, the design of theoretical and computational models to predict the behavior of living structures. She has published more than 250 peer-reviewed journal articles. Ellen is the current Chair of the US Committee on Biomechanics and a Member-Elect of the World Council of Biomechanics. She is a Fellow of the American Society of Mechanical Engineers and of the American Institute for Mechanical and Biological Engineering. She received the NSF Career Award, the Humboldt Research Award, and the ASME Belytschko Award. Ellen is an All American triathlete, a multiple Boston, Chicago, and New York marathon runner, and a Kona Ironman World Championship finisher.

Daniel Rueckert

How AI is changing the future of radiology

This talk will explain how AI is changing the future of radiology. In particular, I will examine the impact of deep learning on the entire medical imaging pipeline: First, I will introduce a framework for reconstructing MR images from undersampled data using a deep cascade of convolutional neural networks to accelerate the data acquisition process. We show that such a method can outperforms state-of-the-art compressed sensing approaches, both in terms of image quality and reconstruction speed. In addition, we will present how deep learning can be used for image enhancement (e.g. super-resolution) and image quantification (e.g. image segmentation). Finally, we will show examples of how deep learning can be used for diagnosis and prognosis of diseases.

Biography

Daniel Rueckert is Alexander von Humboldt Professor for AI in Medicine and Healthcare at the Technical University of Munich. He is also Professor of Visual Information Processing in the Department of Computing at Imperial College London. From 2016 to 2020 he served as Head of the Department of Computing at Imperial College. He gained a MSc from Technical University Berlin in 1993, a PhD from Imperial College in 1997, followed by a post-doc at King's College London. In 1999 he joined Imperial College as a Lecturer, becoming Senior Lecturer in 2003 and full Professor in 2005. At Imperial, he has founded the Biomedical Image Analysis group consisting of four academics, 15 post-docs and 20 PhD students. He has published more than 500 journal and conference articles as well as graduated over 50 PhD students. In his early research career he has worked on the development of non-rigid registration algorithms for the compensation of tissue motion and deformation. The developed registration techniques have been successfully used for the non-rigid registration of various anatomical structures, including in the breast, liver, heart and brain and are currently commercialized by IXICO, an Imperial College spin-out company. Professor Rueckert is an associate editor of IEEE Transactions on Medical Imaging, a member of the editorial board of Medical Image Analysis, Image & Vision Computing, MICCAI/Elsevier Book Series, and a referee for a number of international medical imaging journals and conferences. He has served as a member of organising and programme committees at numerous conferences, e.g. he has been General Co-chair of MMBIA 2006 and FIMH 2013 as well as Programme Co-Chair of MICCAI 2009, ISBI 2012 and WBIR 2012. In 2014, he has been elected as a Fellow of the MICCAI society and in 2015 he was elected as a Fellow of the Royal Academy of Engineering and as fellow of the IEEE. More recently has been elected as Fellow of the Academy of Medical Sciences (2019).

A1.1

AI Boosting the accuracy of Google and public web search engines in recognizing and classifying dental visual assets

Ahmed Kaboudan[1], Sameh Talaat[2], Christoph Bourauel[3]

1   DigiBrain4 Inc., IL, Chicago, United States
2   Future University in Egypt, Orthodontics, Cairo, Egypt
3   Bonn University, Bonn, Germany

Abstract: To assess the accuracy of a propriety AI engine in recognizing, categorizing and classifying dental visual assets as compared to Google Search Engine, one of the largest publicly available search engines and the largest data repository.

Results: The results achieved by the engine for searching dental visual assets were 93% accurate, whereas the results achieved using Google Search Engine were less than 32% accurate.

Keywords: Dental visual assets; Artificial Intelligence; Dental X-Rays; Dental Clinical Images, Dental Classifier; Smart Search Engine; Machine Learning, Deep Learning.

Figure caption: Accurate results as displayed by the new AI search engine.
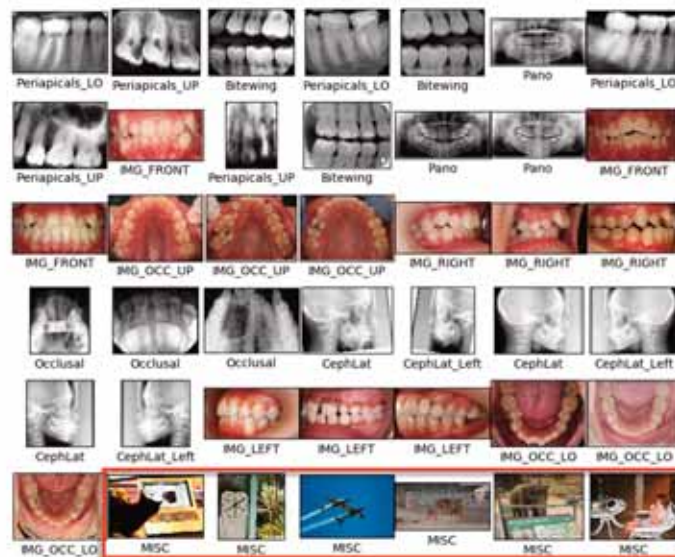
A1.2

Testing the conformity of an AI application with the handicapping labio-lingual deviations index for the assessment of malocclusion severity from clinical images

Christoph Bourauel[1], Sameh Talaat[1,2], Ayu Handono[3], Mohammed Elnagar[4], Flavio Sanchez[4], Budi Kusnoto[4], Ahmed Kaboudan[3]

1   University of Bonn, Oral Technology, Bonn, Germany
2   Future University in Egypt, Department of Orthodontics, Cairo, Egypt
3   Digibrain4 Inc, Chicago, United States
4   University of Illinois at Chicago College of Dentistry, Chicago, United States

Introduction and Aim: The assessment of the severity of malocclusions is a decisive step not only to determine the orthodontic treatment need but also to justify financing of the therapy by the health insurance companies. Computer assisted systems might help to establish objective and impartial systems for treatment assessment. It thus was the aim of this study to assess the conformity of a Convolutional Neural Network (CNN) digital model with the Handicapping Labio-Lingual Deviations (HLD) index, commonly used to assess the severity of malocclusion from intra oral clinical images.

Materials and methods: The sample of this study was composed of the intraoral images of 300 subjects. All images were intraoral clinical images, in one of the following views: Left Occlusion, Right Occlusion, Front Occlusion, Upper Occlusal, and Lower Occlusal. The following malocclusion conditions were localised and counted: crowding, spacing, increased overjet, cross bite, open bite, deep bite. The HLD indices of these cases were calculated in a previous study by an experienced orthodontist. The CNN model that was used for this study was a patented AI application (DR_ANNIE©). This model is capable of detecting, localising and counting multiple malocclusion instances in each image. It is a fully convolutional deep neural network; 24 convolutional layers followed by 2 fully connected layers. This model was implemented using TensorFlow framework freely available from Google.

Results: There was a strong agreement between the created CNN model (DR_ANNIE©) and HLD index (99.3 %). DR_ANNIE© yielded the exact HLD score in 48.2 % of the assessed cases. In 49.6 % of the cases, DR_ANNIE© surpassed the HLD index by only a score of 1. DR_ANNIE© did not under- or overestimate a case by score of 2 in comparison to the measured HLD index.

Conclusions: The built AI application (DR_ANNIE©) proved to be capable of detecting, localising and counting malocclusion instances from different views of intra-oral clinical images accurately. DR_ANNIE© conformed to the HLD index for measuring the severity of malocclusion from intra-oral clinical images.

References:
Patent: Dento-Cranofacial Clinical Cognitive Diagnosis and Treatment System and Method. Patent # 10,878,954 (Dec 29, 2020) – DR_ANNIE© - DigiBrain4, INC

A1.3

Validity of an AI application for assessment of orthodontic treatment need from clinical images

Sameh Talaat[1]

1   Uniklinikum Bonn, Düsseldorf, Germany

Aim: To assess the validity of a Convolutional Neural Network (CNN) digital model to detect and localize orthodontic malocclusions from intra oral clinical images.

Materials and methods: The sample of this study was composed of the intraoral images of 700 Subjects. All images were intraoral clinical images, in one of the following views: Left Occlusion, Right Occlusion, Front Occlusion, Upper Occlusal, and Lower Occlusal. The following malocclusion conditions were localized: crowding, spacing, increased overjet, cross bite, open bite, deep bite. The images annotations were repeated by the same investigator (S.T) with a one week interval (ICC ≥ 0.9).

The CNN model that was used for this research study was the "You Only Look Once" model. This model is capable of detecting and localizing multiple objects, or multiple instances of the same object in each image. It is a fully convolutional deep neural network; 24 convolutional layers followed by 2 fully connected layers. This model was implemented using TensorFlow framework freely available from Google.

Results: The created CNN model was able to detect and localize the malocclusions with an accuracy of 99.99 %, precision of 99.79% and a recall of 100%.

Conclusions: The use of computational deep convolutional neural networks to identify and localize orthodontic problems from clinical images proved to be valid. The built AI engine proved to be capable of detecting and localizing malocclusion from different views of intra-oral clinical images accurately.

A2.1

Influence of the mechanics on 3D muscle-driven predictive simulations of human walking

Antoine Falisse[1]

1   Stanford University, Bioengineering, Stanford, United States

Predictive simulations generate novel movements based on a model of the neuro-musculoskeletal system without relying on experimental data. In the last two decades, researchers have increasingly used such simulations to study human locomotion, by evaluating the effect of changes in the neuro-musculoskeletal system on the predicted gait pattern. Under the assumption that gait optimizes performance, researchers formulated predictive simulations as optimal control problems, commonly using the metabolic cost of transport as optimality criterion such as suggested in experimental studies (e.g., Bertram & Ruina 2001, Selinger et al. 2015).

Although predictive simulations optimizing for metabolic energy can capture the salient features of human gait, they often fail to produce expected knee flexion angle, knee extension torque, and knee extensor activity during early stance (e.g., Song & Geyer 2015, Ong et al. 2019, Falisse et al. 2019). Ackermann and van den Bogert (2010) suggested that other criteria than energy minimization might contribute to human gait. In particular, they showed using two-dimensional (2D) muscle-driven models that optimizing for muscle fatigue rather metabolic energy resulted in more physiological knee flexion angle and knee extensor activity. However, in recent work with three-dimensional (3D) muscle-driven models (Falisse et al. 2019), we found that optimizing for muscle fatigue did not produce the expected knee flexion pattern during early stance, and resulted in excessive trunk sway and step width. Combining energy and fatigue considerations in the cost function improved the realism of our predictions, but the latter still lacked knee flexion angle, knee extension torque, and knee extensor activity during early stance. Overall, it remains unclear whether the optimality criterion alone determines the predicted stance knee pattern.

In this context, we evaluated whether mechanical parameters might contribute to predicting physiological stance knee patterns. In particular, we investigated the effect of enabling foot roll-off, modelled through a toe joint or smaller front-foot contact spheres, on predictive simulations of walking. Interestingly, we found that enabling foot roll-off helped produce knee flexion angle, knee extension torque, and knee extensor activity during early stance. Those results suggest that not only the motor control (i.e., the cost function) but also the mechanics shape the behavior of the knee during walking.

References:
Ackermann M, van den Bogert AJ. J. Biomech. (2010): 43, 1055–1060.
Bertram JEA, Ruina A. J. Theor. Biol. (2001): 209, 445–453.
Falisse A, Serrancoli G, Dembia C, Gillis J, Jonkers I, De Groote F. J. R. Soc. Interface (2019): 16, 20190402.
Ong CF, Geijtenbeek T, Hicks JL, Delp SL. PLoS Comput. Biol. (2019): 15, e1006993.
Selinger JC, O'Connor SM, Wong JD, Donelan JM. Curr. Biol. (2015): 25, 2452–2456.
Song S, Geyer H. J. Physiol. (2015): 593, 3493–3511.

A2.2
Predictive simulations of movement to assess human gait neuromechanics

Friedl De Groote[1]

1   KU Leuven, Department of Movement Sciences, Leuven, Belgium

Locomotion results from complex interactions between the central nervous system and the musculoskeletal system with its many degrees of freedom and muscles. Gaining insight into how the properties of each subsystem shape human gait is challenging as experimental methods to manipulate and assess isolated subsystems are limited. Simulations that predict movement patterns based on a mathematical model of the neuro-musculoskeletal system without relying on experimental data can reveal principles of locomotion by elucidating cause-effect relationships. Simulations of movement are typically based on the assumption that the central nervous system optimizes performance. Under this assumption, predictive simulations can be formulated as optimal control problems. New computational approaches have enabled the use of such predictive simulations with complex neuro-musculoskeletal models [1]. We performed simulations based on a musculoskeletal model that contained 29 degrees of freedom, 92 Hill-type muscles actuating the lower limbs and trunk, and 8 ideal torque actuating the arms to explore optimality principles underlying human gait and the relation between musculoskeletal properties and gait mechanics. We found that a multi-objective cost function combining metabolic energy, muscle activations and joint accelerations, all terms squared, produced a human-like walking pattern. The same optimality criterion also predicted gait deficiencies caused by muscle weakness and prosthesis use. We explored how foot and foot-ground interaction mechanics influenced gait mechanics and found that modeling foot roll-off was important to predict realistic knee flexion and knee extension torques during the stance phase of walking, features that have been hard to capture in predictive simulations. We are currently using predictive simulations in combination with personalized musculoskeletal models to assess how altered neuro-musculoskeletal properties affect gait performance in children with cerebral palsy and Duchenne muscular dystrophy, and for the design of exoskeleton controllers that reduce the metabolic cost of walking in healthy adults. Using a series of case studies, I will discuss insights gained from simulations based on complex musculoskeletal models as well as challenges towards developing more realistic simulations to gain new fundamental insight into motor control of gait, and to help design personalised gait interventions.

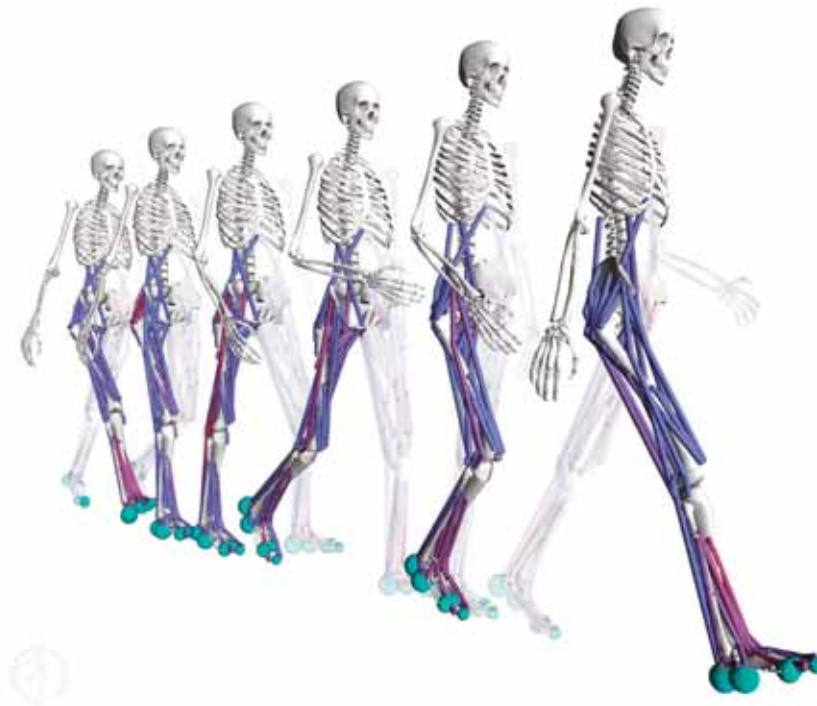*Figure caption: Predictive simulation of human walking. The walking pattern visualised here was generated by trajectory optimization based on a complex OpenSim-based three-dimensional muscle-driven model without relying on experimental data [2]. Blue spheres represent contact geometries. Muscles turn red when active.*

References:
[1]   Falisse et al., J R Soc Interface, 2019;
[2]   Seth et al., PLOS Comput Biol, 2018.

A2.3

A generalizable stochastic optimal control framework to simulate control and movement of non-linear musculoskeletal systems

Tom Van Wouwe[1], Friedl De Groote[1], Lena Ting[2]

1   KU Leuven, Movement Sciences, Leuven, Belgium
2   Emory University & Georgia Tech, Atlanta, United States

Stochastic optimal control (SOC) has been proposed as a theory of motor coordination [1] explaining movement kinematics and variability based on minimizing the effects of physiological noise on movement performance. Due to computational limitations however, SOC has only been applied on simple models that typically do not account for nonlinear inter-segment interactions and muscle mechanics. Yet, non-linear mechanics contribute significantly to the required modulation of feedback and feedforward control to stabilize movement against noise. Here, we present method for SOC that allows efficient simulation of nonlinear stochastic systems. Non-Gaussian distributions of the stochastic state trajectory are approximated by Gaussian distributions, allowing the state space to be described by the mean state and state covariance 'P'. The dynamics of 'P' is described by the continuous Lyapunov equation (cfr. propagation rules of the Extended Kalman Filter). The resulting augmented deterministic optimal control problem is solved using direct collocation and gradient-based optimization.

We applied this SOC method to muscle-driven (Hill-type muscles) simulations of perturbed standing balance (single-joint), reaching (two-joint) and torque driven simulations of walking. In all cases we solved for feedforward controls and feedback gains that minimized expected effort (expected controls squared) while satisfying a specified task goal.

A muscle-driven inverted pendulum model of standing was controlled by proprioceptive and vestibular feedback. In agreement with experiments and SOC simulations with linear models, we predicted sensory reweighting in favor of vestibular information with increasing platform rotation magnitude [2]. In addition, our simulations allowed insight in muscle-level motor control strategies, predicting muscle co-activation, as a minimal effort strategy to withstand platform translations - but not rotations, that was larger when accounting for short-range stiffness in the muscles.

A two-segment muscle-driven arm model of reaching was controlled by time-varying feedback from endpoint kinematics. The simulations predicted experimentally observed reactive muscle activity and kinematic trajectories in response to perturbations depending on target shape [3]. Simulations of perturbed reaching were in better agreement with experiments than simulations based on point mass models.

A torque-driven walker model was controlled by feedforward controls and full-state feedback loops. Stochastic simulations of walking generated realistic gait kinematic patterns but more importantly predict features of sensorimotor control. Similar to the soleus H-reflex [4], simulated local ankle feedback gains are downregulated at increased walking speed.

In conclusion, the framework allowed to demonstrate that SOC predicts task-dependent modulation of feedforward (co-contraction) and feedback muscle controls that is dependent on musculoskeletal dynamics, sensory noise and movement condition. The efficiency of our framework opens the door for stochastic optimal control simulations to study sensorimotor control of human movement using complex models.

[1]   Todorov, Nat Neurosci, , 2004.
[2]   Petarka, J Neurophysiol, 2002.
[3]   Nashed et al. J Neurophysiol, 2012.
[4]   Capaday et al., J. Physiol., 1986

A2.4

Estimating muscle forces and motion kinematics while calibrating muscle parameters : a forward optimization approach

François Bailly[1], *Amedeo Ceglia*[1], *Mickael Begon*[1]

1Campus UdeM in Laval, Laval, Canada

Introduction: Muscle forces feedback is crucial for the evaluation of musculoskeletal disorders as well as for rehabilitation and neuroprostheses control. However, these quantities are almost impossible to measure in-vivo, therefore biomechanists have turned to musculoskeletal simulation to estimate them. In such simulations, one of the most used muscle-tendon unit (MTU) models is the normalized Hill-type, which depends on several parameter, varying non linearly with the anthropometry of the body. Precisely estimating these parameters is therefore a prerequisite for muscle force estimation.

Several methods have been proposed to estimate some or all aforementioned parameters. They rely on the adjustments of the muscle parameters (often through optimization) to match joint torques computed by inverse dynamics (ID). ID is subject to possibly large errors, therefore compromising the accuracy of existing MTUs calibration methods.

We propose, for the first time, a fully forward multiple shooting approach, to simultaneously calibrate MTUs while estimating the whole motion dynamics, from muscle activations to segments kinematics.

Methods: A simplified 2-degrees of freedom arm model actuated by four hill-type MTUs was used as a proof of concept. A 1-second reference motion was simulated with this reference model, paying attention that each of the four MTUs was recruited at some point of the motion. Then, using Bioptim [1], a multiple shooting optimal estimation algorithm was formulated as in [2] to estimate the motion dynamics, with the addition of optimal fiber length and of the isometric force of each MTU as time-independent parameters of the optimal problem. Using a surrogate model (i.e., with randomized MTU parameters around the values of the reference model), this optimization was solved recursively by alternating between optimizing the optimal fiber length (with fixed isometric forces) and vice versa, until convergence to the reference values within a specified tolerance.

Results: After, 70 iterations (50 s), the proposed algorithm was able to retrieve both the dynamics of the motion and the MTUs parameters of the model using a forward optimization approach. Across MTUs, the root mean square error (RMSE) was 29.3 N (3.5 %) for the isometric forces, 6.2 mm (0.6 %) for the optimal fiber length and the mean RMSE was 2.2 N (0.75 %) for muscle forces.

Discussion: This result is promising for MTU calibration and force estimation, as it does not rely on inaccurate inverse methods. As a future work, it needs to be generalized to more complex musculoskeletal models, investigated on experimental data and compared to previous approaches.

References:
[1]   Michaud, B., et al. (2021). Bioptim, a Python framework for Musculoskeletal Optimal Control in Biomechanics. bioRxiv.
[2]   Bailly, F., et al. (2021). Real-time and dynamically consistent estimation of muscle forces using a moving horizon emg-marker tracking algorithm. Frontiers in bioengineering and biotechnology, 9, 112.

A2.5
Model-based estimation of muscle forces during carved turns in alpine skiing

Dieter Heinrich[1], Antonie J. van den Bogert[2], Werner Nachbauer[1]

1   University of Innsbruck, Department of Sport Science, Innsbruck, Austria
2   Cleveland State University, Department of Mechanical Engineering, Cleveland, United States

Introduction: During turning maneuvers in alpine skiing, competitive skiers face a high risk of sustaining a serious knee injury. Musculoskeletal simulation models can estimate individual muscle forces, provide insight into tissue loading and can thus contribute to a better understanding of injury mechanisms. The purpose of the present study was to develop a three-dimensional musculoskeletal model of an alpine skier to estimate muscle forces during turning maneuvers in alpine skiing.

Methods: We developed a three-dimensional musculoskeletal model of an alpine skier and two skis with 53 degrees of freedom (19 for the skier and 17 for each ski) and 94 three-element Hill-type muscles (43 per leg and 8 actuating the lumbar joint). The skier model was based on the full-body OpenSim model of Catelli et al. (2019), where we added additional muscles for the lumbar and hip joints. Each ski was discretized into 18 rigid segments (7 rear segments, 1 center segment and 10 front segments) and connected by revolute joints with spring-damper elements to incorporate mechanical properties (bending stiffness and damping). We modeled the ski-snow contact using three types of forces acting on each ski segment (Mössner et al., 2014). We applied a frictional force, a penetration force acting normal to the snow surface, and a shear force acting parallel to the snow surface, which provided resistance against lateral shearing. To estimate muscle forces during a turning maneuver, we formulated an optimal control problem (OCP), where experimental kinematic data of an alpine skier captured by three cameras was tracked. Muscle redundancy was resolved by minimizing the sum of squared muscle activations. The OCP was solved using direct collocation and the nonlinear optimization solver IPOPT. To increase computational speed, we provided analytical derivatives of the objective function and constraints (van den Bogert et al. 2011).

Results: Tracking the measured kinematics of the skier during the turning maneuver converged in about 40 min of computational time on a single core of a workstation (Thinkstation 330, E-2146 CPU). The speed of the skier was 14 m/s and the turning maneuver lasted 1.5 s. The primary activated muscle groups were the lateral and dorsal trunk muscles, the vasti, hamstrings and glutei of the inner leg as well as the glutei, vasti, soleus and hamstrings of the outer leg.

Conclusion: A novel three-dimensional musculoskeletal model of an alpine skier was developed and successfully applied to determine muscle forces during a turning maneuver in alpine skiing.
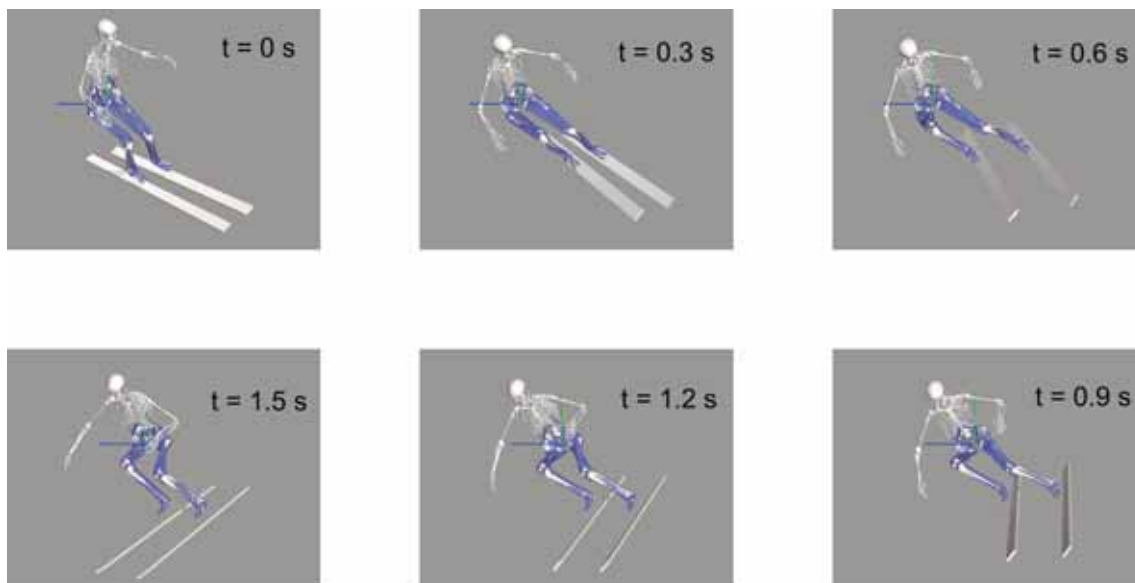

Figure caption: Musculoskeletal skier model visualized in OpenSim

References:
[1]   Catelli DS et al. (2019). Comp Methods Biomech Biomed Engin, 22: 21-24.
[2]   Mössner M et al. (2014). Scand J Sci Sport, 24: 577-585.
[3]   van den Bogert et al. (2011). Procedia IUTAM, 2: 297-316.

A3.1

A continuum approach for the diffusion-compensated ETM model and its application on Neuroblastoma clinical data

Diego Sainz-DeMena[1], Wenfeng Ye[2], Leonor Cerda Alberich[3], Maria Angeles Perez[1], Jose Manuel Garcia-Aznar[1][4]

1   Multiscale in Mechanical and Biological Engineering, Instituto de Investigación en Ingeniería de Aragón (I3A), Universidad de Zaragoza, Zaragoza, Spain
2   ANSYS France, Montigny-le-Bretonneux, France
3   La Fe Health Research Institute, Valencia, Spain
4   nstituto de Investigación Sanitaria Aragón (IIS Aragón), Universidad de Zaragoza, Zaragoza, Spain

Dynamic contrast-enhanced magnetic resonance imaging (DCE-MRI) is a well-stablished method to get an insight on tissues vascularization (specially in cancer). By injecting a contrast agent (CA), we can obtain the concentration-time curves of this CA on each voxel in the tissue.

To obtain more physiological information, pharmacokinetic (PK) models are fitted to these curves. The most common PK models in clinical practice are the Tofts model (TM) and the extended Tofts model (ETM)[1,2]. These models provide physiological information while keeping a low computational cost. Nevertheless, one of their major drawbacks is that they only consider CA arrival to each voxel through active delivery, neglecting CA diffusion between adjacent voxels.

Some authors have proposed updated versions of these models[3,4] to take into account passive delivery of CA. Although their results showed an improvement in the physiological parameters' precision, both models proposed a voxel-wise analysis, which lead to either a prohibitive computational cost[3] or the assumption of some simplifications that limit the application range of the model[4].

Here we propose a continuum approach for the diffusion-compensated ETM (D-ETM) developed by these authors.

Instead of fitting each voxel separately, our work consists of a FE model (ANSYS) of the tumour geometry where the continuum D-ETM equation is implemented:

$$(dC_t)/dt = (\nabla(D\nabla C_e) + K^{Trans}(C_p - C_e))*v_e + v_p * \llbracket dC \rrbracket_p/dt \quad (1)$$

This implementation of the problem allows for a more extensive application of the model: both homogeneous and heterogeneous tissues (such as Neuroblastoma tumours) can be analyzed with this model.

By applying a numerical method, the arterial input function (AIF) measured no longer needs to be fitted to an analytical function; it can be introduced in the model (Cp) directly. Avoiding this previous step of AIF fitting helps increasing the precision of the estimated parameters.

Apart from more precise ETM parameters, our model also returns an estimate of the tissue diffusion coefficient. This information is very useful for further models of tumour growth, species diffusion, etc. By obtaining a precise estimation of the vasculature and the diffusivity, we can identify which regions are less susceptible to treatments (hypoxic or necrotic regions, for example).
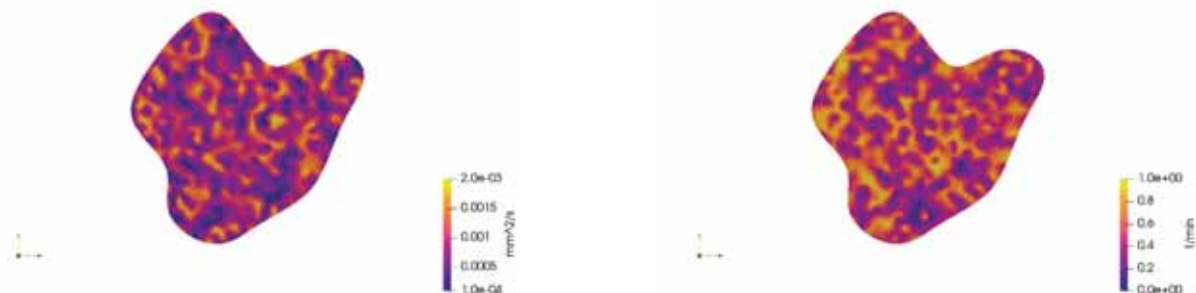
References:
[1]   Tofts, P. S., J. Magn. Reson. Imaging, 1997
[2]   Tofts PS, et al, J Magn Reson Imaging, 1999
[3]   Pellerin, M. et al, Magn. Reson. Med., 2007
[4]   Fluckiger, J. et al, Phys Med Biol, 2013

A3.2

Replicating the mechanical environment of an experimental natural knee simulator in specimen-specific tibiofemoral finite element models for the study of menisci.

Rosti Readioff[1], *Aiqin Liu*[1], *Louise M. Jennings*[1], *Ruth K. Wilcox*[1], *Alison C. Jones*[1]

1   University of Leeds, Institute of Medical and Biological Engineering, School of Mechanical Engineering, Leeds, United Kingdom

Knee osteoarthritis is one of the most prevalent joint diseases [1], hence there are increased efforts in developing early intervention strategies to delay knee degeneration. Experimental simulation using human cadaveric tibiofemoral joints has been developed for the functional investigation of tribology and biomechanics of early intervention strategies, such as meniscal allografts [2]. However, cadaveric studies are costly and time consuming, with each specimen being viable for a limited number of conditions. A collection of specimen-specific tibiofemoral finite element (FE) models provides a means to both expand the set of conditions and the number of samples in a given study, vastly increasing the value gained for each sample. The current study aims to adapt existing human tibiofemoral FE models to match the constraints, kinetics and kinematics used in experimental simulations.

Three specimen-specific FE models of knee joints, previously developed and validated for static contact mechanics experiments, were utilised. The models consisted of femur, tibia, articular cartilage of the femur and tibia, and lateral and medial menisci. Initially, the boundary conditions and ligamentous constraints of an experimental natural knee simulation were replicated on specimen-specific FE models. This involved defining three degrees of freedom (DoF) on the tibia and one DoF on the femur to represent the rotation and translation axes of the tibia and femur relative to each other, matching the experimental simulation conditions (Figure a and b). Springs with experimentally determined stiffness coefficients were used to define the ligamentous constraints in the FE model. Subsequently, contact mechanics of flexed knee were studied using the FE models at discrete flexion angles ranging from 0° to 60° while applying 200N constant load. Contact mechanics parameters of the cartilage were measured.

A challenge with simulating flexion states of knee models was maintaining convergence of the model while representing the complex contact surfaces of the tibiofemoral joint. We overcame this by introducing a spring to provide loose contact between the femur and tibia. Results showed a decrease in contact area with increasing flexion angles (Figure c and d). Future work will focus on kinematic validation and application of the multi-specimen computational modelling capability to investigate the biomechanics of meniscus allograft transplantation.
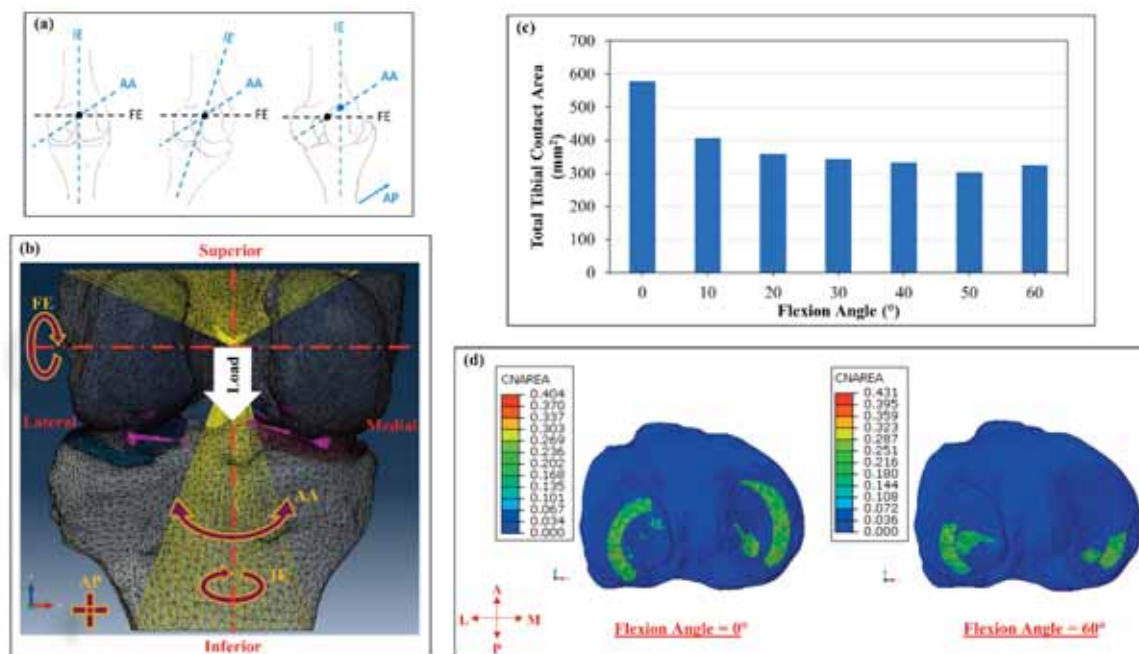

Figure caption: This figure shows (a) the rotation and translation axes replicated in the (b) tibiofemoral FE models, showing internal-external (IE), abduction-adduction (AA) and flexion-extension (FE) axes of rotation and anterior-posterior (AP) axis of translation. (c) Shows the FE predicted total contact area of the tibial articular cartilage at different flexion angles. In addition, (d) shows contact area for the FE simulation at two flexion angles.

References:
[1]   James et al., The Lancet, 2018.
[2]   Liu et al., PLOS ONE, 2020.

A3.3

A subject-specific FEM to predict deep tissue mechanical stresses when lying: A preliminary study of sensitivity to substrate stiffness

Lionel Rayward[1], Peter Pivonka[1], Mark Pearcy[1], Graham Kerr[2], Paige Little[1]

1QUT Gardens Point Campus., Biomechanics and Spine Research Group, Brisbane City, Australia
2QUT Gardens Point Campus., School of Exercise and Nutrition Sciences, Brisbane City, Australia

Deep tissue pressure injuries (DTPI) and superficial pressure injuries (SPI) are caused by sustained pressure to the skin, resulting in shear and hydrostatic stresses which are distributed from the skin into deep tissues interfacing with boney tissue. Prior studies have shown the most common area for DTPI is in muscle over the sacrum [1] with prolonged periods of lying being a potential contributing factor. This study sought to better understand the mechanics of soft tissues of the pelvis while a patient is lying supine. To achieve this, a subject-specific finite element (FE) model was developed, to estimate the influence of substrate stiffness on the magnitude of shear and principal stresses within the muscle interfacing the sacrum (MIS) and skin interfacing with the substrate (SIS).

Both subject-specific anatomy and tissue parameters were developed using a combined approach including 3D imaging (MRI) and biomechanical assessment of the subject when lying. The model geometry was developed using MRI scans of a healthy male subject lying in both the prone and supine position. Scans in both positions enabled tissue deformation due to pelvis weight to be calibrated with the use of a pressure sensor mat (XSensor Tech Corporation, Canada), which measured distribution of torso/pelvis weight beneath the subject. 3D reconstructions for the bone, subcutaneous adipose and skin tissues, and other soft tissue (i.e. muscle and organs) were generated using Amira (Vsn 6.0, Thermo Fisher Scientific FEI, USA). Using ANSYS optimization tools, the constitutive models for the adipose and skin, and soft tissue were calibrated based on displacement/force responses (pressure mat) of the subject lying supine on a soft foam and rigid substrate (MRI mattress substrate). The FE model simulated the pelvis under gravitational load, in frictional contact ($\mu = 1$) with substrates of stiffnesses E=10KPa to 20KPa.

With increasing substrate stiffness, peak MIS Maximum Principal ($\sigma 1$) stress increased minimally (5%), while peak MIS Maximum Shear stress decreased by 25%. Within the SIS, the FEM predicted a non-linear relationship between stiffness and $\sigma 1$, where $\sigma 1$ was minimized at E=15KPa.

The model predictions highlight the importance of accurately calibrated substrate mechanics to produce useful stress estimation. The proposed methodology indicates that there exists an optimal substrate stiffness which reduces the shear stress within skin tissue. Further investigations are underway to explore a broader range of substrate mechanics and to implement pathologically-relevant tissue parameters.

References:
[1] Takahashi et al, 2017, J Tissue Viability, 26(1)

A3.4

Finite element modelling of the human eye crystalline complex under healthy and diseased conditions

Leonor Jud[1], Andre Castro[1], Rui Ruben[2], Bernardo Feijoo[3], Filomena Ribeiro[3], **Paulo Fernandes[1]**

1   *IDMEC, Instituto Superior Tecnico, Universidade de Lisboa, Lisbon, Portugal*
2   *ESTG, CDRSP, Polytechnic Institute of Leiria, Leiria, Portugal*
3   *Departamento de Oftalmologia, Hospital da Luz, Lisbon, Portugal*

The condition of pseudoexfoliation, prevalent in up to 30% of individuals older than 60-years-old [1], can lead to severe conditions such as subluxation or dislocation of the lens, due to the weakening of the supporting zonules i.e., zonulysis. The biomechanical effects of this disease remain poorly studied to this point. In order to address this gap, geometric non-linear FE models for a 62-year-old crystalline lens complex were developed, composed by the capsular bag, cortex and nucleus of the crystalline lens and anterior, equatorial and posterior sets of zonular fibers. The cortex and nucleus were modelled with tetrahedral elements (3D), whereas the capsular bag was modelled as a 2D shell, all with isotropic material properties. The zonules were modelled as membrane elements (2D), with hyperelastic anisotropic material properties. The stretching of the zonules changes the shape of the eye's lens, from an accommodated to a disaccommodated state (near-to-far vision). Healthy (from literature data [2]) and pseudoexfoliative conditions were modelled. Under pseudoexfoliation, the effects of individual and groups of the zonular sets were assessed: the zonulysis origin was examined, as well as its extension throughout the zonular fibers. The moderate zonulysis was considered to pertain 50% of the healthy zonular thickness, whereas the severe condition accounted for 5%, with transitional regions of 50% (see Fig.1).

The equatorial fibers had the lowest impact both on the accommodative capacity and thickness variation of the lens, being this role taken by the posterior zonules. At severe disruption of all zonular sets there is a loss of 86% of the total resulting force in the zonules, and total loss of accommodative response of the lens. In the capsular bag, the average Von Mises stress decreases from a healthy value of 73,4kPa to 12,43 kPa. A similar behavior is observed for the lens, where the maximum Von Mises stress value is reduced by 61%.

The present work allowed for a better understanding of potential routes to zonulysis, through the FE modeling of the effects of zonular dialysis. The source data can be attainable in a clinical setup, by means of measurements of one's accommodative capacity, so this work has the potential to be scaled for clinical practice and evaluation of patient's individual condition.
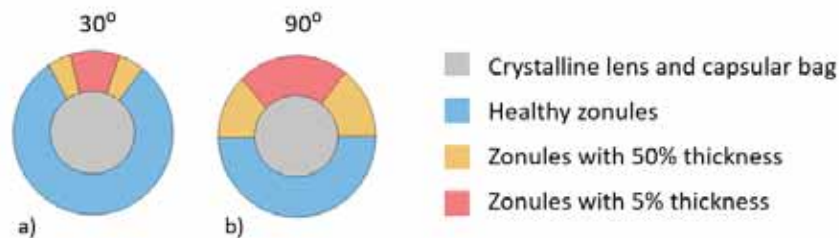

Figure caption: Diseased lens complex. a) Severe superior degeneration of 30 degrees, with 15 degrees of a transitional moderate region, in each side. b) Severe superior degeneration of 90 degrees, with transitional 45 degrees in each side of moderate dialysis.

References:
[1]   *Schöltzer-Schrehardt, U., Naumann, G. 2006. Ocular and systemic pseudoexfoliation syndrome. American journal of ophthalmology 141(5):921–937.*
[2]   *Wang, K. et al. 2019. A Modeling Approach for Investigating Opto-Mechanical Relationships in the Human Eye Lens. IEEE Transactions on Biomedical Engineering 67(4):999–1006.*

A3.5

Biomechanical analysis of intra-articular stresses caused by the reconstruction of the ACL using a section of the patellar tendon in the heel strike phase

Laura Dussan[1], Christian Javier Cifuentes De la Portilla[1], **Mónica Gantiva[1]**

1   Universidad de Los Andes, Ingeniería Biomédica, Bogotá D.C., Colombia

Anterior cruciate ligament (ACL) injury accounts for 50% of knee ligament injuries and 75% of them occur during sports activity [1]. The main treatment for this is ACL reconstruction with autologous tissue such as the patellar tendon. There are different variants of this surgery, however, there is no methodology that allows quantifying the consequences on the biomechanics of the knee. The objective of this study is to identify changes in ACL intra-articular tensions, during the heel strike phase of gait, at which time a force is generated that can move the tibia forward. For this, a finite element computational model has been made that was reconstructed from tomographic images of a healthy patient (Figure 1-A). This initial model was modified by changing the mechanical properties of the ACL to those of the patellar tendon to simulate ACL reconstruction surgery with a section of the patellar tendon. The model was validated simulating compression and flexion and comparing the results of tension in the menisci with the literature [2] [3]. Heel strike simulation was performed by subjecting the distal end of the tibia to a compression force of 574 N and a force of 300 N in the ventral direction in two simulation steps. As a result, it was obtained that the principal maximum stress for the case of the ACL reconstruction surgery model presented a value of 7.39 MPa in the ACL. This represents an increase of 202% with respect to the healthy model, which presented a maximum stress of 3.65 MPa. This increase is a consequence of the change in mechanical properties such as Poisson's radius, from 0.3 to 0.49, and Young's modulus, from 64MPa to 100MPa, which describe a more rigid behavior. In conclusion, there is evidence of a remarkable change in ACL intra-articular tensions related to reconstruction with tendon tissue, which exposes the need to evaluate the biomechanical consequences generated by a graft.

A)   B)   C)
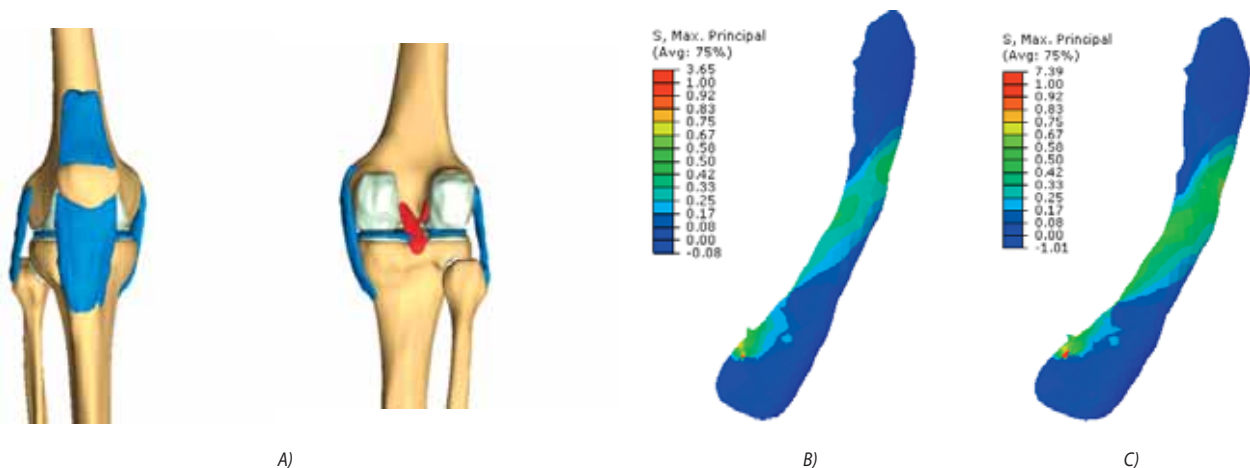
Figure 1: A) Healthy model obtained in 3D.- Maximum principal stress in ACL for B) healthy model and C) modified model subjected to force in the heel strike phase

References:

[1]   Márquez-Arabia J, Márquez-Arabia W. Lesiones del ligamento cruzado anterior de la rodilla. Revista latreia. 2009; 22(3): p. 256-271.
[2]   Peña E, Calvo B, Martínez M, Doblaré M. A three-dimensional finite element analysis of the combined behavior of ligaments and menisci in the healthy human knee joint. Journal of Biomechanics. 2006; 39(9): p.1686–1701.
[3]   Yagi M, Wong E, Kanaromi A, Debski R, Fu F, Woo SL.-Y. Biomechanical analysis of an anatomic anterior cruciate ligament reconstruction. American Journal of Sports and Medicine. 2002; 30: p. 660–666.

A3.6
Finite element analysis of subchondral bone cysts in the tibiotalar joint

Harriet Talbott[1], Richard Wilkins[2 3], Anthony Redmond[2 4], Claire Brockett[1 2 4], Marlène Mengoni[1]

1   Institute of Medical and Biological Engineering, School of Mechanical Engineering, University of Leeds, Leeds, United Kingdom
2   Leeds Institute of Rheumatology & Musculoskeletal Medicine, Leeds, United Kingdom
3   Leeds haemophilia Comprehensive Care Centre, Leeds Teaching Hospitals NHS trust, Leeds, United Kingdom
4   Versus Arthritis Centre for Sports, Exercise and Osteoarthritis, Nottingham, Oxford, Loughborough, Leeds, United Kingdom

Subchondral bone cysts are an indicator of late stage haemophilic joint disease; however, the implication of these cysts on joint health is little understood. The aim of this study was to assess, computationally, the influence of subchondral bone cysts on tissue pressures through their inclusion in patient-specific finite element (FE) models.

Chronologically sequential, non-weightbearing MRI sequences (N=17) were acquired for three people with subchondral bone cysts present in one or more bone of the tibiotalar joint. Segmentation specific FE meshes of bones, cartilage and subchondral bone cysts were created using Simpleware-ScanIP P-2019.09 (Synopsis). FE models were developed to simulate the forces associated with neutral still standing, for each sequence under two cyst conditions: cysts defined as intact bone, and as defacto cystic tissue (Abaqus 2017, Dassault Systèmes). A subsequent study on the effect of the depth of the cyst alone was carried out by creating artificial models from one of the ankles for which the cyst volumes were displaced away from the surface by increments of 0.5mm to a maximum of 3mm (maximum observed distance across all ankles.

Changes in peak and mean contact pressures were measured to investigate the influence of the cystic tissue. Mean contact pressures saw small percentage changes in all ankles, with both tibial and talar cartilage values tending in the same direction, the degree of change appeared to be unrelated to cyst location or volume. However, contact pressure distribution on both cartilage layers changed with the addition of cystic tissue, this was consistent in shape when the cyst was offset to different depths. Mean contact pressure varied minimally with the offset, though peak outputs were affected.

This work demonstrates the importance of cystic tissue in contact pressure distribution in the ankle. Mean contact pressure however is not affected by cysts, whatever their depth or volume. The presence of cysts may affect progression of the disease by redistributing contact between the tibia and the talus.
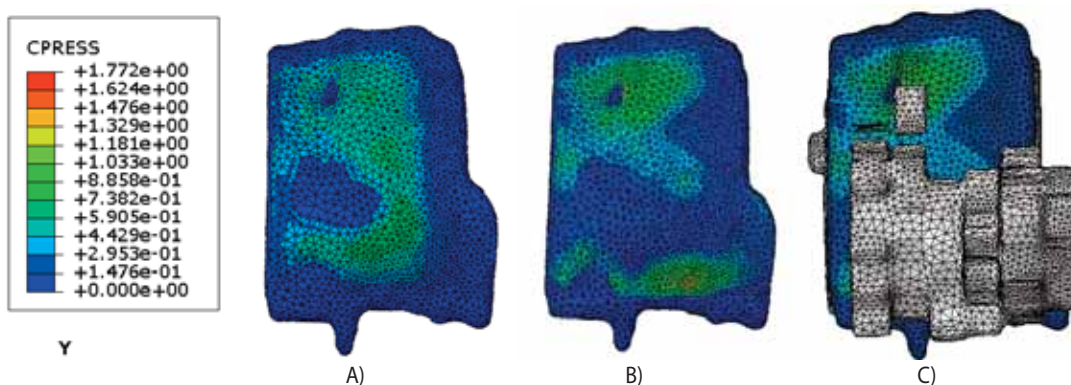

Figure caption: Contact pressure (MPa) on the talar cartilage (A) modelled as intact bone, (B) defacto cystic tissue, (C) tibial cyst overlaid for location reference.

A4.1
Statistical shape modeling to evaluate alterations in female bony pelvis morphology with pregnancy and parturition

Megan Routzong[1], Liam Martin[1], Ghazaleh Rostaminia[2], Pamela Moalli[3], Steven Abramowitch[1]

1   University of Pittsburgh, Bioengineering, Pittsburgh, United States
2   Northshore University Health System, Division of Urogynecology, Skokie, United States
3   University of Pittsburgh, Obstetrics, Gynecology & Reproductive Sciences, Pittsburgh, United States

Background: Although it has been documented that the female bony pelvis undergoes changes during pregnancy, robust pelvic shape quantification has yet to be implemented to study pregnancy and parturition (childbirth). While a wider pelvis is more favorable for vaginal childbirth, it has also been associated with pelvic floor disorders1. Therefore, our goal was to use statistical shape modeling to evaluate alterations in female bony pelvis morphology with pregnancy and parturition by comparing the shapes of nulliparous (have never given birth), pregnant (in the 3rd trimester), and parous (have given birth) women.

Methods: In this retrospective study, the bony pelvis (innominate bones and sacrum) was segmented from pelvic MR and CT images of women age 19-49. To establish corresponding points while simultaneously smoothing each segmentation, a template pelvis was fit to each patient-specific geometry using DeformetricaTM. Then a Procrustes analysis was performed in MathematicaTM to align the shapes, a principal component (PC) analysis identified modes of variation, and a parallel analysis determined which modes described significant shape variance (i.e., more than noise). PC scores—projections of patient-specific data onto eigenvectors—from each significant mode were compared between nulliparous (N=15), pregnant (N=15), and parous (N=17) women with a MANCOVA (controlling for age) and multiple comparisons post-hoc.

Results: The first 2 of 9 modes described significant differences between patient groups (p=0.008 and <0.001, respectively). Pregnant pelvises significantly differed from those of nulliparous and parous women (Figure 1). Modes 1 and 2 described 26.5% and 12.9% of the total shape variance, respectively. Mode 1 demonstrated an overall wider pelvis (particularly at the iliac crests) and straighter sacrum and Mode 2 demonstrated a wider pubic arch and more inferior lumbosacral joint and sacral promontory on average in pregnant compared to nulliparous and parous women.

Conclusions: The bony pelvis undergoes significant changes during pregnancy (in response to altered mechanical loads and hormone levels) that appear to widen the pelvis in preparation for vaginal childbirth. Interestingly, the bony pelvis shape recovers after pregnancy and parturition to nulliparous values (representative of a narrower pelvis), suggesting that these pregnancy-specific shape alterations are generally not permanent. Future studies will evaluate these changes longitudinally and their relationship with the mechanics of childbirth and pelvic floor disorders.
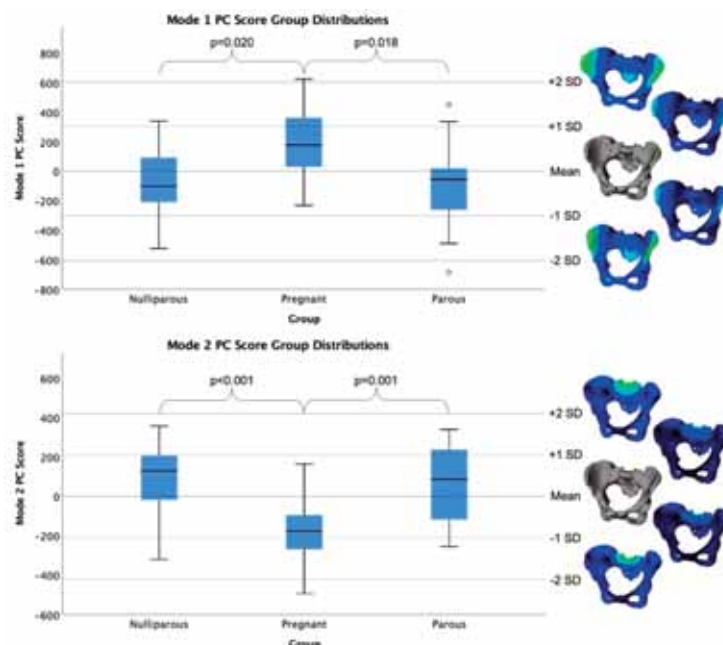

Figure caption: Boxplots displaying mode 1 and 2 PC scores with corresponding pelvic shapes at each standard deviation (SD) from the mean. Significant group differences are denoted with p-values. Lighter colors represent regions of maximal and dark colors regions of minimal displacement from the mean shape.

References:
1. Pavličev M et. al. Am. J. Obstet. Gynecol. 222(1):3-16.2020

A4.2
Novel application of a corresponding point algorithm for unbiased smoothing

Liam Martin[1], Megan Routzong[1], Pamela Moalli[2], Steven Abramowitch[1]

1   University of Pittsburgh - Swanson School of Engineering, Bioenginnering, Pittsburgh, United States
2   UPMC Magee-Womens Hospital, Obstetrics, Gynecology & Reproductive Surgery, Pittsburgh, United States

Background: When geometries obtained from medical images are used in computational analyses, aliasing can cause significant challenges; thus, geometries are smoothed via manual, semi-manual, or fully automated techniques. Manual techniques are time-consuming and potentially introduce bias, and most automated techniques can introduce artifacts, volumetric changes, and/or overly smooth anatomical features. The goal of this study was to develop and evaluate an unbiased, automated smoothing protocol to remove aliasing resulting from MR and CT imaging data while preserving anatomical features with high curvature.

Methods: The pelvic innominate bones and sacrum were chosen for this study due to their geometric complexity. 24 high-resolution CT scans were manually segmented. The geometries were averaged to serve as the template. An additional CT scan served as the "ground truth," representing a patient-specific scan to be segmented and smoothed. Sequences of slices were then removed to introduce various degrees of aliasing, resulting in the inclusion of only 50%, 33%, 25%, 20%, 17%, and 14% of the original image data. The resulting segmented geometries were then smoothed using a large deformation diffeomorphic metric mapping corresponding point algorithm (implemented in Deformetrica1) that smooths by fitting the template geometry to subject-specific segmentations. Each smoothed geometry was then compared to the ground truth via an unsigned point-to-surface distances to determine accuracy. Success was defined a priori as an average surface-to-surface distance of under 1 mm and at least 90% of distances smaller than 2.5 mm.

Results: The template consisted of 25,743 vertices and smoothing of all geometries took 32 hours (single CPU core @ 2.6 GHz, 192 Gb Ram). The protocol was robust to large degrees of aliasing (Figure 1). All aliased pelvises had an average surface-to-surface distance under 1 mm (max 0.79 mm), and over 95% of vertices had an error less that 2.5 mm (min 96% vertices).

Conclusions: This approach demonstrated the capacity to smooth highly aliased pelvises to a level nearly indistinguishable from high-definition CT segmentations. The protocol affords the use of previously unusable datasets (high amount of aliasing) in shape modeling and finite element studies. While the focus of this study was the bony pelvis, future studies will confirm the validity of this protocol and its robustness for other bones, soft tissues, and missing data.
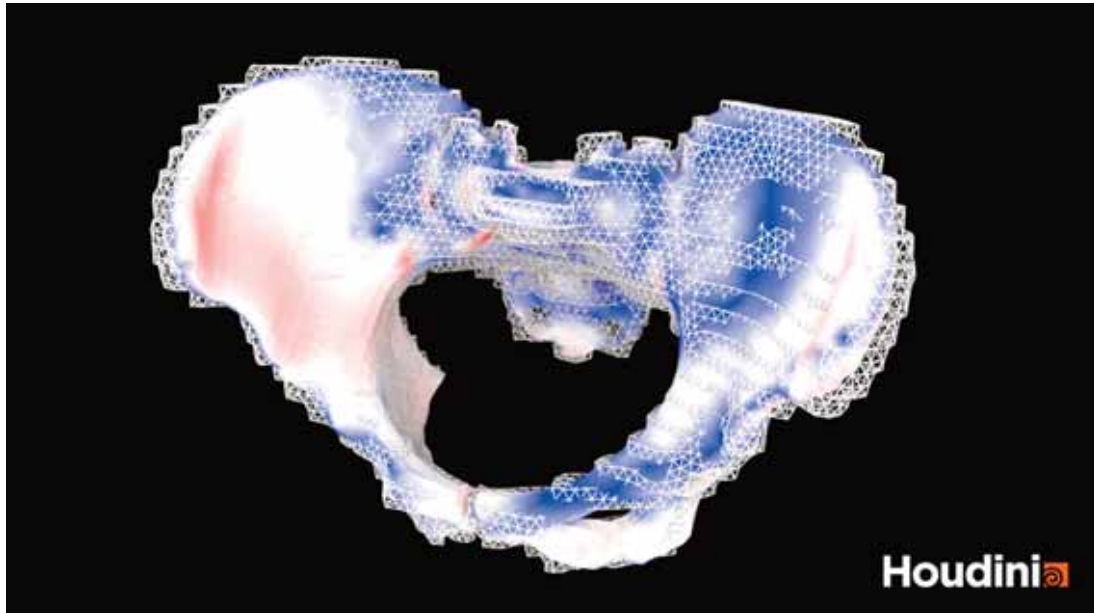

Figure caption: Comparison of the fit of the template (solid object) deformed into the 14% test pelvis (wireframe) to ground truth. The colormap represents distance to ground truth transitioning from red at > 2 mm, to white at 1 mm, and blue at ≈ 0 mm.

References:
1.   Lange C et al. Anisotropic smoothing of point sets. Computer Aided Geometric Design; 2005.

A4.3

Ultrasound-derived finite element models of pregnant women at high- and low-risk for preterm birth

Erin Louwagie[1], Mirella Mourad[2], Ronald Wapner[2], Joy Vink[2], Kristin Myers[1]

1   Columbia University, Mechanical Engineering, New York, United States
2   Columbia University Irving Medical Center, Obstetrics & Gynecology, New York, United States

Globally, 1 in 10 babies is born prematurely, with preterm birth (PTB) defined as delivery before 37 weeks gestation [1]. There is no accurate or universal method to predict or prevent PTB [2,3]. The integrity of cervical tissue is vital to term pregnancy. However, a pervasive lack of knowledge on normal cervical and uterine tissue behavior makes it challenging to identify patients at high risk of PTB [3]. This research aims to investigate the biomechanical environment of patients who delivered preterm and at term using finite element computational methods.

In this study, we measured maternal anatomy and cervical stiffness from two cohorts of women: oneat high-risk for PTB and another at low-risk for PTB. Patients at high risk for PTB were recruited based on cervical length, with an ultrasound cervical length of less than 20mm considered high risk. Patients at low risk for PTB were screened against for indicators of PTB and risks of fetal demise. Cervical stiffness was measured using the Pregnolia system (Pregnolia AG, Schlieren, Switzerland). High-risk subjects were examined at two gestational timepoints (16-24 weeks and 4-9 weeks after initial exam), and low-risk subjects were examined at four gestational timepoints (8-14, 18-20, 24-26, and 34-36 weeks). In each exam, overall dimension measurements of the uterus and cervix were obtained from ultrasounds taken by trained sonographers. 3D models of each patient's anatomy were built using an existing parametric modeling method [4]. These models included the uterus, cervix, fetal membrane, and a supporting abdomen. For comparison, we used the first visit measurements from the high-risk cohort and second visit measurements from the low-risk cohort.

Meshed finite element geometries were generated in Hypermesh 2021 (Altair Engineering Inc., Troy, MI), and finite element analysis (FEA) computed in FEBio Studio (v1.3.0) [5]. The models were fixed in the normal direction in the sagittal plane, on the posterior side, and the superior and inferior faces. Material properties were assigned based on exiting literature [6], and patient-specific cervical properties were found using inverse FEA of the cervical stiffness measurements. An intrauterine pressure of 1kPa was applied. Patients who delivered preterm have higher stretch concentrations at the internal os (opening of cervical canal into uterine cavity) (Fig.).
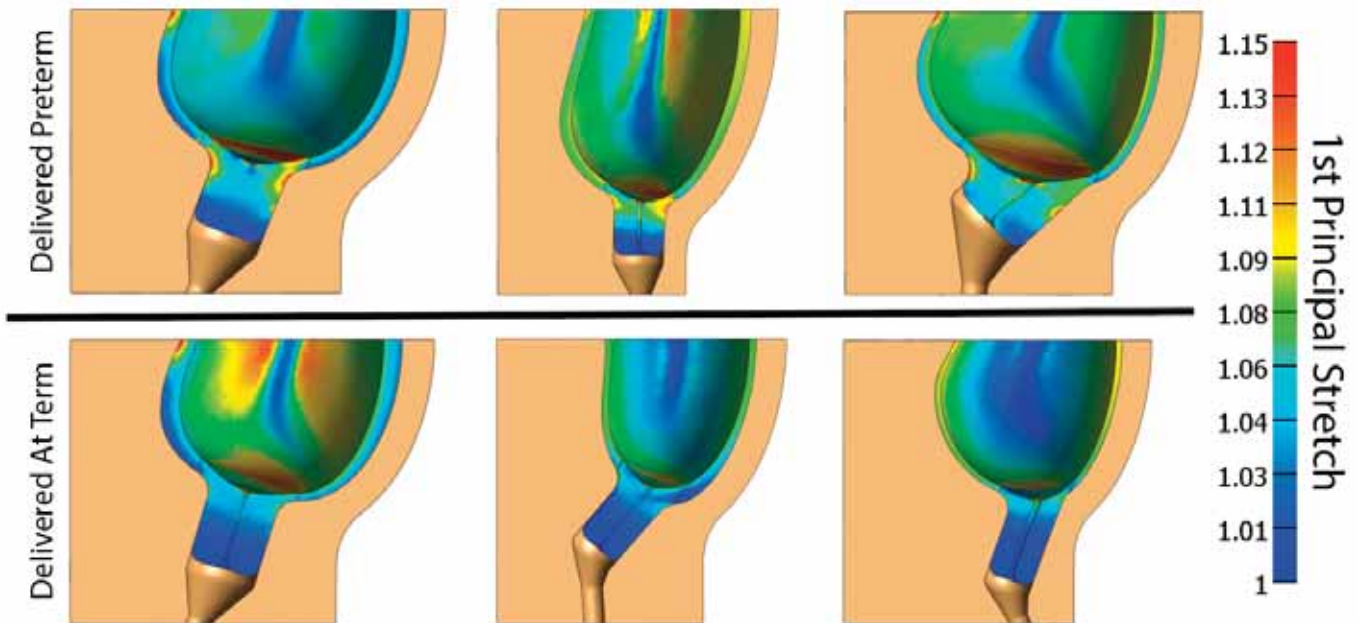

Figure caption: 1st principal stretch maps for patients who delivered preterm and patients who delivered at term.

References:
[1]   The Partnership for Maternal, Newborn & Child Health, "Born Too Soon: The Global Action Report on Preterm Birth", 2021.
[2]   Mayo Clinic, "Premature Birth", 2017.
[3]   Vink, J and Myers, K, Best Pract Res Cl Ob, 52:88-102, 2018.
[4]   Louwagie, E et al., PLOS ONE, 16(1):e0242118, 2021.
[5]   Maas, S et al., J Biomech Eng, 134(5):011005, 2012.
[6]   Westervelt et al., J Biomech Eng, 139(5): 0510041-05100411, 2017.

A5.1

Computational investigation of the effect of bolus stiffness on TMJ loading during chewing

Benedikt Sagl[1], Martina Schmid-Schwap[1], Eva Piehslinger[1], Xiaohui Rausch-Fan[1], Ian Stavness[2]

1   Medical University of Vienna, University Clinic of Dentistry, Wien, Austria
2   University of Saskatchewan, Department of Computer Science, Saskatoon, Canada

The human jaw region is a complex musculoskeletal system, encompassing two joints working in unison together with many muscles in a relatively small area. Mastication is an essential task of human life and produces high muscle activations, which have the potential of producing increased temporomandibular joint (TMJ) loading. While the pathophysiology behind the development of diseases of the TMJ is not fully understood (1), an increased loading of the TMJ has been previously associated with temporomandibular disorders (TMD), which suggests a potential clinical relevance of TMJ mechanics during chewing in TMD treatment (2). Moreover, TMD self-management guidelines suggest eating soft and small pieces of food to reduce TMJ pain (3). TMJ loading cannot be measured in vivo, due to patient safety restrictions, which leaves computer modeling as one of the few tools available for investigations of the potential connection between TMJ loading and TMD. Consequently, the objective of the presented study was to investigate the effect of food bolus stiffness on mechanical TMJ loading.

A combined rigid-body-finite-element model of the jaw region was used to investigate the effect of food bolus stiffness, while keeping bolus position and size stable. The bolus was placed on the right-side first molar and had a size of 10mm. The stiffness was investigated for 0.5 MPa, 0.875 MPa, 1.25 MPa, 1.625 MPa and 2 MPa. Mandibular motion and TMJ disc von Mises stress were reported.

Overall, computed mandibular motion agrees well with previous literature. The mechanical stress of the disc was higher during the closing phase of the chewing cycle and for the non-working side disc at all stiffness levels. Lower stiffness of the food bolus lead to a reduced TMJ loading.

Our, results support the present guidelines regarding bolus stiffness modifications. Overall, our study offers a first in silico investigation of dynamic chewing with detailed TMJ stress for different bolus stiffness values. The results help to strengthen the confidence in TMD self-management recommendations, potentially reducing pain levels of patients.

In the future, we strive to include more bolus variables in our investigation to develop a comprehensive overview of the biomechanical effect of various food bolus variables on mechanical TMJ loading.
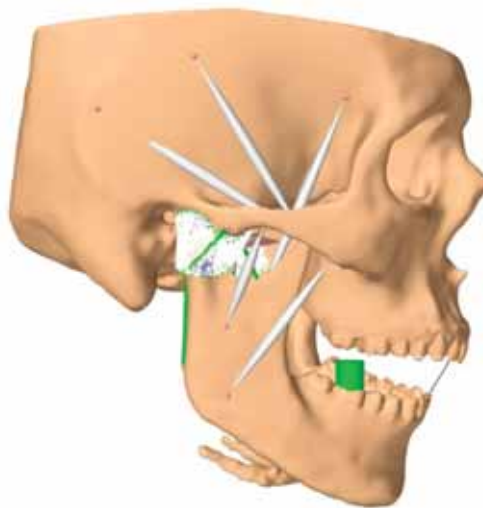

Figure caption: Model used for investigation during a chewing simulation

References:
1.   Ingawalé S, Goswami T. Temporomandibular joint: Disorders, treatments, and biomechanics. Ann Biomed Eng [Internet]. 2009;37(5):976–96. Available from: http://www.ncbi.nlm.nih.gov/pubmed/19252985
2.   Detamore MS, Athanasiou KA. Structure and function of the temporomandibular joint disc: Implications for tissue engineering. J Oral Maxillofac Surg. 2003/04/10. 2003;61(4):494–506.
3.   Story WP, Durham J, Al-Baghdadi M, Steele J, Araujo-Soares V. Self-management in temporomandibular disorders: a systematic review of behavioural components. J Oral Rehabil. 2016;43(10):759–70.

A5.2
Influence of different occlusal contact situations on stress in periimplant bone

Andreas Greuling[1]

1   *Medizinische Hochschule Hannover, Klinik für zahnärztliche Prothetik und biomedizinische Werkstoffkunde, Hannover, Germany*

Nowadays, implant restorations are often used for treatments in dentistry, yet implant losses are still a problem. Several factors play a role here, for instance adverse biological reactions like periimplantitis. Occlusal overload is also a known problem and is often addressed by finite element analysis. In this study [1] the stress distribution in peri-implant bone of a single-tooth implant crown was investigated using the finite element method. The load was applied indirectly via an occluding tooth through a three and five contact setup into the implant crown. The friction coefficient values between the crown and antagonist were varied between 0.1 and 1.0. Additionally, three crowns with cusp inclinations of 20 °, 30 ° and 40 ° were modeled. We found higher stress magnitudes when using cusps with greater inclination. Furthermore, the number of contact areas and the interplay between the different areas with different inclination also played a major role for the stress in the periimplant bone. If the goal is to reduce stress in the periimplant bone, particular attention should be paid to occlusal adjustment so as to prevent oblique loading onto dental implant restorations.
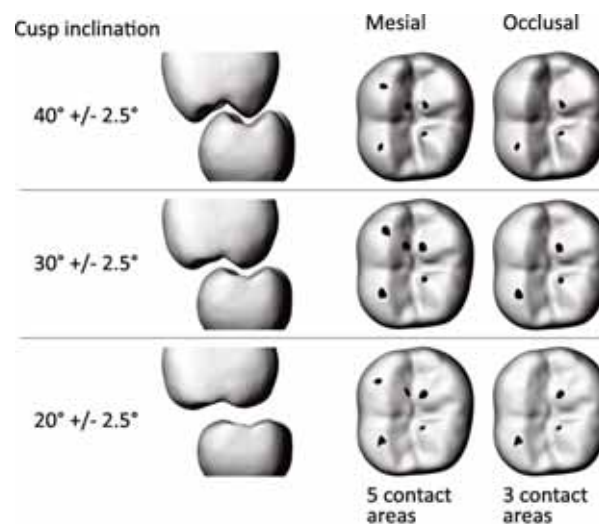

Figure caption: Occlusion schemes used in the FEA. On the left side the different cusp inclination is visualized, on the right the resulting contact areas on tooth 46 for two different contact situations.

References:
[1]   *Brune, A., Stiesch, M., Eisenburger, M. & Greuling, A. (2019) The effect of different occlusal contact situations on peri-implant bone stress - a contact finite element analysis of indirect axial loading. Materials Science & Engineering C-Materials for Biological Applications 99: 367-373.*

A5.3

The effects on temporo-mandibular joint caused by orthodontic inter-arch elastics: a finite element study

Yaqiu Zhang[1], Ludger Keilig[1], Istabrak Dörsam[1], Christoph Bourauel[1]

1   University of Bonn, Oral Technology, Bonn, Germany

Introduction: Temporo-mandibular joint disorder (TMD) is a cranio-facial disease caused by the combination of diverse etiologies. It is reported that TMD followed after orthodontic treatment in some cases. Inter-arch elastics are a common way to apply forces during orthodontic treatment, and it causes mechanical effects on the temporo-mandibular joint (TMJ). It is expected that some adapted remodelling develops to coordinate the relation of maxilla and mandible and the respective teeth. The aim of this study was to analyze whether variations of inter-arch elastics would develop harmful effects on healthy TMJ.

Method: A TMJ model with masticatory system based on Hill type actuators was established [1, 2] with finite element method (see figures 1 and 2) using Mimics and MSC.Marc/Mentat software packages. Mouth opening and closing with and without orthodontic loading were simulated and von Mises stresses and maximum principle stresses on the disc and the displacements of mandible were analyzed.

Results: Comparing the simulations with and without orthodontic force application, there is no significant difference of the stresses on the surface of disc, and the displacement of the mandible is more forward with a clockwise rotation under application of class II long and short elastics, more backward and upward with counterclockwise rotation under class III long and short elastics, no apparent difference under vertical elastics, tend to the opposite side with larger anchorage under oblique elastics and tend to the side with orthodontic loading under interaction elastics.

Conclusion: In our study the stress on the surface of disc with orthodontic loading is in the normal biological range. Comparing with long distance elastics, the short elastics lead to more gentle stresses. It is better to choose short elastics for a part of patients with TMD. Displacement of the mandible is beneficial to the corresponding orthodontic treatment.

Table 1: The stresses on temporo-mandibular discs at the maximum opening position (partial results).

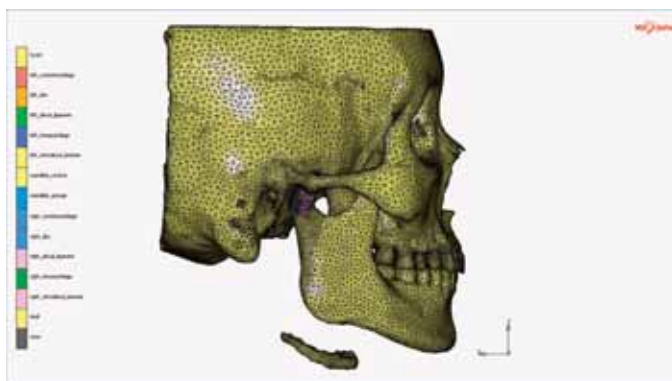|	von Mises Stress		Maxium Principle Stress	
	Left	Right	Left	Right
Without	1.46E-02	5.08E-02	-3.88E+00	-3.34E+00
	3.538E+00	3.823E+00	4.21E+00	3.70E+00
Class II	1.89E-02	4.71E-02	-4.89E+00	-3.82E+00
	4.79E+00	2.77E+00	5.63E+00	3.19E+00
	2.37E-02	5.19E-02	-3.10E+00	-2.49E+00
	3.78E+00	2.70E+00	4.54E+00	4.49E+00

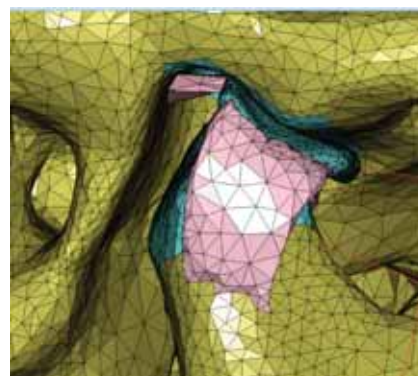Figure 1: Right lateral view. The red lines indicate the direction of the passive muscle forces.

Figure 2: The right teporo-mandibular joint.

References:
[1]   Hill, A.V. et al., Proc. Roy. Soc. B, 126:136-195, 1938.
[2]   Van Ruijven, L. J. et al., Eur. J. Appl. Physiol, 61: 479–485, 1990.

A5.4

Numerical simulation of forces generated during different bodily teeth movements using an orthodontic aligner

Tarek Elshazly[1], Ludger Keilig[1], Ahmed Ghoneima[2], Moosa Abuzayda[2], Christoph Bourauel[1]

1   Bonn University, Oral Technology Department, Bonn, Germany
2   Hamdan Bin Mohammed College of Dental Medicine, MBRU, United Arab Emirates

This study aimed to develop a 3D Finite element (FE) model to understand the biomechanical behaviour of clear aligners. Using the Msc.Marc/Mentat FE system, an idealised FE model consisting of 3 teeth was used to perform sensitivity analysis. Using software packages Materialise Mimics, a realistic 3D model of upper jaw was imported to design different orthodontic cases. A complete aligner with a 0.7 mm thickness was modelled. The full model was exported to Marc/Mentat. 4-noded tetrahedral elements were used for meshing. The number of nodes and elements for each component of the model are shown in Table 1. Material parameters of all structures are shown in Table 2. The forces generated by 0.2 mm bodily movements of the teeth 21, 13, and 15 (facio-lingually, mesio-distally, and extrusion-intrusion) were calculated and compared to standard experimental measurements. A touching condition was established in contact interfaces between the aligner and the tooth surfaces, with a friction coefficient of $\mu=0$, and interference closure - 0.04. The resultant forces in facio-lingual direction were $\approx$25 N, in mesio-distal direction were $\approx$25 N, while in extrusion-intrusion direction were $\approx$2.5 N.

Table 1: Number of nodes and elements of the Components of the finite element model.

Component	No. of Elements	No. of Nodes
Aligner	380308	92570
Cast	223637	55383
Tooth 21	13541	3450
Tooth 13	17451	4299
Tooth 15	11745	4299

Table 2: Material parameters of all structures.

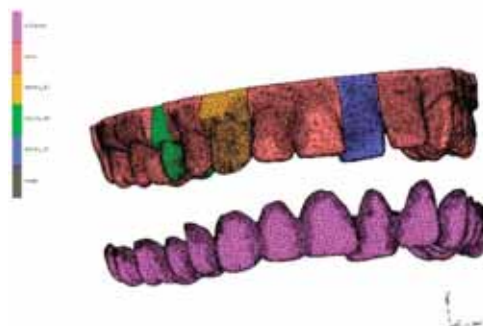| Structure	Young's Modulus (GPa)	Poison's ratio
Aligner	2	0.3
Teeth	80	0.3

Figure 1: A realistic 3D-model of upper jaw with designed 0.7 mm clear aligner used to simulate different orthodontic movements of the teeth 21, 13, and 15.

References:
1.   Elkholy et al, American Journal of Orthodontics and Dentofacial Orthopedics, 151:407 – 415, 2017.
2.   Lee et al, Comput. Methods Biomech. Biomed. Engin., 16:1143–1149, 2013.

A5.5
Finite element estimation of orthodontic tooth movement using stimulus induced node motion

Zumrat Usmanova[1], Emin Sunbuloglu[1]

1   Istanbul Technical University, Mechanical Engineering, Istanbul, Turkey

Load initiated bone adaptation process has been used in orthodontics to treat malocclusions in patients by applying stimuli outside of usual everyday loads, also called orthodontic loads, to promote tooth movement by affecting equilibrium state of the surrounding bone tissue. Accurate modeling of long term orthodontic tooth movement (OTM) is an important aspect of dental biomechanical research since it allows to predict the behavior and interaction of bone-tooth environment in a non-destructive way. Existence of such predictive tools might also help to avoid the adverse effects of OTM on teeth and the surrounding tissues during this clinical procedure. Analyzing long-term OTM via FEA is not an easy task and it is important to correctly set-up the tooth-bone environment and interactions between each constituent of the model. In this study a novel numerical method to simulate long-term OTM is proposed. The method involves external bone remodeling with strain energy density (SED) of the bone taken as the mechanical stimulus, and bone apposition and resorption are modeled by nodal movements at the bone/tooth interface using ABAQUS UMESHMOTION subroutine. Contrary to conventional re-meshing algorithms, where resorbed/apposed bone is being constantly updated and element deletion/creation is performed for each increment, the proposed method only moves the mesh without changing the initial topology. This way, a continuous re-meshing is avoided at each increment and computational power is greatly reduced, which is of great importance during long-term OTM simulations with anatomically exact and complex tooth-bone models. For this study, a 3D model of right central maxillary incisor and its surrounding alveolar bone was used for the modeling of OTM for a duration of 1 week. Displacement controlled orthodontic load was applied to the tooth and the resulting bone remodeling was observed. Results indicated strain energy density values reaching an equilibrium state after a certain period of time. In this study, UMESHMOTION subroutine was successfully implemented and external bone remodeling without change in initial topology has been achieved.
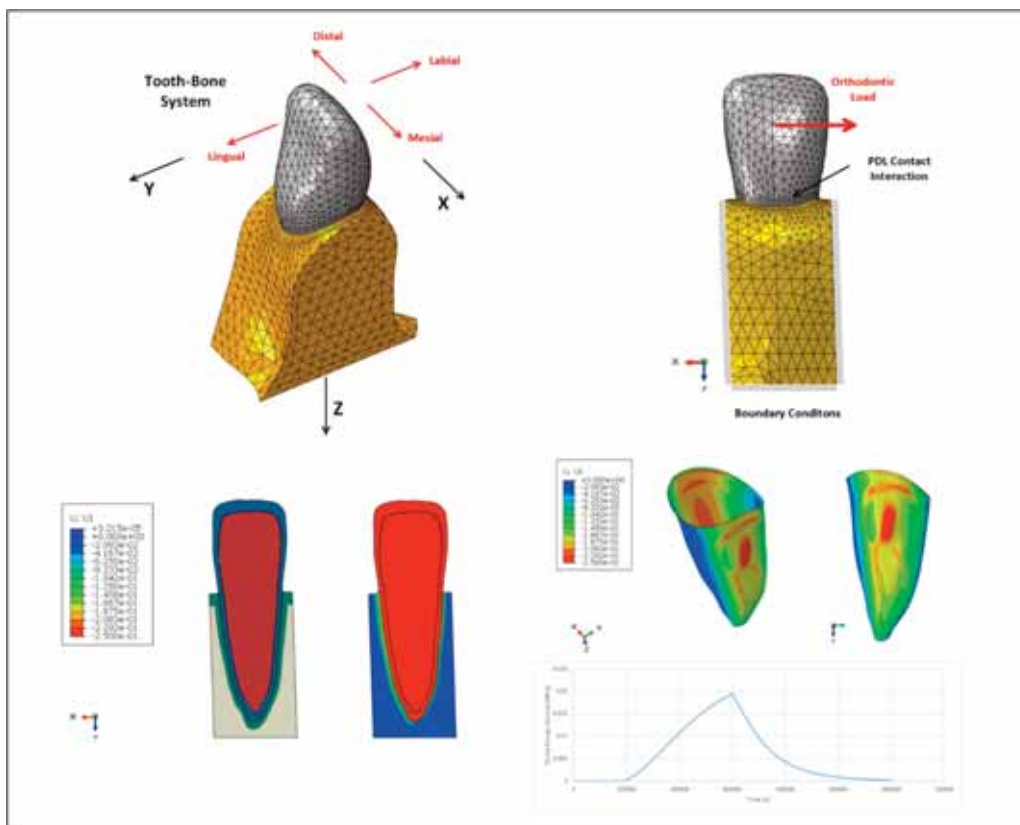

Figure . General overview of the process

A6.1
What metrics should we be using to access implant fixation?

Mark Taylor[1]

1   Flinders University, Medical Device Research Institute, Adelaide, Australia

Finite element analysis has been extensively to assess the fixation of primary and revision joint replacements and fracture fixation devices. The emergence of in silico clinical trials has the potential to lead to a paradigm shift in the evaluation of orthopaedic devices. However, FE has yet to be fully accepted by regulatory agencies as a method to evaluate the performance of existing and new devices. One reason for this is the absence of reliable and robust assessment criteria. A variety of metrics have been used to assess the immediate post-operative and long term mechanical environment including bone stress, strain and strain energy density. Micromotion at the bone-implant interface is also commonly reported to assess the primary stability of cementless devices. Although these metrics are widely used in the literature, there is no consensus as to how these metrics should be reported (peak, mean, percentiles, percentage area or volume experiencing a defined range of the metric), where these metrics should be assessed (defined regions of interest vs whole bone) and what values of the metric are deemed to represent acceptable or unacceptable performance. More importantly, there has been limited research to establish how these metrics, and the method of reporting them, correlates with actual clinical performance.

An example is the assessment of primary stability of cementless implants by predicting the micromotion at the bone-implant interface. Many studies cite the research of Pilliar et al. (Pilliar et al., 1986) that states if micromotions are less than 30 microns bone ingrowth will occur, whereas fibrous tissue formation will occur if micromotions are greater than 150 microns. At first sight, this suggests that a well define performance criteria can be identified, for example that micromotions should be below 30 microns. Historically, the peak micromotion has been commonly reported as the output metric. If peak micromotion is used most implants would fail the performance criteria, as they commonly have regions that exceed not only the 30 micron threshold for bone ingrowth but also the 150 micron threshold for fibrous tissue formation. However, if the mean interface micromotion is reported, there is a greater chance that an implant can be shown to meet this performance criteria. In isolation, reporting the metrics in a different way does not solve the problem of how to develop an effective screening tool. To truly evaluate whether a given metric (e.g. mean or peak micromotion) is effective, it needs to be evaluated and benched marked for a range of implants with known clinical histories, both good and bad.

Through examples, such as assessing primary stability, it will be shown that there is still considerable work needed to identify and verify robust performance metrics which can be used to determine the safety and efficacy of new orthopaedic devices.

References:
Pilliar, R.M., Lee, J.M., Maniatopoulos, C., 1986. Observations on the effect of movement on bone ingrowth into porous-surfaced implants. Clin. Orthop. Relat. Res. 208, 108–113.

A6.2
3D finite element modal analysis of a femoral stem under various bone-implant contact conditions

Anne-Sophie Poudrel[1], Vu-Hieu Nguyen[2 3], Giuseppe Rosi[2 3], Guillaume Haiat[1]

1   MSME, CNRS UMR 8208, Univ Paris Est Creteil, Univ Gustave Eifel, CNRS, 61, Avenue du Général de Gaulle, 94010 Créteil Cedex, France
2   Université Paris-Est Creteil, CNRS, MSME, 94010 Créteil, France
3   Université Gustave Eiffel, MSME, 77454 Marne-la-Vallée, France

Around one million Total Hip Arthroplasty (THA) are carried out yearly worldwide, making it one of the most common surgical procedure [1]. Cementless arthroplasty is more and more frequently performed. The implant is impacted following a press-fit procedure into a slightly under-sized cavity, previously reamed by the surgeon. The primary stability achieved during the surgical procedure is a determinant factor of the success of cementless hip arthroplasty surgery [2]. Some numerical studies have described the effects of the bone cavity properties on the acetabular cup primary stability [3]. However, the biomechanical phenomena occurring at the bone-implant interface during the femoral stem insertion are still poorly understood and it remains difficult to quantify in vivo the optimal insertion state. The aim of this study is to evaluate the influence of biomechanical properties on the frequency response of the bone-implant system as an indicator of the quality of the insertion.

For that purpose, a nonlinear geometrical 3D finite element model of the femoral stem insertion was implemented (Figure 1). A parametric study was carried out by considering changes of cortical and trabecular bone Young's moduli E_c and E_t, of bone thickness and the friction coefficient at the bone-implant interface μ. For each configuration, the numerical simulation was divided into two successive steps. First, a quasi-static analysis involving Coulomb's contact law was used to model the implant insertion into the bone. A loading force ranging from 500N to 2000N characterizing each insertion step was applied at the top of the ancillary which is a rigid cylindrical part used by the surgeon to apply the impacts during implant insertion. Then, after each insertion step, a modal analysis was carried out and the vibrational behavior of the ancillary-femoral stem system was characterized.

The Frequency Response Functions of the system and the corresponding mode shapes were calculated on the frequency range [0-10] kHz. The results show a sensitivity of specific resonance frequencies to (i) the femoral stem driving level in the bone and (ii) to bone-implant interface biomechanical properties. The proposed model should be validated experimentally by comparing the results obtained numerically with experimental modal analysis. This study opens new paths towards the development of noninvasive evaluation methods of the femoral stem stability.

Figure caption: Geometry of the femur and the femoral stem

References:
[4]   Pivec et al, Lancet, 380 (9855), 1768–1777, 2012
[5]   Ulrich et al, International Orthopaedics, 32(5): 597–604, 2008
[6]   Raffa et al, Proc Inst Mech Eng H, 233 (12), 1237–1249, 2019

A6.3
Explicit finite element evaluation of uncemented total hip arthroplasty

Marzieh Ovesy[1], *Philippe Zysset*[1]

1   ARTORG Center, Bern, Switzerland

The term primary stability of total hip arthroplasty (THA) is mainly quantified as the amount of micromotions occurring at the bone-implant interface. Finite element analysis (FEA) could measure the amount of micromotions. However, these models have not considered the damage and the complex material representation of bone [1]. This study aimed to evaluate the effect of implantation on bone in terms of stress and quantify the irreversible micromotions produced during subsequent loading cycle.

A cadaveric right femur (age: 87, gender: female) was scanned using quantitative computed tomography (QCT). Using a pre-operative surgery planning, the Optimys (Mathys Medical, Switzerland) femoral stem was positioned in the bone. The head of the femur was cut accordingly. To simulate the canal opened by the rasping stage, the implant image was shrank by 2 mm and subtracted from the femur. Then, the femur was meshed and the corresponding bone volume fraction (BV/TV) was assigned to each element (Medtool, Austria). Explicit finite element simulation was performed .The material model was chosen to represent the bone as a BV/TV dependent homogenized material having elastic-plastic behavior [2]. Damage was based on the cumulative plastic strain and fully damaged elements were deleted [2]. The implant was assumed to be rigid. Unilateral contact with a friction coefficient of 0.3 was applied. The implantation was simulated by a displacement-based loading protocol defining the position of the implant tip along the femur shaft. Finally, the implant undergoes a loading cycle representing a gait cycle from the Orthoload database. The irreversible micromotions were evaluated as the relative motion between bone and implant at the end of loading cycle [3].

The implantation was simulated successfully. The maximum von Mises stress after the implantation was 141 MPa. The maximum micromotions after the loading stage was 440 μm, respectively showing the highest values at medial and lateral sections of the femur. Existence of friction has led to higher tangential micromotions than normal values.

The developed approach based on explicit FEA and bone damage allows for the first time to model the hip implantation process and evaluate primary stability after the first physiological loading cycle. It also provides the opportunity to quantify the stresses induced by implantation and apply loading protocols on the damaged femur rather than on an intact structure. This first proof of principle opens the path to investigate the effect of press-fit and friction and on the primary stability of THA.

References:
1.   Viceconti et al, J Biomech, 33 1611-1618, 2000.
2.   Ovesy et al, J Biomech, 107 109844, 2020.
3.   Bergmann et al, J Biomech: 34(7) 859-71, 2001.

A6.4
Modelling bone-implant interaction in fracture fixation devices

Pankaj Pankaj[1]

1   The University of Edinburgh, King's Buildings Campus, School of Engineering, Edinburgh, United Kingdom

Fracture fixation devices, such as half-pin fixators, ring fixators and locking plates, are extensively employed to treat fractures. For any fixation device there are three key clinical requirements and consequent mechanical demands arising from them [1]: (a) it must support fracture healing; (b) it must not fail during the healing period; and (c) it should not loosen or cause patient discomfort. It has been shown that the mechanical demands (a) and (b) are related implant stiffness and its fatigue strength. Consequently stiffness of bone-fixation systems has been extensively investigated over several decades. Implant loosening (mechanical demand (c)), which also entails a risk of infection, occurs due to high strains at the bone-implant interface and due to cyclic loads has received considerable little attention. Computational modelling is an apparent tool for such an analysis as it is not straightforward measure strains at the bone-implant interface via an experimental set-up. We discuss different approaches we have employed to evaluate loosening. For cortical bone-implant interaction we consider two approaches. In the first we assume the bone to be linearly elastic but incorporates anisotropy and inhomogeneity [2]; loosening is estimated by evaluating the volume of bone that crosses a strain threshold [3]. The second approach additionally incorporates strain-based plasticity [4] in the models and estimates loosening by evaluating the pattern and the volume of bone that enters the plastic regime [5]. We consider varied approaches for trabecular bone-implant interaction; all assume isotropy. We examine linear elasticity and Drucker-Prager and crushable foam plasticity [6]. Since implants experience cyclic loading which is known to cause implant loosening we also examine two time-dependent criteria: linear viscoelastic [7] and nonlinear viscoelastic and viscoplastic [8]. Our results indicate that with time-independent models, estimates provided by linear elastic approaches are good, particularly when the aim is merely to compare fixation configurations and options. However, loosening due to cyclic loading can only be provided by time-dependent models and our studies show that it is influenced by bone quality and number of cycles (Fig. 1). So time-dependent models can be used not only to predict loosening but also to provide post-op rehabilitation advice.
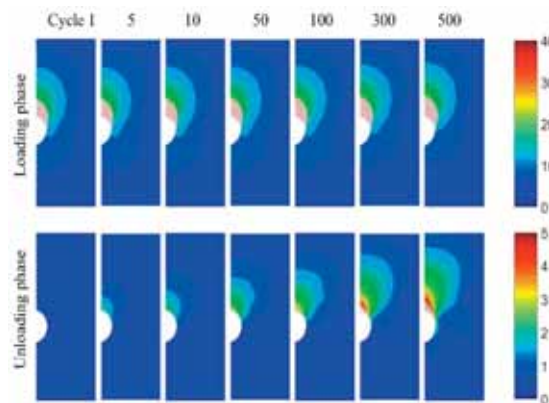

Figure 1: Displacement (µm) contour plots for the section experienced the larger deformation at 7 representative cycles for loading and unloading phases. White semicircle on the left shows symmetric half of a screw.

References:
[1] MacLeod and Pankaj (2014), DOI:10.1007/978-1-4939-0745-8__7;
[2] Donaldson et al. (2011) DOI:10.1177/2041303310395675;
[3] MacLeod et al. (2016) DOI:10.1002/jor.23193;
[4] Pankaj and Donaldson (2012) DOI:10.1002/cnm.2491
[5] Donaldson et al. (2011) DOI:10.1002/jor.21587;
[6] Goffin et al. (2014) DOI:10.1016/j.jbiomech.2013.09.014;
[7] Xie et al. (2019) DOI:10.1177/0954411919877970
[8] Xie et al. (2018) DOI:10.1302/2046-3758.710.BJR-2018-0085.R1

A6.5

Efficient non-linear micro FE: results from trabecular biopsies and human radius sections

Dieter Pahr[1], Philippe Zysset[2], Monika Stipsitz[1]

1   TU-Wien, Institute of Lightweight Design and Structural Biomechanics , Vienna, Austria
2   University of Bern, ARTORG Center for biomedical engineering research, Bern, Switzerland

Micro finite element analysis (2FE) is a special engineering tool for studying the mechanical behavior of bones. The increasing availability of high-resolution CT data as well as computing resources make 2FE more and more attractive. Recently, an efficient solver for large-scale 2FE simulations (ParOSol [1]) was extended for nonlinear material behavior by our group [2]. The material model included damage-based tissue degradation and fracture. The presented study consists of two parts. First, the new framework was applied to 20 trabecular biopsies (see Figure). Tissue material parameters were identified based on two biopsies by comparison with axial tension and compression experiments. An excellent correlation of the maximum apparent stress was found between simulations and experiments (R2 > 0.97), validating the model on the apparent level. A novel elasticity limit was proposed based on the local damage information which show that inelasticity starts very early at apparent strains of 0.26 ± 0.18% in tension and −0.2 ± 0.17% in compression. The obtained damage distributions lead to a good insight into the failure mechanisms of trabecular bone.

In a second part, the 2FE is applied to predict the inelastic behavior of radius segments and compare the result with the well-known Pistoia criterion (PC). The advantage of the PC is that a simple strain threshold can be used to predict the failure behavior, but it must be recalibrated for different bone geometries, loadings, and CT resolutions. The experimentally determined failure load could be predicted well with both the PC and NL simulations. An optimized PC was proposed using experimental data to calibrate the individual volume of the overstressed tissue. The predicted region of damage agrees well with both models (PC and NL), although the optimized PC predicted more diffuse areas. However, the PC relies on an individual calibration requiring the experimental failure load, whereas the nonlinear simulation does not require a priori knowledge of the experimental failure load. The next step is to validate the methodology locally using digital volume correlation and to include a simple contact model for bone-implant investigations. If available, first results on this will be presented at the conference.
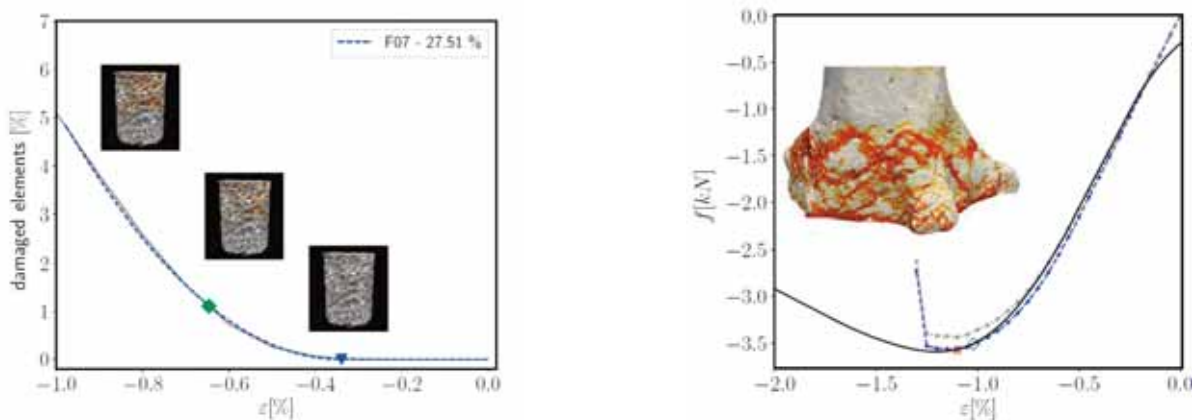

Figure caption:
Left: Damage progression and elasticity limit for one individual sample under compression. New elasticity limit (blue triangle) and 0.2% yield point (green rectangle).
Right: Force-strain curve of a radius section. Experimental curve (black), simulation results (blue), and damage distributions at the last increment.

References:
[1]   Flaig C, Arbenz P (2011) A scalable memory efficient multigrid solver for micro-finite element analyses based on CT images. Parallel Comput 37(12), 846–854.
[2]   Stipsitz M, Zysset PK, Pahr DH (2020) Efficient materially nonlinear μFE solver for simulations of trabecular bone failure. Biomechanics and modeling in mechanobiology 19, 861-874.

A6.6

Bone-implant integration assessed using in-situ mechanical pull-out during synchrotron X-ray tomography

Elin Törnquist[1], Ornella Lohéac[1], Sophie Le Cann[1 2], Deepak Raina[3], Vladimir Novak[4], Jonas Engqvist[5], Stephen Hall[5 6], Hanna Isaksson[1]

1   Lund University, Biomedical Engineering, Lund, Sweden
2   CNRS / MSME: Laboratoire Modélisation et Simulation Multi Echelle: Créteil, Paris, France
3   Lund University, Orthopaedics, Lund, Sweden
4   Paul Scherrer Institute, Villigen, Switzerland
5   Lund University, Solid Mechanics, Lund, Sweden
6   LINXS - Lund Institute of advanced Neutron and X-ray Science, Lund, Sweden

Background and aims: Degenerative disorders and trauma reduce fracture resistance of bone, often resulting in the need for medical interventions involving implants. Long-term implant stability relies on adequate bone-implant integration and depends on the quantity and quality of the newly formed bone. This study employs X-ray microtomography during in-situ loading and advanced image analysis to evaluate how bio-active molecules affect the quantity and quality of newly formed bone around an implant.

Methods: Proximal rat tibiae were implanted with hollow fenestrated PEEK screws left to integrate for 6 weeks (Fig 1A). The screws were filled with a calcium sulphate/hydroxyapatite based biomaterial (Control, N=8) or with the biomaterial mixed bio-active molecules (zoledronic acid and rhBMP-2) (Treated, N=8) [1]. Stepwise in-situ implant pull-outs using a custom-built loading device (rate: 0.3 mm/min, step 0.15 mm) were performed while acquiring X-ray images at unloaded and after each load step (30 keV, 6 ms/projection, 3000 projections, 360° rotation, voxel size 2.75 μm). Mechanical properties (stiffness, peak force, work-to-failure) and amount of newly formed bone close to the implant (Fig 1C) were compared between treatment groups. Tracking of internal deformations was done with Digital Volume Correlation (DVC) using the open-source software TomoWarp2 [2].

Findings and conclusions: Results confirm that the addition of bio-active molecules increases bone formation and leads to better implant integration. Peak force and work-to-failure were higher in the treated group than in the control (p=0.04 and p=0.03, respectively) with stiffness showing the same trend (Fig 1B). The treated group showed more bone close to the implant (55.1±2.9%) than the control (20.9±4.4%). Initial DVC results have helped identify the failure mechanism as fracture of bone grown into the screw threads (Fig 1D). Ongoing DVC analysis will yield insight into failure mechanisms and further assess the quality of the newly formed bone.
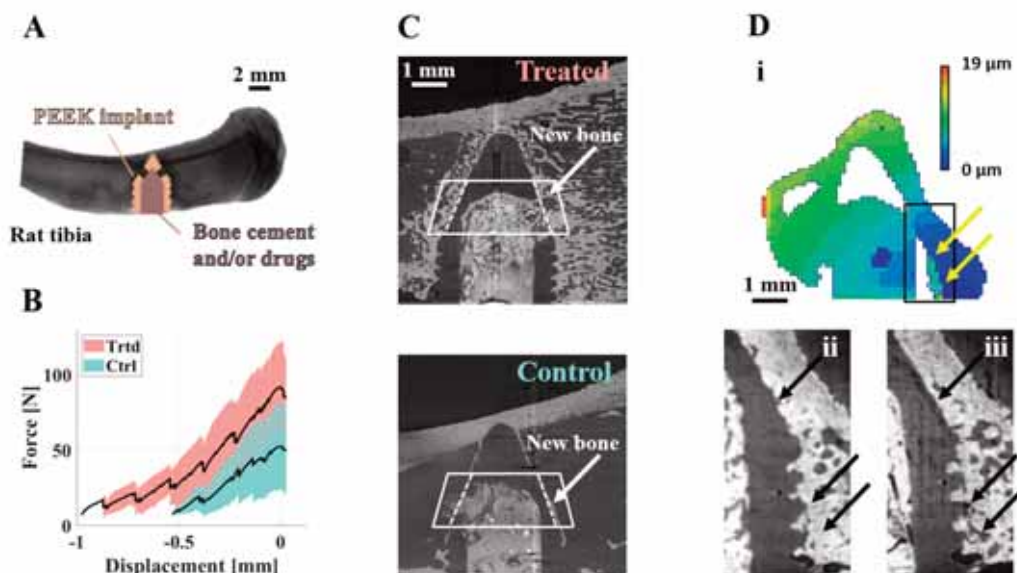

Figure 1: A) Tibia with PEEK implant. B) Load curves with peaks centered at zero, shown as mean (black line) and standard deviation (shaded area) for the two groups. C) Tomographic slices with region of interest for bone volume analysis marked. D) Implant loosening (indicated with arrows), identified through DVC displacement field (i, absolute values), in tomographic images prior to (ii) and after (iii) failure.

References:
1.   Raina, D. B. et al. Acta Biomater. 96 (2019).
2.   Tudisco, E. et al. SoftwareX 6 (2017).

A6.7

Modeling the spatio-temporal evolution of bone-implant interface stiffness via a stochastic numerical approach

*J. Xie[1], Daniel Rittel[2], Keren Shemtov-Yona[3], Furqan A. Shah[4], Anders Palmquist[4]*

1   State Key Laboratory of Explosion Science and Technology, Beijing Institute of Technology, Beijing, China
2   Faculty of Mechanical Engineering, Technion - Israel Institute of Technology, Haifa, Israel
3   The Maurice and Gabriela Goldschleger School of Dental Medicine, Department of Oral Biology, Tel Aviv University, Tel Aviv, Israel
4   Department of Biomaterials, Sahlgrenska Academy, University of Gothenburg, Göteborg, Sweden

Various biochemical, biological, physical and mechanical processes and interactions take place at the bone-implant interface. This interface gradually evolves over time as peri-implant bone gains stiffness. Owing to the multifactorial nature of interfacial processes, a comprehensive numerical model for predicting the mechanical behavior of the bone-implant interface has remained a challenge. Here, we propose a simple mechanical model, starting from an elementary unit cell comprising randomly assigned stiffness (i.e., Young's modulus) and going all the way up to a macroscopic bone-implant interface in a gap healing model (i.e., at the time of implant placement, a space exists between the implant surface and bone). Gap closure and subsequent increase in stiffness are modeled to account for the two main directions of peri-implant bone formation, namely Contact Osteogenesis (CO) and Distance Osteogenesis (DO). This linear elastic stochastic finite element model reveals a highly nonlinear temporal evolution of bone-implant interface stiffness, strongly dictated by the specific kinetics of the contact osteogenesis and distance osteogenesis. Prior to gap closure at the two peri-implant osteogenesis fronts, the bone-implant interface possesses relatively low stiffness. However, following gap closure, the stiffness increases dramatically – reminiscent of a percolation transition whose threshold corresponds to gap closure. Albeit preliminary, the model presented here can be incorporated into future calculations of the bone-implant system where the material properties of bone and biological processes are defined based on quantitative experimental (in vivo) data.
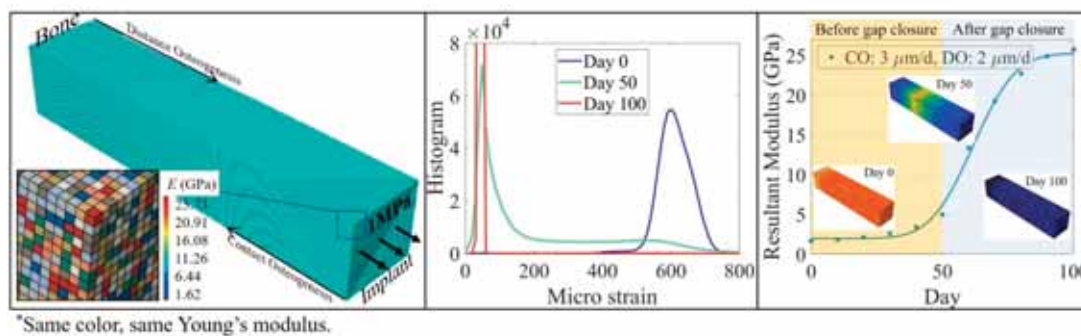
Figure 1: Dimensions of the cuboid bone-implant interface model are set to $50 \times 50 \times 250 \, \mu m3$, divided into three distinct evolving regions: CO region, gap zone (unmineralized region), and DO region. At CO of 3 μm/day and DO of 2 μm/day, micro strain distribution and Young's modulus evolve over the 100-day period, and particularly dramatically following gap closure between the two bone formation fronts (i.e., CO and DO).

A8.1
Mechanical stability and clinical application of polyetherketonketon (PEKK) material

Istabrak Dörsam[1], Ludger Keilig[1], Christoph Bourauel[2]

1   University of Bonn, Oral Technology and Department of Prosthetic Dentistry, Preclinical Education and Materials Science, Bonn, Germany
2   University of Bonn, Oral Technology , Bonn, Germany

Introduction and Aim: Polyetherketonketon (PEKK) is a high-performance polymer that got more applications in dentistry in the last years. The second ketone group promises better mechanical and physical properties as there are polish ability, higher compressive strength, and a bone-like elastic modulus.

The aim of the study was to investigate experimentally, numerically, and clinically various PEKK made dental restorations and compare them with those made from classical dental materials.

Method: Fixed partial prostheses on teeth (crowns and bridges) and removable overdentures on implants (bar system) with a PEKK framework were constructed for patients' treatment. Mechanical stability and repairing requirement caused my fracture or chipping were investigated for a period of two years.

Meanwhile the static fracture and fatigue of PEKK framework for similar clinical restorations were experimentally investigated and compared with dental metal frameworks.

Finally, finite element (FE) analysis of the above mentioned restoration was undergone to analysis the distribution of the stress within the framework and their transfer into the surrounding tissue.

Results: The clinical observations showed good stability of the prosthesis. There was no repairing demand within the period of two years.

The static fracture tests of the fixed partial prostheses with PEKK resulted in 899 (± 96) N. The fatigue limit was 720 N. The polymer framework resulted in reduced framework stresses of 52 MPa in comparison to titanium (76 MPa) and zirconium (80 MPa). Varying the framework material had minimal influence on the loading of surrounding tissue.

The static fracture limits of the bar materials were 1,750 N, 780 N, 310 N for Ti, CoCr, and PEKK, respectively. The fatigue limits for the bar materials were comparable: 200 N for titanium, 160 N for CoCr, and 150 N for PEKK.

The stress within the bar was 2,600 MPa (titanium), 1,000 MPa (CoCr), and 270 MPa (PEKK).

Conclusions: Using soft, novel materials as framework for fixed partial prostheses does not negatively influence biomechanical loading of the involved surrounding structures.

For the overdentures with bar, PEKK showed different mechanical behaviour compared to Ti and CoCr. The distribution of stresses within the PEKK bar was wider than the area of loading and the loading of the implants war higher as well.

PEKK could be considered as a promising material and a good alternative for patients with metal allergy however, intraoral long-term stability is expected to be limited compared to metal restorations.

A8.2
Adhesive layer defects and their impact on indirect dental restoration mechanical behavior

Yannick Yasothan[1 2], *Kyo Shindo*[3], *Elsa Vennat*[1 3], *Nicolas Schmitt*[2 4]

1   Université Paris-Saclay, CentraleSupélec, CNRS, Laboratoire MSSMat, Gif-sur-Yvette, France
2   Université Paris-Saclay, ENS Paris Saclay, CNRS, LMT, France
3   Université Paris Descartes, Faculté de Chirurgie Dentaire, URB2i-EA4462, France
4   Université Paris-Est Créteil, INSPE, France

Caries affect nearly 2.3 billion people worldwide[1]. When the tooth decay lesion is mild, one possible treatment is indirect dental restoration. It consists of bonding a dental prosthesis on a prepared tooth with an adhesive layer. The adhesive layer can, however, debond[2]—thus reducing the indirect dental restoration life span. This debonding can be caused by the presence of defects in the adhesive layer. To better understand how the failure occurs, we propose to investigate: the morphology of the adhesive layer and its defects, as well as the impact of adhesive layer defects on the mechanical behavior of the restored tooth.

Morphological characterization of the adhesive and its defects was performed on three simplified dental assemblies. These assemblies were composed of a Vita Enamic® dental prosthesis, a Maxcem EliteTM adhesive layer, and a dental preparation machined from bovine cortical bone.

The internal structure of the dental assemblies was observed by X-ray micro-Computed. The resolution of the reconstructed 3D images was 7.3 μm.

Image post-treatment was carried out on AVIZO 9 and ImageJ. The objectives of this process were: 1) to enhance the reconstructed 3D image quality, improving the identification of each assembly element - 2) to describe the internal geometry of the respective assemblies.

Two types of defects were observed in the adhesive layer: spherical-shaped defects and "flat" defects at the dental preparation/adhesive layer interface. On the three samples, the average volume of spherical-shaped defects is 0.275 mm3. For "flat" defects, it is 0.073 mm3.

From the 3D images, a finite element model (FEM) was set up to study defect impact on the mechanical behavior of restorations. The development of the FEM involved the implicit description of the assembly geometry, the implementation of elastic properties of the restoration elements, and the use of an adaptive meshing method[3]. We pointed out the most critical defects, their size, and their location leading to the highest stress concentration.

In the proposed FEM, we considered a perfect interface between the different parts of the assemblies. However, to better model and understand the assembly failure, we need to deepen our knowledge of the interface behavior. Our next step will be to set up a method to assess the adhesion between the dental prosthesis and dental preparation experimentally.

References:
1   GBD 2017 Disease and Injury Incidence and Prevalence Collaborators, Lancet 392, 1789 (2018).
2   M. Øilo, A.D. Hardang, A.H. Ulsund, and N.R. Gjerdet, European Journal of Oral Sciences 122, 238 (2014).
3   E. Vennat, A. Hemmati, N. Schmitt, and D. Aubry, Journal of the Mechanical Behavior of Biomedical Materials 116, 104329 (2021).

A8.3

Comparison of different augmentation techniques in maxillary implant placement

Ludger Keilig[1,2], Tabea Winter[1], Istabrak Dörsam[1,2], Helmut Stark[2], Christoph Bourauel[1]

1   Medical Faculty, University of Bonn, Oral Technologies, Bonn, Germany
2   Medical Faculty, University of Bonn, Department of Prosthetic Dentistry, Preclinical Education and Materials Science, Bonn, Germany

Bone atrophy in the edentulous jaw influences bone quality as well as bone geometry. This has to be taken into account when planning implant supported restorations, especially in the lateral region where typically the highest forces within the oral cavity are registered. Mainly two options are available in such cases: using short implants or sinus floor augmentation (SFA). It was the aim of this study to numerically investigate the biomechanical behavior of an implant in the maxilla, using different combinations of bone height, insertion region, augmentation technique, implant length, and healing state.

A CBCT scan of an partially edentulous maxilla with advanced atrophy with a bone height of 9 mm in the region of the missing upper first right premolar was used as base FE model, and further five models were created from this by remodeling the bone height to 2, 4, 6, 8 and 10 mm. Clinically recommended augmentation techniques (internal or external SFA) were then employed to increase the bone height in the virtual models to 10 mm. Depending on the available bone, implants with different length were inserted (7 mm and 9 mm in the original clinical model, 9 mm in the augmented models). To investigate the load transfer in the different augmented structures, a force of 500 N was applied at the implant shoulder in axial direction, and the resulting stresses and strains within the structure were recorded. All simulations were performed with glued contact at the bone-implant-interface to simulate the osseointegrated state. For the models without augmentation, the simulations were additionally performed with sliding contact between implant and bone to simulate immediate loading.

The force of 500 N resulted in a pathological overload in all cases. Stresses were between 98 MPa and 723 MPa. Comparing the two implant length in the clinical model, the 9 mm implant resulted in lower stresses (101 MPa) than the 7 mm implant (136 MPa). With osseointegration, in the non-augmented models stresses of up to 136 MPa were found. For the internal SFA stresses of up to 122 were reached, and for the external SFA up to 356 MPa. Immediate loading of the non-augmented models resulted in stresses up to 723 MPa.

While the force of 500 N that was used in these simulations exceeds the typically expected forces, especially in older patients, it allows us to compare the relative performance of each modeled situation. The results show that the biomechanical loading of the implant after an internal SFA leads to similar load distribution in the bone as in the original, non-atrophied bone. The increased stresses that were observed in the models with external SFA demonstrate the importance of a fully healed augmentation and implantation site to avoid implant failure.

A8.4

A dentin image-based model with 3D fan-like microstructure and curved orthotropic material: is tubule orientation naturally optimized with respect to chewing load?

Elsa Vennat[1], *Aubry Denis*[1]

1   *CentraleSupelec, MSSMat, Gif sur Yvette, France*

Starting from acquired CT images of a tooth, a finite element approach is used to segment the tooth into four smooth regions: the enamel, the dentin, the pulp and the outer domain. The dentin is assumed to be an orthotropic material with the main axis oriented along the tubules in a fan like manner from the pulp towards the enamel. The other materials are assumed to be elastic isotropic. A pressure force is applied at the top of the crown to simulate the action of the food compressed by an upper tooth.

The CT images are directly read by the FEM code into a box while the grey intensity levels are interpolated into a brick uniform mesh. A Helmholtz filter is applied to smooth out the different regions, more particularly at the bottom where the pulp is usually difficult to trace back. The segmentation, i.e. the attribution of a well-defined constant value to each region, is performed using the Chan Piecewise Constant Level-Set Method (1), (2). It consists in using a single level function, constrained to take integer values according to the number of constituents. Then an electrostatic equivalent is proposed where the outer domain and the pulp are set at constant and different potential (3). The current lines show rays which extend like a fan from the pulp to the outer boundary. As shown in Vennat et al. (4) and Jud (5), they are distributed similarly to the tubules in the dentin providing the orthotropic axis.

Finally, the tooth is loaded at the upper boundary by a normal pressure to simulate the chewing load. The study shows that the orientation of the orthotropy axes in the dentin plays a major role in the force transmission from the crown to the underneath bone. The proposed presentation thus provides a fully integrated image-based approach to the dentinal mechanical response with refined microstructural modeling.

References:
(1)   X.C. Tai et al, Image Processing based on Partial Differential Equations, Springer (2000)
(2)   A. Mitiche, I. Ben Ayed, Variational and Level Set Methods in Image Segmentation, Springer (2010)
(3)   R. Allena, D. Aubry, A novel technique to parametrize shell-like deformations inside biological membranes, Computational Mechanics volume 47, pages 409–423 (2011)
(4)   E. Vennat et al, The role of lateral branches on effective stiffness and local overstresses in dentin, J. Mech. Behaviour of Biomed. Mat., 116 (2021)
(5)   C. Jud, Dentinal tubules revealed with X-ray tensor tomography, Dental Materials, 32, 1189-1195 (2016).

A8.5
Finite element analysis of endocrown-restored premolars with different designs

Mostafa Aldesoki[1], Ahmad Aboelfadl[2], Tarek Morsi[2], Christoph Bourauel[1]

1   University of Bonn, Oral Technology , Bonn, Germany
2   Ainshams University, Faculty of Dentistry, Fixed Prosthodontics , Cairo, Egypt

There is no significant difference between survival rates of endocrown-restored molars and molars restored with traditional techni¬ques [1]. However, the clinical performance of endo¬crown-restored premolars is inferior to that of molars [1, 2]. The main cause of failure of premolars restored with endocrowns is the cohesive failure of bonding [1]. The clinical fracture of endocrown-restored teeth has also been reported [3]. The aim of this study was to compare the biomechanical behaviour of endo¬dontically-treated maxillary premolars restored with lithium-disilicate endocrowns and conventional crowns and to evaluate the influence of the endocrown pulp chamber extension depth and the axial extension with a shoulder finish line on the stress distribution along the endocrown/tooth interface. An intact maxillary premolar was digitised with a cone-beam CT. Five models were generated from a sound maxillary premolar (Figure 1). Bone geometry was simplified as a cylinder of compact and trabecular bone. All models were remeshed and imported into a finite element analysis software (ANSYS workbench 14.0, Houston, USA) where the base of the bony cylinder was selected as a fixed support. All material properties were assumed to be linear, elastic and homogenous (Table 1). Axial and oblique forces of 100 N each were applied separately to each model. Comparing the endocrown models to the crown model, the differences in total deformation and von Mises values were not significant regardless to the endocrown design. Von Mises values decreased by 15% in models (B) and (C) with the 5 mm pulpal extension compared with models (D) and (E) with the 3 mm pulpal extension. Von Mises stresses on the tooth structure of models (C) and (E) with the axial extension were 15% lower than that of models (B) and (D) with the butt margin (Figure 2). The results showed that endocrowns are an appropriate restoration for endodontically treated maxillary premolars. Additionally, reduction of the pulpal extension depth to 3 mm yielded more stresses on the restored tooth, while addition of an axial extension, instead of a butt margin produced more favourable stress distribution within the restored tooth.
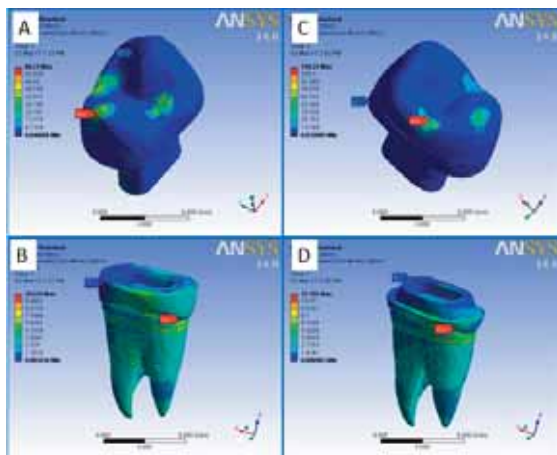

Figure 1 A. Fiber post, composite core and crown B. Endocrown with 5mm pulpal extension. C. Endocrown with 1.5mm axial extension and 5mm pulpal extension. D. Endocrown with 3mm pulpal extension. E. Endocrown with 1.5mm axial extension and 3mm pulpal extension.
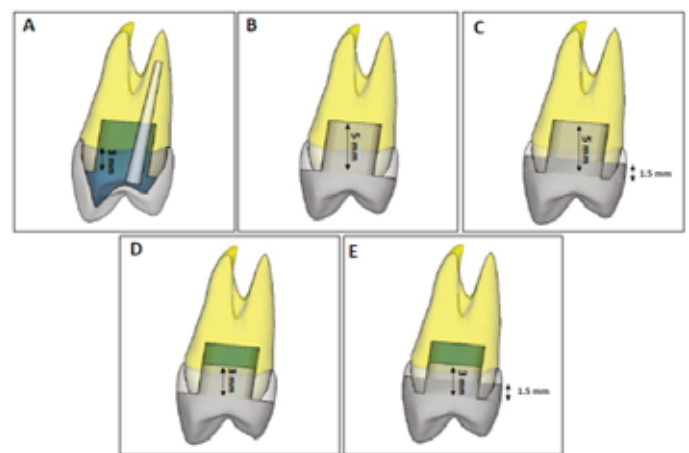

Figure 2 von-Mises stresses in A, B: butt margin; C, D: axial extension.

MATERIAL	ELASTIC MODULUS (GPA)	POISSON'S RATIO
ENAMEL	84.1	0.33
DENTIN	18.6	0.32
TRABECULAR BONE	1.37	0.30
CORTICAL BONE	13.7	0.30
COMPOSITE CORE	22	0.22
IPS E-MAX CAD	100	0.20

References:
1.   Bindl et al, J. Prosthet. Dent, 95:81, 2006.
2.   Biacchi et al, J. Esthet. Restor. Dent, 25: 383–390, 2013.
3.   Bernhart et al, Int. J. Comp. Dent, 13: 141–154, 2010.

A8.6

Comparing the effect of dental implant-abutment connections on crestal bone: three-dimensional finite element analysis

Salih Celik[1 2], Lisa Scherer[3], Florian Sachsenhauser[2], Jan Niewolik[2], Johannes Scherer[2]

1   University of Bonn, Endowed Chair of Oral Technology, Bonn, Germany
2   Advantiqx Dr. Johannes Scherer, Gersthofen, Germany
3   Zahnärzte im Piramid, Gersthofen, Germany

Introduction: Screwed internal connections are the most common solutions since they combine high stability, tightness, easy handling, and are relatively easy to manufacture. However, real-world experience suggests that there is a relationship between the implant-abutment connection and crestal bone decline. To understand the causes, two commercially available implant variants with different geometries were simulated. The purpose of this study was to analyze the effect of different implant-abutment connection (IAC) designs on the bone, using 3-dimensional (3D) finite element (FE) analysis, taking into account the bone adaptation and the setting processes in the IAC due to changing mechanical stress.

Material and Method: For the comparative analysis, two different implants, namely Ankylos and Nobel Active, were respectively assembled, put into a part of a jaw as a 3D tetrahedron half-model and simulated in the Ansys software. Particular emphasis was placed on the display of the pretension of the screw, the adaptation of the bone, and the effect of the contacts between the abutment, implant, and bone. The implants differ in the cone angle (Ankylos 5.7 °, Nobel Active 11.7 °) and in the wall thickness at the upper edge. In each case, a load cycle consisting of assembly (with pre-tensioning screws and adaptation of the bone to the deformation), the chewing load of 250 N under 30 ° from right side, relief and chewing load from the left side was calculated.

Results: If the connection is loosened e.g. while changing from temporary to permanent restoration, critically high tensile stresses arise between the implant and the bone. The contact forces of the IAC lead to an asymmetrical deformation of the implant and thus an uneven distribution of stress in the implant-bone-interface, even with a pre-tensioned connection under changing chewing load. In principle, these effects were stronger if the wall thickness of the implant was smaller. While the chewing load applied to the abutment, compression and tension forces occur on the left implant-bone-interface thus can lead to loosening. This could be the reason for crestal bone loss. In principle, smaller cone angles and greater wall thicknesses, as found in Ankylos, lead to less movement in the connection and more favorable load distribution in the bone during the chewing process.

Discussion: Controlled and randomized clinical studies should be conducted with various biomechanical parameters on more different IAC in implant dentistry. The results indicated that IAC may be a major cause of crestal bone decline. One solution could be to move the IAC away from the crestal area or to use one-piece implants.
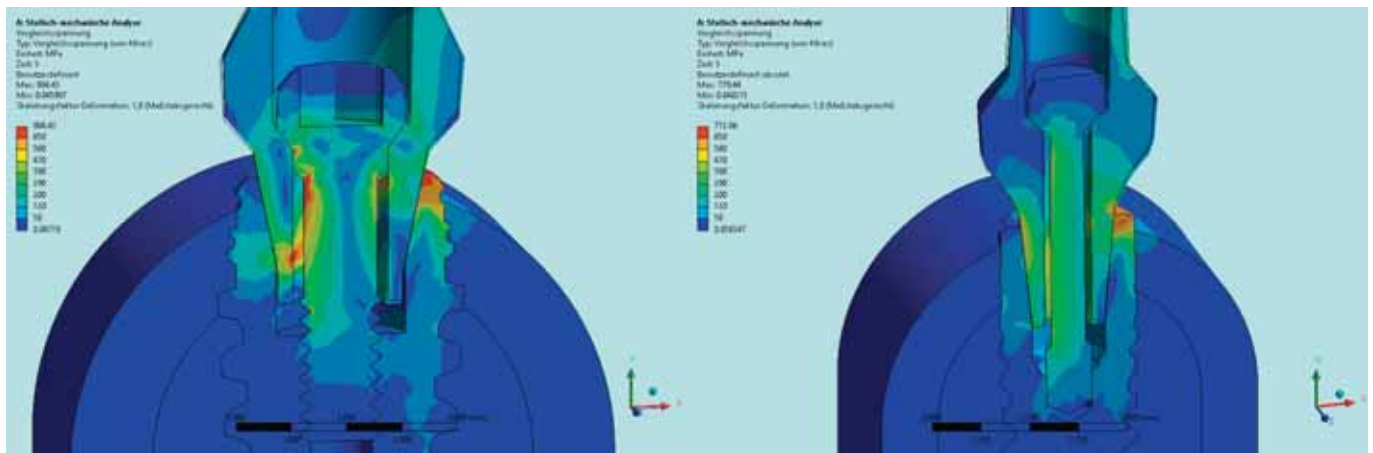

Figure 1: The view of stress distribution (after von Mises) of Ankylos (left) and Nobel Active (right) implants.

A8.7
Towards a reduced order model for the simulation of the periodontal ligament

Albert Heinrich Kaiser[1]

1   Institute for Numerical Sia Institute for Numerical Simulation, University of Bonn, Bonn, Germany

This contribution describes a reduced order model, used to identify parameters for simulation of the periodontal ligament response to force in the initial phase of orthodontic tooth movement, based on two previous investigations, an in vitro experiment with specimens of porcine mandibular premolars and an in vivo experiment on human upper first incisors.

For the curve fit of the in vitro experiment a model function, assuming viscoelasticity, was introduced. The viscoelastic model function was augmented by a ramp rise time term, to account for observed dependence of the response on actuator velocity, and a previous load history term, to account for the effect of the previous tests on the current test. The correlation coefficient of a curve fit for all tests grouped together was $R^2=0.98$. Next, a curve fit of the in vivo experiment was done. Good correlation was found for a simplified model function, without viscoelastic term ($R^2=0.96$). For both tests, in vitro and in vivo, the ramp rise time term improved correlation.

A finite element model of the specimen of the in vitro experiment was created. For the PDL a hyperelastic constitutive model for compressible material was used and model parameters were identified. The present work indicates that the macroscopic response of the periodontal ligament to an external load can be simulated with a poro-visco-hyperelastic model. The simulation showed that poroelastic behaviour will gradually cease when viscoelastic relaxation progresses. This followed also from dimensionless analysis. As a consequence, for slow loading, or if initial response to fast loading is not of interest, a visco-hyperelastic model may suffice.

To identify parameters of the finite element model several optimization problems were solved. The model function, which can be regarded as a reduced order model, allowed a full factorial experiment (analysis) at low cost, to identify initial parameters. The thus found parameters were further refined with an optimum interpolation meta-model. That is, for limited number of parameter combinations the response was simulated with the finite element model and a refined parameter study was conducted by means of optimal interpolation. The thus found optimal parameters were verified by simulation with the finite element model. Optimal interpolation is computationally cheap, which allowed full factorial experiments at low cost.

References:
Kaiser, Albert Heinrich: Simulation of the Periodontal Ligament During the Initial Phase of Orthodontic Tooth Movement. - Bonn, 2020. - Dissertation, Rheinische Friedrich-Wilhelms-Universität Bonn.
Online: https://nbn-resolving.org/urn:nbn:de:hbz:5-59200
Kaiser, Keilig, Klein, Bourauel: Parameter identification for the simulation of the periodontal ligament during the initial phase of orthodontic tooth movement. Computer Methods in Biomechanics and Biomedical Engineering, Taylor & Francis, 2020, doi: 10.1080/10255842.2020.1830275

A9.1
A novel review of temporomandibular joint replacement options

Christine Walck[1], *Yeram Lim*[1], *Seth Rosenstein*[1]

1   Embry-Riddle Aeronautical University, Mechanical Engineering, Daytona Beach, United States

The temporomandibular joint (TMJ) is one of the most complex joints in the human body with its ability to rotate and translate during jaw opening and closing movements. The motion during jaw-closing has two phases: 1) rotation and translation along the mandibular fossa from maximum mouth open (MMO) (32° jaw rotation) to 22°of jaw rotation [2], and 2) pure rotation from 22° until mouth closed position (0° jaw rotation) [1]. The rate of rotation and translation of the mandibular condyle (MC) is assumed linear from MMO to mouth closed position [1]. This motion pattern alters after the jaw undergoes a total open joint arthroplasty where the damaged portions of the joint is removed, and in some cases, replaced with implants.

This study analyzes the motion and torque capabilities associated with the Free Fibula Flap (FFF) procedure, and two types of TMJ implants: 1) a generic implant constrained to pure rotation, and 2) a patient-specific (PS) implant capable of both rotation and translation. Kinematic and kinetic models using subject-specific anthropometric measurements obtained from a model of a 50-65 year old male acquired from the National Institute of Health within a Computer-Aided Three-Dimensional Interactive Application were developed and assessed at one-degree increments of jaw rotation.

Results show the PS implant most resembles the kinematics and kinetics of the healthy jaw due to its ability to rotate and translate. The PS implant had a 34.4 mm inferior displacement at MMO; a 1.15% decrease compared to the healthy jaw's (34.8 mm), and a maximum net torque of 18,600 N-mm; a 29.3% decrease compared to 26,300 N-mm (Figure 1 and 2). The rotation-constrained FFF procedure and generic implant limits the jaw to 70% of MC rotation decreasing the inferior displacement at MMO (FFF/Generic: 22.5 mm) by 35.3% compared to the healthy jaw and prohibits net torque about the MC after the pure rotation phase (Figure 1 and 2).
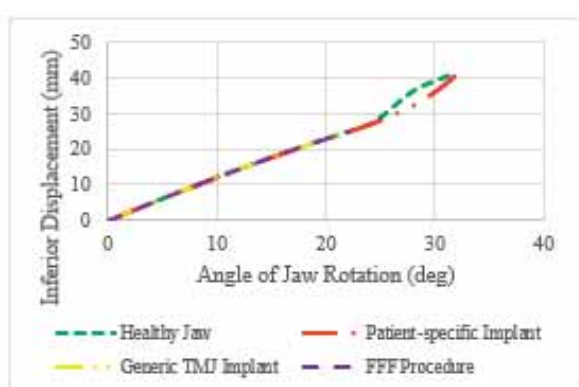
Figure 1. Inferior displacement of the jaw for each system.
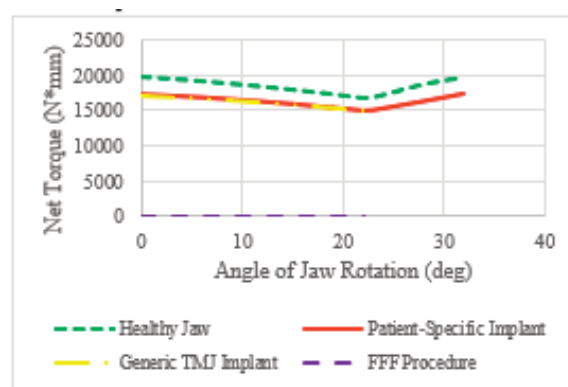
Figure 2. Net moment about the mandibular condyle for each system.

The differences in the PS implant, generic implant, and FFF procedure were influenced by surgical procedures. These results can provide surgeons better insight into the outcomes of a TMJ implant, and a basis on future improvements of the surgical methods used to provide a higher torque about the MC. The surgical methods influence the muscle activation, muscle force, and the moment arm used to generate torque about the MC. With this analysis, an improvement to the method of insertion of TMJ implants can be improved.

References:
[1]   Bermejo, E. et al. (2017). "Genetic Algorithms for Skull-Face Overlay Including Mandible Articulation," Information Sciences, 420, pp. 200-217.
[2]   Naeije, M. (2002). "Local Kinematic and Anthropometric Factors Related to the Maximum Mouth Opening in Healthy Individuals," Journal of Oral Rehabilitation, 29, pp. 534-539

A9.2

Uncertainty in muscle-tendon parameters can greatly influence the accuracy of knee contact force estimates of musculoskeletal models

Seyyed Hamed Hosseini Nasab[1], Colin Smith[1], Pascal Schütz[1], Philipp Damm[2], Adam Trepczynski[2], William R. Taylor[1]

1   Institute for Biomechanics, ETH Zürich, Zürich, Switzerland
2   Julius Wolff Institute, Charité - Universitätsmedizin Berlin, Germany

Musculoskeletal models have been widely used to estimate in-vivo loading conditions within the knee. However, when predictions are compared against in-vivo measurements, substantial errors are common, especially when generic models were used[1]. Here, uncertainty in model parameters likely contributes to the observed modelling errors. This study aimed to quantify the impact of uncertainty in lower-limb muscle parameters on the knee contact force (KCF) estimates of a generic musculoskeletal model during squat.

Skin-marker trajectory, ground reaction force, and in-vivo KCF data measured from six subjects with an instrumented knee implant were obtained from the CAMS-Knee datasets[2]. CT images were used to scale a generic musculoskeletal model[3] to each subject's anthropometry. Maximum isometric force (MIF), pennation angle (PEN), tendon slack-length (TSL), origin and insertion points (OIP), and via-points (VIA) of six major groups of the lower-limb muscles were perturbed around their baseline values to perform a series of Monte-Carlo (MC) simulations (Fig1.A). The random muscle parameters were obtained from Gaussian-distributions based on inter-individual variability reported in literature[4]. For each subject and muscle group, we performed one MC simulation (MCALL) with 2000 iterations where all the five muscle parameters were perturbed and five individual MCs (MCi), each with 500 iterations with only one parameter perturbed.

Skin-marker trajectory and GRF of representative squat trials were input to the OpenSim, where Static Optimization tool and the perturbed models were used to calculate KCF by minimizing sum of the squared muscle activations. KCF estimates were then compared against the in-vivo loads to obtain the corresponding simulation errors. 5-95 percentile range (CB) of the error distribution obtained from MCALL was compared between muscle groups to identify the muscle group with the highest contribution towards the overall KCF uncertainty.

Baseline simulations resulted in peak KCFs of up to 4 times body weight (BW), indicating errors of up to 100% when compared to the in-vivo forces (Fig1.B). The MC simulations revealed that variability in the lower-limb muscle parameters can explain up to 70% of the simulation error. Here, at small flexion angles, knee flexors showed the highest contribution, whereas knee extensors were the main contributors to the overall error at larger flexion angles (Fig1.C). Regarding the increasing contribution of via-points and extensor muscles with increasing knee flexion angle, the observed flexion-dependent errors most likely originate from inaccurate representation of the extensor muscle pathways in the scaled generic models. This study therefore highlights the importance of subject-specific modelling of the muscle pathway geometry when activities with large knee flexions are simulated.
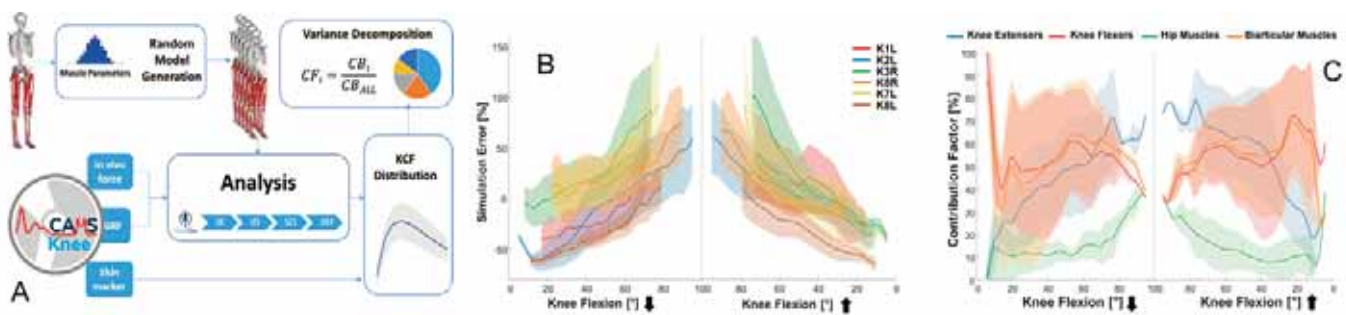

Fig 1: A. Probabilistic modelling flowchart. B. Distribution of the simulation error. C. Contribution of different muscle groups to simulation uncertainty.

References:
1.   Imani-Nejad, Ann.Biomed.Eng. 2020.
2.   Taylor, J.Biomech. 2017.
3.   Rajagopal, IEEE.Trans.Biomed.Eng. 2016.
4. Myers, Ann.Biomed.Eng. 2015.

A9.3

Data-driven models for musculotendon length estimation in individuals with Parkinson's Disease - a statistical parametric mapping analysis

Marco Romanato[1], *Francesca Volpin*[1], *Daniele Volpe*[2], *Massimo Sartori*[3], *Zimi Sawacha*[1]

1   University of Padova, Information Engineering, Padova, Italy
2   Fresco Parkinson Institute, Villa Margherita, S. Stefano, Arcugnano, Italy
3   University of Twente / Universiteit Twente, Department of Biomechanical Engineering, Enschede, Netherlands

Gait alterations are among the most disabling motor-symptoms associated with Parkinson's Disease (PD). Reduced stride length, stride velocity and lower limb joint range of motion are hallmarks of parkinsonian gait [1]. Recently, the authors identified an impaired magnitude on leg muscle forces in PD during gait when compared with healthy control subjects (CS), adopting neuromusculoskeletal electromyography-informed modelling [2]. The aim of the proposed study was to enhance subject-specificity of the previous model, including a scaling technique for the optimization of musculotendon parameters [3]. For our purposes, thirteen CS (age=57.8±5.6 years, BMI=27.3±3.9 kg/m2) and ten PD subjects (age=62.8±11.4 years, BMI=27.1±2.9 kg/m2) were acquired with a 6-cameras motion capture system (60Hz, BTS), synchronized with 2 force plates (960Hz, Bertec) and an 8-channels EMG system (1000Hz, BTS) that recorded bilaterally the activities of 4 muscles: Rectus Femoris, Biceps Femoris, Gastrocnemius Lateralis and Tibialis Anterior. Inverse kinematics, inverse dynamics, and muscle analysis were performed in OpenSim using both a linearly and a muscle-optimized scaled model [3], including 24 lower limb muscles. Muscle-tendon parameters were calibrated to the individual using CEINMS [4]. EMG-assisted neuromusculoskeletal modelling was used to extract normalized muscle fiber lengths of hamstrings and quads muscles. Results obtained with the two scaling approaches were compared. Models' validity has been assessed comparing experimental excitations and simulated activations over the gait cycle using a within-participant analysis of variance with statistical parametric mapping (SPM) methods [5] (p<0.05, Bonferroni post-hoc). Differences between the muscle operating length of both the assessed populations obtained with the muscle-optimizer were compared using two-sample nonparametric t-test with SPM methods (p<0.05). Results reported in the figure below showed a statistically significant reduction of fiber lengths range of motion either for the hamstring muscles and quad muscles in the PD group. The narrower musculotendon operating length detected in persons with PD might indicate the reason of the observed reduction of stride length and range of motion. Moreover, the evidence retrieved with the current analysis could provide a deeper understanding on the biomechanical reason for the impaired muscle forces and joint torques generation in PD.
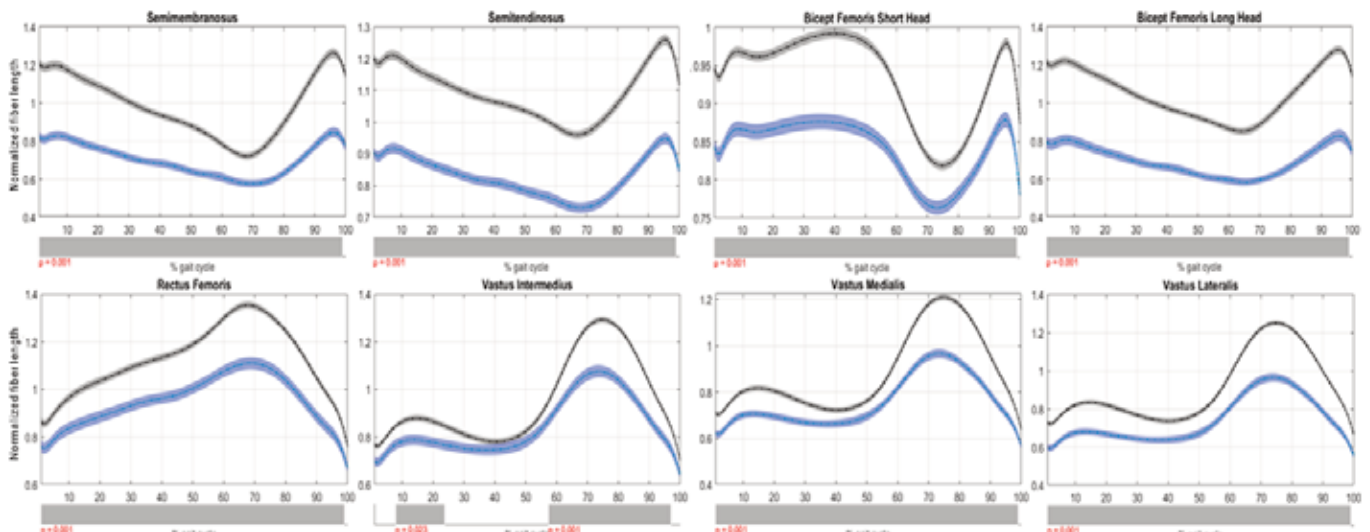

Figure caption: Normalized musculotendon lengths during walking in CS (black line) vs. PD subjects (blue line). Cross-subject mean trajectories with standard error clouds. Hamstrings muscles in the upper row, quads muscles in the bottom row. Lower black bars represent a simplified visualization of the significant areas indicated by the SPM{t} statistic.

References:
1.   Morris et al. Mov. Disord. 2005. 1(20):40–50.
2.   Romanato et al. CMBBE. 2021. Under review.
3.   Modenese et al. 2016. J Biomech. 2016. 49:141-48.
4.   Pizzolato et al. J. Biomech. 2015. 48:3929-3936.
5.   Pataky et al. J Biomech. 2013.

A9.4

An improved artificial neural network to predict three-dimensional position of body joints during various static load-handling activities

Mahdi Mohseni[1], Navid Arjmand[1], Farzad Aghazadeh[1], Majid Zahedian[1], Amin Mohammadi Nasrabadi[1]

1   Sharif University of Technology, Department of Mechanical Engineering, Tehran, Iran

Evaluation of body posture is an essential input into biomechanical models [1]. The common motion analysis techniques to measure body posture are costly and limited to laboratories. As alternatives, posture prediction approaches such as trained artificial neural networks (ANN) based on in vivo measurements are therefore developed. Previous studies have used these ANNs to estimate the body anatomical joint angles during various activities [2,3]. Moreover, we have recently developed and evaluated the capability of ANNs to predict the 3D position of body joints based on the worker's body height, three-dimensional position of the hand load, and its weight [4]. This study aimed to improve the predictive power of this latter ANN by incorporating knee flexion angle (KFA) as an additional input into the ANN [4]. The motion data collected from fifteen healthy individuals during 135 lifting activities by reaching three hand loads (0, 5 or 10 kg) loads from nine different horizontal and five vertical positions [4] were used to train this novel feed-forward ANN. KFA was considered as a three-state input into the ANN: 0 to 30º (i.e., stoop lifting), 30 to 90º (semi-squat), and >90º (full-squat). Based on a trial-and-error approach to achieve the highest predictive power, number of hidden layer neurons in the ANN was set to 40. Output layer included 45 neurons; i.e., the 3D position of fifteen body joints (Figure 1a). 15% of the motion data were used to test the accuracy of the trained ANN. The training stopped after 114 epochs (RMSE = 5.06 cm) and its generalization capability was tested (RMSE = 5.4 cm and R2 = 0.986 (Figure 1b)). The results showed that considering the KFA as an input improved both the training and testing RMSEs by 24.5% and 22.9%, respectively, as compared to the original ANN [4]. In future, deep neural networks will be developed to improve the predictive power of this ANN.
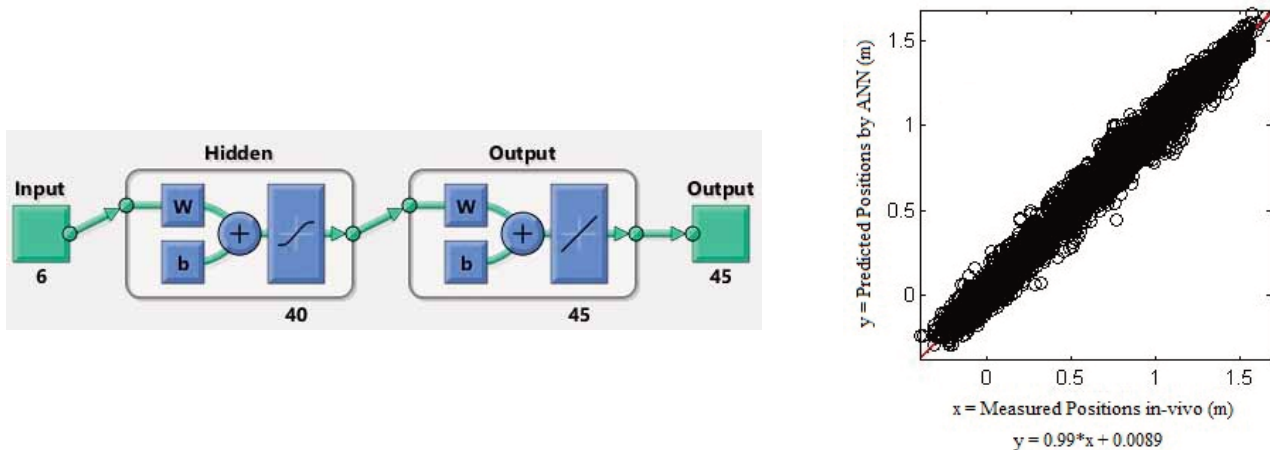
Figure 1: (a) The trained three-layered ANN and (b) scatter plot of all measured and their corresponding predicted values by the trained ANN (15% of motion data).

References:
[1]   Dreischarf M, Shirazi-Adl A, Arjmand N, Rohlmann A, Schmidt H. Estimation of loads on human lumbar spine: A review of in vivo and computational model studies. J Biomech 2016;49:833–45. https://doi.org/10.1016/j.jbiomech.2015.12.038.
[2]   Perez MA, Nussbaum MA. A neural network model for predicting postures during non-repetitive manual materials handling tasks. Ergonomics 2008;51:1549–64. https://doi.org/10.1080/00140130802220570.
[3]   Gholipour A, Arjmand N. Artificial neural networks to predict 3D spinal posture in reaching and lifting activities; Applications in biomechanical models. J Biomech 2016;49:2946–52. https://doi.org/10.1016/j.jbiomech.2016.07.008.
[4]   Aghazadeh F, Arjmand N, Nasrabadi AM. Coupled artificial neural networks to estimate 3D whole-body posture, lumbosacral moments, and spinal loads during load-handling activities. J Biomech 2020;102:109332. https://doi.org/10.1016/j.jbiomech.2019.109332.

A10.1

Exploring the jamming phase transition in a 3D epithelial layer using a deformable cell model

Jef Vangheel[1], *Steven Ongenae*[1], *Maxim Cuvelier*[1], *Bart Smeets*[1]

1   KU Leuven, Department of Biosystems, Leuven, Belgium

In many biological processes such as wound healing, embryonic morphogenesis, and pathological processes like cancer metastasis, a fluid-like to solid-like phase transition occurs, known as the jamming transition. This transition emerges from the interactions between a large number of cells. In turn, these cell-cell interactions depend on single-cell properties such as adhesion and cortical tension. Vertex and Voronoi models have provided crucial insights into how this transition is controlled. These models describe confluent tissue, and have shown that cell jamming depends on the balance between adhesion and cortical tension[1], cell's active motility[2], and cell-cell alignment[3]. Recently, Kim et al.[4] developed a novel 2D model, accounting for porous tissues, and showed that cell-cell adhesion can both unjam or jam tissue depending on its porosity; in confluent tissue cell-cell adhesion favours fluidisation, while in porous tissue cell-cell adhesion promotes solidification. The majority of these models are focused on the 2D apical surface of epithelial sheets. However, cell and tissue shape changes during morphogenesis or cancer metastasis are essentially 3D processes. As a solution, we developed a 3D deformable cell model (DCM), where the 3D shape of each individual cell is accurately represented, and cell-cell interactions are captured by explicit interaction forces[5]. This way, the DCM naturally captures changes in cell shape from squamous to columnar cell types (fig. 1a), and describes the behaviour and properties of both partially and fully confluent tissue.

We study the jamming phase transition in an epithelial layer in function of cell-cell adhesion and cell motility (fig. 1a-b). By measuring dynamics of cell rearrangements (fig. 1c-d), we show that cell motility induces tissue fluidisation, and cell-cell adhesion fluidises tissue in the confluent regime, while it promotes solidfication in porous tissue. Furthermore, we show that tissue fluidisation in confluent tissue is accompanied by cell extrusion (fig. 1e).
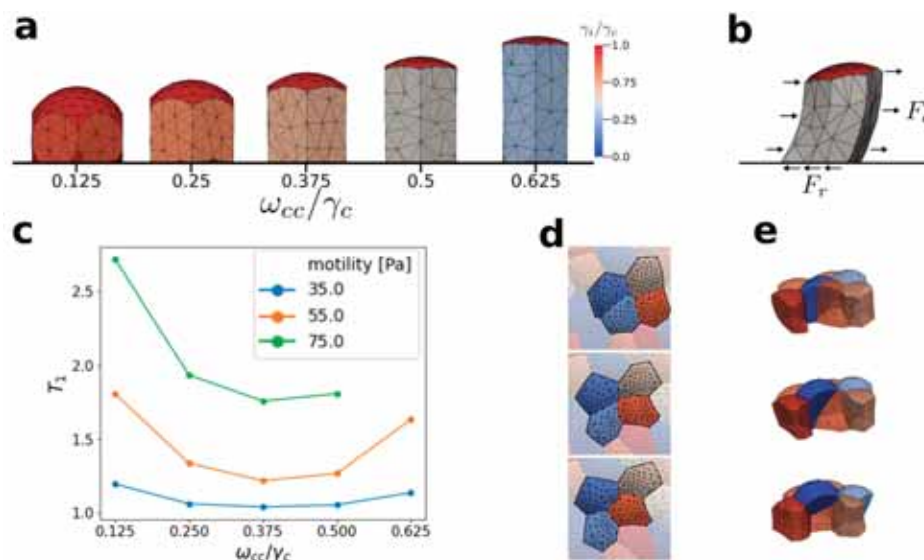
Figure 1: a) Cell shape changes influenced by cell-cell adhesion modeled using the DCM. b) Representation of a motile cell with retraction and protrusion forces Fa and cell-substrate force Fr. c) Cell rearrangements measured by a neighbour exchange rate T1. The more cells rearrange, the more T1 diverges from 1. If no rearrangements occur T1 = 1. d) Example of a T1-transition viewed from the apical side, and e) cell extrusion.

References:
1   Bi, D. et al. Nat. Phys. 11, 1074–1079 (2015)
2   Bi, D. et al. Phys. Rev. X 6, 021011 (2016)
3   Giavazzi, F. et al. Soft Matter 14, 3471–3477 (2018)
4   Kim, S. et al. Nat. Phys. (2021)
5   B. Smeets, M. Cuvelier, J. Pesek, H. R. Biophys. J. 116, 1–9 (2019)

A10.2
Arrested coalescence in tissue spheroid fusion: from tissue rheology to individual cell properties

Steven Ongenae[1], Jef Vangheel[1], Gabriella Nilsson Hall[2], Ioannis Papantoniou[2], Bart Smeets[1]

1   Katholieke Universiteit Leuven, Department of Biosystems, Leuven, Belgium
2   Katholieke Universiteit Leuven, Skeletal Biology and Engineering Research Center, Leuven, Belgium

Fusion of tissue-spheroids is a frequently used unit operation to create larger coherent constructs in bottom-up tissue engineering. Furthermore, the fusion process can be analyzed to study rheology. In the classical liquid description, the dynamics of fusion are related to the spheroid's radius, surface tension and viscosity. Since a liquid droplet minimizes its area due to surface tension, fusion is always complete. However, recent experimental studies indicate that fusion can be inhibited, a phenomenon called arrested coalescence1–3. To account for the arrested coalescence, we propose a viscoelastic description of tissue spheroid fusion dynamics, in which elastic energy gradually builds up counteracting the surface tension-driven area minimization4. By performing simulations with an individual cell-based we show that that higher levels of cell activity result in complete fusion, while at low activity levels arrested coalescence occurs. Additionally, when cell-cell repulsion increases, more cell activity is needed to complete fusion. Finally, to take into account realistic cell shapes and cell mechanical properties, we present simulations of spheroid fusion using a deformable cell model. Using this model, we reveal the relationship between cell-cell connectivity changes and the emergence of arrested coalescence.

Figure caption: Simulation of tissue spheroid fusion using a deformable cell model.

References:
1   Pierzchalska, M. et al. Protoplasma 256, 575–581 (2019)
2   Tsai, A.-C. et al. Tissue Eng. Part A 21, 1705–1719 (2015)
3   Grosser, S. et al. Phys. Rev. X 11, 11033 (2021)
4   Ongenae, S. et al. bioRxiv (2021)

A10.3

Simulations indicate that temporal dynamics differentiate Notch ligands controlling angiogenesis

Tommaso Ristori[1 2], *Laura Tiemeijer*[1 3], *Oscar Stassen*[1 3], *Carlijn Bouten*[1], *Cecilia Sahlgren*[1 3]

1   Eindhoven University of Technology, Department of Biomedical Engineering, Eindhoven, Netherlands
2   Boston University, Department of Biomedical Engineering, Boston, United States
3   Åbo Akademi University, Faculty for Science and Engineering, Turku, Finland

Achieving a full understanding and control of angiogenesis, the formation of new blood vessels from a pre-existing vasculature, is one of the central challenges to advance tissue engineering. This process features endothelial cells sprouting and migrating towards gradients of vascular endothelial growth factor (VEGF). The juxtracrine Notch signaling pathway is a key regulator of this phenomenon. Recently, we have demonstrated that the direction and location of angiogenic sprouts can be controlled via micropatterns of the Notch ligand Dll4 [1]. However, it is unknown if other Notch ligands might be more efficient candidates for angiogenesis control. Moreover, the underlying mechanisms of angiogenesis in tissue engineering are still poorly understood.

Here, we compared the effects of micropatterns of Dll4 versus Jag1, a Notch ligand with pro-angiogenic properties [2]. To this aim, we investigated endothelial cells, seeded in a localized fashion via microfluidic channels, sprouting under the influence of micropatterned lines of Dll4 or Jag1. To understand the sprouting response to patterns, we simulated the experiments by adapting a previous computational model of Notch cross-talking with VEGF signaling [3].

Confirming our previous findings [1], cells only sprouted in between the Dll4 patterns (Fig. A-top). In contrast, Jag1 lines did not have any evident effect, with sprouts occurring randomly (Fig. A-bottom). The computational simulations quantitatively replicated these experimental results. Parameter exploration suggested that the temporal dynamics of Notch signaling versus cell migration determines the differential effects of the Dll4 and Jag1 ligands (Fig. B). More specifically, Dll4-mediated Notch activation is faster than its Jag1 counterpart. The latter is too slow, compared to the cell migration from the patterns, to elicit evident effects on the cellular system.

Concluding, by coupling in vitro experiments with a computational model of Notch signaling, we compared and simulated the potential of different Notch ligands to control the location of angiogenic sprouts. Our experiments indicate that future studies should consider Dll4 as a preferred ligand versus Jag1. In addition, similar to observations reported for native angiogenesis [4], our computational simulations highlight the central role of signaling temporal dynamics in regulating angiogenesis in tissue engineering. The proposed computational framework could be further enhanced and employed to rapidly explore the potential of other Notch proteins and strategies, towards optimizing the control of angiogenesis.
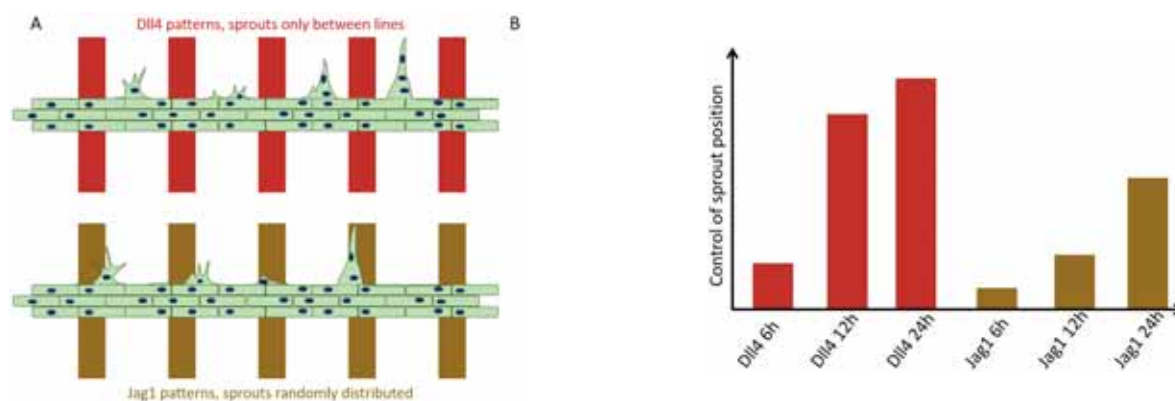
Figure caption: (A) Experiments: Notch ligands had different effects. (B) Simulations: temporal dynamics strongly affects the ligand effects (12h corresponding to experiments).

References:
[1]   Tiemeijer et al., Sci Rep, 8:6392, 2018;
[2]   Benedito et al., Cell, 137(6):1124-1135, 2009;
[3]   Boareto et al., PNAS, 112(29):E3836-E3844, 2015;
[4]   Bentley et al., Philos Trans R Soc Lond B Biol Sci., 372(1720):20150522.2017, 2017

A10.4

Tissue engineering a synthetic urinary bladder - steps towards developing a compliant artificial organ and degradable bio-active scaffold

Virginia Monteiro[1], *Katia Zolotovsky*[2], *Erez Pery*[3], *Ron Weiss*[3]

1   Federal University of Minas Gerais, Cell Biology, Belo Horizonte, Brazil
2   Rhode Island School of Design (RISD), Providence, United States
3   Massachusetts Institute of Technology, Cambridge, United States

Tissue engineering can potentially become a viable option for bladder replacement upon meeting the goal of building a compliant reservoir and adequate urodynamic response. In this project we aim to engineer a synthetic bladder with a bio-active degradable scaffold to deliver optimized urodynamics. To account for optimal urodynamic response, scaffold geometry results from computational analysis. The geometry is initialized from CT or MRI images of the patient's urinary bladder. With the fluid-structure interaction (FSI), we predict and optimize relevant urodynamic parameters, such as pressure-volumes curves, compliance and residual urine [1-2]. The interaction of urine with the organ is modeled with the Particle Finite Element Method, and the non-linear behavior of the synthetic tissue with FEM. The scaffold is fabricated in two steps, first by 3D printing silicone, recreating organ shape, and second by in-situ growth of cellulose. Synthetic gene networks in Gram-negative bacteria Gluconacetobacter xylinus are considered to enable spatial control of cellulose growth and the resulting scaffold's structure, surface functionalization and biodegradation [3]. The multi-step differentiation of stem cells [4] and the design of synthetic gene networks are considered to express ligands for specific cell binding and co-polymerization for faster scaffold biodegradation. The output transcription factors guide the multi-step differentiation of stem cells into different cell types: urothelial, smooth muscle cells, and endothelial cells. CRISPR synthetic guide RNA (sgRNA), miRNA, and mRNA-based developmental genetic programs are used to activate or repress endogenous genes dynamically. A layered organ structure is expected to develop from mesenchymal stromal cell differentiating in muscle layer and urothelial layer. The development of the synthetic bladder using a programmable bioactive scaffold based in bacterial cellulose is achieved from a given lattice structure with graded porosity, designed taking in consideration the mechanical properties of the grown tissue and optimized urodynamics.

References:
1.   V. Monteiro, C. T. Gasser, and K. Moerman, "Subject specific bladder morphology and correspondent 3D mold lattice structure for organ reconstruction," Eur. Urol. Suppl., vol. 18, no. 1, p. e1678, Mar. 2019.
2.   V.Monteiro, E. Oñate, S. Oller, Computational model of the human urinary bladder. Centre Internacional de Mètodes Numèrics en Enginyeria (CIMNE). 2013.
3.   K. Zolotovsky, M. Gazit, and C. Ortiz, "Guided Growth of Bacterial Cellulose Biofilms," in Biomimetic and Biohybrid Systems, 2018, pp. 538–548.
4.   Programming gene and engineered-cell therapies with synthetic biology," Science, vol. 359, no. 6376, p. eaad1067, Feb. 2018."

A10.5

The effect of stress and strain on tissue formation during in situ heart valve tissue engineering

Elmer Middendorp[1 2], Amber Daniels[1], Carlijn Bouten[1 2], Anthal Smits[1 2], Sandra Loerakker[1 2]

1   Eindhoven University of Technology, Department of Biomedical engineering, EINDHOVEN, Netherlands
2   Institute for Complex Molecular Systems, EINDHOVEN, Netherlands

During in situ heart valve tissue engineering (HVTE), a porous polymeric scaffold is implanted at the functional site with the aim to harness the host's regenerative capabilities. In the study of Kluin et al. [1] this technique was employed to replace the pulmonary valve in an ovine model. Although the results were promising, the underlying determinants for tissue formation remain unclear. In an in vitro setting, multiple studies [2-3] have shown that mechanical stimuli influence the ECM production of cells. In this study, we therefore investigated whether mechanical stimuli also relate to tissue production during in situ HVTE by comparing the maximal principal stress and strain with the increase in tissue thickness observed in vivo.

Equibiaxial tensile tests were performed on implants and explants by Kluin et al. [1]. Using their results, parameters for a fiber reinforced material model [4] have been estimated for the implants (n=1) and explants (6 months (n=3) & 12 months (n=2)). Using finite element modeling, we were able to determine the maximal principle stresses and maximal principal true strains averaged over the valve geometry. With these results, we estimated the average stress and strain for each implant over the period from implantation until 6 months and over the period from 6 to 12 months of implantation. From the experimental results, the increases in thickness during both periods (0-6 and 6-12 months) were obtained as well, which served as a measure for tissue production. The Pearson's correlation coefficient between the thickness increases and the stresses and strains were subsequently computed to investigate to what extent mechanical stimuli correlate with tissue production in in situ HVTE.

The stresses and strains in the heart valves were successfully simulated using finite element analysis in five out of six cases. The simulation did not converge in one 6-month explant which was excluded from further analysis. In figure 1 the resulting stresses and strains are visualized. In the current analysis, Pearson's correlation showed no significant correlation for both the principal stress (r=-0.54, p=0.46) and principal strains (r=0.87 p=0.13) with the increases in thickness.

In this study, the influence of mechanical stimulation on thickness increases of in situ tissue engineered ovine pulmonary valves have been investigated. Although no significant relationships have been found so far, local variations in thickness had been observed experimentally. Together with the spatial variations of stresses and strains in heart valves, this may indicate that the current global approach may be insufficient. Future efforts will therefore be dedicated to investigate if mechanical stimuli and heart valve growth correlate at a more local scale.
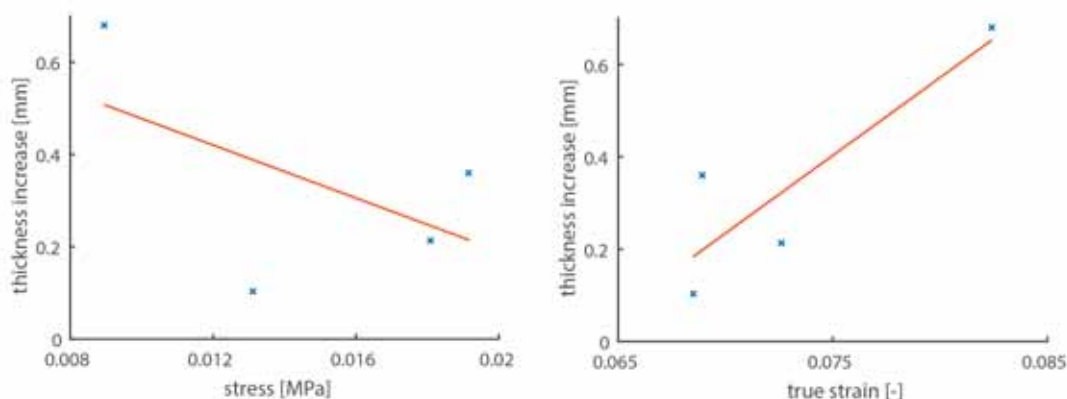
Figure caption: "Time averaged maximal principal stresses and strains against the increase in tissue thickness over six months"

References:
 [1   Doi:10.1016/j.biomaterials.2017.02.007
[2]   Doi:10.1016/j.jmbbm.2016.05.005
[3]   Doi:10.1002/adbi.201900249
[4]   Doi:10.1016/j.jbiomech.2006.01.009"

B1.1
Modelling the spread of COVID

Fred Vermolen[1]

1   *University of Hasselt, Computational Mathematics Group, Department of Science, Diepenbeek, Belgium*

The world is hit by the pandemic COVID-19, which, due to the high mortality among elderly people, has a major impact on our daily life. In this presentation, we consider a Spatial Markov Chain model for the spread of epidemics. The formalism incorporates susceptible, infected, resistant and dead people. The model is based on the principle to represent networks of people by a graph which connects nodes that represent individuals. This modelling can also be generalized to nodes representing villages or communities. The internodal connections represent relations between humans, which may be understood in a generic context regarding distances and all kind of relations. In this way, a graph is connected to the likelihood of infectious spread from person to person. The intensity of contact can be varied over time and by randomness. Several lockdown scenarios have been incorporated in the modelling studies. The developed computational framework aims at predicting probabilities of scenarios, rather than predicting scenarios in particular. The presentation will also list alternative models from the literature and discuss their merits and disadvantages.

B1.2

Analysis and simulation of the second wave of COVID19 in Italy through a time-varying SIRD model

Giuseppe Carlo Calafiore[1], **Tommaso Bradde**[1], Carlo Novara[1], Corrado Possieri[2]

1   Politecnico di Torino, Electronics and Telecommunications, Turin, Italy
2   Consiglio Nazionale delle Ricerche, Istituto di Analisi dei Sistemi ed Informatica "Antonio Ruberti", Rome, Italy

Since the first wave of the COVID19 pandemic, epidemiological models have represented fundamental tools for understanding the contagion, for testing hypotheses, and for implementing control strategies.

In this contribution, we study the second wave of COVID19 in Italy through a modified Susceptible-Infected-Recovered-Deceased (SIRD) discrete-time model [1]. We consider the method proposed in [2], which incorporates time-varying parameters into the SIRD equations, making it possible to explain the dynamics of the infection under different spreading conditions (e.g., sudden imposition of containment measures). This model structure is characterized by a limited number of intelligible parameters, that are estimated from epidemiological data regarding the number of infected, recovered and deceased individuals of the geographical region of interest.

The identification stage consists in estimating the time dependency of the three coefficients entering the SIRD equations, namely the infection, recovery, and mortality rates. To this aim, we represented these parameters through time-dependent basis functions expansions, and we estimate the expansion coefficients during the model identification. We make use of a high number of basis function, and we seek for a sparse solution of the coefficients vector, which retains the components that are useful to reconstruct the observations; the coefficients are found by solving a least-squares problem with $\ell 1$-regularization (LASSO).

We modeled the COVID19 infection in Italy, from August 31st 2020 to January 12th 2021, using the data provided by Italian "Protezione Civile". Gaussian, polynomial and logistic basis functions have been used to identify the transmission, recovery and mortality rates, respectively. The parameters have been identified with 11 basis functions out of the 55 available, setting the regularization factor λ=16. The results show that the model recovers the behavior of the pandemic over the considered time window. The estimated transmission rate is coherent with the increase of the infections which took place in summer and the imposition of containment measures on October 26th. Additionally, we performed predictions of the infection evolution up to February 18th, applying the multi-stage simulation described in [2]. The prediction is accurate and validates the foreseen increasing trend of the recovery rate.

In conclusion, the proposed model structure proves to be a valuable tool to analyze the evolution of the infection and to predict the effect of actual or conceivable reaction strategies.
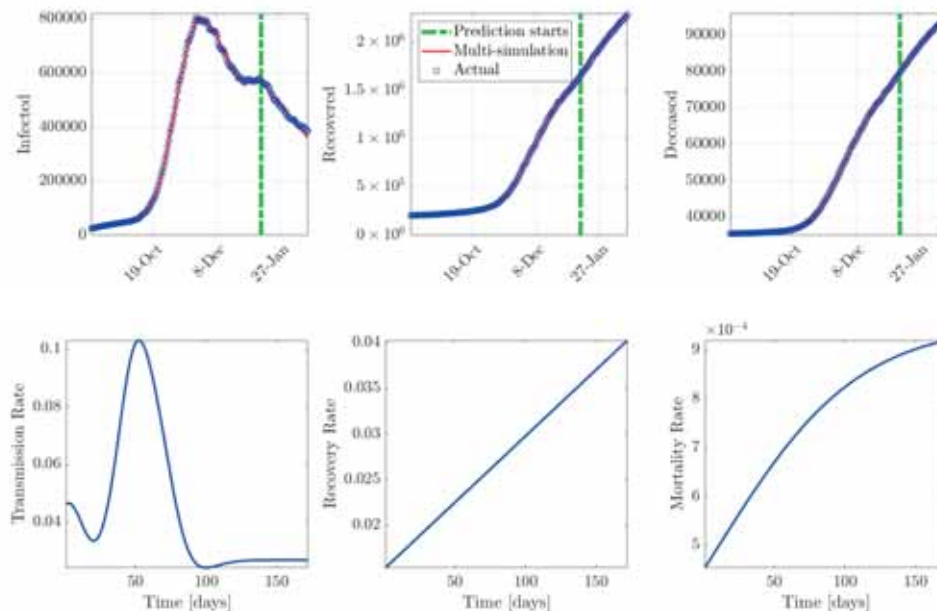
Figure caption: Model validation against data and identified SIRD parameters. Time expressed in days since Aug. 31 2020.

References:
[1]   W. O. Kermack and A. G. McKendrick, «A contribution to the mathematical theory of epidemics» Proceedings of the royal society of London. Series A, vol. 115, n. 772, pp. 700-721, 1927.
[2]   G. C. Calafiore, C. Novara and C. Possieri, «A Time-Varying SIRD Model for the COVID-19 Contagion in Italy» Annual Reviews is Control, vol. 50, pp. 361-372, 2020.

B1.3
The role of asymptomatic individuals on vaccination effectiveness

Paolo Di Giamberardino[1], *Daniela Iacoviello*[1]

[1]   *Sapienza University of Rome, Dept. Computer Control and Management Engineering, Rome, Italy*

Since the beginning of 2020, all the world has been affected by the new virus SARS-CoV-2 that has caused more than 3 million of deaths and more than 141 million of infected patients. This pandemic has a significant characteristic related to the high number of non-diagnosed individuals: they are subjects that do not know to have got the infection but can anyway spread the virus; in some cases, they could also have some symptoms, but they have probably underestimated them. One possibility to have, at least, an estimation on the number of non-diagnosed subjects in a more extended period is to perform a serological test to a significant sample of population; this test provides the information about the presence of COVID-19 antibodies, so it can confirm if the subject has been previously infected, unknowing it. In the period May-July 2020 in Italy there was a serological test campaign from which it is evidenced that about 2.5% of the population (1.501.537 individuals), had, in some ways, met the SARS-CoV-2 without knowing it. The statistical survey has also investigated about the regional distribution of these non-diagnosed cases, showing a large local variability, with ranges from 0.4% for Sicilia to 7.4% for Lombardia (Fig.1). The estimation of the number of infected subjects that have not been diagnosed is useful in the modeling process, since it provides an estimation of the percentage of non-diagnosed subjects with respect to the diagnosed ones, assuming its validity in general, as characteristic of the considered population. The model introduced to study the contribution of the amount of undiagnosed infected individuals to the effectiveness of the vaccination campaign is presented (Fig. 2). The aim in the model design is to let it be able to describe the undiagnosed people dynamics and, at the same time, to maintain it as simple as possible to guarantee a good identification with the available data. The analysis is performed in two steps. The first one is devoted to the choice of some meaningful regions, different for the relationship between the number of persons with a positive serological test and the number of individuals diagnosed (symptomatic or swab test positive) during the infection, for an identification procedure to set the models parameters accordingly. In the second step, the effects of a vaccination strategy in the different cases are analyzed and the best approach depending on the presence of undiagnosed persons is designed. The overall idea is that it is possible to optimize the vaccine distribution over the regions according to the estimated number of asymptomatic patients present to obtain the best global result. Such an evaluation is performed introducing the quantities: the vaccination efficiency the cost of vaccination
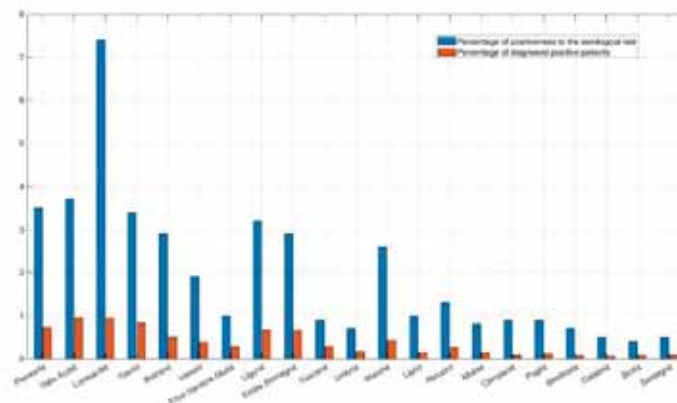
Figure 1: Comparison between the percentage of asymptomatic non diagnosed subjects determined after the serological campaign and the diagnosed positive patients in the Italian regions

$$\dot{S} = B - \beta S I_U - d_S S - vS$$
$$\dot{I}_U = \beta S I_U - \sigma I_U - \gamma_U I_U - d_{IU} I_U$$
$$\dot{I}_D = \sigma I_U - \gamma_D I_D - d_{ID} I_D$$
$$\dot{R}_U = \gamma_U I_U - d_{RU} R_U$$
$$\dot{R}_D = \gamma_D I_D - d_{RD} R_D + vS$$
$$\dot{D}_D = d_{ID} I_D$$

Figure 2: The mathematical model proposed

$$\varepsilon = \frac{\text{Number of susceptible individuals vaccinated}}{\text{Total number of vaccinated persons}} = \frac{S}{S + I_U + R_U}$$

$$\chi = \text{Cost of vaccine for one person} \times \text{Total number of vaccinated persons} = \chi_0 \left(S + I_U + R_U \right)$$

References:
ISTAT, https://www.istat.it/en/
GitHub, https://github.com/pcm-dpc/COVID-19/tree/master/dati-andamento-nazionale.

B2.1
Quantifying cellular forces: a FE-based algorithm for traction force microscopy

*Silvia Hervas-Raluy[1], María José Gómez-Benito[1], Carlos Borau-Zamora[1], Mar Cóndor[2], **José Manuel García-Aznar[1]***

1   Escuela de Ingeniería y Arquitectura de la Universidad de Zaragoza, Zaragoza, Spain
2   KU Leuven Campus Arenberg III, Leuven, Belgium

Cells are able to behave both as active and passive materials. They can bear and transmit physical forces and respond to them through many different mechanisms. There are different tools in the literature [1] that allow quantifying forces exerted by the cells, one of them being Traction Force Microscopy (TFM), that can be developed in 2D or 3D. TFM consists on obtaining the stresses (force per unit area) at the cell surface by measuring the displacements of the surrounding material. This method requires the application of an inverse algorithm that allows estimating these forces from the displacement field and some knowledge regarding the material properties of the surrounding tissue and the cell. This problem becomes more complicated when applied in 3D and the cell is embedded in matrices with a high non-linear and non-affinity behavior. In such conditions, the inverse problem is not well-conditioned and, in most cases, a numerical solution must be implemented. To circumvent these problems, Legant et al. computed 3D traction fields using the Finite Element (FE) Method [2]. Alternatively, Steinwachs et al. developed a continuum approach that incorporates non-affine properties of the matrix [3].

Here we propose a new numerical FE-based strategy to compute 3D traction fields [4,5]. The inverse problem is solved iteratively and can be easily implemented in any FE commercial software. The main advantage of this automatic methodology (Fig.1) is that it can solve problems under the hypothesis of finite deformations and non-linear material formulation. In order to test the proposed methodology, we analyze two cases. First, we solve a theoretical problem to validate the model. Secondly, we evaluate the traction forces in a real cell embedded in a collagen-based matrix.

In conclusion, this work opens new possibilities to improve the quantification of cellular forces.
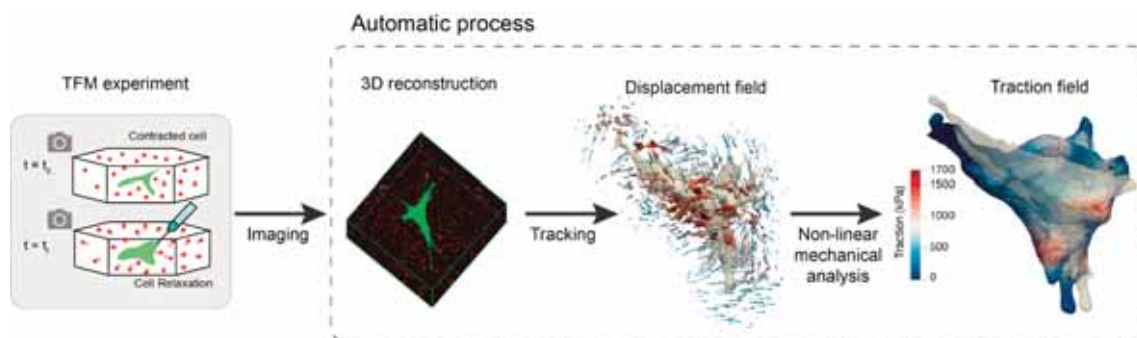
Figure 1: "Workflow for 3D TFM and the numerical algorithm developed [5]. Cellular tractions are obtained via a 3-steps method. First, two pictures during the experiment are captured. Then, the 3D segmentation is obtained through the imaging process. The tracking method computes the displacement field and the cell geometry. At the end, the traction field is obtained via the resolution of the inverse problem."

References:
[1] Roca-Cusachs et al (2017). Nature cell biology, 19(7), 742-751.
[2] Legant et al. Nat. Methods 7:969–71 (2010).
[3] Steinwachs et al. Nat Methods 13:171–6 (2016).
[4] Cóndor & García-Aznar (2019). Computer methods and programs in biomedicine, 182, 105056.
[5] Hervas-Raluy et al. (2021) PlosOne (in press).

B2.2

Cell-based characterization of tissue rheology and mechanics: particle-based computational models

Bart Smeets[1], Steven Ongenae[1], Maxim Cuvelier[1], Jef Vangheel[1]

1   KU Leuven, Leuven, Belgium

3D micro-tissues show great potential for organoid culture or as building blocks for regenerative medicine applications. The predictable and modular behavior of micro-tissues render them practicable for application in engineering purposes. However, for this we need adequate living material models that take into account the active mechanical properties of the underlying cells as they undergo morphological transitions. From the broad spectrum of cell-based models, active foam models are particularly well suited for the mechanical representation of micro-tissues at biologically relevant timescales [1,2]. Cells are considered as active viscous droplets, which are mainly parameterized by surface tension, adhesion and differential interfacial tension, viscosity and fluctuating protrusive and contractile pressure that generates active motility [3]. Using this model, we investigate the mechanical and rheological behavior of small tissue spheroids. By comparing the distribution and propagation of mechanical stress, we show how cortical tension and differential adhesive tension modulate the behavior of the tissue from a liquid droplet to a granular assembly. Next, we investigate the role of active cell migration and cell division in fluidizing the micro-tissues. A fluid-to-glass transition is observed which results in stretched exponential relaxation dynamics of the compaction during tissue self-assembly [4], and in arrested coalescence during spheroid fusion [5]. Finally, we address the compatibility of the underlying computational model to describe various different morphological transitions, thereby demonstrating its broad applicability for modeling 3D tissue structures.
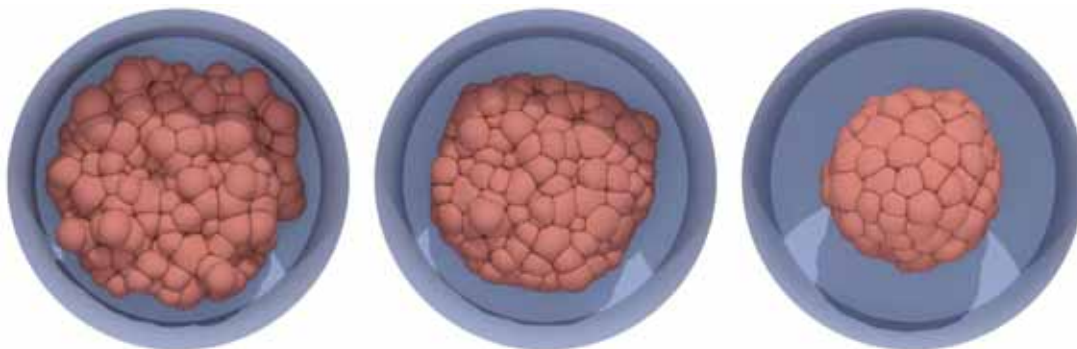
Figure caption: Active foam simulation of aggregate compaction during micro-well self-assembly

References:
[1]   Bi et al. (2015) Nature Physics 11, 1074-1079.
[2]   Kim et al. (2020) bioRxiv 2020.06.17.157909
[3]   Smeets et al. (2019) Biophys J 116(5):930-937
[4]   Smeets et al. (2020) Matter 10.1101/699447.
[5]   Ongenae et al. (2021) bioRxiv 2021.02.26.433001.

B2.3
imMechanoType: imaged-based mechanophenotyping of single cells

Anna Garcia-Sabaté[1], *Jiranuwat Sapudom*[2], *Mei ElGindi*[2], *Rachid Rezgui*[3], *Jeremy Teo*[2]

1   New York University Abu Dhabi, Engineering, Abu Dhabi, United Arab Emirates
2   New York University Abu Dhabi, Engineering, Saadiyat Island, United Arab Emirates
3   New York University Abu Dhabi, Core Technology Platforms, Saadiyat Island, United Arab Emirates

Biomechanical evaluation of cells could reveal their physiological state and many reported methods have successfully differentiated cell types as well as cellular pathophysiology[1–3]. These invasive methods are often end point assays and masks vital information that can only be revealed with biomechanical properties that have temporal resolution. We have developed a platform for assessing cellular biomechanics from live-imaging datasets, thereby providing dynamic biomechanical properties non-invasively [4]. The platform morphs sequential pairs of images in an iterative manner that results in a strain fields that is fitted with viscoelastic models to infer cellular stiffness and viscosity values (Figure). It was formerly demonstrated to be able to detect significant differences in stiffness between human mesenchymal stem cells and stem cells exposed to osteogenic conditions. In this study we challenge the sensitivity of the platform by attempting to detect differences in cellular phenotype, specifically, human antigen presenting cells derived from monocytic cell lines.
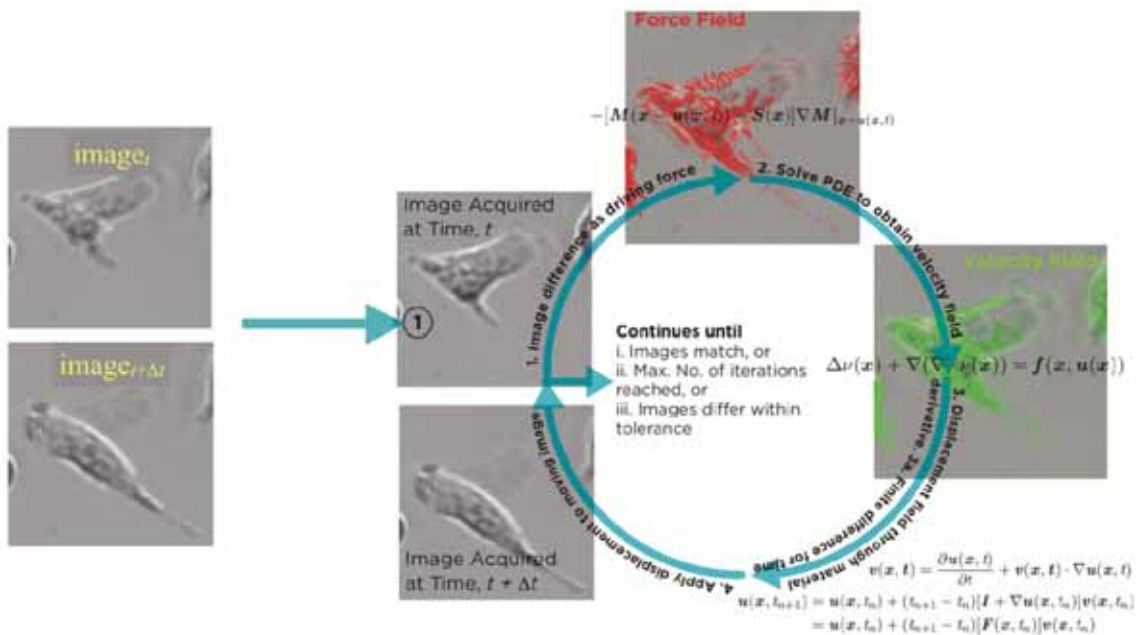
Figure. imMechanotype takes in live-imaging datasets and analyses for cellular mechanical properties for phenotyping purposes.

References:
1.   Lim CT, Bershadsky A, Sheetz MP, Interface JRS. Mechanobiology. J R Soc Interface. 2010;7 Suppl 3:S291----3.
2.   Ekpenyong AE, Whyte G, Chalut K, Pagliara S, Lautenschläger F, Fiddler C, Paschke S, Keyser UF, Chilvers ER, Guck J. Viscoelastic Properties of Differentiating Blood Cells Are Fate- and Function-Dependent. PLoS ONE. 2012;7:e45237.
3.   Kumar S. Cellular mechanotransduction: Stiffness does matter. Nature Materials. 2014;13:918–920.
4.   Pearson YE, Lund AW, Lin AWH, Ng CP, Alsuwaidi A, Azzeh S, Gater DL, Teo JCM. Non-invasive single-cell biomechanical analysis using live-imaging datasets. Journal of Cell Science. 2016;129:3351–3364.

B2.4

On the calibration of vertex and FE models in cell mechanics and cytoskeletal reconstruction from TFM

Jose Munoz[1 2 3]

1   Universitat Politècnica de Catalunya, Mathematics , Barcelona, Spain
2   Centre Internacional de Mètodes Numèrics en Enginyeria (CIMNE), Barcelona, Spain
3   Institu de Matemàtiques de la UPC - BarcelonaTech, Barcelona, Spain

Numerical models depend on a variety of parameters that may be directly or indirectly measurable experimentally, or that are either specific of the model or purely numerical. We will present a three-dimensional vertex model, based on the minimization of a functional, and describe how to calibrate the most common material parameters (or penalty coefficients) that constrain cell volume, minimize cortex area, or impose edge contractility from wound healing experiments and recoil (see [1,2] and Fig. 1). We will also highlight numerical stability related to space discretization of the cortex inherent in vertex models.

Based on this experience, we will also comment on force inference of tissues through Traction Force Microscopy (TFM), and derived results on the indirect measurement of cell adhesion and contractility from combined traction and area measurements. We finally present an inverse method to generate a plausible cytoskeletal network that best matches the traction field computed through TFM, as shown in Fig. 2.

(a)

(b)
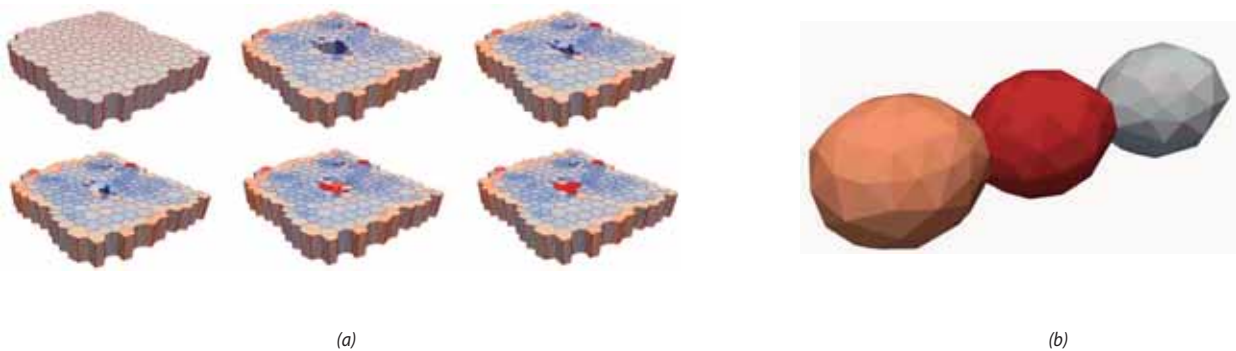
Figure 1: Vertex model applied to simulations of (a) wound healing of cell monolayer, and (b) stretching test of three cells.

(a)

(b)

Figure 2: Example of cytoskeletal Network computed from self-equilibrated dipoles. (a) Contour plot of the norm of tractions from TFM. (b) Set of dipoles that best match the traction field.

References:
[1]   Ioannou, F., Dawi, M.A., Tetley, R.J., Mao, Y., Munoz, J.J. Development of a new 3D hybrid model for epithelia morphogenesis. Frontiers in Bioengineering and Biotechnology, Vol. 8, pp. 1-11, 2020
[2]   Mosaffa, P., Tetley R.J., Rodríguez-Ferran, A., Mao, Y., Muñoz, J.J. Junctional and cytoplasmic contributions in wound healing. Journal of the Royal Society Interface, Vol. 17, Article number: 20200264, 2020

B2.5
Quantifying cellular forces in a 3D in vitro vascular model

Jorge Barrasa Fano[1], *Apeksha Shapeti*[1], *Mar Cóndor*[1], *Janne De Jong*[1], *Alejandro Apolinar-Fernández*[2], *Mojtaba Barzegari*[1], *Jose Antonio Sanz-Herrera*[2], *Hans van Oosterwyck*[1]

1   Katholieke Universiteit Leuven, Leuven, Belgium
2   University of Seville, Sevilla, Spain

Cellular behavior is not only regulated by bio-chemical processes. Cells are affected also by their mechanical microenvironment. For example, stem cells can differentiate into tissue-specific cells depending on the stiffness of the extracellular matrix (ECM)1. Moreover, cells also actively exert forces to shape their environment and perform their (mal)function under physiological as well as pathological conditions. For example, cancer cells can migrate away from the primary tumor causing metastasis by applying pulling forces on the surrounding collagen fibers2. Seeking physiological relevance, biologists often select three-dimensional in vitro models to study cell behavior. Typically, cellular forces are computed by means of Traction Force Microscopy (TFM), a methodology initially developed for 2D cultures and currently being extended to be compatible with 3D in vitro cultures. Currently, there are no 3D TFM software tools that can simultaneously guarantee accurate force calculation and easy usability by non-technical users. In this work, we developed an advanced validation framework to evaluate the accuracy of traction recovery algorithms3. With this framework, we quantified the effect of the inherent sources of error of TFM (such as bead density and focal adhesion size) on the accuracy by comparing the results from our inverse traction recovery method4 and another state of the art forward method to ground truth solutions (see top row of figure). Our simulations showed that our inverse method improves twofold the accuracy of the forward method (average error of 23% vs. 50%). Moreover, we further supported these result by recovering cellular tractions around angiogenic sprouts in an in vitro model of angiogenesis5 (see bottom row of figure). Our inverse method recovered more realistic traction patterns than the forward method, showing clearer pulling patterns at the sprout protrusion tips. Furthermore, we developed TFMLAB, an open source Matlab toolbox that integrates all the necessary computational steps for 3D TFM6. With this toolbox, a user with limited programming experience can input microscopy images, easily tune parameters via graphical user interfaces and obtain output matrix displacements and cellular tractions as an output.
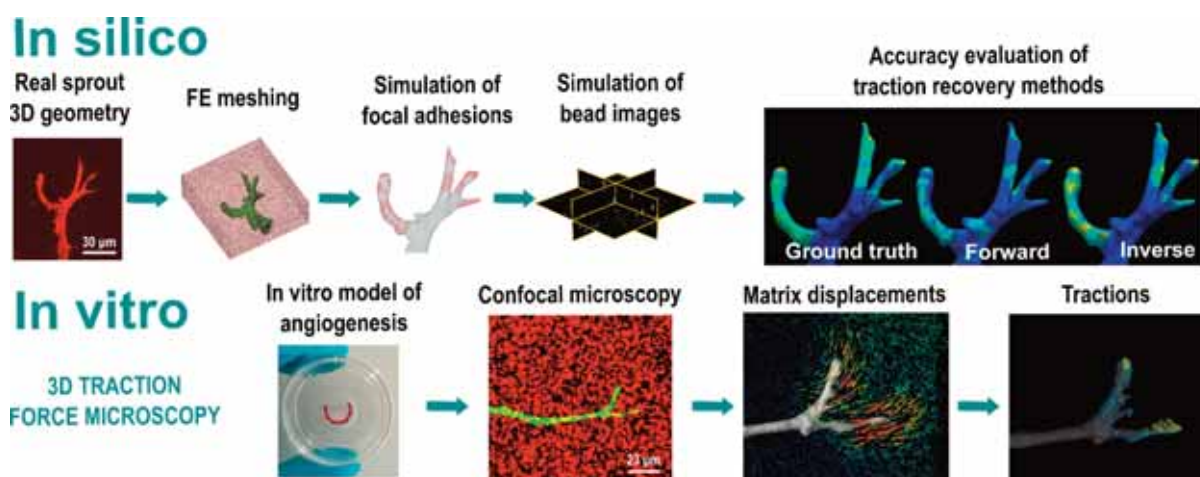
Top row: In silico simulations, involving Finite Element (FE) simulations, and microscopy bead image simulations were conducted to validate the accuracy of traction recovery methods (forward and inverse) with respect to a ground truth solution. Bottom row: Traction recovery around angiogenic sprouts in an in vitro model of angiogenesis3.

References:
1   Engler, A. J. et al. Cell 126, 677–689 (2006)
2   Kopanska, K. S. et al. PLoS One 11, e0156442 (2016)
3   Barrasa-Fano, J. et al. bioRxiv 2020.12.08.411603 (2020)
4   Sanz-Herrera, J. A. et al. Soft Matter (2020)
5   Vaeyens, M.-M. et al. Angiogenesis (2020)
6   Barrasa-Fano, J. et al. bioRxiv 2020.12.18.423056 (2020)

B3.1

The role of fluid removal rates on the flow field of a surrogate system of an artificial kidney

Miguel Pereira[1], Tsvetan Yorov[2 3], Matilde De Pascale[4], Bahram Haddadi[3], Viriato Semiao[5], Maria Norberta de Pinho[1], Margit Gföhler[2], **Michael Harasek[3]**

1   IDMEC, Department of Mechanical Engineering, Instituto Superior Técnico, Universidade de Lisboa,, Portugal
2   Department of Engineering Design and Product Development, TU Wien, Austria
3   Institute of Chemical, Environmental and Bioscience Engineering, Vienna, Austria
4   Department of Civil, Chemical, Environmental and Materials Engineering (DICAM), University of Bologna,, Italy
5   IDMEC, Department of Mechanical Engineering, Instituto Superior Técnico, Universidade de Lisboa, Portugal

Chronic Kidney Disease (CKD) affects 11-13% of the world population and Renal Replacement Therapies (RRTs) stand as a life support for most of these patients. The RRTs generally associated to the Artificial Kidney (AK) are membrane-based treatments which assure the separation functions of the failing kidney in extracorporeal blood circulation. In the 1990s, the progress from conventional hemodialysis (HD) controlled by diffusion and known as low-flux hemodialysis (LFHD) to new RRTs like hemofiltration (HF), hemodiafiltration (HDF) and high-flux HD (HFHD) was due to the introduction of ultrafiltration (UF) membranes characterized by high convective permeation fluxes. However, fluid volume removal and hemodynamic management remains as a matter of concern due to its association to cardiovascular stress and potential organ damage. Despite the understanding of hemodynamics as being directly dependent on fluid mechanics fundamentals, little attention has been given to the main focus of the present work, which is the influence of the fluid removal rates typical of HFHD on the flow field, particularly on the increase of the potentially blood traumatizing shear stresses developed adjacently to the membrane. Its quantification is performed in a surrogate system of an artificial kidney (AK)/hemodialyzer mimicking tangential fluid velocities and membrane removal rates with circulating water.

Two flat-sheet laboratory-made ultrafiltration (UF) hybrid membranes of cellulose acetate(CA)/silica(SiO2) are tested. The experimental setup, comprising the two-compartment AK surrogate where the semi-permeable membrane (surface area of 0.0021 m2) separates the top slit (height, h=600μm «width, W=3cm; length L=25cm) for feed circulation from the bottom chamber receiving the membrane permeating fluid. The feed/water (T=37◦C) pumped

through the slit at volumetric flowrates 40mL/min≤Q≤160mL/min generates pressure drops, ΔP, with uncertainty of ±20%. Pressure sensors are computer connected through the data acquisition program LabVIEW. Transmembrane pressure ranges from 3×10^3 Pa to 1.5×10^4 Pa.

The AK experiments in typical HFHD permeation conditions yielded pressure drops that compared to the ones of an AK with impermeable walls are more than 512% for membrane CA22/5%SiO2 and 576% for CA30/5%SiO2. This reflects the increase on magnitude of the potentially blood-traumatizing shear stresses at the membrane surface.

For the comparison of experimental results with AK fully developed flow, CFD was used. A computational fluid dynamics analysis of the flow channel was performed using OpenFOAM® and an in-house developed solver (membraneFOAM) which accounts for the mass transfer through membranes using multi species driving force models or coupled transport models. The flow channel was fully resolved by a suitably fine finite volume mesh. Flow fields were calculated for all experimental conditions. Results show that HFHD operation significantly affects the flow field and shear stress field.

B3.2

Development of CFD technique to simulate the hemodynamic effects of the Cardioband implantation

Laura Iannetti[1], Emanuele Gasparotti[2], Simona Celi[2], Massimiliano Mariani[3], Sergio Berti[3]

1   BETA CAE Italy , Turin, Italy
2   BioCardioLab, Fondazione Toscana Gabriele Monasterio, Massa, Italy
3   Adult Cardiology Unit, Fondazione Toscana Gabriele Monasterio, Massa, Italy

The mitral valve regurgitation (MVR) disease is caused by the dilatation of mitral annulus thus, during the systole, the blood flows back towards the left atrium decreasing cardiac efficiency [1]. Transcatheter techniques are proposed to correct MVR. The Cardioband® system (Edwards Lifesciences, USA) [2] uses a specific polyester sleeve, fastened on the posterior mitral valve annulus by helicoidal metal anchors, to reshape and contract the mitral annulus and repair the MVR. In a previous study [3] a Cardioband FEA tool was developed to evaluate the structural effect of the Cardioband system. The work aim is to investigate the hemodynamic changes in the left heart after the Cardioband implantation by combining the previous structural results with the fluid dynamic ones. CFD simulations were setup for pre and post deployment stages at two different cardiac phases. The geometries were extracted at the Systolic Peak Flow (SPF) and at the Diastolic Peak Flow (DPF) respectively. The patient specific pre-deployment geometries were segmented from CT-gated dataset. By means of morphing the post-deployment geometries were obtained by deforming the latter ones considering the Cardioband contraction, previously calculated [3]. The four configurations were discretized with 106 tetrahedral elements using ANSA pre-processor and the blood was modeled as a Newtonian fluid with density of 1.060 kg/dm3 and viscosity of 3.5 cP. With regards to the boundary conditions, a flow constraint was imposed at the ventricle surface to reproduce its contraction and the expansion during SPF and SDF. The SPF was simulated by imposing constant inlet flow rate equal to 20 l/min and the outlet pressure at pulmonary veins and at aortic root equal to 10 mmHg and 120 mmHg, respectively. During SDF, similarly, constant outlet flow rate equal to 15 l/min and an inlet pressure of 10 mmHg at pulmonary veins were set. Additionally, wall condition was imposed at aortic root section to mimic the closed aortic valve. For each phase, a comparison between pre and post implantation was performed by analyzing velocity and pressure distributions. Results, referring to the anterior-posterior heart section (Fig 1a), confirm the effectiveness of Cardioband deployment capable to reduce the regurgitation phenomena (-50%) in the SPF (Fig 1b-c). Moreover, as reported, the device implantation leads to an increase of the transvalvular pressure (+30%) during the SDF (Fig 1d-e). In conclusion the Cardioband implant effects on hemodynamics of left heart, at SPF and SDF, were successfully assessed by combining structural and CFD techniques.
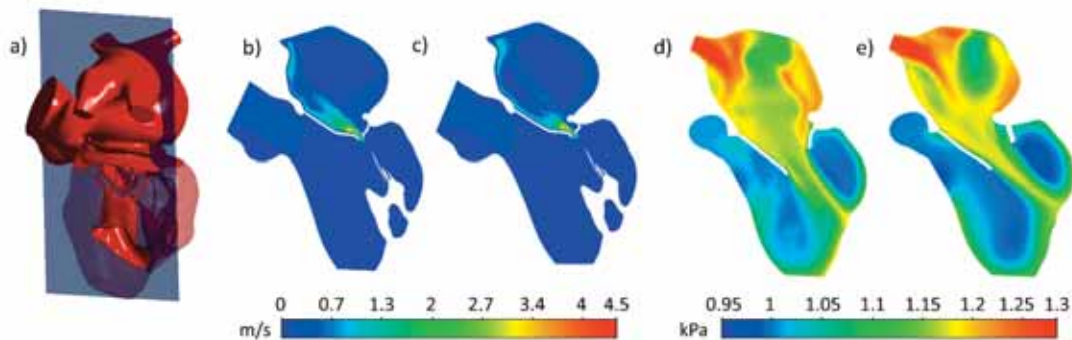
Figure 1: CFD results: diastolic velocity fields and diastolic pressure distribution at pre (b-c) and post (d-e) procedure in the anterior-posterior section (a).

References:
[1]   Douedi, S., & Douedi, H. (2020). Mitral Regurgitation
[2]   Nickenig et al, JACC: Cardiov Interv, 2016.
[3]   E. Gasparotti et al, WCB Conference, 2018.

B3.3

Hemodynamic effects of entry versus exit tear size and tissue stiffness in aortic dissection

Kathrin Baeumler[1], *Judith Zimmermann*[1 2], *Daniel B. Ennis*[1 3 4], *Alison Marsden*[5 6 7], *Dominik Fleischmann*[1]

1   Stanford University, Department of Radiology, Stanford, United States
2   Technical University of Munich, Department of Informatics, Garching, Germany
3   Veterans Affairs Health Care System, Division of Radiology, Palo Alto, CA, United States
4   Stanford University, Cardiovascular Institute, Stanford, United States
5   Stanford University, Department of Pediatrics (Cardiology), Stanford, United States
6   Stanford University, Department of Bioengineering, Stanford, United States
7   Stanford University, Institute for Computational and Mathematical Engineering, Stanford, United States

Aortic dissection is characterized by delamination of the aortic wall, resulting in a new parallel flow channel – the false lumen – which is separated from the true lumen by delaminated aortic tissue – the dissection flap. We investigate the effects of entry and exit tear size and the effect of aortic tissue stiffness on false lumen pressure, which is associated with adverse events.

We created a patient-specific 3D model of a Type B aortic dissection (Model A) based on CT imaging. In Models B and C the entry or exit tear was reduced to 27% of their original area, respectively. In Model D both entry and exit tears were reduced (Figure 1A). CFD simulations with and without fluid structure interaction (FSI) to account for deformability were conducted in all four models. Boundary conditions were informed by 2D phase contrast MRI measurements in a compliant 3D print of Model A [1].

FSI simulations showed increased systolic pressure differences ΔP between true and false lumen in Models B and D with small entry tears. In the distal dissection ΔP reached negative values in Model C due to a reduced exit tear size and associated larger false lumen pressure (Fig 1B). With smaller tears less flow was diverted into the false lumen, and true lumen flow increased from QTL, max of 2.67 L/min in Model A to 4.6 L/min in Model D (Figure 1C). Flow waveforms were dampened in FSI compared to rigid simulations (Figure 1D) and the true lumen flow increased by 30% in Model A in the rigid simulation. ΔP is exacerbated especially in the distal dissection with small exit tears (Models C and D) (Figure 1B).

Our findings suggest that the tear configuration and elasticity of the aortic tissue both influence interluminal pressure differences and flow rates and are likely relevant for a patient-specific prediction of late adverse events.
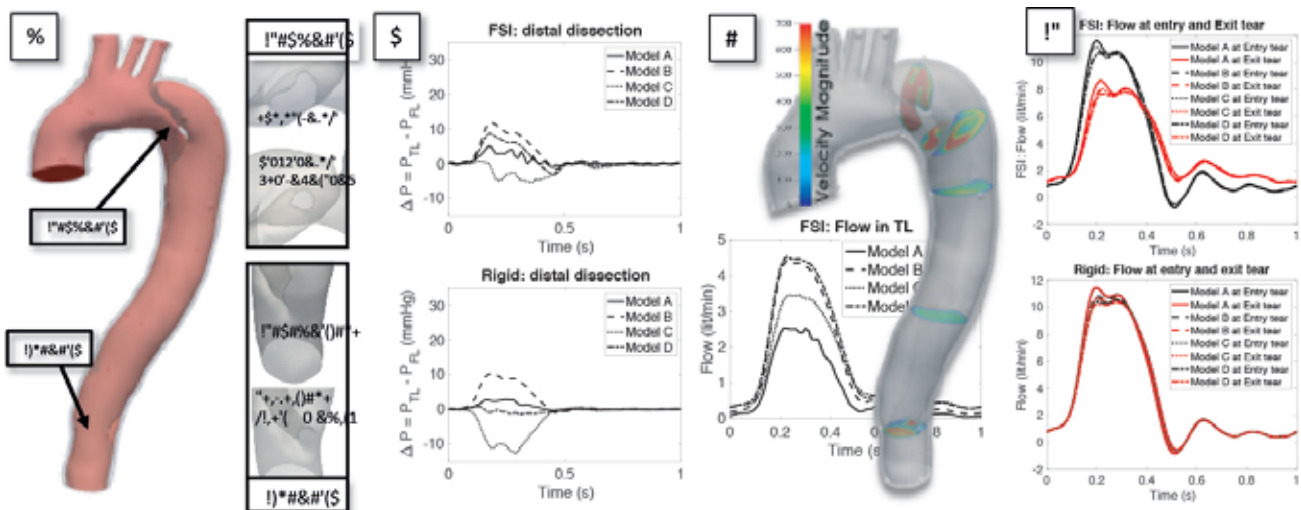
Figure 1: (A) Patient-specific model of aortic dissection and altered entry and exit tears. (B) In the distal dissection, the false lumen pressure exceeds the true lumen pressure only in Model C. Rigid walls increased this effect. (C) True lumen flow varies with tear configuration, and (D) flow rates are dampened when compliance of the arterial wall is included in the simulation.

References:
[1]   J. Zimmermann, K. Baumler, M. Loecher, T. E. Cork, F. O. Kolawole, K. Gifford, A. L. Marsden, D. Fleischmann, and D. B. Ennis: Quantitative Hemodynamics in Aortic Dissection: Comparing in vitro MRI with FSI Simulation in a Compliant Model. Accepted for publication in proceeding of FIMH 2021.

B3.4

A fluid-structure interaction framework for the identification of factors triggering calcification in native and bioprosthetic heart valves

Corso Pascal[1], Elena Tsolaki[2], Inge Herrmann[2], Dominik Obrist[1]

1   ARTORG Center for Biomedical Engineering Research, Bern, Switzerland
2   ETH Zurich - Nanoparticle Systems Engineering, Zurich, Switzerland

Calcification of native or bioprosthetic aortic valves (BAV) represents a major concern since calcific aortic stenosis affects 12% of the population over age 75 and calcification limits bioprosthetic aortic valve durability [5]. Calcification consists of the irregular deposition of mineralised crystals that change both the micro- and macro-scale properties of the tissues [2]. Understanding the mechanisms that lead to calcification in native and BAV leaflets remains challenging. Computational effort has been previously made [e.g. 1] to simulate the flow and the leaflet motion to highlight the key parameters that could be responsible for the structural deterioration of the leaflet but a multi-scale approach has not been proposed so far.

In the present study, the approach considered to tackle the fluid-structure interaction (FSI) problem is based on (i) a finite-element solver for the elastodynamics equation governing the valve mechanics, (ii) a high-order finite-difference solver for the incompressible Navier-Stokes equations governing the blood flow, (iii) a variational transfer for the strong coupling between fluid and structure [4]. The mechanical constitutive law is a fibre-reinforced model [3] for which different degrees of leaflet calcification are taken into account by changing the coefficient for the isotropic term representing the stiffness of the extracellular matrix.

The simulation of the FSI problem allows to focus on the computation of key hemodynamic factors, namely wall shear stress, oscillatory shear index (OSI) as well as mechanics-related parameters such as mechanical stress and the finite-time Lyapunov exponent based on the Cauchy-strain tensor. All these macroscopic parameters are correlated to morphological structures of calcification minerals observed from high-resolution microCT and electron microscopy in order to provide insight into mechanisms of calcification analysing the problem with a multi-scale approach.
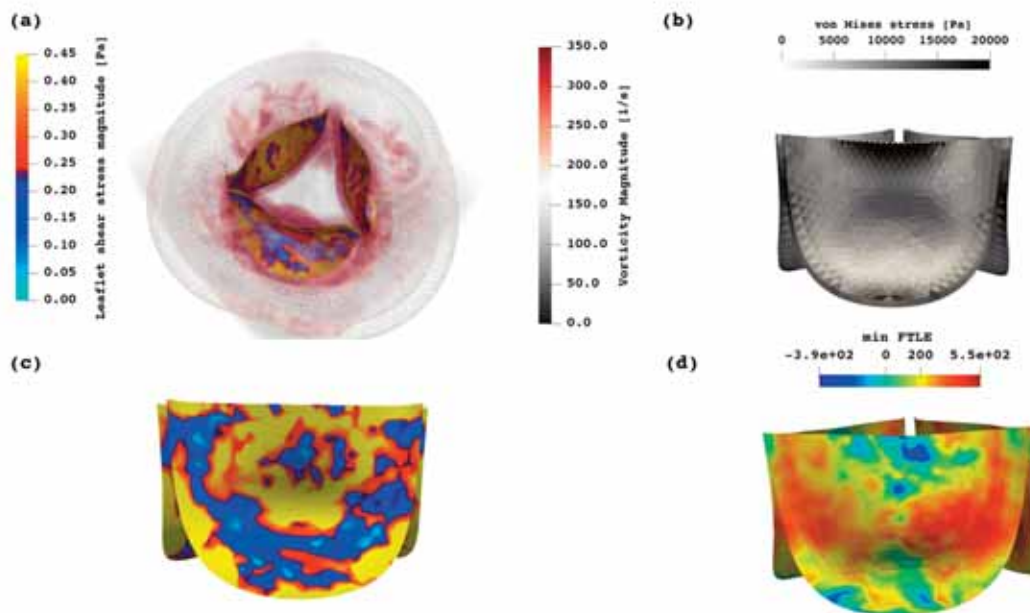
Figure 1 – Key parameters for the correlation of flow, leaflet mechanics and calcification process in the leaflets.

References:
1.   Ge L., Sotiropoulos F., *"Direction and Magnitude of Blood Flow Shear Stresses on the Leaflets of Aortic Valves: Is There a Link with Valve Calcification?"*, J. Biomech. Eng., 2010.
2.   Gomel M. A., Lee R. and Grande-Allen K. J., *"Comparing the Role of Mechanical Forces in Vascular and Valvular Calcification Progression"*, Frontiers in Cardiovas. Med., 5, 2019.
3.   Holzapfel G. A., Gasser Th. C., Ogden R. W., *"A New Constitutive Framework for Arterial Wall Mechanics and a Comparative Study of Material Models"*, Journal of elasticity and the physical science of solids, 61(1):1-48, 2000.
4.   Nestola M., Becsek B., Zolfaghari H., Zulian P., De Marinis D., Krause R., Obrist D., *"An immersed boundary method for fluid-structure interaction based on overlapping domain decomposition"*, J Comp Phys 398, 2019.
5.   Salaun E., Clavel M.-A., Rodés-Cabau J., Pibarot Ph., *"Bioprosthetic aortic valve durability in the era of transcatheter aortic valve implantation"*, Heart, 104(16):1323-1332, 2018.

B3.5

Failure properties of abdominal aortic aneurysm tissue are orientation dependent

Stanislav Polzer[1], Vojtěch Man[2], Robert Vlachovský[3], Luboš Kubíček[3], Jan Kracík[4], Robert Staffa[3], Jiří Burša[2], Madhavan Raghavan[5]

1   Technical University of Ostrava, Department of Applied Mechanics, Ostrava, Czech Republic
2   Brno university of Technology, Institute of Solid Mechanics, Mechatronics and Biomechanics, Brno, Czech Republic
3   St. Anne's University Hospital Brno , 2nd Department of Surgery, Brno, Czech Republic
4   Technical University of Ostrava, Department of Applied Mathematics, Ostrava, Czech Republic
5   University of Iowa, Roy J. Carver Department of Biomedical Engineering, Iowa, United States

Biomechanical rupture risk assessment of abdominal aortic aneurysm (AAA) requires information about failure properties of aneurysmal tissue. There are large differences between reported values even in terms of mean or median values. Among others, studies vary in using either axially or circumferentially oriented samples. This study1 investigates the effect of sample orientation on failure properties of AAA.

Methods: Aneurysmal tissues from 45 patients (11 females) were harvested during open AAA repair performed in St. Ann University Hospital, Brno, Czech Republic. Tissue was cut into uniaxial samples (90) and uniaxial failure tests were performed within three hours from harvesting. If possible, the samples were cut in both axial (49 samples) and circumferential (41 samples) directions. Wall thickness, First Piola-Kirchhoff strength Pult and ultimate tension Tult were recorded. Influence of sample orientation and other clinical parameters were investigated using non parametric.

Results: The subgroup of circumferentially oriented specimens was similar to that of axially oriented specimens in all the investigated parameters (age, AAA size, mean arterial pressure, wall thickness, prevalence of chronic obstruction pulmonary disease, prevalence of hyperlipidemia and portion of women). Medians of Pult (medians of 1100 kPa for circumferential vs. 715 kPa for axial direction, $p<10^{-4}$) and Tult (medians of 17.4 N/cm in circumferential vs. 11.2 N/cm in axial direction, $p<10^{-4}$) were significantly higher in circumferential direction. For paired data (available in 20patients), the median of difference was 411kPa ($p<10^{-3}$) in P_ult and 7.4N/cm ($p<10^{-4}$) in T_ult in favor of circumferential direction. Further, a negative correlation was found between wall thickness and Pult ($\rho=-0,287$, $p=0.006$) and not between wall thickness and T_ult ($\rho=0,07$, $p=0.52$).

Discussion: In this study, we have measured failure properties of aneurysmal tissue in both circumferential and axial direction and obtained paired data for the first time. Thanks to that we were able to remove inter patient variability and clearly showed the circumferential failure properties as by some 400kPa and 7.4N/cm higher in circumferential than axial direction. That at least partially explains the large difference between mean failure properties reported by various groups. Other studies which reports both axial and circumferential failure properties observed similar trend in but they did not reached statistical significance which was likely caused by unpaired data.

Conclusions: In this first study of anisotropy in AAA wall failure properties using paired comparisons, the strength in circumferential orientation was found to be higher than in axial orientation.

References:
1.   Polzer, S. et al. Failure properties of abdominal aortic aneurysm tissue are orientation dependent. J. Mech. Behav. Biomed. Mater. 104181 (2020). doi:10.1016/j.jmbbm.2020.104181

B3.6

Fluid-structure interaction for the simulation of cerebral aneurysm with flow-diverter

Elie Hachem[1], Aurelien Larcher[1], Ramy Nemer[1], Philippe Meliga[1], Augusto Sanches[2], Yigit Özpeynirci[2], Thomas Liebig[2]

1   PSL Mines ParisTech, CFL Research Group at CEMEF, Sophia Antipolis, France
2   Institute of Neuroradiology, University Hospital LMU, Munich, Germany

Fluid-Structure Interaction (FSI) applications are of interest in a wide array of engineering applications, and in particular, biomechanical systems such as blood flow, heart valve, and saccular cerebral aneurysm…. For the latter case, the accurate prediction of rupture should be assessed to choose the appropriate treatment. When in contact with blood, the aneurysm exhibits deformation that may become critical, based on the pressure of its surrounding, and due to the inevitable interaction between both sides. The rupture risk in aneurysms is usually evaluated using hemodynamics. Accurate and precise modeling of such biomechanical system can then serve as an important tool for the diagnostics. We propose a new FSI framework for the analysis of cerebral aneurysm. It is based on an Adaptive Immersed Mesh (AIM) method combining finite element solid dynamics solver with a fully Eulerian fluid-solid framework. It easily handles the insertion of a stent which finally allows us to accurately describe the mechanical exchanges between the blood flow, the surrounding vessel tissue, and the flow-deviator (see Figure 1). The Navier-Stokes equations are solved for the fluid, with the appropriate blood rheology. Hyperplastic solid dynamics equations are solved for the solid, which can handle both compressible and incompressible material. The Variational Multi Scale (VMS) stabilization method is used for both methods. It helps stabilize the advection dominated regime for the fluid flow, and damp out spurious pressure oscillations for the solid problem. 3D results are presented to show the accuracy and robustness of the hybrid method in assessing the behavior of a saccular cerebral aneurysm.
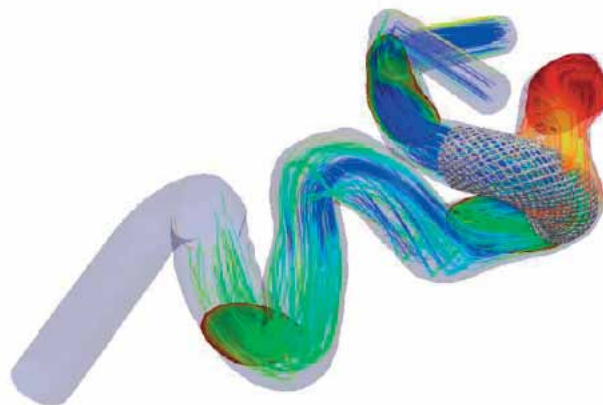
Figure caption: The impact on the flow when using a stent deployed across the aneurysm neck

B4.1
Multiscale modeling of traumatic brain injuries: From brains to atoms

Svein Kleiven[1], *Maryam Majdolhosseini*[1], *Alessandra Villa*[1]

1   KTH - Royal Institute of Technology, Neuroics, stockholm, Sweden

In spite of several preventive strategies, there has not been an important impact on the burden of head injury world-wide. Consequences of head injuries are not limited to the victim alone but have impact on the society as a whole through the large costs involved, not to mention the tragedies and the suffering. It should be noted that very little is understood about the true mechanisms associated with head injury, but many theories exist. Implementation or modification of security systems, such as a new car model, is now a long and complex process. In recent years, biomechanical simulation models of head and human body acquired an increasingly larger place in the design of safety systems. One of the advantages with the finite element (FE) method is the possibility to model the anatomy with great detail, thus it is possible to study the kinematics of the head as well as the stresses and strains in the Central Nervous System (CNS) tissues. This presentation primarily focuses on summarizing current efforts, and to outline future strategies in human head injury modeling. Multiple length scales are involved in the development of traumatic brain injury, where the global mechanics of the head level are responsible for local physiological impairment of brain cells. In a multi-scale approach, finite element models of the head and at the axonal level are coupled, where it is observed that the maximum axonal strains do not always correlate directly with the brain tissue strain levels. The results indicate that cellular level heterogeneities have an important influence on the axonal strain, leading to an orientation and location-dependent sensitivity to mechanical loads.

B4.2

Viscosity reconciles seemingly disparate stiffness measurements under static and dynamic conditions, in vivo and ex vivo

Gergerly Bertalan[1], Heiko Tzschätzsch[1], Kristian Franze[2], Siliva Budday[2], **Ingolf Sack**[1]

1   Charité – Universitätsmedizin Berlin, Berlin, Germany
2   University of Erlangen-Nuremberg, Erlangen, Germany

Brain biomechanics is increasingly recognized as a crucial factor for neuronal integrity and function. However, determination of brain stiffness is challenged by the complexity of brain tissue structures, often unknown boundary conditions, and the time dependence of measurement methods, rendering precise quantification of brain biomechanical parameters difficult. In addition, biomechanical tissue changes post mortem and ex vivo have raised concerns about the generality of stiffness values across measurement techniques such as large-strain quasi-static mechanical measurements, atomic force microscopy (AFM), and magnetic resonance elastography (MRE).

Here, using unconfined compression, tension, and shear measurements, AFM, ex-vivo and in-vivo MRE, we show that stiffness values of the cerebral cortex, hippocampus and corpus callosum of the human and murine brain can differ by orders of magnitude depending on the dynamic range of the measurement and even differ in their relative stiffness values between regions. However, these apparent differences can be explained by standard viscoelastic models, which assume that brain tissue is highly viscous. Remarkably, differences related to in vivo and ex vivo condition changes had little effect on our MRE data of the murine brain.

Collectively, our study combined for the first time a variety of methods over a wide dynamic range from quasi-static to more than a thousand Hz vibration frequency, applied to in vivo and ex vivo brain tissue, and showed that the large dispersion of brain stiffness measurements can be explained by the remarkably high viscosity of brain tissue. In the future perspective, precise determination of viscosity using multi-dynamic MRE could be used to infer the specific microstructure of regional tissue anatomies of the brain.

B4.3
Patient-specific modeling of tau pathology in Alzheimer's disease

Amelie Schaefer[1], *Mathias Peirlinck*[1], *Kevin Linka*[2], *Ellen Kuhl*[1]

1   Stanford University, Mechanical Engineering, Stanford, United States
2   Hamburg University of Technology, Continuum and Materials Mechanics, Hamburg, Germany

In the United States, one out of ten people over the age of 65 is suffering from Alzheimer's disease. As the number of older adults in our society increases, case numbers are projected to more than double over the next 30 years [1]. It has become widely accepted that the cerebral accumulation of hyperphosphorylated tau is one of the disease initiators and closely related to neurodegeneration and cognitive impairment [2]. However, until recently, our understanding of how this pathological protein aggregates and propagates across the brain has relied almost exclusively on postmortem histopathology. Now, the emerging imaging technology of positron emission tomography allows to visualize the distribution of tau protein in the brain in vivo, offering the opportunity to track disease progression in a patient over time. Using the extracted quantitative characteristics of the evolution of tau, data-driven computational models can provide crucial insights into critical factors and time points for early diagnosis and intervention and allow for personalized predictions of disease progression.

We use a network diffusion model on a weighted Laplacian graph to compute the propagation of hyperphosphorylated tau protein across the brain's connectome [3]. We compare our model to longitudinal positron emission tomography images from the Alzheimer's Disease Neuroimaging Initiative, following 76 subjects over three to four annual scans. Using Bayesian hierarchical modeling, we infer model parameters that best reproduce the neuropathological patterns of the image data on subject- and group-levels. This probabilistic approach allows us to quantify the uncertainty associated with the inferred parameters, making optimal use of individual and population evolution data. Propagation of the quantified uncertainty allows us to estimate the credibility of our personalized model predictions. As such, our Bayesian framework provides clinically relevant information on the progression of the disease and may serve as an important tool to optimize the subject-specific scheduling of follow-up imaging with the goal of improving the accuracy of predictions while minimizing cost.
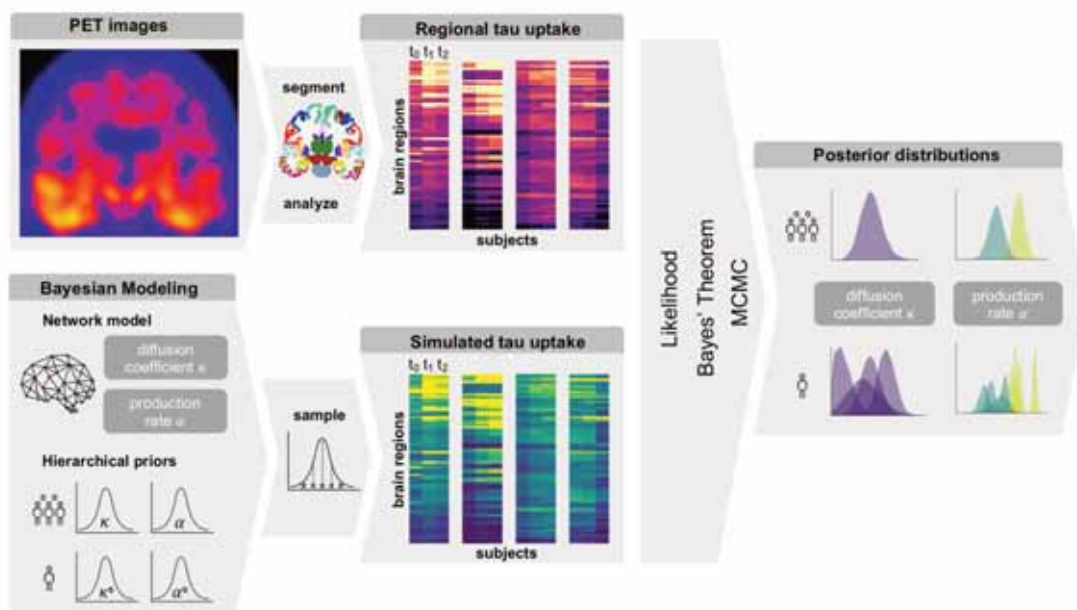
Figure caption: Schematic overview of the methods used in this study

References:
1.   Alzheimer's Association, 2019 Alzheimer's disease facts and figures. Alzheimer's & Dementia, 15(3), pp.321-387.
2.   Bejanin, A., et al., 2017. Tau pathology and neurodegeneration contribute to cognitive impairment in Alzheimer's disease. Brain, 140(12), pp.3286-3300.
3.   Schäfer, A., Mormino, E.C. and Kuhl, E., 2020. Network Diffusion Modeling Explains Longitudinal Tau PET Data. Frontiers in Neuroscience, 14, p.1370.

B4.4

Regional characterization of the dynamic mechanical properties of human brain tissue by microindentation

Andrea Menichetti[1], David B. MacManus[2 3], Michael Gilchrist[3], Bart Depreitere[4], Jos Vander Sloten[1], Nele Famaey[1]

1   KU Leuven, Biomechanics Section - Department of Mechanical Engineering, Leuven, Belgium
2   Dublin City University, School of Mechanical & Manufacturing Engineering, Dublin, Ireland
3   University College Dublin, School of Mechanical & Materials Engineering, Dublin, Ireland
4   University Hospital Leuven, Department of Neurosurgery, Leuven, Belgium

Traumatic brain injury (TBI) is a relevant health concern and a major cause of morbidity and mortality, especially among the elderly population. In the EU alone, 1.37 million TBI and 56,000 TBI-related deaths are estimated annually[1]. Finite element (FE) models of the human head are powerful tools to investigate injury risk and promote TBI prevention. The accuracy of FE simulations relies on the biofidelity of the brain tissues' material properties, however little is known about their mechanical behavior at high rates of deformation, representative of TBI loading scenarios. To the best of the authors' knowledge, this is the first study on the characterization of mechanical properties of human brain tissue using micro-indentation under the largest applied strain (35%) and highest strain rates (10/s) in the literature.

10 human brains were collected from subjects between 64 and 94 years old and tested within 4 ± 1 days post-mortem. A custom-built micro-indentation apparatus[2] was used to characterize the hyper-viscoelastic mechanical properties of 12 different anatomical regions of the brain (Figure). The brain samples were indented up to 35% strain and at 10/s strain rate with a 250 μm diameter probe. On average we performed 5 tests per sample. All experiments were approved by the Medical Ethics committee of KU Leuven.

An inverse FE algorithm was used to fit a neo-Hookean based quasi-linear viscoelastic constitutive model to the experimentally measured force-time data[3]. The mean instantaneous shear modulus (μ_0) and the viscoelastic parameters (e.g. long-term relaxation function g_∞) were compared between the different regions by means of a linear mixed model. μ_0 varied across the regions (Figure): superior mid-frontal cortex and cerebellum exhibited the lowest mean values ($\mu_0=3.53\pm1.27$ kPa and 3.40 ± 0.92 kPa, respectively), while corona radiata ($\mu_0=7.63\pm2.01$ kPa) and basal ganglia ($\mu_0=7.62\pm3.04$ kPa) the highest. Each region was statistically significantly different from at least one other region ($p<0.05$, data not shown). The influence of age, sex and time post-mortem were also assessed, but within the tested cohort none of these factors had a significant effect on the regional μ_0 differences. On average, white matter regions showed 39% higher g_∞ than grey matter regions.

In this study, for the first time, hyper-viscoelastic material properties of human brain tissue under large strain and high strain rates representative of TBI were characterized by means of micro-indentation. These findings address the paucity of data in literature on human brain properties and highlight the differences across the different anatomical regions. These data will help improve the accuracy of 3D FE human head models.
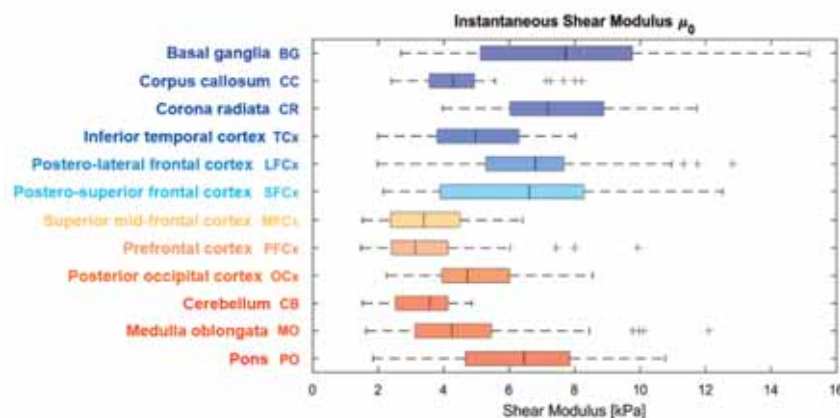
Figure caption: Regional variation of μ_0.

References:
[1]   Majdan et al., Lancet Public Health, 1:e76-83, 2006
[2]   MacManus et al., J.Mech.Behav.Biomed.Mater., 87(11):256-266, 2018
[3]   MacManus et al., Sci.Rep., 7:13729, 2017

B5.1
An innovative rehab robot with real time visual feedback & performance assessment

Fong-Chin Su[1], *Yu-Lin You*[2], *Cheng-Feng Lin*[3], *Li-Chieh Kuo*[4]

1   National Cheng Kung University, Department of Biomedical Engineering & Medical Device Innovation Center, Tainan, Taiwan
2   National Cheng Kung University, Department of Biomedical Engineering, Taiwan,
3   National Cheng Kung University, Department of Physical Therapy, Tainan, Taiwan
4   National Cheng Kung University, Department of Occupational Therapy, Tainan, Taiwan

Rehabilitation robots have been widely designed and used to improve functional movement in persons with impaired physical mobility. The SportsArt pinnacle trainer is a novel-designed fitness equipment for training of stability, body-control, strength and endurance. The Pinnacle is so far the only cross trainer to successfully combine motions in sagittal, coronal, and transverse planes. To extend this trainer for passive rehabilitation of the weak elderly and patients, the motor driven mechanism was redesigned and implemented with adjustable stride width, step strength, variable foot position and unique handle positioning for unprecedented workout of infinite variety. Furthermore, a novel weight support system was developed with in-vivo gait symmetry information for real time visual feedback to the subjects during training.

Knee osteoarthritis (OA) is more affected on the medial compartment. This may related to the greater knee varus moment was found in knee OA patients compared to healthy people. In previous study, a knee valgus moment was found during stepping pinnacle trainer, and this result was expected to reduce knee varus moment and may further delay the disease. We investigated the training effects of pinnacle trainer on biomechanics of lower extremity on clients with knee OA. The knee OA training group received an eight-week pinnacle trainer intervention, three times a week and about 30 minutes per session, and the control group did not have intervention but maintained their exercise habits. The motion analysis during stepping pinnacle trainer were measured at the baseline assessment and after 8 weeks immediately. The joint moment on the frontal plane was changed from varus moment to valgus moment during stepping phase after an eight-week pinnacle trainer intervention for the training group, however, the control group still remain the varus moment during stepping phase after 8 weeks. After the pinnacle trainer intervention, the knee joint moment may be changed from knee varus to knee valgus moment. This may not only reduce the pain intensity and improve the functional performance for the daily living but also delay the disease due to the shift of the knee joint loading from medial side to the lateral side.

Also, thirty stroke patients were also recruited to evaluate the training effects of this novel rehabilitation system. After Pinnacle trainer intervention, walking ability and functional tests were improved significantly. Quality of life was improved significantly in physical function and general health. The innovative rehab robot with real time visual feedback & performance assessment may provide a safe and effective choice for stroke patients and OA patients.

B5.2
Intelligent home-based upper limb rehabilitation for patients with chronic stroke

Li-Chieh Kuo[1], *Yu-Chen Lin*[2], *Yu-Shen Lin*[3], *Chih-Chun Lin*[2], *Tzu-Yu Pan*[2]

1   National Cheng Kung University, Department of Occupational Therapy
2   National Cheng Kung University
3   Southern Taiwan University of Science and Technology

Background: Over 50% stroke survivors might be struggling with multiple temporarily or permanent disabilities due to their restricted functions of motor, cognition and activities of daily living (ADL). Not only hospital-based intervention but home-based training is also crucial for improving or maintaining their functions. However, adherence of home program is always an uncertain and challenging issue for both patients and clinicians due to a lack of suitable strategies for delivering the services. Robotic assistive devices have been proved to be effective for improving motor and ADL function in stroke rehabilitation. In addition, the intelligent home-based rehabilitation has been proposed recently for its convenience and immediacy during these critically pandemic periods. This study thus aimed to develop and investigate the effectiveness of intelligent home-based upper limb rehabilitation system which included remote evaluations and interventions via an Expert Evaluation App, a Home-based Training App, and a robotic assistive device.

Methods: The Expert Evaluation App was developed to assess the patient's motor status before training and then linked to the Home-based Training App for generating training programs. The programs included various daily tasks such as eating with spoon, pouring water with a cup… etc., which could be adjusted directly by clinicians on-line. All the records could be uploaded automatically to cloud database for further storages, computations, and follow-up inspections by clinicians. The robotic assistive device was designed to provide support and force to assist elbow and forearm movements. 11 chronic stroke patients were randomly allocated to experimental (using both robotic assistive device and Home-based Training App) and control groups (using only Home-based Training App). The training was provided 4 weeks, 5 times/week, 30 min/day. The OpenPose, one of the artificial intelligence techniques for determining body segment movements, was used to analyze the patients' motor performances at home and then offered immediately evaluations or training results for both patients and clinicians.

Results: The training outcomes indicated that patients' upper limb motor function (FMA-UE) and affected hand use (Motor Activity Log) improved in both groups. ADL function (Frenchay activities index and Barthel Index) and Quality of Life (WHOQoL-BREF) were also reported with improvements or maintenance in most of the patients. Both the patients and clinicians reported with high satisfaction and convenience while using this intelligent rehabilitation system.

Conclusion: The intelligent home-based upper limb rehabilitation concept and system enables chronic stroke patients to have good adherence for home program, especially during this pandemic time. Most patient and clinician users satisfied with their using experiences. The tentative results also showed its effectiveness of improvements in motor and ADL functions and life quality as well.

B5.3
Development of augmented reality system for supporting motor rehabilitation

Hirokazu Kato[1], Isidro III Butaslac[1], Yuichiro Fujimoto[1], Masayuki Kanbara[1]

1   Nara Institute of Science and Technology, Graduate School of Science and Technology, Ikoma, Japan

Augmented Reality (AR) is a technology for overlaying virtual objects and information in the real world, and has come to be applied in various fields. There are various purposes for using AR. One of the most effective uses of AR is to support the work of the user. Therefore, many AR systems for work support have been proposed so far. In the medical field, AR has also been attempted to be used for supporting difficult tasks of doctors such as surgical operations. We believe that AR can be effectively used in motor rehabilitation and are working on the development of an AR system that supports motor rehabilitation. While there are various display methods in AR, recently high-performance Head Mounted Displays (HMDs) for AR has been developed. Therefore, we are focusing on the development of AR system using HMDs. In supporting motor rehabilitation, we are considering two scenarios. One is a scenario that supports patients in performing motor rehabilitation. Patients need to move their bodies according to the training menu. However, it is difficult to see if it is done properly. There is a way to observe themselves in the mirror, but the available scenes are limited. Also, even if they can observe themselves, it is difficult to judge whether their posture and movement are appropriate. We believe that AR technology can be used to provide real-time, easy-to-understand feedback to patients undergoing training as to whether their postures and movements are appropriate, and we have developed a prototype system to verify this. Specifically, we are developing a system that allows patients undergoing walking training to check the position to move their legs and the height to lift them in real time while facing the front. The other is a system for therapists who assist patients in motor rehabilitation. The therapist must assist the patient in exercising and assess whether the exercise is being performed properly. However, since the evaluation is usually based on observation, it is subjective and difficult to objectively evaluate and record. We have developed a system that combines an AR system with a pose measurement system and other sensing devices to provide the therapist with real-time feedback of patient exercise status. By using this system, it is expected that the therapist will be able to give more appropriate advice to patients. We will introduce these two systems and their uses, and discuss their issues and future potential.
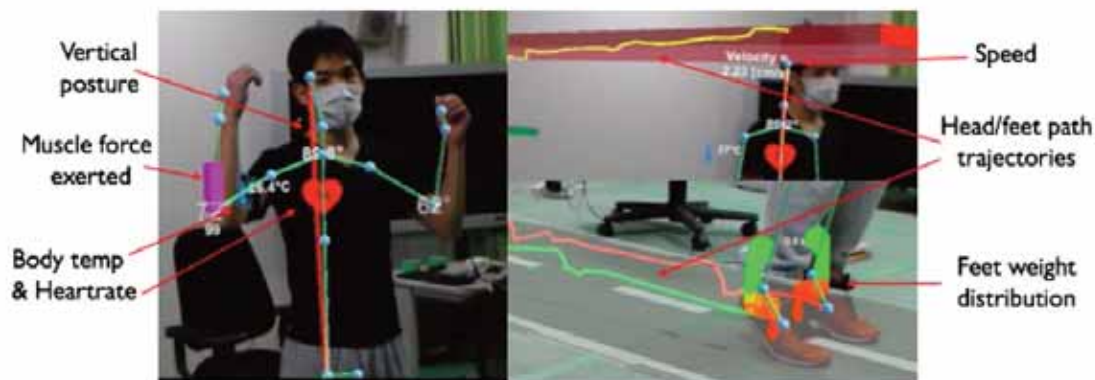
Examples of visualization in our system.

B5.4
Soft robot hand for stroke rehabilitation

Raymond Kai-Yu Tong[1]

1   The Chinese University of Hong Kong, Biomedical Engineering, Hong Kong

Soft robotic hands are proposed for stroke rehabilitation with the new soft material properties and and low inherent stiffness. The clinical efficacy of a soft robotic hand have been evaluated with chronic stroke subjects with different levels of spasticity. Chronic stroke subjects were recruited and underwent 20 sessions of 1-hour EMG-driven soft robotic hand training. The robot hand could actively flex and extend the fingers, and the training effect was evaluated by the pretraining and post-training assessments with the clinical scores: Fugl-Meyer Assessment for Upper Extremity(FMA-UE), Action Research Arm Test(ARAT), Modified Ashworth Scale(MAS), and maximum voluntary grip strength. The results showed significant improvement of upper limb function in ARAT, FMA-UE and maximum voluntary grip strength (increased mean=2.14 kg). EMG-driven rehabilitation training using the soft robotic hand with flexion and extension could be effective for the functional recovery of upper limb in chronic stroke subjects.
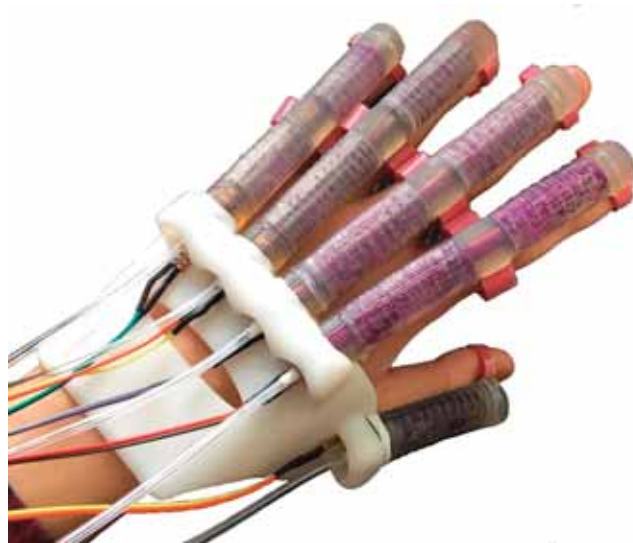
Figure caption: The soft robotic hand can actively flex and extend the fingers

References:
XQ Shi, HL Heung, ZQ Tang, Z Li, KY Tong, Effects of a Soft Robotic Hand for Hand Rehabilitation in Chronic Stroke Survivors, Journal of Stroke and Cerebrovascular Diseases, 30(7), 2021, 105812

B5.5

Concept of a co-simulation model integrating a musculoskeletal human model and models of an exoskeleton and a power tool to identify design options for the technical systems

Carla Molz[1], *Johannes Sänger*[2], *Zhejun Yao*[3], *René Germann*[2], *Sven Matthiesen*[2], *Robert Weidner*[3 4], *Sandro Wartzack*[1], *Jörg Miehling*[1]

1   Engineering Design, Friedrich-Alexander-Universität Erlangen-Nürnberg, Erlangen, Germany
2   IPEK - Institute of Product Engineering, Karlsruhe Institute of Technology (KIT), Karlsruhe, Germany
3   Laboratory of Manufacturing Technology, Helmut-Schmidt University Hamburg, Hamburg , Germany
4   Chair for Production Technology, Institute of Mechatronics, University of Innsbruck, Innsbruck, Austria

Working at and above head height with a power tool, which is particularly common in craft and assembly applications, represents an example of physical work, which can cause musculoskeletal disorders. To protect working people from overload and injuries in these situations, the development and use of application-specific exoskeletons have greatly increased in recent years. Beside user tests, digital human models (DHM) become more popular for developing exoskeletons. Using DHMs to simulate the effects of exoskeletons on the human body can integrate the future user earlier in the product development process. However, the application, the user and the exoskeleton are often greatly simplified. For example, only 2-dimensional motions are analyzed [1] or the exoskeleton's support is simplified as a constant moment acting on a joint [2]. These procedures may be usable for a rough evaluation, but for a more holistic view and a better assessment of design impacts, co-simulation models including a kinematic and dynamic model of the exoskeleton and the power tool should be used.

Consequently, we present a concept for a co-simulation model focusing on activities at and above head height using a power tool. A simplified representation of the concept is shown in Figure 1. The co-simulation model is based on a full-body musculoskeletal human model, which interacts with a model of an arm exoskeleton and a power tool. First, motion capture data of a subject without the exoskeleton are used as input for the co-simulation model. Based on this movement, the interactions with both the exoskeleton and the power tool can be derived and applied to the musculoskeletal human model. By using a musculoskeletal human model, biomechanical parameters such as joint reaction forces, muscle activity or metabolic costs can be used to analyze the impact of the technical systems on the human body in this application. The goal of the co-simulation model is to simulate the interactions between the technical systems and the human as well as to evaluate the effects of design changes of the technical systems on the human body.
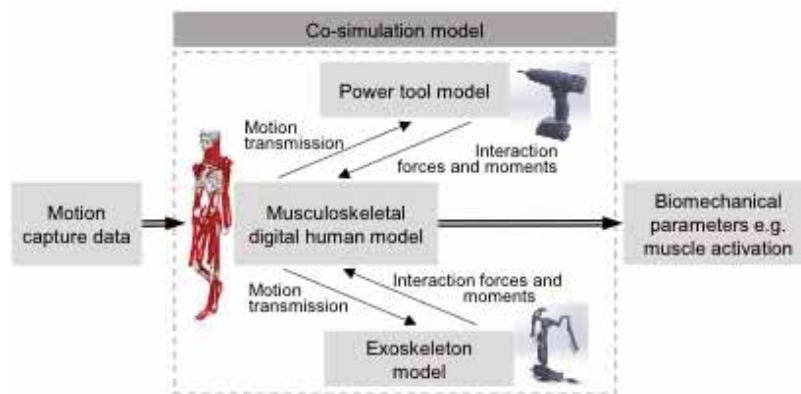
Figure 1: Simplified representation of the concept for a co-simulation model consisting of a musculoskeletal human model, an exoskeleton model and a power tool model.

References
[1]   Manns P, et al. (2017) IEEE Robot. Autom. Lett.; 2: 1564–1570.
[2]   Miehling J, et al. (2018) In: Karafillidis A, Weidner R, editors. Cham: Springer International Publishing: 219–227.

B5.6

A framework to quantify joint kinematics and moments using a subject-specific virtual simulator reproducing exoskeletal-assisted locomotion

Vishnu Chandran[1], Sanghyun Nam[1], David Hexner[2], William Bauman[3], Saikat Pal[1]

1   New Jersey Institute of Technology, Biomedical Engineering, Newark, United States
2   ReWalk Robotics, Yokneam, Israel
3   James J. Peters VA Medical Center, Bronx, United States

Introduction: Robotic exoskeletal devices have vast, but largely untapped, potential to restore mobility to individuals with neurological disorders, including those of spinal cord injury (SCI), stroke, traumatic brain injury, and multiple sclerosis. The growing demand for these devices necessitates the acceleration of technology to develop and systematically characterize the effects of human parameters and robot design variables on the human-robot system during exoskeletal-assisted locomotion (EAL). Such parametric studies are cost-prohibitive and not feasible using experimental methods, but computational simulation remains a viable alternative. As such, our goal was to develop a computational framework to simulate EAL and compare model-predicted joint kinematics and moments from unassisted and exoskeletal-assisted maneuvers.

Methods: An able-bodied subject (41 years, male, 178 cm, 86.2 kgs) was recruited. Prior to participation, the subject provided written informed consent. The subject was trained in a ReWalk P6.0, and his 3-D motion was analyzed during unassisted and exoskeletal-assisted sit-to-stand, stand-to-sit, and walking maneuvers. All 3-D motion data were collected from a single session and included simultaneous measurements of marker trajectories, ground reaction forces, and electromyography (EMG) data.

We adapted a full-body OpenSim model [1] to simulate unassisted and exoskeletal-assisted maneuvers. A full-scale geometry model of the ReWalk P6.0 was integrated with the musculoskeletal model (Figure 1A). The human-robot model had 10 degrees of freedom to represent the exoskeleton (six at the pelvic band to anchor the exoskeleton to the body, two at the hips, and two at the knees) in addition to the 37 degrees of freedom to represent the human. We included constant-distance constraints at the locations where the device was strapped to the body. The generic musculoskeletal model was scaled to match the subject anthropometry. Inverse kinematics were performed to obtain joint kinematics, and inverse dynamics to obtain joint moments.

Results: The virtual simulators reproduced unassisted and exoskeletal-assisted maneuvers within acceptable tolerances (average RMSE 1.2 cm for unassisted and 1.3 cm for exoskeletal-assisted walking). Mean peak flexion angle during exoskeletal-assisted walking was 50.2°, compared to 68.6° unassisted (Figure 1B). Mean peak flexion moment during exoskeletal-assisted walking was 12.1 Nm, compared to 57.1 Nm unassisted (Figure 1C). We compared our model-predicted joint kinematics and moments with measured EMG data (Figure 1D). The findings from sit-to-stand and stand-to-sit maneuvers are not shown.
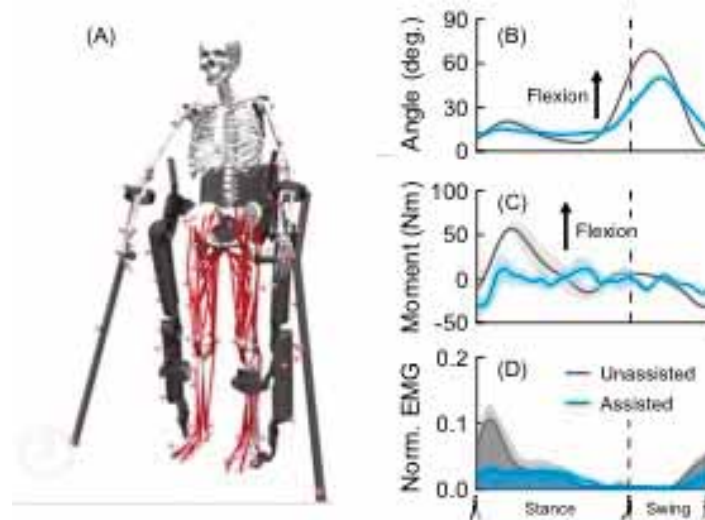
Figure 1. A subject-specific virtual simulator of EAL (A) and average (±1 SD) knee flexion-extension angles (B), moments (C), and (D) normalized vastus medialis EMG from six unassisted and six exoskeletal-assisted walking trials.

Discussion: This work provides a foundation for parametric studies to quantify the effects of perturbations in human and robot variables on the integrated system during EAL. The virtual simulator of EAL provides a data-driven model of human-exoskeleton interaction. This approach provides the potential for a low-risk and cost-effective platform to conduct rapid design-phase evaluation of exoskeleton refinements, but would entail further studies on individuals with SCI.

References:
1) Rajagopal A, et al., IEEE Trans Biomed Eng, 63, 2016.

B6.1
Active contours modeling of respiratory airways using isogeometric analysis

David Ortiz-Puerta[1], *Daniel E. Hurtado*[1]

1   Campus San Joaquín, Pontificia Universidad Catolica de Chile, Department of Structural and Geotechnical Engineering, Macul, Chile

Image-based respiratory airways models have been widely used in physiology studies related to diseases diagnoses, surgery planning, aerosol delivery, and educational purposes. These models require a precise representation when studying chronic obstructive lung diseases characterized by changes in their morphology and mechanical properties due to the remodeling process. To model the intricate branching surface of the airways, we follow the Weibel bipodal model and recursively generate a control point mesh using octagonal templates. These templates are centered in the skeleton of the extracted airways from computerized tomography images. Then, the control point mesh must be adjusted to the real surface of the airways. Usually, this is made by projecting the control points, leading to errors in highly deformed airways. To correct this, we use the energy-based image segmentation Snake model as the adjustment methodology. To this end, the Snake model is formulated as a variational gradient-flow problem, which is solved using IGA as a numerical scheme and multipatch surface NURBS as spatial discretization. Images of COPD and control subjects at End Expiration and End Inspiration are used, and the method is validated by comparing the DICE coefficient of projection methodologies found in the literature, showing accurate results even in highly deformed airways.

(a) real surface.

(b) Adjusted multipatch NURBS.

Figure caption: Results over a COPD patient at End Expiration: (a) real surface, (b) adjusted multipatch NURBS using the Snakes segmentation model.

References:
[1]   GOLD. Global Strategy for the Diagnosis, Management, and Prevention of Chronic Obstructive Pulmonary Disease. (2019).
[2]   Kass, M. et al. Snakes: Active contour models. International journal of computer vision, 1(4), 321-331 (1988).
[3]   Cottrell, J. A., Hughes, T. J., & Bazilevs, Y. Isogeometric analysis: toward integration of CAD and FEA. John Wiley & Sons. (2009).
[4]   Miyawaki, S. et al. Automatic construction of subject-specific human airway geometry including trifurcations based on a CT-segmented airway skeleton and surface. Biomech. Model. Mechanobiol. 16, 583–596 (2017).

B6.2
Whole-lung simulation of aerosol deposition using CFPD

Pantelis Koullapis[1], *Fotos Stylianou*[1], *Stavros Kassinos*[1]

1   University of Cyprus, Mechanical & Manufacturing Engineering Department, Nicosia, Cyprus

Information on aerosol deposition characteristics inside the human airways is important when assessing the dose of an inhaled medication as well as the health effects related to pollutant exposure. Direct in vivo measurements remain limited due to the risks associated to patient's radiation exposure. In addition, in vitro measurements on airway casts although useful, are not easy to conduct and there are also difficulties in manufacturing the finer airway structures (e.g., alveolar ducts with diameters of 300μm). In silico models offer a valuable tool which can be used to study airflow and aerosol transport at all scales of airways inside the human lung. Currently, the majority of three-dimensional computational models of the human lung focus on truncated geometries of either the upper airways or the terminal alveolar regions, as a consequence of the large computational cost to simulate the entire lung.

In this study, a three-dimensional whole-lung airway model is developed which can be used to simulate the airflow and aerosol transport in the entire human respiratory tract. An upper airway model which includes airways from the mouth to around the seventh bronchial generation is derived from MRI and CT scan data. The intermediate airways up to the terminal conducting lung generations are represented by simplified bifurcation models that are merged onto the upper airway geometry. The acinar generations are modeled using three generations of transitional bronchioles and multiple sub-acini models [1]. The methodology developed in [2] is adopted in order to reduce the computational cost of the simulation (tree decomposition of the deep airways). Quiet breathing and a deep inhalation maneuver are simulated using LES to account for the turbulence generated in the upper airways. A Lagrangian tracking scheme is employed for particle transport from the mouth down to the alveolar generations.

The predicted deposition results, both overall and regional, will be compared to available in vivo data from the literature as well as predictions from simpler algebraic models.
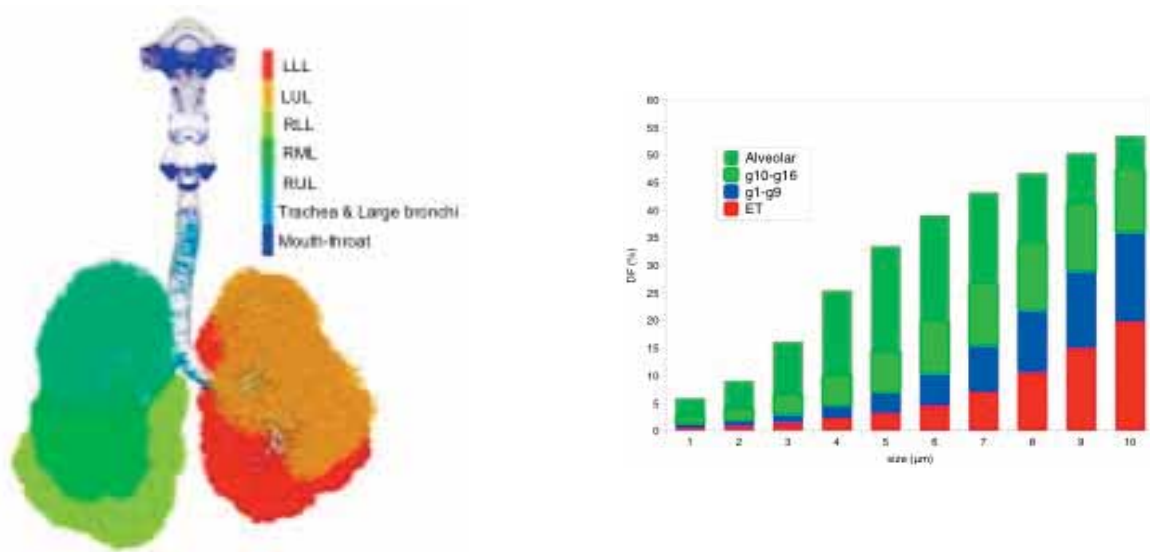
Figure 1. (a) Deposited 5μm particles during the inhalation phase of tidal breathing in the entire respiratory tract (coloured by the location of deposition).
(b) Deposition fraction during the inhalation phase of tidal breathing in the various regions of the respiratory tract.

References:
[1]   P.G. Koullapis, F.S. Stylianou, J. Sznitman, B. Olsson, S.C. Kassinos, Towards whole-lung simula- tions of aerosol deposition: a model of the deep lung, J. Aerosol Sci. 144 (2020).
[2]   P.G. Koullapis, P. Hofemeier, J. Sznitman, S.C. Kassinos, An efficient computational fluid-particle dynamics method to predict deposition in a simplified approximation of the deep lung, Eur. J. Pharm. Sci. 113 (June) (2018) 132144.

B6.3

Inverse finite element modeling of the breathing organ-level lung using digital image correlation

Mohammad Maghsoudi Ganjeh[1], Crystal Mariano[1], Samaneh Sattari[1], **Mona Eskandari**[2]

1   University of California Riverside, Mechanical Engineering
2   University of California Riverside, Mechanical Engineering / BREATHE Center School of Medicine

The international COVID-19 pandemic has driven respiratory biomechanics to the forefront, revealing the underexplored vulnerabilities of pulmonary research. Computational biomechanical models can enable predictive insights to examine fundamental lung physiology and potential load amplifications in diseased states [1, 2]. However, the complex and hierarchical structure of the lung impedes these advancements, and results in the organ's bulk mechanical response to commonly be siloed from its local tissue behavior [3]. To address this knowledge gap, in this study we introduce the first structural inverse finite element model of the breathing lung using a reduced order surface representation, which compounds the role of the intricate bronchial network, parenchymal tissue, and visceral pleura behavior. We design and validate a custom-designed apparatus to imitate inflation and deflation in the ex-vivo lung and interface the system with large deformation digital image correlation capabilities to ultimately connect local strains to global volumes and pressures [4]. The optimized heterogenous and hyperelastic continuum model, which employs adjoint methods, accurately captures the experimentally observed topological lung surface strain distributions for varying pressure levels. The development of this novel multiscale framework can facilitate in-silico investigations to improve ventilation strategies and further examine how chronic endurance of disease alters the load-bearing biomechanics of the lung.

References:
[1]   Herrmann, Jacob, Merryn H. Tawhai, and David W. Kaczka. "Computational modeling of primary blast lung injury: implications for ventilator management." Military medicine 184.Supplement_1 (2019): 273-281.
[2]   Sarabia-Vallejos, Mauricio A., Matias Zuñiga, and Daniel E. Hurtado. "The role of three-dimensionality and alveolar pressure in the distribution and amplification of alveolar stresses." Scientific reports 9.1 (2019): 1-11.
[3]   Arora, Hari, et al. "Correlating Local Volumetric Tissue Strains with Global Lung Mechanics Measurements." Materials 14.2 (2021): 439.
[4]   Mariano, Crystal A., et al. "Novel Mechanical Strain Characterization of Ventilated ex vivo Porcine and Murine Lung using Digital Image Correlation." Frontiers in Physiology 11 (2020): 1536.

B8.1
Patient-specific loading for HR-pQCT based homogenized FE analysis of the distal radius

Denis Elia Schenk[1], *Philippe Zysset*[1]

1   University of Bern, ARTORG Center for Biomedical Engineering Research, Bern, Switzerland

Introduction: Trabecular bone microstructure is known to adapt its morphology to local loading conditions for achieving a safe uniform tissue loading level [1-2]. Previous investigators used this relation to simulate bone remodeling or retrace physiological loading conditions from local density and architecture. The latter inverse approach consists of quantifying bone morphology using micro-computed tomography and computing the relative importance of selected load cases by minimizing the fluctuation of a tissue loading level metric [3]. The present study aimed at identifying a personalized, optimal, multiaxial load case at the distal radius using HR-pQCT-based, isotropic, homogenized finite element (hFE) analysis.

Material and Methods: We used HR-pQCT reconstructions of the 20 mm most distal section of 21 human fresh-frozen distal radii [4]. For each section, we simulated six unit load cases (FX palmar-dorsal force, FY ulnar-radial force, FZ distal-proximal force, MX moment about palmar-dorsal, MY moment about ulnar-radial, MZ moment about distal-proximal) using an efficient linear hFE method based on a single isotropic bone phase. We formulated an optimization problem consisting of minimizing the deviation of the resulting strain tensors $\varepsilon(x)$ to a hydrostatic reference strain ε_0 over the full domain of the model. Both, uniaxial FZ (1 DOF) and optimal (OPT: 6 DOF) load cases were optimized to the same ε_0, and their energies were computed as the scalar product of the resulting forces and displacements.

Results: As expected, the scaling factor in OPT for distal-proximal compressive force FZ was much larger compared to the two other forces, and the moment about the palmar-dorsal axis MX was larger compared to the two other moments. Multiaxial energy of OPT load case was on average 61%±60% (range 2%-227%) higher than for uniaxial FZ load case, and the respective objective function values were on average 2%±1.2% (range 0.3%-4%) lower (Fig.1).

Discussion and Outlook: Compared to previous models, we included canonical load cases in six DOF and used an asymmetric strain metric. The obtained scaling factors for the optimal multiaxial load case compare well to the findings of Smith et al. [5], who investigated forces and moments in the distal radius during different wrist motion patterns. The higher energy and lower objective function values indicate that the optimized load case results in strains closer to a preferred hydrostatic strain state and therefore can absorb more energy compared to uniaxial FZ load case.
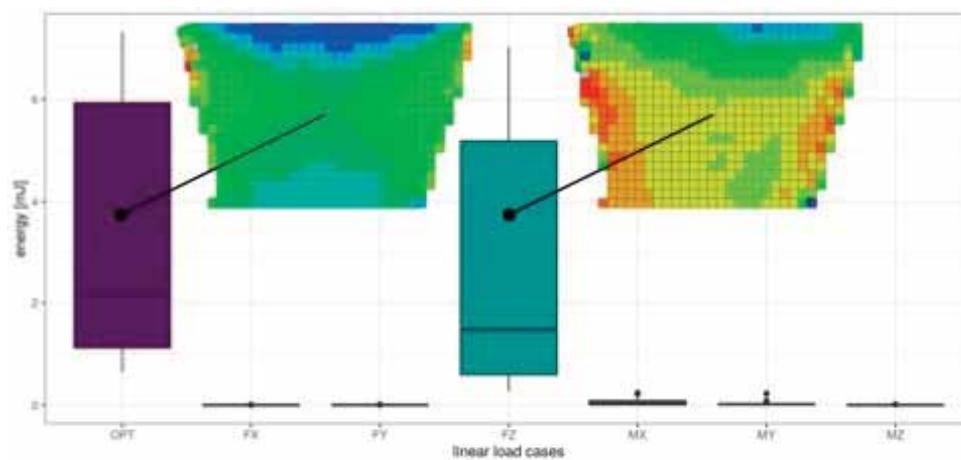
Figure caption: Linear energy of optimized (OPT) and uniaxial FZ load cases with respective maps of objective function values (coronal plane).

References:
[1]   Wolff, 1892
[2]   Frost, Bone Miner, 1987
[3]   Christen, Biomech. Model. Mechanobiol., 2012
[4]   Hosseini, Bone, 2017
[5]   Smith, ASSH, 2017

B8.2

3D+t ultrasound-based fluid-structure interaction modeling for abdominal aortic aneurysm rupture risk analysis incorporating pre-stress

Judith Fonken[1][2], *Esther Maas*[1][2], *Arjet Nievergeld*[1][2], *Marc van Sambeek*[1][2], *Frans van de Vosse*[1], *Richard Lopata*[1]

1   Eindhoven University of Technology, Biomechanical Engineering, Eindhoven, Netherlands
2   Catharina Ziekenhuis, Vascular surgery, Eindhoven, Netherlands

Currently, the prediction of rupture risk in abdominal aortic aneurysms (AAAs) solely relies on maximum AAA diameter. However, wall mechanics and hemodynamics have shown to provide better risk indicators1. Since both highly depend on the AAA geometry, a patient-specific risk assessment is required. To perform a large, longitudinal study on AAA growth and rupture risk, the use of a non-invasive imaging modality combined with fluid-structure interaction (FSI) modeling is required to analyze the interaction between wall mechanics and hemodynamics1. Solid AAA modeling using time-resolved 3-dimensional ultrasound (3D+t US) data was recently demonstrated and allows for simultaneous estimation of wall stresses and stiffness. In this study, the 3D+t US-based modeling framework was advanced to FSI modeling. Furthermore, the effect of including a pre-stress estimation (PSE) to obtain the stresses present in the measured geometry was evaluated.

For this study, 30 patients with AAA diameters ranging from 27-56 mm were included. The established workflows (Fig. 1) use the patient-specific AAA geometry and brachial blood pressure as input for the FSI models. The diastolic 3D+t US-based segmentation was elongated and used to obtain the lumen and wall meshes. In the FSI-PSE workflow, the pre-stress in the solid geometry was estimated using the Backward Incremental Method (BIM)2. At the inlet of the fluid domain, a time-varying flow profile was prescribed. A 3-element Windkessel model was used to prescribe the outlet pressure3. Blood was modeled using the Carreau model, whereas the wall was modeled using the Neo-Hookean model. The FSI simulations were initialized with the diastolic pressure and the results were evaluated on the last of 3 cardiac cycles.

A robust framework to execute FSI simulations using 3D+t US data was developed and successfully employed on a large set of patient data. Omitting the pre-stress results in increased displacements (40-78%), decreased wall stresses (29-54%) and deviating wall shear stress and oscillatory shear index patterns. These results underline the importance of incorporating pre-stress in FSI simulations. After validation, the obtained framework to execute 3D+t US-based FSI simulations provides an important tool for longitudinal studies on AAA growth and rupture risk.
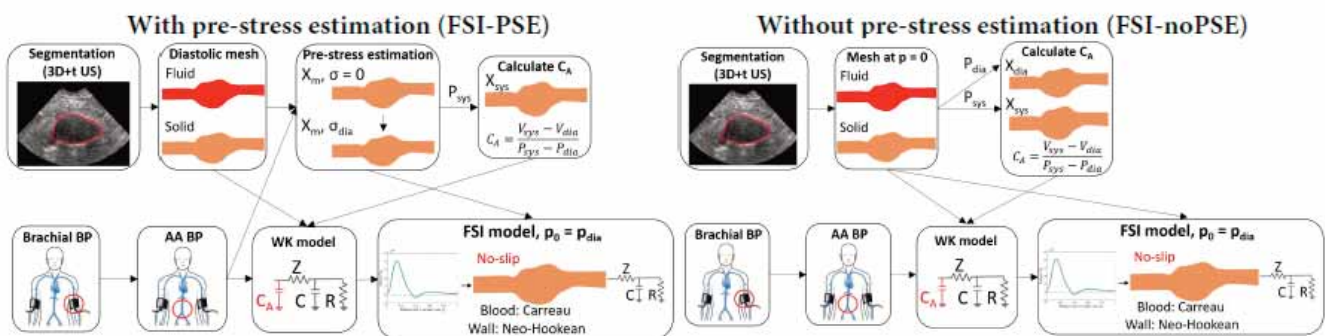
Figure caption: Fig. 1: FSI workflows with (left) and without (right) pre-stress estimation (PSE), using 3D+t US segmentations and brachial blood pressure (BP) as patient-specific input

References:
1.   Salman et al, Front. Bioeng. Biotechnol., 7:111, 2019.
2.   De Putter et al, J. Biomech, 40(5):1081-1090, 2007.
3.   Bessems et al. J. Fluid Mech., 580:145-168, 2007.

B8.3

Patient-specific electrophysiology simulations in single ventricle physiology

Oguz Tikenogullari[1], Mathias Peirlinck[1], Henry Chubb[2], Ellen Kuhl[1], Alison Marsden[2]

1   Stanford University, Mechanical Engineering, Stanford, United States
2   Stanford University, Pediatrics-Cardiology, Stanford, United States

Single ventricle patients often experience dysfunction in the electrical conduction system of the heart particularly after surgical palliation. Treatment is possible; however, a significant portion of patients do not benefit from these treatments due to shortcomings in individualization of treatment methods. Computational modeling provides a promising avenue to understand the causes and treatment of the deterioration in electrical function.

In this study, we simulate the personalized electrical activation in a single ventricle heart model, as the basis for personalized cardiac electrophysiology treatment planning. We created a finite element model of the ventricular geometry from segmentation of cardiac magnetic resonance images of a patient with single ventricle physiology using the SimVascular software (www.simvascular.org).

We employed the Ten Tusscher-Panfilov human myocyte model1 to model how ion mobility at the cell level translates into electrical activation. We accounted for fiber orientations in our model using a rule-based method (Figure 1, Left). We adopted reported anisotropic conductivity values and used a previously proposed algorithm to automatically generate the Purkinje network, which runs from the approximate location of the atrioventricular node along the endocardial surfaces2. We optimized the location of the Purkinje-myocyte junctions3 such that the simulated activation times matched clinically measured personalized activation maps obtained during cardiac catheterization.

The discretized model consists of linearly interpolated tetrahedral elements for the myocardium and line elements for the Purkinje network, coupled at shared nodes that represent the Purkinje-myocyte junctions and solved monolithically in the finite element analysis (Figure 1, Right). We employed a monodomain formulation of the electrophysiology equations and applied an operator split method to numerically decouple the reaction and diffusion terms4. We solve the reaction problem locally at the integration point level and the diffusion problem globally using linear finite elements in space and the second order generalized-alpha method in time. We employ larger time steps compared to the reaction-part of the problem, to take advantage of inherent stability of the diffusion problem. Ultimately, we will extend this framework to optimize personalized cardiac resynchronization therapies in single ventricle patients.
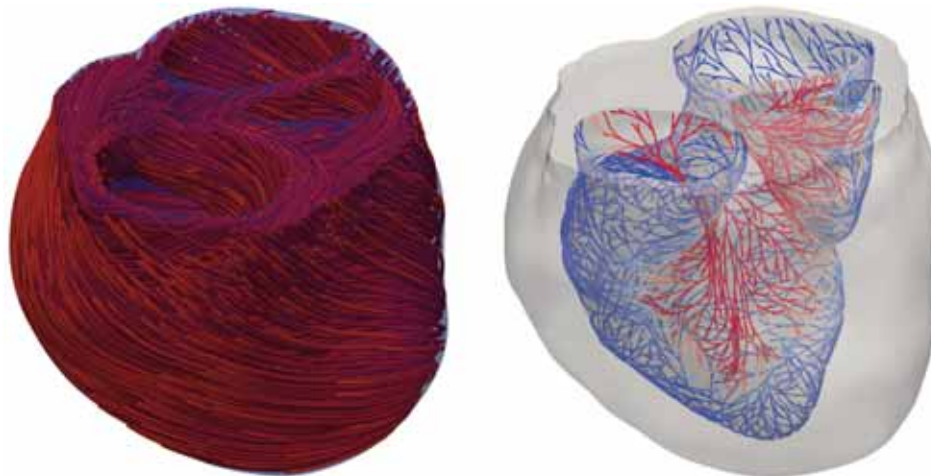
Figure 1: Image–based anatomic model of a SV patient. Left: fiber directions. Right: His Purkinje system in an SV patient.

References:
1:   ten Tusscher, KH et al. (2004). A model for human ventricular tissue. APJHeart, 286(4).
2:   Costabal, FS et al. (2016). Generating Purkinje networks in the human heart. Journal of biomechanics, 49(12).
3:   Vergara, C et al. (2014). Patient-specific generation of the Purkinje network driven by clinical measurements of a normal propagation. MBEC, 52(10).
4:   Qu, Z & Garfinkel, A (1999). An advanced algorithm for solving partial differential equation in cardiac conduction. IEEE Transactions on Biomedical Engineering, 46(9).

B8.4

Bayesian parameter estimation of ligament properties based on tibio-femoral kinematics during squatting

Laura Bartsoen[1], *Matthias Faes*[1], *Michael Skipper Andersen*[2], *Roel Wirix-Speetjens*[3], *David Moens*[1], *Ilse Jonkers*[4], *Jos Vander Sloten*[1]

1   KU Leuven, Mechanical engineering, Leuven, Belgium
2   Aalborg university, Department of Materials and Production, Aalborg, Denmark
3   Materialise NV, Leuven, Belgium
4   KU Leuven, Movement science, Leuven, Belgium

The possible applications of musculoskeletal knee models (MSKMs) in a clinical setting are numerous, e.g. surgical navigation and clinical decision making. Such applications require MSKMs that result in an accurate prediction of kinematics and ligament strains. The objective of this study is to estimate the ligament material properties and attachment sites of an MSKM for seven specimens based on knee rig experimental data during a squatting motion. This allows assessing if ligament properties can be estimated based on squat movement kinematics as well as quantifying their variability between specimens. We used Bayesian parameter estimation to account for uncertainty in the experimental data ($\sigma = 0.5$ mm or ° [1]) by optimization of an input parameter space consistent with all possible solutions. The set of solutions accounts for physiologically relevant ligament strain ($\varepsilon < 6\%$ [2,3]). The transitional Markov Chain Monte Carlo algorithm was used [4,5]. To perform the parameter estimation with feasible computational cost, an artificial neural network of the musculoskeletal knee model was trained. The figure shows the histograms resulting from the parameter estimation for the reference strain and linear stiffness for the AnteroLateral ligament (ALL) and the AnteroLateral (PCL0) and PosteroMedial (PCL1) Posterior cruciate ligaments. Each specimen is assigned a color where the transparency is consistent with the probability of the solution. It can be seen that no unique solution can be found solely based on measured kinematics of a squat motion as multiple solution clusters are found for each of the specimens. This shows that further research is required into alternative (combinations of) movements that would lead to a unique solution and can be accurately measured in vivo. The large variation between specimens shows that a small range of ligament properties that represents the patient population cannot be established. To limit ligament properties uncertainty in clinical applications, research will need to invest in establishing patient specific uncertainty ranges and/or in vivo measuring methods.
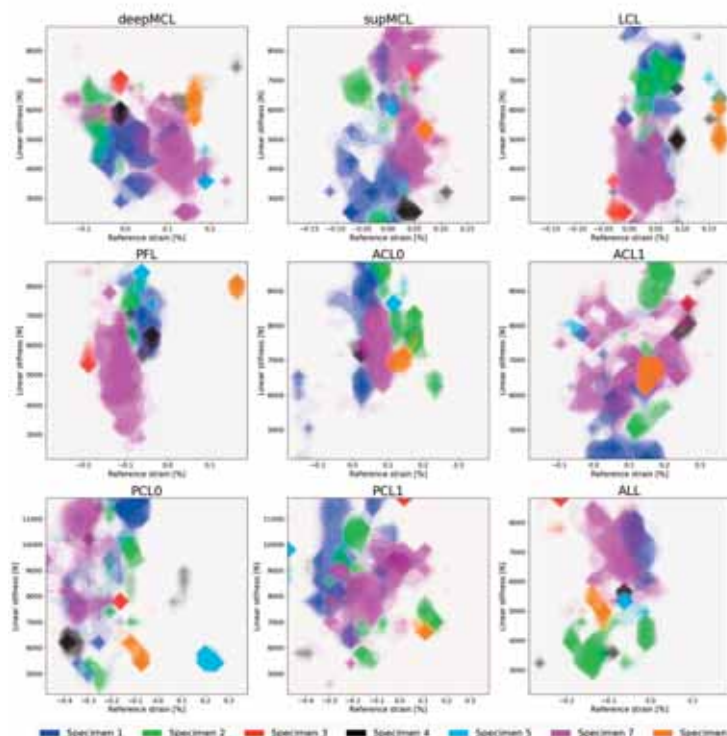
Figure caption: Results of the Bayesian parameter estimation.

References:
[1]   Victor, J., A comparative study on the biomechanics of the native human knee joint and total knee arthroplasty, PhD thesis, KU Leuven, 2009.
[2]   Guo, Zheying, et al. "Quantification of strain induced damage in medial collateral ligaments." Journal of biomechanical engineering 137.7(2015).
[3]   Provenzano, Paolo P., et al. "Subfailure damage in ligament: a structural and cellular evaluation." Journal of Applied Physiology 92.1(2002):362-371.
[4]   Ching, Jianye, et al. "Transitional Markov chain Monte Carlo method for Bayesian model updating, model class selection, and model averaging." Journal of engineering mechanics 133.7(2007):816-832.
[5]   Faes, Matthias, et al. "A multivariate interval approach for inverse uncertainty quantification with limited experimental data." Mechanical Systems and Signal Processing 118(2019):534-548.

B8.5

Biomechanical simulation platform for patient-specific refractive interventions

Malavika Nambiar[1], Harald Studer[2], Abhijit Sinha Roy[3], Philippe Büchler[1]

1   University of Bern, ARTORG Center for Biomedical Engineering Research, Bern, Switzerland
2   Optimo Medical AG, Biel, Switzerland
3   Narayana Nethralaya Eye Hospital, Indira Nagar, Bengaluru, India

Myopia (near sightedness), is the most common yet underestimated ocular impairment affecting global health. Projections suggest nearly 50 % of the world's population will be myopic by 2050, mainly due to lifestyle changes, making it the leading cause of blindness worldwide. Corrective surgeries such as LASIK, SMILE and PRK are becoming increasingly popular but 10-15 % of cases fail to provide the desired correction rates. The foremost drawback in these corrective surgeries arise in the stage of surgical planning itself. The lack of patient specific information leads to a "one size fits all" approach. A possible solution to this problem is the incorporation of patient specific parameters like, patient specific tissue properties along with topography into the surgical planning, for patient specific diagnosis and treatment.

In this regard, a patient specific geometrical model has been developed based on Pentacam (Oculus Optikgeräte GmbH, Germy) elevation maps of 10 patients undergoing LASIK, PRK and SMILE surgeries, respectively. The unique surgical parameters like LASIK flap diameter and SMILE lenticule thickness have been captured using the software GMSH 4.6 in conjunction with Python 3.0. A Holzapfel-Gasser-Ogden hyperelastic mechanical model was implemented using an ABAQUS UMAT subroutine. The current collagen fiber distribution was modelled using a general structural tensor that accounts for two families of fibers. Both family of fibers have an orthogonal orientation in the center of the cornea and are circumferentially oriented in the corneal periphery. Besides fiber orientation, in-plane and out-of-plane fiber dispersions have been considered in the model to account for the fact that the fibers are not perfectly aligned with the main direction of anisotropy3. The model was validated by measuring the corneal curvature from the clinical data and ensuring that it was accurately reproduced at different steps of the modeling procedure. Simulations of the three refractive interventions were then conducted based on the pre-operative clinical data and the corneal curvature were examined and compared.

Condition	Spherical Equivalent
Presurgical - measured	-5 D
Presurgical - model	-5 D
Post-surgical PRK	+ 0.2 D
Post-surgical SMILE	+ 0.8 D
Post-surgical LASIK	-5.4 D
Target correction	0 D
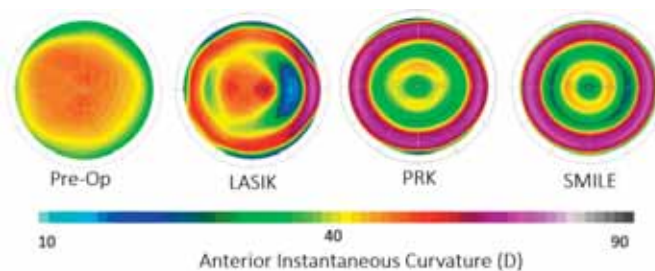
The pre-surgical models are in good agreement with the patient's corneal geometry and topography. This is established by the spherical equivalent of the measured and developed presurgical model. The surgical models capture the targeted correction in spherical equivalent of the PRK and SMILE surgery models, while showing an over-correction of 0.2D – 0.8D. Improvements are required to accurately model LASIK interventions. More patient specific details like biomechanical properties of the corneal tissue will be incorporated in future models. We aim to collect this data using Brillouin imaging. We will further work towards improving the mechanical model and to validate the predictions.

B8.6

Towards quasi-automatic and acurate 3D reconstruction of the scapula from biplanar X-rays

Sandrine Bousigues[1 2], *Wafa Skalli*[2], *Anna Gounot*[2], *Xavier Ohl*[3], *Nicola Hagemeister*[1 4], *Laurent Gajny*[2]

1   Laboratoire de recherche en imagerie et orthopédie (LIO), Montréal, Canada
2   Arts-et-Métiers, Institut de Biomécanique Humaine Georges Charpak, Paris, France
3   Reims - Maison Blanche, Reims, France
4   École de technologie supérieure ÉTS, Montréal, Canada

In clinical routine, scapula's shape and position are of high interest to investigate the scapulo-thoracic and gleno-humeral joints. A previous (V1) 3D reconstruction method of the scapula from biplanar X-rays [1] has been proposed. However, it is not used in clinical routine, due to complex manual annotations and adjustments, thus requiring high operator expertise. Moreover, its accuracy is still to improve. The purpose of this work was to develop an improved (V2) accurate method with minimal manual input and in vitro validation.

The proposed method relied on an initial set of 6 manually annotated landmarks, completed with 2 additional landmarks inferred using a statistical shape model built on a database of 40 cadaveric segmented scapulae. Then a Moving Least Square algorithm deformed a mean model of scapula to fit the eight landmarks. The initial solution was projected on the radiographs allowing the user to adjust the model with control handles and fit the real radiograph bony projection.

In vitro evaluation has been performed on 6 cadaveric CT-scan (1mm slice thickness) with segmented scapulae. Biplanar digitally reconstructed radiographs (DRR) were generated. Each scapula was previously reconstructed using the V1 method by an expert in shoulder anatomy and 3D reconstruction. In the current study, the V2 method was used both by an expert and a non-expert engineer who received a theoretical training of 3 hours and practiced the reconstruction process on independent in-vivo radiographs during approximatively 10 hours. Accuracy was assessed using points-to-surface distances between the CT-based and DRR-based reconstructions.

For the V2 method, expert and non-expert operators obtained similar results. When comparing V2 with a non-expert to V1 with an expert, the average points-to-surface distance between DRR-based reconstructions and the CT segmentations were respectively 1.8 mm for V2 (non-expert) versus 3.2 mm for V1 (expert). The average maximum value was 8.9 mm against 11.6 mm. Focusing on the glenoid region, the average error was 1.3 mm, and 1.8mm, with a maximum value of respectively 3.4 versus 4.4 mm.

The V2 method appears more accurate and robust requiring only a limited training even for non-shoulder specialists. The manual annotations have been selected to enable user-friendly operation, and for their potential for future automatic detection. The initial solution proposed is improved regarding the V1 method, allowing minimizing user input in the adjustment process. The proposed method still requires further validation such as an in vivo reproducibility study. Nevertheless, it constitutes a consistent step towards routine quasi-automatic use of scapular 3D reconstruction in clinics.

References:
[1]   C. Bascans et al. 'Bi-planar low dose X-Ray method for personalised 3D modeling of the scapula and automated computation of morphological parameters', Int J CARS, vol. 13, no. S1, pp. 1–273, Jun. 2018, doi: 10.1007/s11548-018-1766-y.

B9.1

A formalism for modelling traction forces and cell shape evolution during cell migration in various biomedical processes

Qiyao Peng[1], Fred Vermolen[2], Daphne Weihs[3]

1   *Delft University of Technology, Delft Institute of Applied Mathematics, Delft, Netherlands*
2   *Hasselt University, Faculty of Science, Diepenbeek, Belgium*
3   *Techonion-Israel Institute of Technology, Faculty of Biomedical Engineering, Haifa, Israel*

It has been widely documented that cell geometry influences cellular activities like cell growth and death, cell mobility and adhesion to the direct environment. The shape of a motile cell is determined by its boundaries, which dynamically vary with a local balance between retraction and protrusion. During wound healing, epidermal cells alter their shape for re-epithelialization and fibroblasts (spindle shape) differentiate into myofibroblasts (dendric shape) to regenerate collagen bundles in the extracellular matrix, while they exert traction forces causing wound contractions. For cancer cell metastasis, cancer cells need to deform to adapt to obstacles during invasion and they apply traction forces on their immediate environment.

We developed a phenomenological model to simulate cell shape evolution during cell migration, based on [1] and [2], where the traction forces exerted by the cells were not yet considered. Plastic deformations of the direct environment of cells are modeled by morphoelasticity theory, which results into momentum balance equation over the cell boundary. In our model, the cell boundary is split into line segments by nodal points, and each point is connected to the cell center by an elastic spring to maintain the cell cytoskeleton (see Figure 1). Together with chemotaxis/mechanotaxis, passive convection and random walk, the displacement of the nodal point is determined. Hence, the cell shape evolves over time.

To validate the model, we managed to reproduce the most important trends observed in the experiment [3]. The model can be applied to mimic various (microscopic) biological observations with several equilibrium shapes of cell. Furthermore, the current model provides a basis that can be expanded to describe more experimentally observed phenomena in cell geometry. For more details about this part of work, we refer to [4].
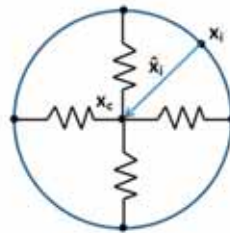
Figure 1. A schematic of the distribution of the nodal points on the cell membrane

References:
[1]   *Chen J, Weihs D, Dijk MV, Vermolen FJ (2018) A phenomenological model for cell and nucleus deformation during cancer metastasis. Biomechanics and Modeling in Mechanobiology 17(5):1429–1450.*
[2]   *Vermolen FJ, Gefen A (2012) A phenomenological model for chemico-mechanically induced cell shape changes during migration and cell–cell contacts. Biomechanics and Modeling in Mechanobiology 12(2):301–323.*
[3]   *Mak M, Reinhart-King CA, Erickson D (2013) Elucidating mechanical transition effects of invading cancer cells with a subnucleus-scaled microfluidic serial dimensional modulation device.*
[4]   *Peng Q, Vermolen, FJ and Weihs D (2020) A Formalism for Modelling Traction forces and Cell Shape Evolution during Cell Migration in Various Biomedical Processes. arXiv preprint arXiv:2012.05538.*

B9.2

A combined continuum-tensegrity FE model to describe the mechanical behaviour of a chondrocyte cell: definition, identification and validation by means of AFM indentation and micropipette aspiration

Alessandro Arduino[1], Sofia Pettenuzzo[1 2], Alice Berardo[1 3], Emanuele Luigi Carniel[2], Carmelo Majorana[1]

1   University of Padova, Department of Civil Environmental and Architectural Engineering, Padova, Italy
2   University of Padova, Department of Industrial Engineering, Padova, Italy
3   University of Padova, Department of Biomedical Sciences, Padova, Italy

The mechanical properties of human cells and their subcomponents play a key role in the mechanotransduction of external stimuli into physiological processes such as proliferation, differentiation and migration. As a result, the interest in the mechanical behaviour of living cells has drawn a lot of attention within the scientific community in recent years. Indeed, the experimental investigation of their mechanical properties has always been challenging since many parameters can affect the in-vivo as well as in-vitro tests. Moreover, these issues are particularly relevant in the study of tumour cells due to their intra and inter tumour variability. For the above reasons, the use of computational models might become a helpful and powerful tool in addressing cell biomechanics.

Here we present a Finite Element (FE) Model (Abaqus/CAE 2019, Dassault Systems) to illustrate the mechanical behaviour of a cell, by simulating both an AFM indentation and a micropipette aspiration. The cell has been described combining a continuous part (nucleus, cytoplasm and membrane) and a tensegrity structure (cytoskeleton). This approach has been applied in previous works [1], providing the main features of cells mechanics, e.g., the strain hardening due to the cytoskeleton prestress.

The model parameters were identified with AFM indentation experimental data on chondrocytes and chondrosarcoma cells (e.g. [2]) and then validated by simulating micropipette aspiration of living cells and comparing the results with experimental observations from the literature [3].

Our results and validations suggest that this model may represent both the experimental setups with a good deal of accuracy. Indeed, this FE model represents a useful tool for the mechanical investigation of both living and cancer cells also in the studies of the mechanical processes that undergo during the different stages of tumour cells.
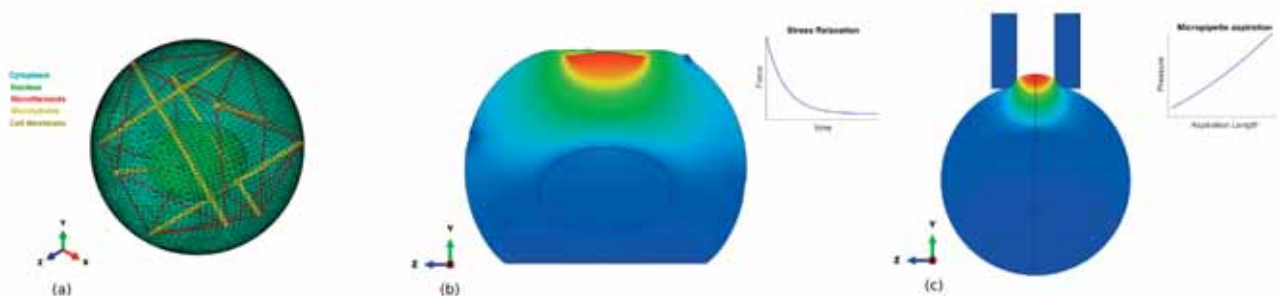
Figure caption: (a) Chondrocyte discretization with a continuum-tensegrity approach, (b) Displacement contour field during AFM indentation and stress relaxation data, (c) Displacement contour during micropipette aspiration and length vs aspiration data.

References:
[1]   McGarry J. G. and Prendergast P. J., 2004. A three-dimensional finite element model of an adherent eukaryotic cell. European Cells and Material, 7, 27-34.
[2]   Darling E. M., Zauscher S., et al., 2007. A Thin-Layer Model for Viscoelastic, Stress- Relaxation Testing of Cells Using Atomic Force Microscopy: Do Cell Properties Reflec Metastatic Potential? Biophysical Journal, 92, 1784-1791.
[3]   Zhou, E. H., Lim, C. T., & Quek, S. T. (2005). Finite element simulation of the micropipette aspiration of a living cell undergoing large viscoelastic deformation. Mechanics of Advanced Materials and Structures, 12(6), 501-512.

B9.3

Axon model generated from ssTEM images predicts microstructural failure under mechanical loading

Lucy Wang[1], *Miriam Goodman*[2], *Ellen Kuhl*[1]

1   Stanford University, Mechanical Engineering, Stanford, United States
2   Stanford University, Molecular and Cellular Physiology, Stanford, United States

In the United States, over 1.7 million people sustain a traumatic brain injury each year, and about 5.3 million people are currently living with a traumatic brain injury-related disability [1]. While the trauma itself occurs at the head level, the damage can be traced to the smaller scale of individual axons within the brain. Currently, computational head trauma models predict axon injury by applying a damage threshold on the calculated strains. However, the current roadblock in accurate predictive injury simulation is the selection of the appropriate safety level threshold for axonal failure. To address this problem, studies have looked to the cytoskeleton of the axon for insight. While previous studies have used computational models of the axon cytoskeleton to study how the axon fails under applied loads, these studies have all assumed an idealized geometry with regularly spaced microtubules and constant cross-sectional areas [2]. This idealized geometry tends to overestimate axon strength since failure is determined by the weakest cross section along the length of the axon. To address this issue, we analyzed serial section transmission electron micrographs taken of a 15-um long section of a C. elegans touch receptor neuron [3]. We established a semiautomated procedure to identify microtubules in these images and reconstructed the structure of the microtubule bundle within the neurite. We then discretized the microtubule geometry using beam elements in Abaqus Standard and added truss elements to represent crosslinking proteins. Simulations of tensile loading revealed localized regions of high strain corresponding to the weaker cross sections with fewer microtubules. This failure mode cannot be captured by an idealized model with constant cross-sectional area. We anticipate that our new axon model more accurately represents the microstructural failure mode of the axon under mechanical loading.
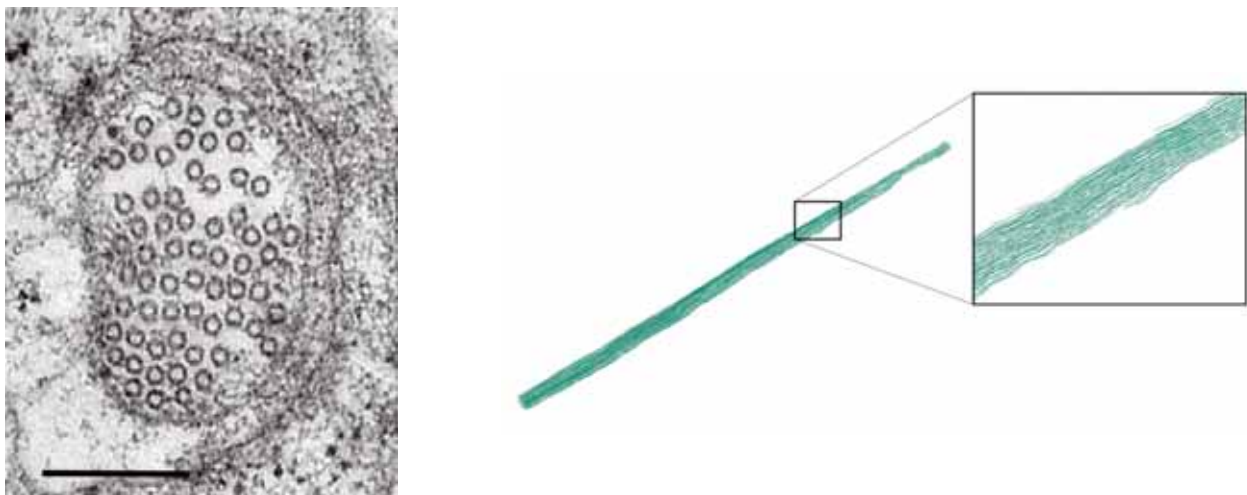
Figure caption: (left) Transmission electron micrograph of the microtubule arrangement in a C. elegans neurite cross section. Scale bar: 200nm [3]. (right) Reconstruction of the microtubule bundle structure over a 15-um long section of the neurite.

References:
[1]   Roozenbeek B, Maas AIR, Menon DK (2013) Changing patterns in the epidemiology of traumatic brain injury. Nat Rev Neurol 9:231-236
[2]   de Rooij R, Kuhl E (2018) Physical biology of axonal damage. Front Cell Neurosci 12:144
[3]   Cueva JG, Goodman MB (2007) Serial section electron microscopy data of touch receptor neurons from wild type animals using a mouse polyclonal antibody against MEC-2. Stanford Digital Repository.

B9.4

Temperature influence on the compression and breakage behaviour of yeast cells

Achim Overbeck[1], Jan-Henrik Finke[1 2], Ingo Kampen[1 2], Arno Kwade[1 2]

1   Technische Universität Braunschweig, Institute for Particle Technology, Braunschweig, Germany
2   Technische Universität Braunschweig, PVZ - Center of Pharmaceutical Engineering, Braunschweig, Germany

Industrial biotechnology uses microbiological cells to produce a wide range of products.

Whilst the organisms in question are well understood regarding their genetic and molecular properties, less is known about their mechanical properties. Previous work has established a testing procedure for single yeast cells using a commercial nanoindentation instrument equipped with a Flat Punch probe, allowing the compression of single cells (Saccharomyces cerevisiae, baker's yeast) between two parallel surfaces. The resulting force-displacement curves clearly showed the bursting of the cells and served to determine characteristic values such as the bursting force, bursting energy and the relative deformation at the bursting point. Other studies have investigated the influences of growth conditions and of measurement conditions (compression speed, osmotic pressure and multiple deformations) on the characteristic mechanical values [1]. Recent studies examined the mechanical characteristics according to the temperature during compression. Temperature from 0°C to 25°C has no significant influence on the micromechanical characteristics. Raising temperature up to 35°C caused lower strengths of the cells. At even higher temperatures up to 50°C the bursting force and energy increase significantly. By applying a simple deformation geometry model [2] the cell wall tensile strength depending on the temperature was calculated. The findings of these studies can facilitate the identification of efficient conditions for the cell breakup and product recovery in biotechnological downstream processes, e.g. for the production of active pharmaceutical ingredients.

References:
[1]   Overbeck, A., Kampen, I., & Kwade, A. (2015). Mechanical characterization of yeast cells: Effects of growth conditions. Letters in applied microbiology, 61(4), 333-338.
[2]   Overbeck, A., Günther, S., Kampen, I., & Kwade, A. (2017). Compression Testing and Modeling of Spherical Cells–Comparison of Yeast and Algae. Chemical Engineering & Technology, 40(6), 1158-1164.

B10.1

Dynamic analysis of the dissipative response of intervertebral discs about a nonlinear prestressed state

Jean-Baptiste Garcher[1], *Deü Jean-François*[1], *Rouleau Lucie*[1]

1   Conservatoire national des arts et métiers, LMSSC, Paris, France

Due to their critical location in the human anatomy, intervertebral discs (IVD) are subject to complex loading conditions. Experimental and numerical studies on intervertebral discs under static loading are widely analysed in the literature, giving insight into the mechanical characteristics of IVD. Nevertheless, due to complex experimental protocols and challenging simulations, their dynamic behaviour is scarcely studied. Further studies are necessary to better understand the mechanisms in degenerative disc disease and support the design of robust disc prothesis. The goal of this work is to examine the nonlinear effects of time-dependent loading on the mechanical response of IVD, through numerical simulations.

The first step consists in developing a finite element model which accounts for the complexity of the IVD (heterogeneity, fibre anisotropy, hyperelasticity, viscoelasticity). The hyperelastic Holzapfel-Gasser-Ogden (HGO) material model (Gasser, Ogden, et Holzapfel 2006) was implemented to describe the nonlinear behaviour of the annulus fibrosus. The dissipative behaviour of the fibres is also considered through a finite strain viscoelasticity model, compatible with the hyperelastic formulation (Govindjee et Simo 1992). The proposed finite element model is validated with numerical results from the literature, by performing quasi-static simulations under compression loading on healthy IVD. Figure 1 evidences the important fibre contribution to the stress distribution at organ-level scale.

The second contribution aims at characterising the dynamic response of the IVD in time domain. Vibrations about a nonlinear prestressed state will be considered to model physiological dynamic loading such as whole body vibration. A complementary aspect focuses on the viscoelastic behaviour of the IVD, by quantifying the dissipated energy through hysteresis loops. The influence of inputs parameters (preload, strain-rate and excitation frequency) on the dynamic responses will be also analysed (Marini et Ferguson 2014).
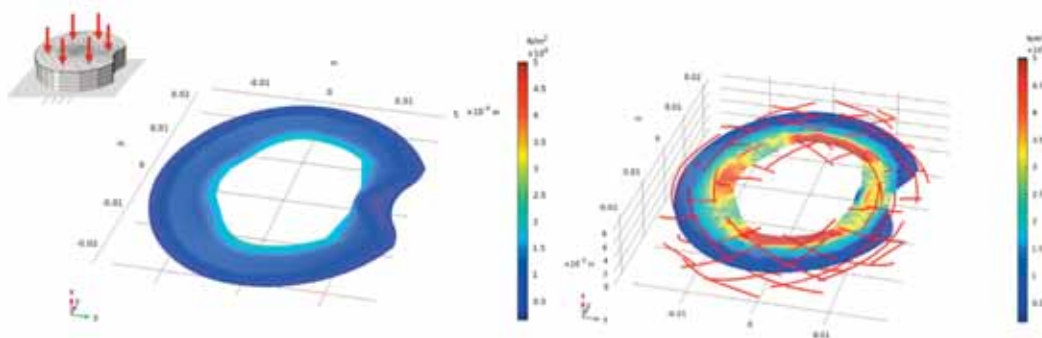
Figure caption: Von Mises stress on a cross section of annulus fibrosus (circumferential part of the IVD). On the left: without fiber contribution. On the right: with fiber contribution. Geometry of L4/5 lumbar disc (Little, Pearcy, et Pettet 2007)

References :
Gasser, T. C., Ogden, R. W., Holzapfel, G. A., 2006. « Hyperelastic Modelling of Arterial Layers with Distributed Collagen Fibre Orientations ». *Journal of The Royal Society Interface 3 (6): 15-35.*
Govindjee, S., Simo, J. C., 1992. « Mullins' Effect and the Strain Amplitude Dependence of the Storage Modulus ». *International Journal of Solids and Structures 29 (14-15): 1737-51.*
Little, J. P., Pearcy, M. J., Pettet, G. J., 2007. « Parametric Equations to Represent the Profile of the Human Intervertebral Disc in the Transverse Plane ». *Medical & Biological Engineering & Computing 45 (10).*
Marini, G., Ferguson, S. J., 2014. « Nonlinear Numerical Analysis of the Structural Response of the Intervertebral Disc to Impact Loading ». *Computer Methods in Biomechanics and Biomedical Engineering 17 (9).*

B10.2

Influence of indentation speed on the response of porcine spinal cord white and gray matters

Yvan Petit[1 2 3], *Eric Wagnac*[1 2 3], *Lucien Diotalevi*[1 2 3], *Annie Levasseur*[2 3], *Nicolas Bailly*[1 2 3 4]

1   Ecole de technologie superieure, mechanical engineering, Montréal, Canada
2   CIUSS Nord-de-l'ile-de-Montreal, Research center, Montreal, Canada
3   International Research Lab on imaging and biomechanics of the spine, Marseille, France
4   Laboratoire de Biomécanique Appliquée UMR T24, Marseille, France

Abstract: Knowledge of the spinal cord behavior is important to better understand spinal cord injuries. Its behavior is generally considered as hyper-viscoelastic. However, describing the specific properties of spinal cord white and gray matters under different loading condition is challenging using traditional tests such as tensile, compression, shear. As a result, the stiffness and relaxation behavior of white matter (WM) compared to gray matter (GM) is still debated and only few studies have investigated the effect of strain rate on the response of WM and GM[1,3,5]. The specific purpose of this study is to investigate the effect of loading speed on the stiffness and relaxation response of the porcine spinal cord WM and GM using micro-indentation.

Seven samples of thoracic spinal cord were extracted from 6 animals, fixed into agarose and sliced into 4 mm thick transverse slices. The samples were glued into a petri dish, submerged into phosphate buffer solution and 150 μm axial indents were performed with a 500 μm diameter flat punch. Six to eight (2-4 in GM and 4-6 in WM) indentation locations were tested at 7 loading speeds (1.25, 5, 20, 80, 320, 1280, 5120 and 12480 μm/s) in random order of location and loading speed. Each indentation was followed by 10s holding time, unloading and 90s relaxation period. All samples were tested within 12 hours post-mortem. Based on previous studies on porcine brain[2,4], quasi-linear elastic modulus was extracted between 55% and 85% indentation depth and 2 terms Prony series were used to obtain the relaxation time.

Kruskall-Wallis tests and factorial ANOVA were performed on a total of 442 indentations (n=15-40/group) to investigate the effect of loading speed on the elastic modulus and relaxation time of WM and GM. The elastic modulus was significantly higher (p<0.0001) for GM (1.2±0.4kPa) than WM (0.7±0.7kPa) and increased significantly (p<0.0001) with indentation speed (figure). Long (3_1) and short (3_2) relaxation times reduced with indentation speed up to 1280 μm/s and remained stable above. Stabilized relaxation times significantly differ (p<=0.0012) between WM (3_1=3,3±0.4s, 3_2=0.23±0.05s) and GM (3_1=3,4±0.3s, 3_2=0.26±0.04s).

This study shows loading speed dependent behavior of the spinal cord and suggests slightly stiffer GM with longer relaxation time than WM. Future work will investigate the hyperplastic behavior of WM and GM and include these findings into finite element modelling of the spinal cord to improve their biofidelity.
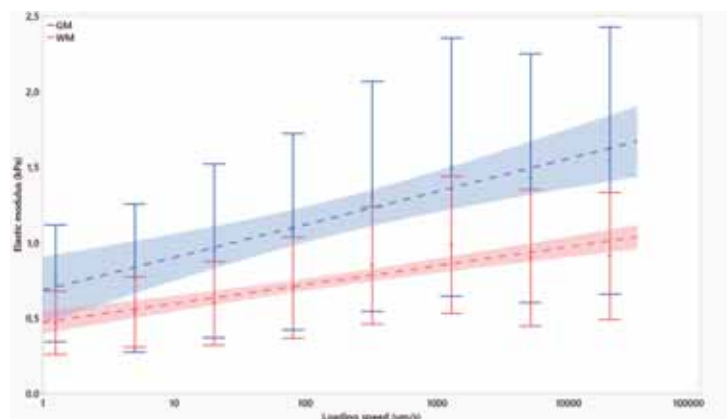
Figure caption: Effect of indentation speed on WM and GM elastic moduli

References:
1.   Ichihara et al. 2003.
2.   Qian et al. 2018.
3.   Sparrey et al. 2009.
4.   Weickenmeier et al. 2016. 5. Yu et al. 2020.

B10.3

Relationship between the cross-sectional distribution of spinal cord gray and white matter mechanical properties and its microstructure

Nicolas Bailly[1 2 3 4], Eric Wagnac[2 3 4], Annie Levasseur[3], Yvan Petit[2 3 4]

1   Université Gustave Eiffel, Laboratoire de Biomécanique appliquée, Marseille, France
2   ETS, Department of Mechanical Engineering, Montréal, Canada
3   Hôpital du Sacré-Coeur de Montréal, Research Center, Montréal, Canada
4   iLab-Spine, Laboratoire International en Imagerie et Biomécanique du Rachis

The capacity of finite element modeling to reproduce spinal-cord injury strongly depends on gray and white matter material properties[1]. Yet the rigidity and viscoelasticity of these materials are still debated[2,3] and might not be homogeneous as great variability in axon morphometries and density was described within spinal-cord white matter[4]. Moreover, the microstructure and especially the myelin content were shown to affect the mechanical properties of the white matter in the brain[5]. The goal of this study is to characterize the cross-sectional distribution of mechanical properties in the spinal-cord by micro-indentation and to study if that distribution correlates with spinal-cord microstructure.

Transverse slices (5 mm thick) of 10 freshly harvested porcine thoracic spinal-cord were prepared within 12 hours post-mortem, submerged into PBS and mounted into a Hysitron TI950 TriboIndenterTM. Indentations were performed with 0.5 mm diameter flat punch with a maximum displacement of 300μm, and loading rate of 2.5 μm/s. The elastic modulus was obtained from the slope of the loading curve at an indentation depth of 100 ± 10 μm. Indents were performed all over the surface of the slice and were separated by at least 1 mm (~25 indents/sample). The effect of the type of material was evaluated using (1) kruskal Wallis test and (2) factorial ANOVA. To visualize the cross-sectional rigidity variations, elastic moduli were divided by their sample mean (normalization) and merged into one reference spinal-cord (figure 1a). Histologic staining (LFB and H&E) were performed to obtain the distribution of myelin content and the glial content respectively in the transverse slices with a resolution of 0.5mm2. Myelin and glial content distribution were correlated with the normalized elastic modulus distribution.

No significant difference was found between the elastic modulus (E) of white matter (n=183, E=0.51 ±0.21 kPa) and gray matter (n=51, E=0.53 ±0.25 kPa). Figure 1a shows the cross-sectional distribution of elastic modulus in the spinal-cord: the white matter displayed large variation of elastic modulus and was stiffer in the gray matter vicinity (figure 1a). Glial content was weakly correlated (r=0,2 ; p<0,01) with elastic modulus in the white matter (figure 1b) but no correlation was found between rigidity and myelin content.

The large rigidity variation within the white matter might partly explain differences in reported rigidity of the spinal-cord materials[2,3]. Those variations might have an impact on stress and strain within the spinal-cord. This study also provides knowledge on the relationship between microstructure and mechanical properties and is a first step toward a microstructure informed model of the spinal-cord.
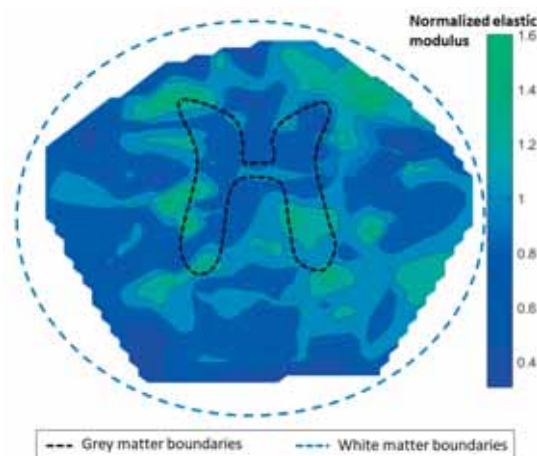
Figure caption: Contour map of normalized elastic modulus in the spinal-cord

References:
1.   Sparrey et al. 2009,
2.   Ozawa et al. 2001,
3.   Yu et al. 2020,
4.   Duval et al., 2018,
5.   Weickenmeier et al. 2016

B10.4

Evaluation of the main spatial angles in adolescent idiopathic scoliosis optically diagnosed

Sasa Cukovic[1], William R. Taylor[1], Vanja Luković[2], Christoph Heidt[3], Radu Petruse[4], Subburaj Karupppasamy[5]

1   Institute for Biomechanics, ETH Zürich, Laboratory for Movement Biomechanics, Zürich, Switzerland
2   University of Kragujevac, Faculty of Technical Sciences Čačak, , Cacak, Serbia
3   University Children Hospital - UKBB Basel, Basel,
4   "Lucian Blaga" University of Sibiu, Sibiu, Romania
5   Singapore University of Technology and Design, Singapore, Singapore

Clinical evaluation of Adolescent Idiopathic Scoliosis (AIS) is performed on standing PA X-ray images, and Cobb angle (CA) is considered the "golden" standard for 2D diagnosis. This study aims to examine optically-assessed spatial angles of AIS as CA inadequately capture the spatial aspects of the deformity. Most relevant angles to capture the complexity of the spinal geometric alignment and facilitates the development of a new method for classifying AIS in 3D are between vertebrae Th1-Th3, Th3-Th12, and Th12-L4 describing proximal thoracic (PT), main thoracic (MT) and lumbar (L) regions.

Descriptive Statistics

Females	N	Min.	Max.	Mean	Std. Deviation
3DAngle L4Th12, deg		3.83	30.37	11.41	6.57
3DAngle Th3Th12, deg		2.95	55.49	16.30	12.10
3DAngle Th1Th3, deg		1.53	16.28	7.36	4.11
Primary Cobb, deg		10.26	36.25	19.90	8.42
Age		8.00	12.00	10.57	1.38
Valid N (listwise)	19				

Males	N	Min.	Max.	Mean	Std. Deviation
3DAngle L4Th12, deg		4.23	31.95	13.86	9.19
3DAngle Th3Th12, deg		3.32	37.46	15.20	12.94
3DAngle Th1Th3, deg		1.91	28.99	10.29	9.48
Primary Cobb, deg		11.73	47.20	25.13	11.27
Age		9.00	16.00	12.14	2.73
Valid N (listwise)	7				

Fig.1: Spatial angles defined through Th1, Th3, Th12, and L4 vertebrae in a subject-specific model of AIS generated by ScolioSIM tool – Back and 3D view of AIS and descriptive statistics of the measurements

Introduction: AIS is the most common type of spinal deformity in adolescents [1]. Current diagnostic and monitoring methods are based on harmful ionizing radiation. To overcome this potential threat, non-invasive 3D optical measurements offer a powerful solution. One of the latest diagnostic solution that automatically generates deformity parameters is ScolioSIM1.0 [2]. It relies on a multiscale and registerable 3D generic spinal model that auto-adapts to various shapes and sizes of the subject's back (Figure 1).

Methods: Retrospective analysis of 3D optical datasets of 26 AIS patients' back surfaces (19 females and 7 males; 10.5±1.3 and 12.1±2.7 years old, CA >10deg, 19.9±8.4deg and 25.1±11.2deg) was performed using ScolioSIM1.0 tool. Diagnostic indicators were processed using SPSS with a primary focus on three critical spatial angles that describe the three most important segments of the deformed curve (3DAngleL4Th12 3DAngleTh3Th12, and 3DAngleTh1Th3).

Results and discussion: By measuring spatial angles of the deformity it is possible to evaluate a level of helicoidal torsion of the 3D spinal alignment in certain regions: PT and MT as well as L segments. This analysis showed that the MT region had the highest angular values in females and males (16.3±12.1 and 15.2±12.9). These angles also devide 3D spinal alignement in 3 most significant curvature segments through exact vertebrae centroids suitable for AIS 3D classification.

Conclusions: The clinical relevance of this surface-based approach is high considering the generated deformity angles are suitable for characterizing the most relevant segments of the 3D spinal alignment compared to 2D CA. These findings also reinforce the need to investigate other measurements, especially spatial inflection points and angles in mid-thoracic and thoracolumbar regions and their correlation with axial vertebral rotations.

References:
[1]   Luković et al. (2019). Comput Meth P Bio, 178: 247-263.
[2]   Ćuković S. (2015) PhD Thesis; University of Kragujevac.

B10.5

Identifying and assessing subject-specific lumbar spinal motion by finite helical axis evolution

Robert Rockenfeller[1], Andreas Müller[2][3]

1   Universität Koblenz • Landau - Campus Koblenz, Mathematisches Institut, Koblenz, Germany
2   Universität Koblenz • Landau - Campus Koblenz, Institut für Medizintechnik und Informationsverarbeitung (MTI), Koblenz, Germany
3   Swiss Federal Laboratories for Materials Science and Technology, EMPA, Dübendorf, Switzerland

Degenerative changes particularly in the lumbar region of the spine are closely related to the origin of lower back pain and are known to go hand in hand with alterations in spinal kinematics during daily motion. The full cause-and-effect interaction hereof is barely resolved, as dynamic information is difficult to access. Further, there exist no reliable measures to clearly distinguish the degree of pathological issues from mere kinematics. Hence, conventional and surgical treatments of lower back pain commonly aim at restoring static configurations, such as pelvic incidents or the C7 plumb line. One possible dynamic criterion for the identification and assessment of lumbar spinal motion is thought to be found in the finite center of rotation between two vertebrae, or its temporal evolution (the centrode), respectively. However, there are several issues regarding this quantity. For example, as we will show, centrodes originating from in vivo motion are inherently different from those measured in vitro. Thus, in silico predictions from recreating in vitro experiments may not hold under in vivo conditions. Further, the center of rotation is usually calculated by projecting the corresponding finite helical axis on suitable physiological planes, e.g. the sagittal plane for flexion-extension movements. As a direct consequence, it is not possible to describe complex multi-plane motion with the help of centrodes. In addition, such projections drastically diminish the dimensionality of available kinematic information from seven to three. Several approaches on visualizing the relative motion of two vertebrae with increasing dimensionality of information are presented.

Regarding the full temporal evolution of finite helical axes corresponding to millisecond time changes, we show how agglomerative hierarchical clustering techniques can be used to identify and group similar movements. The L-method is utilized to find a suitably small number of existing clusters. A representative axis from each cluster is finally equipped with visual information regarding the amount of rotation around and translation along this axis. The final result, the quiver principal axis plot (QPAP) allows for an intuitive gathering of complex lumbar spinal motion over time, see Figure. The influence of several modeled surgical procedures, such as inter-laminar framing and laminectomy, on the corresponding QPAP are shown.
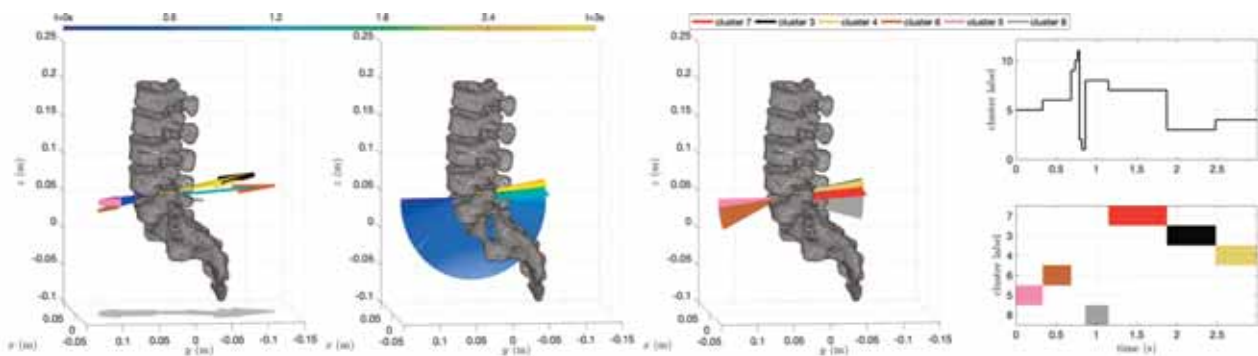
Figure caption: From left to right: (a) QPAP of a right-left lateral bending between vertebrae L4 and L5. (b) Temporal evolution of finite helical axes. (c) Clustered finite helical axes. (d) Assignment of clusters over time.

C2.1
Modelling osteochondral grafts within a human tibiofemoral joint

Gavin Day[1], *Alison Jones*[1], *Marlène Mengoni*[1], *Ruth Wilcox*[1]

1   University of Leeds, Mechanical Engineering, Leeds, United Kingdom

Osteoarthritis is the most prevalent chronic rheumatic disease worldwide with knee osteoarthritis having an estimated lifetime risk of approximately 14 % [1]. Autologous osteochondral (cartilage-bone) grafting has demonstrated positive outcomes in terms of pain and function in some patients [2], however, understanding of the biomechanical function and how the treatment can be optimised remains limited, especially for factors affecting short term stability of the graft. The aim of this study was to develop a robust method for generating specimen-specific finite element (FE) models of osteochondral grafts within a full tibia-femoral joint, prior to bone integration.

In vitro tests were conducted on a cadaveric human tibiofemoral joint, which was tested using a materials testing machine and knee-specific fixtures [3]. Six defects were created in the femoral condyles using a drill bit; two of which were treated with osteochondral autografts and two received metal pins as a control. Contact pressure measurements were obtained using flexible sensors, applying load to the joint before drilling the hole, after hole (defect) creation and after osteochondral repair (or metal pin insertion). FE models were created by segmenting and meshing registered μCT scans captured pre- and post-test. Models of the osteochondral grafts were specimen-specific and bone material properties were calibrated and based on the μCT background. FE model setup created pre-strain in the graft and surrounding area that mimicked the experimental pressfit. Boundary conditions and loading conditions matched the experimental setup. Pressure maps for the tibial cartilage layers, mean pressure values and contact area, were measured and compared to the experimental data.

Experimentally, repairs either successfully created a flush, continuous cartilage layer, or the graft was inserted too deep. The resultant pressure map changes were well represented in the FE models. Cartilage defects were measurable in the experimental pressure data with good agreement in the FE model pressure maps (Fig1).

The FE models are based upon extensive validation and calibration testing, including validation of contact pressure maps in tibiofemoral models under static loads, material property calibration and data from graft push-in tests. Experimentally, the graft depth varied, this positioning and alignment was well replicated in FE and evidenced by good agreement between the in vitro and model contact pressure maps. A robust method of creating osteochondral graft models within femoral condyles within full tibiofemoral joints has been developed that can be used to investigate a range of grafting parameters.
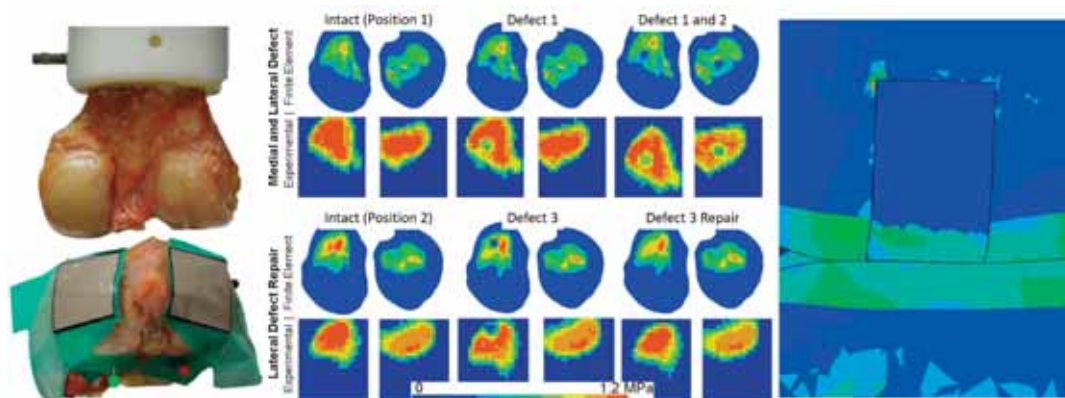
Figure caption: Experimental testing setup (left), FE and experimental contact pressure distributions for defect and repair cases (middle), example FE strain map for the graft repair case (right).

References:
1.   Bortoluzzi et al., 2018. Autoimmun Rev
2.   Pareek et al. 2016. Arthroscopy
3.   Cooper et al. 2020 J.Mech.Behav.Biomed

C2.2
Endochondral ossification of long bones

Mahsa Sadeghian[1], *Sandra Shefelbine*[1]

1   Northeastern University, Mechanical Engineering Department, Boston, United States

Endochondral ossification is the process in which the cartilage in the growing bones is replaced by calcified bone. In long bones this process takes place in the epiphyses (at each end of the bone) and forms the secondary ossification centers. Mechanical loading plays a crucial role in this process and affects the morphology of the developing bones. In the absence of mechanical loading the rate of ossification decreases [1]. Mechanobiological theory suggests that cyclic octahedral shear stress and hydrostatic tensile stress promote ossification while cyclic hydrostatic compression inhibits it [2]. In this study we utilized this theory to simulate the ossification in the epiphyseal cartilage and to predict the formation of the secondary ossification center and morphology of the growth plate (physis) that remains as cartilage. The longitudinal growth was then simulated in the growth plate for several years while the secondary center was expanding. The proposed algorithm includes the contribution of the biological factors in the ossification process, modeled as diffusion from the surrounding bone, and mechanobiological factors, calculated from stresses due to loading. This algorithm was implemented in generic finite element models of a diarthrodial joint under dynamic loading. The effects of geometry and loading condition on progression of the physeal – metaphyseal growth front and secondary center were investigated. In all models the ossification of the secondary center initiated in the middle of the cartilage, beneath the loading surface. The results also showed that the presence of a stiff secondary center protects the growth plate cartilage from ossification. Under an asymmetric loading condition, the predicted growth plate tilted perpendicular to the load. When the load was applied in multiple steps over a wide region, the growth rate over the growth plate was more uniform compared to the concentrated axial load. In conclusion, this model integrates together many previous computational models of endochondral ossification in different stages of skeletal development into a single algorithm and is a step towards a better understanding of bone growth mechanoadaptation.
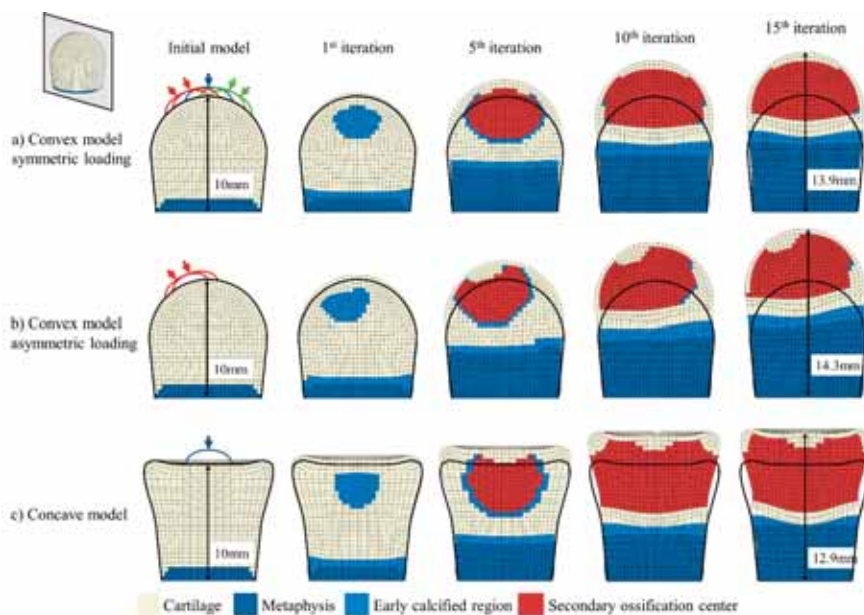
Figure caption: Endochondral ossification of the epiphyseal cartilage. Cross-sections of the 3D geometries are shown. a) symmetric loading on a convex geometry, b) asymmetric loading on a convex geometry, c) axial loading on a concave geometry. The growth plate and articular cartilage were preserved.

References:
1.   S. Sundaramurthy, J. J. Mao, Modulation of endochondral development of the distal femoral condyle by mechanical loading, Journal of orthopaedic research 24 (2006) 229–241.
2.   D. R. Carter, M. Wong, The role of mechanical loading histories in the development of diarthrodial joints, Journal of Orthopaedic Research 6 (1988) 804–816.

C2.3

Effect of osteoporosis severity on the acetabular fracture during a sideways fall: A finite element study

Shahab Khakpour[1], Petri Tanska[2], Mika E. Mononen[2], Rami Korhonen[2], Timo Jämsä[1]

1   University of Oulu, Medical Faculty, Medical imaging, physics, and technology, Oulu, Finland
2   University of Eastern Finland, Department of Applied Physics, Kuopio, Finland

1.5 million osteoporotic fractures happen per year [1] and every one of two women and one of three men has an osteoporotic fracture history [2]. While the incidence of low-energy hip fracture has been declined in the developed country during the last decades, the incidence of low-energy acetabular fracture has been increased notably [3]. Low-energy acetabular fracture generally happens during a non-traumatic and mostly is observed in the geriatric population who mostly suffer from osteoporosis [3]. Owing to a higher incidence, previous research mostly focused on hip fracture rather than acetabular fracture and there is a research gap in the biomechanics of the low-energy acetabular fracture [4]. This study applied a CT-based (median male) finite element analysis to investigate the effect of cortical and trabecular osteoporosis severity bone on the acetabular fracture. Bones were modeled as heterogeneous strain-rate-dependent materials with different behavior in tension and compression. Also, pelvic soft tissues and a simple representation of whole-body segments were included to enhance the model prediction. The body configuration was changed from supine (CT- imaging) to sideways fall. The obtained model was meshed and analyzed in LS-DYNA. Results showed that while trabecular osteoporosis affects only trabecular bone failure, cortical osteoporosis influences both cortical and trabecular bone failure substantially. Whereas the type of acetabular fracture at low severity of osteoporosis is elementary, it will be changed to more complicated fracture patterns(associated) at the higher severity levels of osteoporosis. This study suggests that at the early stage of osteoporosis, treatment should be focused on the trabecular bone, and at a more advanced stage, the treatment should target the cortical bone to prevent the low-energy acetabular fracture. Also, according to the results, early action against acetabular osteoporosis can decrease the risk of the more complicated (associated) fracture types.

References:
[1]   C. Cooper et al., "The crippling consequences of fractures and their impact on quality of life," Am. J. Med., vol. 103, no. 2 A, 1997, doi: 10.1016/s0002-9343(97)90022-x.
[2]   E. Seeman and J. A. Eisman, "7: Treatment of osteoporosis: Why, whom, when and how to treat," Med. J. Aust., vol. 180, no. 6, pp. 298–303, 2004, doi: 10.5694/j.1326-5377.2004.tb05931.x.
[3]   T. A. Ferguson, R. Patel, M. Bhandari, and J. M. Matta, "Fractures of the acetabulum in patients aged 60 years and older: An epidemiological and radiological study," J. Bone Jt. Surg. - Ser. B, vol. 92, no. 2, pp. 250–257, 2010, doi: 10.1302/0301-620X.92B2.22488.
[4]   C. Cooper, Z. A. Cole, C. R. Holroyd, and S. C. Earl, "Secular trends in the incidence of hip and other osteoporotic fractures," pp. 1277–1288, 2011, doi: 10.1007/s00198-011-1601-6.

C2.4

Biomechanical characterization of bone marrow lesions using a combined experimental and computational approach

Oluwasegun Kayode[1], Nagitha Wijayathunga[1], Gavin Day[1], Marlene Mengoni[1], Ruth Wilcox[1]

1   Institute of Medical and Biological Engineering, University of Leeds, Leeds, United Kingdom

Introduction: Osteoarthritis (OA) is a degenerative disease affecting joints and is one of the lead causes of pain and disability in adults [1]. Bone marrow lesions (BMLs) are one feature of subchondral bone involvement in OA. BMLs are radiological features defined on fat suppressed T2 MRI images as areas of ill-delineated hyper signal intensities in comparison to unaffected areas [2] suggesting a change in tissue content and properties in the affected regions. Both bone volume fraction and mineral density within the lesion have been seen to alter [3], but there have been no studies investigating the material properties of the bone within these lesions.

The aim of this study was to characterize the mechanical elastic properties of BMLs, using a combined experimental and computational approach.

Methods: Six human cadaveric patellae from donors aged 56-76 were used in this study; all exhibited BML regions under MRI. Osteochondral bone plugs were taken from non-BML (n = 6) and BML (n = 7) regions within the patellae, with guidance from the MRI scans. Micro computed tomography (μCT) images were obtained for each bone plug at 82μm resolution and the plugs were then tested under uniaxial compression until failure.

Images were segmented in ScanIP (ScanIP P-2019.09, Synopsys-Simpleware), downsampled to 164μm and models were generated such that each voxel greyscale value was proportional to the bone volume fraction in that region. Finite element (FE) models of each bone plug were created, and each bone element was assigned individual material properties based on the assigned greyscale value. An optimization toolkit [4] was used to calibrate the greyscale density–material property relationship for both the BML and non-BML groups such that; $\llbracket Young's\ Modulus\rrbracket_{(bone\ element)} (GPa) = \alpha \times \llbracket Assigned\ Greyscale\rrbracket_{(bone\ element)} (0\text{-}255)$.

Results and discussion: Using the specimen-specific FE models, different α values were found for the BML and non-BML group, with the BML group having a lower α, as shown in Figure 1.
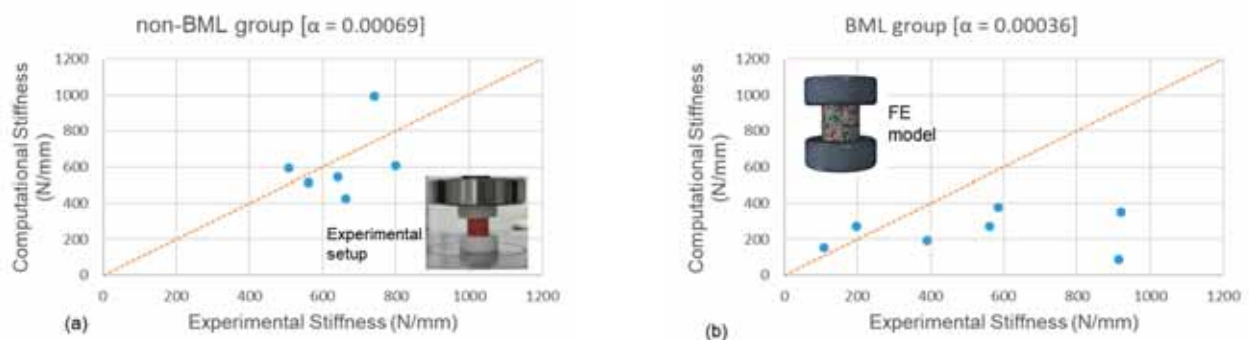
Figure 1: (a) calibration graph for non-BML group and experimental setup, (b) calibration graph for BML group and example finite element model.

This suggests a different greyscale-stiffness relationship in the BML region, which may be due to poorly organized or less stiff bone tissue in comparison to non-BML regions. The poor agreement between computational and experimental stiffness in the BML group may also account for the difference in α values.

References:
(1)   Arthritis Research UK. State of Musculoskeletal Health, 2018.
(2)   Roemer et al. Osteoarthritis Cartilage, 2009.
(3)   Hunter at al. Arthritis Res Ther, 2009.
(4   Mengoni, M. eprints.whiterose.ac.uk, 2015.

C2.5

Assessment of local displacement predictions generated by MicroFEMs of trabecular bone cores retrieved from the shoulder

Jonathan Kusins[1], Nikolas Knowles[2], Melanie Columbus[2], George Athwal[3], Louis Ferreira[1]

1   Western University, Mechanical and Materials Engineering, Canada
2   University of Calgary, Cumming School of Medicine, Calgary, Canada
3   Western University, Schulich School of Medicine and Dentistry, London, Canada

Micro finite element models (µFEM) of the shoulder can be used to evaluate bone strength which is important for preclinical joint replacement design evaluation [1]. However, the predictive outcomes generated by µFEMs are influenced by underlying modelling assumptions. Therefore, experimental validation is necessary to ensure clinically relevant conclusions are achieved [2]. The aim of the current study was to assess local displacements predicted by shoulder trabecular bone core µFEMs compared to full-field experimental displacements quantified using digital volume correlation (DVC) techniques.

Six humeral osteotomies were collected from patients that had undergone total shoulder arthroplasty due to end-stage osteoarthritis. Cubic trabecular bone cores (edge length of 5.5 mm) were excised from the humeral osteotomies. Stepwise compressive loading was performed within a microCT scanner (image resolution = 4.75 µm) and volumetric images were captured at varying loading steps (Figure 1). DaVis DVC was used to quantify full-field experimental local displacements.

MicroFEMs with voxel sizes of 20 and 40 µm were generated for each trabecular bone core using the pre-loaded microCT image. Homogeneous and heterogeneous material properties were assigned. Local DVC displacements were prescribed to the medial and lateral surfaces [3]. Linear regression was performed on the pooled results to quantify the agreement between µFEM predicted local displacements to the experimental results. Comparisons between experimental and µFEM predicted forces were also computed.

The µFEMs were able to replicate the experimental local displacements with high accuracy (slope ≥ 0.85, R2 ≥ 0.88) (Table 1). At a voxel size of 20 µm, higher errors in axial force were predicted for all six µFEMs using homogeneous material properties (225% mean difference [range: 85-385%]) compared to heterogeneous material properties (85% mean difference [range: 4-235%]). Similar trends were observed with a voxel size of 40 µm.

The results of this study indicate that accurate local displacement predictions can be obtained with shoulder µFEMs generated using either homogeneous or heterogeneous material properties with varying voxel sizes. These findings may be useful to reduce the computational resources associated with the µFEM approach, but other outcome measures (e.g., yield strength, trabecular strains) should also be evaluated in this context. The accuracy of predicted axial force was improved with the use of heterogeneous material properties, but the relative error was still high (85% difference). Future work should investigate varying methodologies associated with heterogeneous material mapping at the tissue-level, to improve these relationships. Nevertheless, continual development of shoulder µFEMs combined with full-field DVC validation techniques can improve the predictive capabilities to efficiently screen joint replacement designs prior to clinical adoption.
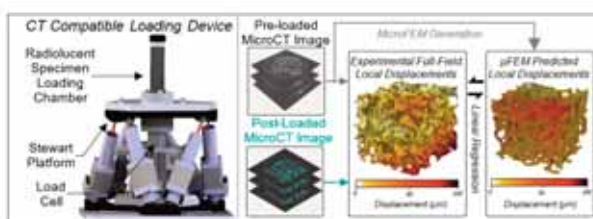
Figure 1: A CT-compatible loading device was used to apply stepwise compressive loads to trabecular bone cores within a microCT scanner. Full-field experimental local displacements were quantified using DVC and compared to µFEM predictions generated from corresponding pre-loaded microCT scans.

Table 1: Pooled linear regression results comparing predicted µFEM local displacements to experimental DVC results.

Material Properties Assigned to µFEM	Voxel Size [µm]	Slope (m)	Intercept (b) [µm]	Coefficient of Determination (R²)	Root Mean Square Error [µm]
Homogeneous	20	0.86	-1.1	0.90	10.9
	40	0.89	-1.5	0.91	10.2
Heterogeneous	20	0.85	-2.3	0.88	11.4
	40	0.88	-2.5	0.91	10.6

References:
[1]   Chevalier et al. J Biomech 2016.
[2]   ASME Verification & Validation 40 – 2018.
[3]   Chen et al. J Mech Behav Biomed Mater 2017.

C2.6

Variations in the osteocyte lacuna morphology result in a nonuniform local bone tissue strain distribution

Haniyeh Hemmatian[1 2 3], Astrid D. Bakker[2], Jenneke Klein-Nulend[2], G. Harry van Lenthe[1]

1   KU Leuven, Department of Mechanical Engineering, Biomechanics section, Leuven, Belgium
2   Vrije Universiteit Amsterdam, Department of Oral Cell Biology, Academic Centre for Dentistry Amsterdam (ACTA), Amsterdam, Netherlands
3   University Medical Center Hamburg-Eppendorf, Department of Osteology and Biomechanics, Hamburg, Germany

State-of-the-art imaging techniques have implicated that bones' mechanosensing cells, osteocytes, play a major role in bone maintenance via orchestrating bone remodeling. Osteocytes are embedded in lacunae, connected via canaliculi and form a lacuno-canalicular network that allows osteocytes to sense and transduce mechanobiological signals. We previously found links between osteocyte mechanotransduction and its lacuna network architecture1. Yet, it remains unknown how osteocyte lacuna network architecture may affect the micromechanical environment of osteocytes. This study aimed to quantify the effect of alterations in osteocyte lacunar morphology on peri-lacunar bone tissue strains. To this end, the actual lacunar network morphology in fibulae of six young-adult (5-month) and six old (23-month) mice, quantified by high-resolution micro-computed tomography, was related to microscopic strains, analyzed by micro-finite element (μFE) modeling2. μFE models of the bone extra cellular matrix (ECM), the pericellular matrix (PCM) and osteocyte cell bodies (OCYs) were created by a direct conversion of μCT-image isotropic voxels with a size of 0.7 μm to 8-node linear hexahedral elements (Fig 1A). The micromechanical environment of each osteocyte and its surrounding matrix was characterized in terms of effective strains3 (EFF) and strain amplification under 1% uniaxial compressive strain (Fig 1B,C). Our analysis determined that increased lacuna volume from 100-200 μm3 to 500-600 μm3 led to 12.6% increase in maximum effective strains in OCYs, 9.6% in PCM, and 5.3% in ECM. Lacunae which are more closely aligned with the longitudinal axis of the bone (< 8°) are exposed to 8% lower strains in OCYs, 6.5% in PCM, 4.2% in ECM than lacunae with a deviation in orientation above 8 degrees. Moreover, by increasing lacuna sphericity from 0-0.5 to 0.7-1, maximum effective strain decreased by 25% in OCYs, 23% in PCM, and 13% in ECM. We further showed that due to the presence of larger and more elongated lacunae in young mice, local bone tissue strains are on average 5% higher in the vicinity of lacunae and their osteocytes compared to lacunae in old mice. Understanding how changes in lacunar morphology affect the micromechanical environment of osteocytes presents a first step in unraveling their potential role in the amount of strains that the osteocyte cell bodies are exposed to.
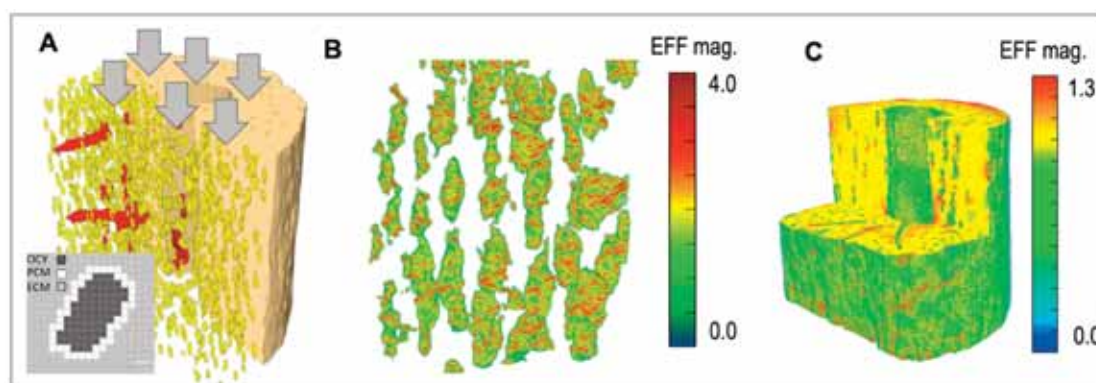
Fig 1. (A) Representation of the micro-FE model of a fibula midshaft. (B) Effective strain distribution over osteocytes. (C) Effective strain distribution over the extracellular matrix. Scale bar=100 μm.

References:
1.   Hemmatian et al., 2018.
2.   van Rietbergen et al., 1995.
3.   Pistoia et al., 2002.

C2.7

Comparison of patient femoral quantitative computed tomography measures calibrated at different distances to isocenter

Carla Winsor[1]

1   University of Wisconsin-Madison, Mechanical Engineering, Madison, United States

Computed tomography (CT) Numbers in Hounsfield Units [HU] change as a function of positioning within the CT scanner1. Scanning an inline bone mineral density (BMD) phantom with the patient is the clinical gold standard for calibrating CT-based patient-specific finite element models. Including a phantom in the x-ray path is known to affect BMD measurements2. This study compared patient-specific femoral strength (FS) and BMD results derived using calibration information captured at three different distances from the isocenter: under the patient (UP), pelvis distance (OR), and head distance (IR). Five patients and a Model 3 BMD inline phantom (Mindways, Austin, TX, USA) were scanned at the University of Wisconsin-Madison hospital on a GE LightSpeed series CT scanner at 120 kVp with a standard reconstruction kernel. A Model 062M phantom (CIRS Inc., Norfolk, VA, USA) with bone density reference plugs was scanned on a GE Revolution CT scanner at Queen's University in Kingston, Ontario, CAN. Calibration data were segmented in Mimics v.23 (Materialise, Leuven, Belgium) and CT Number [HU] to BMD [mg/cc] relationships were derived by plotting BMD [mg/cc] on the x-axis and measured CT Numbers [HU] on the y-axis, and linearly regressing. The calibration equation was then rearranged to solve for BMD [mg/cc] in terms of CT Numbers [HU]. The OR calibration equation was y [mg/cc] $=1.011*x$ [HU] -34.99, and the IR calibration equation was y[mg/cc]$=1.036*x$[HU]-56.43. When compared with UP calibration results, OR and IR calibration resulted in average differences across patients of 7.48±8.06% and 14.4±11.9% in FS [N] (using a Maximum Principal Strain failure criterion, tension limit 0.73% and compression limit 1.04%) and 7.34±7.74% and 17.1±9.03% in composite integral BMD [mg/cc] contained within the patient model (Figure 1). Results derived from OR or IR were not statistically significantly different from the results from UP calibration when evaluated by a paired t-test.
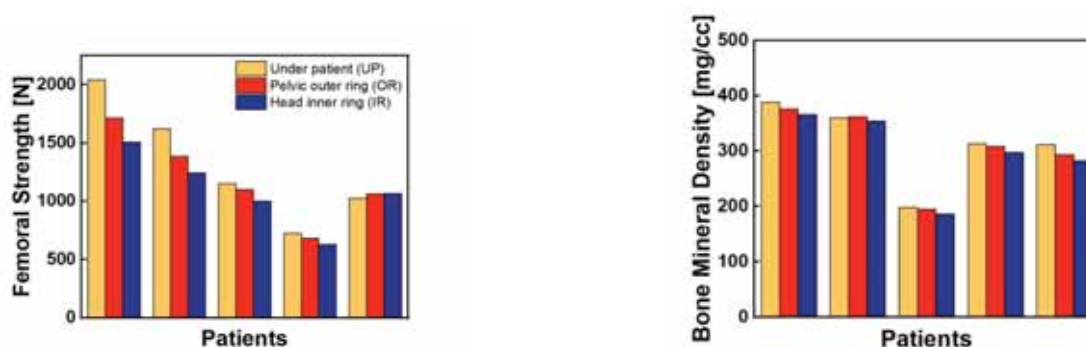
Figure 1: Patient-specific femoral strength [N] and composite integral bone mineral density [mg/cc] results calculated using under the patient (UP), pelvis distance (OR), and head distance (IR) calibration data.

References:
1.   Szczykutowicz TP, et al. Am J Roentgenol. 2017;208(5):1064-1072. doi:10.2214/AJR.16.17215
2.   Brown JK, et al. J Clin Densitom. 2017;20(2):216-225. doi:10.1016/j.jocd.2015.11.001

C2.8

An automated approach for 3D reconstruction of femur from CT data via pixel clustering

Dipannoy Das Gupta[1], Mahmuda Naznin[1], Tanvir Faisal[2]

1   Bangladesh University of Engineering & Technology, Computer Science & Engineering, Dhaka, Bangladesh
2   University of Louisiana at Lafayette, Mechanical Engineering, Lafayette, United States

3D reconstruction from 2D image dataset is a fundamental task in image based computational biomechanics. 3D reconstruction of femur from its DICOM dataset is primarily a manual process, which is a setback in computational modeling such as Finite Element Analysis (FEA). Furthermore, it requires expensive biomedical image processing software, skill set and considerable time. Hence, we are introducing a coupled automated 3D reconstruction and mesh generation process to resolve these issues. Currently, available works are too generic and scattered while our proposed process represents a specific solution to this problem. To execute this task, we have designed a pixel-based clustering method to dig out the femur profile that eventually propagates point cloud.

Here, pixel clustering method was employed to collect femur features to generate 3D bone geometry (Figure 1(a)). A cluster can be stated as a disjoint set of pixels where two sets are disconnected. The clusters were created horizontally and vertically across the CT slices to keep the proximity of the neighbors as close as possible. Concurrently, it ensured smaller cluster size, which prevented the influence of outliers. Each cluster had a particular measure of central tendency. However, due to the intersection of this measure found in regions like femoral head, acetabulum socket, it failed to provide optimal clustering for those regions. Hence, the shapes of the slices were configured to make femoral head clusters larger. Thus, a complex shape like the femoral head was distinguished from its neighboring pelvis and acetabulum. This procedure was applied to the distal part of the femur to remove the patella. Furthermore, the pixel clustering method can efficiently eradicate isolated pixels. The method is further beneficial as it is able to preserve the actual pixel value while extracting femur profile, and thereby facilitating proper mesh generation, which was later accomplished by mesh generation algorithm [1, 2].

With our proposed method, we can generate the perfect 3D shape of femur (Figure 1(b)). Obtaining the femoral head shape was a challenging task because of its position. Nevertheless, our approach can identify non-femoral pixel positions and turn them into "don't care". Moreover, its noise removal rate is approximately 100%. Yet, some expected pixels are found missing which are needed to be populated.

We have developed a CT-based image processing framework for 3D reconstruction and subsequent mesh generation of a femur. We find the preliminary results promising. We are exploring further to use this technique efficiently for patient specific FE modeling for predicting femoral fracture.
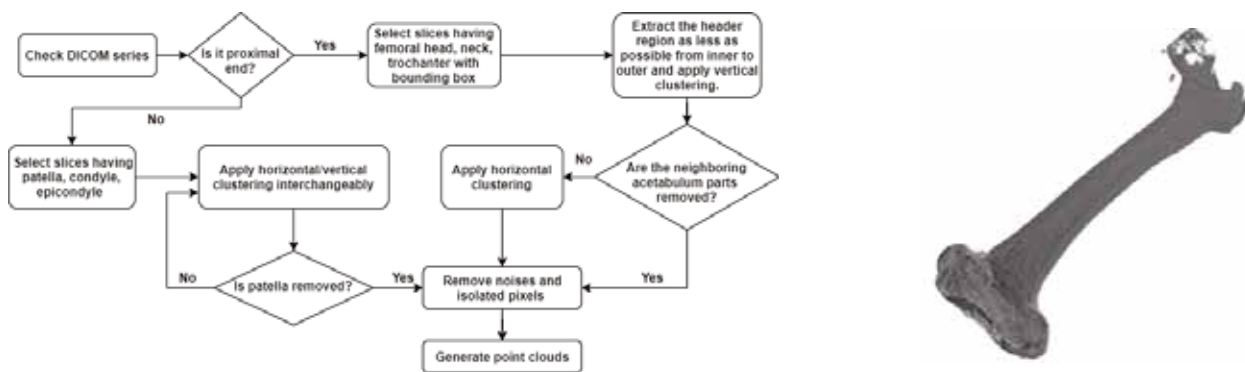
Figure 1: (a) The flow diagram of pixel clustering method and (b) reconstructed femur from DICOM images

References:
1.   Stéfan van der Walt et al., scikit-image: Image processing in Python (2014).
2.   Dawson-Haggerty et al., "trimesh", version-3.2.0 (2019).

C3.1
Recent progress in mathematical modelling of tumor-induced angiogenesis

Tomas Alarcon[1]

1   *ICREA-Centre de Recerca Matematica, Cancer Modelling Group, Bellaterra, Spain*

In this talk, I will review recent progress in mathematical modelling of tumour-induced angiogenesis, i.e. the process whereby tumours acquire a vascular network which supplies them with enough nutrients to support their growth. I will focus on two different issues. First, I will report our results regarding a new multiscale model of early pattern formation in angiogenesis, where we explore the role of complex behaviour of the endothelial cells (i.e. the cells that make up blood vessels) regarding overtaking and phenotype switch. I will then move on to fully formed angiogenic networks to report recent results of how the structural abnormalities of such networks profoundly affect the patterns of blood flow within them and provide ground for the emergence in intra-tumoral heterogeneity.

C3.2
Patient-specific tumor forecasting through imaging-based mathematical modeling

David Hormuth Hormuth[1], Ernesto A.B.F. Lima Lima[1], Guillermo Lorenzo Lorenzo[2], Chengyue Wu[1], **Thomas Yankeelov**[1] [3]

1   The University of Texas at Austin
2   University of Pavia
3   MD Anderson Cancer Center

The focus of our team's efforts is to develop biomathematical and biophysical models of tumor initiation, growth, and invasion to establish a sound clinical-computational framework describing the hallmarks of cancer, and to use this knowledge to develop tumor forecasting methods to improve diagnosis and optimize treatment for the individual patient.

In this presentation, we will discuss: 1) building mechanism-based models of tumor growth and treatment response, 2) calibrating those models with time-resolved imaging data, and 3) applying the resulting experimental-computational methodology to problems in clinical oncology. More specifically, we will provide five short vignettes on ongoing efforts in our lab to:
1) predict the response of breast cancer to neoadjuvant therapy using quantitative MRI data
2) predict the response of brain cancer to radiation therapy using quantitative MRI data
3) develop image-guided computational fluid dynamics for characterizing tumor hemodynamics
4) build a model of breast cancer response to treatment incorporating in vitro and in vivo data
5) predict the spatiotemporal distribution of radiolabeled liposomes for treating of brain cancer

For each vignette, we will begin by developing the model equations, and then describing the data types required by the models. Then, we will summarize how the data are processed and employed to calibrate and initialize the mathematical models. We will continue by illustrating the types of predictions that our models enable for each individual patient. Finally, we will evaluate the model predictions by comparing them to clinical outcomes and enumerate areas for improvement.

A re-occurring theme in the presentation will be how integrating advanced imaging techniques with patient-specific bio-mathematical models enable patient-specific predictions of therapeutic outcomes. In this way, we hope to assist the field of clinical oncology to move away from population-based assessments to patient-specific predictions.

C3.3
Multiphysics modeling of tumoral spheroid evolution

Ana Carrasco Mantis[1], *Jose Antonio Sanz-Herrera*[1], *Manuel Doblaré*[2], *Ignacio Ochoa*[2], *Teodora Randelovic*[2], *Héctor Castro Abril*[2]

1   University of Seville, Spain
2   University of Zaragoza, Spain

In recent years, spheroids have become popular in modulating biological experiments. They have a unique 3D quasi-spherical morphology and are used as a useful surrogate model of many cell processes that include signaling and communication [1]. Besides the interaction with external cues and diffusion mechanisms of nutrients, oxygen or drugs, their morphology influences on cells proliferation, differentiation, migration, cell death or changes in the phenotype. In particular, spheroids represent a versatile tool in the study of the cancer evolution and their response to treatments [2].

In this paper, we show firstly the experimental tests of 1000-cell spheroids made from two glioblastoma cell lines with clearly different phenotypes: U-251 MG and U-87 MG. Glioblastoma (GBM) is a highly heterogeneous tumor that originates in glial cells and is characterized by a strong invasive capacity and proliferation. They can promote necrosis, giving rise to areas of high cell concentration, close to a necrotic core, known as 'pseudopalisades' and also microvascular hyperplasia.
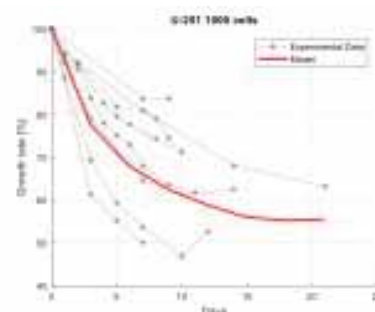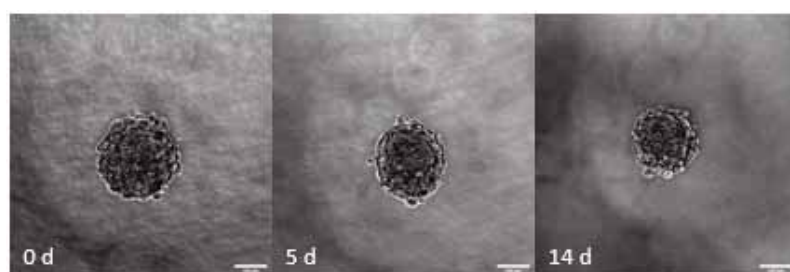
Figure 1. Left: images of the evolution of U-251 1000 cells line in 0, 5, and 14 days. Results show a reduced cross section evolution over time. Right: plot of the cross section evolution of the spheroid when comparing the results of the model versus the reported experimental range.

Second, we present a mathematical model that considers the most important phenomena that take place in the referred experiments, which include GBM spheroids immersed in cell culture medium. The coupled physics of the model accounts for: (i) diffusion of nutrients and oxygen from the medium through the spheroid, (ii) cell growth and death dynamics, and (iii) cell active contractility. The mathematical model is implemented in a finite element framework. The output of the simulation allows quantifying, along the spheroid domain, the evolution of nutrients concentration, cell dynamics, spheroid contractility and cells' active stresses. After a proper model calibration eventually based on the data from literature [3], our simulations are able to capture both the expanding and decreasing (contractile) profile of the spheroids (see fig. 1). These findings will allow investigating and quantifying, in silico, some relevant issues in GBM tumor evolution.

References
1.   Ayuso et al, PloS one, 10 (10), e0139515, 2015.
2.   Bull et al, PLoS computational biology, 16 (8), e1007961, 2020.
3.   Ayensa-Jiménez et al, Scientific Reports, 10 (1): 1-21, 2020.

C3.4
The effect of a necrotic core on the interstitial fluid pressure in solid tumors

Hooman Salavati[1 2 3], *Pim Pullens*[4 5], *Wim Ceelen*[1 3], *Charlotte Debbaut*[2 3]

1   Ghent University, Department of Human Structure and Repair, Ghent, Belgium
2   Ghent University, IBiTech– Biommeda, Ghent, Belgium
3   Cancer Research Institute Ghent (CRIG), Ghent, Belgium
4   University Hospital Ghent, Department of Radiology, Ghent, Belgium
5   Ghent University, Ghent Institute of Functional and Metabolic Imaging (GIFMI), Ghent, Belgium

Previous theoretical and experimental research showed that the interstitial fluid pressure (IFP) is typically higher in solid tumors compared to normal tissue, resulting in a poor prognosis and treatment resistance. Elevated IFP is correlated with disorders in the tumor microenvironment, such as tumor-related angiogenesis and solid hypertension. These disorders are often accompanied by cellular necrosis and the formation of a necrotic core in the central region of tumor [1]. In this study, we present a 3D computational fluid dynamics modelling approach to better understand the link between the presence of a necrotic core and the IFP in solid tumors.

The interstitial fluid flow throughout tumors was simulated in COMSOL Multiphysics (Inc., Burlington) using idealized spherical 3D geometries with total (D) and necrotic core diameters (Ø) ranging between 3-16mm and 1.5-8mm, respectively (Fig.1a). Furthermore, a realistic 3D geometry of a peritoneal necrotic tumor of a mouse was obtained from MRI T2-weighted imaging (Bruker, Billerica) (Fig.1c). The interstitial flow in the tumors was described by Darcy's law and the fluid continuity equation, in which the interstitial fluid source was expressed by Starling's law accounting for high tumor vascular permeability [2]. This source term was set to zero (no functional blood vessels) in the necrotic core. A parameter study allowed investigating the impact of the necrotic core on the IFP (Fig.1b & d).

The results show that IFP values noticeably decrease in small spherical tumors (D<1cm) due to the presence of a necrotic core (Fig.1b). Moreover, a larger necrotic core reduces the IFP more profoundly. Although the highest IFP in tumors does not directly correlate with the tumor size, the IFP profile is considerably affected in the periphery of the tumors by the tumor size and necrotic core presence (Fig.1b). However, in large tumors (D>1cm) IFP is only sensitive to the necrotic core when necrosis extends to 80% of the tumor volume. Fig.1d shows the IFP profile in the middle of the realistic tumor (along the dashed line in Fig.1c). The presence of the necrotic core clearly reduced the highest IFP values in the center of the tumor. Interestingly, results showed that even a small necrotic core can alter the IFP profile depending on the tumor and necrotic core shapes (Fig.1d).

The presence of a necrotic core can noticeably affect the IFP, and this may affect anticancer drug delivery. Therefore, current work highlights the importance of a comprehensive study on the properties and extent of necrotic core in solid tumors.
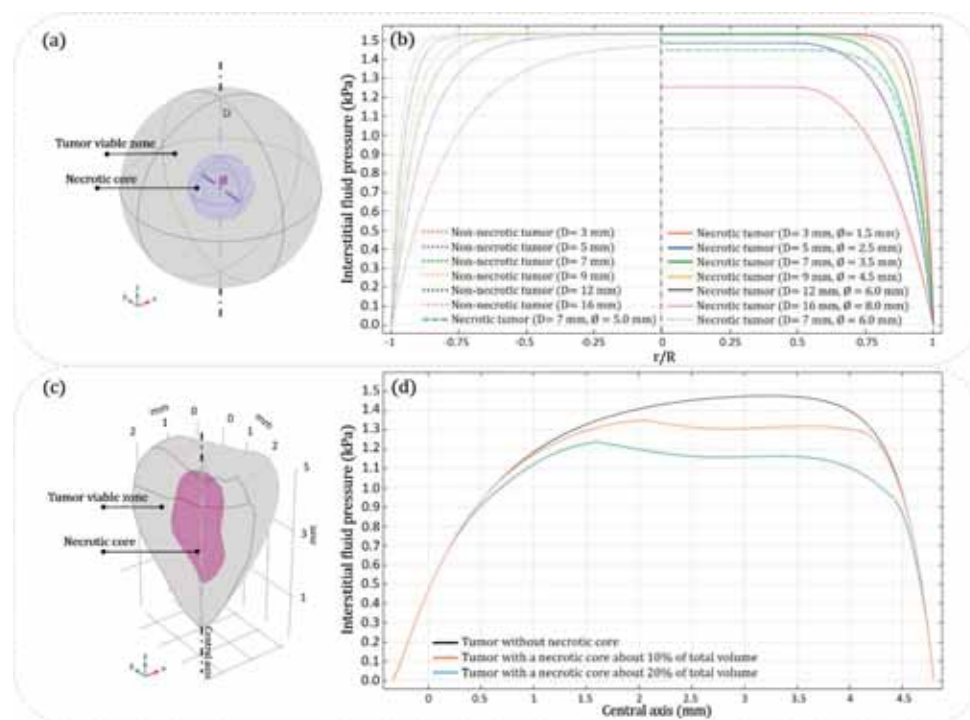
Figure caption: Fig1.The impact of a necrotic core on the IFP profile in solid tumors: (a) spherical tumor geometry (b & d) the effect of necrotic core presence on IFP (c) realistic tumor geometry.

References:
[1]   Baxter (1990).Microvasc.Res.40(2):246-263.
[2]   Steuperaert (2019).Drug Deliv.26(1):404-415.

C3.5
Computational epigenetics: simulating the acquisition of drug resistance in glioblastoma

Marina Pérez-Aliacar[1 2], *Jacobo Ayensa-Jiménez*[1 2], *Teodora Randelovic*[1 3], *Mohamed H. Doweidar*[1 2 4], *Manuel Doblaré*[1 3 4]

1   Aragon Institute of Engineering Research (I3A), Zaragoza, Spain
2   University of Zaragoza, Mechanical Engineering , Zaragoza, Spain
3   Aragon Institute of Health Research (IISA), Zaragoza, Spain
4   Centro de Investigación Biomédica en Red en Bioingeniería,Biomateriales y Nanomedicina (CIBER-BBN), Spain

Glioblastoma (GBM) is the most frequent primary brain tumour. Unfortunately, it is also the most lethal and recalcitrant, with a 5-year survival rate of only 5% [1]. Despite being a rare tumour, it is one of the most challenging malignancies to treat in oncology. Little advances have been made in the last years towards prolonged survival of GBM patients, despite the considerable effort.

The current standard of care for this tumour is surgical resection, followed by radiotherapy and concomitant and adjuvant chemotherapy. Temozolomide (TMZ) is the only chemotherapeutic drug currently used for GBM treatment. However, at least 50% of patients treated with TMZ develop resistance and do not respond to the treatment [2]. Understanding the mechanisms that lead to resistance acquisition is crucial for the understanding of the process and for the development of optimal treatment strategies.

Mathematical models are powerful tools to better understand complex mechanisms, as those governing the acquisition of resistance in GBM, and provide a cheap and quick way of testing hypothesis or what if situations. Although the evolution of GBM has already been simulated with continuum models [3,4], these existent models do not consider how cells keep in memory their past states and adapt to the changes in the environment. That is, they are not able to reproduce the epigenetic changes that lead to TMZ resistance.

Based on the concept of internal variables, and inspired by the ideas of continuum mechanics, we propose a new approach for modelling GBM evolution when treated with TMZ, capturing the change in cell behaviour that occurs during the acquisition of resistance. Our model is able to reproduce the trends that have been experimentally observed in literature, where tumour cells initially respond to TMZ and then resume proliferation as they become resistant [5], and could eventually be used in the optimisation of the dose and timing of therapies.

References:
[7]   Alexander and Cloughesy (2017) J. Clin. Oncol., 35(21), 2402-2409.
[8]   Lee (2016), Gen. & Dis., 3(3), 198-210.
[9]   Zade et al. (2020), Comput. Meht. Programs. Biomed.193, 105443.
[10] Ayensa-Jiménez et al. (2020), Sci. Rep., 10(1),1-21.
[11] Ricard et al. (2007), Ann. Neurol., 61(5) 484-490.

C4.1

Assessing the role of hemodynamics on tissue engineered vascular graft growth and remodeling: a tale of two scaffolds

Stephanie Lindsey[1], John Kelly[2], Jason Szafron[1], Christopher Breuer[2], Jay Humphrey[3], Alison Marsden[4]

1   Stanford University, Pediatric Cardiology and Institute for Computational & Mathematical Engineering, Stanford, United States
2   Nationwide Children's Hospital, Center for Regenerative Medicine, Columbus, United States
3   Yale University, Department of Biomedical Engineering, New Haven, United States
4   Stanford University, Pediatric Cardiology and Bioengineering; Institute for Computational and Mathematical Engineering, Stanford, United States

Introduction: Single ventricle palliation requires the use of a vascular graft to connect the inferior vena cava (IVC) to the pulmonary arteries. While this procedure typically employs prosthetic grafts, tissue engineered vascular grafts (TEVGs) offer a promising alternative, as they possess the ability to grow and remodel. The propensity for TEVGs to stenose[1], however, impedes their acceptance as an industry standard. Here, in linear studies involving grafts consisting of PGA (polyglycolic acid) versus a PLLA (poly-L-lactic acid) fibers, we study the role of hemodynamics in graft degradation, neotissue and stenosis formation. Using an ovine surrogate model, we compare the propensity of the PLLA scaffold to stenose to that of PGA models. MRI serial-imaging revealed that sheep implanted with PLLA TEVGs experience a more gradual stenosis that runs along a longer length of the graft and retains a larger luminal cross-sectional area. Because TEVG growth and remodeling is both an immuno-driven and mechano-mediated response[2], stenosed graft structure was hypothesized to be an initial driver of changing hemodynamic forces, with changes in pressure and wall-shear stress resulting from the stenosed TEVG geometry. Following endothelization of the TEVG neotissue, hemodynamic forces were hypothesized to play a large role in subsequent graft thinning and remodeling.

Methods: Anatomic models of the native vessel and TEVG region were reconstructed for each animal at 1-week, 6-week, and 1-year post TEVG implantation via SimVascular[3], with additional 12-week and 24-week timepoints added for a subset of PLLA animals. Image registration techniques were used to combine MRI and intravascular ultrasound measurements to capture wall thickening that led to TEVG stenosis. We performed subject-specific FSI simulations using the Arbitrary Lagrangian Eulerian method, in which both the vessel wall material properties and zero-dimensional boundary parameters were tuned to match in-vivo deformation, flow, and pressure data. Pre-stress and external tissue support was accounted[4][5].

Results & conclusions: Within six weeks of TEVG implantation, stenosis formation caused a 73%-88% reduction in PGA lumen cross-sectional area and a 25%-40% reduction in PLLA lumens. PGA grafts focal stenosis was consistently 77% of the way along the graph between the proximal and distal anastomosis and was met by a dramatic shift in pressure and wall shear stress magnitude, while PLLA grafts experienced small to negligible pressure and shear shifts with stenosis. Results confirmed that the immune response dominates early (1-week to 6-week) TEVG growth and remodeling, before giving way to a more hemodynamic-driven response. PLLA fibers degraded more slowly than their PGA counterparts, stress-shielding neotissue for a longer period of time and affecting surrounding IVC tissue mechanics.
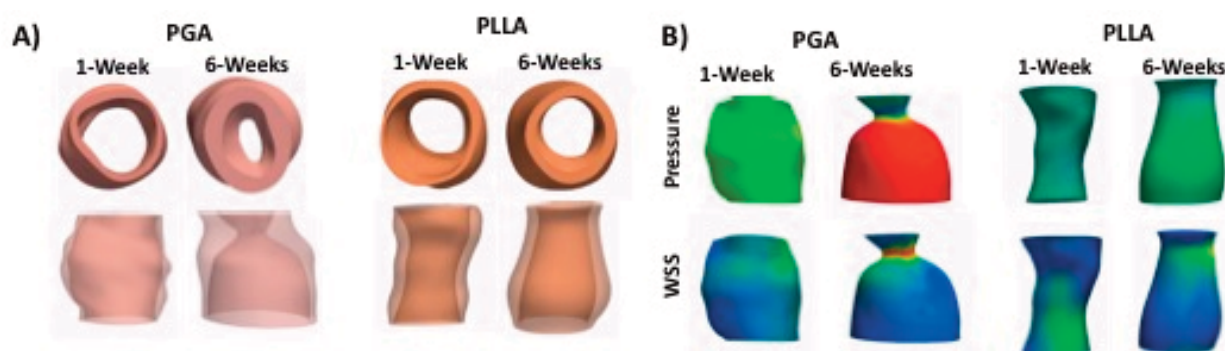
Figure caption: A) Representative 1-week to 6-week TEVG models' morphology (top-down and side-view) B) corresponding pressure and wall-shear stress (WSS) maps

References:
1.   Hibino+J.Thorac.Cardiovasc.Surg 2010;
2.   Szafron+Ann.Biomed.Eng 2018;
3.   Updegrove+Ann.BiomedEng2017; Hsu+FiniteElem.Anal.Des.2011; Moireau+BMMB2012

C4.2
Investigating biomechanic effects of rheumatic heart disease on the thoracic aorta

Hannah Cebull[1], Radhika Kulkarni[1], Ntobeko Ntusi[2 3 4], Craig Goergen[1]

1   Purdue University, Weldon School of Biomedical Engineering, West Lafayette, United States
2   Groote Schuur Hospital, Division of Cardiology, Cape Town, South Africa
3   University of Cape Town, Hatter Institute for Cardiovascular Research in Africa, Cape Town, South Africa
4   University of Cape Town, Cape Universities Body Imaging Centre (CUBIC), Cape Town, South Africa

While many aortic biomechanics studies exist, we aim to address the following gaps: 1) develop a clinically-feasible method of modeling blood flow, and 2) improve understanding of rheumatic heart disease's (RHD) affect on the thoracic aorta. RHD disproportionately affects low- to middle-income countries with minimal research conducted, compared to the global health burden of this disease. RHD research was the most underfunded when considering the global burden of the 16 major tropical diseases evaluated.1

RHD is diagnosed with echocardiography and cardiovascular magnetic resonance (CMR). RHD is associated with dysfunction of the valves and myocardium, often requiring valve replacement surgery to improve symptoms and extend survival. Valve lesion severity determines the type and level of surgical intervention. Therefore, there is a need to further characterize aortic valve lesions in RHD to understand which patients are most likely to benefit from surgery, while using affordable and accessible imaging modalities. We aimed to simulate the effects of RHD aortic valve lesions from CMR on the aortic wall using computational fluid dynamics (CFD).

This study used previously collected CMR data of RHD patients at Groote Schuur Hospital in Cape Town, South Africa. While many CFD studies use costly methods such as 4D flow MRI, we present a method using phase contrast-MRI (PC-MRI) and rapidly-acquired HASTE on 12 RHD patients and 12 matched controls (power analysis: α=0.05, β=0.2) using a 3T Siemens Skyra. We used SimVascular3 and MedViso4 for image analysis and simulation.

We segmented and obtained average flow from the CMR data. Outlet boundary conditions were estimated using Murray's law and age-matched blood pressure values. We ran each simulation using parabolic velocity inlet profiles and compared it to patient-specific velocity inlet profiles. Sensitivity analyses were conducted to ensure no artificial modeling effects influenced results.

We compared our patient-specific velocity inlet profiles to the commonly used parabolic profiles and found patient-specific more closely matched PC-MRI mean velocities. We also found altered wall shear stress (WSS) and blood flow patterns when comparing the two methods, as shown in Figure 1. Increased peak velocity (+22 cm/s) and WSS (+62 dyn/cm2) was observed in RHD compared to the control. Future work will include a deformable vessel wall and statistical analyses to quantify differences between using parabolic and patient-specific profiles and differences between RHD and non-RHD patients.
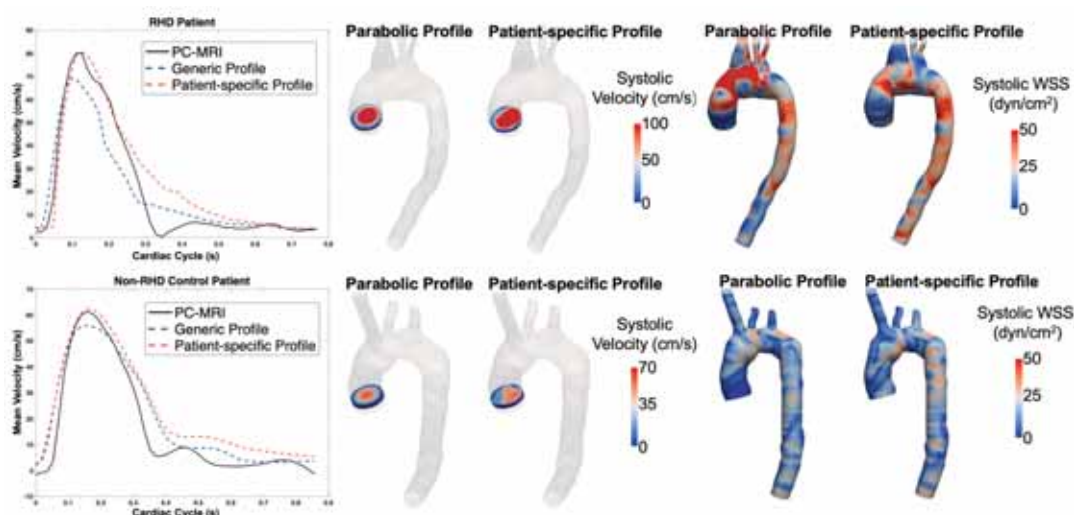
Figure 1: Representative CFD results of RHD patient with severe aortic regurgitation and one control patient.

References:
[1]   Marijon E, et al. N Engl J Med. 2017.
[2]   Updegrove A, et al. Ann Biomed Eng. 2017.
[3]   Heiberg E, et al. BMC Med Img. 2010.

C4.3

A pilot study with the National Children's Research Centre at Crumlin utilising computational fluid dynamics in the treatment of congenital heart disease

Malachy O'Rourke[1], Colin McMahon[2], Kevin Walsh[2], **Doireann Shaffrey**[1]

1   University College Dublin, Mechanical Engineering, Dublin, Ireland
2   National Children's Research Centre (NCRC), Paediatric Cardiology, Dublin, Ireland

Nearly 1% of children born today will be diagnosed with a form of congenital heart disease (CHD).[1] Despite the vast spectrum of morphology and variation that exists within each defect, personalised care for these patients is not yet possible. In recent years, computational fluid dynamics (CFD) has emerged as a useful technology that could potentially solve this issue. By incorporating patient-specific data into in silico simulations, clinicians can be provided with a detailed understanding of hemodynamic environments, therefore, improving their ability to plan effective interventions. Although existing literature shows great promise, widespread integration of CFD into clinical practice remains years away. A large effort from the bioengineering community is required in order to validate the accuracy of these methods.

In a pilot study between University College Dublin (UCD) and the National Children's Research Centre (NCRC) at Crumlin, a patient-specific CFD analysis was conducted for a pre-repair case of Tetralogy of Fallot, the most common form of complex CHD.[2] First, a 3D model of the pulmonary artery was reconstructed from computed tomography images using an open source software, 3D Slicer. A quantitative inspection with in vivo measurements confirmed the accuracy of the segmentation. A periodic velocity profile was extracted from the Doppler echocardiogram and applied as an inlet boundary condition. Blood was modelled as an incompressible, Newtonian fluid and a laminar viscosity model was imposed. Computational results for a variety of hemodynamic parameters were analysed and their corresponding significance was made apparent. For example, peak systolic velocity and pressure measurements were used to diagnose the severity of the pulmonary stenosis, in accordance with the European Society of Cardiology.[3]

Finally, in an effort to better represent in vivo behaviour, the compliance of the arterial wall was taken into account during a fluid-structure interaction (FSI) simulation. Discrepancies between the two computational methods were seen, although comparison with clinical data is required before a final conclusion can be made with regards to the accuracy of either method.

Overall, this study has illustrated that integration of a patient-specific computational analysis into the clinical treatment of CHD is possible using standard medical imaging modalities. A strong collaboration has been established between engineers at UCD and clinicians at the NCRC for work to continue into the future.

References:
[1]   Hoffman JL, Kaplan S. The incidence of congenital heart disease. J Am Coll Cardiol. 2002;39(12):1890-1900.
[2]   Chern, M.J., Wu, M.T. and Her, S.W., 2012. Numerical study for blood flow in pulmonary arteries after repair of Tetralogy of Fallot. Computational and mathematical methods in medicine, 2012.
[3]   Escardio.org. 2021. 4.2 - Quantification of severity. [online] Available at: ¡https://www.escardio.org/Education/Practice-Tools/EACVItoolboxes/Valvular-Imaging/Atlas-of-valvular-imaging/4-2-Quantification-ofseverity: :text=Continous%20Doppler%20evaluation%20of%20the,velocity%20rules%20out%20pulmonary%20st

C4.4

Development and case studies of a trans-Reynolds-number computational modeling approach for thrombosis and thromboembolism

Nicolas Tobin[1], *Keefe Manning*[1 2]

1   The Pennsylvania State University, Biomedical Engineering, University Park, United States
2   Penn State Hershey Medical Center, Surgery, Hershey, United States

Thrombosis and thromboembolism are potentially lethal processes that can lead to events such as stroke, pulmonary embolism, or the failure of a blood-contacting device such as artificial valves, stents, and blood pumps. The development of a computational fluid dynamics approach to model the growth and embolization of blood clots is detailed and simulations are presented of growth and embolization in a sudden expansion geometry at varying Reynolds number, highlighting the mechanical and biochemical insights made possible by such an approach.

Written as a solver in OpenFOAM [1], the modeling approach described includes a reduced-order representation of the coagulation cascade for the biochemical pathways leading to thrombosis, and a viscoelastic representation of the mechanics of thrombus material, allowing for the investigation of both formation and embolization of blood clots.

Case studies are presented of variations on an experimentally established clot growth problem in a sudden expansion, depicted in Figure 1 with a simulated clot. Previous work has observed clot growth in the recirculation region of this geometry in the case of laminar flow at a Reynolds number of 388. After training the model on this benchmark case, extrapolated behavior at varying Reynolds numbers indicates a strong trend toward clot volume decreasing with higher (laminar) Reynolds number, and no clot growth in transitional or turbulent flows, which is attributed to the transient nature of low-shear regions in the recirculation.

Additional simulations are presented of embolization in the same geometry. Simulations are initiated with a clot in the sudden expansion representative of one grown at the benchmark Re = 388 case, and the clot is then subjected to increased flow rates. At Reynolds number 5000, embolization is initiated with the clot being peeled away at the upper corner of the step. The clot then fully detaches from the wall and is carried by the flow out of the domain.

Figure 1: Sudden expansion geometry used in case study simulations, with red clot grown in recirculation region at Re = 388. Flow is from left to right.

References:
[1]   www.openfoam.org

C5.1

Random forest and wavelet for sleep scoring: a deeper analysis in age subjects and early-late sleep

Eugenia Moris[1], *Cecilia Forcato*[2], *Ignacio Larrabide*[1]

1   Pladema, Tandil, Argentina
2   Instituto Tecnológico de Buenos Aires, Laboratorio de Sueño y Memoria, Depto de Ciencias de la Vida, Capital Federal, Argentina

Sleep scoring it is a common method used by experts to monitor the quality and quantity of sleep in people [2]. But it is a time-consuming and labour-intense task [3]. Because of this, automatic sleep scoring has been recently studied using machine learning techniques. However, it is important to know whether the age of the patients influences sleep classification. As well as whether the use of early-late sleep can influence as well

We present a Random Forest algorithm that uses discrete wavelets to extract features from each epoch and classify them into Stage 1, Stage 2 or Slow Sleep Stage (SWS). The wavelets provide information in both the time and frequency domain. Only one channel (Fpz-Cz), from the public Sleep-EDF dataset, was used[1].

This data set provides two-night sleep records of 71 healthy patients aged 25-101 years, without any sleep-related medication. The subjects were divided into four groups, Group 1 (26-35 years), Group 2 (50-60 years), Group 3 (66-75 years) and Group 4 (85-101 years).

First, we train our random forest with one group and classify the rest, getting an idea of how age affects classification. As a result, we observe that classification is better when the random forest is trained with young subjects. However, it is interesting to note that with older subjects, Stage 1 results are improved. On the other hand, the SWS stage declines significantly with increasing age.

Finally, we trained with early sleep (first 4 hours) and late sleep (last 4 hours) separately using only Group 1. In this case we appreciate that the classification improves when the model is trained with early sleep, even classifying late stage.

We conclude that, in general, classification improves if we train our model using younger subjects, even if testing is performed on older subjects. Moreover, it is better to look for early sleep if we want a higher accuracy.
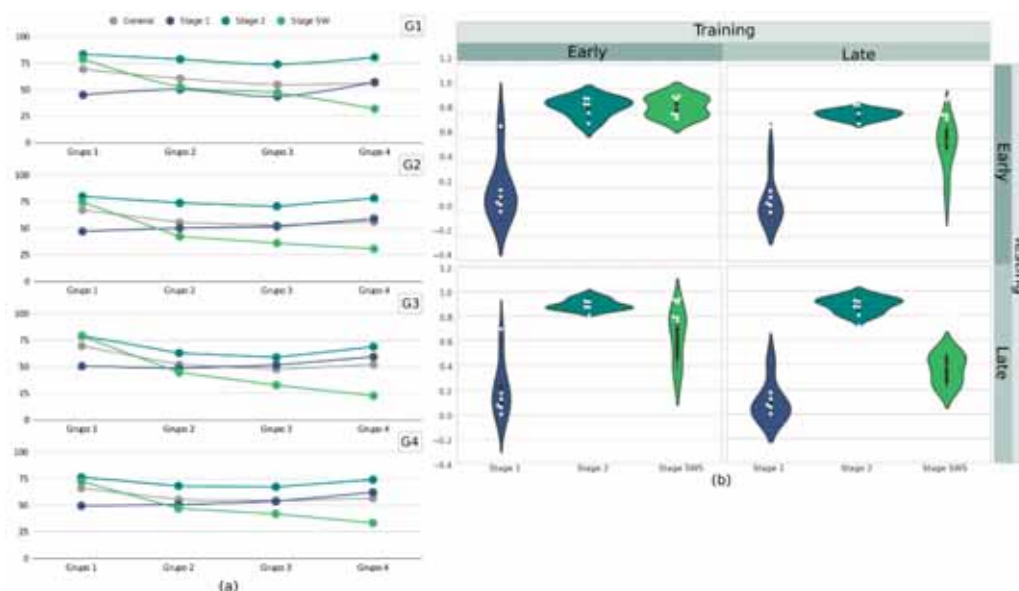
Figure caption: Figure (a) shows the change in classification when the test group is changed. The box on the right indicates with which group each model was trained. Figure (b) shows the differences when we train or test over the early or late sleep.

References:
[1]   Goldberger, A., et al. PhysioBank, PhysioToolkit, and PhysioNet: Components of a new research resource for complex physiologic signals. Circulation. [Online] (2000).
[2]   McKinley, S., et al. Sleep and psychological health during early recovery from critical illness: an observational study. Journal of psychosomatic research (2013).
[3]   Michael H Silber et al. The visual scoring of sleep in adults, Journal of clinical sleep medicine (2007)

C5.2

Retinal nerve fiber layer as a biomarker of disability progression in multiple sclerosis patients using machine learning techniques

Alberto Montolío[1], José Cegoñino[1], Elena Garcia-Martin[2], Amaya Pérez del Palomar[1]

1   Group of Biomaterials, Aragon Institute of Engineering Research (I3A), Department of Mechanical Engineering, University of Zaragoza, Zaragoza, Spain
2   GIMSO Research and Innovative Group, Aragon Institute for Health Research (IIS Aragon), Ophthalmology Department, Miguel Servet University Hospital, Zaragoza, Spain

Introduction: Multiple sclerosis (MS) is a chronic disease of the central nervous system (CNS) in which axonal loss is considered the main cause of disability [1]. This disease is characterized by its high heterogeneity and unpredictable course. Neuroretina could be a reliable MS biomarker, as the visual pathway is one of the most affected systems in MS patients. Optical coherence tomography (OCT) is a non-invasive, objective and reproducible method to monitor axonal damage by measuring peripapillary retinal nerve fiber layer (pRNFL) and macular RNFL (mRNFL) thicknesses [2]. The use of OCT protocols, in combination with machine learning techniques, is a useful method to predict the disability course in MS patients.

Material and methods: 72 MS patients underwent neuro-ophthalmological evaluations over ten years of follow-up. Structural measurements of RNFL were performed using the different protocols of Spectralis OCT. This data was used to develop two machine learning models capable of predicting the disability state in MS patients. The first one uses date from the first two years of the follow-up to predict the disability state nine years later and the second one uses the first three years to predict eight years later.

Results: With two-year follow-up, the best classifier was decision tree with both fast macular thickness and fast RNFL-N thickness protocol: an area under curve (AUC) of 0.863. With three-year follow up, decision tree performed best for fast macular thickness protocol and support vector machine for fast RNFL-N thickness protocol: an AUC of 0.913 (see Figure 1).
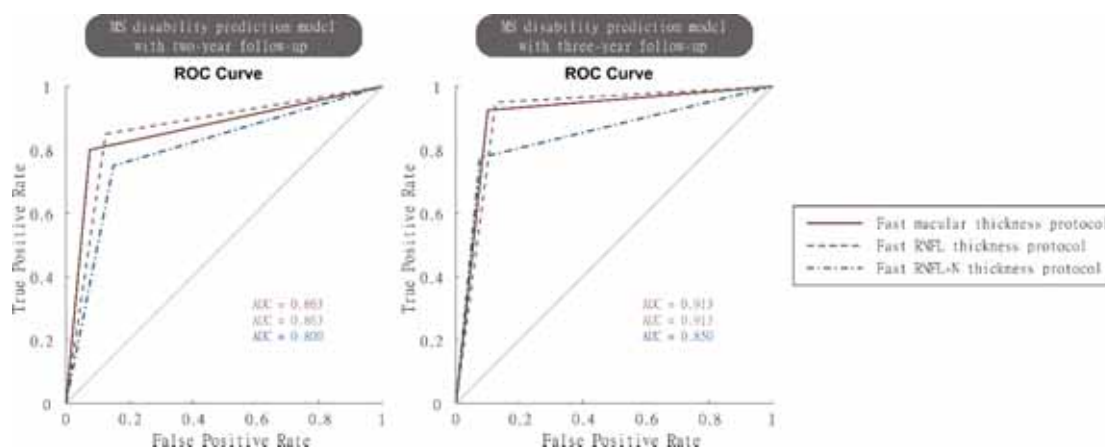
Figure 1. Receiver operating characteristic (ROC) curve with area under curve (AUC) for the best algorithm.

Discussion: With this work, our proposal is to promote the use of OCT data, in combination with artificial intelligence, to make an early diagnosis and predict MS course. This would be of significant benefit to clinicians, who would be able to select more specific treatments based on the predicted disease course for a given patient.

References:
[1]   Y. You et al., "Chronic demyelination exacerbates neuroaxonal loss in patients with MS with unilateral optic neuritis," Neurol. Neuroimmunol. neuroinflammation, vol. 7, no. 3, 2020
[2]   F. London et al., "Optical coherence tomography: a window to the optic nerve in clinically isolated syndrome," Brain, vol. 142, no. 4, pp. 903–915, Apr. 2019

C5.3

Automated segmentation and landmarking of scapulae to assess the outcome of total shoulder arthroplasty using convolutional neural networks

Osman Berk Satir[1], Alexandre Terrier[2], Fabio Becce[3], Frédéric Vauclair[4], Philippe Büchler[1]

1   University of Bern, ARTORG Center for Biomedical Engineering Research, Bern, Switzerland
2   École Polytechnique Fédérale de Lausanne, Laboratory of Biomechanical Orthopedics, Lausanne, Switzerland
3   Lausanne University Hospital (CHUV), Department of Diagnostic and Interventional Radiology, Lausanne, Switzerland
4   Lausanne University Hospital (CHUV), Service of Orthopedics and Traumatology, Lausanne, Switzerland

Glenohumeral osteoarthritis (OA) is increasing worldwide because of the aging population. Total shoulder arthroplasty (TSA) is becoming a common surgical procedure to relieve pain and disability associated with OA. Despite satisfactory outcome and good long-term survivorship, there is a lack of clear indicators to predict the long-term success and revision risk of TSA particularly in young patients. Biomechanical configuration of the glenohumeral joint could influence survivorship and potential causes for the observed complications have been proposed, such as the pre-surgical state of rotator cuff muscles, the shape/orientation of the degenerated glenoid cavity and the acromion, or the bone quality. Manually exploring the glenohumeral joint or the potential causes is a repetitive and time-consuming process. Therefore, in this study, we developed image analysis and deep learning-based approaches to quantify several potential preoperative morphological markers automatically and objectively.

Distance between original and predicted surface mesh (in mm)
0   0.1 0.2 0.3 0.4 0.5 0.6 0.7 0.8 0.9 1
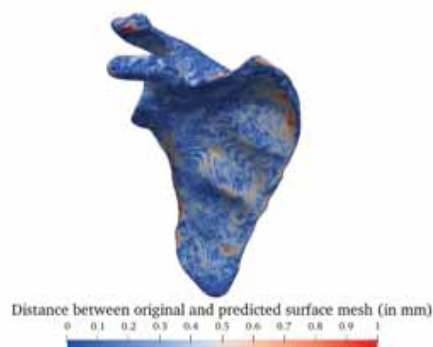
First, the scapula is segmented from Computed Tomography scans of healthy and pathological shoulders using a Convolutional Neural Network (CNN) based segmentation network (U-Net). Validation on healthy and pathological scapulae showed a high segmentation accuracy with Dice coefficients of 0.956 and 0.931, Hausdorff distances of 3.61 and 5.94 mm, and average surface distances of 0.14 and 0.29 mm for the healthy and pathological cases, respectively.

Shoulder arthroplasty planning is based on the anatomical axes of the scapula that are used to quantify glenoid version and inclination, and improve the position accuracy of the implants to correct glenoid erosion. Therefore, specific landmarks identified on the scapula could be used to quantify its 3D anatomy. Thus, based on segmented scapulae, we are proposing an algorithm for the detection of landmark points on scapulae to quantify several morphometric parameters that can potentially be related to TSA outcome, such as glenoid orientation, acromion index and critical shoulder angle.

To predict the landmarks, we currently investigate Graph Neural Networks. This allows us to make the predictions directly on the surface meshes obtained from the segmentation. We utilize Dynamic Graph CNN as our architecture, with surface meshes of scapulae to predict the geodesic distance of each vertex to the desired landmark. On the predicted distance map, the vertex with the lowest predicted distance is considered as a landmark. Currently, this approach is tested with a few landmarks placed on healthy scapulae. The current average prediction error strongly depends on the landmark position and ranges from about 2 mm up to 8 mm.

Actual Geodesic Distance Map
0   50   100 150 200

Predicted Geodesic Distance Map
0   50   100 150 200
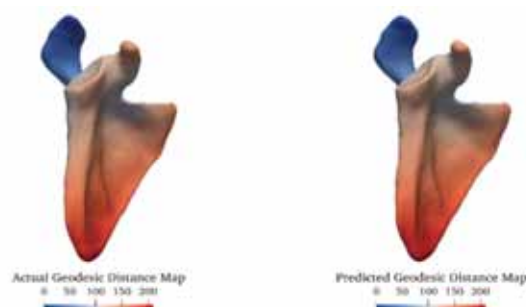
The initial results for landmark detection are suboptimal yet promising, given that due to current mesh density, the distance between neighbour vertices vary between 1-3 mm. In the next steps, we plan to improve these results by including additional features, modifying the mesh density and investigating different architectures.

C5.4

Discovering cell behaviour using physically-guided neural networks. Application to the simulation of glioblastoma invasion process

Jacobo Ayensa-Jiménez[1 2], *Mohamed H. Doweidar*[1 2 3], *Manuel Doblaré*[1 2 3 4]

1   Escuela de Ingeniería y Arquitectura de la Universidad de Zaragoza, Mechanical Engineering, Zaragoza, Spain
2   Aragon Institute of Engineering Research, Zaragoza,
3   CIBER - Center for Biomedical Research Network, Bioingeniería, Biomateriales y Nanomedicina, Madrid, Spain
4   Institute for Health Research Aragon, Zaragoza, Spain

The broad possibilities offered by microfluidic devices for massive data monitoring and acquisition open the door to the use of Artificial Intelligence methods and technologies in a very promising field: cell culture monitoring [1]. It is common to focus the scientific interest on a particular biological mechanism, such as the response of GBM cells to hypoxia, known in the literature as the go or grow paradigm. Recently, some mathematical models have been able to capture the cell culture progression using transport partial differential equations, combined with a mathematical description of the different biological phenomena involved, such as cell migration, proliferation and oxygen consumption [2].

However, these models are corseted to the population-based parametric description of the involved mechanistic processes suffered by the individual cell, related to its metabolic activity. This modelling bias often darkens the underlying biochemical mechanisms that are of interest for scientific purposes and makes it difficult to target them when designing drugs and therapies in the fight against cancer. Besides, this bias error propagates to the predictions of the cell evolution under different stimuli and in different environments.

In response to this, a recent family of methods, coined as Physically-Guided Neural Networks with Internal Variables (PGNNIV) have arisen, where some of the problem physics are known and others are sought to be discovered [3]. PGNNIV allow building non-parametric models relating internal variables of interest, bringing together the predictive power of data science and the interpretability of physically-based models. When these internal variables are associated with cell stimuli and responses, it is possible to unravel cell metabolic changes in a quantitative fashion without making any modelling bias beyond the involved variables.

We apply PGNNIV to both discover and predict cell behaviour under different oxygen levels. Their explanatory capacity can unravel the cell metabolism changes in response to hypoxia, outperforming the estimations given by standard parametric fitting (Fig. A). This improvement is consequently translated into a better prediction of cell culture evolution, and ultimately of tumour progression (Fig. B) under oxygen gradients. This strategy of in silico testing is quick and cheap and can strongly reduce animal experimentation, therefore facilitating research in areas such as biotechnology and biomedical engineering.
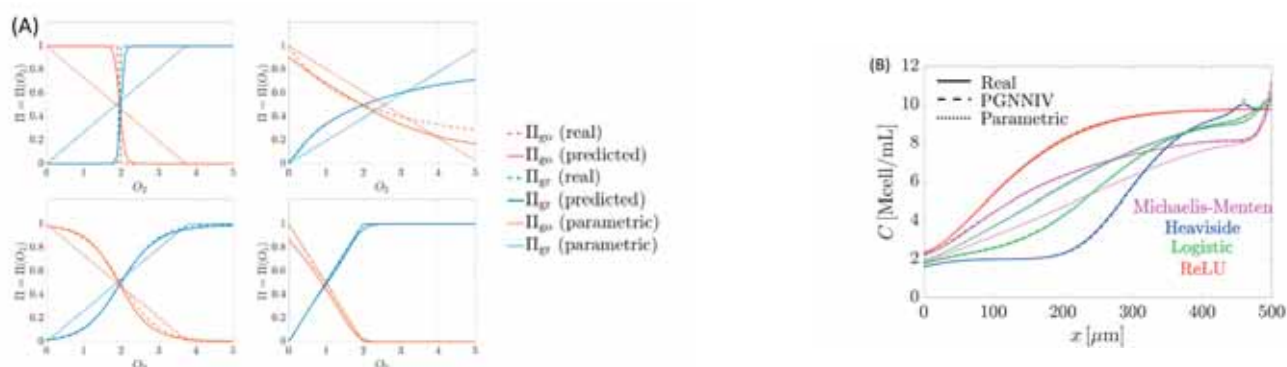
Figure caption: PGNNIV performance: (A) Unravelling capacity. (B) Predictive capacity.

References:
[12] Galan et al. (2020), Matter, 3(6), 1893-1922.
[13] Ayensa-Jiménez et al. (2020), Sci. Rep., 10(1),1-21, 2020.
[14] Ayensa-Jiménez et al. (2021), Comput. Meth. Appl. Mech. Eng., 381, 113816.

C5.5
Left ventricular elastance estimation from brachial pressure waveform

Vasiliki Bikia[1], Marija Lazaroska[1], Deborah Scherrer[1], Méline Zhao[1], Georgios Rovas[1], Nikolaos Stergiopulos[1]

1   Laboratory of Hemodynamics and Cardiovascular Technology, Swiss Federal Institute of Technology,, Institute of Bioengineering, Lausanne, Switzerland

Introduction: Left ventricular (LV) end-systolic elastance (Ees) is a major determinant of cardiac systolic function [1] and hemodynamical state [2]. Yet, its bedside use is not established due to the invasive and expensive nature of its measurement [3]. The goal of the present study is to introduce a method for the assessment of cardiac contractility, using as sole measurement arterial blood pressure (BP) waveform recordings.

Methods: Concretely, we aim to provide evidence of the potential in using the morphology of the brachial BP waveform and its time derivative for predicting LV Ees via convolution neural networks (CNNs). The requirement of a large training dataset is addressed by the use of a previously validated one-dimensional cardiovascular simulator [4] that allows for the generation of a large in-silico cohort (n=4,018) [5]. We evaluated two CNN configurations: (i) using one channel (CNN1C), namely only the raw brachial BP signal as an input, and (ii) using as inputs both the brachial BP wave and its time derivative (CNN2C).

Results: For the CNN1C, Pearson's correlation coefficient (r) and RMSE were equal to 0.91 and 0.1 mmHg/mL, respectively. For CNN2C, accuracy was found to be higher (r=0.97 and RMSE=0.05 mmHg/mL). The Bland-Altman analysis showed that the estimated Ees had low bias, while limits of agreement were narrow (Figure 1).
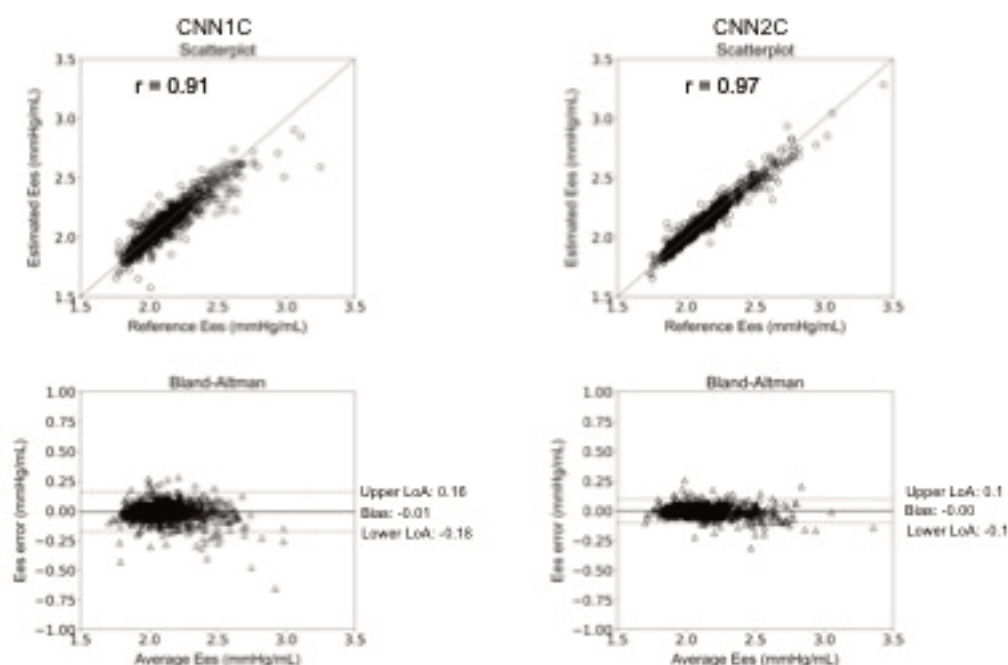
Figure caption: Comparison of the estimated and the reference Ees values.

Conclusion: The arterial BP wave appeared to be a promising source of information for assessing Ees. Predictions were found to be in good agreement with the reference Ees values over an extensive range of LV contractility values and loading conditions. The proposed methodology could be easily transferred to the bedside and potentially facilitate the clinical use of Ees for monitoring the contractile state of the heart in the real-life setting.

References:
[1]   K. Sagawa, et al., "End-systolic pressure/volume ratio: a new index of ventricular contractility," Am. J. Cardiol., 1977.
[2]   M. Cecconi, et al., "Consensus on circulatory shock and hemodynamic monitoring. Task force of the European Society of Intensive Care Medicine," Intensive Care Med, 2014.
[3]   K. Sagawa, "The end-systolic pressure-volume relation of the ventricle: definition, modifications and clinical use.," Circulation, 1981.
[4]   P. Reymond, et al, "Validation of a one-dimensional model of the systemic arterial tree," Am. J. Physiol. Heart Circ. Physiol., 2009.
[5]   V. Bikia et al., "Noninvasive estimation of aortic hemodynamics and cardiac contractility using machine learning," Sci Rep, 2020.

C6.1

A microvessel near the sacral skin surface is closed by pressure but not shear of a polyurethane foam mattress: a plane-stress finite-element model study

Hiroshi Yamada[1], *Makiko Tanaka*[2]

1   Kyushu Institute of Technology, Department of Biological Functions Engineering, Kitakyushu, Japan
2   Yamaguchi Prefectural University, Faculty of Nursing and Human Nutrition, Yamaguchi, Japan

Aims: The combination of prolonged pressure and shear on a body surface over a bony prominence causes pressure injury. The injury is mainly due to pressure, but shear has also been suggested to play a role in pressure injury. Yamada et al. conducted finite element (FE) analysis of the closure of a microvessel near the surface of sacral skin under plane stress and identified the Young' modulus of the skin as 23 kPa so that the vessel closes at a skin surface pressure of 10 kPa (1). Here, the microvessel shape was investigated numerically for vertical and horizontal displacements of a body with respect to a polyurethane foam mattress.

Methods: The FE model was modified. The skin was 2 mm thick, the microvessel was located on the symmetric axis of the model 0.2 mm from the skin surface, and the mattress was 50 mm thick. A strain energy density function was used for a high-repulsive polyurethane foam mattress with a modification of the Poisson's ratio as 0 (2). The Young's modulus of the subcutaneous tissue was also modified to be 1/5 that of skin to express a loose connection to the skin layer. The blood pressure for the microvessel was set to 4 kPa with a vertical displacement of 35 mm and subsequent horizontal displacements of 10 mm and 20 mm of the sacral bone. Results and discussion: The figure shows the distribution of in-plane minimum principal stress and the luminal shape of a microvessel in the skin under compressive and shear stresses. The microvessel was 10.8 ꭢm in diameter under blood pressure only; under a compressive stress of 7.1 kPa on the skin surface near the vessel, it closed to a height of 3.1 ꭢm, with the width remaining almost constant. During horizontal motion, the body weight of the model was almost constant, and the vessel opened slightly with an increase in height of 0.8 ꭢm for a combination of compressive stress of 6.5 kPa and shear stress of 1.5 kPa on the skin surface near the vessel. The opening of the vessel may have been because it was located away from the most deformed region of the mattress.

Conclusion: FE analysis of a microvessel in the sacral skin indicated that the pressure of the mattress on the skin surface markedly decreased the height of the microvessel, while shear did not.
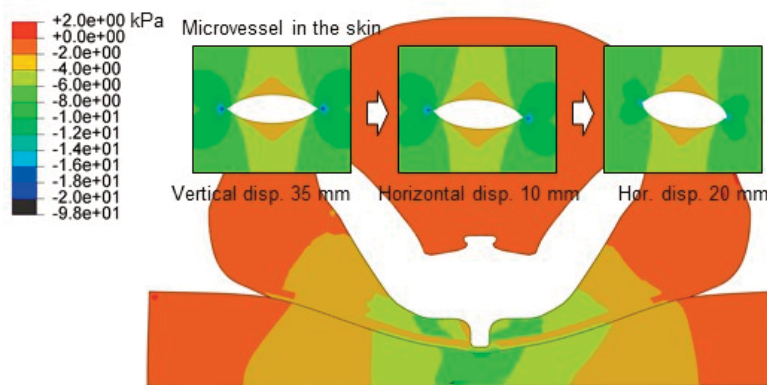
Figure caption: Distribution of in-plane minimum principal stress and the luminal shape of a microvessel in the skin under compressive and shear stresses.

References:
(1)   Yamada H, et al, Med Biol Eng Comput, 55(1), 79-88, 2017.
(2)   Fuwa Y, et al, J Mech Med Biol, 20(5), 2050031, 2020.

C6.2

An anisotropic hyperelastic model for human skin: finite element modelling, identification of parameters, mechanical tests

Wael Alliliche[1], Christine Renaud[1], Jean Michel Cros[1], Zhi Qiang Feng[1]

1   Université Paris-Saclay, Univ Evry,, LMEE, , Évry-Courcouronnes, France

The skin is a living organ which behaves like a hyperelastic and almost incompressible material. The dermis contains collagen fibers that make the biomaterial anisotropic. A modified HGO model [1] is used to describe the skin. This model has an isotropic part expressed as a polynomial sum [2], an anisotropic part composed of an exponential part to describe the effect of the fibres according to their orientation. Since the materials are nearly incompressible, a third term appears to describe the behaviour of compressibility.

The constructive model is a function of strain and material's parameters, the latter are identified by an optimization method. The optimisation algoritm minimize the error between experimentals datas and analytical developement . The model is implemented in the "Finite Element Research" (FER) code developed by the LMEE.

In order to make a simulation of a skin indentation, we use the bipotential contact law [3]. This law is a combination of contact and friction coupled in a single non-differentiable potential called bipotential.

We performed a simulation of an experimental trial of uni-axial tensile test on the skin. The curves of stress according to the strain are plotted, we compare the obtained numerical results from FER code with experimental curves (figure 1). We noticed that the maximum relative error between numerical datas and the experimental ones is less than 3% (figure 2). Then, we make several simulations by changing the orientation fibers angle at each time, we concluded that only the tangentiel component to tensile direction of the orientation vector works, because the fibers only work in traction.

For the next test, we applied an indentation of a rigid circular indenter into skin (figure 3). Then, we modified the fibers orientation and made differents numerical simulations (Figure 4).

Figure caption:
  Figure 1 : Coincidence of the experimental curve with the numerical curve.
  Figure 2 : Absolute error between experimental and analytical curves.
  Figure 3 : Original and deformed shape of the model after indentation test.
  Figure 4 : Evolution of stress with respect to orientation angle

References:
[1]   Holzapfel GA, Gasser TC, Ogden RW. 2001. A new constitutive framework for arterial wall mechanics and a comparative study of material models. Dordrecht: Springer Netherlands. chap. 61.
[2]   Yeoh O. 1993. Some forms of the strain energy function for rubber. Rubber Chemistry and Technology. 66:754-771.
[3]   De Saxcé G, Feng Z.-Q. 1998. The bipotential method: A constructive approach to design the complete contact law with friction and improved numerical algorithms. Mathematical and Computer Modelling. 28(4):225-245.

C6.3

Peri-wound skin loads are considerably more sensitive to the pressure level than to the dressing stiffness in a negative pressure wound therapy

Aleksei Orlov[1], Amit Gefen[1]

1   Tel Aviv-Yafo, Biomedical Engineering, Tel Aviv-Yafo, Israel

Negative pressure wound therapy (NPWT) is an established adjunctive modality for treatment of both acute and chronic wounds. However, little is known about the optimal settings and combination of treatment parameters and importantly, how these translate to target tissue strains and stresses that would result the fastest healing and buildup of good-quality tissues. In this study we have developed a computational modelling framework for better understanding of the mechanobiology of tissues at the peri-wound and wound-bed under NPWT. We specifically developed a three-dimensional open wound finite element (FE) model that contains viscoelastic skin, adipose and skeletal muscle tissue components for determining the states of tissue strains and stresses in and around the wound when subjected to NPWT without primary suture closure. This FE modelling further facilitates studies of the influence of the foam dressing (FD) properties such as its stiffness on the dynamic strain and stress states generated in the tissues. The highest tissue strains occurred at the wound-bed whereas tissue stresses maximized in peri-wound skin. An increase in the negative pressure level within the 10-175 mmHg range caused both the effective tissue strain and stress values to rise. Specifically, for the above pressure range, strains in the wound-bed increased from 3% to 43% and strains in peri-wound skin increased from 0.3% to 3%; the effective wound-bed and peri-wound tissue stresses increased from 0.3 kPa to 5 kPa and from 96 kPa to 1250 kPa, respectively. The most important finding of the present study is that the skin strain state is considerably more sensitive to the pressure level than to the stiffness of the FD within a 8.25 to 99 kPa stiffness range, which covers the current industry standard. This computational simulation data demonstrated that the strain and stress states in peri-wound skin are considerably more sensitive to the pressure level set in the NPWT device/protocol than to the stiffness of the FD. Stiffer and softer FD over an order of magnitude around the mean industry standard (for a dry dressing) yielded indistinguishable tissue strains and stresses, particularly in peri-wound skin which forms the biological reservoir for healing, being the source for immune and tissue-repairing cells, as well as of vascular supply. Accordingly, peri-wound skin strains and stresses which stimulate cell proliferation/migration and angiogenesis and thereby, healing of the wound, can be more effectively controlled by adjusting the pressure level than by varying the stiffness of the foam dressing.
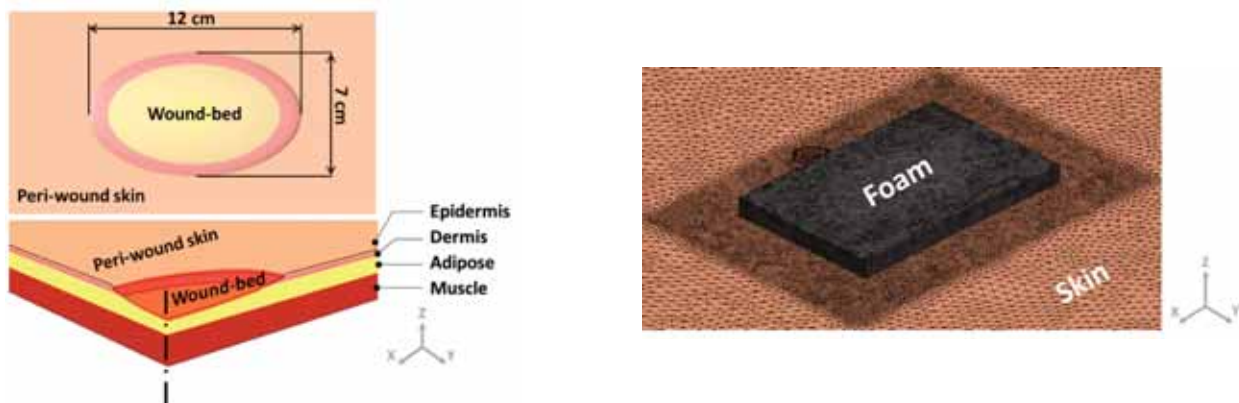
Figure captions: 1) Geometry of the wound model with its tissue and wound components. 2) The FE mesh around the wound-bed with the applied foam.

C8.1

The Coupled Momentum Method revisited: formulation, higher-order elements, solver technology, and verification

Ingrid Lan[1], Ju Liu[2], Weiguang Yang[3], Alison Marsden[1 3 4]

1   Stanford University, Department of Bioengineering, Stanford, United States
2   Southern University of Science and Technology, Department of Mechanics and Aerospace Engineering, Shenzhen, China
3   Stanford University, Department of Pediatrics (Cardiology), Stanford, United States
4   Stanford University, Institute for Computational and Mathematical Engineering, Stanford, United States

Compared to the arbitrary Lagrangian-Eulerian (ALE) method, the coupled momentum method (CMM)1 offers a computationally efficient approach for modeling fluid-structure interaction (FSI), which is critical for capturing wave propagation phenomena in three-dimensional cardiovascular simulations. In brief, CMM allows an Eulerian fluid description and models the wall as a transverse-shear-enhanced linear elastic membrane. While the original CMM derivation achieved coupling via a fictitious body force, we instead start from a unified continuum ALE formulation2. Without resorting to this fictitious body force, we arrive at a similar FSI formulation via the small-strain and thin-wall assumptions.

Given recent advances in computational methods, we propose enhancements to the discrete problem in several aspects, including the spatiotemporal discretization, structural dynamics, preconditioner design, membrane boundary conditions, and use of higher-order elements. In particular, we employed the residual-based variational multiscale formulation for stabilized spatial discretization rather than the classical Streamline Upwind Petrov-Galerkin method. Additionally, contrary to the ubiquitous approach of collocating pressure at time step tn+1, we evaluated pressure at the intermediate time step in the generalized-α method to achieve second-order temporal accuracy of pressure. To introduce numerical damping at high-frequency modes and unify temporal integration of the FSI system, we computed the membrane displacement from its velocity via the generalized-α method, rather than the Newmark-β method. A segregated algorithm was designed to allow the implicit solver to retain the same block structure as that of the Navier-Stokes problem, which we exploited in our nested block preconditioner. Furthermore, instead of prescribing homogeneous Dirichlet boundary conditions on the wall, we implemented conditions enabling motion of the wall boundary nodes in the tangential plane. Elimination of such clamping is critical for mitigating spurious wave reflections introduced by artificial boundaries in future 3D-1D-0D coupling efforts.

In conjunction with quadratic tetrahedral elements, our methodology offers improved performance and higher-order accuracy for quantities of clinical interest, including pressure and wall shear stress. Using relatively coarse linear and quadratic meshes, we verified our method against Womersley's deformable wall theory3 and observed excellent agreement between numerical and analytical solutions for fluid velocity profiles, flows, pressures, and wall displacement. Finally, given the nonzero internal stress state of the vessel wall at configurations obtained from medical imaging, tissue prestressing will be presented in CMM for the first time. The merits of our combined technology will be demonstrated through a suite of patient-specific FSI simulations.

References
[1]   C.A. Figueroa et al. A coupled momentum method for modeling blood flow in three-dimensional deformable arteries. CMAME. 195:5685-5706, 2006.
[2]   J. Liu, A.L. Marsden. A unified continuum and variational multiscale formulation for fluids, solids, and fluid-structure interaction. CMAME. 337:549-597, 2018.
[3]   V. Filonova et al. Verification of the coupled-momentum method with Womersley's Deformable Wall analytical solution. IJNMBE. 36:e3266, 2019.

C8.2
Synchrotron imaging based computational models of blood flow dynamics in the ventral aorta of adult zebrafish

Matthias Van Impe[1], Marco Stampanoni[2], Julie De Backer[3 4], Patrick Sips[4], Patrick Segers[1]

1   Ghent University, IBiTech-bioMMeda, Belgium
2   Paul Scherrer Institute, Villigen, Switzerland
3   Ghent University Hospital, Department of Cardiology, Ghent, Belgium
4   Ghent University Hospital, Center for Medical Genetics, Ghent, Belgium

Zebrafish have emerged as a valuable model organism to study the pathophysiological mechanisms leading to human disease, including cardiovascular disorders. Genetic tractability and optical transparency favor efficient visualization of cardiovascular structures during early developmental stages, leading to a number of bio-engineering reports on embryonic ventricular fluid dynamics. Also fluid dynamics analyses in adult zebrafish could provide important information related to the pathophysiology and mechanobiology of progressive conditions, and could be used for the validation of results obtained in large-scale embryonic or larval studies, but options to study the adult cardiovascular phenotype are limited [1]. Therefore, we applied synchrotron imaging to adult zebrafish allowing efficient integration of three-dimensional cardiovascular information, while still providing sufficient soft tissue contrast to develop sample-specific fluid dynamics models of the zebrafish circulation. We show that synchrotron-based image stacks provide sufficient detail to set up unprecedented finite element computational fluid dynamics (CFD) and fluid-structure interaction (FSI) models of the ventral aorta. A key output of these models is the shear stress exerted on the endothelium lining the vessel wall, wall shear stress (WSS), playing an important role in cardiovascular mechanobiology.

Phase-contrast synchrotron X-ray imaging, performed at the Paul Scherrer Institute in Villigen (Switzerland), allowed us to visualize major cardiovascular structures including the atrium, ventricle, bulbus arteriosus, and, depicted below on the left, the ventral aorta, afferent and efferent branches and gill vasculature, all at $1.625\ \mu m^3$ voxel size and within a $4.16\ mm^2$ field-of-view. Blood flow dynamics in the ventral aorta was modelled for N = 5 wild-type, 13 months old zebrafish, starting from Pulsed Wave Doppler measurements (in vivo) and the acquired synchrotron data (ex vivo). Image stacks were segmented into 3D blood and soft tissue volumes using Mimics software and three cardiac cycles were simulated in COMSOL Multiphysics. CFD and FSI studies revealed consistent WSS patterns, and, as expected, blood pressure and WSS were overestimated for CFD cases, compared to the preliminary FSI results (one case is depicted below on the right). Lowest WSS locations were found near the branching regions. Effects of different outlet boundary conditions, blood viscosity, gill vasculature sprouting from the branches and aortic wall constitutive models were investigated and quantified. Overall, this study provides a first reference for aortic biomechanics in adult zebrafish and shows potential to significantly advance (computational) cardiovascular phenotyping.
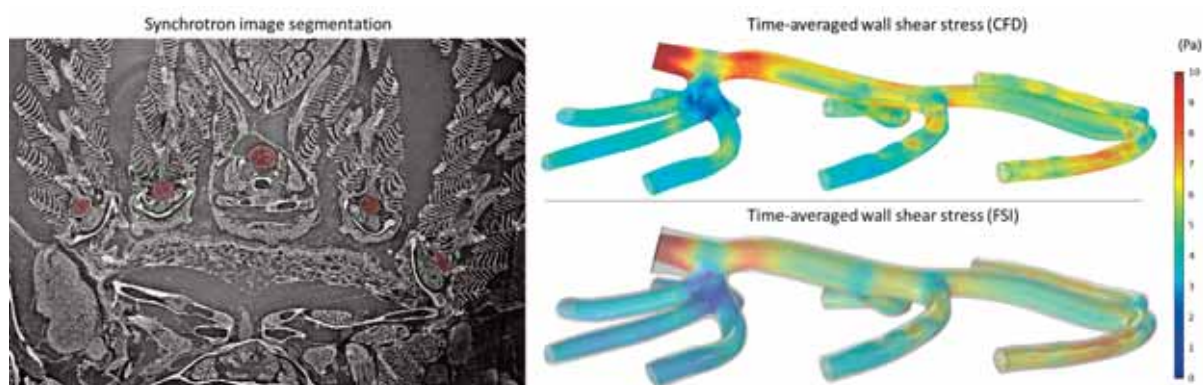
Figure caption: Synchrotron imaging allows segmentation (shaded red, left) and 3D reconstruction of the ventral aorta and can be used as input for sample-specific geometries computational models (right).

References:
[1]   De Spiegelaere et al., Anat. Histol. Embryol., 2020

C8.3
Pulsatility indices can inform on distal perfusion following ischaemic stroke

Ivan Benemerito[1 2 3], Ana Paula Narata[4], Andrew Narracott[1 3], Alberto Marzo[1 2]

1   The University of Sheffield, INSIGNEO Institute for in silico medicine, Sheffield, United Kingdom
2   The University of Sheffield, Department of Mechanical Engineering, Sheffield, United Kingdom
3   The University of Sheffield, Deparment of Infection, Immunity and Cardiovascular Disease, Sheffield, United Kingdom
4   Southampton University Hospital, Department of Radiology, Southampton, United Kingdom

Ischaemic stroke (IS) is an occlusion in the brain circulation which reduces blood supply to the affected regions [1]. Leptomeningeal anastomoses (LMAs) provide alternative pathways for the blood to bypass the occlusion and perfuse peripheral regions. LMAs connect the middle cerebral artery (MCA) to the anterior (ACA) and posterior cerebral arteries (PCA), and divert flow when either is occluded [2]. Larger LMAs are associated with greater distal perfusion and better clinical outcomes after stroke [3]. Characterisation of LMAs can indicate distal perfusion levels and guide clinical intervention, but is impractical as the imaging required is only available during stroke. Blood velocities in the ACA and PCA, measurable using Doppler ultrasound, are affected by the size of the LMAs and potentially related to the status of distal perfusion. In this study we examine how well the pulsatility index (API) of the ACA and PCA can predict levels of distal perfusion following MCA occlusion.

A 1D model of the brain circulation, extended from [4] to include LMAs, was used to simulate the effects of variation of the radii of LMA, ACA, PCA, and distal MCA (within ±40% of their baseline value) on distal perfusion and API of the ACA and PCA. The influence of input parameters on model outputs was assessed using Sobol's sensitivity indices. The robustness of API in predicting the perfusion was tested in two cases: i) 40% uncertainty for all the input parameters; ii) 10% uncertainty for radii of the ACA and PCA alone, 40% uncertainty for all remaining variables.

Sobol's indices show that variability in LMA radii contributes to 90% of the variability in perfusion and to 60% of API's variability. Despite the relation API/perfusion is weaker than LMA radii/perfusion, the significance of the effect of LMA radii on both perfusion and API makes API a surrogate variable for perfusion.

API/perfusion scatter plots show that high uncertainty in ACA and PCA radii do not allow for precise estimate of perfusion (Figure 1). With ACA and PCA radii uncertainty at 10%, API<1.15 indicates perfusion >60%. For API>1.15 the corresponding perfusion level cannot be predicted unequivocally, as it ranges from 25% to 80%.

Reducing uncertainty on ACA/PCA radii has the potential to improve the use of API metrics in indicating the level of distal perfusion. Results suggest that API could be used as a tool preliminary evaluation for identifying higher level of perfusion and to inform clinical decision making.
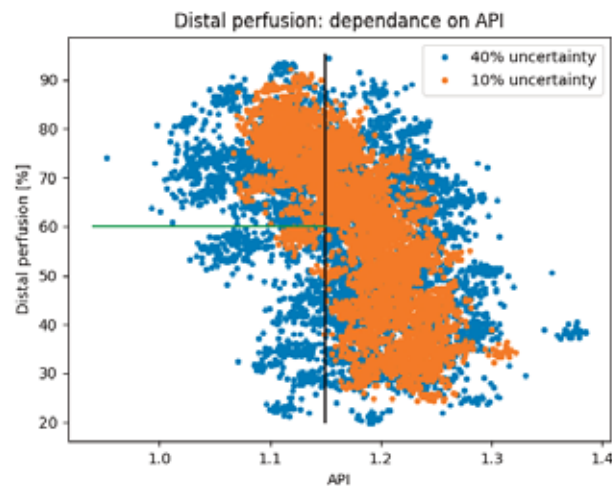
Figure caption: Lower values of API (<1.15, black line) indicate high level of perfusion (>60%, green line)

References:
[1]   Dimagl et al, 1999;
[2]   Brozici et al, 2003;
[3]   Wu et al, 2017;
[4]   Melis et al, 2019;

C8.4

Leaflet fluttering and turbulent systolic blood flow after bioprosthetic heart valves

*Corso Pascal[1], Silje E. Jahren[1], Barnhard Vennemann[2], **Dominik Obrist**[1]*

1   University of Bern, Bern, Switzerland
2   ETH Zürich, Zürich, Switzerland

Aortic valve replacement with bioprosthetic heart valves (BHV) is a successful treatment for elderly patients with moderate to severe aortic stenosis. The performance and durability of BHV has been connected to a dynamic process known as leaflet fluttering. Leaflet fluttering is the result of an instability mechanism which may contribute to laminar-turbulent transition behind the valve leading to unphysiological blood flow in the ascending aorta and increased trans-valvular pressure gradient (Becsek, Pietrasanta, and Obrist 2020). Furthermore, leaflet fluttering may be related to fatigue and structural valve deterioration which limits BHV durability (Johnson et al. 2020). Therefore, leaflet fluttering is a process that needs to be better understood to help designing better BHV which suppress fluttering.

We will present experimental and computational data to characterize and quantify leaflet fluttering in a state-of-the-art BHV design. The results indicate the presence of different fluttering modes including modes with trailing edge oscillations and travelling wave modes. These fluttering modes will be analyzed and connected to laminar-turbulent transition mechanisms. Furthermore, we will show computational results illustrating the role of valve tissue mechanics and geometry on leaflet fluttering.

Results of this study provide a better understanding of the main determinants of leaflet fluttering and may give indications for better BHV designs with reduced leaflet fluttering.
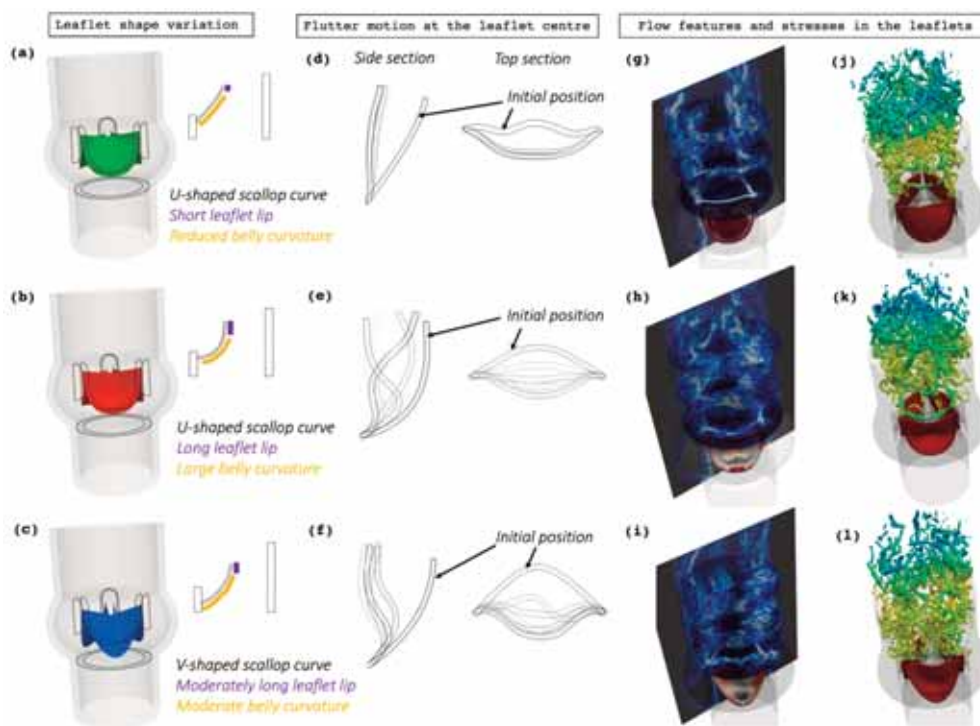
Figure caption: Characterization of leaflet fluttering for three different valve designs

References:
Becsek, B., L. Pietrasanta, and D. Obrist. 2020. "Turbulent Systolic Flow Downstream of a Bioprosthetic Aortic Valve: Velocity Spectra, Wall Shear Stresses, and Turbulent Dissipation Rates." *Frontiers in Physiology* 11. https://doi.org/10.3389/fphys.2020.577188.
Johnson, Emily L, Michael C H Wu, Fei Xu, Nelson M Wiese, Manoj R Rajanna, Austin J Herrema, Baskar Ganapathysubramanian, Thomas J R Hughes, Michael S Sacks, and Ming-Chen Hsu. 2020. "Thinner Biological Tissues Induce Leaflet Flutter in Aortic Heart Valve Replacements." *Proceedings of the National Academy of Sciences* 117 (32): 19007–16.

C8.5
The effect of an aneurysm on particle paths in a 3D vessel geometry

Dániel Gyürki[1], *István Szikora*[2], *György Paál*[1]

1   Budapest University of Technology and Economics, Department of Hydrodynamic Systems, Budapest, Hungary
2   National Institute of Clinical Neurosciences, Department of Neurointerventions, Budapest, Hungary

Intracranial aneurysms are saccular malformations on the wall of brain arteries, mainly found on the Circle of Willis. They carry a serious health risk as their rupture may cause stroke which can even result in death. Therefore, investigating the reasons behind the formation and rupture of these bulges is a major topic of research. In our study we numerically follow the paths of small particles placed inside the blood flow. Závodszky et al. [1] showed that the particle paths display a chaotic nature, in which the presence of the aneurysm plays an important role.

To investigate the effect of the aneurysm sac, first we removed the aneurysm from a real 3D vessel geometry. The geometry can be seen in part A of the figure, with the removed sac in blue. The flow fields for the two geometries were obtained with a lattice-Boltzmann simulations. The simulations were time-dependent; the prescribed inlet velocity is a generalized 1-second-long signal; the data were saved at every 0.01 second. The spatial resolution is uniform, resulting in around 5M fluid voxels. Last, 1M massless passive tracers were placed in the flow at the inlet (red cross-section in figure) and their paths were followed. A fourth order Runge-Kutta method was used to integrate the flow field. The time it takes for the particle to leave the domain (residence time) and the reached outlets were recorded until 10 seconds.

In part B of the figure the residence times and the reached outlets were plotted at the starting section. The green and yellow outlets are painted in part A of the figure accordingly, and the dark blue color means that the particle was stuck at the wall. It is conspicuous from the residence times, that compared to the case when there was no aneurysm, regions with large residence times appear in the middle. The effect of the aneurysm is more significant on the reached outlets. The prominent outlet changed in the presence of the malformation.

These results show that removing the aneurysm greatly influences the particle paths. These particles may model those that play important roles in biological processes, like platelets in hemostasis or chemicals from medicines. Therefore, the effects of vessel wall malformations should be investigated, since the particles may leave in different vessels or can be trapped inside the aneurysm for a long time.
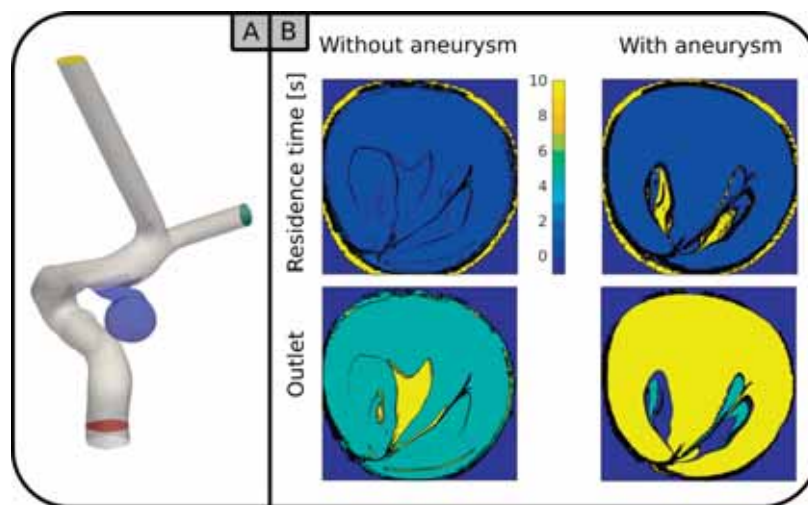
Figure caption: The investigated geometry; tracer residence times and reached outlets with and without the aneurysm.

References:
[1] Závodszky G., Károlyi Gy., Paál Gy. Emerging fractal patterns in a real 3D cerebral aneurysm, Journal of Theoretical Biology. Elsevier, 2015, Vol. 368,pp. 95-101.

C8.6

Computational modeling for understanding cerebral vasculopathy during early childhood in sickle cell disease

Lazaros Papamanolis[1], Valentin Amar[1], Suzanne Verlhac[2], Pablo Bartolucci[3], Irene Vignon-Clementel[1]

1   Inria, Paris, France
2   Robert Debré Hospital, APHP, Pediatric Imaging Department, Reference Center for Sickle Cell Disease, Paris, France
3   Hôpital Henri-Mondor, APHP, Centre De Référence Des Syndromes Drépanocytaires Majeurs, Créteil, France

Sickle cell disease (SCD) is the most common inherited disease due to a single mutation, often leading to stenosis in cerebral arteries (cerebral vasculopathy). Previous work has established a critical cerebral blood flow velocity threshold (time-averaged mean maximum velocity (TMMV) = 200 cm/s), putting SCD children exceeding it at increased risk of stroke [1]. However, it still remains poorly understood why critical blood velocities are encountered disproportionately in children below the age of 10, while they rarely appear in adults. This study aims to elucidate the underlying biomechanical factors that promote stenosis and differentiate risk between children and adults in SCD.

The intracranial internal carotid artery (ICA) with its terminal branches was segmented from MRI images of 3 patients (aged 4.5, 6 and 23) with TMMV measurements < 200 cm/s, and 1 patient (aged 5) with TMMV > 200 cm/s, as measured by transcranial Doppler. Blood flow was numerically simulated using the Navier-Stokes equations with varying inlet flow rates for each patient. TMMV and wall shear stress (WSS) were calculated at regions of interest from simulation results.

Simulated TMMV results demonstrated that the level of inlet flow rate required to reach the critical TMMV threshold remained within pathophysiological range for pediatric patients but fell outside realistic ranges for the adult patient (Fig. 1) [2]. At the same time, contrarily to healthy patients, diameters between children and adults remain the same in SCD [2]. Thus, given the diameter similarity between age groups, hyperflow appears to be the primary factor for elevated cerebral velocities and stroke risk in early childhood.

The patient with measured critical TMMV presents a case where the occlusion process has already begun. Simulated WSS results for this case showed an alternation of high WSS and low WSS areas in the ICA indicating areas of vasculopathy development. This is coherent with the literature on stenosis formation and consistent with longitudinal MRI scans of the same patient at later stages of the occlusion process.

Future work is needed to validate these hypotheses of geometry-flow interaction mechanisms on a large cohort of patients.
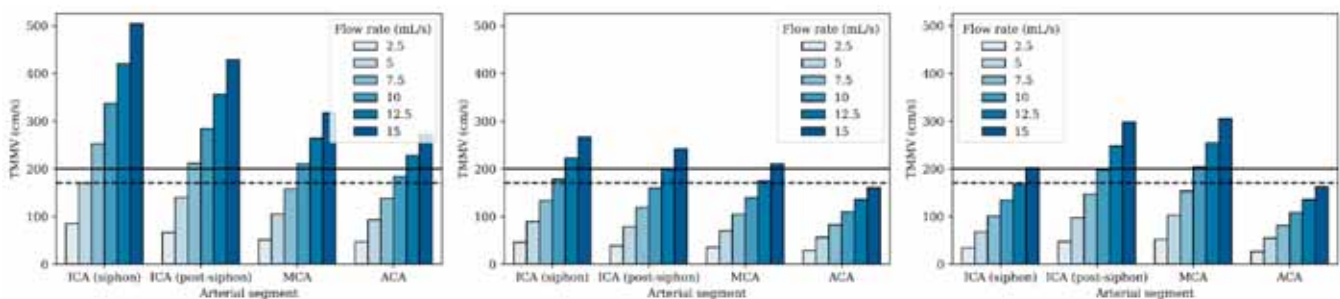
Figure 1: "Simulated TMMV results for varying inlet flow rates for 3 SCD patients with non-critical measured TMMV, aged 4.5 (left), 6 (middle), 23 (right). TMMV computation regions: ICA, middle cerebral artery (MCA), anterior cerebral artery (ACA). The straight and dotted horizontal lines represent the critical (200 cm/s) and conditional (170 cm/s) risk thresholds respectively".

References:

[1]   Adams, R J et al. "Long-term stroke risk in children with sickle cell disease screened with transcranial Doppler." Annals of neurology vol. 42,5 (1997): 699-704.
[2]   Vaclavu, L et al. "Intracranial 4d flow magnetic resonance imaging reveals altered haemodynamics in sickle cell disease." British Journal of Haematology, 180(3):432–442, 2018.

C8.7

Dense-discrete phase simulations of blood flow in a stenotic coronary artery

Violeta Carvalho[1], Nelson Rodrigues[1], Rui A. Lima[1], José Carlos Teixeira[1], Senhorinha FCF Teixeira[2]

1   University of MInho, Department of Mechanical Engineering, Guimarães, Portugal
2   University of MInho, Production and Systems Department , Guimarães, Portugal

Atherosclerotic cardiovascular disease is a silent and common pathology that affects millions of people around the world. Over time, lipids are deposited in the arterial walls reducing blood flow which in turn can result in several dangerous and life-threatening cardiovascular issues including myocardial infarction [1,2]. Due to the high mortality caused by this disease, over the years, great progress was achieved in its understanding through extensive experimental and numerical research. Although in vivo and in vitro experiments have played an important role in the validity of new treatment techniques, due to the great progress that has been made in computational power, numerical methods have been frequently applied in atherosclerosis' research. Typically, blood flow modeling is performed considering the blood as a homogeneous Newtonian or non-Newtonian fluid, however, blood is a complex mixture of plasma, red blood cells, white blood cells, and platelets. Accordingly, in the present study, numerical simulations were performed in Ansys® software by using the dense-discrete phase model (DDPM). This model consists of a hybrid Eulerian-Lagrangian method and it is used to simulate the presence of Red Blood Cells in blood when flowing inside stenotic coronary arteries. Moreover, the same simulation was performed resorting to the Mixture model in which both phases are treated as continuous fluids, in order to verify if the differences are considerable. In Figure 1, the velocity of the RBCs (A), the velocity streamlines of the plasma (B) predicted by the DDPM model, and the velocity streamlines computed by using the Mixture model are presented for instants 0.02 s and 0.2 s.

In general, it was found that the plasma and mixture streamlines are similar for both multiphase models when t = 0.02 s. However, when t = 0.2 s, the DDPM model predicts more small vortices while in the Mixture model the recirculation zones tend to be more regular. In terms of velocity magnitude, the differences are minor, with the DDPM model predicting vortices with slightly higher velocities. From these results, it can be observed that the presence of particles affects significantly the blood flow, creating more disturbed and irregular recirculation zones, but the mixture model allows obtaining a good approximation of what occurs when a discrete solid phase is considered.
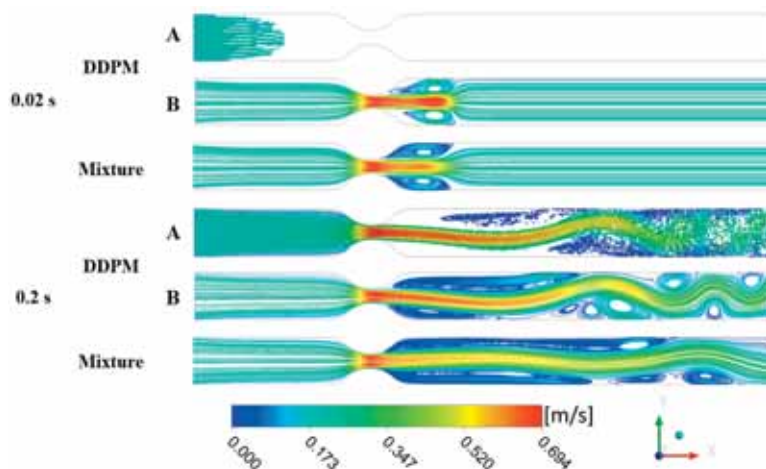
Figure 1: Velocity of RBCs (A), plasma (B) and mixture, when t = 0.02 s and t = 0.2 s in the two multiphase models.

References:
[1]   T. Wang, Pathogenesis of atherosclerosis, Diagnostic Histopathol. 23 (2017) 473–478. https://doi.org/10.1016/j.mpdhp.2017.11.009.
[2]   V. Carvalho, I. Maia, A. Souza, J. Ribeiro, P. Costa, H. Puga, S.F.C.F. Teixeira, R.A. Lima, In vitro stenotic arteries to perform blood analogues flow visualizations and measurements: a Review, Open Biomed. Eng. J. 14 (2020) 87–102. https://doi.org/10.2174/1874120702014010087.

C8.8

Towards a fast alternatives to optimise the implantation of left atrial appendage occluder devices

Carlos Albors[1], *Eric Planas*[1], *Jordi Mill*[1], *Andy Olivares*[1], *Oscar Cámara*[1]

1   Pompeu Fabra University. Poblenou Campus, Barcelona, Spain

Introduction: Device-related thrombosis (DRT) is a feared complication after left atrial appendage occlusion (LAAO), where the optimal occlusion device configuration (e.g., type, size, deployment position) for each patient-specific LAA geometry remains open. In-silico flow models can help describe haemodynamics to understand the risk of thrombus formation. Most published studies are based on Computational Fluid Dynamics (CFD), which are associated with large computational times, unfitting for clinical routine [1]. The recent appearance of faster flow solvers such as GPU-based Lattice Boltzmann method (LBM) could allow decrease computational times to minutes. In this manuscript we present a first comparison of CFD and LBM methods in two patient-specific LA geometries cases with two different LAAO devices deployed in two positions to compare their performances.

Methods: We analyzed two different patient-specific geometries where two different occluder devices (Amplatzer Amulet and Watchman FLX) were implanted in two positions: covering and uncovering the pulmonary vein ridge (PR), a potential factor for DRT [1]. Flow simulations were performed with the CFD solver Ansys Fluent 2019R3 (Ansys Inc., USA) and with the GPU-based LBM method in Ansys Discovery Live (ANSYS Inc, USA). In both solvers, fixed wall conditions, an extracted velocity curve from Doppler echo at the mitral valve; and a generic pressure measurement from an AF patient at the pulmonary veins were implemented as a boundary conditions. Velocities and re-circulations near the device were assessed, and vorticity was detected through the Lambda-2 vortex criterion.

Results: GPU-based LBM simulations lasted much less time than CFD solver (~10 minutes for LBM and ~2 days for CFD simulations) and similar results were observed when assessing flow patterns. According to the computed in-silico indices, the disc in the Amplatzer Amulet device can protect better towards DRT, if it covers the PR, than Watchman FLX device.

Conclusion: GPU-based LBM approach has potential to be an alternative to CFD for certain tasks such as leak detection for LAAO implantation since it provides qualitatively similar blood flow patterns than CFD simulations in a matter of minutes. Further research would be needed to validate this approach in a larger cohort.

Figure caption: Computational Fluid Dynamics and Lattice-Boltzmann method fluid simulations obtained for 2 geometries and configurations of the occluder devices.

References:
1.   Mill, J., et al.: Impact of flow dynamics on device-related thrombosis after left atrial appendage occlusion. Canadian Journal of Cardiology 36 (2020).
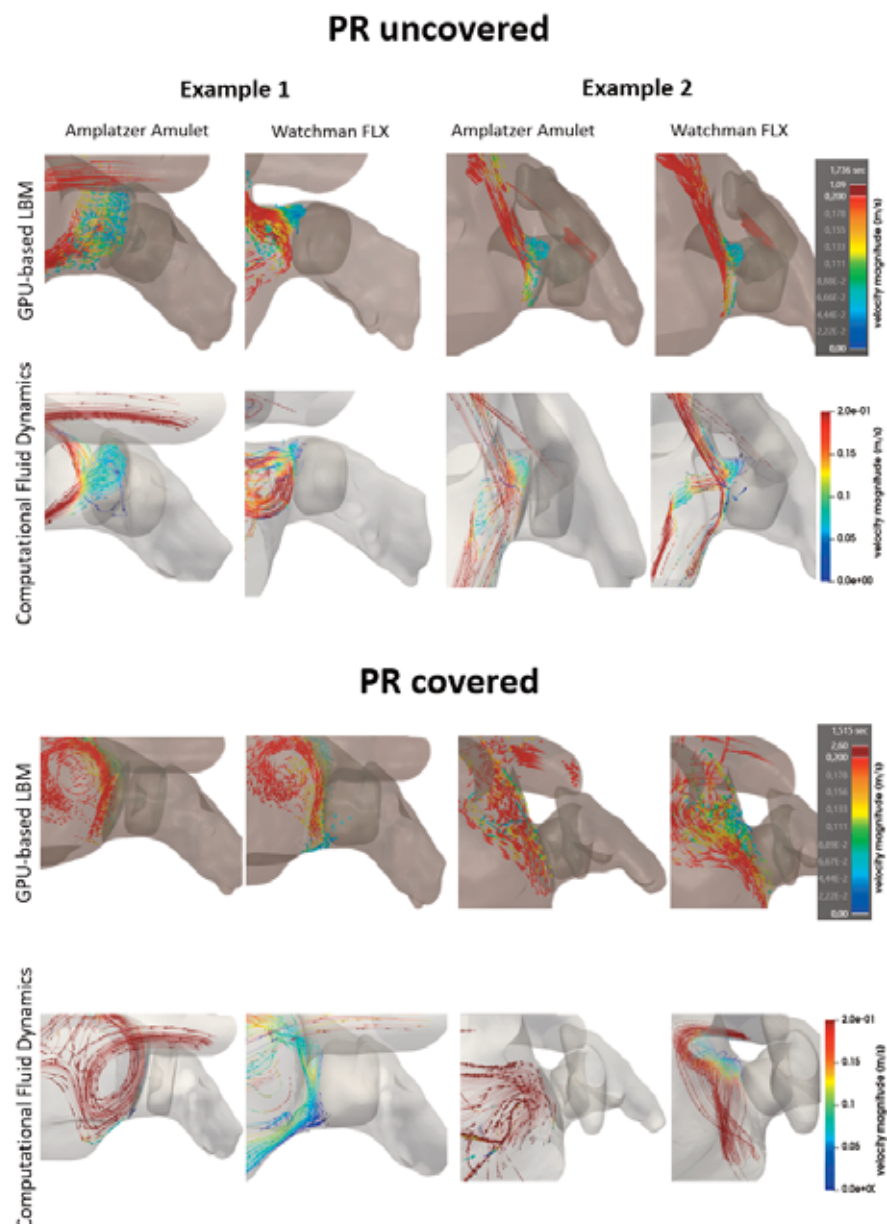
C9.1

Monoaxial stretch of an edge-bound in-silico epithelial tissue by bubbly vertex model

Yukitaka Ishimoto[1]

1   Akita Prefectural University, Department of Mechanical Engineering, Yurihonjo, Japan

Epithelial tissue is essential for animal body plan and ubiquitous inside and outside body, mostly wrapping organs. Partially due to its ubiquity and potential for future medical applications, many works have been devoted to mathematical models for representing morphology and dynamics of epithelial tissues. One of such is the well-known cell vertex model [1] which frequently used to capture the morphology of a tissue or show some idea behind observed morphological events such as growth and isotropy/anisotropy. It was followed by many other related models using polygonal approximation of cell shapes. However, in such models, curvatures of the cell boundaries were omitted and cell internal pressures had not been even discussed, which may mechanically account for the cell shape with cell boundary tensions. We have established a model with the curvature as the bubbly vertex model [2] and discussed its potential of representing tissue dynamics and dynamical properties of the tissue in our past work [3].

In this work, we focus on the dynamical properties of the in-silico epithelial tissue by the bubbly vertex model, and examine them by stretching monoaxially without attaching to a substrate-like background. To detach the in-silico tissue from the background, one has to define some appropriate boundary condition between vertices since surrounding cells and vertices are the main source of frictions to a vertex in question. There exist a few different sorts of friction terms in dynamical equations of cells, such as those in the vertex models for soap froth, the friction term in a continuous form for wound healing [4], and an affine way of introducing it to the three-dimensional vertex model [5]. We examine them and show our results of oscillating monoaxial stretch of the tissue. We found there are nontrivial differences between the results and our previous work [3] on the in-silico tissue attached on a substrate. We also discuss possible applications to in vitro epithelial tissues.

References:
[1]   H. Honda, Int. Rev. Cytol. 81, 191 (1983).
[2]   Y. Ishimoto and Y. Morishita, Phys. Rev. E 90, 052711 (2014).
[3]   T. Toyoshima and Y. Ishimoto, Lect. Notes Comput. Vis. Biomech. 36, 632 (2020).
[4]   O. C.-Escartin, J. Ranft, P. Silberzan, and P. Marcq, Biophys J. 106, 65 (2014).
[5]   S. Okuda, Y. Inoue, M. Eiraku, T. Adachi, and Y. Sasai, Biomech. Model Mechanobiol 14 413 (2015).

C9.2

Numerical approach for the in-silico modelization of the endothelial glycocalyx with divergence-conforming immersed boundary method

Antonio Cerrato[1], *Hugo Casquero*[2], *Carles Bona Casas*[1], *Joan Josep Cerda*[1]

1   Universitat de les Illes Balears, Departament de Física & Institut d'Aplicacions Computacionals de Codi Comunitari (IAC3), Palma, Spain
2   University of Michigan, Department of Mechanical Engineering, Dearborn, United States

The endothelial glycocalyx (EG) is a thin layer made of proteoglycans and glycoproteins anchored to the endothelial cells that recovers the luminal surface of all blood vessels throughout the body. This organ, that has the appearance of a brush, accounts for a good number of essential functions to keep us alive: it acts as a selective barrier for flowing particles, as a lubrifying layer for the transport of red blood cells, as a controller of the appearance of thrombosis, inflammations and oxidative stress. Moreover, it has a crucial role as a mechanotransductor of information from the blood flow towards the endothelial cells so they can change their shape and other properties allowing the body to have dynamic control over the blood transport and pressure[1]. Loss or degradation of the EG has an important impact on the appearance or development of a myriad of diseases like atherosclerosis, ictus, hypertension, among others [2].

Due to the crucial role of EG for the correct function of the circulatory system, its numerical modelization has been the object of several works in recent years[3]. The numerical approach of the microcirculation including the EG involves the solution of the Navier-Stokes equations for incompressible fluids interacting with solids with complex geometries and constitutive models. In our work we present a new numerical strategy to tackle this problem, our model uses a formulation based on the Isogeometric Divergence-Conforming Immersed Boundary method (DCIB)[4,5] which is coupled to a coarse grain particle model (managed by ESPResSo [6]) that can include a great variety of potential interactions. For instance, we focus our numerical studies on the behavior of brush-type structures made of bonded deformable particles under shear-flow and their resistance to being penetrated by an external object.

The results of our simulations have shown that the proposed numerical approach to this FSI problem can capture complex behaviors of the fluid flow within the brush structure. Thus, the model is able to reproduce the expected physical behavior of the brush under shear flow according to previous works. Furthermore, we study the influence of the stiffness of filaments on the penetration of external particles together with the influence of the shear rate.

References:
1.   S. Dognè et al, Arterioscler Thromb Vasc Biol, 38:1427-1439, 2018.
2.   R. Mitra et al, Curr Atheroscler Rep, 19(12):63, 2017.
3.   A. Kabedev et al. Sci Rep. 0;8(1):240, 2018
4.   H. Casquero et al, J of Comp Phys, 374:625-653, 2018.
5.   H. Casquero et al. J of Comp. Phys., 425, 109872, 2021.
6.   HJ Limbach et al, Comp Phys Comm, 174:704-727, 2006.

C9.3

An adaptive in silico cartilage model that predicts degenerative changes in articular cartilage including collagen degeneration and reorientation under multi-axial injurious loading.

Seyed Ali Elahi[1], Petri Tanska[2], Rami Korhonen[2], Rik Lories[3], Nele Famaey[3], Ilse Jonkers[3]

1   KU Leuven, Department of Human Movement Sciences/ Mechanical Engineering Department, Leuven, Belgium
2   University of Eastern Finland
3   KU Leuven, Belgium

During daily-life activities, articular cartilage is subjected to multi-axial mechanical loading, e.g. compression, torsion, sliding or a combination of these. Injurious loading may disrupt cartilage homeostasis and cause progressive cartilage degeneration. Mechanical degeneration plays an important role in the onset and progression of osteoarthritis (OA). Despite extensive studies, the interaction between mechanical loading and cartilage constitutional changes in mechanically induced OA is not yet fully understood. This research aims at studying the onset and progression of degeneration in cartilage subjected to multi-axial injurious loadings using a novel integrative in silico model. A finite element (FE) model of cartilage explant (cylinder: 1.5mm height and radius) was created in Abaqus. A fibril-reinforced poroviscoelastic swelling material model was used to describe the explant with depth-dependent properties (given in [1]). The explant was subjected to four different loadings: (i) injurious unconfined compression (4MPa pressure in 0.1s [2] on the top surface) and loading in (i) followed by (ii) 4mm sliding in the x-direction (parallel to the fibrils at surface), (iii) 4mm sliding in the z-direction (perpendicular to the fibrils at surface) and (iv) 15 degrees torsion. A Cartilage Adaptive REorientation Degeneration (CARED) model was introduced to predict the interaction between collagen fibril disorganization and degradation and proteoglycan (PG) depletion. The CARED model runs FE simulations within an iterative process. Using the FE model output, fibrils are reoriented towards a preferred direction modulated by tensile principal strains [3]. The collagen content is degraded when the strain in the fibril direction exceeded 10% [4] while the PG content is degraded when the maximum shear strain exceeded 30% [1]. Fixed charge density (FCD) loss and increase in tissue hydration were linearly related to the decrease in PG content. The variations in cartilage constituents before and after degeneration under each of the simulated loadings are shown in figure. Adding the sliding and torsion loadings decreased the fibril reorientation in the explant surface and increased fibril disorganization in the middle zone. These also changed the location of intense collagen degradation in surface and increased PG depletion, in terms of FCD loss and increase in tissue hydration. For all loadings, the collagen and PG degradations were the greatest in the middle zone, which is in agreement with recent experiments [5]."
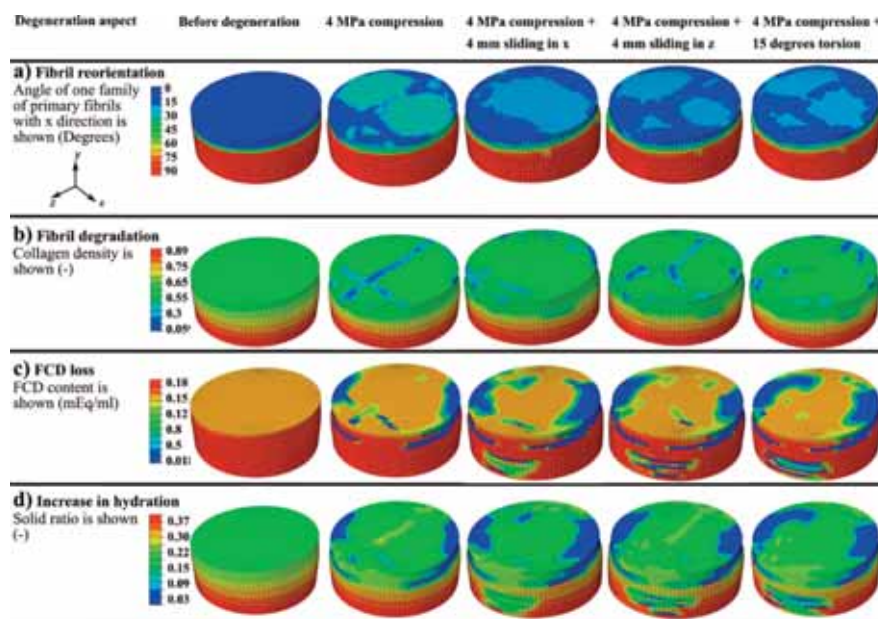
Figure caption: "The constituents of the cartilage explants before and after degeneration."

References:
[1]   Eskelinen et al, Biomech Model Mechan 18, 2019.
[2]   Loening et al, Trans Orthop Res Soc 24, 1999.
[3]   Tanska et al, Biomech Model Mechanobiol 17, 2018.
[4]   Valentín et al, Int J Numer Method Biomed Eng 29, 2013.
[5]   Durney et al, J Biomech 23, 2020.

C9.4
Cellular force generation during sprouting angiogenesis

Mar Cóndor[1], *David Böhringer*[2], *Alejandro Apolinar-Fernández*[3], *Jorge Barrasa Fano*[1], *Jose Antonio Sanz-Herrera*[3], *Ben Fabry*[2], *Hans van Oosterwyck*[4]

1　KU Leuven, Mechanical engineering - Biomechanics section, Leuven, Belgium
2　Friedrich-Alexander-Universität Erlangen-Nürnberg, Department für Physik, Zentrum für Medizin, Physik und Technik, Erlangen, Germany
3　Escuela técnica superior de ingeniería, Área Mecánica de Medios Continuos y Teoría de Estructuras, Sevilla, Spain
1　KU Leuven, Mechanical engineering - Biomechanics section, Leuven, Belgium

Most, if not all, organs are dependent on the formation of a functional blood circulatory network for development, growth and regeneration. The mechanisms that control the ingrowth of vessels during angiogenesis have attracted much attention given its importance in the pathogenesis of various disease conditions such as ischemia, cancer and diabetes [1].

Previous in vitro studies have demonstrated that angiogenesis is strongly affected by ECM stiffness, and depending on the hydrogel used, angiogenesis was found to increase with increasing hydrogel stiffness or to peak at intermediate stiffness. However, the force fields during angiogenesis for different ECM matrix stiffness values has thus far not been quantified.

We adapted an existing model of endothelial invasion into collagen type I hydrogels for Traction Force Microscopy (TFM) procedures [2]. By performing second harmonic generation time-lapse imaging of both invasive endothelial sprouts and collagen fibers, we measured 3D collagen deformation fields (see Fig. 1, left) for three different concentrations of reconstituted collagen gels (2.4, 1.2 and 0.6 mg/ml), which are used to infer cellular tractions during sprouting angiogenesis. By examining collagen deformations we have observed how endothelial cells mechanically interact with the collagen network at the sprout tip.
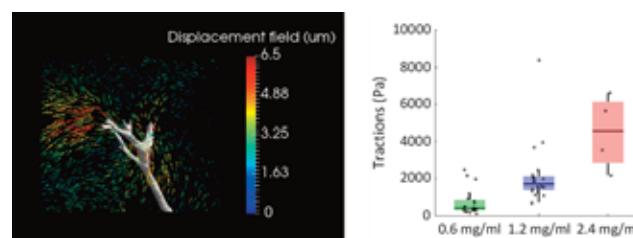
Figure 1: Displacement field (left) generated by a HUVEC-based sprout invading a 1.2 mg/ml collagen gel and differences in tractions (right) for the different collagen concentrations.

When comparing the different collagen stiffness values, we have observed that sprouts formed within the softest collagen gels (0.6 mg/ml) are able to exert the same amount of deformations in the gels than those formed in the stiffest gels (2.4 mg/ml), implying that the cells generated considerably larger tractions in the denser and stiffer gels (see Fig. 1, right). In addition, we have observed how cells forming sprouts in the softer collagen gels invade at higher rates than those formed in the stiffest gels and sprouts are composed of larger number of cells.

Previous studies have shown how individual cells -when invading the surrounding ECM- are able to compensate for the steric hindrance, imposed by different matrix stiffness, by using cellular forces in a more efficient way [3]. By observing the process of endothelial sprout formation in hydrogels with different densities and stiffnesses in combination with 3D TFM techniques, we are now able to investigate in detail how multicellular cell systems and their tip cells exert forces to invade the surrounding ECM.

References:
1.　Potente, M., et al., Cell, 2011.
2.　Vaeyens, M. et al. Angiogenesis, 2020.
3.　Cóndor, M.; et al. Biophysical Journal, 2019.

C9.5

Computational modelling to predict how fibroblast senses extracellular matrix stiffness and cell crosstalk in different mechanical environment

Jinju Chen[1]

1   Newcastle University, Engineering , Newcastle Upon Tyne, United Kingdom

Cells can feel the physical attributes of their surrounding material. The materials provide support for cell adhesion. In turn, the cells exert forces on their substrates in response to the external stimuli. This process is termed as mechanosensitivity of cells, which has been reported to regulate cellular processes [1-2]. For example, when hepatic myofibroblasts in liver are cultured on a soft matrix with Young's modulus of below 2kPa (akin to normal liver) [3], they are less fibrotic in phenotype compared to those cultured on stiffer gels with moduli above 8kPa (fibrosis liver) [4]. Most of studies assumed that the intrinsic elastic modulus affected cellular responses. However, it is important to point out that the stiffness a cell senses not only depends on the intrinsic elastic properties but also the materials thickness.

To address these, we have developed a finite element (FE) model to study the effect of substrate thickness and stiffness on cell responses. Bio-chemo-mechanical models for the stress fibre (SF) and focal adhesion (FA) formation have been implemented in our FE model. In our computational modelling, we have demonstrated that fibroblast cell senses deeper into the substrates with lower elastic moduli. Our modelling also revealed that fibroblast cells of different sizes were very responsive to substrate thickness for hydrogels with stiffness below 2kPa (see Fig.1a). While, such thickness sensing effect became insignificant for hydrogels stiffer than 6kPa (see Fig.1a). We also investigated the cell crosstalk in different mechanical environment. This has important implications for understanding of wound healing process and designing biomaterials for tissue engineering.
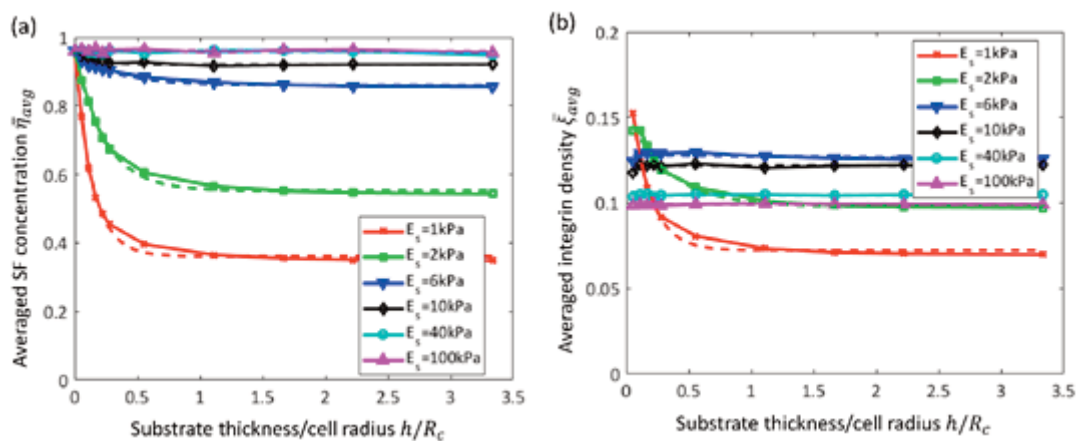
Figure 1: Effect of substrate stiffness and thickness on (a) averaged SF concentration, and (b) averaged integrin density along cell radius.

References:
[1]   Engler AJ. et al, Cell. 2006; 126 : 677. [2] Dalby MJ. et al , Nat. Mater. 2007; 6: 997.
[3]   Wells RG. J. Clin. Gastroenterol. 2005; 39: S158. [4] Wells RG. Biochim. Biophys. Acta. 2013; 1832: 884. [5] Deshpande VS. et al, Proc. Natl. Acad. Sci. 2006; 103:14015

C10.1

Sensitivity of the shear wave speed-stress relationship in connective tissues to material properties and microstructure - a probabilistic finite element study

Jonathon Blank[1], Darryl Thelen[1], Matthew Allen[2], Joshua Roth[3]

1   University of Wisconsin-Madison, Mechanical Engineering, Madison, United States
2   Brigham Young University, Mechanical Engineering, Provo, United States
3   University of Wisconsin-Madison, Orthopedics and Rehabilitation, Madison, United States

Background: Shear wave tensiometry is used to gauge the axial stress in tendon[1,2] and ligament[3] using the shear wave speed (SWS) propagating along the loaded tissue. However, variations in the composition and structure of tendons and ligaments, such as their collagen content and fiber alignment, can affect the tissue's material properties and response to loading. The effect this has on shear wave tensiometry is unknown. Accordingly, the objectives of this study were to use a probabilistic finite element model to determine the sensitivity of SWSs to (1) constitutive properties and (2) simulated fiber malalignment.

Methods: All finite element models were implemented in FEBio v.3.04 and executed on a high-throughput computing grid. The tissue was modeled as a Mooney-Rivlin transversely isotropic rectangular prism with distributed fibers.[5,6] We generated two cohorts of 10,000 models to vary constitutive properties (A) and fiber alignment (B). We stretched each model to an axial strain between 0-10% and excited a shear wave. The SWS was computed using the time delay in wave arrival at two nodes. Based on a tensioned beam model, we fit linear relationships between the axial stress and squared SWS, where the slope and intercept theoretically represent the tissue density and unloaded apparent shear modulus of the tissue.[1]

Results and discussion: SWSs were in range with those measured in previous studies (10-150 m/s).[2,3] As predicted by an analytical tensioned beam model, the slope of the squared SWS-stress relationship was sensitive to the tissue density ($R^2 = 0.99$) (Fig. 1.ii). Other constitutive properties changed the SWS to the extent that they changed the axial stress. At low loads, the SWS increased with fiber malalignment due to an increase in the tissue's unloaded apparent shear modulus with less well-aligned fibers (i.e., low kf). The microstructure-dependent shear modulus converged to the average unloaded apparent shear modulus observed in cohort A as fibers became more well-aligned (i.e., high kf) (Fig 1.iii).

Conclusions: SWSs are sensitive to changes in tissue microstructure and track axial stress predictably despite changes to constitutive properties that govern the tissue's stress-strain behavior. With this modeling pipeline we can evaluate cause-effect relationships in experimental tensiometry data.

Figure 1: We varied constitutive properties in cohort A according to a random uniform distribution (kf=500).6 In cohort B, we also varied the fiber distribution in the XZ plane (kf=0-500). Shown are measurements from the finite element model (i.e., fem) and those predicted using the analytical model (i.e., pred).

References:
[1]   Martin, Nat. Commun., 2018.
[2]   Martin, J. Biomech., 2019.
[3]   Blank, J. Mech. Behav. Biomed. Mat., 2020.
[4]   Maas, J. Biomech. Eng., 2012.
[5]   Gouget, Biomech. Model. Mechanobiol., 2012.
[6]   Stender, Biomech. Model. Mechanobiol., 2018.

C10.2
A rat muscle finite-element model to account for transverse loading effects

Mohamed Maamir[1 2 3], Tobias Siebert[4], André Tomalka[4], Yoann Lafon[1 2 3], Bertrand Fréchède[1 2 3]

1   Claude Bernard University Lyon 1, Villeurbanne, France
2   Université Gustave Eiffel, Champs-sur-Marne, France
3   IFSTTAR - French Institute of Science and Technology for Transport, Development and Networks, Champs-sur-Marne, France
4   University of Stuttgart, Stuttgart, Germany

Introduction: Previously reported experimental results on single rat Gastrocnemius Medialis (GM) muscles showed a macroscopic coupling between applied external transversal loads and force generation: activation generated transversal bulging, while increasing the transverse load tended to concurrently reduce the axial contraction force of the muscle [1]. The availability of these experimental results offered the possibility to explore the influence of fibre orientation on this coupling numerically.

Methods: The measured surface geometry of muscle, aponeurosis and tendons, as well as internal muscle fibres orientations, were used to reconstruct the 3D solid mesh of a rat GM muscle. Multiple Finite Element models were developed (A) with fibres directions interpolated from the experimental data and (B) with unidirectional pennation angles ranging from 0 to 30° from the longitudinal axis. We implemented a user-defined material formulation combining a Mooney-Rivlin function and active Hill-type fibre model in LS-DYNA. The rat GM muscle material properties were first calibrated through static optimisation against experimental data [2] obtained during isometric maximum induced contraction force (MVC) and passive transverse compression tests. The active transverse loading experiment [1] was then reproduced, where the muscle lay on a plate while a plunger was applied with increased weights on the muscle belly. Force at MVC and plunger vertical displacement were computed and compared to experimental results.

Results and discussion: As reported earlier [3], increased pennation angles heavily influenced the MVC force level. Both plunger lifting height and muscle MVC force were reduced with increased weight, albeit to a lesser extent than in the experiments. Simulating higher weight levels confirmed these trends. When the weight increased from 65g to 265g, in case B at 0° the reduction in simulated lifting height (resp. MVC force) was 19 % (resp. 31 %) of the experimental result. Other scenarios, including case A, resulted in smaller variations. Finally, global patterns of deformation (and thus, the lifting height) were very sensitive not only to pennation angle but also to boundary conditions and small variations in plunger lateral position. This may explain the difficulty to fully model a phenomenon which causes may be multi-factorial (as opposed to purely mechanical).
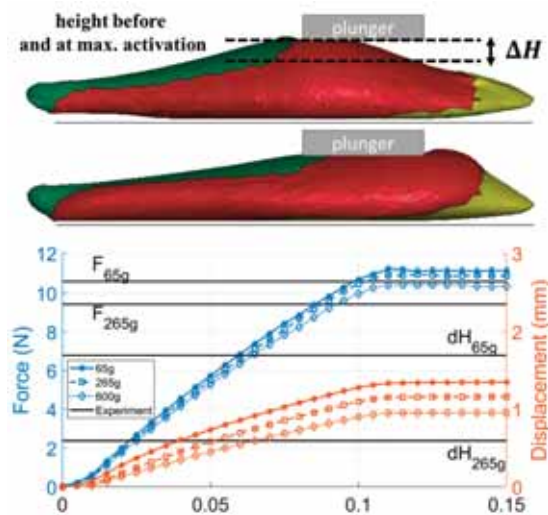
Figure caption: "muscle bulging at MVC with models B (at 0° and 15°, top). Transverse lifting height / longitudinal MVC force (bottom)"

References:
[15] Siebert et al. (2014). J Biomech, 47: 1822-28.
[16] Siebert et al. (2018). J Biomech, 66: 57-62.
[17] Wakeling et al. (2020). Front Physio, 11: 813

C10.3

Use of 3D ultrasound imaging with speckle tracking to identify calcified areas in abdominal aortic aneurysms

Achim Hegner[1], Christopher Blase[1], Andreas Wittek[1], Wojciech Derwich[2]

1   Frankfurt University of Applied Sciences, Personalized Biomedical Engineering Laboratory (PBE), Frankfurt am Main, Germany
2   University Hospital Frankfurt am Main, Clinic for Vascular and Endovascular Surgery, Frankfurt am Main, Germany

Introduction: For progress monitoring of an abdominal aortic aneurysm (AAA) mainly computed tomography (CT) and ultrasound imaging (US) are used. US imaging equipped with speckle-tracking provides dynamic information of small parts of the vessel and CT imaging the geometry of the whole AAA including calcifications. Our group uses 3D ultrasound for in vivo material characterization, as a performance test of the speckle-tracking algorithm we investigated if US imaging is capable to distinguish calcified areas from areas which are not calcified.

Methods: To this moment, CT and US images were obtained from ten AAA patients at the University Hospital Frankfurt (Germany). 3D vessel models of the aneurysmatic areas were reconstructed based on both imaging modalities. Three different strain components were calculated based on the US models using finite element analysis. For this purpose, US models based on a single segmentation were evaluated. Averaged models were also created, for which ten segmentations of the diseased vessel were averaged in each case. Calcifications were separately reconstructed based on CT imaging. A previously successfully implemented ICP algorithm for registration problems was used for the registration of the CT and US vessel geometries and calcifications. After registration, the deformations obtained by US imaging were mapped onto the CT geometry. The material points describing the surface of the US geometry could now be divided into "point with or without calcification" based on the reconstructed calcification and registration. To compare different strain components based on two individual calculation methods, a two-sample Kolmogorov-Smirnov test was used.

Results: The registration results of the patient specific geometries show a mean ± sd root mean squared error (RMSE) of 2.27 ± 0.44 mm and a mean ± sd Modified Hausdorff distance (HD) of 1.80 ± 0.37 mm for the registrations. Circumferential-, principal-, and equivalent-strains are significantly smaller in areas with calcification than in areas without calcification with mean p-values of p_Circ=0,00, p_Princ=0,00 and p_Equi=0,01.

Conclusion: Using 3D ultrasound with speckle-tracking, it is possible to distinguish calcified areas from areas which are not. The results are to be confirmed by the evaluation of further data sets.

References:
S. Matl, R. Brosig, M. Baust, N. Navab, S. Demirci, Vascular image registration techniques: A living review. Medical Image Analysis, Vol 35, pp. 1Є17, 2017.
D. Farotto, P. Segers, B. Meuris, J. Vander Sloten, N. Famaey, The role of biomechanics in aortic aneurysm management. J Mech Behav Biomed Mater., Vol. 77, pp. 295Є307, 2018.

C10.4

Elastic properties of normal breast tissues using an indentation protocol - a preliminary study

Ana Margarida Teixeira[1], *António André*[1], *Maria da Luz Barroso*[2], *Horácio Costa*[2], *Pedro Martins*[1 3]

1   INEGI, Porto, Portugal
2   Centro Hospitalar de Gaia/Espinho, Serviço de Cirurgia Plástica, Reconstrutiva, Craneomaxilofacial , Mão e Unidade de Microcirurgia, , Vila Nova de Gaia, Portugal
3   LAETA, Portugal

The mechanical properties of breast tissues are important for medical diagnose since the stiffness changes with a pathology. This has been investigated, however the experimental protocols are not standardized and for example the need of preconditioning is still debatable [1]. Thus, this study aims to evaluate the elastic properties of normal breast tissues, considering the effect of preconditioning. Two adjacent specimens (~12x12x5mm3) were collected from one patient, who underwent mammary reduction surgery, and they were tested using an indenter with diameter of 5mm, a strain amplitude of 0.5mm and a speed rate of 1.2mm/min for 14 cycles. As expected from literature [1], hysteresis was observed (Figure 1). The models proposed by Delaine-Smith et al. [2] were applied in the two linear regions of the loading curve of the last cycle. Young's modulus ranged from 3.2±0.4kPa to 8.8±1.1kPa and from 43.0±5.2kPa to 117.6±14.2kPa in the first and second linear regions, respectively, which is consistent with literature [3]–[6]. Moreover, comparing with [2], different concentrations of agarose can present similar elastic moduli of normal breast tissues. Regarding the effect of preconditioning, adding 6 cycles to one of the samples only had an impact on the first linear region, increasing the stiffness. Krouskop et al. [7] also reported that preconditioning increases the elastic modulus. Despite being a preliminary study, important considerations about the experimental protocol were obtained.
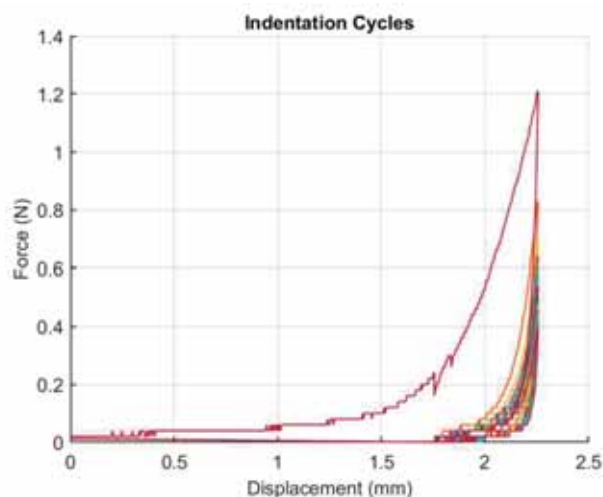
Figure 1: Force-displacement data for 14 cycles.

References:
[1]   N. Ramião et al., "Biomechanical Properties of Breast Tissue, a State-of-the-art Review.," Biomech. Model. Mechanobiol., vol. 15, no. 5, pp. 1307–23, 2016.
[2]   R. M. Delaine-Smith et al., "Experimental validation of a flat punch indentation methodology calibrated against unconfined compression tests for determination of soft tissue biomechanics," J. Mech. Behav. Biomed. Mater., vol. 60, pp. 401–415, 2016.
[3]   P. S. Wellman et al., "Breast Tissue Stiffness in Compression is Correlated to Histological Diagnosis," Tech. Report. Harvard BioRobotics Lab., pp. 1–15, 1999.
[4]   A. Samani et al., "Measuring the elastic modulus of ex vivo small tissue samples," Phys. Med. Biol., vol. 48, pp. 2183–2198, 2003.
[5]   A. Samani et al., "Elastic moduli of normal and pathological human breast tissues: an inversion-technique-based investigation of 169 samples," Phys. Med. Biol., vol. 52, no. 6, pp. 1565–1576, 2007.
[6]   T. Matsumura et al., "Measurement of elastic property of breast tissue for elasticity imaging," Proc. - IEEE Ultrason. Symp., pp. 1451–1454, 2009.
[7]   T. A. Krouskop et al., "Elastic Moduli of Breast and Prostate Tissues under Compression," Ultrason. Imaging, vol. 20, no. 4, pp. 260–274, 1998.

C10.5

Maternal pushes during the second stage labor: a biomechanical study of fatigue damage accumulation

Maria Vila Pouca[1 2], *João Pedro Sousa Ferreira*[1 2], *Marco P. L. Parente*[1 2], *Renato M. Natal Jorge*[1 2]

1   FEUP - Faculdade de Engenharia da Universidade do Porto, Porto, Portugal
2   INEGI - Institute of Science and Innovation in Mechanical and Industrial Engineering, Porto, Portugal

Although vaginal delivery is supposedly a natural event in a women's life, it is not risk free. In fact, pelvic floor muscle injuries have been reported to occur up to 66% and will cause an increase risk to develop pelvic floor disorders later in life.

Recently, it has been showed that a similar mechanism to mechanical fatigue can occur in soft tissues. This has been seen in the anterior cruciate ligament 4 and also in sheep pelvic floor muscle3. The implications of these discoveries are that tissue tears might occur, not only due to a single maximal load, but also due to an accumulation of several sub-maximal loads.

In the second stage of labor, due to the combination of the uterine contractions and maternal pushes, which are necessary to achieve the fetal expulsion, the pelvic floor muscles are subjected to repetitive loads. This raises the question whether the maternal pushes might cause an excessive damage accumulation in the pelvic tissue, if not managed accurately.

There are commonly two possible managements of labor: a spontaneous or a directed/coached pushing. In the coached pushing, women are instructed to inhale deeply and to push for a duration of 10s (gives ~3 pushes per contraction)2. In the spontaneous pushing, this is carried out naturally by the woman according to their desire (gives ~3-5 pushes per contraction for 3-5 seconds or 1 longer push near the contraction peak)1.

In this work, we developed a biomechanical model of the second stage of labor, implementing a visco-hyperelastic constitutive model including fatigue damage, to test the hypothesis that the different maternal pushing patterns influence the damage accumulation in the pelvic tissue. Our final aim is to analyze the best approach in terms of minimizing the damage accumulation. We hope this work will bring a new light into how labor is managed, ultimately helping to improve the labor experience for women.

References:
1.   Hanson L. Second-stage labor care: challenges in spontaneous bearing down. J Perinat Neonatal Nurs. 2009;23(1):31. doi:10.1097/JPN.0b013e318196526b.
2.   Lee N, Gao Y, Lotz L, Kildea S. Maternal and neonatal outcomes from a comparison of spontaneous and directed pushing in second stage. Women and Birth. 2019;32(4):e433-e440. doi:https://doi.org/10.1016/j.wombi.2018.10.005.
3.   Vila Pouca MCP, Parente MPL, Natal Jorge RM, Ashton-Miller JA. Investigating the birth-related caudal maternal pelvic floor muscle injury: The consequences of low cycle fatigue damage. J Mech Behav Biomed Mater. 2020;110:103956. doi:https://doi.org/10.1016/j.jmbbm.2020.103956.
4.   Wojtys EM, Beaulieu ML, Ashton-Miller JA. New perspectives on ACL injury: On the role of repetitive sub-maximal knee loading in causing ACL fatigue failure. J Orthop Res. 2016;34(12):2059-2068. doi:10.1002/jor.23441.

C10.6
Patient specific modelling of respiratory PPE interacting with the soft tissues of the face

Sam Evans[1], Bethany Keenan[1], Peter Worsley[2], Silvia Caggiari[2], Dan Bader[2]

1Cardiff School of Engineering, Cardiff, United Kingdom
2University of Southampton, Southampton, United Kingdom

Masks and respirators to protect against inhalation of particles and aerosols have become very important during the Covid-19 pandemic. Discomfort and soft tissue injuries from prolonged use of poorly fitting respirators are common among healthcare workers and others and pose a threefold danger: as well as the risk of injury, discomfort often leads users to remove respirators, increasing infection risk, and poor fit can lead to leaks and lack of protection. A significant cause of these problems is that most commercial respirators and testing standards are made in a single size designed for a white, male workforce (in fact many can be traced back to a study on US Air Force pilots in the 1950s). This means that women, other ethnic groups and those with unusual face shapes more often experience problems.

The aim of this study is to investigate the interaction of different mask designs with different face shapes and with the soft tissues of the face in order to improve their design, develop better guidelines for users and better inform testing standards. We are approaching this in three ways, through clinical studies and skin microenvironment measurents, by using MRI to quantify soft tissue strains and through finite element modelling, which is the subject of this abstract.

Masks were modelled using FEBio, based on measurements for flexible designs such as the 3M 9330+ and using 3D laser scans (Artec Spider) to capture the geometry of rigid designs such as the Easimask and HY 9632. Meshes were created using Meshlab and GMsh together with meshing tools in FEBio Studio. Masks were represented using shell elements combined with 3D solid elements to represent foam padding and other features where through-thickness deformation is significant. Subjects were MRI scanned (3T Siemens Magnetom Prisma) and models were created using Simpleware, segmenting the skin, fat, cartilage and muscle and treating the bones, teeth and irrelevant parts of the head as a rigid body.

Modelling flexible masks in particular is exceptionally difficult because buckling and wrinkling of the soft material creates numerous bifurcations and instabilities, as well as very large deformations, numerous difficult contacts and complex material models including plastic deformation of metal components. An implicit dynamic solution algorithm can help to reduce instabilities and improve convergence.

Work is ongoing to increase the number of subjects and validate the models using digital volume correlation measurements.
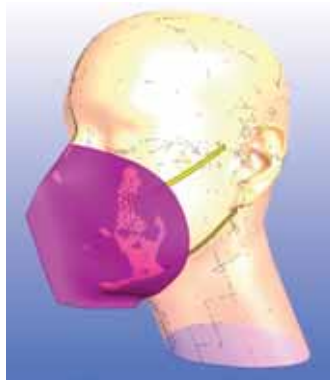
Figure caption: Ree KN95 mask virtually fitted to a NIOSH standard headform.

139

D-01

Necessity and importance of high-performance computing to address the scalability issue of biomedical-related computational studies

CMBBE 2021

A b s t r a c t   b o o k

D1.1
Taking blood flow simulation towards the exascale with HemeLB

Jon McCullough[1], Ioannis Zacharoudiou[1], Peter Coveney[1 2]

1   University College London, Department of Chemistry, London, United Kingdom
2   University of Amsterdam, Institute for Informatics, Amsterdam, Netherlands

As the performance and scale of computing power continues to increase, the ambition of simulations that can be conducted likewise grows. In the field of computational biomedicine, this often focuses on the introduction of more realistic physics models, the analysis of larger data sets and the study of more detailed physiological domains. With the first exascale computers scheduled for arrival in the next 12 months, the ambition of creating a virtual human simulation – a personalized digital model of an individual to assess and predict health outcomes - comes closer to reality. However, taking full advantage of such performance demands that applications can efficiently extend their operation to very large computational scales. Achieving this requires substantial effort from both scientists and developers. Many areas of biomedical simulation are making significant strides towards human-scale simulation, the domain of blood flow modelling being a particular example. The open-source application HemeLB[1] solves 3D macroscopic blood flow in complex vascular geometries using the lattice Boltzmann method. Its performance has been optimized to handle the sparse domains characteristic of blood vessels and has been shown to deliver excellent parallel performance on both CPU and GPU architectures. We have demonstrated strong scaling performance to over 300,000 CPU cores on SuperMUC-NG (Germany) and 18,000 GPUs on Summit (USA) - some of the fastest supercomputers of the current generation. In this presentation, we will discuss some of the challenges of obtaining scaling performance at this scale using a code focused on biomedical simulation and will provide an outlook on taking HemeLB towards exascale computation.

References:
1. hemelb.org

140

D-01

Necessity and importance of high-performance computing to address the scalability issue of biomedical-related computational studies

CMBBE 2021
Abstract book

D1.2
Current scaling limits of a large-scale cellular blood flow simulation

Gabor Zavodszky[1], Max van der Kolk[1], Jelle van Dijk[1], Ana Varbanescu[1], Alfons Hoekstra[1]

1   University of Amsterdam, Computational Science Lab, Amsterdam, Netherlands

Blood is the single most important biological fluid in the human body. Modelling its behavior accurately on the cellular level is gaining importance in the recent years. Resolving the deformation of single cells and their trafficking in bulk is fundamental for various domains ranging from rheology, through microfluidics, to applied disease-specific research (e.g., diabetic blood flows or tumor cell circulation). The complexity and the computational cost of these simulations keep increasing as well, on the one hand due to more and more included detail, and on the other hand due to the larger domain sizes of interest. In this work a detailed performance and scaling analysis will be presented for large-scale simulation scenarios (>10k cores) of HemoCell , our open-source cellular blood flow simulation library. The library is thoroughly validated [1,2] and has been applied to a large set of research questions (e.g., Fig.1 and [3,4]). The typical performance bottlenecks (for instance, the communication overhead, load-imbalance, strong-scaling limits) arising when running at scale are discussed, together with the currently implemented mitigation strategies, such as code optimizations [5], and dynamic load-balancing [6], and their shortcomings. HemoCell is among the most performant cellular suspension codes, and the current strong-scaling analyses indicate that the performance is limited by the size of the communication envelope, which yields the optimum point at O(10) cells per computing-core domain decomposition on the current HPC architectures (e.g., Cartesius, SURF, Netherlands; SuperMUC, LRZ, Garching). A single mm3 of human blood contains approximately 5 million red blood cells, which implies that the accurate and efficient modelling of a single microliter of blood requires O(500,000) computing cores, that positions the problem to exascale territory. This can have far reaching consequences regarding future numerical models and applications and shows the importance of the presented techniques that aim to mitigate performance bottlenecks in large-scale cellular simulations.

Figure caption: Simulation of cellular blood flow over an artificial stenosis in a microfluidic chamber (image from [4]).

References:
[1]   Závodszky et al. (2017). Frontiers in physiology, 8, 563.
[2]   de Vries et al. (2020). International Journal for Uncertainty Quantification, 10(4).
[3]   De Haan et al. (2018). Applied Sciences, 8(9), 1616.
[4]   van Rooij et al. (2021). Interface Focus, 11(1), 20190126.
[5]   Tarksalooyeh et al. (2019). In International Conference on Computational Science (pp. 537-547). Springer, Cham.
[6]   Alowayyed et al. (2018). Journal of computational science, 24, 1-7.

141

D-01

Necessity and importance of high-performance computing to address the scalability issue of biomedical-related computational studies

CMBBE 2021
Abstract book

D1.3

Numerical models as regulatory evidence: gathering credibility evidence through VVUQ

Alfonso Santiago[1 2]

1 Barcelona Supercomputing Center - Centre Nacional de Supercomputació, Computer Applications in Science and Engineering, Barcelona, Spain
2 ELEM biotech, R+D+I, Barcelona, Spain

Although numerical models have been ubiquitous for industries like aerospace during the last 30 years, such models are just beginning to revolutionize the biomedical devices industry. This has recently been addressed in published protocols, such as the ASME V&V 40, which provide guidance on gathering credible evidence for regulatory review. Such transition is also being seen in the regulatory side. The U.S. Food and Drug Administration (FDA) launched the Medical Device Development Tool (MDDT) programme that allows considering modeling tools as review evidence during device submissions.

Today, the novel medical devices review process is mostly a qualitative one, relying on expensive and time consuming animal testing and etically questionable human clinical trials. Numerical modelling opens the door for a highly scalable quantitative process, a comparatively cheaper pipeline, and a more ethical way of improving device design and providing review evidence. But, compared to purely mechanical systems as in aerospace, numerical models for the biomedical industry have to deal with an extremely large variability of the test samples and underlying systems that are not fully understood. It is our maximum priority as numerical modelers provide a complete and thorough set of credibility evidence to accelerate the application of simulation to complex biomechanical systems. While it is for certain that populations of subjects are required to provide reliable credibility evidence, they involve a high computational cost making high performance computing (HPC) architectures mandatory. At the same time, data mining techniques are required to analyse these populations and drive conclusions out of them.

In this talk we walk through the different codes and standards to provide credibility evidence and show multiple examples of this process.

142

D-01

Necessity and importance of high-performance computing to address the scalability issue of biomedical-related computational studies

CMBBE2021

Abstract book

D1.4

A penalty contact implementation on a highly parallelisable cartesian mesh finite element solver

Frederik Trommer[1 2], Pinaki Bhattacharya[1 2]

1   The University of Sheffield, Department of Mechanical Engineering, Sheffield, United Kingdom
2   The University of Sheffield, Insigneo Institute for in silico Medicine, Sheffield, United Kingdom

Introduction: Micro finite element analysis (uFE) is a validated tool for non-invasively quantifying bone mechanics using high resolution computed tomography (CT) images. uFE solvers for for voxel models, such as ParOSol [1], can efficiently solve problems with billions of degrees of freedom. As yet, such solvers do not accurately compute contact induced stresses. The novel SS-SC formulation [2] resulted in a reduction of errors associated with contact in voxel-based meshes from 42% to 2%. As an intermediate step towards implementing the SS-SC formulation in the highly parallelized octree-based multigrid solver ParOSol, the present study implements the standard penalty contact formulation in this solver.

Methods: An incremental solution strategy is implemented. Within each increment, contact iterations are performed to solve the nonlinear contact boundary conditions. Specifically, the contributions from the tangent contact stiffness and the contact reaction forces are updated. These contributions are computed based on [3]. The implementation was used to analyse the problem of two linear elastic, homogeneous and isotropic bodies (A and B) with hard, frictionless contact (Figure 1). The nine nodes on the bottom plane of body B (comprising four voxels) are fixed in all dimensions; the 4 nodes on the top of body A, comprising a single voxel, are restricted in x and y directions; body A is displaced in -z direction onto body B such that they penetrate by 10% of the voxel size. Two equally weighted master–slave pairs were defined with the opposing surfaces of A and B as master and slave respectively and vice versa. Model prediction is verified against an identical formulation in the commercial FEA solver Abaqus v6.14.

Figure 1 compares the predictions from ParOSol and Abaqus for the displacement of the bodies.

Conclusions: The implemented penalty contact formulation converged, and predicted deformations comparable to a commercial solver. The solution obtained by Abaqus shows more overclosure and a larger bulge in body B, probably owing to numerical artifacts due to the small size and the constrained nature of the problem. Future implementations will engage the multigrid cycles in the solution process and include a simulated smooth surface definition, thus improving the prediction of surface interactions and integrating the SS-SC formulation more completely into ParOSol.
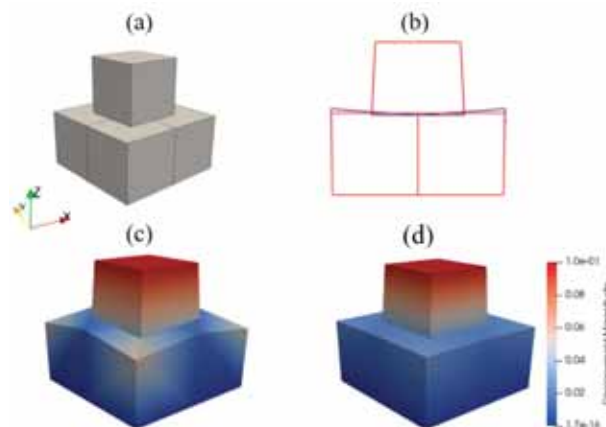
Figure 1: a) Model geometry in reference configuration. b) Outlines of the solutions at a central cross section, blue: Abaqus, red: ParOSol. Magnitude of contact induced displacements predicted by c) Abaqus and d) ParOSol.

References:
[1]   Flaig (2012) PhD Thesis ETH Zürich.
[2]   Bhattacharya et al. (2018) Int J Numer Meth Eng, 115(4):411–26.
[3]   Parisch (1989) Int J Numer Meth Eng, 28:1803–12.

D2.1

Efficient identification of myocardial material parameters and the stress-free reference configuration for patient-specific models

Justyna Anna Niestrawska[1], Laura Marx[2], Matthias A.F. Gsell[2], Federica Caforio[2], Gernot Plank[2], Christoph M. Augustin[2]

1   Gottfried Schatz Research Center for Cell Signaling, Metabolism and Aging - Division of Macroscopic and Clinical Anatomy, Graz, Austria
2   Gottfried Schatz Research Center for Cell Signaling, Metabolism and Aging - Division of Biophysics, Medical University of Graz, Graz, Austria

Image-based computational models are a powerful tool to understand mechanisms of physiological and pathological conditions in cardiac function. Driven by recent advances in medical imaging and simulation technologies, a translational trend is emerging geared towards employing cardiac modelling as a clinically useful diagnostic modality. However, the personalization of these in silico models remains a challenging task requiring the automatization of complex parameterization techniques of various model components such as anatomy, active stresses within the myocardium and passive biomechanical tissue properties.

There have been numerous contributions in experimental and computational biomechanics to characterize the passive behavior of the myocardium. However, many of these studies suffer from severe limitations and are not applicable to high-resolution geometries. Therefore, we propose a novel methodology for an automated identification of in vivo properties of passive cardiac biomechanics: An efficient model function based fitting method to find personalized passive material parameters while simultaneously generating a stress-free reference configuration [1]. Latter is a crucial step for image-based biomechanical modeling. In this regard we were able to present an improved algorithm to find this stress-free reference configuration with a novel fail-safe feature.

The model based fitting algorithm was tested on a cohort on previously published LV meshes [2] and showed excellent fittings to the personalized empirical Klotz end diastolic pressure volume relation [3] for all cases. As fitting and the generation of the stress-free reference configuration was performed simultaneously the method only required a small number of forwards simulations (<10 for all cases) and was very efficient (around two to three times faster than a standard inflation experiment). The workflow is applicable to a large variability of constitutive models, model functions and FE formulations and can be established in FE software packages with ease. Additionally, the robustness of the algorithm with respect to initial input parameters was shown by sensitivity analysis.
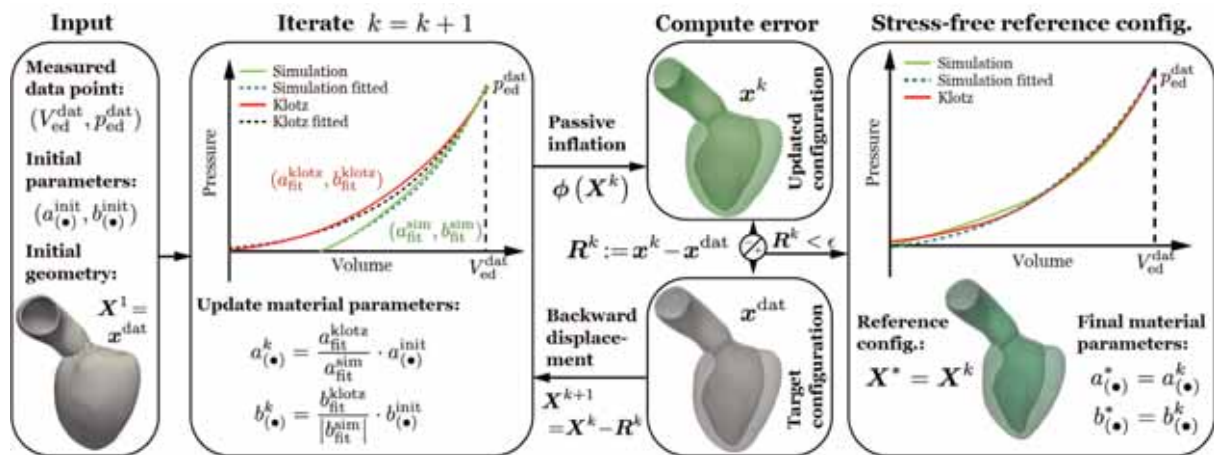
Figure caption: Workflow showing the simultaneous unloading and fitting of patient specific passive biomechanical properties.

References:
[1]   L. Marx, J.A. Niestrawska, M.A.F. Gsell, F. Caforio, G. Plank, C.M. Augustin (2021). Efficient identification of myocardial material parameters and the stress-free reference configuration for patient-specific human heart models. arXiv preprint arXiv:2101.04411.
[2]   L. Marx, M.A.F. Gsell, A. Rund, F. Caforio, A.J. Prassl, G. Toth-Gayor, T. Kuehne, C.M. Augustin, G. Plank, Personalization of electro-mechanical models of the pressure- overloaded left ventricle: fitting of Windkessel-type afterload models, Philosophical Transactions of the Royal Society A: Mathematical, Physical and Engineering Sciences 378 (2020) 20190342.
[3]   S. Klotz, M. L. Dickstein, D. Burkhoff, A computational method of prediction of the end-diastolic pressure–volume relationship by single beat, Nature Protocols 2 (2007) 2152–2158.

D2.2

Reconstructing cardiac action potential waves from tissue deformations using the ensemble transform Kalman filter

Christopher Beam[1], *Cristian Linte*[2,3], *Laura Muñoz*[1], *Niels Otani*[1]

1 Rochester Institute of Technology, School of Mathematical Sciences, Rochester, United States
2 Rochester Institute of Technology, Biomedical Engineering, Rochester, United States
3 Rochester Institute of Technology, Center for Imaging Sciences, Rochester, United States

Many models have been proposed which describe the propagation of membrane potentials through muscle tissue within the heart. These membrane potentials encode the concentrations of various ions inside and outside the myocytes and the motion of these ions is what triggers the deformation of cardiac tissue. Direct measurement of these action potentials and the resulting active stresses that cause the tissue to contract is highly invasive, as it interferes significantly with the function of the tissue. Thus, non-invasive in vivo measurements of tissue motion using medical imaging are thus preferred. Theoretically, it is possible to solve an inverse problem to recover the membrane potentials and active stresses, given the deformations, in a naïve manner using a QR solver. However, since this problem is ill-posed, the presence of noise and uncertainty in the measurements precludes the naïve QR-based solution as a practical method.

Here we propose to use the Ensemble Transform Kalman Filter (ETKF) to overcome the effects of these measurement uncertainties. The ETKF allows for the assimilation of uncertain measurement data with mathematical models of the quantities being measured. The ETKF allows for the reconstruction of quantities which are derived from those being measured. The ETKF can produce membrane potential and active stress estimates even when the model used in the estimation process differs from the system model used to generate the original data. Furthermore, parameter estimation can be used to further refine the estimates produced by the ETKF by allowing it to tune the parameters used in the reconstruction model to better approximate the data produced by the ground truth model.

Using the naïve QR-based method, we found that a measurement noise coefficient of 0.05 produced reconstruction errors with a standard deviation of 1.67 for the (normalized) active stress. However, when utilizing the ETKF in conjunction with the model used in generating the ground truth data, the reconstruction error distribution was characterized by a standard deviation of 0.28. This precision was refined by replacing the model used in the ETKF prediction step and additionally incorporating parameter estimation. These changes further reduced the standard deviation of the error to 0.15.

In summary, the ETKF is a robust and efficient technique for reconstructing the membrane potentials and active stresses from tissue deformations. Additionally, parameter estimation can be further used to refine the estimates produced by the ETKF by enabling further tuning of the parameters used in the reconstruction model to better approximate the ground truth model.

D2.3

A coupling strategy for a 3D-1D model of the cardiovascular system to study the effects of pulse wave propagation on cardiac function

Federica Caforio[1 2], Christoph Augustin[2], Jordi Alastruey[3 4], Gernot Plank[2]

1   Institute of Mathematics and Scientific Computing, NAWI Graz, University of Graz, Graz, Austria
2   Gottfried Schatz Research Center: Division of Biophysics, Medical University of Graz, Graz, Austria
3   Department of Biomedical Engineering, Division of Imaging Sciences and Biomedical Engineering, King's College London, King's Health Partners, St. Thomas' Hospital, London , United Kingdom
4   World-Class Research Center "Digital Biodesign and Personalized Healthcare", Sechenov University, Moscow, Russian Federation

The impact of increased stiffness and pulsatile load on the circulation and the heart performance is documented not only for cardiovascular events but also for ventricular dysfunctions. Therefore, computer models of cardiac electromechanics (EM) shall integrate effects of the circulatory system on heart function for clinical applications. To ensure a satisfactory tradeoff between accuracy and computational cost, simplified representations of the circulation are used.

In this talk, we describe a novel strategy for a coupled model based on a 3D EM model of the heart function [2,4], together with a 1D model of blood flow in the arterial system [1]. The coupling approach is based on the resolution of a saddle-point problem for the volume and pressure in the cavity.

As an illustration, we consider a system composed by a 3D model of the Left Ventricle (LV) coupled to an arterial outflow consisting of a 1D viscoelastic tube and lumped terminal boundary conditions. To explore the effect of vessel stiffening, we consider three scenarios: a baseline case, with model parameters calibrated with clinical data, and two cases with aortic wall stiffness E increased by a factor 2 and 3, respectively. The increase in E results in an augmentation of the peak LV and pulse pressure and a variation in the pulse pressure profile. The augmentation in E also leads to an increase in End-Systolic Volume, resulting in a reduction in Stroke Volume.

The use of 1D arterial models enables to efficiently capture the effects of vascular changes and distributed properties, since they allow for a more detailed representation of the impact of pulse wave transmission on the circulation and cardiac function. Consequently, the use of this coupled model has great potential in understanding a broad spectrum of cardiovascular pathologies. An application to aortic coarctation using a stenosis model [3] will be shown during the talk.
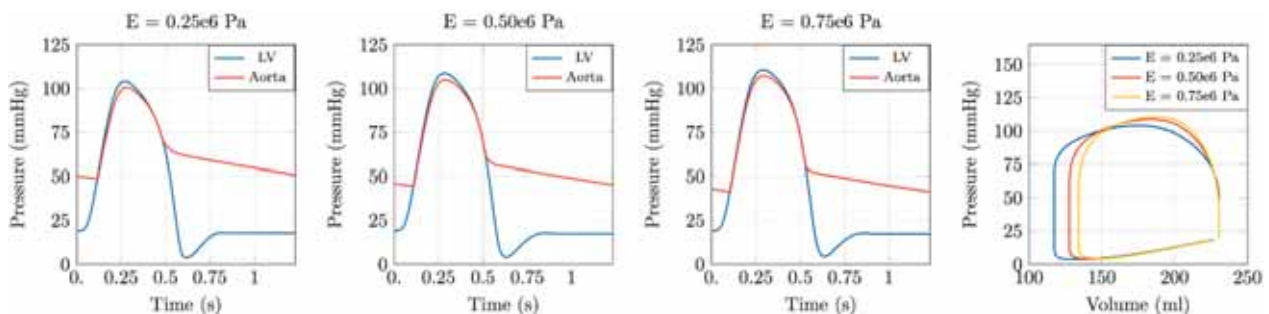
Figure caption: Illustration of model predictions. Left: Pressure trace in the LV and at the aortic inlet. Right: Pressure-volume loop in the LV.

References:
[1]   J Alastruey, KH Parker, and SJ Sherwin. BHR Group - 11th Int. Conf. on Pressure Surges, 401–442, 2012.
[2]   CM Augustin, A Neic, M Liebmann, AJ Prassl, SA Niederer, G Haase, and G Plank. JCP, 305:622–646, 2016.
[3]   W Jin, J Alastruey, JRSI, 18: 20200881, 2021.
[4]   A Neic, FO Campos, AJ Prassl, SA Niederer, MJ Bishop, EJ Vigmond, and G Plank. JCP, 346:191–211, 2017.

D2.4

Developing drugs that are safe for the female heart: a novel sex-specific torsadogenic risk classifier

Mathias Peirlinck[1], *Francisco Sahli Costabal*[2 3 4], *Ellen Kuhl*[1]

1   Stanford University, Mechanical Engineering, Stanford, United States
2   Pontificia Universidad Catolica de Chile, Department of Mechanical and Metallurgical Engineering, Chile
3   Pontificia Universidad Catolica de Chile, Santiago, Institute for Biological and Medical Engineering, Chile
4   Millennium Nucleus for Cardiovascular Magnetic Resonance, Chile

About a century ago, sex differences in cardiac electrophysiology were reported for the first time[1]. At this point, female sex is recognized to be an essential risk factor for multiple adverse cardiac events. Especially for Torsades de Pointes (TdP), a particular type of polymorphic ventricular tachycardia known to precipitate into ventricular fibrillation and sudden cardiac death, women turn out to be impacted twice as much as men[2]. Unfortunately, some drugs interact with specific ionic channels in cardiac cells, predisposing the heart to develop these Torsades de Pointes. Consequently, a pro-arrhythmic risk assessment is mandatory before a drug can enter the market. Over the last years, in silico modeling has emerged to play an increasingly important role in this assessment. Computational models provide novel biomarkers with improved sensitivity and specificity compared to experimental cell and animal studies[3]. However, female sex is mostly overlooked as an independent risk factor.

In this study, we develop a novel sex-specific torsadogenic risk classifier through multiscale modeling and machine learning. We first build an individual male and female multiscale exposure-response simulator[4] taking into account sex differences in subcellular ion channel activity, tissue-level conductivity, and organ-scale geometry. Secondly, we use latin hypercube sampling and logistic regression to explore the arrhythmic sensitivity of the male and female heart to drug-specific ion channel blocking. Based on this, we establish an exploratory ion channel blocking parameter space and combine low-fidelity cell-scale and high-fidelity multiscale modeling to delineate TdP risk classification boundaries, using multi-fidelity Gausian process classification and active learning procedures[5]. Our results quantitatively confirm and delineate women's intrinsically higher risk for drug-induced TdP development both on the cell and organ scale. Using our male and female multi-fidelity risk classifiers, we study the sex-specific torsadogenicity risk of high, intermediate, and low risk drugs, showcasing significant differences in critical drug concentrations between men and women.
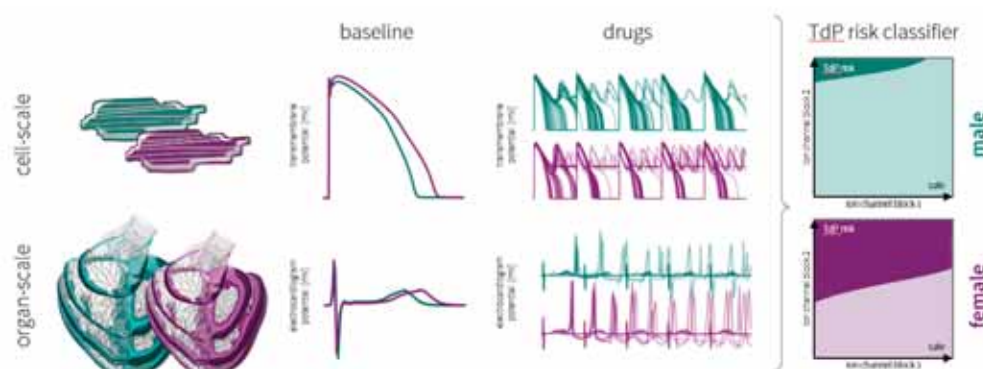
Figure caption: Schematic overview of our study.

References:

1   Bazett, HC (1920) "An analysis of the time relations of electrocardiograms" Heart 7
2   Makkar, RR et al. (1993) "Female gender as a risk factor for torsades de pointes associated with cardiovascular drugs" JAMA 270 (21)
3   Passini, E et al. (2017) "Human In Silico Drug Trials Demonstrate Higher Accuracy than Animal Models in Predicting Clinical Pro-Arrhythmic Cardiotoxicity" Front. Physiol. 8 (668)
4   Sahli Costabal, F et al. (2018) "Predicting the cardiac toxicity of drugs using a novel multiscale exposure-response simulator" Comput. Methods Biomech. Biomed. Engin. 21 (3)
5   Sahli Costabal, F et al. (2019) "Multi-fidelity classification using Gaussian processes: accelerating the prediction of large-scale computational models" Computer Methods in Applied Mechanics and Engineering 357

D2.5
Hemodynamic modeling for mitral regurgitation

Mia Bonini[1], Marc Hirschvogel[2], Yunus Ahmed[3], Paul Tang[3], Hao Xu[2], Alistair Young[2], David Nordsletten[1 2 3]

1   University of Michigan, Biomedical Engineering, Ann Arbor, United States
2   King's College London, Department of Biomedical Engineering and Imaging Sciences, United Kingdom
3   University of Michigan, Department of Cardiac Surgery, Ann Arbor, United States

Mitral regurgitation (MR) is a common valvular disease and can lead to pulmonary hypertension, atrial fibrillation, and heart failure. It is understood that MR causes a decrease in systolic outflow and an increase in left atrial pressure as well as dilation of the left ventricle and left atria [1]. However, the impact of MR the entire cardiovascular system, in particular the right heart, is incompletely understood. Specifically, the impact of the degree of regurgitation and the variation in the regurgitant jet on the load in the right heart is unclear. This study aims to predict the effect of MR on cardiovascular hemodynamics and right ventricular function using state-of-the art imaging and hemodynamics modeling.

We developed a pipeline to create patient-specific computational fluid dynamic models of the left heart to analyze MR (see Figure 1). Gated CT data was collected retrospectively, and a neural network was used to segment the images. The segmentation masks were converted into dynamic STL surfaces and meshes were constructed. We propose an arbitrary Lagrangian-Eulerian boundary energy-driven left atrial and left ventricular fluid dynamics model [2]. Patient specific pressure measurements were collected and used to drive the energy-boundary motion. This method allows for the motion of the left heart to adapt and respond to changes to the cardiovascular system. The 3D model of the left atrium and left ventricle is coupled to a closed-loop lumped parameter model of the systemic and pulmonary circulation [3]. Varying degrees of mitral valve stenosis were introduced into the model to assess the potential hemodynamic impact of MR on the cardiovascular system and on the right ventricular workload.

This process makes it possible to further understand the effect that mitral regurgitation has on right heart function and assist in predicting the risks associated with MR for individual patients. This is particularly important for patients who require a left ventricular assist device in which right heart failure, linked with MR, is a common complication [4].
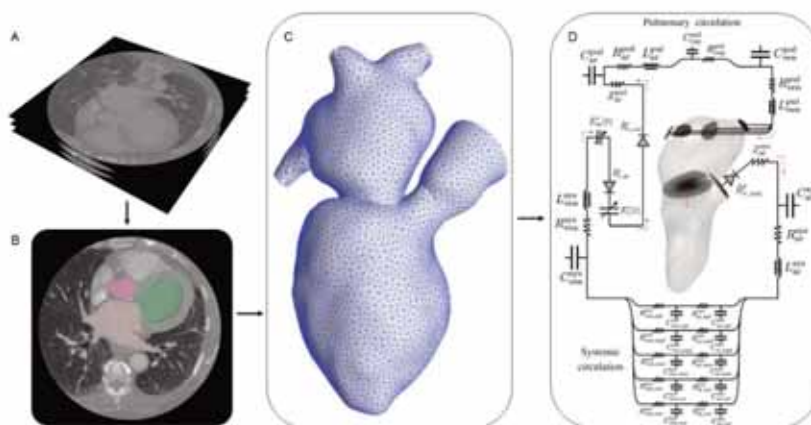
Figure 1: Personalized hemodynamic modeling pipeline of atrioventricular flow. (A) Medical imaging and data acquisition, (B) neural network anatomical segmentation and labelling, (C) 3D model reconstruction and mesh generation, (D) 0D-3D coupling.

References:
[1]   Douedi, Steven. and Hani Douedi. "Mitral Regurgitation." StatPearls, StatPearls Publishing, 10 March 2021.
[2]   Lee, Jack, et al. "Multiphysics computational modeling in CHeart." SIAM Journal on Scientific Computing 38.3 (2016): C150-C178.
[3]   Balmus, Maximilian, et al. "A partition of unity approach to fluid mechanics and fluid–structure interaction." Computer Methods in Applied Mechanics and Engineering 362 (2020): 112842.
[4]   Kassis, Hayah et al. "Significance of Residual Mitral Regurgitation After Continuous Flow Left Ventricular Assist Device Implantation." JACC. Heart failure vol. 5,2 (2017): 81-88. doi:10.1016/j.jchf.2016.09.014

D2.6
Computational modelling of subepicardial mechanics in desmoplakin cardiomyopathy

Javiera Jilberto[1], Marc Hirschvogel[2], Renee Miller[2], Adam Helms[3], David Nordsletten[1 2]

1   University of Michigan, Biomedical Engineering, Ann Arbor, United States
2   King's College London, Biomedical Engineering and Imaging Sciences, London, United Kingdom
3   University of Michigan, Internal Medicine, Division of Cardiovascular Medicine, Ann Arbor, United States

Desmoplakin cardiomyopathy is a genetic disease produced by a mutation of the desmoplakin (DSP) gene, a component of the desmosome that provides cell-to-cell adhesion. Patients with this genetic mutation commonly suffer from systolic dysfunction due to progressive injury and fibrosis in the subepicardial layer of the left ventricular myocardium [1]. Considering that the mechanical link between cells is impaired, it follows that the magnitude of the subepicardial layer's stretch as well as the workload that cells can bear may play a critical role in DSP cardiomyopathy. We hypothesize that the unique mechanical environment of the subepicardium (particularly stretch and myocardial work) negatively impacts the tissue, causing injury and later fibrosis. This study investigates the variations in subepicardial stretch due to modifications in hemodynamic loading conditions using a computational biomechanical model of the left ventricle (LV). The model consists of an idealized LV geometry coupled with a 0D model of the circulatory system [2]. The parameters are tweaked to reflect changes in heart rate, afterload, and contractility, among others. Further, an Eikonal problem was used to provide realistic activation patterns across the LV muscle. The amount of stretch in the subepicardial layer was studied in a healthy LV and a diseased LV with subepicardial fibrosis. Idealized versions of the most common fibrosis patterns in DSP cardiomyopathy affecting the mid-inferior region and the whole circumference of the LV are studied. A third, more realistic case, created from the fibrosis pattern measured using medical image data, is also considered. This study systematically assesses variations in subepicardial stretch due to changes in hemodynamic loading and fibrosis patterns. It represents an important input for investigating more complex, patient-specific models with the final objective of understanding the development of DSP cardiomyopathy.
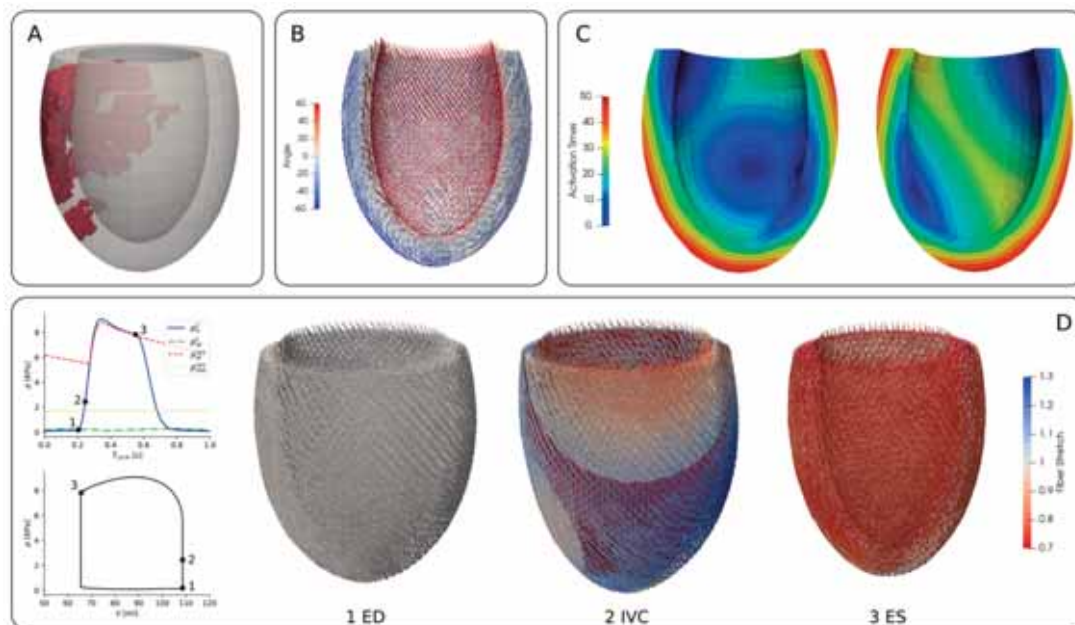
Figure caption: A LV model with subepicardial fibrosis. B Rule-based fiber field. C Activation times. D Healthy LV simulation at end-diastole (ED), isovolumic contraction (IVC), and end-systole (ES). During IVC, the activation wave is shown as a red contour. Left plots show the Wiggers diagram and P-V loop for one cardiac cycle. Black dots refer to time points before mentioned.

References:
[1]   Smith, E. et al. (2020). Desmoplakin Cardiomyopathy, a Fibrotic and Inflammatory Form of Cardiomyopathy Distinct From Typical Dilated or Arrhythmogenic Right Ventricular Cardiomyopathy. Circulation, 141(23), 1872–1884.
[2]   Hirschvogel, M. et al. (2017). A monolithic 3D-0D coupled closed-loop model of the heart and the vascular system: Experiment-based parameter estimation for patient-specific cardiac mechanics. International Journal for Numerical Methods in Biomedical Engineering, 33(8), 1–22.

D2.7

Preliminary results of >bi-axial characterization of the left atrium

Wendy Silva-Verissimo[1], Fedoua El Louali[2], Stanislas Rapacchi[3], Yves Godio-Raboutet[2], Yannick Tillier[4], Morgane Evin[2]

1   Aix-Marseille Univ, Univ Gustave Eiffel, LBA, TS2, Marseille, France
2   Aix-Marseille Univ, Univ Gustave Eiffel, LBA, Marseille, France
3   Centre de Résonance Magnétique Biologique et Médicale - UMR 7339, Marseille, France
4   Cemef, Sophia Antipolis, France

By its function, the left atrium (LA) plays a central role in cardiac mechanics. It contributes to 20% of ventricular filling and is the site of atrial fibrillation with an prevalence of 10% in the population over 80 years old [1]. Numerous factors, such as age or obesity [2], can cause LA dilation and dysfunction creating blood stasis also known as thrombus mostly located in the left appendage (LAA). The thrombus formation is one of the risk factor of atrial fibrillation especially in LAA [3]. While passive myocardium of the LV has been well characterized, little data exists concerning LA. This arrangement leads to a mechanical behaviour of LA as an incompressible, non-linear, elastic and anisotropic material. Bi-axial characterization allow to consider the different orientation of fibres and the anisotropic behaviour whereas uni-axial characterization may not adequately represent deformation of that kind of tissue.

Methods: 5 samples (7mm squared) of left atrium were tested biaxially from one Yucatan swine including two samples at different location of the LAA and 3 samples surrounding the pulmonary veins. Thickness measurements were performed after testing including variation of the thickness through the sample. Th tested conditions included 5 conditions with displacement of 0.05 mm.s-1 with condition of (1:1, 1:2, 2:1, 1:4 and 4:1) the ratio between perpendicular tested axis. As previously described by Di Martino [5], a non linear, hyperelastic, nearly incompressible and transversally isotropic model was used changing the neo Hookean model of the isotropic term into a Yeoh model:

$$W = c_{10}(I_{\bar{c}} - 3) + +C_{20}(I_1 - 3)^2 + \frac{k_1}{2k_2}\left(e^{k_2(I_{4c}-1)^2} - 1\right) + \frac{k_3}{2k_4}\left(e^{k_4(I_{6c}-1)^2} - 1\right)$$

Thickness measurements was 1.14 to 3.1mm in the LAA samples and 2.4 to 3.6mm in the PV samples. The constitutive model fitting resulting in different orientation for LAA and PV location (0.62±0.76 and 0.72±0.75 rad for LAA and 0.94±0.86 and 0.83±0.77 rad for PV).

Taking into consideration the variability of the thickness within the computation of the model parameters, the constitutive model changes mainly the k2 and k4 coefficients. Those results highlighted the significance of the thickness measurements as well as the necessity of performing several testing conditions.

References:
[1]   W. Kannel, , p. 25, 2008.
[2]   M. Evin et al., Cardiovasc Diabetol, vol. 15, no 1, p. 164, déc. 2016, doi: 10.1186/s12933-016-0481-7.
[3]   L. D. Biase et al., vol. 68, no 18, p. 12, 2016.
[4]   S. Ho, Cardiovascular Research, vol. 54, no 2, p. 325 -336, mai 2002, doi: 10.1016/S0008-6363(02)00226-2.
[5]   C. Bellini et E. S. Di Martino, Journal of Biomechanical Engineering, vol. 134, no 2, p. 021008, févr. 2012, doi: 10.1115/1.4006026.

D3.1

Myocardial stiffness assessment by ultrafast ultrasound imaging

Olivier Villemain[1]

1   *The Hospital for Sick Children, Division of Cardiology, Toronto, Canada*

Ultrafast ultrasound imaging (UF) is a recent imaging technique with possible important novel clinical applications for cardiovascular imaging. Increasing temporal resolution allows exploration of novel domains in cardiovascular physiology and pathology. By increasing frame rates to >1000 fps, it has become feasible to observe and analyze very short-lived tissue movements that were not possible to detect by other imaging techniques. A recent application has been the use of UF imaging to study shear wave propagation in the myocardium to assess mechanical tissue properties. Different techniques have been proposed using either natural shear waves associated with cardiac mechanical events or external shear waves generated by ultrasound energy. Myocardial stiffness (MS) can be assessed from the estimation of the shear wave propagation velocity through the relationship between shear velocity and tissue viscoelastic properties. Physical concepts, ultrasounds techniques, and clinical results will be presented.

D3.2

Intracardiac 3-D vector flow imaging by triplane color Doppler echocardiography

Florian Vixège[1], Simon Mendez[2], Franck Nicoud[2], Didier Vray[1], **Damien Garcia**[1]

1 CREATIS, Villeurbanne, France
2 Université Montpellier, Montpellier, France

During left ventricular filling (diastole), the mitral inlet forces intraventricular flow to form a vortex. When cardiac filling is impaired (diastolic dysfunction), a change in blood flow occurs, with a significant impact on the intraventricular vortex. Our goal is to evaluate this intraventricular vortex to better assess cardiac filling. The clinical accessibility of echocardiography makes ultrasound the preferred technique to analyze intracardiac blood flow. Doppler echocardiography, however, only returns velocity projections along the ultrasound beams. We therefore introduced iVFM ("intraventricular Vector Flow Mapping") by conventional 2-D Doppler echocardiography [1]. The current 2-D iVFM technique does not allow recovery of the three-dimensional structure of intraventricular blood flow. With the goal of obtaining a full-volume three-dimensional field, we therefore upgraded 2D-iVFM to 3D-iVFM. We used triplane Doppler echocardiography, which returns three apical long-axis planes (color Doppler + B-mode) separated by a 60° angle with good temporal resolution. To recover a three-component volumetric velocity field, we derived a constrained least-squares problem, which was solved by the Lagrange multiplier method. We used fluid dynamics-based hemodynamic properties to constrain the problem, such as conservation of mass (divergence-free flow) and free-slip boundary conditions on the endocardial wall. We validated 3D-iVFM in a patient-specific CFD model of intracardiac flow [2]. Intracardiac velocimetry by 3D-iVFM could be an effective tool to quantify intraventricular vortex and to assess blood flow during heart filling. Fast and clinically compatible, 3D-iVFM could offer new echocardiographic insights into left ventricular hemodynamics.
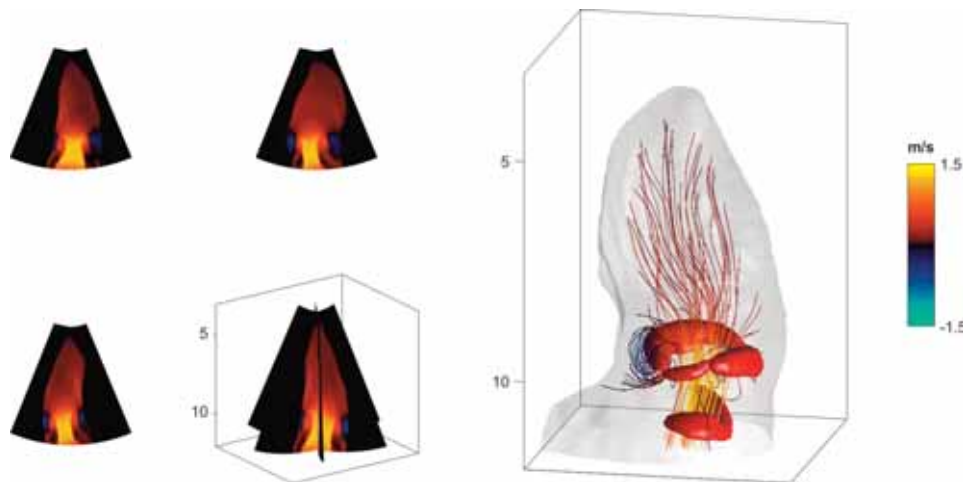
Figure caption: Three-dimensional 3-D triplane iVFM validated in a patient-specific CFD model of left heart flow. The figures on the left represent the simulated triplane Doppler velocities. The figure on the right represents the velocity field reconstructed by the 3-D iVFM constrained method. The vortex ring that forms at the beginning of the filling is visible.

References:
[1] Assi KC, Gay E, Chnafa C, et al. Intraventricular vector flow mapping-a Doppler-based regularized problem with automatic model selection. Phys Med Biol. 2017;62(17):7131-7147. doi:10.1088/1361-6560/aa7fe7
[2] Chnafa C, Mendez S, Nicoud F. Image-based large-eddy simulation in a realistic left heart. Computers & Fluids. 2014;94:173-187. doi:10.1016/j.compfluid.2014.01.030

D3.3
Myocardial perfusion simulation: an image-based coupled patient-specific multiscale model

Irene Vignon-Clementel[1], Lazaros Papamanolis[1], Clara Jaquet[2], Matthew Sinclair[3], Hugues Talbot[2 4]

1   Inria, Palaiseau, France
2   Université Gustave Eiffel, Marne la Vallée, France
3   Heartflow, Redwood City, United States
4   Ecole Centrale Supelec, Saclay, France

Image-based models derived from CT angiography are being used clinically to simulate blood flow in the coronary arteries of individual patients to aid in the diagnosis of disease and planning treatments. However, image resolution limits vessel segmentation to larger epicardial arteries. Although blood flow simulations have been carried out in such image-based models, a remaining challenge is bridging scales from flow in the coronary arteries to the micro-circulation supplying the myocardium. Previous models developed for that purpose are descriptive rather than predictive.

We propose a multi-scale patient-specific model enabling blood flow simulation from the large coronary arteries to myocardial tissue [1] (Fig1). The aorta, coronary arteries and left ventricle are segmented from coronary CT angiography (A,B). A patient-specific synthetic vascular network is then generated starting from segmented epicardial vessels down to the arterioles [2] (C). The tree generation method, named constrained constructive optimization, satisfies functional principles to account for multiple, competing vascular trees. The algorithm simulates angiogenesis under vascular volume minimization with flow-related and geometrical constraints. It adapts the simultaneous growth of trees from multiple epicardial vessel outlets to patient priors, with a first phase on the epicardium, followed by growth inside the myocardium. Blood flow is then simulated in the segmented arteries and the synthetic arterial network with a 1-D reduced-order model that is coupled to a porous model representing blood flow in the myocardium (D). During post-processing, the myocardium is divided into 17 segments as proposed by the American Heart Association (AHA), where Myocardial Blood Flow (MBF) is calculated (D). The spatial distribution of MBF is evaluated by computing the corresponding perfusion polar map, a 2D representation of the 3D myocardial volume to compare the results to [15O]H2O PET MBFpolar maps (E). Additionally, Fractional Flow Reserve (FFRCT) resulting from the coupled model is computed (D).
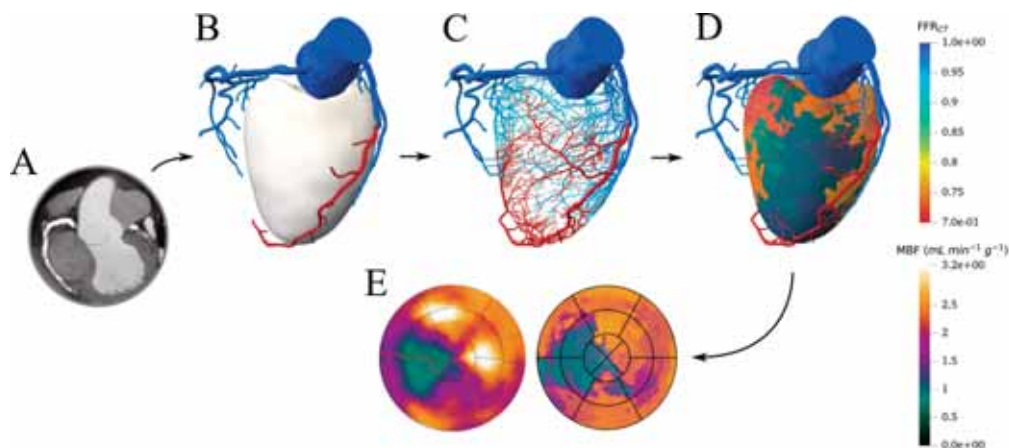
Figure: Illustration of method for a diseased patient

We applied this method to a small cohort of patients with suspected CAD who underwent CCTA and [^15 O]H_2 O PET prior to invasive coronary angiography. We will demonstrate how far this novel multiscale method for simulation of coronary and myocardial blood flow results in matching PET data.

References:
[1]   Papamanolis L, Kim HJ, Jaquet C, Sinclair M, Schaap M, Danad I, van Diemen P, Knaapen P, Najman L, Talbot H, Taylor CA & Vignon-Clementel, I (2021). Myocardial Perfusion Simulation for Coronary Artery Disease: A Coupled Patient-Specific Multiscale Model. Annals of Biomedical Engineering, 1-16
[2]   Jaquet C, Najman L, Talbot H, Grady L, Schaap M, Spain B, Kim HJ, Vignon-Clementel IE & Taylor CA (2019). Generation of patient-specific cardiac vascular networks: a hybrid image-based and synthetic geometric model. IEEE Transactions on Biomedical Engineering, 66(4), 946-955.

D3.4
In silico time-resolved 3D phase-contrast magnetic resonance imaging

*Thomas Puiseux[1], Anou Sewonu[1], Moreno Ramiro[1], Simon Mendez[2], **Franck Nicoud**[2]*

1   *Spin Up !, Toulouse, France*
2   *IMAG, University Montpellier, CNRS, Montpellier, France*

A numerical pipeline is presented to produce in silico time-resolved 3D phase-contrast Magnetic Resonance Imaging (or 4D Flow MRI) under realistic flow conditions. The method relies on an Eulerian- Lagrangian formalism where a finite-volume method solves the Navier-Stokes equations over a fixed computational grid and massless particles with proper source terms represent the evolution of spins immersed into a time-dependent, external magnetic field, as dictated by the Bloch equations. Two ingredients were specifically developed to reduce the computational burden and make 4D Flow MRI generation affordable in silico: first of all, a semi-analytic solution for the Bloch equations valid as long as the radio-frequency is off is used to relax the very small time-stepping constrain imposed by the characteristic time response of the spins; second of all, a periodic particle seeding strategy avoids the issue of heterogeneous spin density while allowing the computation of the magnetic signal without storing the spins trajectory history over the whole duration of the virtual MRI exam (several minutes). After being validated by considering a Poiseuille flow configuration, the procedure is applied to the flow within an in vitro flow phantom typical of the cardiovascular system and recently used to reconcile Computational Fluid Dynamics and 4D Flow MRI data [1]. The simulated MR velocity images compare favorably to both the flow computed by solving the Navier-Stokes equations, as illustrated in the Figure, and experimental 4D Flow MRI measurements [2]. More details can be found in [2] where the in silico MRI strategy is notably used to identify the origins of the MRI measurement errors, as a first step towards a fully integrated quality control strategy of 4D Flow MRI."
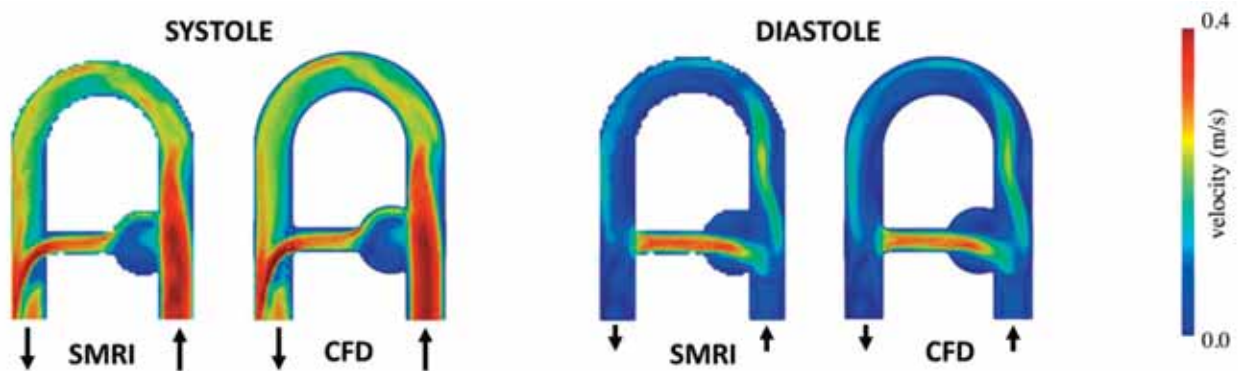
Figure caption: "Velocity magnitude from CFD (reference) and the in silico 4D Flow MRI pipeline presented. The arrows represent the inlet/outlet at systole and diastole."

References:
1-   Puiseux, Thomas, Anou Sewonu, Olivier Meyrignac, Hervé Rousseau, Franck Nicoud, Simon Mendez, and Ramiro Moreno. 2019. "Reconciling PC-MRI and CFD: An in-Vitro Study." NMR in Biomedicine 32 (5): e4063. https://doi.org/10.1002/nbm.4063.
2-   Puiseux, Thomas, Anou Sewonu, Ramiro Moreno, Simon Mendez, and Franck Nicoud. 2021. "Numerical Simulation of Time-Resolved 3D Phase-Contrast Magnetic Resonance Imaging." PLoS ONE 16 (3 March): 1–32. https://doi.org/10.1371/journal.pone.0248816.

D3.5

Predicting rupture location in ascending aortic aneurysms using patient-specific finite element models: a preliminary analysis

Dermot O'Rourke[1], Timothy Surman[2], John Abrahams[2], James Edwards[2], Karen Reynolds[1]

1   Flinders University, Medical Device Research Institute, Adelaide, Australia
2   Royal Adelaide Hospital, D'Arcy Sutherland Cardiothoracic Surgical Unit, Adelaide, Australia

Introduction: Ascending aortic aneurysms are a localised dilation that present a significant clinical risk if untreated. Surgical repair to prevent rupture is recommended for patients with a diameter > 5.5 cm. However, aorta size alone has limited ability in predicting rupture [1]. Finite element (FE) models improve rupture risk prediction by providing an estimation of strength [2]. However, the accuracy in predicting rupture location ascending aorta FE models remains unclear. The aim of this study was to investigate CT-based FE models in predicting regions in the ascending aorta likely to rupture.

Methods: Pre-rupture and post-rupture CT scans were obtained for 7 patients (5 males) who underwent emergency repair following an ascending aortic rupture. All geometries were retrieved using segmentation and applying a surface mesh. Visible contrast extravasation on the post-rupture image was considered a rupture site. Pre-rupture FE models were characterised with a hyperelastic constitutive model [3] and assigned a 2 mm wall thickness [4]. The equivalent strain from the continuum tissue damage theory was calculated using the backward displacement method [5]. The post-rupture model was registered to the pre-rupture model with a rigid iterative closest point algorithm. The rupture site was projected onto the FE model (Figure). Rupture was predicted if the peak equivalent strain value within the rupture site was greater than the 99th percentile.

Results: The peak equivalent strain within the rupture sites across the patients was 7.81 – 14.96 kPa1/2. Registration failed in 1 patient due to misalignment of the models. The models predicted rupture in 3/6 remaining patients.

Discussion: The results indicated that the FE models predicted high equivalent strain in regions that coincided with locations of rupture. A limitation was the rigid registration gave only an approximate alignment of the models and failed in one instance. Current preliminary work is investigating the accuracy of patient-specific FE models to aid surgical guidelines for preventing ascending aortic rupture.

Patient	Rupture Site Peak Eq Strain (kPa1/2)	99th Percentile (kPa1/2)	Rupture	Time between scans (Months)
1	14.66	11.67	Y	1
2	7.81	11.25	N	7
3	14.96	14.15	Y	22
4	10.47	19.81	N	46
5	8.58	12.89	N	48
6		Registration failed		59
7	11.85	11.00	Y	64
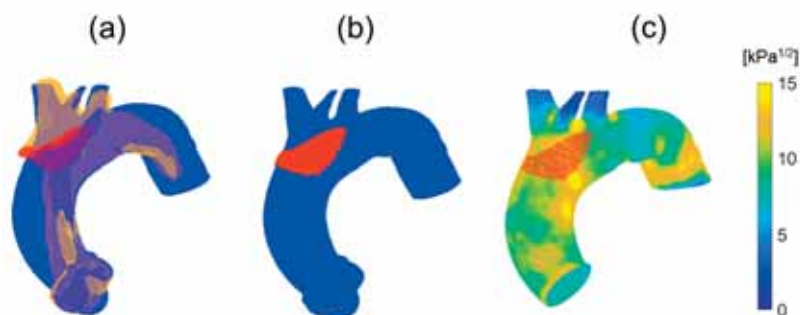
Figure caption: Registering the post-rupture (yellow) and rupture site (red) onto the pre-rupture model (blue) (a) Rigid registration, (b) projecting the rupture site, (c) equivalent strain distribution with rupture site overlaid.

References:
1.   Elefteriades et al. J Am Coll Cardiol, 2010
2.   Polzer et al., J Vasc Surg, 2020.
3.   Gasser et al. J R Soc Interface, 2006
4.   Martin et al. Am J Physiol Heart Circ Physiol, 2015
5.   Liang et al. Biomech Model Mechan, 2017.

D4.1
A computational framework for crack propagation in spatially heterogeneous materials

Lukasz Kaczmarczyk[1], Karol Lewandowski[1], Chris Pearce[1]

1   University of Glasgow, James Watt School of Engineering, Glasgow, United Kingdom

Bone adapts in response to its mechanical environment. This evolution of bone density is one of the most important mechanisms for developing fracture resistance. A finite element framework for simulating bone adaptation, commonly called bone remodelling, is presented. This is followed by a novel method to both quantify fracture resistance and to simulate fracture propagation. The authors' previous work on the application of configurational mechanics for modelling fracture is extended to include the influence of heterogeneous bone density distribution. The main advantage of this approach is that configurational forces, and fracture energy release rate, are expressed exclusively in terms of nodal quantities. This approach avoids the need for post-processing and enables a fully implicit formulation for modelling the evolving crack front. In this paper density fields are generated from both (a) bone adaptation analysis and (b) subject-specific geometry and material properties obtained from CT scans. It is shown that, in order to correctly evaluate the configurational forces at the crack front, it is necessary to have a spatially smooth density field with higher regularity than if the field is directly approximated on the finite element mesh. Therefore, discrete density data is approximated as a smooth density field using a Moving Weighted Least Squares method. Performance of the framework is demonstrated using numerical simulations for bone adaptation and subsequent crack propagation, including consideration of an equine 3rd metacarpal bone. The degree of bone adaption is shown to influence both fracture resistance and the resulting crack path.

a) Density mapping.   b) Bone adaptation.   c) Crack propagation analysis.
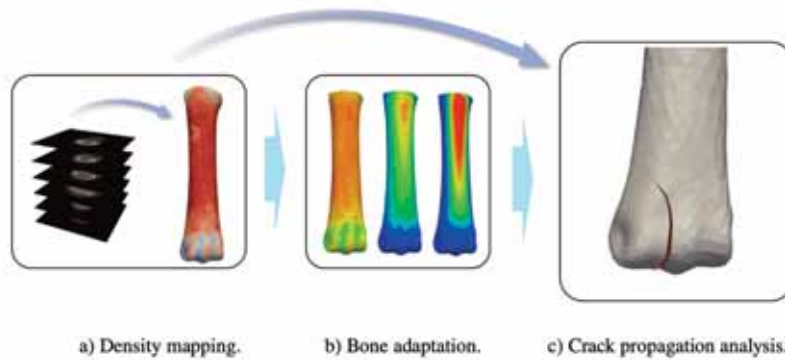
Figure caption: Figure caption: Framework for estimating bone fracture resistance in MoFEM [1]. a) Density derived from Quantitative Computed Tomography (qCT) is mapped onto finite element mesh; (b) bone adaptation analysis; (c) fracture mechanics to evaluate the fracture energy release rate of an initial crack at different time steps c).

References:
[1]   Kaczmarczyk et al., (2020). MoFEM: An open source, parallel finite element library. Journal of Open Source Software, 5(45), 1441, https://doi.org/10.21105/joss.01441

D4.2
Recent advances in bone remodeling applications to clinical bone research

Peter Pivonka[1]

1   Queensland University of Technology, Mechanical, Medical and Process Engineering, Brisbane, Australia

Osteoporosis (OP) is a chronic progressive bone disease which affects a large portion of the elderly population worldwide. OP is characterized by a slow reduction of bone matrix and changes in the bone matrix properties which ultimately leads to whole (organ) bone fractures [1].

Novel drug treatments are developed to more effectively reduce the risk of bone fractures. Assessing the effects of novel and existing treatments on OP is challenging due to the complexity of the bone remodeling process, its effects on the bone matrix and the different spatial and temporal scales involved. Identification and characterization of various bone biomarkers has significantly improved our understanding of OP pathophysiology. The bone matrix and its constituents are specific bone biomarkers measured at a particular bone site. One the other hand, biochemical ligands released during bone remodeling and measured in blood or urine are non-specific bone biomarkers. These biomarkers can be used to characterize the underlying bone mechanobiological system and drug treatment effects [1].

Recently, disease system analysis (DSA) has been proposed as a novel approach to quantitatively characterize drug effects on disease progression [1]. DSA integrates physiology, disease progression and drug treatment in a comprehensive mechanism-based modelling framework using a large amount of complementary biomarker data. In this work, I will present latest mechanistic pharmacokinetic-pharmacodynamic (PK/PD) models of osteoporosis treatment. Examples of currently used drug interventions including denosumab [2,3] romozosumab [4], and PTH [5] treatments will serve as discussion points on which mechanisms are essential for accurate bone remodeling simulations. Bone matrix mineralization turns out to be an essential model feature that is required to predict BV/TV changes for the case of anti-catabolic drug treatments of OP [3].

References:
[1]   S. Trichilo and P. Pivonka, Disease systems analysis in osteoporosis and mechanobiology, in Multiscale mechanobiology of bone remodelling and adaptation, Editor P. Pivonka, CISM Courses and Lectures No. 1406, Springer, 2017;
[2]   S. Scheiner et al.. Mathematical modeling of postmenopausal osteoporosis and its treatment by the anti-catabolic denosumab, Int. Journal for Numerical Methods in Biomedical Engineering, 30(1), pp1-27, 2014;
[3]   J. Martinez-Reina and P. Pivonka, Effects of long-term treatment of denosumab on bone mineral density: insights from an in-sillico model of bone mineralization, Bone, 125, pp87-95, 2019;
[4]   M. Martin et al., Assessment of Romozosumab efficacy in the treatment of postmenopausal osteoporosis: results from a mechanistic PK-PD mechanostat model of bone remodeling, Bone, 133, pp1-16, 2020;
[5]   M. Lavaill et al., Effects of PTH treatment in osteoporosis – insights from a mechanistic PK-PD model, BMMB, pp1-16, 2020.

D4.3
A nonlocal formulation for bone remodelling using peridynamics

Emely Schaller[1], Ali Javili[2], Ina Schmidt[3], Areti Papastavrou[3], Paul Steinmann[1]

1   Institute of Applied Mechanics, University of Erlangen-Nuremberg, Erlangen, Germany
2   Department of Mechanical Engineering, Bilkent University, Ankara, Turkey
3   Faculty of Mechanical Engineering, Nuremberg Tech, Nuremberg, Germany

Bone tissue has the ability to adapt its external and internal structure to both mechanical and biological alterations via bone formation and resorption. In this regard, the biomechanically coupled subprocesses of bone remodelling are influenced by the mechanical and biological environment. Although some biomechanical correlations are well known, the complex process of bone remodelling is not yet fully understood.

In recent years, a variety of mathematical formulations have been established to model the process of bone remodelling. Previous studies focused, for example, on the porosity of bone structure, availability of nutrition or the biological stimulus, which mainly controls the bone density evolution. The latter was defined as an age-dependent, diffusive or nonlocal quantity due to the nonlocal cell to cell communication. Although the biological stimulus has already been established as a nonlocal quantity, the governing equations for the mechanical evolution equations have been realized only in a local form.

To capture fully nonlocal material behaviour, we introduce a peridynamic formulation for the remodelling process of bone tissue at the macroscale for the first time. For this purpose, we reformulate the local evolution equations of [1] in a peridynamic sense [2]. In contrast to the classical theory, the governing equations in peridynamics are obtained in integrodifferential forms. Thus, every point of the continuum is influenced by its finite-size neighbourhood. First, we justify the suitability of our nonlocal formulation with a simple biaxial deformation test. As a second numerical example, we demonstrate the density evolution throughout the proximal femur, that evolves due to a prescribed deformation at the femoral head and at the greater trochanter. Furthermore, we compare both numerical examples with local finite element simulations using a Saint Venant-Kirchhoff material model, appropriate to compare with the harmonic pairwise energy density in our peridynamic formulation.

The resulting density evolution of our peridynamic model is in good agreement with the local finite element model for both numerical examples when a small neighbourhood is chosen compared to the domain size. Increasing the size of the neighbourhood for the proximal femur simulation highlights the nonlocality sensitivity and results in an enhanced interaction of bone tissue throughout the femur.

We have shown that our peridynamic formulation can be used to model nonlocal bone remodelling. In future, the biomechanically coupled phenomena of bone formation and resorption can be further examined on its nonlocal characteristic using our presented nonlocal formulation.

References:
[1]   Kuhl, E., Steinmann, P., 2003. Theory and numerics of geometrically non-linear open system mechanics. Int. J. Numer. Meth. Eng. 58 (11), S. 1593–1615. DOI: 10.1002/nme.827.
[2]   Javili, A., McBride, A. T., Steinmann, P., 2019. Continuum-kinematics-inspired peridynamics. Mechanical problems. Journal of the Mechanics and Physics of Solids 131 (5), S. 125–146. DOI: 10.1016/j.jmps.2019.06.016.

D4.4
The impact of non-mechanical factors on bone remodelling

Areti Papastavrou[1], Ina Schmidt[1], Paul Steinmann[2]

1   Nuremberg Tech, Faculty of Mechanical Engineering, Nürnberg, Germany
2   FAU Erlangen-Nürnberg, Erlangen, Germany

As a living material bone is able to adapt to external stimuli by changing its trabecular architecture and density. This process is referred to as bone remodelling. In addition to the mechanical stimulus, this process is also influenced by other non-mechanical factors. These include, for example, age, gender, availability of nutrients and hormones and possible degenerative diseases.

In this presentation we discuss a novel computational model for bone remodelling based on the framework of Kuhl and Steinmann [3], which not only considers the mechanical stimulus, but also the influence of age and biological availability, see [4],[5].

We adopt the concept advocated by Oller and Bellomo [1] for soft tissues, which has a metabolism-limited, stress-induced growth rate characterized by phenomenological parameters that represent the biological availability for tissue growth, see [2]. Different approaches to take age into account in the development of bone density are presented. Based on the implementation of our novel model within a non-linear finite element setting, a variety of illuminating examples will be presented.

References:
[1]   F.J. Bellomo, S. Oller, F. Armero, L.G. Nallim, A general constitutive model for vascular tissue considering stress driven growth and biological availability. Computer Modeling in Engineering and Sciences. 80-1:21, 2011.
[2]   E. Comellas Sanfeliu, Numerical modelling of the growth and remodelling phenomena in biological tissues [dissertation], Barcelona TECH, 2015
[3]   E. Kuhl, P. Steinmann, Theory and numerics of geometrically non-linear open system mechanics. Int J Numer Meth Engng. 58(11):1593-1615, 2003
[4]   A. Papastavrou, I. Schmidt, K. Deng, P. Steinmann, On age-dependent bone remodeling, Journal of Biomechanics, DOI 10.1016/j.jbiomech.2020.109701
[5]   A. Papastavrou, I. Schmidt, P. Steinmann, On biological availability dependent bone remodeling, Computer Methods in Biomechanics and Biomedical Engineering, DOI 10.1080/10255842.2020. 1736050

D5.1

Modelling the functional heterogeneity of skeletal muscles: enriching continuum-mechanical models on a motor-unit level

Harnoor Saini[1], Thomas Klotz[1], Oliver Roehrle[1]

1   University of Stuttgart, Institute for Modeling and Simulation of Biomechanical Systems, Stuttgart, Germany

Motor-units (MUs) are often restricted to sub-regions of a skeletal muscle, and their selective recruitment is partly responsible for the "functional heterogeneity" of muscles, i.e., the same muscle may produce various "lines of action" depending on the subset of recruited MUs. To capture this phenomenon, we present a method to incorporate micromechanically based MU activity and distribution within continuum-mechanical muscle models and then demonstrate the method via a prototype musculoskeletal model.

Methods: The mechanical behaviour of skeletal muscle is based on [1] and additively splits the active S_ACT (α_M) and passive stress responses. To incorporate MU information, the muscle activation parameter $\alpha\_M \in [1,0]$ is decomposed according to

$$\alpha_M(t, \boldsymbol{X}) = \sum_i^{N_{MU}} \alpha_i(t)\, \kappa_i(\boldsymbol{X}),$$

where α_i and κ_i are the temporal activity and spatial (fractional) distribution of MU i, and N_MU is the number of MUs, respectively.

Taking a scalar excitatory drive as an input to the MU pool, individual MU activities $\alpha\_i(t)$ are computed via a recruitment model coupled with cross-bridge and calcium-dynamics models, e.g., [2]. MU distributions are computed by (i) reconstructing the microstructure in the muscle, (ii) assigning the (reconstructed) fibres to MUs via a novel algorithm (controlling MU position, overlap, size, etc.) and (iii) homogenising the innervated microstructure within the finite-element mesh to obtain the fractional distribution $\kappa\_i(X)$.

A masticatory system model, including the mandible and masseters, was used to simulate sub-maximal static bites (34/50 MUs recruited). Only the MU distribution was varied between trials, and the bite forces were used to quantify variations in motor-output. An additional model with spatially uniform MUs was simulated, representing the status-quo modelling approach.

Results: The distribution of the recruited MUs dictated active muscle stress (Figure 1). The range in peak bite forces for all MU distributions was 5N with a mean of 146N. Bite force angle (in the horizontal plane) was more drastically affected, with a range of 40° and a mean of -86° (-90°is oriented to the left). Changes in bite force can be explained by MU territory and masseter architecture, i.e., since masseter fibre-orientation and geometry are not uniform, regional contraction influences bite force. The traditional modelling approach yielded a steadier force, directed along the "average" fibre orientation of the masseters.

Conclusion: Our method to enrich a continuum-mechanical model with MUs captured nuances in motor-output that were not possible with a traditional modelling approach.
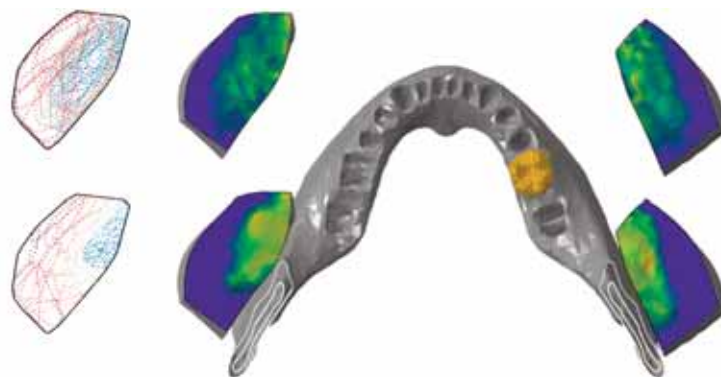
Figure 1: (a) MU territories in right masseter; MU 1 (dark blue) to 50 (dark red); MUs 1-34 are active. (b) S_ACT over the masseter cross-section at the same time instance; 0MPa (blue) to 1MPa (yellow).

References:
[1]   Röhrle et al. (2017). Biomech. Model. Mechan., 16(3): 743-762
[2]   Hiedlauf et al. (2017). PLoS Comput. Biol., 13(10): e1005773

D5.2

Biomechanical analysis of the lower-extremity during golf-swing: A comparative study of a healthy subject against patients with total knee arthroplasty and knee osteoarthritis

Iman Soodmand[1], Maeruan Kebbach[1], Xiping Ren[1], Christoph Lutter[1], Prof.Dr. Sven Bruhn[2], Prof. Dr. Med. Thomas Tischer[1], Rainer Bader[1]

1   Department of Orthopaedics, Rostock University Medical Center, Rostock, Germany
2   Institute of Sport Science , University of Rostock, Rostock, Germany

Patients who undergo orthopedic surgeries such as partial meniscectomy or total knee arthroplasty (TKA) usually want to retain their activity level. It is reported that rates of return to golf after TKA ranges 30-57% [1] and 69.6% after meniscus transplantation [2]. Nevertheless, according to reports 53.7% of assessed golfers after TKA experienced radiographic loosening [3]. Considering the limitations of the literature in this field, further studies are required [4] and muscle forces which are not well-studied so far require special attention. Therefore, the purpose of this study is to compare the range of motion, muscle forces and joint reaction forces among healthy and pathological golfers. Hence, a healthy subject, a patient with osteoarthritis (OA) in both knees, and a patient who underwent TKA in both knees were included. All participants were right-handed male golfers with a handicap index of 15-30; each performed five swings with a nine-iron club and without specific restriction on their swing. Ground reaction forces and 3D motion of subjects were captured by the Gait Real-time Analysis Interactive Lab System (GRAIL, Motekforce Link, Amsterdam, Netherlands). A lower-extremity musculoskeletal model from AnyBody Modeling System (v.7.3.1, AnyBody Technology A/S, Aalborg, Denmark) was adapted with two degrees-of-freedom in the knee joint to perform inverse dynamic analyses. The comparison study revealed that in contrast to the healthy and OA subjects, the TKA subject followed an inconsistent swing technique, known as one of the common causes of golf injuries [4]. The OA and TKA subjects showed a greater mean range of knee flexion angle compared to the healthy subject (44.28°, 41.58°, and 38.17°, respectively). The healthy subject showed the largest peak value of the mean knee compression force (Figure 1a), which was higher for the TKA subject compared to the OA subject (32.05±3.28, 29.97±7.95, and 29.02±2.77 N/kg, respectively). The peak value of the M. gluteus maximus mean force (Figure 1b) was higher for the TKA subject compared to OA and healthy subjects (15.42±5.03, 11.98±2.25, and 10.35±1.17 N/kg, respectively). The reported results should be considered in the light of the limitations in subjects' number. These insights might enhance the understanding of the golf-swing characteristics and provide clinicians and coaches a better vision to help injured-patients to retain activity and health.
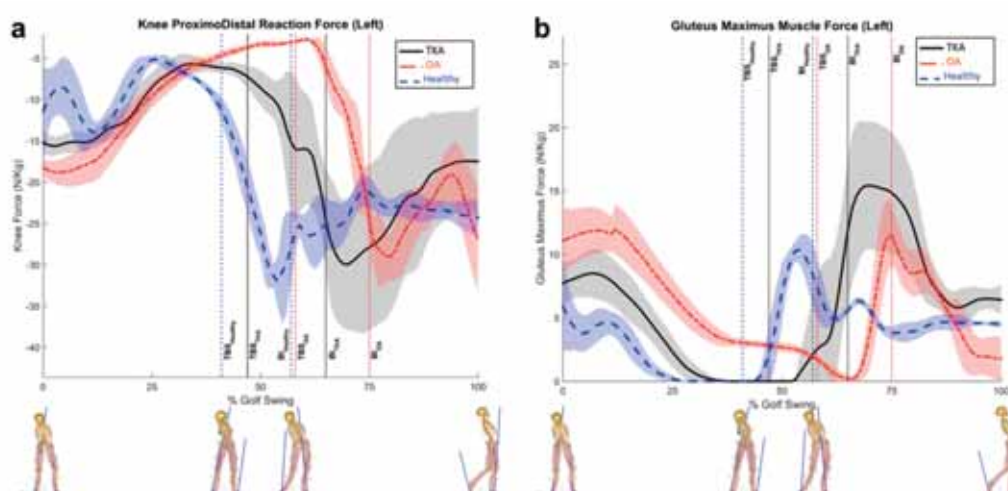
Figure caption: Figure 1. Mean value of the a) knee proximodistal reaction force b) M. gluteus maximus force- The vertical lines show top-of-backswing (TBS) and ball-impact (BI) events

References:
[1]   Baker, M.L., et al. Sports Medicine 47.12 (2017): 2621-2639.
[2]   Cvetanovich, G.L., et al. The Journal of Arthroscopic & Related Surgery 36.9 (2020): 2456-2463.
[3]   Mallon, W.J., et al. The Journal of arthroplasty 8.3 (1993): 299-306.
[4]   Cabri, J., et al. European Journal of Sport Science 9.6 (2009): 353-366.

D5.3

Integrating clinical data and computational modeling to quantify knee mechanics in athletes at increased risk of noncontact ACL rupture

Swithin Razu[1], Dan Sturnick[1], Bruce Beynnon[2], Thomas Santner[3], **Carl Imhauser[1]**

1   Hospital for Special Surgery, Biomechanics Department, New York, United States
2   University of Vermont, Department of Orthopaedics and Rehabilitation, Burlington, United States
3   The Ohio State University, Department of Statistics, Columbus, United States

Clinical studies have linked both tibiofemoral geometry and knee laxity with increased risk of noncontact injury to the anterior cruciate ligament (ACL)[1]. Clinical studies, however, do not provide insight into knee mechanics, including ACL force, nor the complex mechanical interactions between tibiofemoral geometry and knee laxity. Computational knee models and uncertainty analyses overcome these limitations. Unfortunately, they have not included knee geometries from individuals at elevated risk of noncontact ACL injury. Therefore, we integrated tibiofemoral geometries derived from MRI from an age- and team-matched pair of female athletes into an established computational modeling pipeline. The female pair was selected based on having the greatest difference in risk of ACL injury using a multivariable risk model[1]. The multibody dynamic knee model included the cruciates, collaterals, and discretized menisci with their root attachments (ADAMS, MSC, Inc.)[2]. We simulated the clinical pivot shift exam, which loads the ACL[3] via serially applied compression (100 N), valgus torque (8 Nm), internal rotation torque (2 Nm), and an anterior force (30 N) at 15° of flexion. Ligament slack length, toe region, and stiffness were varied to span the space of ligament properties using a Latin Hypercube design[4] (Fig. 1A). The effect of varying these properties on ACL force at the peak applied pivoting load was determined by calculating main effect and joint effect sensitivity indices and 2-way interaction plots using flexible non-parametric kriging predictors and Gaussian Process Models[4]. ACL slack length accounted for 62% of the variability in ACL force for the case knee model, but only 4% in the control (Fig. 1B). Joint effects explained 34% of the variability in ACL force for the control knee model, but only 11% in the case. The joint effects in the control knee model were nonlinear and stemmed from interactions of ACL slack with PCL slack and with ALL slack (Fig. 1C). ACL force in the ACL-injured case knee model was highly dependent on ACL slack, while the control exhibited pronounced interactions among ligament properties. Our computational framework may identify athletes who are ACL-dependent and, therefore, may be at elevated risk of noncontact ACL rupture.
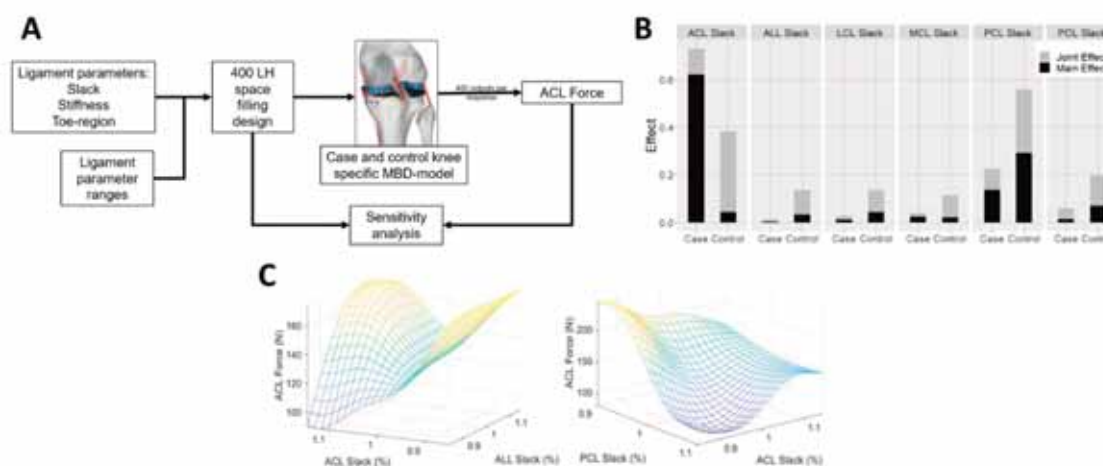
Figure caption: Figure 1. A. Twenty-six ligament parameters created a Latin-hypercube (LH) design as multibody (MBD) model inputs and ACL force was output to conduct the sensitivity analyses. B. Main and joint effects for the female ACL-injured case and uninjured control knee models. C. Two-way interaction plots for the uninjured control knee model.

References:
1.   Sturnick. 2015. AJSM. 2. Kia. 2016. J Biomech Eng. 3. Kanamori. 2000. Arthroscopy.
4.   Santner. 2003. The Design and Analysis of Computer Experiments. "

D5.4

Application of an articulated statistical shape model of the hip to predict clinical measures of coverage

Penny Atkins[1], Praful Agrawal[1], Joseph Mozingo[1], Keisuke Uemura[2], Andrew Anderson[1]

1   The University of Utah, Salt Lake City, United States
2   Nara Institute of Science and Technology, Ikoma, Japan

Developmental dysplasia of the hip (DDH), or under-coverage of the femoral head by the acetabulum, can result in mechanical instability and osteoarthritis. DDH is most commonly diagnosed using two-dimensional measurements on plain film radiographs or single CT/MRI image slices. However, these planar measurements are unable to adequately capture 3D coverage. Statistical shape modeling (SSM) provides an unbiased measure of shape variation. To date, orthopaedic applications of SSM have been largely relegated to analysis of single bones, rather than multi-bone complexes. Herein, we applied SSM to the femur and hemi-pelvis of patients with DDH and then evaluated whether model outputs could predict femoral head coverage.

CT images of 83 hips from 47 female subjects with DDH were acquired with the legs and pelvis neutrally aligned. Femurs and hemi-pelvii were semi-automatically segmented and surfaces were reconstructed and smoothed (Amira v6.0, Visage Imaging). The combined surfaces of each hip were aligned via iterative closest point surface matching prior to input into a multi-domain SSM (ShapeWorks v5.3, University of Utah) [1]. Correspondence particles were automatically placed over the femur (n=4096) and hemi-pelvis (n=2048). In addition to the full bone model, a subset of correspondences were isolated on the femoral head (n=339) and acetabulum (n=119) for a joint-specific model. Principal component analysis (PCA) of the correspondences identified modes of shape variation for both models. Coverage was calculated by determining the element-based area of the femoral head that was intersected by an opposing surface normal of the acetabulum (Figure), and expressed as a percent of the total femoral head surface area. To evaluate the ability of the model to predict coverage, the data was divided into training (n=73) and test (n=10) datasets. Linear regression with Lasso regularization was used to identify the most relevant PCA modes for predicting coverage. Selected modes were then used to train and evaluate a cross-validated linear regression model.

Eight and 13 modes, which represented 6.1% and 39.6% of the overall shape variation, were selected for the full bone and joint-specific models, respectively. The trained regression models generalized well on the test data (full bone: Q2=0.785; joint-specific: Q2=0.886) with mean prediction errors of 0.9% and 0.6% coverage, respectively. For both models, the selected modes represented the depth of the acetabulum and oblateness of the femoral head, aligning well with the clinical description of DDH, while the full bone model also captured morphological and pose-related differences potentially related to altered muscle paths or differences in femoral torsion (Figure).
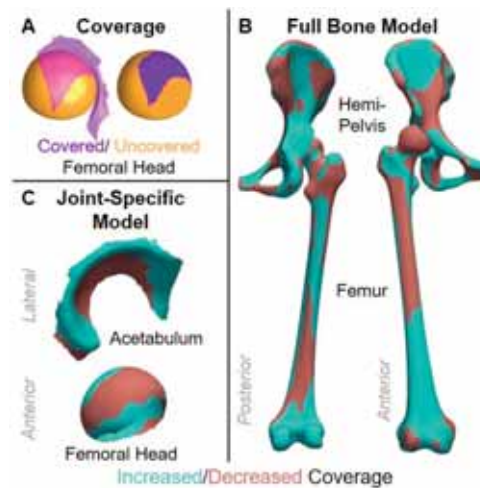
Figure caption: Femoral head coverage (A); regression-based surface reconstructions for the full bone (B) and joint-specific (C) models highlighting regions of increased (cyan) or decreased (red) coverage.

References:
[1] Agrawal P, et al. ShapeMI2020: 111-121.

D5.5
An anatomically-realistic computational modeling framework for testing protective vests

Maayan Lustig[1], Yoram Epstein[2 3], Amit Gefen[1]

1   Tel Aviv University, Department of Biomedical Engineering, Faculty of Engineering, Tel Aviv, Israel
2   Sheba Medical Center, Tel Hashomer, Heller Institute of Medical Research, Ramat Gan, Israel
3   Tel Aviv University, Sackler Faculty of Medicine, Tel Aviv, Israel

In a combat environment Injuries in the torso area (chest, abdomen and spine) are relatively common and constitute about 30% of all injuries. Although a penetrative injury, resulting in mechanical damage and internal organ disruption is known to be potentially debilitating or fatal, a non-penetrative blunt trauma might be lethal as well. The latter is due to the fact that blocking a bullet or other ballistic threats by protective gear, always involves instantaneous, rapid deformations of the armor, which are translated to potentially injurious mechanical energy that is absorbed in the tissues behind the armor. This type of injury is referred to as Behind Armor Blunt Trauma (BABT). The usefulness of the current method for testing the capabilities of protective armors (according to the USA National Institute of Justice, Standard 1010.06) is debated due its reliance on animal experiments, soft protective armor, and shooting by handguns. Other than the animals not being representative of the human anatomy and physiology, the existing method does not provide information regarding magnitudes and distributions of tissue strains and stresses that develop during the impact episode, which is the basis for evaluating the probability of irreversible BABT-related tissue damage. The objective of the present work is to develop a computational platform for comparing the protective performances of existing and possibly future bullet-resistant vest designs, using finite element (FE) modeling. We developed a three-dimensional, anatomically realistic, biomimetic torso model, which includes the protective plates. The FE simulations further consider the velocity of the projective and its specific shape, e.g. a 5.56 NATO ammunition. The performance of each vest is quantitatively evaluated and objectively rated based on a set of biomechanical metrics of vital organs (e.g. the heart, lungs, aorta, liver, kidneys, gastrointestinal system, all are included in the modeling) during and immediately after the ballistic impact. Validation of our FE modeling framework has been achieved by comparing its predictions to experimental findings obtained from a physical phantom system with embedded pressure sensors, which is subjected to pendulum-generated impacts. Noteworthy, this study has immediate practical implications such as shortening the development of new protective vest designs, as well as optimizing live ammunition experimental protocols and costs of testing, following an initial evaluation process using our computational modeling framework.
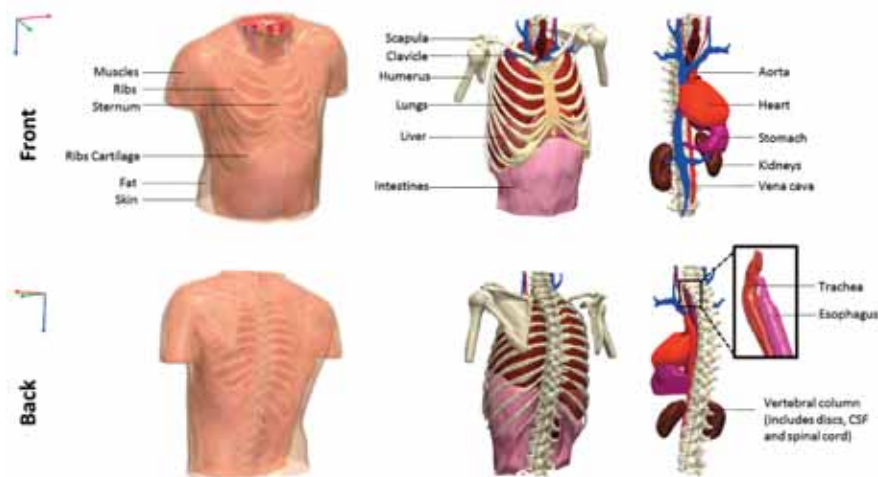
•   Fig. 1 – The 3D bio-mimetic model which is based on of the Visible Human Project
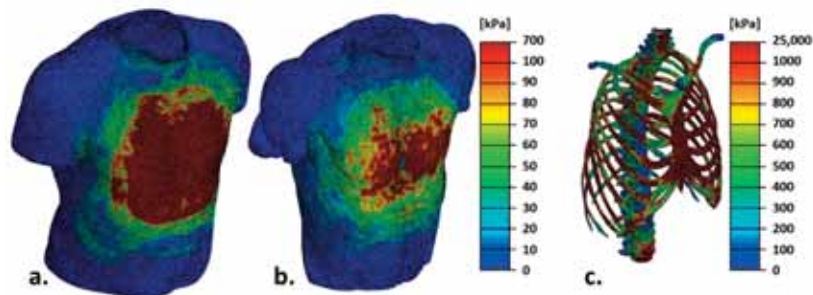
•   Fig. 2 – Effective stress pattern in the: a. Skin, b. Muscles and c. Ribs, ribs cartilage, sternum, and vertebral column, 1.5 [msec] after impact with 5.56 bullet at a velocity of 500 [m/s]

D5.6

Incapacitation prediction for readiness in expeditionary domains: an integrated computational tool (I-PREDICT) - an update and preliminary results

Lance Frazer[1], Matthew Davis[2], Derek Jones[2], Jeremy Schap[2], Corina Espelien[3], Brian Stemper[4], Timothy Bentley[5], Daniel Nicolella[1]

1   Southwest Research Institute, United States
2   Elemance, LLC, United States
3   University of Virginia, United States
4   Medical College of Wisconsin, United States
5   Office of Naval Research, United States

The overarching objective of the I-PREDICT program is to provide a high fidelity, validated, finite element model of the Warfighter's body for injury prediction and incapacitation assessment. This program has been designed to address limitations of existing government supplied total human body finite element models (FEMs) with regard to material property viscoelasticity, high-rate loading, and injury validation using experimental testing and advanced finite element modeling. To this end, a full-body human finite element model has been developed in FEBio. As an initial demonstration of the model, we performed an analysis investigating the potential role of active musculature in maintaining posture and resulting lumbar spine mechanics that may indicate potential injury mechanisms during long-duration flight. We applied a 100 Nm torque to the C1 vertebra, which caused a flexion of the spine into a "slumped" position and deactivated active muscle contraction. The torque was then followed by 20 minutes of vibrational loading on the pelvis to simulate flight loading. In the next simulation, we applied the same torque and vibration, activated torso and neck musculature, and utilized partial-integral-derivative (PID) controllers to coordinate muscle active contraction in order to maintain an erect posture of the spine. We hypothesized that the active muscle controlled erect spine would have lower peak stresses in the intervertebral discs (and thus, potential lower risk of injury), even though a higher total combined force (i.e., applied torque and active muscle forces) is applied to the spine with the muscle contraction. In the slumped model, peak stresses reached 7 MPa and occurred in the lumbar spine (L5) with average stresses of approximately 1 MPa throughout the entirety of the intervertebral discs (IVDs). When the muscles are activated and controlled by the PID controller to maintain improved posture, average stresses in the IVDs increased to 1.3 MPa but peak stresses were lowered to 6 MPa and occurred in the T1-T2 IVD. Stresses in the L5 IVD were reduced more than tenfold to 300 kPa resulting from active musculature maintaining posture. The slumped model approximates the posture an aviator may take if muscle fatigue sets in, and/or the seat is not conducive to proper posture. These preliminary simulations demonstrate the importance of including accurate 3D active musculature in full-body models, the importance of maintaining good posture during long-duration flights, and may indicate potential injury mechanisms leading to the high incidence of lumbar pain among military aviators. In future work, we will investigate the role of uncertainty and variability in tissue properties and environmental factors on warfighter response using probabilistic analysis methods.

Figure caption: FEBio Full body model in development for this program.

D6.1
Multiphysics optimisation of plasmonic photoacoustic contrast agents

Dmitry Chigrin[1][2]

1   RWTH Aachen University, I. Physikalisches Institut (1A), Aachen, Germany
2   DWI – Leibniz-Institut für Interaktive Materialien e.V., Aachen, Germany

Photoacoustic imaging represents a method for deep tissue imaging with high relevance for clinical visualization applications [1,2]. The principle is based on a pulsed near-infrared laser, which is guided into the relevant tissue. The laser radiation is absorbed by biological entities, therefore heating up the exposed tissue or biological fluids. The resulting time-dependent temperature profile leads to the expansion and contraction of the surrounding medium, which can be detected and spatially mapped by an ultrasound transducer [3]. However, suitable contrast agents need to be developed to increase the contrast for in vivo imaging. Gold nanoparticles are often discussed as potential contract agent [4,5]. We have recently developed a theoretical model for the photoacoustic response of gold nanoparticles, considering their size and shape [6]. This model allows to formulate two simple constraints for nanoparticle properties, to obtain an optimal photoacoustic performance in the tissue transparency window. The model demonstrates good agreement with experimental observations and also provides a mean to derive guidelines to development nanoparticle shapes and materials for photoacoustic imaging applications. Two of the most promising nanoparticle geometries have been identified, namely, high aspect ratio gold nanorods and gold nanostars. However, gold nanoparticles with sharp edges can demonstrate low biocompatibility [7]. It has been also demonstrated that biocompatibility can be improved by coating the gold nanoparticles with melanin [8]. In order to adequately describe experimentally observed photoacoustic response of melanin coated nanoparticles, we have developed a multiphysics model self-consistently coupling optical, heat transfer and mechanical deformation analysis [8]. Our work revealed that covering gold nanoparticles with melanin layer not only dramatically improve biocompatibility, but also further enhance photoacoustic signal due to thermal confinement effect [8].

References:
1.   M. Xu and L. V. Wang, Review of Scientific Instruments 77, 041101 (2006).
2.   K. E. Wilson, et al., Journal of Nuclear Medicine 54, 1851 (2013).
3.   C. Li and L. V. Wang, Phys. Med. Biol. 54, R59 (2009).
4.   E. C. Dreaden, et al., Chem. Soc. Rev. 41, 2740 (2012).
5.   W. Li and X. Chen,, Nanomedicine 10, 299 (2015).
6.   R. Garcia-Alvarez, et al., ACS Photonics 7, 646-652 (2020).
7.   R. Narayanan and M. A. El-Sayed, J. Phys. Chem. B 109, 12663 (2005).
8.   T. Repenko, et al. Adv. Funct. Mater. 28, 1705607 (2018)."

D6.2

A multiscale model of restenosis for investigating the effects of tissue damage and hemodynamics on cellular activity after percutaneous transluminal angioplasty

Anna Corti[1], Monika Colombo[1], Scott A. Berceli[2 3], Jose F. Rodriguez Matas[1], Claudio Chiastra[1 4]

1   Politecnico di Milano, Dept. of Chemistry, Materials and Chemical Engineering "Giulio Natta", Milano, Italy
2   University of Florida, Dept. of Surgery, Gainesville, United States
3   Malcom Randall VAMC , Gainesville, United States
4   Politecnico di Torino, Dept. of Mechanical and Aerospace Engineering, Torino, Italy

The restenosis following percutaneous transluminal angioplasty (PTA) for the treatment of peripheral artery disease is a serious shortcoming of the procedure potentially leading to the failure of the intervention. Both the arterial wall damage induced by the balloon expansion and the hemodynamic alteration following PTA are thought to play a major role in the activation of cellular response, leading to excessive intimal re-growth and lumen re-narrowing [1]. In this work, a multiscale computational framework was developed to simulate the arterial response following PTA, by integrating solid mechanics, fluid dynamics and cellular activities, with the aim of providing insights in the mechanobiological processes governing the restenosis and testing the outcome of the procedure under different scenarios.

The framework was based on the combination of three modules consisting of (1) finite element (FEM) simulation of PTA, (2) computational fluid dynamics (CFD) simulations of the post-operative vessel geometry, and (3) agent-based model (ABM) simulations of cellular dynamics in response to the FEM-computed damage and CFD-computed wall shear stress (WSS) [2]. The proposed framework was applied to an idealized three-dimensional model of femoral artery presenting with an eccentric stenosis (Fig.1A). The FEM simulation of PTA was performed considering an Armada balloon model (Abbott Vascular, USA). Data from healthy femoral arteries and heavily calcified femoral plaques were used to calibrate the material model parameters of the healthy intima, media and adventitia and diseased intima, respectively [3]. To describe the material softening due to mechanical damage experienced during the PTA procedure, a damage model was included in the material model formulation. A CFD simulation in the post-operative configuration was then performed and WSS was computed. Five cross-sections in the diseased region were selected for the subsequent ABM analysis. Specifically, the two-dimensional ABM of each section was initialized with the corresponding FEM-computed damage and CFD-computed WSS and simulated cell mitosis and apoptosis, and extracellular matrix production and degradation as function of the mechanical and hemodynamic inputs.

Figure 1B shows the FEM-simulated PTA procedure and the arterial wall remodeling of one exemplifying cross-section in response to the damage input only. The ABM predicted enhanced intimal growth at the damaged regions, with up to 20% lumen area reduction at 1-month.

Future work comprises applying the framework to a realistic vessel geometry and analyzing the impact of plaque size and composition on vessel remodeling.
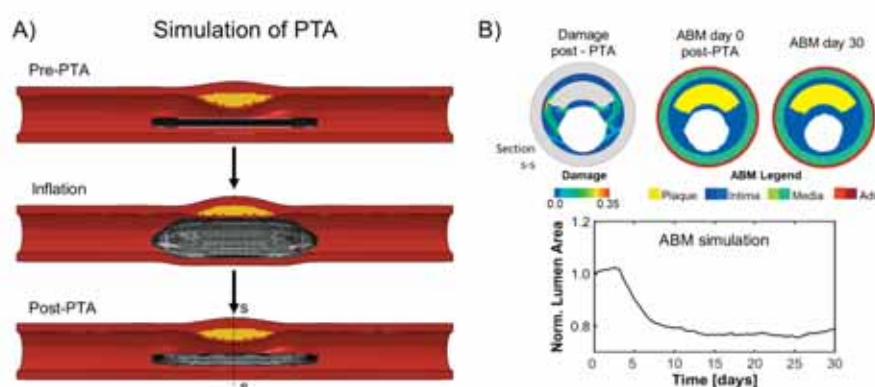
Figure caption: A) Simulation of PTA; B) Results of the FEM-ABM framework.

References:
1.   DeSart et al. J Vasc Surg 64:766-778.e5, 2016.
2.   Corti et al. Comput Biol Med 118:103623, 2020.
3.   Cunnane et al. Acta Biomater. 11:295–303, 2015.

D6.3

Gyroid VS strut-like scaffolds for bone regeneration: AN in silico comparitive analysis of healing in large bone defects

Mahdi Jaber[1], *Sara Checa*[1]

1   Berlin Institute of Health at Charité – Universitätsmedizin Berlin, Julius Wolff Institute, Berlin, Germany

Introduction: Large bone defect treatment remains a clinical challenge. Scaffolds have high potential for the treatment of large defects since they are able to provide biomechanical cues for guiding bone regeneration [1, 2]. However, to date the optimal scaffold design remains to be determined. Gyroid scaffolds have been suggested as a promising design due to their high surface area to volume ratio, which has been shown to increase cell adhesion [3]; however, their regeneration potential remains to be investigated. The aim of this study was 1) to investigate the bone regeneration process within gyroid scaffolds and 2) to determine potential bone regeneration alterations induced within this scaffold design.

Methods: An in silico approach was used to investigate the bone regeneration process within gyroid and strut-like scaffolds. The in silico models combined finite element (FE) analysis, to determine the mechanical environment within the scaffolds, and agent-based models (ABM) describing the biological processes taking place during bone regeneration [4]. Both gyroid and strut-like scaffolds had the same overall geometry: 5mm height (large defect in a small animal [5]) and 79% porosity [Fig. 1]. Scaffold pores were initially filled with granulation tissue, while PCL material properties were assigned to the scaffold. Moreover, scaffold pores were assumed to be filled with bone graft material [4]. A vertical load of 15 N was applied at the top surface, while the bottom surface was fixed.

Results: Initial mechanical stimuli within the gyroid and strut-like scaffold were considerably different, despite being under the same mechanical load [Fig. 2a, b]. Initially, most of the tissue volume within the gyroid scaffold was under mechanical stimuli beneficial for cartilage or fibrous tissue formation. The strut-like scaffold resulted in lower initial mechanical stimuli, with large tissue volumes under mechanical signals beneficial for bone formation. Initially, in both scaffolds, bone started to form from the top and bottom surfaces and slowly progressed towards the center region by intramembraneous ossification. Healing outcome, however was considerably different between the two scaffolds. While in the strut-like scaffold bony bridging was observed, the gyroid scaffold showed a thick layer of fibrous tissue within the scaffold core.

Discussion: Our results show that computer model predictions of bone regeneration are influenced by scaffold structure. This is in accordance with experimental studies showing different healing outcomes for different scaffold designs. Computer model predictions showed distinct initial mechanical environments within the scaffold pores in the gyroid versus the strut-like scaffold. However, the high elasticity of the gyroid scaffold induced high mechanical signals within the scaffold core at the late stages of healing, resulting in fibrous tissue formation. Future studies will investigate the effect of other scaffold designs and combine computer models with experimental data
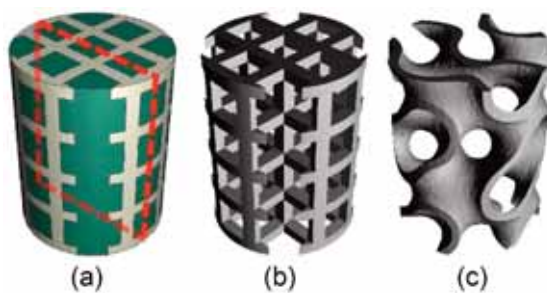
Figure 1: (a) CAD model consisting of regenerating tissue and scaffold, (b) strut-like and (c) gyroid scaffolds
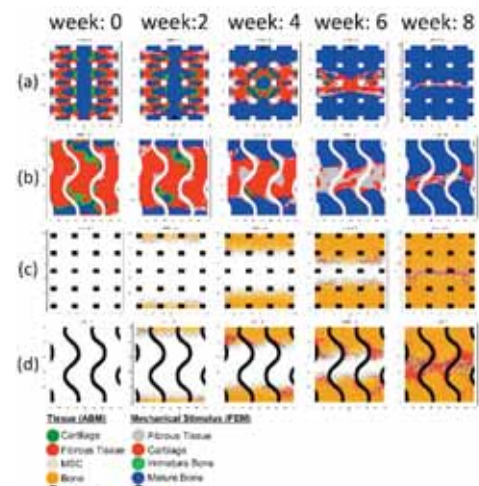
Figure 2: Cross section of the regenerating tissue-scaffold complex as marked in Fig. 1a. (a) and (b) Mechanical stimulus distribution at different stages of bone healing within the strut-like and gyroid scaffolds, respectively. (c) and (d) Tissue patterning at different stages of bone healing within the gyroid and strut-like scaffold, respectively. ABM results of the tissue patterning.

References:
[18]   Werner, M et al., Advanced science, 2017. 4(2): p. 1600347.
[19]   Bidan, C.M et al., PLoS ONE, 2012. 7(5): p. e36336.
[20]   Yoo et al, Int J Precis Eng Manuf 2014 15:1657–1666.
[21]   Perier-Metz et al, Front. Bioeng. Biotechnol 2020, 8:585799
[22]   Mehta et al, Arch Orthop Trauma Surg (2011) 131:121–129

D6.4

Effect of muscle volume on Finite element-based predictions of femoral neck strain using a virtual population

Zainab Altai[1], *Erica Montefiori*[1], *Claudia Mazzà*[1], *Xinshan Li*[1], *Pinaki Bhattacharya*[1]

1   The University of Sheffield, INSIGNEO Institute for In-Silico Medicine, Department of Mechanical Engineering, Sheffield, United Kingdom

Introduction: In older individuals, the variation in muscle anatomy and muscle forces remains unexplained by anthropometric parameters (e.g. body mass or body mass index) [1]. This variability is expected to result in a variation in femoral loading, which is an important determinant of bone remodelling. Yet, a full quantification of this variation has been limited by the small number of subjects recruited in previous observational studies. In this study, the variability is investigated using a virtual population model, by coupling musculoskeletal model (MSKM) with finite element model (FEM) [2].

Methods: Gait analysis, CT (0.79mm x 0.79mm x 0.63mm) and MRI (1.08mm x 1.08mm x 3mm) scans were collected from one woman (70.5years, 61.4kg, 1.64m). Mono-lateral personalised MSKMs of the lower limb were build from MRI segmentations [3]: maximal isometric force was computed as $F_{max} = \sigma V/l_{opt}$, where specific tension σ=61N/cm2, optimal fibre length l_{opt} was estimated from [3], and muscle volume V was assigned from 100 samples drawn from uncorrelated normal distributions. Distribution mean and standard deviations were based on MRI measurements of 11 elderly women [1]. These 100 MSKMs (considered here as models of 100 "virtual subjects") were analysed for one walking trial using OpenSim (https://simtk.org/) to obtain muscle forces and joint contact forces (JCFs). Specific gait frames, first (P1) and second (P2) peak of hip JCF, were identified. Using as input the muscle forces and JCFs at these frames, the peak principal strains (e1 and e3) at the femoral neck were predicted for each virtual subject, following CT-based FEM (using ANSYS APDL 19.1) and body-organ coupling models from [2]. The peak element strain energy density (SED) over the full femur volume were also computed at these frames per virtual subject.

Results: Hip JCFs estimated by the 100 MSKMs varied by up to 0.8 body weight (BW) at P1 and 3.1 BW at P2. The mean ± SD peak e1 and e3 at P1 were 0.37 ± 0.016 % and 0.41 ± 0.016 % respectively, and at P2 were 0.22 ± 0.038 % and 0.27 ± 0.044 % respectively. The mean ± SD peak of SED was 4.57 ± 0.46 GPa at P1 and 10.73 ± 4.43 GPa at P2 (Figure 1).
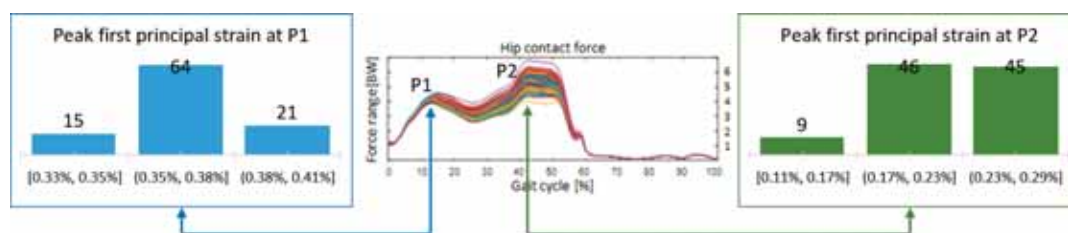
Figure 1: Right and left, distribution of virtual subjects in respect of the peak first principal strains predicted at the two peaks (P1 and P2) of the hip JCF gait frames. Middle, hip JCFs corresponding to the distribution of F_{max}

Discussion: Changes in individual muscle Fmax caused variations in JCF estimates larger than what has been previously reported [4]. Associated variations in peak principal strain were considerably higher than previous observations based on a much smaller cohort (20 subjects) [5].

References
1.   *Montefiori et al, PlosONE, 2020.*
2.   *Altai et al, PlosONE, 2021.*
3.   *Modenese et al, J Biomech, 2018.*
4.   *Valente et al, PlosONE, 9: e112625, 2014.*
5.   *Kersh et al, JBMR, 33: 1999-2006, 2018.*

D6.5
A micromechanical elasto-viscoplastic material model for cold-water coral skeletons

Ewan Smith[1], Marta Peña-Fernandez[1], Janina Büscher[2], Jürgen Titschack[2], Sebastian Hennige[3], Uwe Wolfram[1]

1   Heriot-Watt University, Edinburgh Campus, School of Engineering and Physical Sciences, Edinburgh, United Kingdom
2   University of Bremen, Marum Center for Marine Science, Bremen, Germany
3   University of Edinburgh, School of GeoSciences, Edinburgh, United Kingdom

Increased porosity in structural parts of deep-sea coral reefs due to ocean acidification is a threat which could lead to dramatic and rapid loss of fish biodiversity [1]. In situ evidence highlights that cold-water coral (CWC) can survive in aragonite sparse waters, but in a different way to what is currently considered a biogenic reef due to a majority loss of habitat [1]. The weakening mechanism has a striking similarity with osteoporosis [2] and similar population-based 'fracture risk' analyses could help to investigate 'tipping points' in reefs. No suitable computational framework exists to facilitate this for a range of coral specimen. This study aims to implement a multiscale constitutive model to simulate the mechanical consequences of ocean acidification upon CWCs and use this model to investigate degenerative impacts on a set of specimens by population-based statistical analysis.

Materials and methods: We developed a micromechanical model to scale up stiffness and strength. The skeletal wall was modelled as a polycrystalline material with randomly oriented aragonite needles [3] and dissolution porosity was included via a Mori-Tanaka scheme [4]. We used a Mohr-Coulomb strength criterion [3] for the aragonite crystals to identify a porosity dependent strength criterion [5] at skeletal length scale to incorporate strength loss due to acidification. The elasto-viscoplastic model was implemented in FEA and validated using nanoindentation and micropillar tests. To investigate the effect of varying morphology, exposure and boundary conditions, we analysed CT data-based FE models (Fig 1d) from five CWCs with significantly different morphologies.

Results and discussion: SEM and EBSD images confirmed that crystal arrangement is random. Unacidified polycrystalline stiffness was comparable to nanoindentation results. Increasing porosity due to ocean acidification (Fig 1a) did not significantly affect the underlying material properties of the polycrystal (p=0.08), it has a detrimental effect upon macroscopic stiffness and strength (Fig 1b and 1c). This may cause structural collapse and a shift from high 3-dimensional complexity habitats to a habitat restricted primarily to coral colonies of lower 3-dimensional complexity. This implementation may help to determine biodiversity 'tipping points' for management of these vulnerable ecosystems.
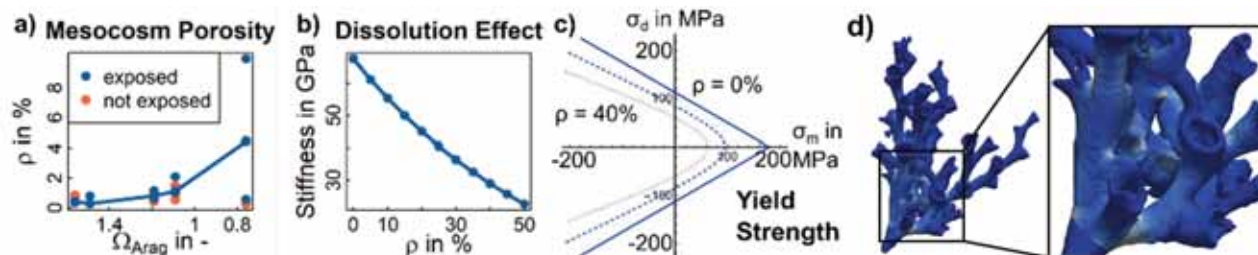
Figure 1: Porosity (ρ) significantly increased with aragonite concentration (ΩArag) (a) for exposed CWC skeletons in experiments simulating future oceanic conditions [1]. Porosities reached up to ~40% so that stiffness (b) and strength (c) were significantly decreased. (d) FE model of a representative CWC sample.

References
[23] Hennige et al. Sci Adv, In review (MS available)
[24] Hernlund et al. Arch Osteopor 2013.
[25] Sanahuja et al. J Eng Mech 2010, 136(2): 239-253.
[26] Speed et al. JMBBM in press
[27] Schwiedrzik et al. BMMB 2013, 12(6): 1155-1168.

D6.6
Multiscale modelling of advection-diffusion processes in perfused tissues

Eduard Rohan[1], Vladimír Lukeš[2], Jana Camprová-Turjanicová[2]

1   University of West Bohemia in Pilsen, Department of Mechanics, Faculty of Applied Sciences, Pilsen, Czech Republic
2   University of West Bohemia in Pilsen, Czech Republic

Physiological processes in tissues, such the growth, remodelling, or detoxification, are driven by the transport of oxygen and nutrients which both depend on the blood microcirculation. Its assessment is usually realized due imaging techniques applied to reconstruct a flow model using the data collected in a time interval during dynamic perfusion tests such as the dynamic contrast-enhanced computed tomography or magnetic resonance. These methods monitor time-space distribution of the contrast fluid which is injected in the form of a time bolus of the contrast fluid concentration. The present paper contributes to the development of a complex multiscale hierarchical model of the tissue perfusion by several aspects: a) The homogenization-based models of the microcirculation derived previously [1,2] are revised and adapted for a new interface condition coupling the flow in precapillary networks (two mutually disconnected systems) with the capillary porosity described by the Darcy flow while respecting the deformation; in this way a new double porosity flow model is derived which provides remedies to drawbacks of the models proposed previously; b) We derive a homogenized model of the contrast fluid (CF) transport in the vasculature. This yields a problem for the CF saturation which is transported due to advection along with the blood. For this, the multiscale advection velocity fields are given by the perfusion model which is decoupled. While in the larger (precapillary) vasculature, the diffusion is very small and provides the model regularization, in the capillary porosity it is used to account for the CF penetration to the space of Disse through the capillary wall fenestration. Furthermore, it is shown how the homogenized models of the flow and the CF transport are coupled with the upper hierarchies of the vascular trees. In this respect, we focus on the situation in the liver tissue. The homogenized models are derived for this lobular structure, whereby flows and the advection-diffusion in vascular trees of the upper hierarchies are described by the multi-compartment Darcy flow model [3].

Figure caption: Representative periodic cell of the liver tissue and the microflow illustration.

References:
[1]   Rohan E., Cimrman R. Two-scale modeling of tissue perfusion problem using homogenization of dual porous media. Int J Multiscale Computational Engineering, 8(1), 2010.
[2]   Rohan E., Turjanicová, J., Lukeš, V. Multiscale modelling and simulations of tissue perfusion using the Biot-Darcy-Brinkman model. Comp & Struct, 251, 106404, 2021.
[3]   Rohan E., Lukeš, V., Jonášová, A. Modeling of the contrast-enhanced perfusion test in liver based on the multi-compartment flow in porous media. J Math Biol., 77:421-454, 2018.

D6.7

Multiscale modeling of the knee joint pathophysiology: differential effect of mechanical loading on the cartilage zones

Satanik Mukherjee[1 2], Raphaëlle Lesage[1 2], Liesbet Geris[1 2 3]

1   Biomechanics Section, Department of Mechanical Engineering, KU Leuven, Leuven , Belgium
2   Prometheus, Division of Skeletal Tissue Engineering, KU Leuven, Leuven , Belgium
3   GIGA In silico Medicine, University of Liege, Liège , Belgium

Optimum mechanical signals are necessary to maintain homeostasis of chondrocytes, the primary cells residing in articular cartilage. Any departure of mechanical signals from optimum values (due to obesity, traumatic injuries etc.) can lead to destabilization articular chondrocyte homeostasis and a switch to hypertrophy, as observed in osteoarthritis (OA). In this context, multiscale models can be used to delineate the translation of mechanical signals from the macro-scale joint level to the micro-scale cell level, as a result of (patho)physiological loading at the joint level, and how these mechanical signals transduce intracellular biochemical processes.

In this study, a coupled multiscale model of the human knee joint was developed to estimate the changes in cell phenotype and activity of the relevant cell secreted factors as a result of (patho)physiological loading at the joint-level1,2. The multiscale model incorporates in-silico models at three different length scales (Figure1)   : 1) Finite element (FE) model of the knee joint, 2) FE model of the chondrocyte, and 3) Intracellular gene/protein regulatory network for mechanotransduction3. Integrins, the mechanosensors for the chondrocytes were modeled as linear springs between the cell and pericellular matrix interface. Using this multiscale model, a pathological case, i.e. the effect of meniscectomy on the progression of OA was studied.

It was observed that meniscectomy leads to increased strains in the articular cartilage as compared to a healthy joint, resulting in higher forces sensed by the chondrocytes in all the zones of cartilage. However, the forces sensed in the superficial zone (SZ) chondrocytes were higher as compared to the deep zone (DZ). This increased mechanical loading in the SZ led to subsequent buildup of inflammatory cytokines over time, which together with the mechanical loading led to a phenotypic switch of SZ chondrocytes to hypertrophy (as evident from the high activity of the pro-hypertrophic biomarkers RUNX2, Coll-X, MMP13). The DZ chondrocytes underwent hypertrophy at a later stage after the SZ had degenerated considerably. Hence, by using the multiscale model, we were able to elucidate the differential behavior of the SZ and DZ chondrocytes in the knee joint due to meniscectomy. This multiscale model has huge potential in not only unraveling the role of mechanical loading in progression of OA, but also to suggest suitable therapeutic regimes to arrest cartilage degeneration in OA.
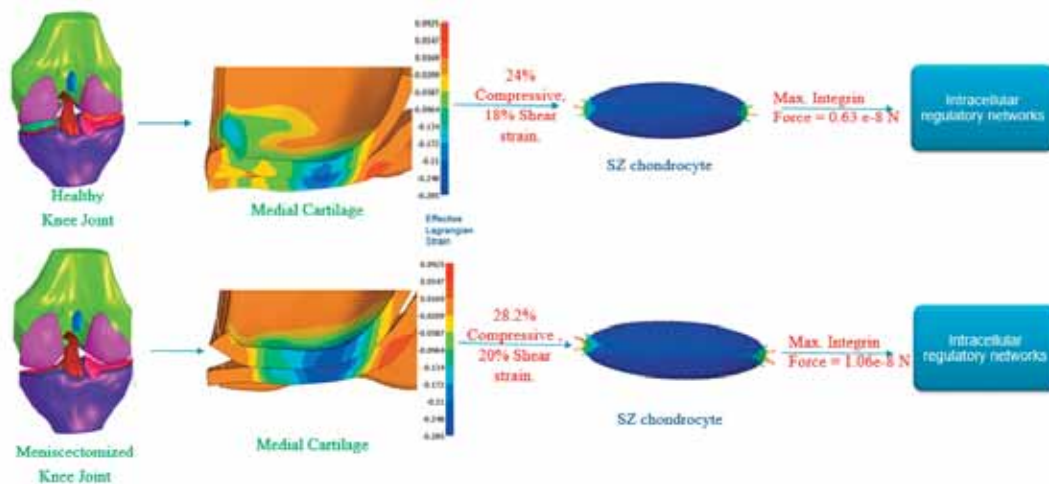
Figure 1: Multiscale model workflow for the SZ chondrocyte.

References:
1.   Erdemir A. J. Med Device.7(4):0409101–409101, 2013.
2.   Wilson W, van Donkelaar CC, van Rietbergen B, Huiskes. J. Biomech. 38, 1195–1204, 2005.
3.   Kerkhofs J, Geris L. Plos One. 10:e0130033, 2015.

D6.8

Biomechanical modeling of soft tissue multiphysics using hybrid machine learning and finite element analysis

Seyed Shayan Sajjadinia[1], *Bruno Carpentieri*[1], *Duraisamy Shriram*[2], *Gerhard A. Holzapfel*[3] [4]

1   Faculty of Computer Science, Free University of Bozen-Bolzano, Bolzano, Italy
2   Engineering Product Development (EPD) Pillar, Singapore University of Technology and Design (SUTD), Singapore
3   Institute of Biomechanics, Graz University of Technology, Graz, Austria
4   Norwegian University of Science and Technology (NTNU), Department of Structural Engineering, Trondheim, Norway

The numerical analysis of soft tissues may require the application of highly nonlinear differential equations coupled with multiphysics theories, which in the context of biomechanics are usually formulated by multiphasic models, see, e.g., [1,2]. These systems of equations are implemented by expensive numerical solvers, e.g., using nonlinear finite element methods, which may be completely inefficient in time-sensitive clinical decision-making process. A common remedy is to first generate a data set of the numerical results that are used for subsequent training a machine learning (ML) model, i.e., ML-based surrogates [3], with the numerical solver being replaced by this efficient data-driven model. However, they still need to be extensive in numerical data generation. Here, we propose a hybrid ML (HML) method with the basic idea of inserting a highly efficient low-fidelity (LF) model prior to an ML model so that the numerical part is able to model a rough estimation of bulk responses, without considering all the physics involved. In this way, the ML part can only focus on improving the LF results to the fidelity of the expensive multiphysics models, while the parameters that can complicate the ML part can now be managed numerically. Figure 1 illustrates the evaluation results for some examples of low- and large-scale simulations, demonstrating that the HML implementations can improve the performance, especially in small training data regimes, so that no further numerical data creation is required. We conclude that the proposed HML method, which is a completely different alternative to the models defined by physics-based loss functions and traditional model-order-reduction techniques, may efficiently increase the accuracy of the ML-based surrogate modeling, in which the multiphysics equations play an important role in the biomechanical analysis of soft tissues.
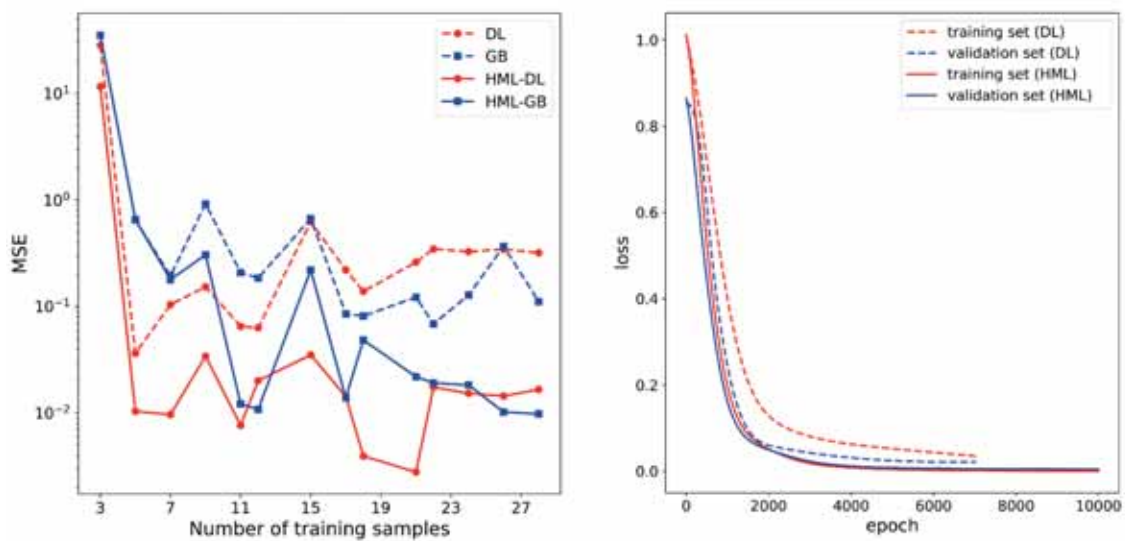
Figure 1: Comparison of hybrid and purely data-driven approaches: mean squared errors (MSEs) for each tuned model of a 2D axial problem (left), and recorded loss functions' values in each epoch for a 3D cartilage problem (right); Abbreviations: DL: deep learning, GB: gradient boosting, HML: hybrid machine learning.

References:
[1]   Arbabi, V. et al., J. Biomech. 49:1510–1517 (2016)
[2]   Sajjadinia, S.S. et al., Proc. Inst. Mech. Eng. Part H J. Eng. Med. 233:871–882 (2019)
[3]   Phellan, R. et al., Med. Phys. 48:7–18 (2021)

D8.1

Including the subtalar joint within lower-limb skeletal models significantly affects ankle, knee, and hip joint kinematics

Erica Montefiori[1], *Claude Fiifi Hayford*[1], *Claudia Mazzà*[1]

1   Department of Mechanical Engineering & INSIGNEO Institute for in silico Medicine, University of Sheffield

Lower-limb skeletal models (SKMs) usually include hip, knee, and ankle, with the latter referring to one or multiple joints, i.e. tibiotalar and subtalar, depending on the application. Different modelling choices and resulting ankle kinematics have been extensively studied. Only few postural studies reported on the relationship between ankle joint alignment and knee and hip kinematics [1], with associated clinical implications. The aim of this study was to use an image-based SKMs to quantify the effect of neglecting the subtalar motion on the estimated lower-limb kinematics.

Gait analysis and lower-limb medical resonance imaging (MRI) were collected from seven juvenile participants (15.3(1.5)y.o., 62(8)kg, 160(2)cm), and thirteen mono-lateral datasets were included in this study. A marker-set including thirteen markers in the foot [2] was used to record gait analysis data and register them with the MRI. Two lower-limb SKMs (M1 and M2) were built from each dataset, including a ball-and-socket hip joint and hinge knee, tibiotalar, and subtalar joints. The joint axes were morphologically fitted [2]. In M2 the subtalar joint was locked in the neutral anatomic position (standing gait trial), hence not allowing for inversion/eversion movement during the dynamic simulations. Inverse Kinematics was run in OpenSim3.3 (https://simtk.org) to estimate joint angles during walking. Root mean square deviation (RMSD) between kinematics from M1 and M2 was evaluated for each participant. Differences between kinematics curves were assessed by non-parametric paired t-test ($\alpha=0.05$) using the Statistical Parametric Mapping (https://spm1d.org) package.

RMSD between models are reported in Table. Ignoring subtalar motion (M2) significantly underestimated tibiotalar plantarflexion and hip internal rotation (6° and 7°, respectively) during late stance and early swing (Figure). A smaller, but significant effect was also found for the other degrees of freedom.

Experimental errors associated with subtalar joint kinematics (up to 3.3° [3]) often lead to neglecting this joint within SKMs. The variations observed in this study, however, were considerably higher than this value. This suggests that the subtalar joint should indeed be included within SKMs to prevent unwanted effects on the estimate of hip, knee, and ankle kinematics.

Table: Maximum and mean±SD RMSD between kinematics from M1 and M2."

RMSD [°]	Hip Fl/Ex	Hip Ab/Ad	Hip Int/Ext	Knee	Tibiotalar	Subtalar
Max	1.4	2.2	5.1	2.1	6.5	18.0
Mean ± SD	0.6 ± 0.4	1.4 ± 0.5	3 ± 1.2	1.1 ± 0.5	4.2 ± 1.0	11.0 ± 3.4
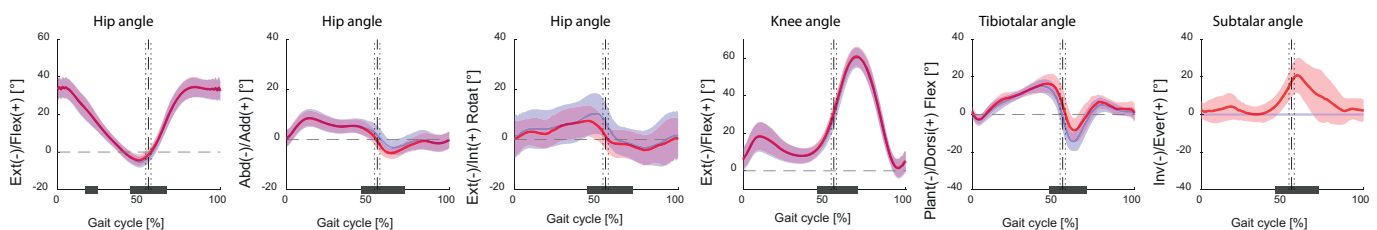
Figure caption: "Mean±1SD lower-limb kinematics using M1 (red) and M2 (blue) over the thirteen simulated limbs. Significant difference indicated by dark grey bars (paired t-test)."

References:
[1]   Khamis, S. et al., 2007. Gait Posture;
[2]   Montefiori, E. et al., 2019. J Biomech;
[3]   Westblad, P. et al., 2002. Foot Ankle Int."

D8.2
EMG signals as a way to control soft actuators

António André[1], *Ana Margarida Teixeira*[1], *Pedro Martins*[2 3]

1   INEGI, 4200-465, Portugal
2   INEGI-LAETA, 4200-465, Portugal
3   FEUP, 4200-465, Portugal

Currently, physical impairments are very common since they have multiple causes: normal aging process [1], neurodegenerative diseases [2] and accidents [3]. These locomotion disorders are very known from society long time ago, reason why researches and engineers [4] have been trying to mitigate the consequences of this problem. Nowadays, solutions such as exoskeletons and exosuits are in constant development and improvement, which may represent a reliable option to help people in circumstances of lack of mobility or in rehabilitation scenarios.

However, both alternatives need a control system acting as a "bridge" between the external device (actuators) and the user. Among all possibilities [5,6], the prediction of user movement intention is prioritized over movement reaction. A possibility is to capture biological signals from the body.

Assuming that premise and in an attempt to achieve the goal, electromyographic (EMG) signals are captured from muscles using a BITalino device [7] and treated in a software like Matlab [8]. After, the signal is sent to a function generator, which sends it, as input, to a soft actuator with piezoelectric properties (materials which have the ability to change the shape and size when electrically stimulated).

This procedure (Figure 1) is intended to be executed in real time.
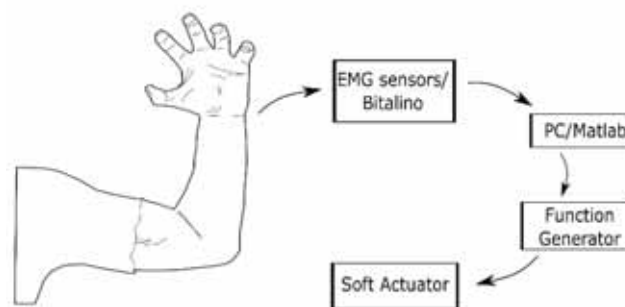
Figure 1. Procedure adopted.

References:
[1]   Chen B., Zi B., Qin L., and Pan Q. State-of-the-art research in robotic hip exoskeletons: A general review. Journal of Orthopaedic Translation, pages 4–13, 2020
[2]   Moreno J. C., Mohammed S., Sharma N., and del Ama A. J. Hybrid Wearable Robotic Exoskeletons for Human Walking. Wearable Robotics Systems and Applications, pages 347–364, 2020
[3]   Nas K., Yazmalar L., Sah V., Aydin A., and Ones K. Rehabilitation of Spinal Cord Injuries. World Journal Of Orthopedics, pages 8–16, 2015
[4]   Kim Y. S., Lee J., Lee S., and Kim M. A Force Reflected Exoskeleton-Type Masterarm for Human-Robot Interaction. IEEE TRANSACTIONS ON SYSTEMS, MAN, AND CYBERNETICS—PART A: SYSTEMS AND HUMANS, 35(2):198–212, 2005
[5]   Anam K. and Al-Jumaily A. A. Active Exoskeleton Control Systems: State of the Art. Procedia Engineering, pages 988–994, 2012
[6]   T. Proietti, V. Crocher, A. Roby-Brami, and N. Jarrasse. Upper-limb robotic exoskeletons for ´neurorehabilitation: A review on control strategies. IEEE Reviews in Biomedical Engineering, 9:4–14, 2016
[7]   BITalino, https://bitalino.com/
[8]   MathWorks, https://www.mathworks.com/products/matlab.html

D8.3

Movement optimization through musculoskeletal modeling and multidimensional surface interpolation

*Christine Walck[1], **Christopher Lamb**[1], Tyler Farnese[1], Jennifer Perskin[1]*

1   Embry–Riddle Aeronautical University, Mechanical Engineering, Daytona Beach, United States

In an effort to enhance medical decision-making and precision treatment, biomechanical modeling and computer simulations originating from observations of human movements are being implemented. Such a combination allows for the establishment of cause-and-effect relationships providing a unique, non-invasive method of evaluation into internal joint and muscle function, as well as athletic performance and neuromuscular coordination. While these are beneficial, the need for optimizing remains. For example, when preventing physiological deconditioning (i.e., muscle atrophy, bone decalcification, and poor cardiovascular health) within the musculoskeletal (MSK) system, current methods rely on a multitude of movements. This is seen on the International Space Station (ISS) as each astronaut uses different exercise machines in the hopes of minimizing the gap between pre- and post-flight syndrome. To reduce the number of exercises and the time spent on each machine while combating space-deconditioning syndrome, an optimized solution is needed. Therefore, the goal of this study is to pair biomechanical modeling and computer simulations with a multidimensional surface interpolation creating an aid in the development of an optimized singular exercise movement. The interpolation uses a radial basis function (RBF) derived from the proper orthogonal decomposition (POD) for a series of biomechanical responses (joint angles and muscle forces), which come from several dynamic exercises (Figure 1). Kinematic and kinetic data for each exercise was collected using motion capture and force plate technology, and processed in OpenSim through an inverse dynamic analysis resulting in the biomechanical responses. Using these responses, the interpolation algorithm learns from progressive calculations outputting the ideal response that will then interpolate a set of new parameters [1]. These new parameters will then aid in the development of a singular movement yielding an optimized exercise machine. To test the code's accuracy, the POD-RBF was specified to interpolate to a dataset for 41 lower extremity muscle forces during a squat movement using the ISS's Advanced Resistive Exercise Device (ARED). Initial results (Figure 2) show an average difference between the interpolation and the OpenSim static optimization results of 1.30% with larger errors seen at datasets having non-zero minimum forces. Optimizing movements will revolutionize countermeasures in fight against the progressive intensity of space-deconditioning syndrome. Future studies will use the new parameters to develop the singular movement and then use inverse dynamics within a biomechanical modeling environment dependent on MSK properties ranging from short- to long-term exposure to validate the singular movement suggested by interpolation.
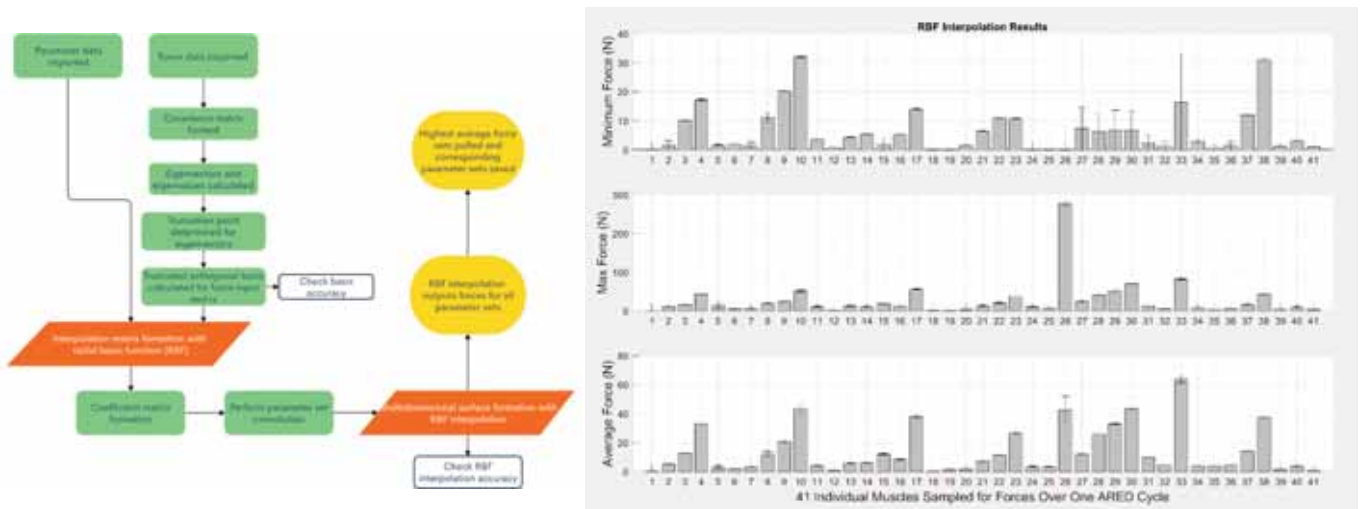
Figure caption: POD-RBF interpolation workflow.

RBF interpolation results found in 41 lower extremity muscles during a ARED squat.

References:
[1]   Rogers, C. A., Kassab, A. J., Divo, E. A., Ostrowski, Z., & Bialecki, R. A. (2012). An inverse POD-RBF network approach to parameter estimation in mechanics. *Inverse Problems in Science and Engineering, 20*(5), 749-767.

D8.4

Could a exoskeleton-driven rehabilitation treatment improve muscle forces generation in PD? A pilot study

Marco Romanato[1], *Fulvia Fichera*[2], *Fabiola Spolaor*[1], *Daniele Volpe*[2], *Zimi Sawacha*[1]

1   University of Padova, Information Engineering, Padova, Italy
2   Fresco Parkinson Center, Villa Margherita, S. Stefano, Arcugnano (VI), Italy

Research focusing on optimal rehabilitation methods has been directed towards powered lower-limb exoskeletons which combines the advantages delivered from the grounded robotic devices with the ability to train the patient in a real-world environment [1]. In this contest literature has highlighted the benefit of coupling gait analysis and musculoskeletal modeling (MSM) for treatment planning, supplementing this approach with robotic rehabilitation [2]. Recently this combined approach has been successfully applied to detect the alterations in motor control related to Parkinson's Disease (PD) [3]. However, no study has reported about the effects of an overground wearable exoskeleton in terms of both gait analysis and MSM derived parameters in PD subjects. The aim of this study was to quantitatively assess the effect of an overground rehabilitation treatment on a PD subject both in terms of gait parameters and muscle forces. Thus, after written informed consent, one PD subject (age=69 years, BMI=22.8kg/m2) has been enrolled (ClinicalTrials.gov Identifier: NCT04778852) and gait analysis was performed before and after a 4-weeks gait training intervention with an overground exoskeleton. Several gait cycles were collected with an 8-cameras optoelectronic system (120-240Hz, Vicon, USA), synchronized with two force plates (1080Hz, AMTI, USA) and an 8-channel electromyographic system (2000Hz, Cometa, Italy); the protocol described in [3] was adopted and the activity of 4 muscles was acquired bilaterally (Biceps Femoris, Rectus Femoris, Gastrocnemius Lateralis, Tibialis Anterior). Three left and three right gait cycles were extracted, inverse kinematics, inverse dynamics, and static optimization were performed in OpenSim using a muscle-optimized scaled model [4]. Results from joint moments and muscle forces were compared with healthy controls (age=57.8±5.6years, BMI=27.3±3.9kg/m2) and reported respectively in figure A and B. It is worth noticing that after the therapy joint loads in both ankle and knee joints were reduced during the whole stance phase and muscle forces displayed an increased magnitude in correspondence with the force peak after the treatment. For the best of our knowledge, the presented case study is the first attempt to track rehabilitation improvement via muscle forces assessment. Further studies should focus on increasing the sample size to generalize the outcomes.
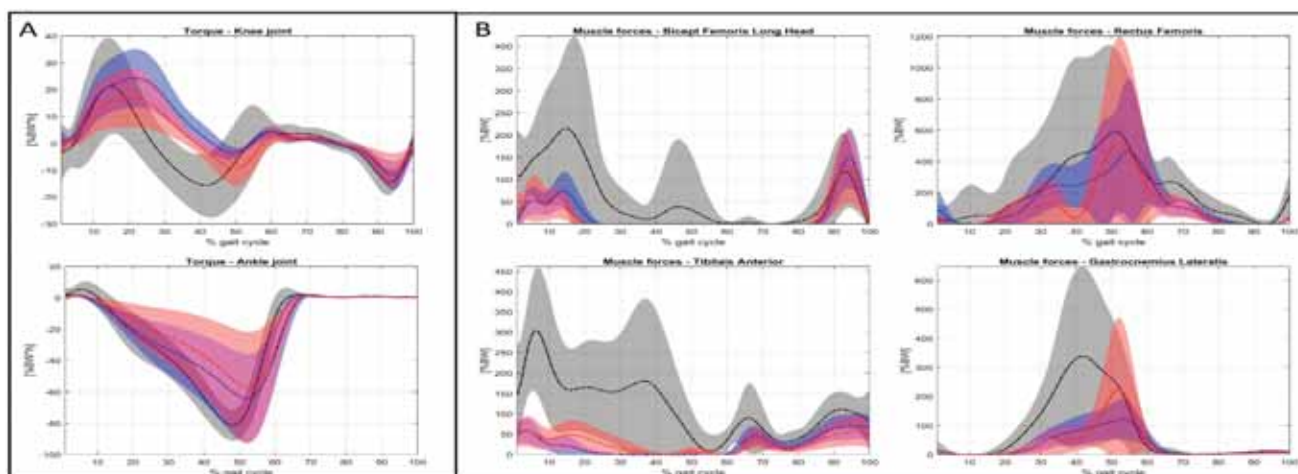
Figure caption: A) Knee and ankle joint moments. B) Biceps Femoris, Rectus Femoris Tibialis Anterior and Gastrocnemius Lateralis muscle forces. Control subjects (black, average ± standard deviation), before treatment PD subject average (blue, average ± standard deviation), after treatment PD subject average (red, average ± standard deviation).

References:
1.   M. Bortole et al, Journal of NeuroEngineering and Rehabilitation, 2015; (12) 54.
2.   M. Sartori et al, WIREs Syst. Biol. Med, 2016; E1368.
3.   M. Romanato et al, CMBBE, 2021; 10.1080/10255842.2021.1925887.
4.   Modenese et al. 2016. J Biomech. 2016. 49:141-48.

D8.5

Simulating the dynamics of a human-exoskeleton system using kinematic data with misalignment between the human and exoskeleton joints

Divyaksh Subhash Chander[1], Max Böhme[2], Michael Skipper Andersen[3], John Rasmussen[3], Maria Pia Cavatorta[1]

1   Politecnico di Torino, Department of Mechanical and Aerospace Engineering, Turin, Italy
2   Leipzig University of Applied Sciences, Faculty of Engineering, Leipzig, Germany
3   Aalborg University, Department of Materials and Production, Aalborg, Denmark

Musculoskeletal model-based simulation can be a powerful tool in the design and evaluation of exoskeletons [1]. They are used extensively during the virtual prototyping stage using motion data of the human without the exoskeleton. An ideal exoskeleton model, perfectly aligned with the human joint axes, can be used to co-simulate the human and exoskeleton dynamics. However, misalignment between the human and exoskeleton joints is commonly observed during the use of an exoskeleton, potentially leading to a loss in the effective assistance received by the user [2]. Motion data collected with the user wearing the exoskeleton should, normally, be able to capture the misalignment between the human and exoskeleton joints. Using misaligned motion data in the combined human-exoskeleton model can lead to complications in the virtual model and unrealistic outputs. One way to tackle these complications is to assume alignment between the human and exoskeleton joints in the model by kinematically constraining it.

This work presents a new method that facilitates the analysis of misaligned human-exoskeleton systems. This is achieved by introducing artificial segments between the human and exoskeleton models. These artificial segments, the so-called dummy segments, ensure kinetic alignment between the human and exoskeleton joints in the model without altering the observed kinematics from the actual trial. The method is demonstrated using an active lower-limb exoskeleton that aims to assist the elderly in stair negotiation. A single subject performed eight trials with the exoskeleton in a laboratory. Motion data of both the subject and exoskeleton were recorded using an optical marker-based motion capture system. Further, the measured ground reaction force and the exoskeleton assistive force were used as inputs in the combined human-exoskeleton model. The outputs from the inverse dynamics analysis of the model with the dummy segments were compared to those from a reference model, where the measured external forces were applied directly to the human model at the corresponding reference points, bypassing the human-exoskeleton interface model completely. The results of the knee compression force, knee flexion moment, and activation of vastus lateralis from the model with the dummy segments showed good agreement with the reference model. The use of the dummy segments allows the study of aligned kinetics and misaligned kinematics from the same model.

References:
[1]   M. Tröster, D. Wagner, F. Müller-Graf, C. Maufroy, U. Schneider, and T. Bauernhansl, "Biomechanical model-based development of an active occupational upper-limb exoskeleton to support healthcare workers in the surgery waiting room," Int. J. Environ. Res. Public Health, vol. 17, no. 14, pp. 1–16, 2020, doi: 10.3390/ijerph17145140.
[2]   R. Mallat, M. Khalil, G. Venture, V. Bonnet, and S. Mohammed, "Human-Exoskeleton Joint Misalignment: A Systematic Review," Int. Conf. Adv. Biomed. Eng. ICABME, vol. 2019-Octob, pp. 1–4, 2019, doi: 10.1109/ICABME47164.2019.8940321.

D8.6

Computational analysis of the load's effect on deliveries cyclists, and the consequence of delivery backpack's design on the cyclist

Nicolás Yanguma Muñoz[1], Brayan David Solórzano Quevedo[1], Kevin Alejandro Giraldo Rodriguez[1], Christian Javier Cifuentes De la Portilla[1]

1   Universidad de los Andes, Biomedical engineering, Biomechanics group (IBIOMECH), Bogota, Colombia

The rapid virtuality transition due to the covid-19 pandemic has increased web or mobile apps to deliver food and essential needs. This also has produced rapid growth in the number of deliveries cyclists. For instance, in Colombia, there are approximately 27 thousand deliveries cyclists on the streets, and another 45 thousand waiting on the food delivery apps services. Although cycling brings benefits to people's health, this labor can have severe injuries and consequences on cyclist well-being [1,2,3]. Hence, this work aimed to analyze the load effect on deliveries cyclists and the kinetic variation with distinct backpacks designs, implementing mathematical models in the software COMSOL Multiphysics. The computational model was constructed in COMSOL Multiphysics using standard male thoracic, and delivery backpack measures. Variations of the original backpack were developed combining additional straps, and new backpack designs were elaborate by changing measurements and appending new tools to optimize loading and reduce lumbar compression. The human geometry model includes thorax, shoulders, and arms; and the backpack geometry model includes a rigid bar, a set of straps depending on the model. Simulations were carried out emulating loads of 4, 8, and 16 kg (5%,10%, and 20% body weight of 80 kg subject). The simulations were evaluated comparing the first and third principal stress on the lumbar and shoulder area. Model validation was done using pressure sensors in the lumbar back area with 10% and 20% of the subject's body, weight 80 kg. The implemented model' results suggest that the forces involved, the moment of inertia, and the torque generated in the rigid bar at the bottom of the backpack result in critical tension and compression forces on the delivery cyclist lumbar area; generating shear displacement in lumbar vertebrates, and consequently potentially causing injuries. Moreover, the new designs successfully optimize compressive and tensile lumbar forces, compensating these by spreading on the shoulders. Further, the computational model shows promising alternatives to evaluate kinetic analysis with low percentage error respecting experimental data.
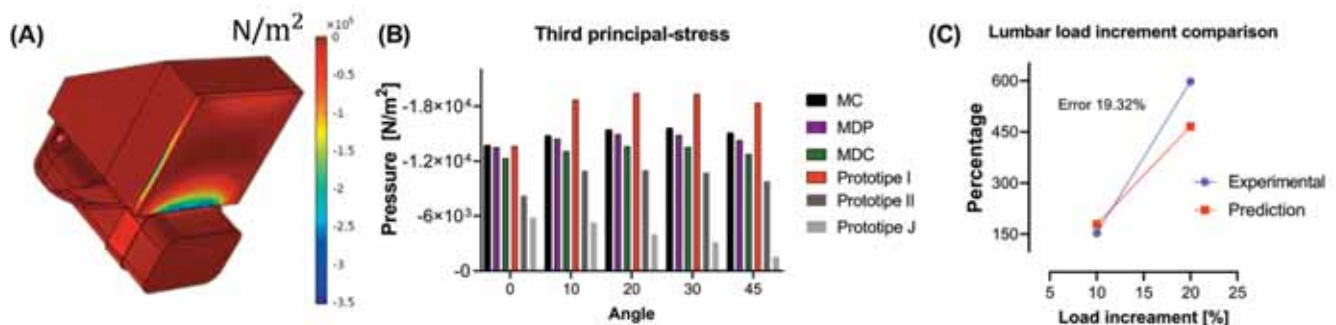
Figure. A) Third principal- stress results, B) Models comparison Third principal-stress, C) Comparison experimental data and in-silico data.

References:
1.   Atreya, S., Joshi, D., Anand, S., Singh, U., & Ribeiro, R. (2010). Effects of Backpack Carriage on Gait and Posture-Design Studies. In the 6th World Congress of Biomechanics (WCB 2010). August 1-6, 2010 Singapore (pp. 155-158). Springer, Berlin, Heidelberg.
2.   Ren, L., Jones, R. K., & Howard, D. (2005). Dynamic analysis of load carriage biomechanics during level walking. Journal of Biomechanics, 38(4), 853-863.
3.   Goh, J. H., Thambyah, A., & Bose, K. (1998). Effects of varying backpack loads on peak forces in the lumbosacral spine during walking. Clinical Biomechanics, 13(1), S26-S31.

D9.1

Insights from applying measured in vivo knee kinematics and contact forces as wear simulation boundary conditions

Michael Dreyer[1 2], Bernhard Weisse[2], William R. Taylor[1], Colin Smith[1]

1   ETH Zürich, Laboratory for Movement Biomechanics, Institute for Biomechanics, Zürich, Switzerland
2   Empa - Swiss Federal Laboratories for Materials Science and Technology, Laboratory for Mechanical Systems Engineering, Dübendorf, Switzerland

Knee implant inlay wear is commonly tested using the ISO 14243 force- and displacement-controlled boundary conditions (BCs). The novel CAMS-knee dataset includes synchronized knee implant kinetics and kinematics obtained from instrumented implants and a moving fluoroscope [1]. We assessed whether in vivo and ISO standard BCs lead to different predictions of implant wear.

We created finite-element models of the ISO force controlled (FC) and displacement controlled (DC) knee implant wear tests using the Innex FIXUC implant (Zimmer Biomet). The DC model prescribed knee flexion angle, axial force, anterior-posterior (AP) displacement and internal-external (IE) rotation. The FC model prescribed AP force and IE torque instead and contained nonlinear AP and IE spring restraints. Representative in vivo knee loads and kinematics were generated for the CAMS walking dataset using the HIGH100 averaging method [2]. The ISO standard (FC, DC), CAMS-Knee (FC, DC), and HIGH100 (FC) BCs were then applied to the models. An elastic-plastic material model was used for the inlay, while the femoral component was rigid. Mesh density was chosen based on a convergence study. Inlay geometry change was predicted for 5 million cycles using a cross-shear and contact-pressure dependent wear model and a compressive creep model. The DC ISO model predicted unrealistic contact and was excluded.

The FC ISO model showed the highest wear rates (Table 1). Wear increased with increasing contact area and slip and decreasing contact pressure. A small average cross-shear-ratio (≤0.02) in all models indicated mostly unidirectional sliding, likely due to the highly constrained implant design. Comparing the CAMS models, contact was generally more posterior and less conforming for the DC model than for the FC model, resulting in reduced contact areas and thus wear. All FC models could not replicate the IE rotation and under-predicted the posterior displacement observed in vivo. Consequently, the wear scar centroids were located ~10mm more anteriorly in the FC compared to the DC CAMS model (Figure 1). Although the medial compartment force was only 1.5x larger, the medial wear scar showed 2–5x more wear than the lateral scar for all models.

The FC ISO model predicted similar wear volume compared to the FC CAMS model. However, none of the FC BCs resulted in kinematics and wear locations that matched the DC CAMS model. This demonstrates the importance of fluoroscopy measurements for validation and model development, and a need for improved methods to predict wear for novel implant designs where implant-specific fluoroscopy measurements are not yet available.

	wear rate [mm³/Mc]	
CAMS DC	9.9	
CAMS FC	12.9	
HIGH100 FC	11.4	
ISO FC	14.1	

Table 1: Predicted wear rate

Figure 1: Wear scar depth and centroid after 5 million cycles (Mc).

References:
[1]   Taylor (2017) J. Biomech.
[2]   Bergmann (2014) PLoS ONE

D9.2

How does the absorption process influence the mechanical stability of a biodegradable MgYREZr screw?

Sabrina Söntgen[1], **Ludger Keilig**[1], Koroush Kabir[2], Anna Weber[1], Susanne Reimann[1], Kristian Welle[2], Christoph Bourauel[1]

1   Medical Faculty, University of Bonn, Oral Technology, Bonn, Germany
2   Medical Faculty, University of Bonn, Department of Orthopedic and Trauma Surgery, Bonn, Germany

Absorbable materials offer many advantages in medical application. Among these are a reduced number of required surgical interventions to retrieve medical implants and therefore reduced risks associated with explantation and surgery in general. Such materials are for example used in screws used for small fracture treatment. Theoretically, the screws are absorbed until only the healed bone structure remains. As the absorption process influences the geometry of the screws, their structural stability during this period is of special interest. It was the aim of this study to determine the influence of the absorption process on the mechanical behaviour of a Herbert screw in a combined experimental and numerical approach.

Two absorbable MgYREZr Herbert screws that were explanted for clinical reasons after 6 weeks and 12 weeks in-situ respectively were available in this study, and five new screws from the same manufacturer were used for reference. Current geometries of the partly-absorbed as well as new screws were determined using µCT. To determine the influence of absorption on the mechanical stability we conducted three-point bending tests with all available screws. Additionally, a numerical analysis was performed based on the recorded geometries to examine the screws and possible stability changes throughout the healing/absorption process. For the new screws we used material parameters (Young's modulus 45 GPa, yield limit 235 MPa) from the literature [1]. The material parameters of the partly absorbed screws were determined by fitting numerical to experimental curves using back-calculations.

In the three-point bending test, the new screws were able to withstand higher loads (mean 175 N, standard deviation 6 N) than both explanted screws, which failed at 72.5 N (explanted after 6 weeks) and 74.5 N (12 weeks). For the new screws, the experimental and numerical curves were almost identical using the material data from [1], but curves differed for the partly-resorbed screws. Using back-calculation we estimated a Young's Modulus of 15 GPa (6 weeks) and 8 GPa (12 weeks) as well as a yield limit of 135 MPa for both screws. Moreover, areas under high stress could be identified, such as a hole in the screw explanted after 6 weeks.

Concluding, our findings show that the stability of the absorbable screws is influenced by the change of the geometry due to the absorption process as well as due to changes in the material behaviour of the partly absorbed structure. This has to be taken into account when using such absorbable materials in order to obtain a better overall patient outcome and treatment results due to improved stability.

References:
1   Ezechieli et al., Biomechanical Properties of a Novel Biodegradable Magnesium-Based Interference Screw. Orthop. Rev. 2016, 8, 6445.

D9.3

Evidence for the applicability of musculoskeletal human models to improve outcomes of total hip arthroplasty

David Scherb[1], *Christopher Fleischmann*[2], *Stefan Sesselmann*[2], *Jörg Miehling*[1], *Sandro Wartzack*[1]

1   Engineering Design, Friedrich-Alexander-Universität Erlangen-Nürnberg, Erlangen, Germany
2   Institute for Medical Technology, Technical University of Applied Sciences Amberg-Weiden, Weiden in der Oberpfalz, Germany

The number of worldwide total hip replacements (THR) yearly increases. The choice for an implant depends on the surgeon's preoperative planning. However, the patients´ individual biomechanical situation is widely neglected during the planning process. This can result in a suboptimal implant selection and positioning, especially for patients with complex pathologies as in revision THR, which may cause muscular dysfunction and hence, elongated or even incomplete rehabilitation. Thus, this study provides evidence in the use of musculoskeletal human models (MHM) in preoperative planning to improve the postoperative outcome of THR, especially in case of revision THR.

Therefore, a patient-specific MHM of a patient is created [1, 2] and put in the pose of "single leg stance". The muscular conditions of the model are adapted to three situations: healthy status, after primary THR and after revision THR [3]. The most affected muscle by THR is the gluteus medius, mainly responsible for pelvic stabilization during single leg stance. The gluteal activation and the hip joint contact forces are simulated for all three situations. Subsequently, adjustable implant parameters (neck shaft angle, femoral offset and antetorsion angle) are varied via a parameter study. Simultaneously, gluteal muscle activation and resulting hip joint contact forces are computed to investigate the effect of the parameter variation.

Analyzing these different situations, the activation of the gluteus medius increases from the healthy status to the status after revision THR due to muscle weakening. In particular, the posterior part of the gluteus medius is activated almost completely just to keep the single leg stance pose. Furthermore, hip joint contact forces decrease after primary and even more after revision THR due to rising activation of other hip muscles. The parameter study shows that the activation of the gluteus medius can be influenced considerably by intraoperative adjustable parameters (see figure).

Therefore, MHM not only allow the analysis of a patient's individual biomechanical condition, but also improve biomechanical outcomes by simulating different geometrical THR implant parameters during surgery planning. Consequently, inclusion of MHM in the preoperative planning process provides better opportunities to choose the right implant parameters and to optimize implant positioning from both a biomechanical and a kinematical point of view.
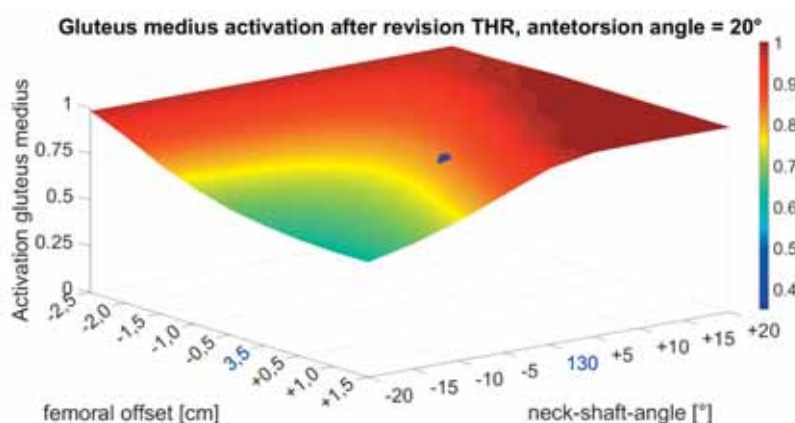
Figure caption: Dependency of gluteus medius activation from intraoperative adjustable hip parameters; Blue point/marks: patient's initial anatomical condition

References:
[1]   Fleischmann C. et al. (2021). In: Ahram; Di Cecco (Hrsg.): Human Interaction, Emerging Technologies and Future Applications III: Springer International Publishing (Advances in Intelligent Systems and Computing), S. 331–337
[2]   Scherb D. et al. (2020). In: Proceedings of the 31st Symposium Design for X (DFX2020): The Design Society, S. 1–10
[3]   Roth P. von et al. (2014). In: The bone & joint journal 96-B, Nr. 12, S. 1618–1622

D9.4

MRSNS: mixed reality guided surgical navigation system using an external electromagnetic tracker and a head-mounted display

Puxun Tu[1], Dongyuan Li[1], Yan Guo[1], Huixiang Wang[2], Xiaojun Chen[1 3]

1   Shanghai Jiao Tong University, School of Mechanical Engineering, Shanghai, China
2   Shanghai Jiao Tong University Affliated Sixth People's Hospital, Department of Orthopedics, Shanghai, China
3   Shanghai Jiao Tong University, Institute of Medical Robotics, Shanghai, China

Accurate registration between virtual space and physical scene is vital when developing any mixed reality based navigation system not only for a high-precision fusion of virtual model and its physical counterpart but also for intra-operative safety. Existing methods, such as the embedded front camera based method [1], still suffer from line-of-sight restriction. The purpose of this study is to propose an accurate registration method for a head-mounted display (Microsoft HoloLens 2) and an external electromagnetic tracker (NDI Aurora), and to develop an integrated navigation system for distal interlocking of intramedullary nail.

The workflow of our proposed MRSNS can be described as the following steps: (1) System connection. The connection between the holographic application running on HoloLens and the computing application running on PC is conducted via TCP/IP. (2) System registration. By matching the customized registration cube with the pre-defined virtual fiducial points, the registration matrix between the HoloLens coordinate system and the electromagnetic tracker coordinate system can be obtained using the absolute orientation quaternion method. (3) Surgical navigation. The virtual nail and the physical one can keep overlapped by updating the matrix T_V^H. An intraoperative warning system can provide intuitive feedback of the real-time deviations and EM disturbances.

To evaluate the performance of the MRSNS, we conducted 20 distal locking trials using 10 tibial models. Experimental results indicated that the distance error was 1.61 ± 0.44 mm and the 3D angular error was $1.46\pm0.46°$. We also conducted a cadaver experiment to evaluate the feasibility of the MRSNS.

Compared with electromagnetic navigation systems and traditional free-hand approaches, the MRSNS has the following potential advantages: (1) No radiation exposure for the whole procedure. (2) Intraoperative hand-eye coordination can be guaranteed. (3) Less time consumption and better stereoscopic visualization. We believe that the MRSNS has great potential in clinical application.
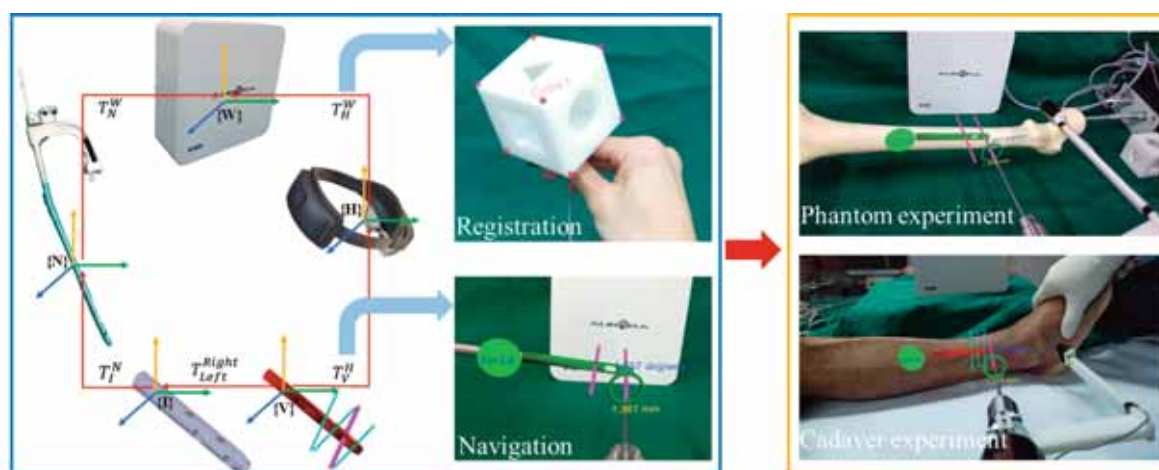
Figure caption: Fig. 1 System architecture and experimental validation.

References:
[1]   F. Liebmann, S. Roner, M. von Atzigen, D. Scaramuzza, R. Sutter, J. Snedeker, M. Farshad, P. Furnstahl, Pedicle screw navigation using surface digitization on the Microsoft HoloLens, Int J Comput Assist Radiol Surg 14 (2019) 1157–1165.

D10.1

On the role of force transmission between migrating endothelial agents in shunt formation during angiogenic remodelling

Lowell Edgar[1], Miguel Bernabeu[1]

1   University of Edinburgh, Usher Institute, College of Medicine and Veterinary Medicine, Edinburgh, United Kingdom

Angiogenic remodelling occurs as endothelial cells (ECs) composing blood vessels rearrange in response to shear stress by migrating against the direction of flow [1]. The mechanisms which prevent vascular shunting during remodelling remain unclear despite being highly relevant to arteriovenous malformations, a leading cause of stroke [2]. We have previously demonstrated that collective signalling may play a role in the remodelling outcome via force transmission between ECs [3]. To elucidate and demonstrate the role of force transmission during shunt formation, we have designed an agent-based model of flow-mediated collective migration. We aim to vary the parameters behind force transmission and to identify which factors push the system towards shunt formation.

We represent individual cells as nested ellipses which migrate against flow and interact via force. Force transmission, based on overlap, consists of extrusive (pushing) forces which maintain spacing and cohesive (pulling) forces which maintain the collective. We simulated migration within an idealised capillary plexus with Poiseuille flow determined by lumen diameter and thus cell number. Agents encountering bifurcations either split apart or combined based on the convergence/divergence of flow.

We found that we could create shunting via the amount of cohesion within the system (Fig. A). Simulations without cohesion maintained an even distribution of cells across the plexus. High levels of cohesion caused ECs to cluster, forming aggregates and depleting cells and flow from other regions of the plexus. Cohesion also prolonged flow reversals as it prevented ECs from intercalating effectively to reduce stress and resolve diameter fluctuations. Flow reversals exert a critical behaviour change within the system by switching the direction of cell migration and flow convergence/divergence at bifurcations; this bifurcation switch acts as the mechanism for cell aggregation and shunt formation (Fig. B).

We have demonstrated the role of EC force transmission during angiogenic remodelling and shunt formation. Extrusive forces allow ECs to intercalate and relieve stress whilst cohesive forces disrupt this intercalation, creating tension within the endothelium and producing diameter imbalances and flow reversals. Our results reveal the dynamic nature of flow direction during remodelling and create new considerations in the study of flow-mediated migration in complex networks. Together these findings provide novel insight into the mechanisms of vascular malformation in vivo and may implicate additional targets for normalisation strategies in the future.
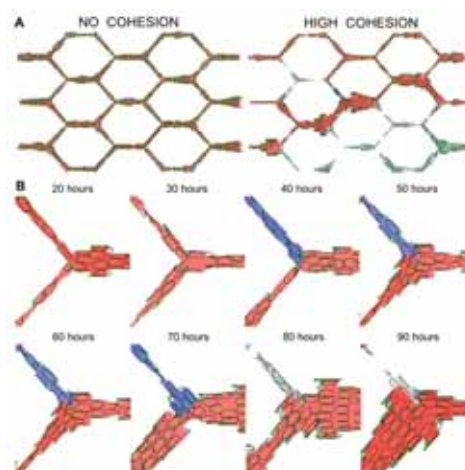
Figure caption: (A) Excess cohesion pushed the system from stable perfusion to shunt formation. (B) Flow reversals at bifurcations cause diverging EC migration paths to instead converge.

References:
[1]   Georgieva PB, et. al. Circ Res. 2019; 125: 262–264;
[2]   Derdeyna, et. al. Stroke 2017; 48(8): e200-e224;
[3]   Edgar LT, et. al. PLoS Comp Biol. 2021; Feb;17(2):e1007715.

D10.2

Deformable ellipsoidal fibril distributions to predict microvascular guidance in response to 3D matrix orientation and anisotropy

Steven LaBelle[1 2], *Shad Dinkins*[1 2], *Adam Rauff*[1 2], *James Hoying*[3], *Jeffrey Weiss*[1 2]

1   University of Utah, Biomedical Engineering, Salt Lake City, United States
2   Scientific Computing and Imaging Institute (SCI Institute), Salt Lake City, United States
3   Advanced Solutions Life Sciences, Manchester, United States

Introduction: Despite the fundamental role of neovessel guidance during angiogenesis in wound healing, graft/implant inosculation, and tumorigenesis, the process by which matrix alignment influences neovessel growth and guidance is poorly understood. Recent studies indicate that both the direction of collagen fibrils and the degree of anisotropy influence collective cellular migration [1]. Although 2D frameworks have taken fibril distribution approaches to modeling guidance, current 3D frameworks calculate guidance cues from discrete vector fields which fail to account for the degree of alignment [2-4]. We propose a 3D ellipsoidal fibril distribution (EFD) representation of collagen orientation during simulations of collective migration phenomena that accounts for matrix anisotropy and realignment due to matrix deformation.

Methods: In vitro alignment studies of angiogenesis - Rat fat microvessels were embedded in type I collagen. Collagen was stretched along the axial direction before polymerization finished to induce low, medium, or high levels of anisotropy (n > 6 ea.). The gel edges were cut from the anchors, gels were cultured for 10 days and then fixed, stained, and imaged. The microvascular density and microvessel orientation distributions were calculated from confocal volumes (n > 18 ea.). Simulations - Mechanical models in FEBio were coupled with AngioFE, a plugin that simulates neovessel growth from parent microvessels [4]. We modified AngioFE to represent fibril distributions as EFDs stored as symmetric positive-definite (SPD) tensors [5]. The directional dependence of growth was based on a persistence term, a direction sampled from the EFD, and the anisotropy of the EFD. Microvessel growth over time was based on in vitro data, the initial matrix density, and the degree of anisotropy. Simulations of growth in low, medium, and high anisotropy were calibrated against experimental data using both our legacy approach (vector field) and our new approach (EFD). Hypothetical distributions of planar isotropy were simulated to compare the predictive capability of each approach.

Results & Discussion: In vitro results – Microvessel density significantly increased at medium and high levels of anisotropy (Fig A, B). Microvascular orientation increased in a dose-dependent manner with matrix anisotropy (Fig C). Simulation results – An EFD field was generated to describe the local fibril orientation distributions (Fig D). A vector-field approach was unable to account for changes in microvascular density based on the degree of anisotropy. Further, a vector-field approach was insufficient to model cases of planar isotropy (Fig E). In contrast, the EFD-based approach was able to predict both changes in growth and guidance based on the degree of alignment. This approach could be extended to other common distributions and nonparametric distributions derived from experiments and imaging data. Further, the degree of anisotropy could control biological activities and cellular signaling to predict matrix-cell mechanobiological interactions during collective guidance, growth and remodeling phenomena.

References:
[1] McCoy, MG., et al., *ACS Biomater. Sci.Eng.* 4(8): 2967-76, 2018. [2] Barocas, VH. & Tranquilo, RT., *J Biomech Eng.* 119(2): 137-45, 1997. [3] Dallon, JC., et al., *J Theor Biol.* 199(4): 449-71, 1999. [4] Maas, SA., et al., *Biophys J.* 115(9): 1630-37, 2018. [5] Fletcher, PT. & Joshi, S., *Signal Process.* 87(2): 250-62, 2007.
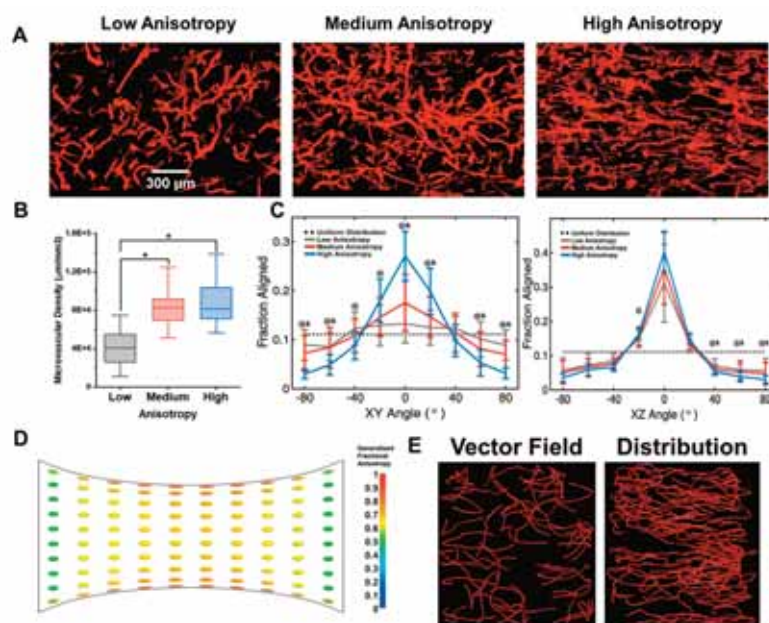
Figure: Medium and high anisotropy increase microvascular density but only high anisotropy significantly influences 3D microvessel orientation. **A)** Representative max intensity Z projections (250 um depth) of confocal images and microvascular density measurements from microvessels grown in aligned matrices. **B)** Microvascular density increases with medium and high anisotropy. 1 Way KW ANOVA. *: p < 0.05. N ≥ 18 per group. **C)** Microvessel orientation distributions in the horizontal (XY, left panel) and vertical (XZ, right panel) planes. Microvessels reoriented along the fibril direction in the XY plane for matrices of high anisotropy but not medium or low anisotropy. There was no appreciable effect of alignment on reorientation in the XZ plane. 1 Way KW ANOVA with Dunn's post hoc performed on each bin. @, & p < 0.05 between low and high or between medium and high respectively. **D)** Demonstration of EFD deformation during uniaxial tension. **E)** Comparison of vector field and distribution (EFD) approaches in predicting growth in highly aligned collagen. The EFD approach allows more stochastic motion and growth increases due to the degree of anisotropy.

D10.3

Theoretical assessment of focused septal growth in hypertrophic cardiomyopathy

Sandra Hager[1], Will Zhang[2], Renee M. Miller[1], Jack Lee[1], David A. Nordsletten[1 2]

1   King's College London, School of Biomedical Engineering & Imaging Science, London, United Kingdom
2   University of Michigan, Department of Biomedical Engineering & Cardiac Surgery, Ann Arbor, United States

The heart grows and remodels (G&R) in response to changes in mechanical loading. The most commonly observed growth types in the left ventricle (LV) are eccentric growth (in the fiber direction) and concentric growth (perpendicular to fibers). However, phenotypical growth patterns in hypertrophic cardiomyopathy (HCM), caused by a genetic mutation of the myocytes' sarcomeric proteins, do not show altered loading conditions yet introduce heterogeneous growth patterns and fiber disarray in the heart. Prior studies have demonstrated promising outcomes for predicting cardiac growth due to increased overload states inside the heart and further modelled inverse G&R after surgery. However, growth patterns in HCM show more complexity than the established models for hypertrophy in the heart, and less research has been done to investigate geometrical changes in this pathological case. By utilizing the kinematic growth approach and adapting previously used kinematic growth tensors from standard growth laws, this study examines tissue related characteristics and their impact on the development of heterogeneous growth patterns in HCM. It was shown that fiber disarray alone might not be the primary driver for the typical growth phenotypes seen in HCM, see Fig. 1. Alternately, an underlying driver for heterogeneous growth might be a consequence of underlying factors, such as inflammation, which stimulates a more isotropic growth pattern. Apart from investigating the geometrical changes, this study details the incompatibility, introduced by growth, associated with residual stress. For quantifying the residual stress in the septal region, the degree of incompatibility was compared with a compatible growth deformation, see Fig. 1. The latter deformation type results in a stress-free grown geometry.
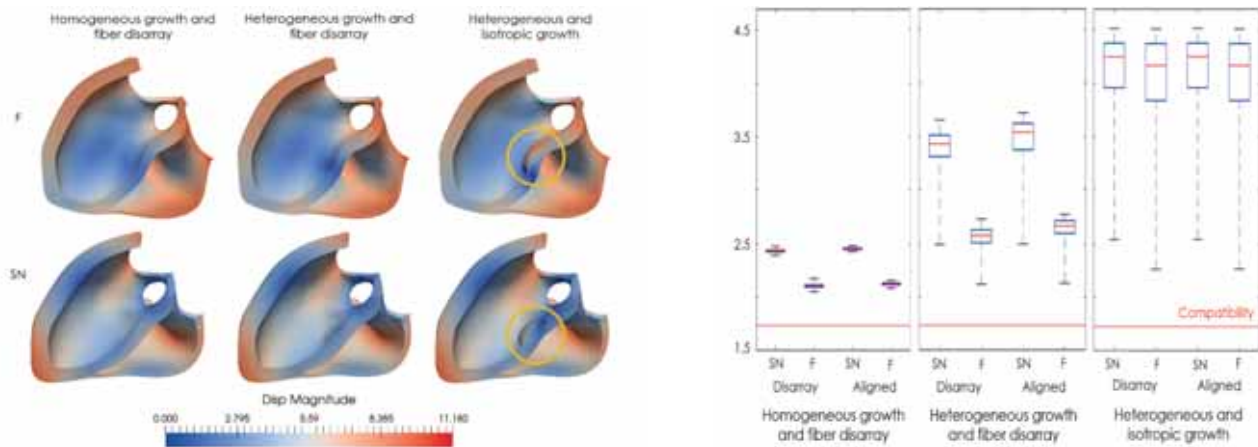
Figure 1: Left: Comparison of the displacement magnitude (mm) between different growth modes and the impact of fiber disarray on the final grown geometry. A phenotypical growth pattern in the septal area stands out when isotropic growth was applied, highlighted with the yellow circle. Right: The degree of incompatibility in the septal region, defined as the Frobenius norm of $F_e F_g$ while compatibility is determined in the grown unloaded state and has to hold $F_e F_g = I$.

References:
Hadjicharalambous, M., Lee, J., Smith, N. P., Nordsletten, D. A.: A displacement-based finite element formulation for incompressible and nearly-incompressible cardiac mechanics. Comput. Methods in Appl. Mech. Eng., 274, 213-236 (2014).
Lee, J., Cookson, A., Roy, I., Kerfoot, E., Asner, L., Vigueras, G., Sochi, T., Deparis, S., Michler, C., Smith, N.P., Nordsletten, D. A.: Multiphysics computational modeling in CHeart. SIAM J. Comput., 38(3), C150-C178 (2016)

D10.4
Computational modeling of trabecular bone micro-structure

Mahtab Vafaeefar[1], Kevin Moerman[1 2], Ted Vaughan[1]

1   National University of Ireland Galway, Galway, Ireland
2   Massachusetts Institute of Technology, Media Lab, Biomechatronics, Cambridge, United States

This study analyses a set of algorithms for the creation of digital models of trabecular bone architecture and compared them to porcine and human bone. The structures investigated are the: Gyroid (GY), Stochastic Microstructure (STM) [1], and Spinodoid (SP) [2]. The Gyroid is regular and (triply) periodic (Fig D1) , while, like bone, the STM (Fig D2) and SP (Fig D3) structures are non-periodic and stochastic. The latter two are derived from isotropic and anisotropic Cahn-Hilliard phase separation algorithms respectively. Using image processing tools [3], we investigated morphometric and topological indices describing the computational bone structures, and compared them to CT derived (Fig A) porcine talar subchondral (PTS), and human femoral head (FH) bone structures (Fig B). The following morphometric indices were considered: bone volume fraction (BV/TV), trabecular thickness (Tb.Th), trabecular separation (Tb.Sp), and the ellipsoid factor (EF) (Fig E), which defines spatial distribution of plate and rod elements. In terms of topological indices, we considered the degree of anisotropy (DA), connectivity density (Conn.D.), intertrabecular angle (ITA), nodal degree of connectivity of the skeleton network [4] (Fig F-H). For each structure, a suitable representative volume element size was determined by considering independence of mechanical behavior and morphometric indices from voxel size and sample size. The effective Young's modulus was computed for each structure through linear homogenization and finite element analysis [4] (Fig C). Through appropriate parameter adjustment this work demonstrates that the computational structures can be made to closely resemble many of the structural and morphometric and topological indices as well as the mechanical properties of bone (Fig I). Hence, the computational structures represent flexible methods for creating artificial bone architectures. Preliminary analysis indicates plate-like elements (as reflected in EF) and connectivity (as reflected in Conn.D) are important contributors to stiffness. This work presents three computationally efficient mathematical techniques to develop trabecular bone-like structures. The algorithms are sufficiently flexible to allow one to capture the heterogeneity in trabecular bone. Furthermore, the algorithms can be used to study the influence of morphometric and topological parameters on bone structural stiffness and fracture and failure characteristics.

Sample	PTS1	PTS2	FH1	FH2	STM	SP	GY
BV (mm^3)	43.36	58.81	35.65	46.88	10.07	10.14	10.04
TV (mm3)	192.37	192.37	170.02	170.02	27.00	27.00	27.00
BV/TV	0.23	0.31	0.21	0.28	0.37	0.38	0.37
Tb.Th mean (mm)	0.17	0.19	0.17	0.17	0.16	0.15	0.17
Tb.Sp Mean (mm)	1.46	1.42	0.59	0.48	0.24	0.19	0.21
Conn. D. (mm^3)	11.64	14.05	10.44	14.87	40.93	34.46	47.44
DA	0.65	0.54	0.51	0.42	0.62	0.80	0.52
Median EF	-0.50	-0.50	-0.25	-0.32	0.08	0.16	0.16
E33 (Mpa)	1227.01	1520.65	549.20	810.68	706.52	918.97	2501.78

Figure caption: CT image segmentation (A) for bone geometry extraction (B), Von Mises stress on STM (C), computational structures (D1-3). Ellipsoid factor distribution (E), nodal connectivity on skeleton (F), and its histogram (G), and ITA distribution (H1-3) for a bone sample. Summary of parameters (I).

References:
[1] Soyarslan et al. (2018a), Acta Mater. 149, 326–340.
[2] Kumar et al., npj Comput Mater 6, 73 (2020).
[3] Doube et al., (2010), Bone 47:1076-9,
[4] Moerman, (2018). JOSS, 3(22), 506.

D10.5
Identification of constitutive material parameters of degenerative menisci using inverse finite element analysis

Jonas Schwer[1], Fabio Galbusera[1], Anita Ignatius[1], Lutz Dürselen[1], Andreas Seitz[1]

1   Institute of Orthopaedic Research and Biomechanics, Centre for Trauma Research Ulm, Ulm University Medical Centre, Ulm, Germany

Introduction: Osteoarthritis of the knee joint is one of the most widespread diseases and therefore of great clinical and socioeconomic importance. Besides the articular cartilage, it affects the menisci, which are crucial for the load transfer and distribution in the knee joint. Thus, identifying alterations in the mechanical properties of meniscal tissue that are associated with progressive degeneration is of particular interest for OA research. Therefore, the objective of this study was to determine the material properties of degenerative human menisci using inverse finite element analysis (FEA).

Methods: Twenty-four cadaveric human knee joints were equally divided into a mild and severe degeneration group and MRI-scanned under loaded (25%, 50%, 100% bodyweight) and unloaded conditions. Then the geometry and 3D displacement of the lateral and medial menisci were assessed ([1], Figure A). Based on a previously introduced method [2] individual FE models of the menisci were created, utilizing an anisotropic, hyperelastic strain energy function [3] to simulate the meniscus matrix in a poroelastic model. As boundary conditions, the superficial displacements, estimated by non-rigid registration were applied to the menisci. During a nature-inspired particle swarm optimization (PSO), the difference between the reaction force of the femoral meniscal surface at equilibrium and the force applied during the experiment was minimized by varying four sensitive constitutive material parameters in a physiologically range [2]. A normalized root mean squared error (NRMSE) was chosen as cost function covering all three load levels. The optimized parameters described the stiffness (C10) and compressibility (D) of the nonfibrillar matrix as well as the nonlinear fiber behavior (k1) and the permeability (k).

Preliminary results: The optimized parameters indicate a decrease in stiffness (C10) as well as impaired compressive properties (D) in severe degenerated menisci (Figure B). Further, the contribution of fibers (k1) changes markedly with progressive degeneration, while the permeability (k) is less affected.

Discussion: The parameters of an anisotropic, hyperelastic material formulation of both, mild and severe degenerated menisci were successfully obtained by a combination of noninvasively measured 3D displacements and inverse FEA. Ongoing calculations will show which parameters respond most sensitive to progressive degeneration. Further, we found that severe degenerated menisci exhibited a significantly higher axial compression than mild degenerated menisci [1]. Therefore, we hypothesize that the compressibility of the nonfibrillar matrix (D) will be higher in severe degenerated knee joints.
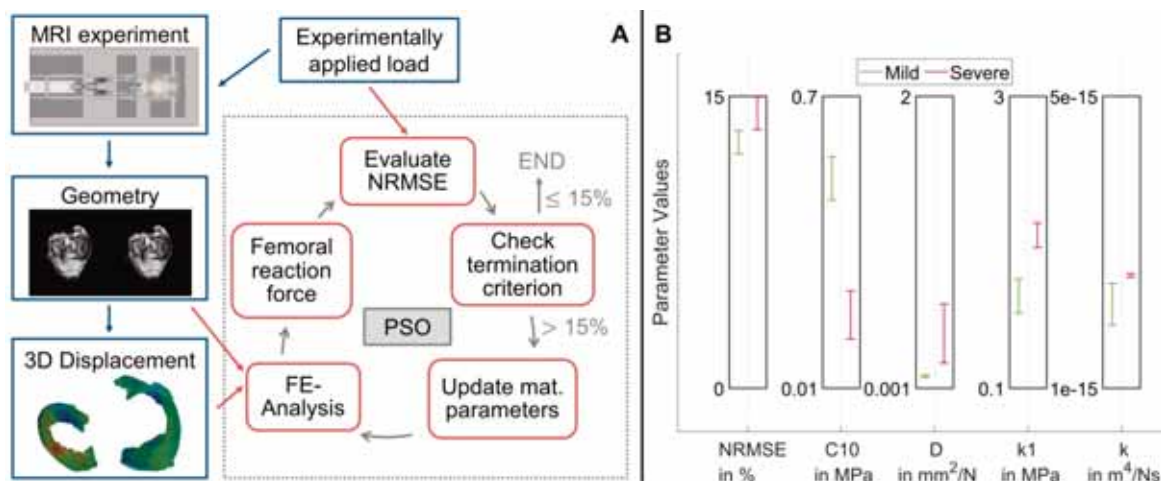
Figure: Schematic illustration of the PSO (A) and preliminary results (n=4) of optimized material parameters of mild and severe degenerated lateral menisci (B).

References:
[28] Schwer et al., Front. Bioeng. Biotechnol., 8, 1106, 2020
[29] Freutel et al., J. Biomech., 48, 1343-1349, 2015
[30] Holzapfel et al., J. Elast., 61, 1-48, 2000

D10.6

Reproducibility of in vivo constitutive parameter identification based on 4D ultrasound strain imaging

Andreas Wittek[1], *Claus-Peter Fritzen*[2], *Armin Huss*[1], *Christopher Blase*[1]

1   Frankfurt University of Applied Sciences, Computer Science and Engineering, Frankfurt am Main, Germany
2   University of Siegen, Engineering, Siegen, Germany

Time-resolved three-dimensional ultrasound combined with speckle tracking algorithms (4D ultrasound) is a non-invasive medical imaging technique that provides full field displacement and strain data of aortic and aneurysmal wall motion in vivo [1]. We have developed a Finite Element Model Updating (FEMU) approach to determine the individual nonlinear and anisotropic constitutive behavior of human aortae and AAA in vivo based on 4D ultrasound data and blood pressure measurement [2].

In an in vitro validation study by our group, the measurement uncertainty of 4D ultrasound strain measurement was examined. The 95%-confidence interval (CI) of the random error of local strain measurement (for tissue segments with a size of about 1.5 x 1.5 mm) was determined to be $\pm$ 2.1%. The uncertainty of the mean of the local strains was slightly smaller ($\pm$ 1.6%). However, the random error of the mean in repeated measurements is the possible systematic error of local strain values in a single measurement.

In the current study, we have performed a numerical experiment to examine the reproducibility and uniqueness of the results of the inverse approach to parameter identification based on the observation of just two load cases (diastolic and systolic blood pressure). In a further numerical experiment, we have tested the effect of the possible random and systematic error of a single 4D ultrasound strain measurement on the identified constitutive behavior.

The repeated identification of the constitutive behavior based on strain data that were not corrupted by measurement uncertainty indicates that the solution of the inverse problem is unique with regard to the identified stretch-CAUCHY stress curves at finite deformations ($R2 \geq 0.978$), but non-unique with regard to the parameters of the chosen Holzapfel-Gasser-Ogden constitutive equation. These results were confirmed by the parameter identification based on strain field data with overlaid random error ($R2 \geq 0.912$). In contrast, the increase of the mean strain by 1.6% (systematic error) resulted in the identification of a decisively softer constitutive behavior. The performed numerical verification experiment shows that it is feasible to identify the non-linear and orthotropic constitutive behaviour of the geometrically irregular aortic wall based on the observation of just two load-cases if reliable measurements of heterogeneous fields are available.

References:

[1]   K. Karatolios,*; A. Wittek* et al. (2013): Method for Aortic Wall Strain Measurement with Three-Dimensional Ultrasound Speckle Tracking and Fitted Finite Element Analysis. In: Ann Thorac Surg 96 (5), 1664–1671, *equal contribution.
[2]   A. Wittek, W. Derwich, K. Karatolios, C.-P. Fritzen, S. Vogt, T. Schmitz-Rixen, C. Blase (2016), A finite element updating approach for identification of the anisotropic hyperelastic properties of normal and diseased aortic walls from 4D ultrasound strain imaging, J Mech Behav Biomed Mater 58, 122–138.

E1.1
Frontiers for innovation in fracture healing simulation

Tianyi Ren[1], Salim Darwiche[2 3], **Hannah Dailey**[1]

1   Lehigh University, Department of Mechanical Engineering and Mechanics, Bethlehem, United States
2   Musculoskeletal Research Unit, Zurich, Switzerland
3   Center for Applied Biotechnology and Molecular Medicine (CABMM), Zurich, Switzerland

Mechanoregulatory models have been used to predict the progression of diaphyseal bone fracture healing for more than two decades. These models can successfully predict the classical sigmoid (S-shaped) recovery curve of bone rigidity over the healing period, but with some notable limitations. In most models, callus development proceeds within a pre-defined domain that both restricts and directs healing, leading to some non-physiologic healing patterns. These undesirable model behaviors can include nucleation of bone healing at the domain extents due to strain artifacts, flooding of the healing domain with bone or cartilage, and unrealistic predictions of nonunion due to extreme sensitivity to distortional strains. Solving these problems will require close collaboration between computationalists and veterinary or clinical teams to identify model shortcomings and strategies for model development. Possible new approaches could include innovations in model geometry definition, new constraint sets in the mechanoregulatory models themselves, and above all, creative approaches to model tuning and validation that leverage in vivo data. In this talk, we will present a few short case studies of our experiences developing mechanoregulatory models and new techniques for 3D imaging data extraction that are directly relevant to the persistent need for translation-ready simulation tools that can predict fracture healing.1–3 For example, in one study we examined the spatial patterning of tissue formation from histology in plated ovine tibial osteotomies. Using this data, we developed a set of geometric constraint equations for the localization of callus near the fracture line (see Figure). This approach was successful in mitigating domain-dependency in the computational models, but the results also introduce new questions about which physiologic features may be missing from the models, such as coupled remodeling during early-stage healing or the biological diversity in healing responses in vivo. This talk will focus on recent successes, new opportunities, and future challenges in the field of numerical modeling of bone healing and ask the big-picture question, "Why are these models not yet in widespread preclinical or clinical translation and what can we do to move them forward?"

Baseline Model   Improved Mechanoregulation Model with Proximity Control
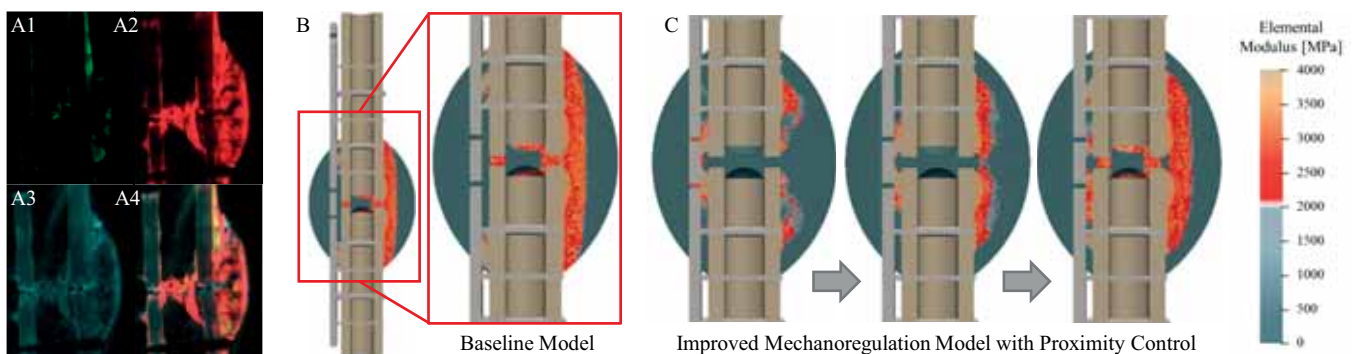
Figure caption: a) Intravital fluorescence images show calcium deposition kinetics of ovine fracture callus at 3 weeks (calcein green, A1), 6 weeks (xylenol orange, A2), 9 weeks (oxytetracycline, A3), and merged (A4). b) Without proximity control, the baseline healing simulation was domain dependent with a non-physiologic callus shape. c) With fracture-line proximity control, the simulation produced a far-cortical bridging pattern like that seen in sheep in vivo.

References:
1.   Ren T, Dailey HL. Mechanoregulation Modeling of Bone Healing in Realistic Fracture Geometries. Biomech Model Mechanobiol. 2020;19(6):2307-2322. PMID: 32524288.
2.   Schwarzenberg P, Ren T, Klein K, Rechenberg B Von, Darwiche S, Dailey HL. Domain-independent simulation of physiologically relevant callus shape in mechanoregulated models of fracture healing. J Biomech. 2021;118:110300.
3.   Ren T, Schwarzenberg P, Klein K, von Rechenberg B, Darwiche S, Dailey H. Nondestructive Image-Based Quantification of Structural Remodeling at the Bone-Callus Interface in Sheep. In: Orthopaedic Research Society (ORS) Annual Meeting. Virtual; 2021.

E1.2
Modeles as microscopes: observations, provocations and opportunities for bone healing simulations

Cameron J. Wilson[1]

1   Cameron Wilson Research Services, Australia

Simulations of fracture healing mechanobiology are increasingly sophisticated, but validation data remain scarce. This limits our ability to produce the "plug and play" predictions sought by clinicians, but computational models are nonetheless valuable tools to explore complex phenomena. Here, I focus on the qualitative patterns the simulations produce over time, and what they might tell us.

In these case studies, finite element models of simple bone fracture geometries were implemented in ABAQUS, with healing algorithms and elastic material properties derived from the University of Ulm models [1]. Snapshots from multiple simulations are presented, emphasising principal strains and tissue distributions. My observations suggest five areas for investigation: (1) validation of individual processes, (2) stress concentrations and artefacts, (3) stability vs callus morphology, (4) interfacial mechanics and (5) growth processes and anisotropy.

Examining early model iterations reveals how unphysiological tissue changes (e.g. widespread cartilage formation) [2–4] direct the course of the simulation. The effect is striking when running simulations between observed intermediate stages of healing [4]. Adding biological constraints to the mechanical rules may address such anomalies, but demands extra validation data. Discrepancies also arise from idealised geometries and interfaces. Stress concentrations depend on the initial soft tissue geometry [2]. In mechanically regulated simulations, these stress concentrations direct callus formation away from the fracture site, which is contrary to experimental observations [5] and callus as a stabilising structure. Modelling has assumed that soft and hard tissues remain attached. The fragility of granulation tissue makes this unlikely, and rupture at this interface will radically alter the local mechanical environment. Explicitly modelling soft tissue growth may mitigate these artefacts and presents a novel research direction. Rather than being a "blank canvas" in-filled by bone and cartilage, preliminary models [6] and experiments [7] suggest that "granulation tissue" can direct patterns of bone formation.

The intermediate stages of iterative simulations represent a "microscope", through which we can appraise the functioning of each component process and sensitivity to inherent assumptions. I propose that each is essential if we are to consider a model truly validated.

References:
[1]   Simon et al. (2011) Comput. Methods Biomech. Biomed. Engin.
[2]   Wilson et al. (2015) Biomech. Model. Mechanobiol.
[3]   Wilson et al. (2017) Biomech. Model. Mechanobiol.
[4]   Terrill (2016) BEB802 report, QUT.
[5]   Wilson et al. (2021) Injury.
[6]   Wilson et al. (2015) Australasian Orthopaedic Trauma Society Annual Scientific Meeting.
[7]   Paris et al. (2017) Acta Biomaterialia.

E1.3
Numerical multiscale modeling of bone mechanobiology

JM García-Aznar[1], G Nasello[1 2], S. Hervas-Raluy[1], MA Pérez[1], MJ Gómez-Benito[1]

1   University of Zaragoza, Multiscale in Mechanical and Biological Engineering, Instituto de Investigación en Ingeniería de Aragón , Zaragoza, Spain
2   KU Leuven, Biomechanics Section,, Leuven, Belgium

Mechanobiology plays a crucial role in bone response from bone morphogenesis to bone fracture healing, remodeling and regeneration [1]. This regulatory role is modulated by a complex system of multiple physical stimuli that involve mechanical loads, and other biological or biochemical factors, such as, hormones, ageing and nutrition. This complexity is not only due to the multiphysics-based signals perceived by cells, but to the hierarchical multiscale organization of the tissue [2] (see Figure 1). This fact has motivated that numerical simulation and mathematical modeling are common tools used to advance in the understanding of this bone complexity focused on bone mechanobiology [2]. It is hard to summarize the large amount of excellent research works existent in the literature to simulate multiscale bone behavior with a special emphasis in bone mechanobiology. In this work, we aim to present a particular perspective of computer-based modeling of bone mechanobiology, focusing on the effect that stimuli associated to the mechanical micro-environment induce in bone healing and remodeling, implant design and scaffold-driven bone regeneration [3].
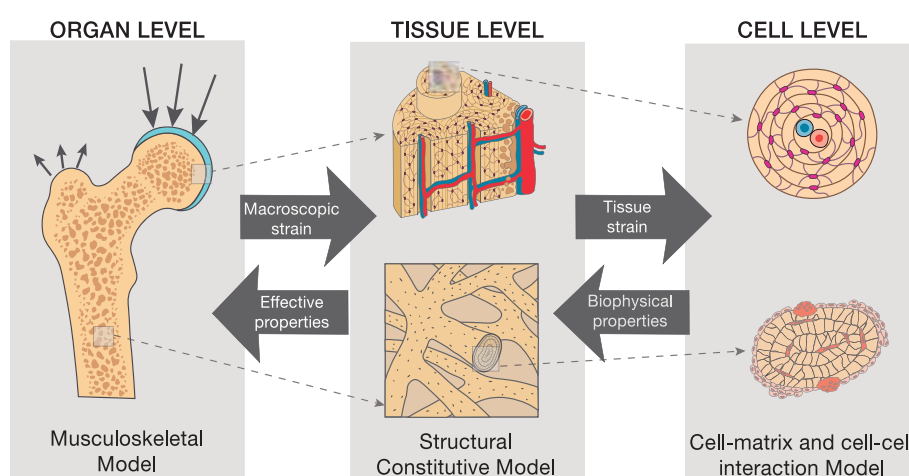
Figure 1: Numerical multiscale approach for advance simulation of bone mechanobiology (image taken with permission from [2]).

Although computer-based simulation allows the modeling of multiple conditions at different scales, their impact is certainly minor without validation. Therefore, validation is crucial for models to acquire predictive value in their performance. Different strategies are being used to develop strong validation: in-vivo image analysis [4] and in-vitro quantification [5]. A comparison of both strategies is discussed as final conclusion of this work.

References:
[1]   J. Klein-Nulend et al, Pathol. Biol. (2005), DOI: 10.1016/j.patbio.2004.12.005.
[2]   JM García-Aznar et al. (2021), Bone, DOI: 10.1016/j.bone.2021.116032.
[3]   G. Nasello et al. (2020), Bone, DOI: 10.1016/j.bone.2020.115769
[4]   AF van Tol et al (2020), PNAS, DOI: 10.1073/pnas.2011504117
[5]   G. Nasello et al. (2020), Front Bioeng Biotechnol, DOI: 10.3389/fbioe.2020.00336

E1.4
3D fracture healing simulations of metaphyseal distal radius fractures

Lucas Engelhardt[1 2], Laura Wundke[1], Frank Niemeyer[2], Anita Ignatius[2], Ulrich Simon[1]

1   Scientific Computing Centre Ulm, Ulm University, Ulm, Germany
2   Institute of Orthopaedic Research and Biomechanics Centre for Trauma Research Ulm, Ulm University, Ulm,

Currently, fracture-healing simulations are primarily applied to diaphyseal fractures. In order to simulate metaphyseal fracture healing, we extended the previously developed and tested computational model for diaphyseal fractures [1] to metaphyseal fractures [2. Up to now, the investigations were analyzed in 2D rotational symmetric geometries. Recent algorithmic enhancements enabled the possibility to simulate complex three dimensional geometries in reasonable timescales. The fracture healing model represents the homogenized local tissue composition as a mixture of the tissue types "soft tissue", "cartilage", "woven bone", "lamellar bone" and "crushed trabecular bone".

Patient-specific HR-pQCT scans are used to determine the outer geometry of the cortical shell, the compression fracture alignment and a trabecular bone concentration evident from the bone density from imaging data. As confirmed in [2] the same tissue differentiation formulations as used in previous models for diaphyseal healing [1] can be used in this case, resulting in a healing prediction course over time.

Figure 1: Patient-individual bone geometry and fractured area (blue). Articular surface (orange), where compression load is applied

Applying a constant global load of 351 N predicted a bony healing of the fracture area within the same timescale as the scans indicated. Computational runtimes of 25 min per iteration and a total time of 233 hours obtained the results, that the Ulm healing model is also well suited for the calculation of three-dimensional metaphyseal fractures. In the model, bone formation starts from the trabecular region. Small parts of the cortex get filled with osseous tissue (yellow circles). Further, some osseous tissue appears at the edges of the fracture site (green arrows).
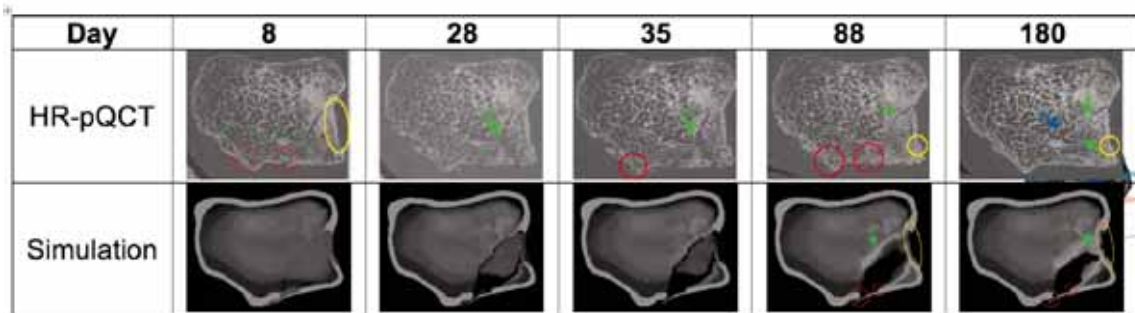
Figure 2: Healing pattern over time in comparison with in vivo data. View in cutting plane (blue)

In the simulation, intramembranous ossification is dominant for bone formation. Little cartilage formation was observed which corresponds well with other studies [3]. Dependencies for the predicted course and distribution of the tissue concentrations may include the geometry of the bones their defined fracture areas and the applied boundary conditions. Further validation and calibration of this 3D metaphyseal healing model in many clinical cases of distal radius fractures will be carried out.

References:
[1]   U. Simon et al. (2011), CMBBE
[2]   L. Engelhardt et al. (2021), MDPI Biomechanics
[3]   P. Aspenberg and O. Sandberg. (2013), Acta orthopaedica

E1.5

Integrated spatial-temporal model for the prediction of interplay between biomechanics and cell kinetics in fibrotic wall formation

Jieling Zhao[1 2], Seddik Hammad[3], Mathieu de Langlard[1], Steven Dooley[3], Dirk Drasdo[1 2]

1   Inria de Saclay, SIMBIOTX
2   IfADo, Dortmund, Germany
3   UMM Heidelberg University, Medicine II, Germany

Liver fibrosis is characterized by the accumulation of extracellular matrix (ECM) caused by repeated liver injuries. Upon different types of injury, there are distinct patterns of fibrosis developed, such as collagen septa connecting two pericentral areas due to toxic injury or septa connecting two portal compartments due to biliary injury.

Since liver fibrosis is a complex process and difficult to capture for biological models, computational models may shed light on exploring the mechanisms behind particular pattern formation. In this work, we present a novel computational liver model that permits to assess the potential role of biomechanics in the formation of fibrotic walls. Our model incorporates the collagen fiber mechanics. For the first time, it studies the orchestration of cell types during fibrosis development and the interaction of cell populations with the collagen network in liver lobules. Our model results are quantitatively confronted experimental findings.

The determination of the pattern-characterizing parameters in this study e.g. the density of hepatic stellate cells (HSC) and macrophages were obtained through image analysis of 2D bright-field and 3D confocal images from mouse experiments. Together with a model of collagen networks, these non-parenchymal cell types and their intercellular signaling were integrated as new elements into a previous computational model of basic liver micro-architecture that includes the hepatocytes (the main parenchymal liver cell), hepatic sinusoids (liver capillaries), the central vein (CV) and the portal vein (PV). The new model is applied to test possible mechanism of formation of fibrotic wall during liver fibrosis in space and time, starting from healthy, then acutely and chronically perturbed livers under consideration of the biomechanical properties of cells and the collagen matrix.

Using this strategy, we proposed a potential scenario distinguishing regeneration after acute toxic insult and repeated toxic exposure leading to formation of characteristic fibrotic walls: 1) The spatial pattern of the cytochrom 450-enzyme CYP2E1 expression indicated the location for the deposition of fibrotic collagens. Briefly, the spatial-temporal pattern of certain signaling molecules (e.g., DAMPs) are governed by the spatial distribution of CYP2E1-positive hepatocyte and this leads to attraction of activated, hence collagen producing, HSCs, and degrading macrophages; 2) The proliferating hepatocytes surrounding the CYP2E1 region compress the fibrotic collagen network into "walls"-like shape. Model simulations of specific perturbations permit its validation.

Figure caption: All components of our model. White: collagen fibres; Red: sinusoids; Green: quiescent hepatocytes; Blue: dividing hepatocytes; Yellow: necrotic hepatocytes; Cyan: HSCs; Dark blue: macrophages.

References:
Jieling Zhaoa,b‡, Seddik Hammadc‡, Mathieu de Langlarda, Steven Dooleyc*, and Dirk Drasdoa,b*
aInria, Saclay; bIfADo, Dortmund; cUMM, Heidelberg University, Mannheim
‡These authors contribute equally to this work
*Corresponding authors: steven.dooley@medma.uni-heidelberg.de & dirk.drasdo@inria.fr
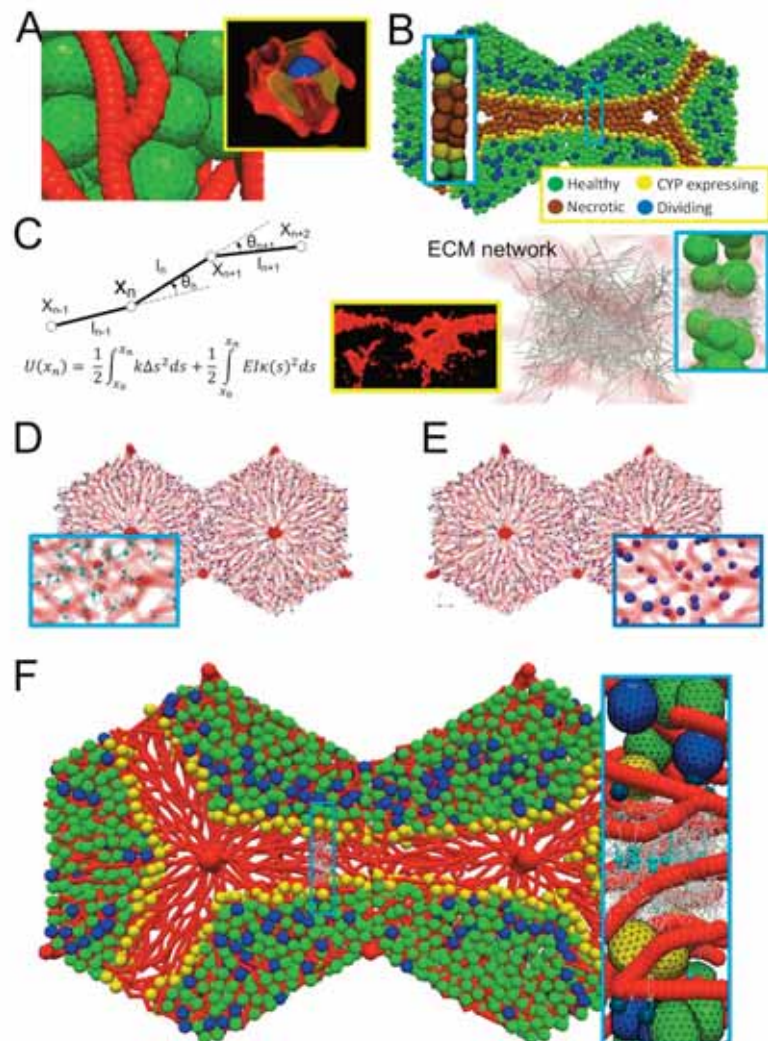
E2.1
Optimization of microCT and contrast-enhanced microCT for cardiovascular applications

Lisa Leyssens[1 2], *Maïté Pétré*[1 2 3], *Greet Kerckhofs*[1 2 4 5]

1   UCLouvain - Institute of Mechanics, Materials and Civil Engineering , Mechatronic, Electrical Energy, and Dynamic Systems, Ottignies-Louvain-la-Neuve, Belgium

2   UCLouvain, Institute of Experimental and Clinical Research, MORF, Woluwe-Saint-Lambert, Belgium

3   KU Leuven, Department of Mechanical Engineering - BioMechanics, Leuven, Belgium

4   KU Leuven, Dept. Materials Engineering, Leuven, Belgium

5   KU Leuven, Prometheus, Division of Skeletal Tissue Engineering, Leuven, Belgium

Atherosclerosis is still a leading cause of death worldwide. To better understand and treat this disease, it is important to evaluate the changes in blood vessel wall microstructure during disease development and to link these microstructural changes to changes in mechanical properties. Microfocus X-ray computed tomography (microCT) combined with contrast-enhancing staining agents (CESAs), a technique referred to as contrast-enhanced microCT (CE-CT), allows non-invasive assessment of the 3D microstructure of soft tissues. Monolacunary and Hafnium-substituted Wells-Dawson polyoxometalate (Mono-WD and Hf-WD POM respectively) have shown their potential for non-destructive staining of kidney and soft skeletal tissues [1]. The aim of this study was to show the potential of CE-CT for high-resolution analysis of the different vessel wall layers and their composition.

First, we have shown with planar biaxial testing that Mono-WD and Hf-WD POM have a negligible effect on the mechanical properties of the tissue. Then, these CESAs were evaluated for their staining potential of the porcine aorta. It was concluded that Hf-WD POM stains with much higher intensity while Mono-WD POM stains less bright and more homogeneously but diffuses much faster than Hf-WD POM (Fig. 1, A-B). The optimized staining parameters were then applied to other types of porcine blood vessels (elastic artery, muscular artery, and vein) and allowed to observe the differences in the 3D microstructure of different tissue constituents (i.e. elastin and collagen) of the vessel wall in these tissues. We also showed important species-related (porcine, rat, human) differences in the vessel wall microstructure of the aorta (Fig. 1, C-D), which could have an important impact on their functional behavior, and hence this is important information when running animal experiments to evaluate disease treatments. From the data mentioned above, 3D morphometrical parameters have been computed such as elastin volume fraction and elastic fiber waviness and separation, and this without altering the native structure of the tissue. Finally, healthy and atherosclerotic human femoral arteries were compared. Plaques and onsets of calcifications could be identified and parameters such as calcification volume fraction could be quantified. The novelty of this study lies in the high-detailed comparison of the microstructure of different types of blood vessels (healthy and diseased) in different species, and this, in a non-destructive 3D manner.
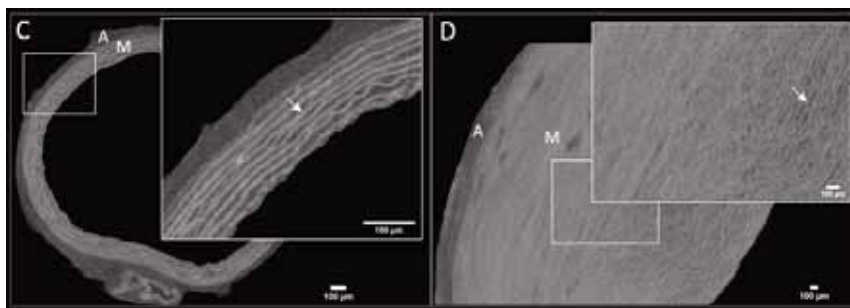
Figure caption: Fig. 1: Normalized gray value in function of time for different locations (x) inside the tissue and fitted with an exponential decay curve for (A) Hf-WD POM and (B) Mono-WD POM. CE-CT-based images of the rat aorta (C) and the porcine aorta (D) stained with Hf-WD POM. A=adventitia, M=media, arrow=elastic lamellae.

References:
[1]   de Bournonville et al, Acta Biomater., 105:253-62, 2020
[2]   Balint et al, PloS One, 11(4):e0153552, 2016

E2.2
4D X-ray microfocus computed tomography for cardiovascular application

Alice Coirbay[1 2], *Grzegorz Pyka*[1 2], *Greet Kerckhofs*[1 2 3 4], *Valérie Lacroix*[2 5]

1   Institute of Mechanics, Materials, and Civil Engineering, UCLouvain, Louvain-la-Neuve, Belgium
2   Institute of Experimental and Clinical Research, UCLouvain, Brussels, Belgium
3   Dept. Materials Science and Engineering, KU Leuven, Leuven, Belgium
4   Prometheus, Division of Skeletal Tissue Engineering, KU Leuven, Leuven, Belgium
5   Faculty of Medicine and Dentistry, UCLouvain, Brussels, Belgium

A typical treatment of atherosclerosis, a frequent cardiovascular disease, involves the placement of a bypass made of synthetic grafts, such as Dacron or Gore-Tex. However, the still existing mismatch in the global but also local mechanical properties between the native tissue and the graft could result in complications [1]. Therefore, detailed analysis of synthetic graft materials, compared to native tissue, is essential to improve vascular graft properties.

In this study, we applied 4D X-ray microfocus computed tomography (4D XCT) to a Dacron graft. In-situ experiments were performed using a Phoenix Nanotom M XCT system combined with a Deben CT5000 mechanical loading stage. 3D image data was generated at consecutive tensile deformation steps (both in the longitudinal and circumferential direction of the graft) with a displacement of 0.2 mm. Avizo software was used to calculate the local strain maps based on conventional Digital Volume Correlation (DVC). Three incremental DVC methods were compared: the "fixed reference image" conventional DVC, using the same fixed reference image volume for all strain steps, the "sequential" incremental DVC, updating the reference volume at each step, and the "preconditioned" incremental DVC, updating the reference volume once severe decorrelation occurs.

The longitudinal and circumferential stiffness of 5.75 MPa and 13.65 MPa respectively, highlighted an anisotropy in Dacron mechanical properties, already identified in literature [2]. From the three incremental DVC methods, the "fixed reference image" conventional DVC enabled a reliable visualization of the strain maps evolution until a maximal displacement of 0.6 mm. For this elongation, the strains in the longitudinal direction were ranging from -0.8% to 12%, with the highest tensile strain mainly located at the front and backwards folds of the graft, highlighting the potential failure location (Fig.1A). In the circumferential direction, the maximal tensile strains (9.04%) were mostly situated in between the longitudinally warp knitted yarns (Fig.1B).

This preliminary work enabled to highlight the intrinsic mechanical properties of Dacron, and to identify the region of highest deformation and possible failure in its microstructure. Furthermore, it paved the way to ongoing similar experiments on native arterial tissue using 4D contrast-enhanced XCT [3]. A high spatial resolution and a non-destructive contrast enhancing staining agent (CESA) already arose as important for sufficient image quality and for not altering the mechanical properties of the tissue. Overcoming these challenges will enable to compare the local mechanical behavior between native tissue and synthetic grafts, information that is still lacking nowadays.
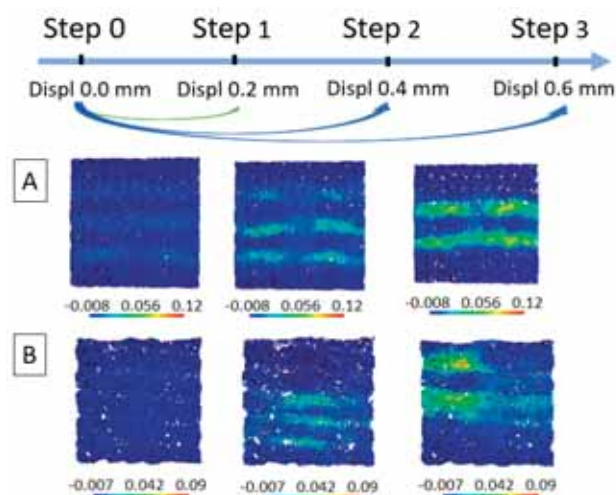
Figure caption: Figure 1: Visualization of Dacron volumetric strains map loaded in the (A) longitudinal direction and (B) circumferential direction.

References:
1.   J. Chlupác et al., Physiological research, 2009.
2.   D. Tremblay et al., The Annals of thoracic surgery, 2009.
3.   L. Leyssens et al., International Journal of Molecular Sciences, 2021.

E2.3

High resolution microfocus computed tomography and POM-based contrast-enhanced computed tomography applied to the heart and its constituents

Camille Pestiaux[1 2], Greet Kerckhofs[1 2 3 4]

1   UCLouvain, iMMC, Louvain-la-Neuve, Belgium
2   UCLouvain, IREC, Woluwe-Saint-Lambert, Belgium
3   KU Leuven, Department of Materials Engineering, Leuven, Belgium
4   KU Leuven, Prometheus, Division of Skeletal Tissue Engineering, Leuven, Belgium

The heart is a highly complex and heterogeneous organ. It is composed of a dense muscle network, cavities, vessels, cells and extracellular matrix including collagen and elastin. The proper organization of the muscle fibers in the myocardium prescribes the heart contraction rate and the spatial organization of the collagen and elastin in the heart valves allows them to ensure the one-way flow of the blood. They are some microstructural examples that guarantee the proper functioning of the heart. An accurate structural analysis of the heart valves, the connection of the chambers, the organization of the muscle fibers and the main vessels will provide a better knowledge of the heart and the effect of diseases on its proper functioning. By consequent, a 3D and non-destructive imaging protocol of the heart and its constituents is crucial to visualize their native microstructure, while not preventing further analysis. To this end, ex vivo microfocus computed tomography (microCT) is already known as a powerful technique to image biological tissues and especially mineralized tissues [1]. The detailed visualization of soft tissues is achieved by the addition of a contrast-enhancing staining agent (CESA), further referred to as contrast-enhanced computed tomography (CE-CT) [2]. Currently, Lugol's iodine is the most popular CESA to image the heart and its constituents. Nevertheless, it is known to induce substantial tissue shrinkage. CE-CT should be optimized in order to provide accurate morphometric measurements of heart constituents such as heart valves on which it has never been applied.

The goal of this study was three-fold. First, we applied high resolution ex vivo microCT on explanted human stenotic aortic valves to better characterize the calcifications within the soft tissues. This technique provided detailed information about their volume, density and spatial distribution, and we were able to distinguish different densities of calcification. Linking this structural characterization with the in vivo performance of the heart will help to better understand the pathology. Second, we demonstrated the potential of Hafnium-substituted Wells-Dawson polyoxometalate (Hf-WD POM), an emerging CESA, to perform CE-CT on the whole heart. We were able to render the complexity of the heart with a close respect to its native anatomy and we compared this imaging protocol with Lugol's iodine staining. Finally, we evaluated the potential of Hf-WD POM-based CE-CT to provide a quantitative characterization of heart valves.
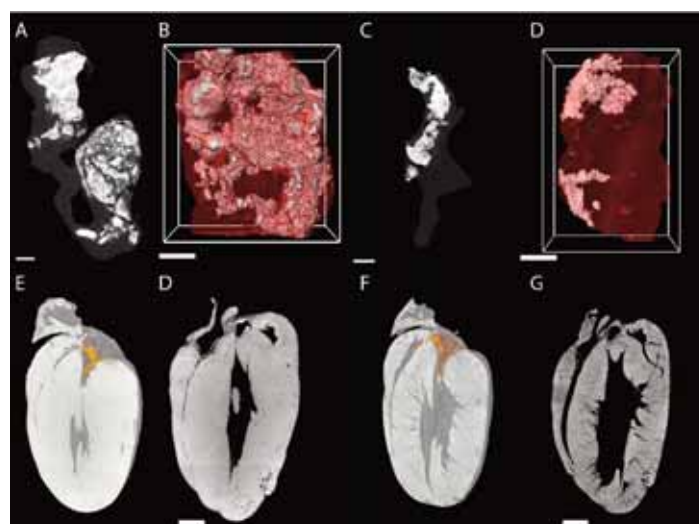
Figure caption: A-D: MicroCT images of human aortic valves explanted for replacement; E-G: CE-CT images of a mouse heart successively stained by Hf-WD POM and Lugol's iodine. Scale bars = 1 mm. Adapted from [3].

References:
1. Rawson et al., BMC Biol, 18:21, 2020 ;
2. de Bournonville et al., Contrast Media Mol Imaging, 2019 ;
3. Pestiaux et al., Int. J. Mol. Sci., 22(6), 2021

E2.5

Development of an automated mass-customisation pipeline for knee replacement surgery using bi-planar X-rays: a critical evaluation

Thomas Burge[1], *Connor Myant*[1]

1   *Imperial College London, Dyson School of Design Engineering, London, United Kingdom*

For standard 'off-the-shelf' knee replacement procedures surgeons use X-ray images to aid implant selection from a limited number of models and sizes. This can lead to complications and the need for implant revision due to poor implant fit. 'Customised' or 'personalised' solutions have been shown to improve results but require increased preoperative assessment (CT or MRI), longer lead times and higher costs. In addition, no commercially available method is believed to be completely automated, requiring some level of manual design and/or image processing. It is viewed that the combination of these factors has prevented widespread adoption of patient-specific implants.

To attain the benefits of patient-specific implants, whilst avoiding the limitations of currently available solutions, a fully automated pipeline, capable of developing personalised implant designs for fabrication via additive manufacturing from calibrated X-rays, has been developed. The novel pipeline uses several AI based techniques including convolutional neural networks to process bi-planar X-ray images, pre-trained point depth and statistical shape models to create a 3D prediction of the subject's anatomy, as well as CAD application programming interface scripts to generate different personalised implant designs. It is not believed that a comparable process has been outlined in the literature to date.

The various modules of the automated pipeline were trained using 2D and 3D image data from the 'Korea Institute of Science and Technology Information' and the 'Osteoarthritis Initiative'. Independent subjects were then selected to test the accuracy of the anatomical reconstruction of the pipeline across different genders, ages, racial groups and arthritis severities. The robustness of the pipeline was further evaluated by studying the effect of parameters such as input X-ray alignment to characterise its limitations.

The proposed presentation will detail the development, training and testing of the novel pipeline and demonstrate that automatic personalisation of knee replacement implants is feasible from 2D medical imaging.

References:
The authors are currently awaiting feedback on their paper titled: 'Development of an Automated Mass-Customisation Pipeline for Knee Replacement Surgery Using Bi-Planar X-rays' which has been submitted to the ASME Journal of Mechanical Design (special issue on 'AI and Engineering Design').

E3.1
Simultaneous mechanical and microstructural analysis of brain tissue

Nina Reiter[1], *Friedrich Paulsen*[2 3], *Silvia Budday*[1]

1   Friedrich-Alexander-University Erlangen-Nürnberg, Institute of Applied Mechanics, Erlangen, Germany
2   Friedrich-Alexander-University Erlangen-Nürnberg, Institute of Functional and Clinical Anatomy, Erlangen, Germany
3   Sechenov University, Department of Operative Surgery and Topographic Anatomy, Moscow, Russian Federation

Mechanical aspects play an important role in brain development, function and disease. Computational models based on nonlinear continuum mechanics can valuably advance our understanding of brain mechanics and can serve as a tool to assist diagnosis and treatment of neurological disorders. Currently, mainly phenomenological material models are used to predict the behavior of brain tissue through numerical simulations. The model parameters often lack physical interpretation and only provide adequate estimates for brain regions that have a similar microstructure as the ones that were used for calibration. Recent efforts towards advanced, microstructurally motivated material models include cell-density dependent material parameters to capture the regional heterogeneity of brain tissue [1]. However, further improvements of such models require new insights into the microstructural mechanisms occurring during mechanical loading of brain tissue. To date, these mechanisms remain poorly understood: it is still unclear how forces are transferred to microstructural elements and how those elements contribute to the characteristic viscoelastic tissue response.

This study examines the relationship between the mechanical response and microstructural rearrangements in porcine brain tissue. First, we visualize cell bodies and nuclei in fresh tissue samples using methylene blue. Subsequently, we subject the stained specimens to cyclic loading and unloading as well as relaxation experiments and simultaneously track microstructural components through a microscope.

On the microscopic level, we observe that the cells move with the network of intercellular connections and extracellular matrix as it is deformed under loading. Interestingly, relative movements between neighboring cells are minor compared to the overall cell displacement; the cell bodies hardly experience any deformation. Our experiments distinctly allow us to track viscoelastic effects, as the cells keep moving during the holding period of stress relaxation tests. Based on these findings, we determine a microstructure-based time constant that is related to the viscoelasticity of the network of intercellular connections and extracellular matrix and develop a microstructure-informed viscoelastic constitutive model for brain tissue [2]. Our analyses show how rearrangements on the cellular scale translate into viscoelastic effects on the tissue scale and indicate that the network of intercellular connections and extracellular matrix as well as its interactions with the cells and fluid phase seem to have a significant effect on the overall tissue mechanics.

References:
[1]   Budday, S., Sarem, M., Starck, L., Sommer, G., Pfefferle, J., Phunchago, N., Kuhl, E., Paulsen, F., Steinmann, P., Shastri, V., Holzapfel, G.: Towards microstructure-informed material models for human brain tissue. Acta Biomater. 104, 53–65 (2020).
[2]   Reiter, N., Roy, B., Paulsen, F., Budday, S.: Insights into the Microstructural Origin of Brain Viscoelasticity. J Elast (2021).

E3.2

Exploring the role of the outer subventricular zone during cortical folding in the developing brain through a physics-based multifield model.

Mohammad Saeed Zarzor[1], Stefan Kaessmair[1], Paul Steinmann[1], Ingmar Blümcke[2], Silvia Budday[1]

1 LTM - Lehrstuhl für Technische Mechanik, Erlangen, Germany
2 Neuropathologie, Erlangen, Germany

The human brain has an extremely complex structure both on the microscopic and macroscopic scale. The strong relation between brain structure and its function has attracted the attention of researchers from different fields with the goal to understand the mechanisms underlying normal and abnormal brain cortical folding. In the past few decades, more and more evidence has emphasized the role of mechanical forces which seem to control cortical folding. However, the link between the cellular processes on the microscale and the mechanical forces on the macroscale still remains insufficiently understood. On the microscale, the radial unit hypothesis supposes that the radial glial cell fibers organize the migration process. During migration, cells move along radial glial cell fibers from the inner layers of our brain around the ventricles, where progenitor cells divide into radial glial cells, intermediate progenitor cells, and neurons, toward the outer surface to form a six-layered cortex. Importantly, the intermediate progenitor cells accumulate above the ventricular zone and form a new layer called subventricular zone (SVZ). Recent findings suggest that the outer layer of the subventricular zone (OSVZ) contributes significantly to the size and complexity of the human cortex [1], but the underlying mechanisms remain largely elusive. It is known that the intermediate progenitor cells divide to produce radial glial-like cells called outer radial glial cells (ORGCs). These cells generate additional scaffolds for cellular migration around gestational week 17 [1]. To capture the effects of the OSVZ and ORGCs on the formation of cortical folds, we establish a multifield computational model. To model the coupling between cellular processes including cell division and migration on the cell scale with cortical folding on the organ scale, we combine an advection-diffusion model with the theory of finite growth [2]. The cell density is introduced as additional field, controlling isotropic growth of the subcortical layers and the circumferential expansion of the cortical layer. Our work emphasizes the role of the OSVZ during the formation of normal cortical folds. We further highlight how disrupted OSVZ formation leads to malformations of cortical development. We demonstrate that the reduced division rate of ORGCs may cause a thicker cortex resulting in the absence of normal folds in patients with lissencephaly. The presented framework could eventually help diagnose and treat neuronal disorders arising from disruptions in cellular development.

References:
[1] Hansen, D. V., Lui, J. H., Parker, P. R., & Kriegstein, A. R. (2010). Neurogenic radial glia in the outer subventricular zone of human neocortex. Nature, 464(7288), 554-561.
[2] de Rooij, R., & Kuhl, E. (2018). A physical multifield model predicts the development of volume and structure in the human brain. Journal of the Mechanics and Physics of Solids, 112, 563-576.

E3.3
Nonlocal wrinkling instabilities in bilayered systems using peridynamics

Marie Laurien[1], Ali Javili[2], Silvia Budday[1], Paul Steinmann[1]

1   Institute of Applied Mechanics, University of Erlangen-Nuremberg, Erlangen, Germany
2   Department of Mechanical Engineering, Bilkent University, Ankara, Turkey

The human brain is a highly wrinkled organ whose complex folding pattern is evidentially linked to not only intelligence but also neurological disorders, including autism, epilepsy and schizophrenia. The formation of surface wrinkles results from differential growth of the gray matter on top of the white matter, which can be modeled as a bilayer consisting of a slightly stiffer film bonded to an elastic substrate. Constrained film growth leads to residual stresses in the film which initiate buckling into a sinusoidal wave pattern.

During the past decades, the wrinkling of bilayers has been analyzed at length through local models based on classical continuum mechanics. However, the influence of nonlocal effects remains mostly unknown. Thus, our goal is to fill this gap from a computational perspective by investigating nonlocal wrinkling instabilities in a film-substrate system. Peridynamics, a nonlocal continuum formulation, provides a tool to model nonlocal material behavior [1].

This contribution presents a numerical procedure to precisely predict the critical conditions of primary wrinkling by employing an eigenvalue analysis. We induce compression in the film by applying the film layer to a prestretched substrate and gradually releasing the prestretch, as it is customary in experiments to model film growth [2]. Our results approach the local solution when the nonlocality parameter, the horizon size, approaches zero. The nonlocal model is able to reproduce an experimentally observed influence of the boundaries on the wave pattern, while this effect is not captured in finite element simulations [3]. Our results suggest that the level of nonlocality of a material model manifests itself in quantitative differences of the main features of the wrinkling behavior, while the influence of most controlling parameters qualitatively follows the same trends as in the local theory. However, an effect of the film thickness on the critical compression is found that is not covered by local predictions.

This contribution, for the first time, shows that adding a nonlocal perspective to the analysis of wrinkling instabilities provides new insights into the nature of the phenomenon.

References:

[1]   Silling, S. A. (2000). Reformulation of elasticity theory for discontinuities and long-range forces. Journal of the Mechanics and Physics of Solids, 48(1), 175-209.
[2]   Budday, S., Andres, S., Walter, B., Steinmann, P., & Kuhl, E. (2017). Wrinkling instabilities in soft bilayered systems. Philosophical Transactions of the Royal Society A: Mathematical, Physical and Engineering Sciences, 375(2093), 20160163.
[3]   Laurien, M., Javili, A., & Steinmann, P. (2021). Nonlocal wrinkling instabilities in bilayered systems using peridynamics [Manuscript submitted for publication].

E3.4

Implementation of novel region-specific human brain material properties into state-of-the-art FE head models

Thibault Vervenne[1], Andrea Menichetti[1], Paulien Vandemaele[1], Michael Gilchrist[2], Aisling Ní Annaidh[2], David B. MacManus[2], Svein Kleiven[3], Bart Depreitere[4], Jos Vander Sloten[1], Nele Famaey[1]

1   KU Leuven, Department of Mechanical Engineering, Biomechanics Section, Leuven, Belgium
2   University College Dublin, School of Mechanical & Materials Engineering, Dublin, Ireland
3   Royal Institute of Technology (KTH), Division of Neuronic Engineering, Huddinge, Sweden
4   KU Leuven - University Hospital Gasthuisberg, Department of Neurosurgery, Leuven, Belgium

Finite element (FE) human head models are commonly used to investigate the biomechanics of head trauma. The reliability of such computational models strongly depends on the accuracy of the mechanical properties assigned to the different brain components. Those mechanical properties generally used in FE head models are either derived from animal tissue or from non-dynamic mechanical tests, not representative of head impacts. Recently, the parameters of a neo-Hookean quasi-linear viscoelastic material model were obtained for twelve specific brain regions, from dynamic microindentation tests on human tissue [1]. This study aims to implement these region-specific mechanical properties into two state-of-the-art FE head models: University College Dublin Brain Trauma Model (UCDBTM) [2] and KTH head model [3].

To assess the performance of the FE head models updated with the human brain material properties, impact experiments on cadavers are simulated [4,5]. FE-predicted relative brain displacements can then be compared with experimentally measured brain motions. The C380 cadaver head of [4] is considered, with impact tests C380-T4 and C380-T5, where reported linear and rotational accelerations are used as boundary conditions for the FE models. Regarding [5], the coronal impact case (40rad/s – 30ms) is applied, represented by a single rotational acceleration. CORrelation and Analysis (CORA) ratings are calculated for the resulting brain displacements in order to quantify the biofidelity of the models.

An overall increase in biofidelity is observed when updating the material properties into the UCDBTM. Original and updated UCDBTM ratings are closely related, mainly because similar neo-Hookean quasi-linear viscoelastic material parameters were used for the original UCDBTM brain tissues. In contrast, a general decrease in biofidelity for all experiments is observed with the KTH model. A potential reason for this decrease is the different material definition originally used for gray matter in the KTH model: a nonlinear second-order Ogden hyperelastic constitutive law combined with higher-order viscoelastic parameters. For both FE models, the CORA-ratings relative to the experimental data of [4] are higher than those relative to [5].

Future work will extend the validation process of updating brain material properties of FE head models, by (i) considering more experimental data tests from [4] and [5], and (ii) predicting brain contusions after bicycle accidents using injury thresholds. Implementing more accurate brain mechanical properties into FE head models will moreover contribute to significant advantages when identifying such thresholds.

(a) UCDBTM   (b) KTH model

Experimental test	FE model	Implemented material properties	
		Original	Updated
[4]: C380-T4	UCDBTM	6.02	6.06
	KTH model	7.06	6.58
[4]: C380-T5	UCDBTM	6.01	6.03
	KTH model	6.79	6.72
[5]: Coronal (40rad/s - 30ms)	UCDBTM	5.40	5.43
	KTH model	6.76	6.35

(c) Results
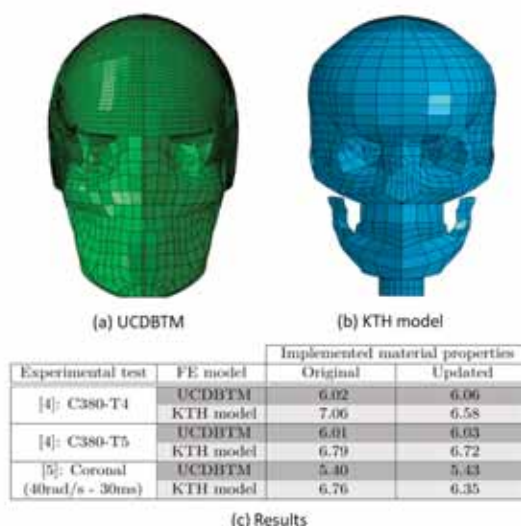
Figure caption: a) & b) FE head models; c) CORA-ratings based on the relative brain displacements. Biofidelity scales as follows: unacceptable (0.0 – 2.5), marginal (2.6 – 4.3), fair (4.4 – 6.4), good (6.5 – 8.5) and excellent (8.6 – 10.0).

References:
[1]   Menichetti et al., IntJEngSci, 155:103355, 2020;
[2]   Trotta et al., IntJMechSci., 173:105448, 2020;
[3]   Zhou et al., JBiomech., 105:109787, 2020;
[4]   Hardy et al., StappCarCrashJ, 51:17-80, 2007;
[5]   Alshareef et al., JNeurotrauma, 35:780-789, 2017.

E3.5

Uncertainty analysis of tissue-level injury metrics for cerebral contusion by means of machine learning surrogate model of the porcine brain undergoing controlled cortical impact

Andrea Menichetti[1], *Laura Bartsoen*[1], *Bart Depreitere*[2], *Jos Vander Sloten*[1], *Nele Famaey*[1]

1   KU Leuven, Biomechanics Section - Department of Mechanical Engineering, Leuven, Belgium
2   University Hospital Leuven, Department of Neurosurgery, Leuven, Belgium

Cerebral contusion (CC) is a frequent type of traumatic brain injury (TBI) found across all age groups, often associated with lifelong disability and mortality. Controlled cortical impact (CCI) is commonly performed on pigs as model of brain trauma to investigate the mechanopathology of CC. The large variability and the uncertainty associated with some CCI experimental parameters contribute to the uncertainty of the intracranial response to the impacts, which is predicted with a finite element (FE) model of the porcine brain[1]. This study investigates the effect of the experimental and modelling parameters on 4 tissue-level injury predictors of CC, i.e. maximum principal strain (MPS), maximum principal strain rate (MPSR), the product of MPS and MPSR (MPSXSR) and maximum shear strain (MSS).

The parameters considered for the uncertainty analysis include the dimension and shape of the probe, the velocity and depth of indentation, the friction and the inclination angle between the meninges and the probe, and the thickness of the meninges. We computed the 95th percentile of the peak MPS, MPSR, MPSXSR and MSS of the brain region underneath the impactor. 80 different sets of values of the 7 input parameters were used in the FE simulations of the CCI. The results were used to train a machine learning surrogate (Artificial Neural Network) of the porcine brain FE model. Monte Carlo simulations (MCS) were performed on the surrogate to evaluate the uncertainty of the injury metrics in a computationally convenient way. The cortical damage data were obtained from the magnetic resonance images and histology assessments post-CCI performed in-vivo on pigs[2]. These data were fit with logistic regression models, which yielded the CC injury risk curves for the 4 FE-derived metrics.

The uncertainty analysis (Figure) highlights that depth of indentation is the most important parameter for MPS and MSS, while MPSR and MPSXSR are most sensitive to the velocity of impact. Conversely, friction, angle of indentation and meninges thickness show very little influence on the injury predictors. All 4 metrics are statistically correlated with the probability of CC ($p<0.05$), however MPS shows the least variability to different loading conditions, suggesting that is a good candidate as tissue-level injury criterion for CC. Future work will include a larger experimental dataset for more reliable CC injury tolerances. These results provide guidelines to optimize the design of CCI tests and bring new insights to the understanding of the mechanical response of brain tissue to focal TBI.
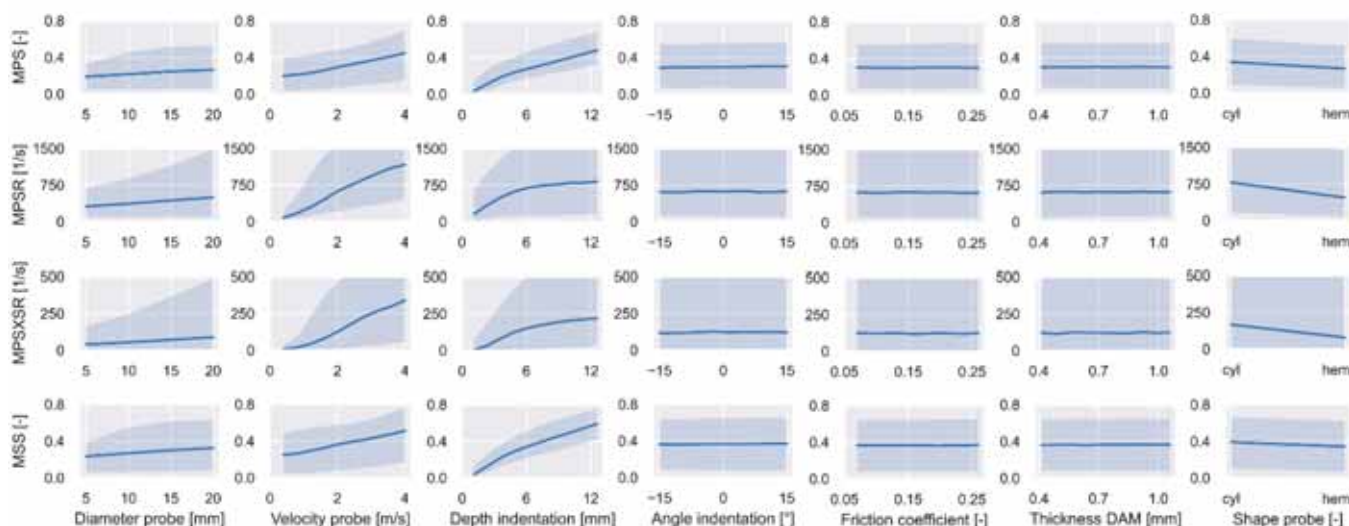
Figure caption: Variability of the CC injury predictors (MPS, MPSR, MPSXSR, MSS) with respect to the input parameters, obtained with the MCS performed on the surrogate of the FE porcine brain model.

References:
[1]   Menichetti et al., CMBBE 2019
[2]   DeKegel et al., TrafficInj.Prev., 2021(in press)

E3.6

Using in-vivo surface morphological measurements of cerebral aneurysm blebs to predict aneurysm rupture risk

Ronald Fortunato[1], *Juan Cebral*[2 3], *Anne Robertson*[1 4], *Spandan Maiti*[1 4 5]

1   University of Pittsburgh, Department of Mechanical Engineering and Materials Science, Pittsburgh, United States
2   George Mason University, Department of Bioengineering, Fairfax, United States
3   George Mason University, Department of Mechanical Engineering, Fairfax, United States
4   University of Pittsburgh, Department of Bioengineering, Pittsburgh, United States
5   University of Pittsburgh, Department of Chemical Engineering, Pittsburgh, United States

Introduction: Biomechanical failure of cerebral aneurysms, a pathology of cerebral arteries (CAs), is a catastrophic clinical event with a fatality rate of 45% [1]. Thus, physicians must balance the risk of rupture under close clinical observation and the risks associated with brain surgery [2,3]. Currently published rupture risk probability models are based on patient and aneurysm characteristics, such as aneurysm size and aspect ratio, but do not include surface morphological information [4,5]. However, currently a topic of research is evaluating statistical models that include hemodynamic and morphological parameters [6-8] as discriminating predictors of rupture. While these models investigate shape indices as they relate to the aneurysm dome, we hypothesize incorporation of bleb-specific surface morphological information can better stratify aneurysms at risk of rupture.

Methods: A total of 35 patients with three-dimensional rotational angiography or computed tomographic angiography that had a patient record of rupture status and bleb presence were included in this study. From those images' patient-specific cerebral vasculature surfaces were segmented. We calculated surface curvature using a least-squares quadratic patch method using a 3-ring vertex neighborhood to construct the patch. We used an inter-observant agreed method to identify which elements on the vasculature surface belonged to the bleb, then calculated surface curvature both Gaussian and Mean at each vertex on the bleb surface. Finally, we calculated two global surface curvature metrics: the L2-norm of the Gaussian curvature (GLN) and L2-norm of the mean curvature (MLN) of blebs. A receiver operator curve and thereby area under curve (AUC) was calculated using global metrics for each patient in either the rupture or unruptured cohorts.

Results: We found statistical significance in MLN (p=0.0003) and GLN (p=0.0007) between ruptured and unruptured cohorts. This contributed to a high AUC for the MLN (AUC=0.8013) and GLN (AUC=0.8147) in rupture and unruptured cohorts.

Conclusions: The significant difference in MLN and GLN in blebs that have records of rupture status provides a good non-invasive discriminating factor and predictor of aneurysm rupture. Additionally, we are investigating the relationship between surface morphological measurements and their effects on biomechanics of the aneurysm wall.
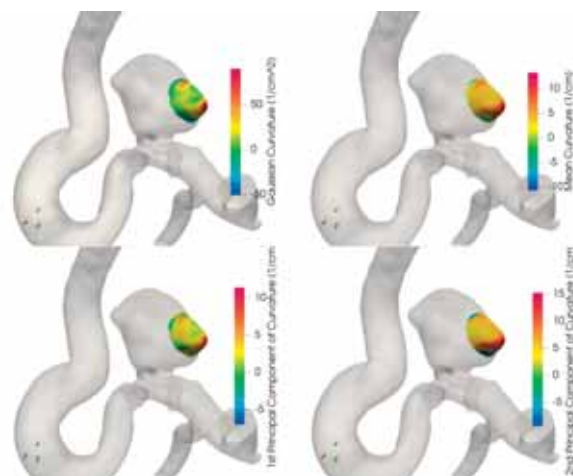
Figure 1. One representative aneurysm with bleb region only contour map of Gaussian (a), Mean (b), and principal components (c-d) of curvature

References:
[1]   Kelly et al., Stroke, 32(2):530-534, 2001
[2]   Broderick et al., Stroke 40(6):1952-7, 2009
[3]   Juvela et al., Stroke, 44(9): 2413-21, 2013
[4]   Greving et al., Lancet, 13(1): 59-66, 2014
[5]   Etminan et al., Neurology, 85(10): 881-889, 2015
[6]   Detmer et al., Acta Neurochirurgica, 160:1643-52, 2018
[7]   Detmer et al., Int J CARS, 13:1767-79 (2018)
[8]   Raghavan et al., J. Neurosurg., 102:355-362, 2005

E4.1

Creating your own TPMS-based functionally graded scaffolds for 3D-printing

Fernando Perez-Boerema[1], Mojtaba Barzegari[1], Liesbet Geris[1 2 3]

1   KU Leuven, Biomechanics Section, Leuven, Belgium
2   KU Leuven, Skeletal Biology and Engineering Research Center, Leuven, Belgium
3   University of Liège, Biomechanics Research Unit, Liège, Belgium

Triply Periodic Minimal Surface (TPMS) based lattices have started to receive more and more attention. This is in large part due to the advances in Additive Manufacturing (AM) technologies that have taken place over the last decade or two. These advances have led to unprecedented control over the materials microstructure, which in turn has made it feasible to manufacture complex structures such as those of TPMS-based lattices. Surprisingly, despite the attention TPMS-based lattices have been getting, and despite the technology to manufacture them with relative ease in different kind of materials, a simple, easy-to-use and affordable tool to create complex functionally graded TPMS-based scaffolds still seems to be lacking.

Within the field of Skeletal Tissue Engineering (STE), TPMS-based lattices have received increasing interest because unlike many other types of lattices, they can provide a biomorphic environment that is suitable for tissue growth[1]. Out of a need to create TPMS-based lattice infills for STE applications, ASLI (A Simple Lattice Infiller) was born. ASLI is a tool that gives users the ability to provide complex functionally graded infills to 3D-objects of any shape (see Figure). This is accomplished by using level-set equations to describe the infill implicitly. Functional grading is introduced by specifying the desired unit cell types, sizes and/or features on a set of discrete points throughout the volume, an input method that makes it easy and straightforward to tune the scaffolds properties to local requirements. To ensure a continuous transition between different unit cell types a filter is used in transition regions. The object, with its implicitly defined infill, is discretized using the MMG[2] or CGAL[3] library. The choice of library is left to the user. If needed, the parallel capabilities of CGAL can be used to speed up discretization. The generated structure is saved as an STL file, which is suitable for 3D-printing. If the user needs to perform Finite Element (FE) simulations, there is also the possibility to generate volume meshes suitable for FE-analyses. ASLI is published under an open-source license and will be available for download, from the starting day of the conference onwards, at www.biomech.ulg.ac.be/ASLI.

Object   +   Graded lattice infill   →   Object with its infill
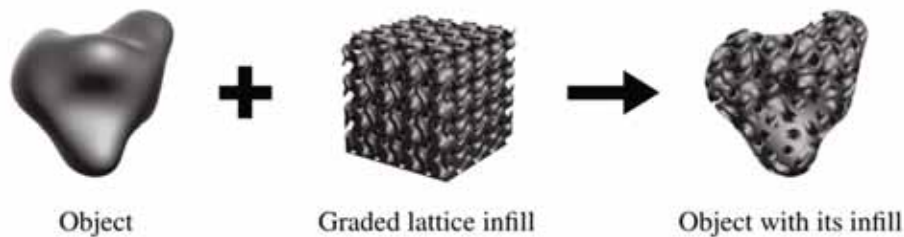
Figure caption: ASLI can be used to provide complex functionally graded infills to objects of any shape.

References:
[1]   S. Rajagopalan, et al., Medical Image Analysis, Vol. 10, No. 5, 2006.
[2]   C. Dapogny, et al., Mmg Platform v5.5.1., 2020
[3]   The CGAL Project, CGAL User and Reference Manual. CGAL Editorial Board, v5.1.1, 2020.

E4.2
Aeva: software suite for annotation and exchange of virtual anatomy

Ahmet Erdemir[1], *Andinet Enquobahrie*[2]

1   Cleveland Clinic, Department of Biomedical Engineering, United States
2   Kitware Inc., Medical Computing, United States

Representation and annotation of anatomy in a virtual form are foundational in biomedical research, particularly for physics-based simulations. Contemporary analysis requires effortless generation, modification, and exchange of virtual anatomy and effective interactive means to work with these digital assets. A unified software, however, to deal with anatomy in a highly fragmented ecosystem of scientific and clinical applications, is missing. With this abstract, we present aeva, a free and open source software suite for annotation and exchange of virtual anatomy. The aeva suite contains two applications: aevaSlicer for reconstruction of mesh-based anatomy from images and aevaCMB for harmonization of anatomical data in support of annotation and exchange of mesh-based anatomy. aevaSlicer and aevaCMB leverage built-in libraries available in Slicer and ParaView/CMB and also add support for new libraries such as Netgen to enhance functionalities available for application users. Current version (2.0.0) supports basic functionality to generate, modify, annotate, and exchange anatomy at multiple platforms (Windows, macOS, Linux). Specifically, users can load and visualize medical images, meshes, and CAD; segment organs and tissues from images; create surface representations; generate volumetric meshes; export anatomical objects in common formats; and annotate anatomical objects, i.e., selecting regions and assigning attributes. An internal data structure and storage format (based on JSON) assimilates heterogeneous representations (aevaCMB). In aevaCMB, a powerful set of interactive region selection tools assist detection of mesh regions by spatial organization or rules: by normals, proximity, freehand, etc. Using aevaCMB, one can perform freeform annotation to set attributes of mesh objects or their regions; assign mesh field data from image intensity; assign organs, tissues, spatial relations, interactions; and set point and line landmarks. A variety of image formats are supported: DICOM (aevaSlicer), NIfTI, NRRD. CAD formats can be loaded to aevaCMB (step, igs). aevaSlicer supports image segmentation, and generation and import/export of surface and volume meshes, e.g., stl, vtk. aevaCMB provides added capability for import/export of MED format and export of FEBio format (feb). Tetrahedral volumetric meshing and surface remeshing are provided. Online documentation, tutorials and video clips are available to help new users get started with the software.

Figure caption: aevaSlicer (top panel) provides various features and an interface amenable to generation of mesh-based anatomy from images. aevaCMB (bottom panel) has features for region selection and annotation of meshes plus import/export of mesh formats.

References:
Download aeva resources at https://simtk.org/projects/aeva-apps.
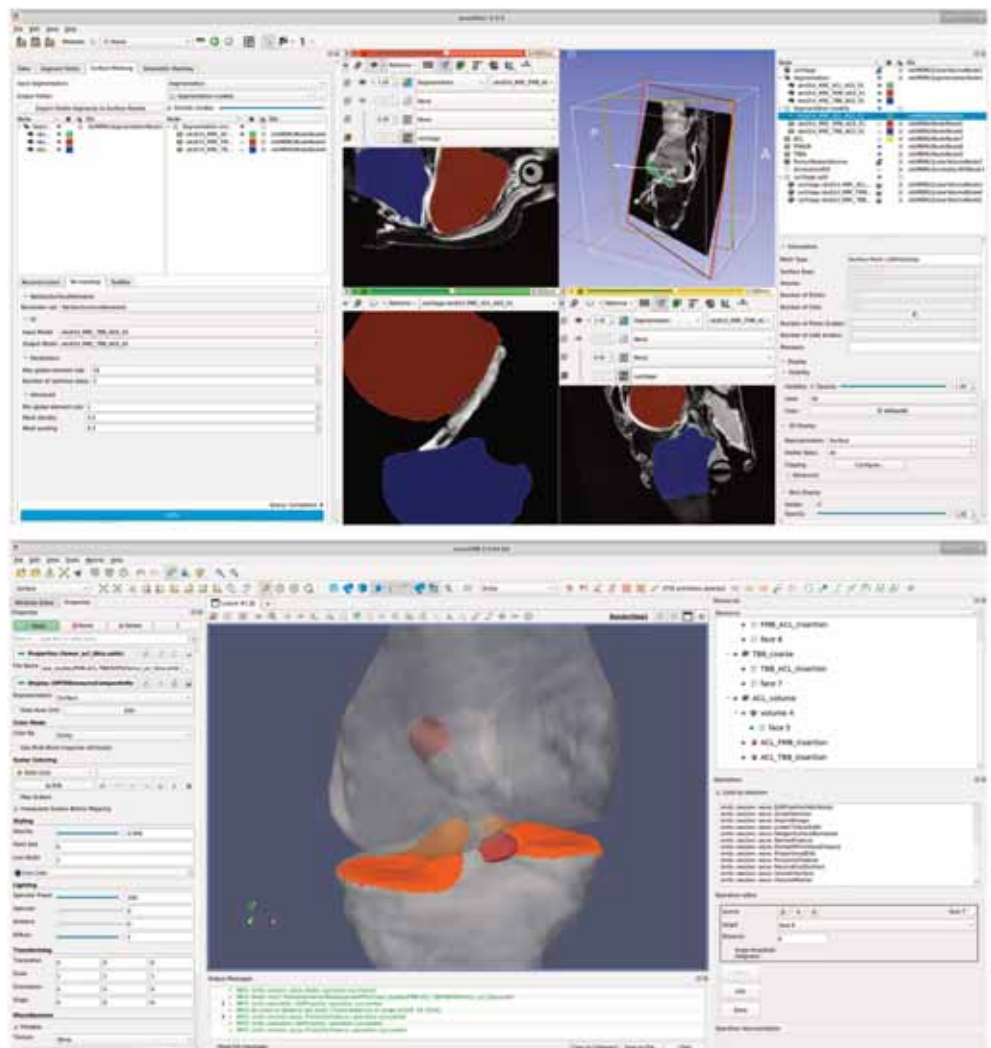
E4.3

3D visualization and automated segmentation of osteocyte cellular components using focused ion beam-scanning electron microscopy (FIB-SEM) and deep learning neural networks

Haniyeh Hemmatian[1], Imke A.K. Fiedler[1], Christine Plumeyer[1], Katharina Jähn-Rickert[1], Björn Busse[1]

1   University Medical Center Hamburg-Eppendorf, Department of Osteology and Biomechanics, Hamburg, Germany

Osteocytes, mechanosensitive bone cells, reside in fluid-filled lacunae within the mineralized bone matrix with their cell-bodies linked to the perilacunar matrix via so-called tethering elements. Sensing of and responding to mechanical stimuli occur via mechanoreceptors and rearrangement of the cytoskeleton. Stimulated osteocytes release second messengers in response to either bone tissue strain, fluid flow-induced shear stress or hydrostatic pressure. This mechanoregulation is intimately linked to the osteocyte morphology, and its immediate microenvironment[1,2], affecting the movement of interstitial fluid, subsequent shear stresses applied to osteocyte membranes, and the drag forces on the pericellular tethering elements. Thus, osteocytes experiencing a locally modified mechanical environment will react with a modified/individual mechanoresponse[3]. To fully understand the significance of morphological changes of osteocytes and the lacuno-canalicular network for mechanosensory function, it is crucial to quantify the osteocyte ultrastructural morphology, i.e. cell membrane and dimension, pericellular space, peri-lacunar and -canalicular space, and tethering elements. To this end, this study aimed to develop protocols for sample preparation and tools for 3D imaging, automated segmentation of the osteocyte cytoplasmic organelles and its lacuno-canalicular network using FIB-SEM and deep learning convolutional neural networks (CNNs). Murine femora were fixed in 3%-glutaraldehyde and 4%-formaldehyde and decalcified in 10%-EDTA. Post-fixation with osmium tetroxide, ferrocyanide and thiocarbohydrazide was followed by embedding in epon resin. Using FIB-SEM, a volume of $20 \times 20 \times 15\mu m$ was milled using a focused gallium ion beam at 30 kV acceleration voltage and 1.5 nA beam current with a slice thickness of 16 nm and imaged at 2 kV in both secondary and backscattered electron modes with a pixel size of 8 nm. After serial image acquisition, osteocyte cellular components were automatically segmented using CNNs (Fig 1). A U-NET architecture was trained to enable visual discrimination between phases based on shape information despite identical gray values. Thus, by developing special staining protocols and using FIB-SEM 3D imaging and deep learning techniques, we were able to (i) visualize the osteocyte lacunao-canalicular network and its cytoplasmic organelles, (ii) decompose it into cell body and its dendrites, nucleus, mitochondria, reticulum, and tethering elements (Fig 1C) as well as collagen fibrils in perilacunar matrix (Fig 1D). We conclude that FIB-SEM, employing a special block-staining protocol and deep learning neural networks, is a promising technique to quantify the 3D characteristics of osteocyte cellular components to enhance our understanding of osteocyte mechanosensory function.
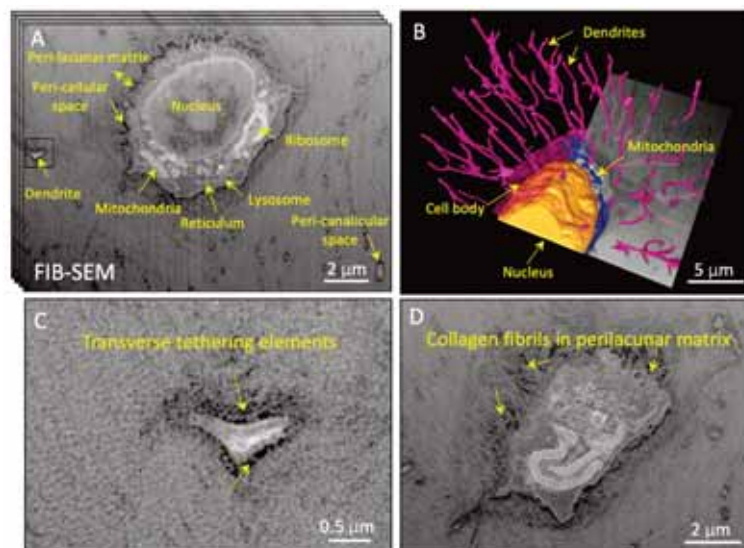
Fig. 1. (A)FIB-SEM imaging of the osteocyte ultracellular components. (B)3D reconstruction of a mouse osteocyte and its dendrites. (C)Visualization of transvers tethering elements. (D)Visualization of collagen fibrils in peri-lacunar matrix.

References:
1.   Hemmatian et al.,2018. 2.Bacabac, et al.,2008. 3.Van Tol et al.,2020.

E4.4

Development of machine learning tool for segmentation and parameter extraction in cardiac left ventricle ultrasound images of patients with cardiomyopathy

Tijana Šušteršič[1 2], *Andjela Blagojević*[1 2], *Stefan Simović*[2 3], *Lazar Velicki*[4 5], *Nenad Filipovic*[1 2]

1   Faculty of Engineering, University of Kragujevac, Kragujevac, Serbia
2   Bioengineering Research and Development Center (BioIRC) , Kragujevac, Serbia
3   Faculty of Medical Sciences, University of Kragujevac, Clinic for Cardiology, Kragujevac, Serbia
4   Faculty of Medicine, University of Novi Sad, Novi Sad, Serbia
5   Institute of Cardiovascular Diseases in Sremska Kamenica, Sremska Kamenica, Serbia

This abstract presents development of an automatic diagnostic tool based on machine learning that analyses cardiac ultrasound images of patients with cardiomyopathy in several views (4 chamber apical, 2 chamber apical and M mode view). This process is generally done manually, where a cardiologist manually extracts a region of interest (ROI), which is a time-consuming and error-prone task [1]. The main aim of the developed tool is to perform automatic left ventricle (LV) segmentation and to extract relevant parameters in order to estimate the severeness of cardiomyopathy in patients. Dataset included 1809 images with apical view and 53 images with M view from real patients collected at three Clinical Centres in UK and Serbia. Separate methodologies have been implemented for analysing apical and M mode view, including U-net for segmentation, after which parameters such as left ventricular length (LVL), internal dimension (LVID), posterior wall thickness (LVPW) and interventricular septum thickness (IVS) are calculated, both in systole and diastole (Fig. 1). The tool has also been implemented on the platform with a user-friendly interface, which allows these two modules to be used either separately or combined. In order to validate the model and compare the results between gold standard and developed methodology, two cardiology specialists have independently manually annotated LV and measured relevant parameters. The results show that the model achieves dice coefficient of 92.091% for segmentation and average root mean square error (RMSE) of 0.3052cm for parameter extraction in apical view images and average RMSE of 1.3548cm for parameter extraction in M mode view. Fully automatic detection of cardiomyopathy in cardiac LV ultrasound images can help clinicians in supporting diagnostic decision making and prescribing adequate therapy.
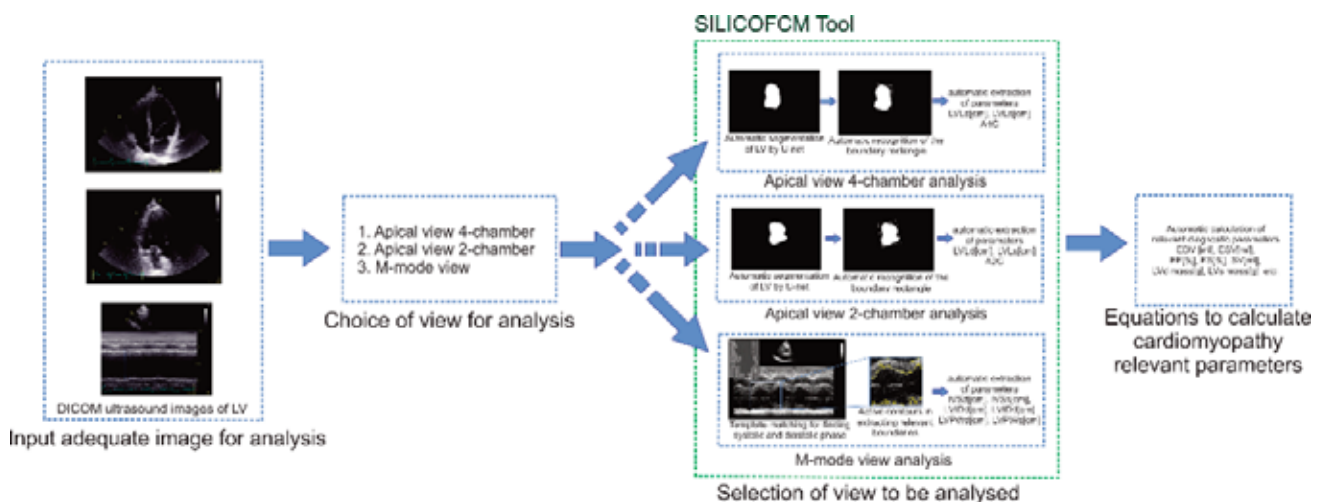
Fig. 1. Workflow of the proposed methodology

References:
[1]   G. Carneiro, J. Nascimento and A. Freitas, "The segmentation of the left ventricle of the heart from ultrasound data using deep learning architectures and derivative-based search methods," IEEE Transactions on Image Processing, vol. 21, no. 3, pp. 968-982, 2011.

E4.5

Thermography as a nonionizing quantitative tool for diagnosing periapical inflammatory lesions

Mohamed Aboushady[1], *Wael Talaat*[2], *Christoph Bourauel*[3], *Sameh Talaat*[4]

1   Future University in Egypt, Endodontics, Cairo, Egypt
2   Sharjah University, United Arab Emirates
3   Uniklinikum Bonn, Germany
4   Future University in Egypt, Orthodontics, Cairo, Egypt

Thermography is a contemporary imaging modality based on acquiring and analyzing thermal data using non-contact devices. The aim of the present study was to assess the validity of thermography, compared with that of the reference standard, for the diagnosis of periapical inflammatory lesions and to evaluate the temperature ranges for acute pulpitis with apical periodontitis (AAP), acute periapical abscess (AA) and chronic periapical abscess (CA). AAP, AA and CA were diagnosed based on clinical and radiographic criteria. Thermographic data were acquired using the FLIR E-5 Infrared Camera. Extraoral thermal images were taken from the front and right and left sides of patients whose mouths were closed, and one intraoral thermal image was taken from the palatal perspective. Agreement in the diagnoses based on the combination of clinical and radiographic assessments and the thermographic evaluation was calculated. The temperature ranges of the three subdiagnostic groups were also measured. A total of 80 patients were enrolled in this study. The mean intraoral thermal image temperature for AA was 37.26 ± 0.36, that for CA was 35.03 ± 0.63 and that for AAP was 36.07 ± 0.45. The differences between the mean intraoral thermal temperatures of the three diagnostic groups were statistically significant ($P<0.001$). The result of the Kappa coefficient of agreement between the combination of clinical and radiographic assessments and the thermographic evaluation was significant ($P<0.001$).

Thermography is an effective, quantitative and nonionizing approach that can be used for the diagnosis of periapical inflammatory lesions. The results of the present study indicated that the highest thermal image temperatures were recorded for AA. Thermography might be able to detect inflammatory reactions during the preclinical stage, leading to early diagnosis.

E4.6
Use of a 3D hand-held scanner to capture trochlear groove shape, a proof of concept study

Jatin Mistry[1], *Caroline Hing*[2], *Simon Harris*[3]

1   Institute of Medical and Biomedical Education, St George's University of London, United Kingdom
2   St George's University Hospitals NHS Foundation Trust, United Kingdom
3   Faculty of Medicine, Department of Surgery & Cancer, Imperial College London, United Kingdom

Introduction: Trochleoplasty is a surgical procedure used to treat patellar instability in patients with severe trochlear dysplasia. Trochlear dysplasia is defined as an abnormality of the depth and shape of the trochlear groove which is modified during trochleoplasty. The aim of this study was to establish whether we could use a 3D hand-held scanner to accurately measure trochlear depth, sulcus angle, trochlear facet ratio, trochlear angle and lateral trochlear inclination angle and establish inter- and intra-rater reliability for each knee model. Analysis of the groove with a hand-held scanner would enable accurate real time planning and facilitate tailor made correction.

Methods: The trochlear groove of the knee models were scanned by two investigators and 3D reference models created. The trochlear groove scans and reference models were surface matched and custom software was written to analyse the trochlear groove surface. This trochlear analyser generated Excel CSV files which were utilised to determine the desired trochlear groove parameters. Intraclass correlation coefficient (ICC) was used for test-retest reliability and to determine which trochlear groove parameter results, for each knee model, showed the best reproducibility.

Results: The differences seen between most trochlear groove parameters measured by the two investigators were small demonstrating good inter-observer reliability - trochlear depth (1.0 mm), sulcus angle (2.7°), trochlear angle (4.0°) and lateral trochlear inclination angle (4.0°), apart from trochlear facet ratio (32.0%) of one knee model. With outliers removed ICC was moderate-excellent in (73.34%) of measurements, with trochlear depth showing the best reproducibility.

Conclusion: This feasibility study showed that the hand-held scanner in conjunction with the supporting software can measure trochlear parameters in a carefully controlled environment and justifies extending research into its use in trochleoplasty.

Colour	Difference (mm)
Red-Orange	0 – 0.1
Orange-Yellow	0.1 – 0.2
Lime green-Green	0.2 – 0.3
Green-Cyan	0.3 – 0.4
Cyan-Light blue	0.4 – 0.5
Light blue-Dark blue	0.5 – 0.8
Dark blue-Magenta	0.8 - ≥1.0 / surface not present
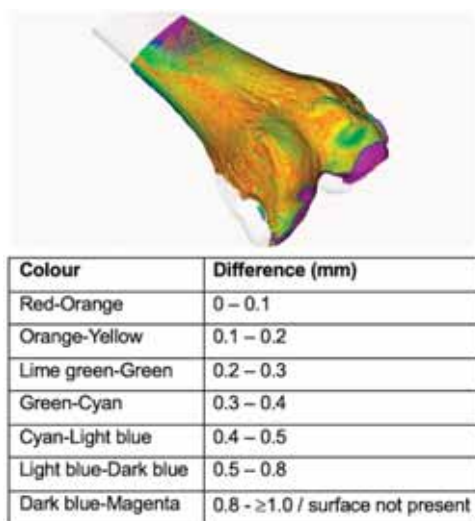
Figure 1: Colour coded difference in the surface of the reference model and trochlear groove scan
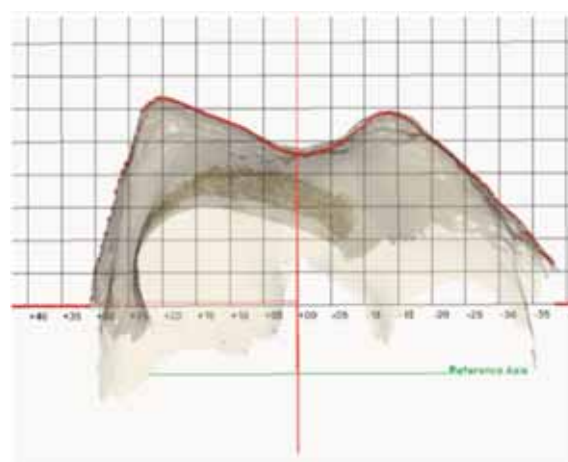
Figure 2: The trochlear contour

E5.1
3D characterization of pelvic floor muscle fascicle orientation for biomechanical modeling

Shaniel Bowen[1], Pamela Moalli[1 2], Steven Abramowitch[1]

1   University of Pittsburgh, Bioengineering, Pittsburgh, United States
2   Magee Women's Research Institute, Obstetrics, Gynecology & Reproductive Sciences, Pittsburgh, United States

Background: Physiologic fascicle orientation is needed for biomechanical models of the pelvic floor muscles (PFMs) to improve simulation of mechanical function. Current methods of quantifying PFM fascicle direction have used 2D/surface-based calculations or diffusion tensor imaging. The objective of this study was to create a semi-automated approach to calculate and visualize 3D PFM fascicle orientation using cryo-sectioned images from the Visible Korean Project.

Methods: Spatially registered, high-resolution cryo-sectioned images of a female cadaveric pelvis (pixel size, 0.1 mm; interval, 0.1 mm) were obtained from a premenopausal donor without history of pelvic floor disorders (age, 43; weight, 54 kg; height, 1.53 m). Using PhotoshopTM, the PFMs were manually segmented from the images. The segmented images were then exported to a custom MathematicaTM script to extricate the muscle fascicle directions in the PFM volume.

The algorithm performed color-to-grayscale conversion and intensity normalization on the images and stacked them to construct a 3D image volume. The image volume was then partitioned into subvolumes (voxel size, 4 mm).

For each subvolume, a Gaussian filter ($\sigma = 0.5$) was applied prior to computing the following at each voxel: gradient magnitude (scalar value) and gradient orientation (unit vector parallel to the gradient). After normalizing the gradient orientation by the gradient magnitude, principal component analysis was performed where the eigenvector with the smallest eigenvalue corresponded to the preferred fascicle direction and the ratio between the smallest eigenvalue and sum of all eigenvalues denoted the confidence of that direction.

Lastly, a 3D vector field was generated from the subvolumes and visualized in 3D using Houdini FXTM.

Results: The following pelvic muscles were assessed: coccygeus (C), iliococcygeus (IC), constrictor urethrae muscle (CUM), superficial perineal muscles (SPM), pubovisceral muscle (PVM), puborectalis (PR), and external anal sphincter (EAS). Figure 1 provides a pictorial overview of the fascicle direction calculation and visualization methods.

In the 3D vector field, local fascicle directions were described by vectors colored by their orientation and scaled by their confidence value (larger vector signifies greater confidence). The PFM groups were delineated by the vector field, with a circular field in the EAS about the anus, inferior-superior orientation (blue/purple) in the PR, PVM, and IC, anterior-posterior orientation (green/yellow) in the SPM, lateral orientation (red/orange) in the CUM and C.

Conclusions: The proposed semi-automated method successfully quantified and visualized PFM fascicle orientation. Future work will compare these data with previous studies and use the data to develop computational simulations of in-vivo muscle function.
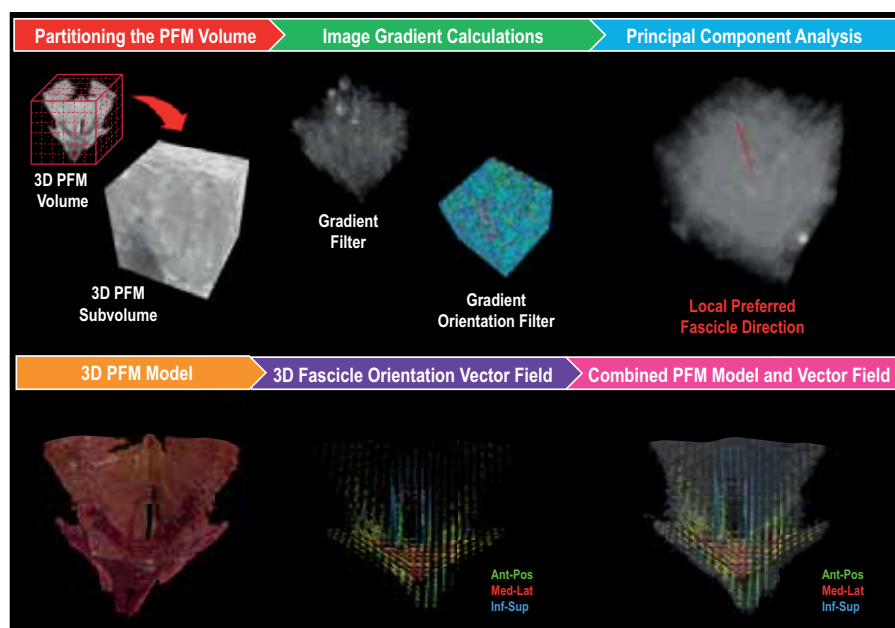
Figure caption: Summary of the calculation (top) and visualization (bottom) of the PFM fascicle orientation methods. Vector field color code: green/yellow, anterior-posterior orientation; red/orange, medial-lateral orientation; blue/purple, inferior superior orientation. Abbreviations: PFM, pelvic floor muscle.

E5.2
Reconstructing 3D lungs from a single chest X-ray with statistical shape and appearance models

Josh Williams[1], Andrew Kirby[2], Steve Cunningham[3], Ali Ozel[1], Uwe Wolfram[1]

1   Heriot-Watt University, School of Engineering and Physical Sciences, Edinburgh, United Kingdom
2   Royal Hospital for Children and Young People, Radiology Department, Edinburgh, United Kingdom
3   University of Edinburgh, Centre for Inflammation Research, Edinburgh, United Kingdom

Introduction: Respiratory patients frequently have poor inhaler technique which impacts their disease management [1]. Treatment efficacy could be improved using predictive models for therapeutic response from patient technique. Widely applying personalised models requires a rapid and cost-effective image processing approach. Statistical shape and appearance models (SSAMs) have been used to reconstruct bones from X-rays [2] and show promise in reconstructing lungs for deposition models. Here, we present our developed lung SSAM and discuss its accuracy in reconstructing the lung volumes.

Materials and methods: Our dataset used computed tomography (CT) scans and radiologist validated segmentations (ground truth) of 51 patient lungs and airways taken from the LUNA16 challenge [3,4]. We used ray-tracing to create digitally reconstructed radiographs (DRRs) for each patient (Fig. 1a). We established shape correspondence using automated landmarking on the lung lobes [5]. Gray-value at the landmark location on the DRR formed our appearance model. Principal component analysis was performed to parameterise the shape model. To reconstruct the lungs we optimised SSAM parameters by minimising the differences between the X-ray and modelled shape's outline and gray-value in Python 3.7 (Fig. 1a). We evaluated our reconstruction by comparing volume difference between the ground truth and reconstructed lungs, excluding the airways. We tested using DRRs, as separate X-rays would introduce error caused by changes in patient breathing and posture.

Results and discussion: Our SSAM reconstructed the total lung volume to a median error of 8% compared to the ground truth (maximum error 20%, Fig. 1b). Lobar reconstruction was less accurate (median 15%, maximum 60%) as the lobar fissures are not visible on frontal X-rays. Our median error was 10 times smaller than the estimated 80% volume increase during deep breathing used in deposition studies [6]. Therefore, our SSAM can be used to calculate pressure change caused by lung expansion for deposition models. Such models will enable clinicians to monitor treatment efficacy.
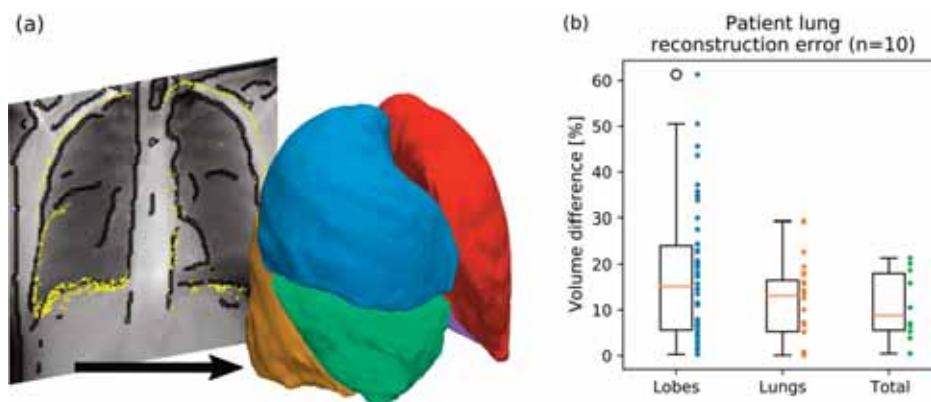
Figure caption: Lung reconstruction error. (a) Input X-ray with fitted outline and reconstructed lung. (b) Volume difference in reconstructed lung volumes compared to the ground truth.

References:
[1]   van Boven, J.F. et al., 2018. NPJ Prim Care Resp M, 28(1), pp.1-3.
[2]   Väänänen, S.P. et al., 2015. Med Image Anal, 24(1), pp.125-134.
[3]   Setio, A.A.A. et al., 2017. Med Image Anal, 42, pp.1-13.
[4]   Tang, H. et al., 2019, In ISBI 2019, IEEE, pp. 1225-1228.
[5]   Ferrarini, L. et al., 2007. Med Image Anal, 11(3), pp.302-314.
[6]   Koullapis, P.G. et al., 2020. J Aerosol Sci, 144, pp.105541.

E5.3

Measurement of soft tissue interactions with respiratory PPE using MRI and digital volume correlation

Sam Evans[1], **Bethany Keenan**[1], Silvia Caggiari[2], Peter Worsley[2], Dan Bader[2]

1   Cardiff School of Engineering, Cardiff, United Kingdom
2   University of Southampton, Southampton, United Kingdom

Since the onset of the Covid-19 pandemic, skin and soft tissue injuries related to the use of respiratory protective equipment (RPE) have been very common, particularly in females or those with smaller face shapes. Tight-fitting respirators such as disposable FFP3 masks, rely on a good seal around the nose and mouth to effectively protect the user from infection. To ensure the RPE protects the user, a face fit test is carried out to identify the correct shape, size, and material for the worker. However, current designs for face masks have solely been centered around a white male workforce, providing a limited range of size and geometry. The use of a 'standard' male face shape in the manufacture of RPE has meant that most women as well as men from black and minority ethnic groups or with facial hair have experienced problems in finding suitable and comfortable personal protective equipment [1]. There is therefore a critical need to better understand the soft tissue injuries occurring at the mask – face interface to not only reduce injury but to aid our understanding in developing an appropriate design template for future RPE devices.

To the best of the authors' knowledge there have been no studies to date which have utilized MRI techniques to measure the facial soft tissue deformation with different types of masks. Thus, the methods employed in this study are twofold. Firstly, an MRI compatible head phantom was designed and SLS printed in order to identify which masks were MR safe for the volunteer (i.e., all ferromagnetic components were removed to avoid any risk of burns). An internal grid structure was incorporated into the design to measure the geometric distortion in the 3T Siemens Magnetom Prisma scanner. The head phantom was also used to capture the surface geometry of the RPE masks using an Artec Eva-S handheld 3D scanner (Figure 1). Secondly, a high-resolution 3D MRI sequence was developed to clearly identify the anatomical face geometry in an unloaded (without a mask) and loaded (with a mask) state for a group of healthy volunteers. All volunteers were quantitively fit tested prior to their MRI examination and each underwent several MRI scans with different types of masks.

Regions of interest were manually segmented from the MRI data in order to define the nasal cartilage and surrounding soft tissue in the cheeks and mouth. Intrasubject elastic registration was performed using custom code developed in MATLAB to extract the soft tissue deformation.

This study is part of a larger study which aims to inform international testing standards and create intelligent software to support mask fitting that can be used in both clinical and industrial sectors.

Figure 1: MRI compatible face phantom (left); volunteer undergoing a face MRI scan with a 3T Siemens system and 64 channel-head and neck coil (middle); and corresponding 3D face scan of volunteer.

References:

1] TUC Report, 2017. Personal protective equipment and women. www.tuc.org.uk
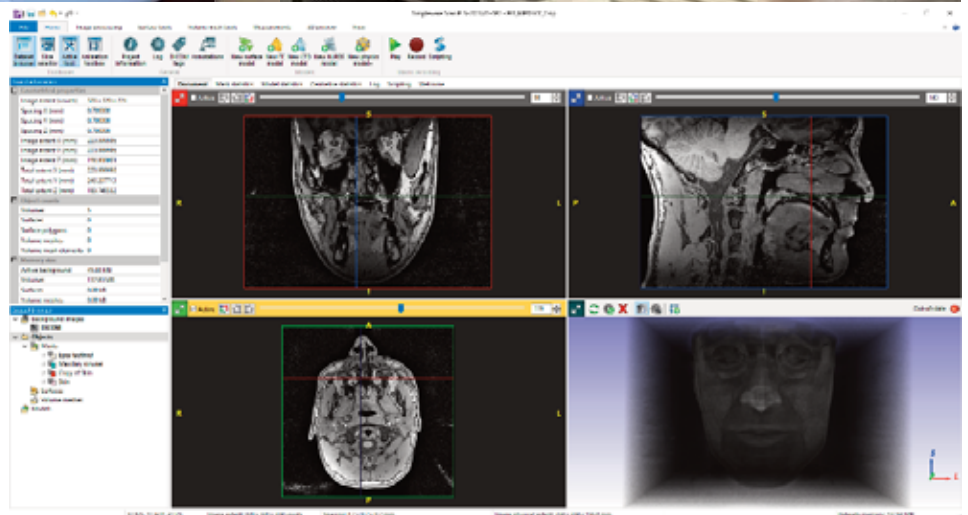
E5.4
Automatic muscle segmentation through deformable image registration

William Henson[1 2], E. Dall'Ara [2 3], Claudia Mazzà[1 2]

1   The University of Sheffield, Department of Mechanical Engineering, Sheffield, United Kingdom
2   The University of Sheffield, INSIGNEO institute for in silico medicine, Sheffield, United Kingdom
3   The University of Sheffield, Department of Oncology and Metabolism, Sheffield, United Kingdom

Introduction: Muscle segmentation is a process relied upon to gather image-based muscle characterisation, useful in assessing muscle health directly and feeding into musculoskeletal modelling pipelines. Semi-automatic techniques are typically employed within modelling pipelines to quantify muscle properties, requiring significant manual labour and thus are associated to operator repeatability issues. An automatic process is proposed to counter these limitations.

Methods: Lower limb T1- weighted Magnetic Resonance (MR) images were taken from three women (Age: 56-69 y.o., Height: 154.0-164.0 cm, BMI: 21.2-27.6) after gaining informed consent. The Sheffield Image Registration Toolkit, proven to be capable of automatically detecting tissue boundaries within medical images [1], was employed as a segmentation tool. Segmentation was achieved by applying the toolkit to a set of reference segmentations [2] (see figure) gathered by using Mimics (Materialise) to automatically segment the images and then manually correcting them where needed. Two tasks were performed to vary the complexity of registration. First, registering left and right limbs of each subject, and second, registering the right limb of each subject to the right limb of the other subjects. Both registration tasks were re-run with pre-processed MR images, in which automatic morphological processes were used to remove the skin and homogenise the fat, aiming to shift the focus of registration to the muscles (example in figure). Resulting automatically generated segmentations were compared to those from semi-automatic segmentation. The DICE similarity score [3], calculated as the ratio of the overlapping volume to the total volume of the two segmentations, was used to account for differences in the shapes segmented muscles, and a volumetric comparison was drawn.
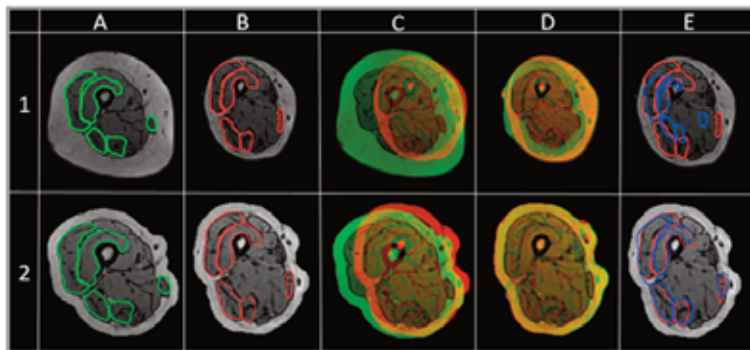
Figure caption: Comparison of registration quality between raw, unmasked images (row 1) and masked images (row 2). The reference data (column A) and target data (B) are registered (pre- and post-registration, C and D respectively) giving the segmentation results (E), where semi-automatic and automatic segmentations are shown in red and blue respectively to allow visual comparison.

Results & discussion: Exploring first the left to right segmentation results, the mean (± standard deviation) DICE scores of the three segmentations before and after masking were 0.74 ±0.13 and 0.81 ±0.09, respectively. The average absolute volumetric accuracy before and after masking was 88.6% ±13.8% and 90.6% ±13.0% respectively, similar to the confidence level of the semi-automatic process [2]. Comparing with the inter-subject registration, there is a significant decrease in the average DICE scores, 0.47 ±0.23 before masking and 0.68 ±0.14 after masking and an increase in the volumetric accuracy, 69.4% ±29.8% before masking, 88.7% ±11.0% after masking. The variability in muscle architecture/anatomy between subjects causes the disparity in accuracy between left to right registration and inter-subject registration.

Conclusion: There is promise in the routine to perform automatic segmentation of muscles, given that left to right segmentation is comparable to the level of confidence of the semi-automatic approach. Possible routes to increase accuracy are using a large database of reference subjects and/or additional post-processing registration tasks using edge detection filters, which could enhance the accuracy of segmentation.

References:
1.   Barber D. C., Hose, D. R., J Med. Eng. Technology, 2005
2.   Montefiori E. et al., PLOSONE, 2020
3.   Dice L. R., Ecological Society of America, 1945

E5.5

Organ segmentation of male pelvic CTs with large artifacts caused by femoral bone prostheses

Gonçalo Almeida[1], Joao Tavares[2]

1   FEUP - Faculdade de Engenharia da Universidade do Porto, Instituto de Ciencia e Inovacao em Engenharia Mecanica e Engenharia Industrial, Porto, Portugal
2   FEUP - Faculdade de Engenharia da Universidade do Porto, Departamento de Engenharia Mecânica, Porto, Portugal

Image artifacts are common in computed tomography due to bone prosthetics, fiducial markers and other surgical implants. These cause large changes in the image due to the way X-rays are absorbed and transmitted by the metal. Although there have been considerable advances [1], the algorithms used in image reconstruction are often unable to remove the resultant cones of shadow and high intensity streaks. In these cases, image analysis becomes very difficult. Organ segmentation must rely on shape prior knowledge and subtle cues from the whole slice and adjacent slices.

We collected 93 CT scans of patients who underwent radiotherapy for prostate cancer, all of whom had previously been implanted with femoral head prosthetics. There were 24 patients with bilateral prostheses, which exhibit particularly bad CT scans, with regions of complete shadow. The goal was to perform segmentation of prostate, bladder and rectum, essential for radiation treatment planning. The scans were manually segmented by medical experts, used as ground-truth. The dataset was split 80/13 for training/validation, and 6 in the validation set had bilateral prostheses.

We trained a three-dimensional fully convolutional neural network with an encoder-decoder architecture using dilated convolutions cascades in the skip pathways connecting the encoding and decoding arms. Dilated convolutions have the benefit of increasing the receptive field of the network without increasing computational complexity too much [2]. Furthermore, they help to extract useful information at different scales, from the finer details in organ boundaries to overall organ shape features.

Despite poor image features, the results are promising, with volumetric Dice scores of 80.1%, 94.4%, and 81.6% and average boundary distances (ABD) of 2.31mm, 1.07mm, and 2.22mm for prostate, bladder and rectum, respectively. This is an improvement over the results achieved by a 3D implementation of the original U-net [3]: Dice 77.3%, 92.4%, and 73.0% and ABD 2.62mm, 1.52mm, and 3.48mm.

Although far from a complete solution, this study shows that a properly trained, well designed deep learning model can elicit the overall shape of the organs and learn to disregard conflicting image artifacts to achieve good segmentations. Further improvements in network architecture, use of a larger training sets, and other training techniques are expected to lead to even better outcomes.

References:
1.   Meyer, E., et al. "Normalized metal artifact reduction in computed tomography." Medical physics 37 10 (2010): 5482-5493.
2.   Dumoulin, V., Visin, F.. "A guide to convolution arithmetic for deep learning." ArXiv abs/1603.07285 (2016).
3.   Çiçek, Ö. et al. "3D U-Net: Learning Dense Volumetric Segmentation from Sparse Annotation." ArXiv abs/1606.06650 (2016).

Figure caption: Example CT slice of patient with bilateral prostheses. Top: ground-truth, middle: U-net, bottom: our model.
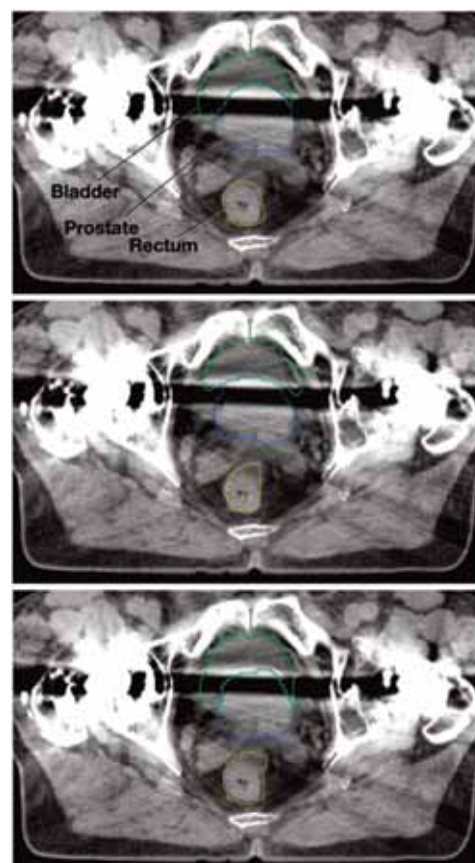
E5.6

Statistical shape modelling of muscle fiber arrangement to characterize soleus muscle architecture in pediatric cerebral palsy

Salim Bin Ghouth[1], Thor Besier[1 2], Geoffrey Handsfield[1]

1   Auckland Bioengineering Institute, University of Auckland, Auckland, New Zealand
2   Department of Engineering Science, Universty of Auckland, Auckland, New Zealand

Introduction: Cerebral palsy (CP) is a common cause of disability in pediatric populations [1], [2]. Although CP is caused by an early-stage, single-event neural damage, it is characterized by life-long movement impairments in the affected child [1]. To better understand the muscle architecture and associated biomechanics altering movement in children with CP, a quantitative investigation of soleus muscle fiber arrangement is important. Here, we introduce an unbiased and quantitative assessment of fiber arrangement in CP via statistical shape modelling of muscle fiber tracts. This novel approach provides a robust and data-driven understanding of muscle architecture in CP from diffusion tensor imaging (DTI). Using DTI data of the soleus muscle combined with a statistical shape model (SSM), we characterized the dominant fiber orientations within and between populations of CP and typically developing (TD).

Methods: We obtained the DTI data of the soleus muscle of 9 children with CP and 8 TD children from a previous study [3]. We removed the size variation within each population. We then generated SSM's of the muscle fiber tracts based on the SSM workflow developed by Zhang et al. [4]. A mean geometry and modes of variations in each population were acquired. The muscle fiber distributions within and between the two populations were quantified.

Results: The CP and TD population-based models can compactly capture the dominant features of each population with a few principal components, or modes. However, the two populations differ in both the dominant features and the variance of the dominant feature within each population. Principal components demonstrate the variability of fiber tracts density and orientation in the soleus muscle (Figure 1). Conclusion: We generated shape models of the muscle fiber distributions in populations of children with CP and TD children. The shape models can describe fiber tracts' variations within and between the two populations. The differences may elucidate the functional impairments of the soleus muscle associated with CP. Future studies will investigate the regional fiber tracts within and between CP and TD populations and use finite element modelling to predict the functional abilities of the soleus muscle in CP and TD populations.
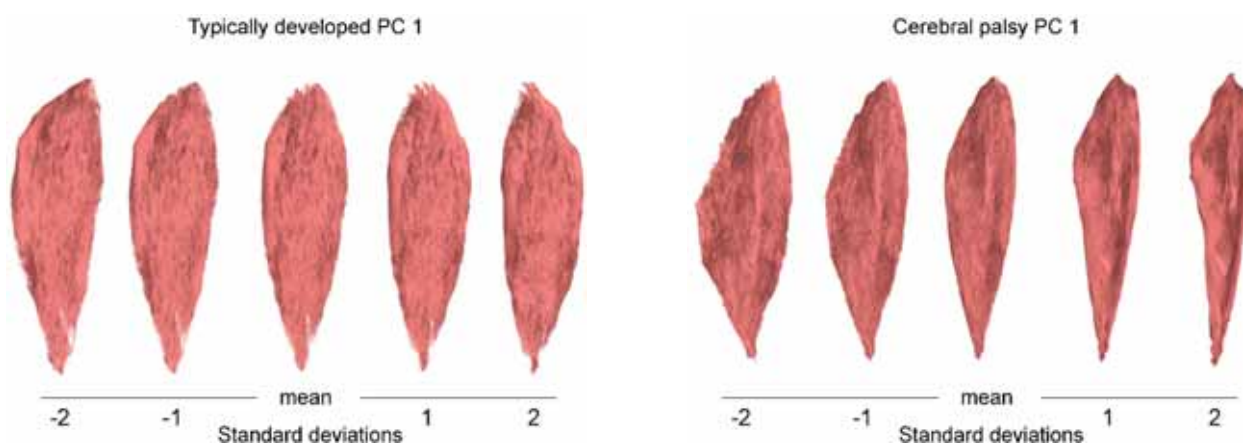
Figure caption: The first PC of TD and CP size-normalized models characterizing the fiber tracts within each population. Tract density and muscle morphology differ between populations, indicating architectural impairments in CP.

References:
[1]   H. K. Graham et al., Nat. Rev. Dis. Prim., vol. 2, 2016.
[2]   M. Oskoui et al., Dev. Med. Child Neurol., vol. 55, no. 6, pp. 509–519, 2013.
[3]   A. S. Sahrmann et al., PLoS One, vol. 14, no. 2, pp. 1–16, 2019.
[4]   J. Zhang et al., Comput. Methods Biomech. Biomed. Eng. Imaging Vis., vol. 2, no. 3, pp. 176–185, 2014.

E6.1

Time-dependent constitutive description of collagenous soft biological tissue. Microstructurally-motivated bottom-up approaches

T. Christian Gasser[1 2], *Christopher Miller*[1]

1   KTH Royal Institute of Technology, Solid Mechanics, Department of Engineering Mechanics, Sweden
2   University of Southern Denmark, Faculty of Health Sciences, Denmark

A versatile constitutive model for load-carrying soft biological tissue should incorporate salient microstructural deformation mechanisms and be able to reliably predict complex non-linear viscoelastic behavior. The advancement of treatment and rehabilitation strategies for soft tissue injuries is inextricably linked to our understanding of the underlying tissue microstructure and how this defines its macroscopic material properties. Towards this long-term objective, we present a generalized multiscale constitutive framework based on a novel description of collagen, the most mechanically significant extracellular matrix protein. The description accounts for the gradual recruitment of undulated collagen fibrils and introduces proteoglycan mediated time-dependent fibrillar sliding. Crucially, the proteoglycan deformation allows for the reduction of overstressed fibrils towards a preferential homeostatic stress. Implicit Finite Element implementations of the models in the multipurpose software FEAP uses an interpolation strategy towards collagen fiber stress determination and results in a memory-efficient representation of the model. A number of test cases, including patient-specific geometries, establish the efficiency of the description and demonstrate its ability to explain qualitative properties reported from macroscopic experimental studies for tendon and vascular tissue.
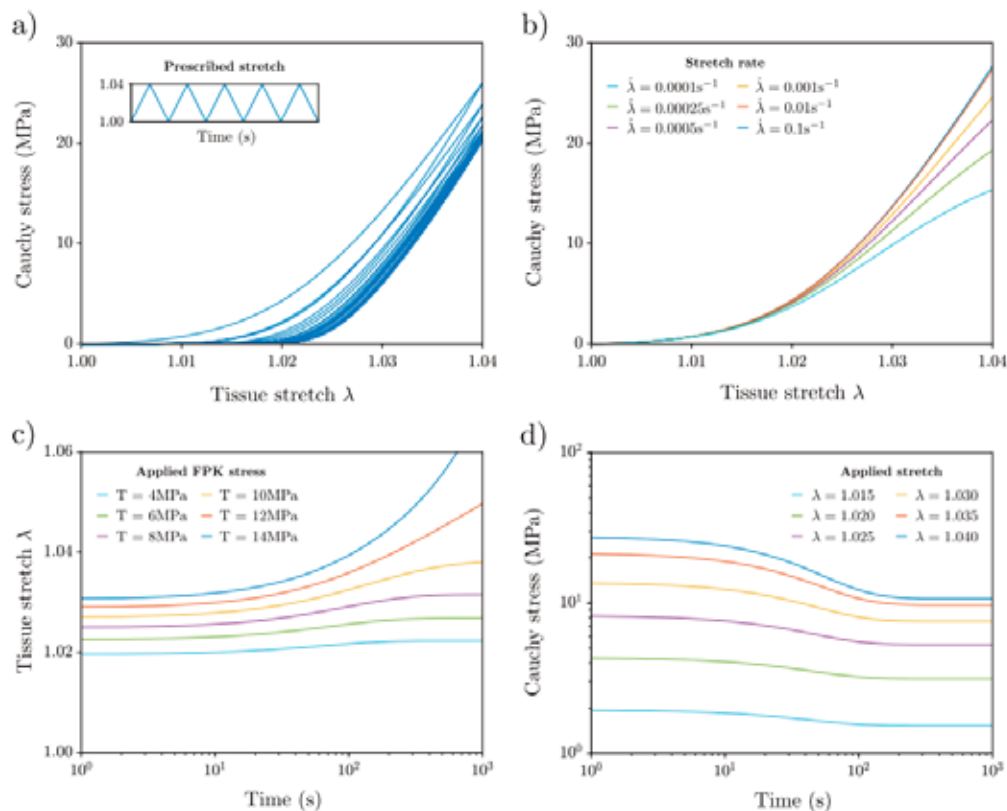
Figure caption: Example: Uniaxial extension of the Achilles tendon for a variety of testing protocols. a) Cyclic stretching; Cauchy stress as a function of tissue stretch (The stretch is cycled continuously between $\lambda = 1.00$ and $\lambda = 1.04$), b) Strain rate stiffening; Cauchy stress as a function of tissue stretch for varying stretch rates, c) Creep; evolution of tissue stretch with time for varying applied fixed FPK stresses, d) Stress relaxation; evolution of Cauchy stress with time for varying fixed applied stretches.

References:

Christopher Miller and T. Christian Gasser, A microstructurally motivated constitutive description of collagenous soft biological tissue towards the description of their non-linear and time-dependent properties, Journal of the Mechanics and Physics of Solids (in press)

G. Martufi and T.C Gasser. Turnover of fibrillar collagen in soft biological tissue with application to the expansion of abdominal aortic aneurysms. Journal of The Royal Society Interface 9 (77), 3366-3377, 2012.

T.C. Gasser. The Biomechanical Rupture Risk Assessment of Abdominal Aortic Aneurysms - Method and Clinical Relevance. In: P. Wriggers and T. Lenarz (eds.) Biomedical Technology; Lecture Notes in Applied and Computational Mechanics, Springer Science+Business Media, 2017.

E6.2

Patient-specific 3D strain field evaluation of abdominal aortic aneurysms using 4D ultrasound

Mirunalini Thirugnanasambandam[1], Esther Maas[1], Arjet Nievergeld[1], Richard Lopata[1]

1   Eindhoven University of Technology, Eindhoven, Netherlands

Abstract: Abdominal aortic aneurysm (AAA) is a pathology of the abdominal aorta, which causes its maximum diameter to increase by at least 50% of its physiological diameter. On rupture, AAAs have a 90% mortality rate, thus making it crucial to identify markers that characterize their growth and rupture. Constant evolution of the vascular wall composition leads to corresponding regional variation in material behavior, which in turn affects the biomechanics of the wall. To account for the inability to non-invasively evaluate the variation of patient-specific material properties across the AAA wall, the current study exploits the use of 4D ultrasound (US) to generate 3D finite strain field of the wall, which will provide direct information on material deformation, but can also be used for inverse material characterization.

Implementation: 4D-US images of patients were recorded in supine position during multiple heartbeats at an acquisition rate of 4 - 8 volumes per second, to ensure that the peak systolic and end diastolic phases were captured in the data. The US image volumes were segmented in the end-diastolic phase and the aortic geometry of the inner wall was regularized. The inner wall was tracked over the cardiac cycle using a 3D speckle tracking algorithm, and the 3D displacement of the wall between the diastolic and systolic phases was evaluated. A 3D least squares based strain estimation (3D LSQSE) algorithm[1,2] was used to fit displacement gradients to displacement data at each central grid point based on those at the neighboring grid points. Following the evaluation of the Green-Lagrange strain tensor at each grid point, the corresponding principal strains and principal directions were evaluated as eigenvalues and eigenvectors of the tensor as shown in Figure 1. This 3D strain map will be used as input to VFM3 for non-invasive, pointwise, material property evaluation of the AAA wall.
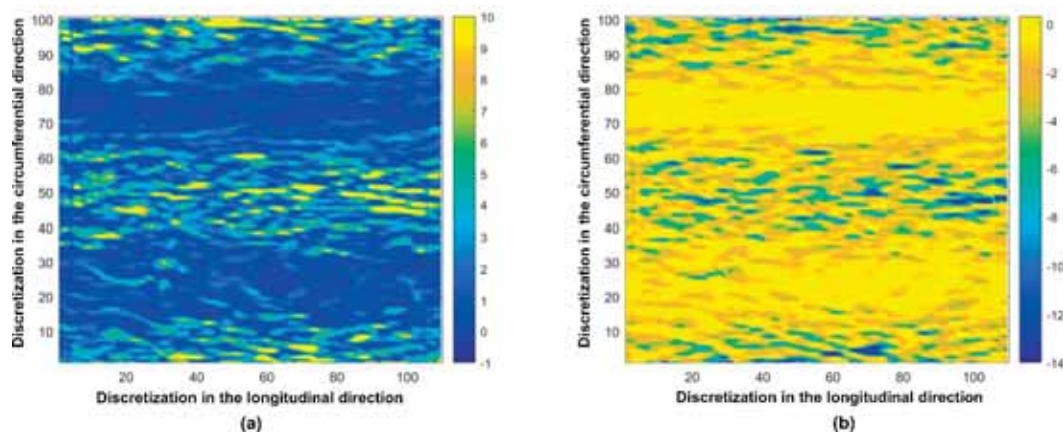
Figure 1: (a) Maximum and (b) minimum principal strain distribution on the AAA wall represented on a Cartesian grid.

References:

1   Lopata RG et al., "Three-dimensional cardiac strain imaging in healthy children using RF-data". Ultrasound Med Biol. 37(9):1399-408 (2011).

2   Cruz Perez, B et al., "Mapping 3D Strains with Ultrasound Speckle Tracking: Method Validation and Initial Results in Porcine Scleral Inflation". Ann Biomed Eng 44, 2302–2312 (2016).

3   Bersi, MR et al., "Multimodality Imaging-Based Characterization of Regional Material Properties in a Murine Model of Aortic Dissection". Sci Rep 10, 9244 (2020).

E6.3

Left ventricular strain mapping in murine models of hypertrophy and infarction from 4D ultrasound

Craig Goergen[1]

1   Purdue University, Biomedical Engineering, West Lafayette, United States

Cardiac disease remains a major cause of morbidity and mortality around the world, prompting a continued effort to better understand the various factors that exacerbate heart disease. To this end, murine models of cardiac disease have become crucial for studying disease factors. Routine evaluation of cardiac function in mice is often conducted using high-frequency ultrasound; however, cardiac function metrics drawn from conventional imaging rely heavily on measurements obtained from one or more representative slices and idealized chamber geometry. While high-field cine-MRI can be used for volumetric imaging, our group has recently developed and validated a high frequency four-dimensional ultrasound (4DUS) technique that uses temporally-gated volumetric imaging (3D plus time) that outperforms cine-MRI [1, 2]. We have also developed standardized analysis methods for left-ventricular 4DUS data, including a custom interactive toolbox with machine learning segmentation techniques [3]. We first used our three-dimensional strain mapping technique to longitudinally characterize left ventricular (LV) mechanics within and around myocardial infarctions (MI) in order to study the post-MI remodeling process in mice [4]. To induce infarcts with varying severities, we used the following groups: sham, 30-minute ischemia-reperfusion, and permanent ligation of the left coronary artery. 3D myocardial strain maps showed that strain profiles at the infarct border followed a reproducible sigmoidal pattern. We also found that mice with mild remodeling had significantly higher strains in the infarcted myocardium than those with severe injury. Finally, we developed a new approach to non-invasively estimate infarct size from strain maps that correlates well with histology. Next, we applied these strain mapping tools to study disease progression in two murine models of pathological cardiac hypertrophy (i.e. CPT2M-/- [5] and Nkx2-5183P/+ [6]). Comparison of strain metric changes suggest that circumferential strain at the base and longitudinal strain along the posterior wall of the LV were most sensitive. We further introduce a novel Hybrid Strain Index (HSI) that incorporates information from these two regions and may have greater utility to characterize disease progression relative to ejection fraction and other common metrics. In summary, the imaging and analysis methods described here show promise for early detection of cardiac disease development and may provide insight into the development of novel clinical imaging biomarkers.
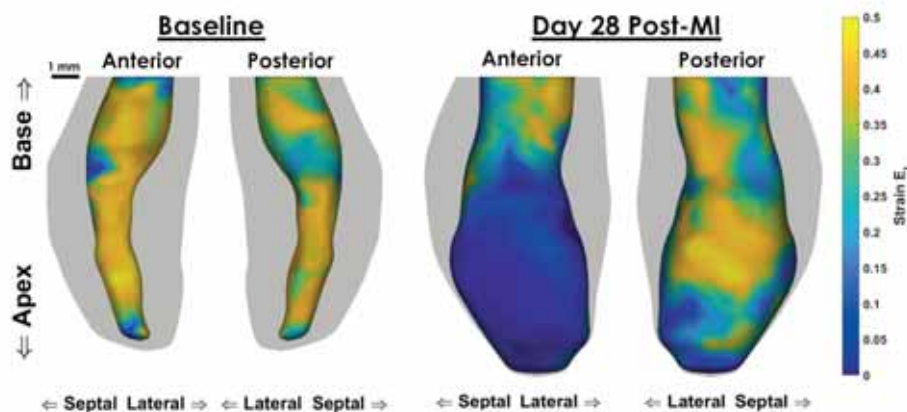
Figure caption: Volumetric representations of peak-systolic LV boundaries with maximum principal 3D Green–Lagrange myocardial strain (EI).

References:
[1]   F. W. Damen et al., 2017, doi:10.18383/j.tom.2017.00016.
[2]   A. H. Soepriatna et al., 2017, doi:10.1007/s10554-017-1283-z.
[3]   F. W. Damen et al., 2021, doi:10.3390/app11041690.
[4]   A. H. Soepriatna et al., 2019, doi:10.1098/rsif.2019.0570.
[5]   A. S. Pereyra et al., 2017, doi:10.1074/jbc.M117.800839.
[6]   M. B. Furtado et al., 2017, doi:10.1172/jci.insight.88271.

E6.4

Assessing rupture risk in ascending thoracic aortic aneurysms using MRI and biomechanics

Stéphane Avril[1]

1   Mines Saint-Etienne, Saint-Etienne, France

Ascending thoracic aortic aneurysm (ATAA) is a life-threatening cardiovascular disease, leading to weakening of the aortic wall and permanent dilation. ATAA affects approximately 10 out of 100,000 persons per year in the general population, and this disease is associated to high risk of mortality and morbidity [1].

The degeneration of the arterial wall at the basis of ATAA is a complex multifactorial process. Individual genetic, biological or hemodynamic factors are inadequate to explain the heterogeneity of ATAA development/progression mechanisms, thus stimulating the analysis of their complex interplay.

Quantifying local aortic stiffness properties in vivo was acknowledged as essential to assess the severity of an ascending thoracic aortic aneurysm [2]. Recently, we established a methodology to quantify non-invasively local stiffness properties of ATAAs using electrocardiographic-gated computed tomography (ECG-gated CT) scans. We showed strong relationship between the extensional stiffness and the rupture stretch of the aortic tissue, supported by biomechanical explanations. However, the interrelationship between the obtained local stiffness with other established markers of aortic function remains unclear and this currently limits the methodology's potential impact [3].

In this context, we have proposed a framework combining these personalized in vivo estimates of the local aortic stiffness with 4D flow magnetic resonance imaging (4DMRI), patient-specific computational fluid dynamics (CFD), and advanced fluid mechanics analysis. The aims were to decipher the existing links between near-wall features, intravascular flow structures and ATAA wall stiffness that may indicate the risk of rupture. Spatial correlations with WSS features were extracted [4] from the topological skeleton analysis to ultimately associate ATAA complex hemodynamic features and wall mechanical properties (see figure).

The obtained results on 2 patients showed existing links between arterial wall degeneration and hemodynamic insult, which corroborate computational predictions of ATAA progression coupling hemodynamics with mechanobiology [5]. This is very promising for achieving patient-specific diagnosis of ATAA progression. Future work will focus on validating these results on more significant cohorts.
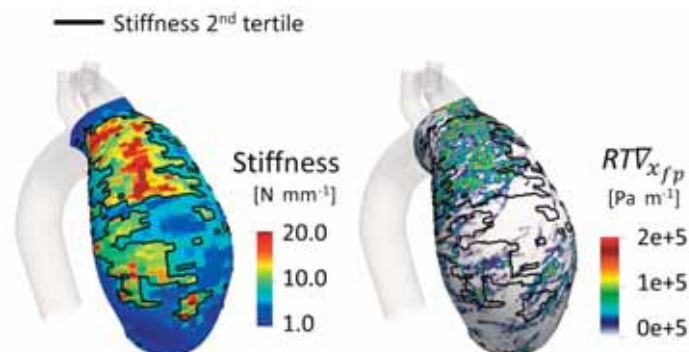
Figure caption: Wall stiffness vs. weighted residence time analysis estimated at the luminal surface of ATAA.

References:
[1]   Elefteriades, J.A., Farkas, E.A., 2010. Journal of the American College of Cardiology 55, 841-857.
[2]   Farzaneh, S., Trabelsi, O., Chavent, B., Avril, S. (2019). Annals of Biomedical Engineering 47, 1038-1050.
[3]   Di Giuseppe, M., Farzaneh, S., Zingales, M., Pasta, S., & Avril, S. (2021). Journal of Biomechanics, 119, 110321.
[4]   De Nisco, G., ... & Morbiducci, U. (2020). Medical Engineering & Physics, 82, 119-129.
[5]   Mousavi, S. J., Jayendiran, R., ..., & Avril, S. (2021). Computer Methods and Programs in Biomedicine, 106107.

E6.5

A CFD and MRI arterial spin labeling modeling strategy to quantify patient-specific cerebral hemodynamics in cerebrovascular occlusive disease

C. Alberto Figueroa[1 2], *Jonas Schollenberger*[1], *Luis Hernandez-Garcia*[1], *Nicholas Osborne*[2]

1   University of Michigan, Biomedical Engineering, Ann Arbor, United States
2   University of Michigan, Surgery, Ann Arbor, United States

Cerebral hemodynamics in the presence of cerebrovascular occlusive disease (CVOD) are influenced by the anatomy of the intracranial arteries, the degree of stenosis, the patency of collateral pathways, and the condition of the cerebral microvasculature. Accurate characterization of cerebral hemodynamics is a challenging problem. In this work, we present a strategy to quantify cerebral hemodynamics using computational fluid dynamics (CFD) in combination with arterial spin labeling MRI (ASL). First, we calibrated patient-specific CFD outflow boundary conditions using ASL-derived flow splits in the Circle of Willis. Following, we validated the calibrated CFD model by evaluating the fractional blood supply from the main neck arteries to the vascular territories using Lagrangian particle tracking and comparing the results against vessel-selective ASL (VS-ASL) (see figure). Finally, the feasibility and capability of our proposed method were demonstrated in two patients with CVOD and a healthy control subject. We showed that the calibrated CFD model accurately reproduced the fractional blood supply to the vascular territories, as obtained from VS-ASL. The two patients revealed significant differences in pressure drop over the stenosis, collateral flow, and resistance of the distal vasculature, despite similar degrees of clinical stenosis severity. Our results demonstrated the advantages of a patient-specific CFD analysis for assessing the hemodynamic impact of stenosis.
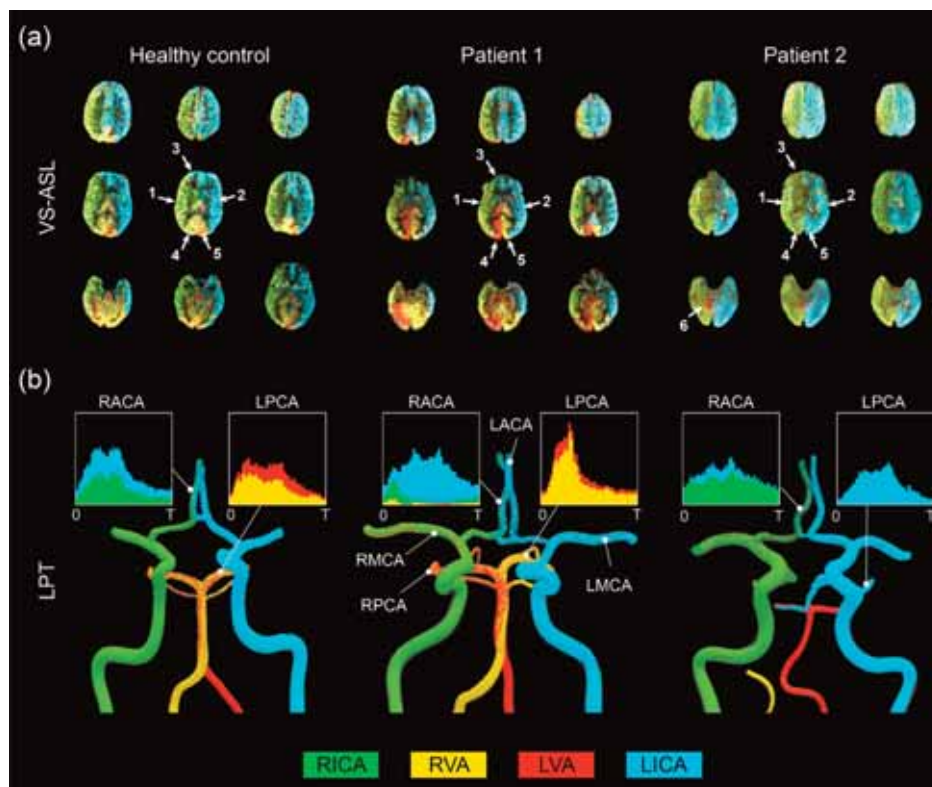
Figure caption: *Qualitative comparison between FBS obtained from VS-ASL and CFD LPT (a) VS-ASL images show the perfusion territories of the main neck arteries from the inferior of the cranium (bottom row slices) to the superior (top row slices). The images were created by color-coding the FBS maps of the main neck arteries on a voxel-by-voxel basis. For visualization purposes, we limited the fractional contributions of each neck artery to a positive range between 0 and 1. The arrows indicate the vascular territories of the 1) RMCA, 2) LMCA, 3) RACA, 4) RPCA, 5) LPCA, and 6) cerebellum. (b) LPT analyses show the advection of particles in the large arteries of the CoW. Particles are color-coded based on the artery of origin in the neck. Histograms demonstrate mixed supply in the RACA and LPCA over the cardiac cycle T.*

References:
A combined computational fluid dynamics and MRI Arterial Spin Labeling modeling strategy to quantify patient-specific cerebral hemodynamics in cerebrovascular occlusive disease. J. Schollenberger, N.H. Osborne, L. Hernandez-Garcia, C.A. Figueroa doi: https://doi.org/10.1101/2021.01.21.426887

E6.6
Processing of ultrasound images by using convolutional neural networks for carotid artery detection and segmentation

Branko Arsic[1 2], **Smiljana Djorovic**[2 3], Milos Anic[2 3], Igor Koncar[4], Nenad Filipovic[2 3]

1   Faculty of Science, University of Kragujevac, Kragujevac, Serbia
2   Bioengineering Research and Development Center (BioIRC), Kragujevac, Serbia
3   Faculty of Engineering, University of Kragujevac, Kragujevac, Serbia
4   Faculty of Medicine, University of Belgrade, Belgrade, Serbia

In the era of personalized medicine, the cardiovascular diseases such as carotid atherosclerosis have to be analyzed by using advanced machine learning techniques in order to better estimate the patient's condition and visualize the carotid artery. The ultrasound (US) images were used in this study for the detection and segmentation of carotid artery lumen and wall, as the US technique is widespread in clinical practice.

The U-Net based Convolutional Neural Networks (CNNs) were applied on the US images, as this methodology is promising in processing of US data [1]. The used US dataset consisted of 108 patients who underwent the US examination (baseline time point), where each patient had captured carotid branches and bifurcation in transversal and longitudinal projections. The difference between the whole transversal carotid surface and lumen area represents the segmented patient-specific carotid wall. The US images had been preprocessed including resizing, classification (grayscale and color US images), as well as the annotation of US images by clinical experts. The obtained results for lumen showed high accuracy in region detection and segmentation (Precision 0.90, Recall 0.92, Dice coefficient 0.91). The segmentation of carotid wall included training and validation of two models, giving the U-Net results of high accuracy - first model (grayscale US images): Precision 0.9636, Recall 0.9634, Dice coefficient 0.9634; second model (color US images): Precision 0.9874, Recall 0.987, Dice coefficient 0.9872. The presented methodology based on automatic extraction of carotid lumen and wall gives the segmentation of individual patient-specific anatomy (Figure 1) and can be used for further analysis of the patient [2]. Development of these deep learning techniques, together with computer-based modelling can contribute to better risk stratification of patients with carotid atherosclerotic disease.
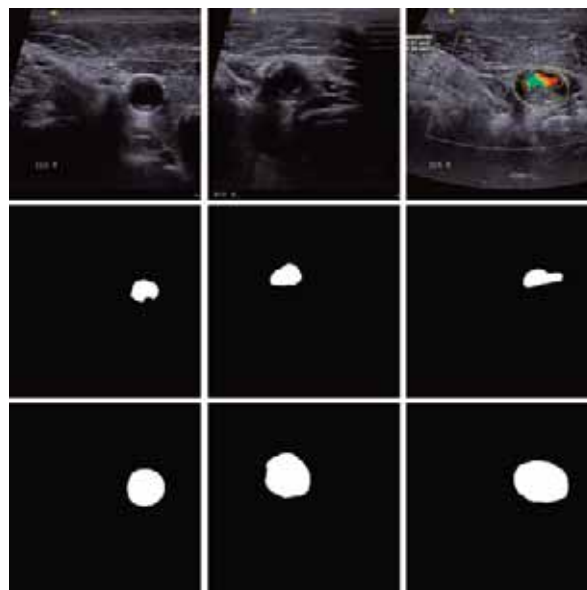
Figure 1. The carotid US images for one patient: original images (a), predicted lumen (b) and wall regions (c).

References:
[1]   Hashimoto, H., Tagaya, M., Niki, H., Etani, H.: Computer-assisted analysis of heterogeneity on B-mode imaging predicts instability of asymptomatic carotid plaque, Cerebrovasc. Dis., (2009).
[2]   Xie, M., Li, Y., Xue, Y. et al: Vessel lumen segmentation in internal carotid artery ultra-sounds with deep convolutional neural networks. IEEE International Conference on Bioinformatics and Biomedicine (BIBM), San Diego, CA, USA, 2019, pp. 2393-2398.

E7.1
Immuno-mechanics: modeling soft tissue growth and remodeling

Jay Humphrey[1]

1   Yale University, Biomedical Engineering, New Haven, United States

Soft tissues exhibit a remarkable ability to adapt to changing mechanical loads, often consistent with mechanical homeostasis. It is becoming increasingly evident, however, that inflammation can either promote or prevent such homeostatic responses. There is, therefore, a pressing need to understand better the potentially complementary or competitive interactions between mechanobiology and immunobiology. In this talk, we will draw from two examples within vascular biomechanics to begin to formulate a general approach to computationally model immuno-mechanics. Toward this end we will consider experimental data from and associated modeling of the in vivo development of a vascular graft from an implanted polymeric scaffold as well as hypertensive aortic remodeling in a common mouse model of hypertension (1-3). We will see that such computational modeling can be accommodated naturally by a general constrained mixture formulation (4), though with important additions.

References:
1.   Latorre M, Humphrey JD (2018) Modeling mechano-driven and immuno-mediated aortic maladaptation in hypertension Biomech Model Mechanobiol 17: 1497-1511.
2.   Szafron J, Khosravi R, Reinhardt J, Best CA, Bersi MR, Yi T, Breuer CK, Humphrey JD (2018) Immuno-driven and mechano-mediated neotissue formation in tissue engineered vascular grafts. Annl Biomed Engr 46: 1938-1950.
3.   Latorre M, Spronck B, Humphrey JD (2021) Complementary roles of mechanotransduction and inflammation in vascular homeostasis. Proceed R Soc A 477:20200622.
4.   Humphrey JD (2021) Constrained mixture models of tissue growth and remodeling – Twenty years after. J Elasticity (ePub ahead of print)

E7.2

Chemo-mechano-biological modelling of tissue growth and remodelling during healing induced by mechanical damage

Michele Marino[1], Meike Gierig[2], Peter Wriggers[2]

1   University of Rome Tor Vergata, Department of Civil Engineering and Computer Science, Rome, Italy
2   Leibniz University of Hannover, Institute of Continuum Mechanics, Garbsen, Germany

Loading conditions above their physiological limits, as during trauma or surgical procedures, cause damage in biological tissues. This initiates repair mechanisms at cell- and molecular-level leading to healing, consisting in growth and remodelling mechanisms (G&R). Healing mechanisms interact with mechanobiology-driven G&R aiming to maintain a homeostatic mechanical state. The balance between functional and dysfunctional G&R is then delicate. This work presents a continuum-based model coupling the description of elasto-plastic damage mechanisms [1], the activation of molecular and cellular events activated by damage, and the repair and re-adaptation (i.e., G&R) of tissues activated by such mechanobiological mechanisms [2-4].

To account for the different mechanisms, the deformation gradient is multiplicatively decomposed into damage, growth, remodelling and elastic deformation gradients. Once a physiological stretch threshold is exceeded, damage evolves. The induced damage influences the stress-stretch response in tissues and initiates the production of biologically-active molecules (e.g., proteinases and growth factors), in turn related to chemotaxis and differentiation of fibroblasts of smooth muscle cells. Cells replace damaged tissues and remodel the new/existing one aiming to maintain a preferred homeostatic level of tissue stretch.

References:
[1]   Marino, M., Converse, M.I., Monson, K.L. and Wriggers, P. "Molecular-level collagen damage explains softening and failure of arterial tissues: A quantitative interpretation of CHP data with a novel elasto-damage model", J Mech Behav Biomed Mat 97:254-271, 2019.
[2]   Cyron, C.J., Aydin, R.C. and Humphrey, J.D. "A homogenized constrained mixture (and mechanical analog) model for growth and remodeling of soft tissue", Biomech Model Mechanobiol 15:1389-1403, 2016.
[3]   Braeu, F.A., Seitz, A., Aydin, R.C. and Cyron, C.J. "Homogenized constrained mixture models for anisotropic volumetric growth and remodeling", Biomech Model Mechanobiol 16:889-906, 2017.
[4]   Marino, M., Pontrelli, G., Vairo, G. and Wriggers, P. "A chemo-mechano- biological formulation for the effects of biochemical alterations on arterial mechanics: the role of molecular transport and multiscale tissue remodelling". J. R. Soc. Interface 14:20170615(17), 2017.

E7.3

Personalized biomechanical models of abdominal aortic aneurysms based on advanced 3-D functional ultrasound imaging

Richard Lopata[1], Emiel v. Disseldorp[1], Niels Petterson[1], Judith Fonken[1], Hein de Hoop[1], Arjet Nievergeld[1], Frans van de Vosse[1]

1   Eindhoven University of Technology, Biomedical Engineering, Eindhoven, Netherlands

Abdominal aortic aneurysms (AAAs), local dilatations in the aorta, lead to a life-threatening hemorrhage when ruptured. Current clinical practice comprises of watchful waiting until the diameter reaches 5.0 – 5.5 cm. This criterion is evidence-based but not tailored to the individual patient. Over the years, image-based wall stress analysis of AAAs has been investigated extensively. Finite element (FE) analysis is used to assess peak wall stresses in a patient-specific geometry. However, translation to the clinic (and longitudinal studies on growth) is hampered by the use of either costly (MR) or harmful (CT) imaging modalities.

In recent years, we have developed a modeling framework that starts with transabdominal, 3-D, ultrasound acquisitions, followed by automatic segmentation and geometry discretization, and finally FE analysis to assess peak wall stresses. Ultrasound (US) functional imaging has many advantages for AAA characterization. One can perform multiple measurements at low cost without the use of ionizing radiation or contrast. The high spatial and temporal resolution allow for not only the assessment of a patient-specific geometry but also the measurement of wall motion and strain, which can serve as valuable input for model personalization and the assessment of global tissue properties, such as the wall stiffness. However, US has some disadvantages such as the anisotropy in image quality and contrast, and the limited field-of-view. In this presentation, the latest advances in ultrafast, multiperspective, 3-D imaging are presented, as well as our work on US-based, patient-specific, fluid-structure-interaction modeling of AAAs.

E7.4

A computational framework for growth and remodeling of thick-walled tissue-engineered vascular grafts

Erica Schwarz[1], Stephanie Lindsey[1], Jason Szafron[1], Jay Humphrey[2], Alison Marsden[1]

1   Stanford University, Stanford, United States
2   Yale University, New Haven, United States

Tissue-engineered vascular grafts (TEVGs) offer a promising alternative to traditional synthetic materials, especially in congenital heart disease applications where growth potential is of increased importance. While studies of TEVG use in Fontan patients have demonstrated their effectiveness, the growth and remodeling (GR) of TEVGs from a cell-seeded scaffold to a neovessel is not fully understood and TEVGs have been shown to develop stenosis, necessitating clinical intervention. Previous studies have proposed 3D fluid-solid-growth (FSG) frameworks for predicting vascular GR, but have been primarily formulated for axisymmetrical, thin-walled vessels, which limits their applicability to TEVGs.[1] In this study, we propose a subject-specific 3D FSG framework for thick-walled, non-axisymmetrical vessels that simulates the evolution of TEVG morphology and hemodynamics in an ovine model.

Our framework employs a handshake between 3D fluid-solid interaction (FSI) hemodynamic simulations and simulations of GR at geometrical control points on the lumen and outer surface of the vessel of interest, $x_i \in \Omega$. These control points are parameterized in terms of vessel abscissa s_i, angular position θ_i, radius $R_i(\tau)$, and thickness $h_i(\tau)$ where τ is time post-implantation. Tetrahedral meshes of the vessel lumen and wall are created from control points using previously defined methods.[2] We then run a hemodynamic simulation of the model using the SimVascular Arbitrary Lagrangian-Eularian solver, svFSI.

After the hemodynamic simulation converges, we query the wall shear stress and pressure at the control point locations, $x_i(\tau)$, and use the constrained mixture-model of GR to calculate local changes in $R_i(\tau)$ and $h_i(\tau)$. This model of TEVG GR is driven by immuno- and mechano-mediated processes which mimic interstitial neotissue deposition during the initial foreign body response that gives way to mechano-mediated neotissue removal as the graft scaffold degrades.[3] From these GR results, $x_i(\tau)$ is updated to create a new vessel geometry. This handshaking procedure is continued, alternating FSI and GR simulations, over a total timeframe of 6 months.

Using this framework, we captured key features of TEVG GR including stenosis formation and resolution. We observed that the mechano-mediated responses alone do not capture the clinically-observed curvilinear asymmetry of stenosis, implying this asymmetry is primarily mediated through an asymmetric immune response. We showed that varying the gain of the transient immune response, which is hypothesized to be asymmetric due to varying rates of endothelization along the graft abscissa, can capture trends in ovine TEVG GR and demonstrate clinically relevant pressure gradients and wall shear stresses. With additional parameter finding and optimization, this work could hold relevance for human patients and further our understanding of how TEVGs can be used to replace traditional graft materials.

References:
1   Figuero, A. (Comput Method Appl M, 2009)
2   Updegrove, A. (Ann Biomed. Eng, 2016)
3   Drews, J. (Sci Transl Med, 2020)

226

E-08
Imaging and visualization 5: Computational challenges in analyzing pediatric musculoskeletal medical imaging

CMBBE 2021
Abstract book

E8.1
Current concepts in pediatric computational anatomy: a medical imaging perspective

Bhushan Borotikar[1]

1   Symbiosis International University, Symbiosis Centre for Medical Image Analysis, Pune, India

Pediatric disorders are on the rise worldwide, partially due to advances in the diagnostic medical technology coupled with outreach and health awareness projects run by organizations like WHO. Among these, neuromusculoskeletal disorders are a common cause of disability, pain, and reduced quality of life. Medical imaging has played a crucial role in the management of these disorders in terms of diagnosis, surgical planning, clinical decision making, and optimal rehabilitation treatment. However, pediatric anatomy, by virtue of its growth potential leading to high temporal variability in its structure, poses multiple challenges in the use of medical imaging. These challenges are faced in all the three sub-domains of medical imaging which are image acquisition, analysis, and synthesis. For example, preclusion of follow-up image acquisition to reduce exposure to ionizing radiation, or image registration problems due to structural growth while performing pre-post treatment comparisons, or scarcity of imaging databases to build deep learning-based algorithms for image analysis (outlier detection) or image synthesis (MRI to synthetic CT).

Computational anatomy is an emerging discipline that derives inferences from a multi-domain interface of geometry, statistics, and medicine and aims at analyzing and modeling the biological variability of organs' shapes at the population level. This discipline includes mathematical algorithms from computer vision and pattern theory, partial differential equations, statistical and manifold spaces, and statistical field theories to compare, pool, and average anatomical data across populations. Such mathematical representation and manipulation of a biological object (human anatomy) is possible based on two simple, yet powerful rules found in nature: 1) nature is organized by symmetry, and 2) nature is organized by scale. Computational anatomical models have been routinely used by healthcare professionals and have been recognized as powerful tools at the hands of clinicians and surgeons to assist them in decision-making.

When building computational models for pediatric applications using medical imaging datasets, the above-mentioned challenges have proven to be non-trivial. The ultimate goal of computational anatomy is to model the mean anatomy, its normal variation, its motion/evolution, and to discover morphological differences between normal and pathological groups. Current computational anatomy models are built on the assumptions of shape homogeneity and use available deformations to model displacement fields. However, simply encoding deformations with a vector space of displacement fields is not sufficient in pediatric datasets. To preserve and analyze the topological space correctly, one needs to model diffeomorphic transformations as well as cater to temporal topological changes that may be non-homogeneous with the starting shape.

In this speech, I will cover recent advances in medical image processing and synthesis that leverage emerging concepts of computational anatomy and how it can be applied to understand the pathomechanics of pediatric musculoskeletal disorders such as Duchenne muscular dystrophy or Cerebral Palsy.

E8.2

Novel approaches to skeletal maturation assessment through modern medical imaging

Dana Duren[1]

1   *University of Missouri, Department of Orthopaedic Surgery, Columbia, MO, United States*

The assessment of skeletal maturation has been a staple in human biology and clinical tracking of pediatric growth and development for over a century. Skeletal maturation assessment provides a window into the biology of a child to determine if they are growing and developing on track with respect to their age-matched peers or it they are experiencing a systematic delay or acceleration in maturation, thus influencing the amount of growth potential remaining. Methodology for the assessment of skeletal maturation ranges from atlas methods (matching a patient's radiograph to a set of standards; Greulich-Pyle) to evaluation of a single bone (Risser sign) to complex evaluation of maturity indicators in a group of bones (Tanner-Whitehouse, Fels Hand-Wrist, RWT Knee Method). Each method has its place in research and clinical practice according to needs and situations, but all rely on the plain radiograph. Over time there has become a desire to assess maturation using other imaging modalities. These offer great promise to the field, with some reducing the patients' exposure to ionizing radiation, some eliminating a step and thus reducing the financial burden of treatment. Extending the assessment of maturation to these other modalities also carries new challenges, primarily the creation of new standards and the adoption of those standards by clinicians. The most attractive aspect of new imaging for skeletal maturation assessment is the ability to develop new quantitative methods that maximize the amount and quality of captured morphology associated with maturation (and distinguishing it from the process of growth). Efforts to date with DXA, MRI, and CT have been promising but have yet to yield the precision and adoption standards of the historic techniques. The potential of these and other applications to revolutionize skeletal maturation assessment relies on biologists and engineers working together to devise the most efficient (therefore readily adoptable) and informative mode of determining maturity.

E8.3

Opportunities and challenges in computational modelling of the pediatric knee

Trent Guess[1]

1   University of Missouri, Columbia, United States

Musculoskeletal knee injury and subsequent surgical treatment is increasing in pediatric and adolescent populations (1, 2). Children who incur these injuries, particularly patellofemoral dislocation and anterior cruciate ligament (ACL) tears, are vulnerable to early-onset osteoarthritis and chronic musculoskeletal impairment through their lifetime (3, 4). Improved morphological and biomechanical information of the pediatric knee (Fig. 1) would enhance the evaluation, diagnosis, and treatment of pediatric sport injury and musculoskeletal disease. Computational modeling can provide insight into knee biomechanics and loading on musculoskeletal tissue during movement. But, the pediatric knee cannot be treated as just a smaller version of an adult knee and there are important differences that should be considered when analyzing knee biomechanics and tissue response. Knee morphology changes during maturation and growth, altering bone shape and ligament origin and insertions sites. Biomechanics in the same individual will change with growth and bone age should be a consideration. Although changing morphology provides a challenge, knee morphology can be determined through medical imaging. A greater challenge for computational analysis of the pediatric knee lies in a lack of information on tissue properties. Material properties used in computational models of the adult knee are often derived experimentally from cadaveric testing, typically from older specimens, and from animal tissue. Medical imaging may provide a means for non-invasive characterization of tissue deformation which could then be used to extrapolate bone age tissue properties from animal and cadaveric specimens. Ligaments and tendons are viscoelastic and this property varies with age. Characterizing the strain rate response of developing ligaments may be important for analyzing injury biomechanics, which can involve high strain rates. Pediatric knees have greater laxity than adult knees. The length at which ligament bundles start to carry force, the zero-load length, can have a large influence on menisci and ligament loading and cartilage contact location during movement. With respect to whole joint mechanics, the zero-load length may be more significant than ligament stiffness properties. Information on pediatric multidirectional knee laxity is scarce and ligament bundle zero-load lengths for an individual are particularly difficult to determine. In the developing knee, the influence of the physis on knee biomechanics should be included. A physis that has not reached full calcification creates a deformable region in the bone that can affect knee tissue loading as well as energy absorption during landing. Like other knee tissues, there is a paucity if information on physis material properties during growth. Finally, anatomical differences in children may influence the prediction of joint center locations as well as muscle anatomy used in gait analyses and movement simulations. For example, linear scaling of adult bone length and adult hip regression equations may not be appropriate for pediatric populations.
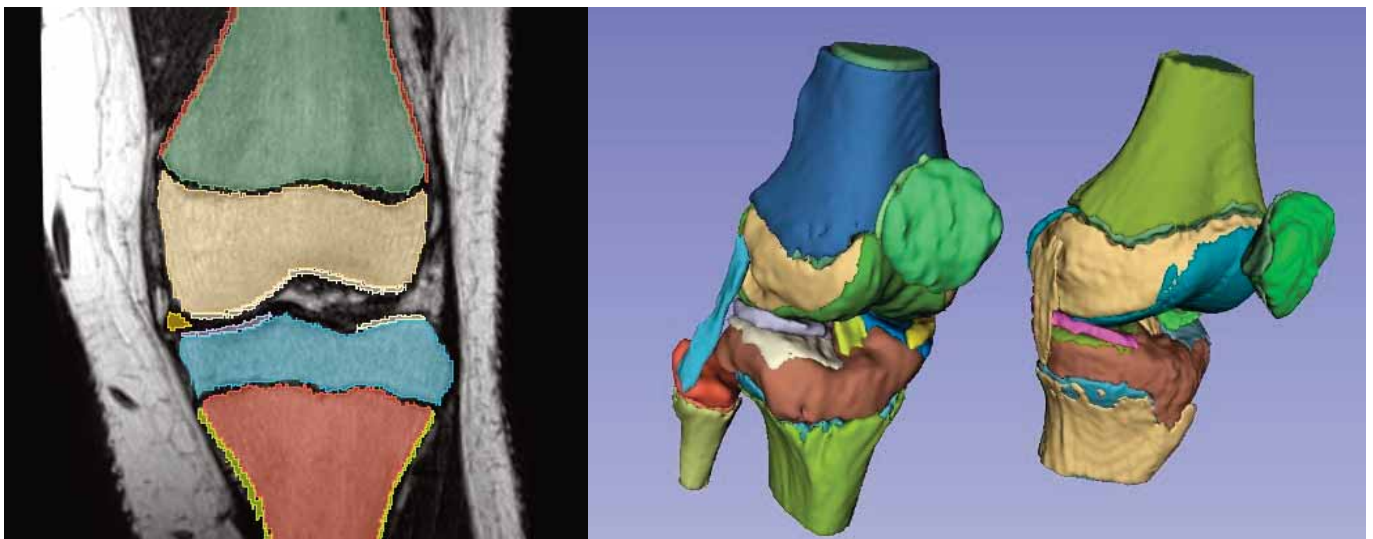
References: **1.** Fabricant, and Kocher (2016), Orthop Clin North Am, **2.** Arshi, et al (2016), Orthop J Sports Med, **3.** Clark et al (2017), Bone Joint J., **4.** Mansson, et al (2015), Am J Sports Med.

E9.1
Deep learning for CT metal artifact reduction

Chuang Niu[1], Ge Wang[1]

1   Rensselaer Polytechnic Institute, BME, Troy, United States

Metal artifact reduction (MAR) is a long-standing problem in the CT field, without a clinically satisfactory solution in challenging cases. Over the past decades [1], many methods were proposed for MAR, including projection data correction [2], iterative reconstruction [3], and image post-processing [4]. Recently, deep learning MAR techniques achieved promising results. However, there are several issues in this area. First, massive labeled data are required for training deep neural networks, while little ground truth data are available for metal artifact-affected images. Second, the current deep learning methods still need to be further improved in image quality and rigorously evaluated to reflect the performance in real scenarios. To address these challenges, here we develop a systematic deep solution that is innovative in three aspects: large-scale realistic simulation, dual-domain learning, and comprehensive evaluation. Specifically, we use CatSim [5] to simulate a large number of artifact-affected data based on the corresponding ground-truth. Empowered by this large-scale dataset, a new dual-domain learning scheme is proposed aided by visual transformer [6]. Finally, comprehensive evaluation is performed on both simulated data and real clinical images. The experimental results demonstrate that our proposed method can effectively reduce metal artifacts and improve the image quality and clinical performance.
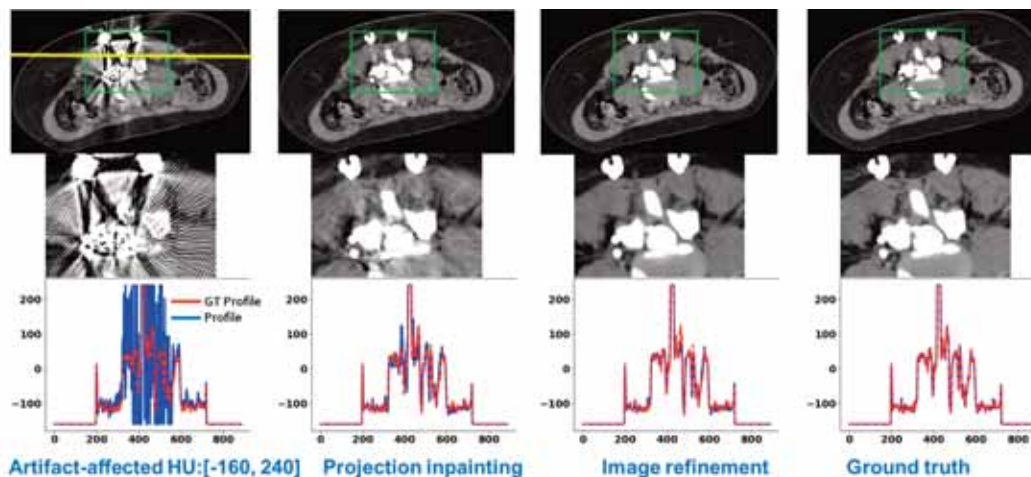
Figure caption: Metal artifact reduction results. In the first row, the images from left to right represent the original image with metal artifacts, the reconstructed images after projection inpainting, the final result after refinement, and the ground truth, respectively. The second row shows the zoomed-in ROIs corresponding to the green bounding boxes in the first row. The third row plots the profiles along the yellow line.

References:
[1]   L. Gjesteby et al., "Metal Artifact Reduction in CT: Where Are We After Four Decades?" in IEEE Access, vol. 4, pp. 5826-5849, 2016.
[2]   Verburg JM, Seco J. CT metal artifact reduction method correcting for beam hardening and missing projections. Phys Med Biol. 57(9):2803-18, 2012.
[3]   H. Zhang, B. Dong, and B. Liu. "A reweighted joint spatial-radon domain ct image reconstruction model for metal artifact reduction." SIAM J. Imaging Sciences, 11:707–733, 2018.
[4]   H. Liao, W. -A. Lin, S. K. Zhou and J. Luo, "ADN: Artifact Disentanglement Network for Unsupervised Metal Artifact Reduction," in IEEE Transactions on Medical Imaging, vol. 39, no. 3, pp. 634-643, March 2020.
[5]   Bruno De Man, et al., "CatSim: a new computer assisted tomography simulation environment," Proc. SPIE 6510, Medical Imaging 2007.
[6]   A. Dosovitskiy et al., "An Image is Worth 16x16 Words: Transformers for Image Recognition at Scale", ICLR 2021.

E9.2
Recent advances in deep learning for CT imaging

Yi Zhang[1]

[1]   *Sichuan University, College of Computer Science, China*

In this talk, we will briefly introduce recent advances in deep learning for medical imaging in the deep imaging group (DIG) of Sichuan University, China. The main content covers several interesting topics, including semi- or weak- supervised learning for medical imaging, graph network for image reconstruction. Hopefully, we can share some experience in this field with our colleagues.

E9.3

Learning-based reconstruction algorithm of radially sampled interventional MRI

Zhao He[1], Ya-Nan Zhu[2], Xiaoqun Zhang[2], **Yuan Feng**[1]

1   Shanghai Jiao Tong University, School of Biomedical Engineering, Shanghai, China
2   Shanghai Jiao Tong University, School of Mathematical Sicences, Shanghai, China

Interventional MRI (i-MRI) is crucial for MR image-guided therapy. However, most of the current reconstruction algorithms designed for fast MR imaging are for dynamic image reconstruction, which may not be suitable for i-MRI. To achieve reconstruction of fast imaging the non-cyclic motion from i-MRI, we addressed this problem by using learning-based algorithms and a golden-angle radial sampling. First, we proposed a feature-based convolutional neural network (FbCNN) to reconstruction images. The method includes two steps: reconstruction of the interventional feature, and feature refinement and post-processing. We showed with only 5 radially sampled spoke, the interventional feature could be reconstructed. Another way is to use a low-rank and sparsity (LS) decomposition algorithm with framelet transform to reconstruct the interventional feature with a high temporal resolution. Different from the existing LS based algorithm, we utilized the spatial sparsity of both the low-rank and sparsity components. We proposed a Low-rank and Spares decomposition with a primal dual Fixed Point (LSFP) method for optimization of the objective function to avoid solving sub-problems. Gelatin and brain phantoms experiments showed with only 10 radial spokes, we could achieve a temporal resolution of 60 ms.
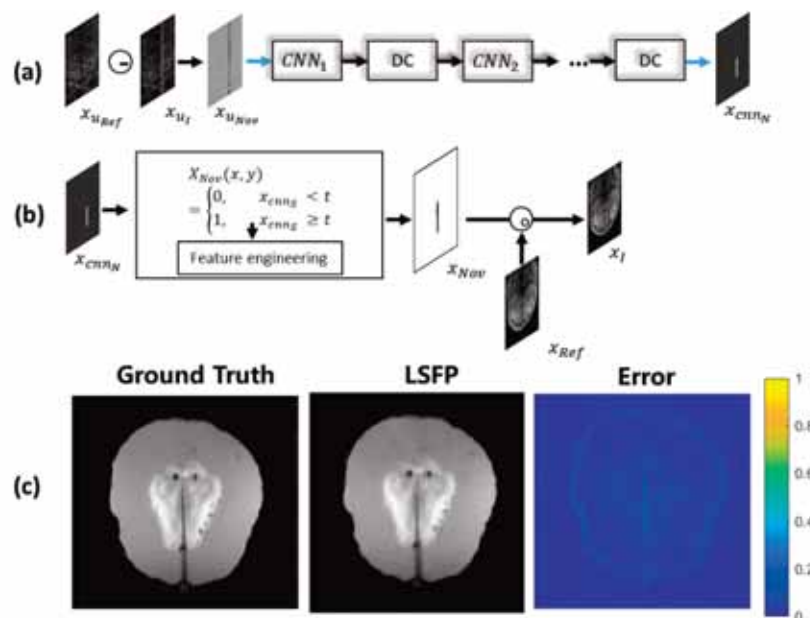
Figure caption: (a) The first stage of FbCNN is the reconstruction of interventional feature, $x_{(\llbracket cnn \rrbracket \_ N)}$. (b) The second stage of FbCNN is feature engineering to refine the shape of the interventional feature. (c) Reconstruction results and error map based on LSFP algorithm.

References:

Hernando D, Haldar J, Ying L, King K, Xu D, Liang Z-P. Interventional MRI with sparse sampling: an application of compressed sensing. Proceedings 16th Scientific Meeting, International Society for Magnetic Resonance in Medicine; 2008; Toronto.

Schlemper J, Caballero J, Hajnal JV, Price AN, Rueckert D. A Deep Cascade of Convolutional Neural Networks for Dynamic MR Image Reconstruction. IEEE T Med Imaging. 2018;37(2):491-503.

Feng L, Grim R, Block KT et al. Golden-angle radial sparse parallel MRI: Combination of compressed sensing, parallel imaging, and golden-angle radial sampling for fast and flexible dynamic volumetric MRI. Magn Reson Med. 2014;72(3):707-717.

E9.4

Impact of automatic versus manual calibration reference segmentation on CT-based finite element analyses

Ashley Pernsteiner[1], Carla Winsor[1], Perry J. Pickhardt[2], Corinne R. Henak[1], Heidi-Lynn Ploeg[3]

1   University of Wisconsin - Madison , Mechanical Engineering, Madison, United States
2   University of Wisconsin - Madison , Radiology, Madison, United States
3   Queen's University, Mechanical and Materials Engineering, Kingston, Canada

CT scanning a densitometric reference facilitates the derivation of a density calibration equation relating the segmented reference's mean CT Number [HU] to its physical density [mg/cc]. Young's modulus is an exponential function of ash density, which can be linearly related to radiological density[1] Therefore, calibration equation variations may cause exponential variations in calculations based on Young's modulus like femoral strength (FS)[1], In addition to CT scan acquisition and post-processing details, calibration equation variations can be introduced by using different segmentation methods. Manual segmentation results from Mimics v.23 (Materialise, Leuven, BEL) and 3D Slicer v.4.10.2 (3D Slicer, Boston, MA) were compared with machine learning automated segmentation results created in Dragonfly v.2020.1 (ORS, Montreal CAN). CT scans of four densitometric references submerged in water were segmented in each software (Fig.1.A). After deriving calibration equations (Fig.1.D), each equation was retrospectively applied to five patients scanned at University of Wisconsin-Madison hospital on a GE LightSpeed series CT scanner at 120 [kVP] and variable current, reconstructed with a Standard kernel. Intra-patient BMD and FS results were visually similar across patients (Fig.1.B,E). Using paired t-tests(α=0.01), significant differences were found between Dragonfly-Mimics and Dragonfly-Slicer. There were no significant differences in BMD between Mimics-Slicer. Therefore, calibration equations derived from Dragonfly may produce different BMD results and that methodological refinement and a larger sample size for may be required in future analysis. There were no significant differences between FS results between Dragonfly-Mimics, Dragonfly-Slicer, and Mimics-Slicer (Fig.1.C,E). Automated segmentation produced higher FS calculations than manual segmentation for all patients. This suggests that the machine learning automated segmentation is a promising method but was not equivalent to manual segmentation for calculation of clinical measures of bone health BMD and FS.

Software	Calibration Equation
Dragonfly (D)	y[HU]=1.12*x[mg/cc]-1.36
Mimics (M)	y[HU]=1.12*x[mg/cc]+7.82
Slicer (S)	y[HU]=1.10*x[mg/cc]+11.7

	1	2	3	4	5
BMD [mg/cm³]	0.290, 0.281, 0.280	0.364, 0.354, 0.353	0.347. 0.338, 0.338	0.197, 0.190, 0.188	0.304, 0.295, 0.294
FS [N]	1990, 1870, 1830	1630, 1520, 1510	1150, 1100, 1090	715, 682, 674	949, 930, 935
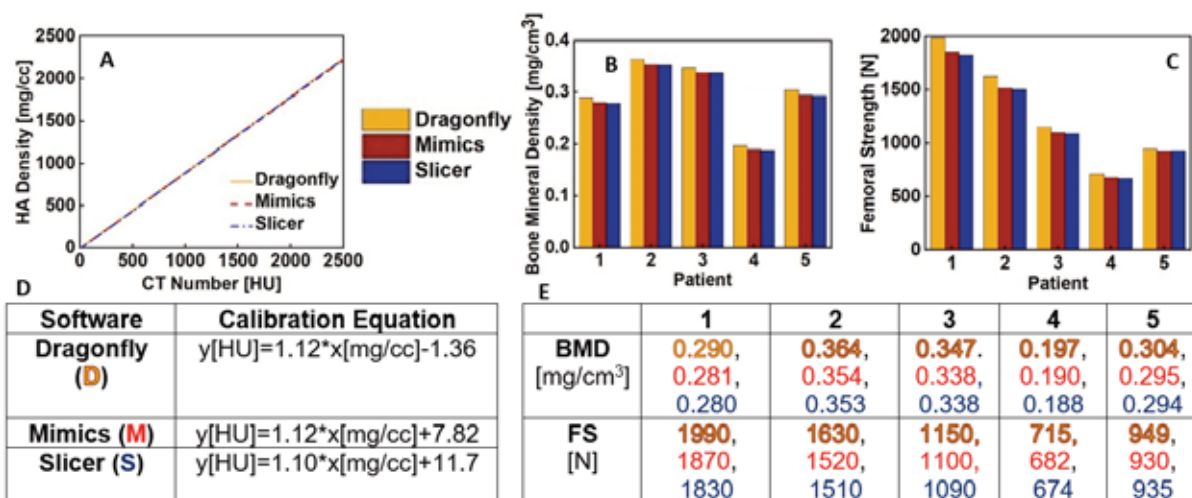
Figure caption: (A) Overlaid calibration equations for a phantom scanned in water for three segmentation software packages. (B) BMD [mg/cc3] results calculated using data for five patients (C) Patient-specific FS[N] using a principal strain failure criterion of 0.73%(tension) and 1.04%(compression). (D) Calibration equations tabulated for each segmentation software. (E) BMD and FS calculations for each patient for each calibration equation.

References:
[1]   Winsor C et al. Bone. 2021;143(July 2020). doi:10.1016/j.bone.2020.115759

E9.5

Quantitative classification of calcifications in diseased tissues

Mehdi Ramezanpour[1], Yasutaka Tobe[1 2], Juan Cebral[3 4], Spandan Maiti[1 2 5], Anne Robertson[1 2]

1   University of Pittsburgh, PA, USA, Department of Mechanical Engineering, Pittsburgh, United States
2   University of Pittsburgh, PA, USA, Department of Bioengineering Engineering, Pittsburgh, United States
3   George Mason University, Fairfax, Virginia, USA, Department of Bioengineering, Virginia, United States
4   George Mason University, Fairfax, Virginia, USA, Department of Mechanical Engineering, Virginia, United States
5   University of Pittsburgh, PA, USA, Department of Chemical Engineering, Pittsburgh, United States

Arterial calcifications are linked to adverse cardiovascular events [1]. Studies have revealed the importance of calcification in the mechanical stability of diseased tissues, including plaques in arterial stenosis and cerebral aneurysms [2, 3, 4]. Understanding the diverse role of calcification in tissue failure requires the classification of calcification based on its association with lipid pools (atherosclerotic or non-atherosclerotic) [3, 4]. The current methods of performing such a classification are highly laborious and time-consuming. Here, we present novel algorithms that enable the semi-automatic classification of calcification within stacks of thousands of 2D images obtained from micro-CT analysis, reducing the classification time from days to hours.

The 3D reconstruction of the tissue (entire domain) and the subdomains including the calcification, and lipid pools are required to perform the aforementioned classification. To this end, the calcifications and the tissue regions were first segmented out from the micro-CT images by filtration, while that of the lipid pool is performed using an efficient supervised machine learning model. After completing the segmentations, the 3D reconstructions were created using the Alpha Shape algorithm. By determining the intersection of calcifications and lipid pool volumes, the fraction of atherosclerotic calcification versus non-atherosclerotic calcification was calculated.

Figure 1 shows an example application of this pipeline on an intracranial aneurysm specimen. For this case, the machine learning model was trained on 30 hand-labeled images and then tested on 300 manually segmented images (selected randomly). A volume fraction of 79.6% of calcifications are located inside the lipid pool; and therefore classified as atherosclerotic. The lipid was found to lie closer to the abluminal side of the wall. The 3D patient-specific reconstruction was used to create a finite element model of this tissue specimen, including lipid pool and calcifications.

Novel algorithms were developed to classify tissues based on the co-localization of calcification and lipid pool. The proposed pipeline enables segmentation of tissue, lipid pools and calcifications in micro-CT images in a semi-automatic manner for a 3D domain reconstruction for the first time. Such a tool makes it feasible to perform comprehensive analyses on impact of calcifications type, for example, in promoting tissue rupture [4].
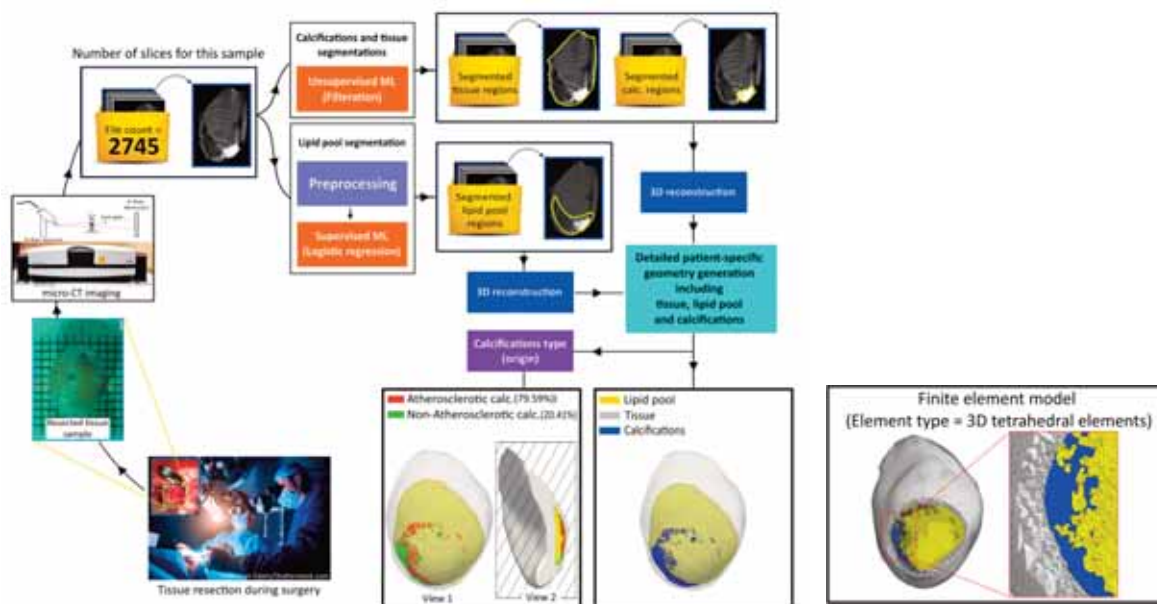
Figure caption: Figure 1. Illustration of different steps in the proposed pipeline for the classification of tissues based on their calcification characteristics.

References:
[1]   J. L. Ruiz et al., J Physiol, vol. 594, no. 11, pp. 2915-2927, 2016.
[2]   J. D. Hutcheson et al., Nat Mater, vol. 15, no. 3, pp. 335-43, Mar 2016.
[3]   P. S. Gade et al., ATVB, vol. 39, no. 10, pp. 2157-2167, 2019,
[4]   R. N. Fortunato et al., Experimental Mechanics, vol. 61, no. 1, pp. 5-18, 2021/01/01 2021.

E10.1
A novel method for quantitative and statistical comparison of local differences in bone morphometry

Sebastian Bachmann[1], *Synek Alexander*[1], *Dieter Pahr*[1 2]

1   TU Wien, Institute for Lightweight Design and Structural Biomechanics, Vienna, Austria
2   Karl Landsteiner University of Health Sciences, Department of Anatomy and Biomechanics, Division Biomechanics, Krems, Austria

Bone can adapt its inner structure, for example, due to changes in external loadings, aging, or diseases. The inner structure can be quantified using CT-based morphometry. Comparisons are typically performed in regions of interest (ROI). Another method is holistic bone morphometry analysis (HMA) [1], which maps such quantities onto finite element (FE) meshes of whole bones. However, HMA lacked a method of quantifying differences across individuals in homologous regions.

In this study, we present an extension of HMA using statistical deformation models (SDM) [2]: (1) a canonical bone image is created using SDM, (2) all bone images are registered onto the canonical bone, (3) the mesh is created on the canonical bone, and (4) the mesh is transformed back onto the individual bones. Finally, morphometric evaluations and statistical analysis can be performed per element across all individuals. As a proof of concept, the method was applied to 18 HR-pQCT scanned cadaveric left distal radii from a previous study [3]. Lengths were normalized by using 1.5 times the maximal width, as total limb length was not available. BVTV was evaluated by sex (Female n=8, Male n=10) and two equally sized age groups (Group I: 76-97, Group II: 54-75). The BVTV differences (Female-Male and age group I-II) were calculated per element and two-sample t-tests with permutation tests for family-wise error (FWER) control were used to evaluate the statistical significance ($\alpha=0.05$).

Age-related bone loss, as well as sex-related differences, could be observed. 10% of the elements containing the largest differences were visualized. However, no elements were significant for age, and only 54 of 50724 elements remained significant for sex.

These preliminary results show that the improved HMA method can display and analyze the spatial distribution of differences between age groups and sexes using a canonical bone as a common basis without additional image annotation such as landmarks or ROIs. In the future, the method can be applied to other bones and larger datasets to reveal significant local differences in morphometry between sex and age but also to reveal local effects of pathologies and treatments. Furthermore, it could be used for fast creation of topologically consistent meshes as a basis for FE analysis.
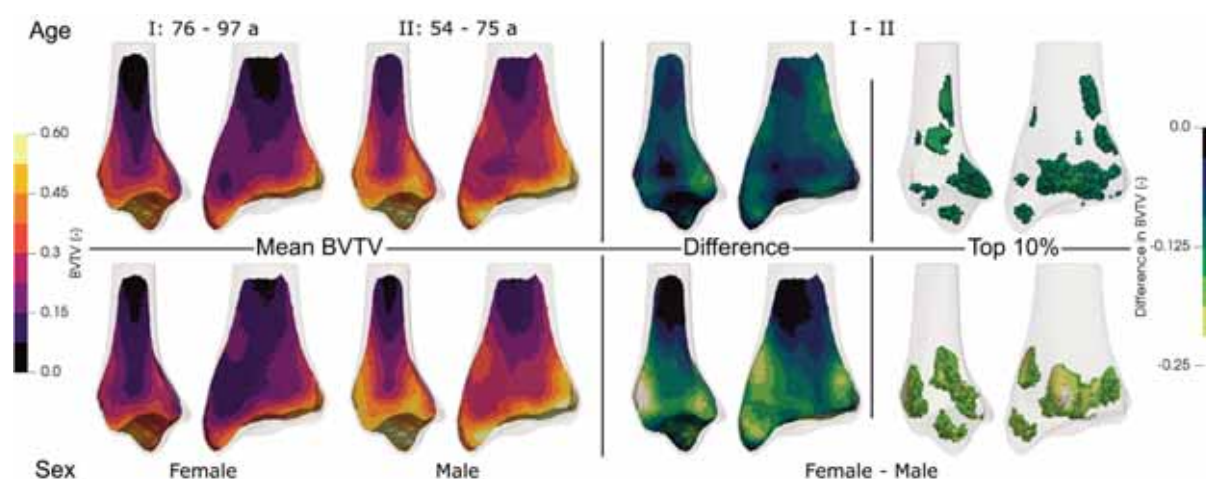
Figure caption: Mean BVTV maps for age groups (top row) and sex (bottom row), difference plots, and thresholded elements showing 10% of the bone volume with the largest differences.

References:
[1]   Gross, T. et al. Palaeontologia Electronica (2014)
[2]   Rueckert, D. et al. IEEE Transactions on Medical Imaging 22, 1014–1025 (2003)
[3]   Synek, A. et al. Journal of Biomechanics 48, 4116–4123 (2015)

E10.2

Feasibility of supervised machine learning for identification of plates and rods in human trabecular bone

Annika vom Scheidt[1], Vera Schulz[2], Marcel Bengs[3], Schlaefer Alexander[3], Björn Busse[2]

1   Medical University of Graz, Gottfried Schatz Research Center, Department of Macroscopic and Clinical Anatomy, Graz, Austria
2   University Medical Center Hamburg-Eppendorf, Department of Osteology and Biomechanics, Hamburg, Germany
3   Hamburg University of Technology, Institute of Medical Technology and Intelligent Systems, Hamburg, Germany

Introduction: Over 200 million people are estimated to be at high risk for bone fracture from osteoporosis worldwide [1]. Fracture risk is determined by bone mass but also by bone microstructure, which can rarely be assessed clinically. Microstructural changes in cortical and trabecular bone drive bone loss and fragility. The amount of trabecular rods and plates is linked to bone fracture [2]. Machine learning methods have proven their suitability for medical image analysis. Hence, we study supervised learning and a multi-class classification task to identify rods and plates in micro-CT images. Moreover, we evaluate to which extent different machine learning methods can help to assess trabecular bone microstructure.

Materials and methods: We used microCT scans of trabecular bone cores from human vertebrae from a post mortem study (obtained in accordance with local ethics guidelines) and considered both strong and deteriorated trabecular microstructure in bones from differently aged women (38, 67, 79, 81 years). We manually annotated rods and plates voxel-wise in grayscale microCT scans (MATLAB, Image Labeler) as ground truth datasets. For our conventional training pipeline, we compared different methods for feature extraction (HOG, Haralick) and classification (SVM, random forests) with varying hyperparameters. For our deep learning approach, we compared different configurations of a convolutional neural network (CNN; U-Net 3D, MATLAB) with pre-processing (binary vs. grayscale), augmentation, and varying masking and loss functions (standard vs. weighted). Dice coefficient, accuracy, sensitivity, and specificity were used as performance metrics.

Results: In pipeline comparison, feature extraction with Haralick outperformed HOG with a 30% higher dice coefficient for rods. For classifiers, SVM with a linear kernel outperformed random forest with a 63% higher dice coefficient. Overall, the identification of plates and rods using our conventional learning algorithm was sufficient for the validation data but lacking for the test data. The CNN approach labeled a higher amount of bone correctly in the test data with the best performing configuration using binary input data, weighted loss and masking.

Discussion: Both methods generated promising results with good generalization to new patient data but conventional feature extraction-based methods were clearly outperformed by the CNN architecture. Consequently, using machine learning to evaluate trabecular microstructure is feasible, preferably using 3D CNNs. As a proof of concept, our study is limited by the small input data set. Using a greater set of volumetric input data for further investigations, machine learning on 3D microCT images should allow an accurate and reproducible classification of trabecular plate-rod microarchitecture aiding the understanding of bone fragility and its treatment.

References:
[1]   Odén et al. Osteoporos Int 26:2243–2248 (2015). https://doi.org/10.1007/s00198-015-3154-6
[2]   Liu et al. JBMR 27(2):263-272, https://doi.org/10.1002/jbmr.562

E10.3
Development of a numerical analysis applied to the bones of the forearm by means of a flexural load

Daniel Maya Anaya[1], *Guillermo Urriolagoitia Sosa*[1], *Beatriz Romero Ángeles*[1], *Belén Alejandra Contreras Mendoza*[1], *Martin Ivan Correa Corona*[1], *Alfonso Trejo Ramírez*[1], *Francisco Javier Gallegos Funes*[1], *Guillermo Manuel Urriolagoitia Calderón*[1]

1   Instituto Politécnico Nacional, Sección de Estudios de Posgrado e Investigación, Ciudad de México, Mexico

The recreation of biomodels through the use of Computer Aided Design (CAD) programs, allow a different foundation for the study of mechanical behavior in bone systems in a non-invasive way. The development of these kind of models are of great importance for the development for preventive and corrective treatments, since it provides a better perspective of the affected area [1]. In this case study, the three-dimensional reconstruction of the ulna and radius bones which belong to the forearm is presented by means of a computerized axial tomography (CT) [2-3]. Applying the Scan Ip® and Power Shape® software's, from which the file obtained is exported to the Solid Works® and ANSYS® computer packages, since they are digital tools that use the Finite Element Method (FEM), with the aim of identify the area where bone injury could occur under flexion loading. The numerical analysis of the model is performed by the ANSYS® computer program. The exemplified geometry is defined by importing the bio-model generated by the Power Shape® program. For the simulation, the cortical and trabecular bone is taken into account as a solid component of both the ulna and the radius. The study considers the material behavior as linear-elastic, continuous, homogeneous and isotropic. A high-order three-dimensional solid element (20 nodes) is established, which has 6 degrees of freedom, displacement in the X, Y and Z axis and rotation in the XY, YZ and XZ planes (Figure 1). It is important to note that the proposed system will work as an embedded beam, that is, it will be restricted in all degrees of freedom in the proximal area of both bones, so that the external agent will be applied in the opposite area, that is, in the area distal, with a value of 196.2 N on the axis parallel to the cross section. Exemplifying that the forearm is in a position at 90 degrees with respect to the transverse side of the individual. For this research case, a displacement of 6.19 mm on their longitudinal axis can be observed in both bones (Figure 2) and a Von Mises stress with a magnitude of 104.4 MPa, which occurs in the proximal area of the cortical bone of the radius (Figure 3). This indicates that this portion of the bone is the most prone to injury or fracture
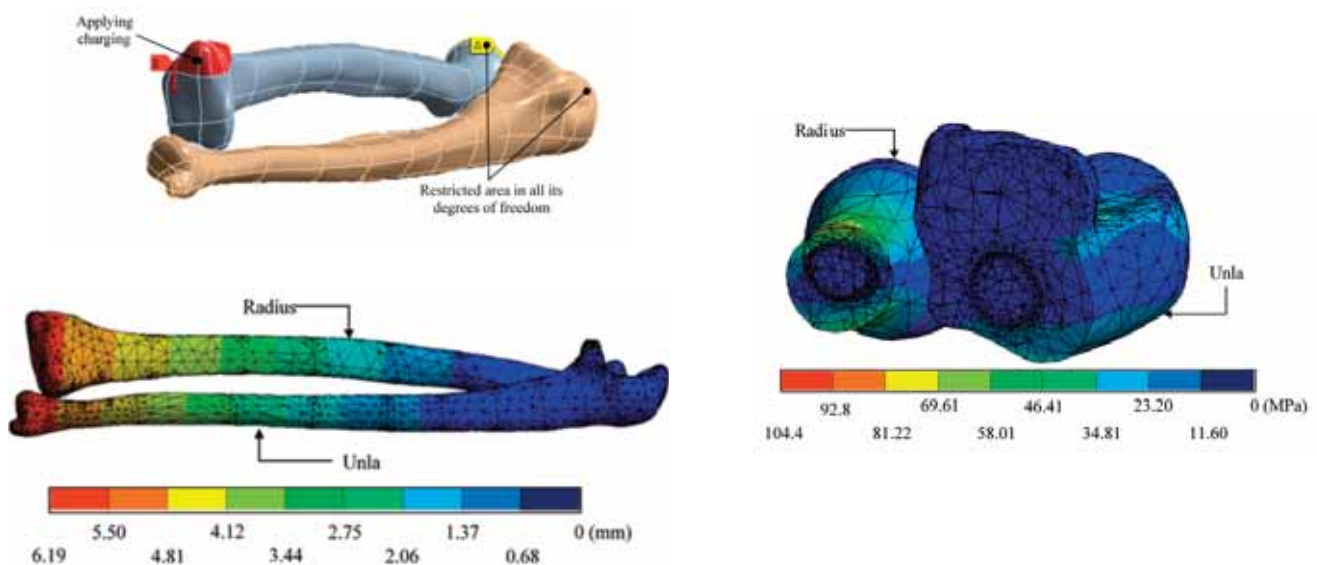
Figure 1: Application of load and restrictions to the biomodel.
Figure 2: Total displacement of both bones on the longitudinal axis.
Figure 3: Von Mises stress of the bone as a whole (corticaltrabecular), section of the proximal zone in the YZ plane.

References

1.   Bosh E. Godfrey Newbold Hounsfield: History and impact of computed tomography, Argentina's Journal of Radiology vol. 76, núm. 4, pp. 331-341, 2012.
2.   Gamarra, V. y Da Silva, F., Proposal of 3D virtual biomodeling using free software, Engineering Magazine; Science, Technology and Innovation, Vol. 1, No. 2, pp 52-59, 2014.
3.   Ramírez, V., Análisis Numérico de Fractura en Huesos Largos en Pacientes Afectados con Osteogénesis Imperfecta, Tesis Maestría, SEPI ESIME Zacatenco, Instituto Politécnico Nacional, pp 45-54, 2017.

E10.4
Radiographic changes in the vertebral column with the practice of yoga postures: a review

Sandeep Mudgal[1], *Chitra Chand*[1], *Sandeep Singh*[1], *Vinod Katiyar*[1]

1   University of Patanjali, Department of Yoga Sciences, Haridwar, India

Physical exercises and practices tend to redefine bone shape and structure at micro and possibly macro-architectural levels. Bone cells metabolism forcefully adapts to training thus resulting in the physical adaptation of bones (in terms of shape, mass and strength) (Lombardi et al., 2019). Yogic postures under Hatha Yoga are considered a good form of weight-bearing exercises. According to Haṭhayoga-pradīpikā,

<p style="text-align:center">"kuryāttadāsanaṃ sthairyamārogyaṃ cāṅgalāghavam"</p>

Above shloka is translated by Muktibodhananda (2013, p. 67) as practising the yoga asanas brings stability (steadiness) to the mind and body; improves the overall health and flexibility of the limbs. Biomedical image analysis and processing is an efficient method to observe radiographic changes in the mechanical structure of bones. Therefore, this review will put forth the critical analysis of the studies related to the effects of the practice of yoga postures on the mechanical structure of the vertebral column. This review aims to examine the existing literature on the effects of yoga postures on bone structural changes in the vertebral column where radiographic imaging is used as an assessment tool. The electronic databases namely; PubMed, Science Direct, Cochrane Library, Wiley Online Library, and Google Scholar were searched with year limit from 2011 to 2021, where both the years are included, using the keywords "yoga", "vertebral column", and "radiography". The research articles and case reports which were published in the English language were included in the review. The studies were not restricted on the basis of age, gender, ethnicity, and socioeconomic status of the participants. The studies which used surgery as an intervention, book chapters, letter-to-editor, review articles, conference proceedings, indexes were excluded. A total of 210 studies were found. After a narrowed search through applying the criteria, two articles were analysed in the review.

It was concluded that posture-based yoga may or may not have any effect on bone structure. However, due to limited studies conducted on the concerned topic, further studies with a longer duration of Yoga practice can be performed to assess the effectiveness of the Yoga postures as an adjunctive treatment for a clinical and/or healthy population.
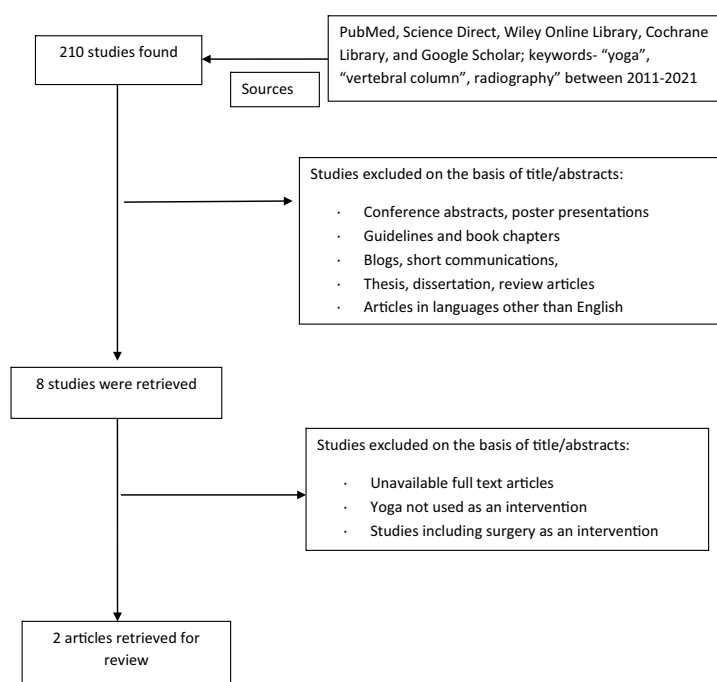
Figure caption (Figure 1): Flow Chart Depicting the Selection of Studies Included in the Review

References:
Lombardi, G., Ziemann, E., & Banfi, G. (2019). Physical Activity and Bone Health: What Is the Role of Immune System? A Narrative Review of the Third Way. Frontiers in Endocrinology, 10, 1. https://doi.org/10.3389/fendo.2019.00060
Muktibodhananda, S. (2013). Hatha Yoga Pradipika (3rd ed.). Bihar School of Yoga. ISBN: 978-8-18-578738-1

E10.5
Comparison of male and female pelvic symmetry and shape

Robyn de Wet[1], Maha Ead[1], Jacob Jaremko[2], Lindsey Westover[1], Kajsa Duke[1]

1   University of Alberta, Mechanical Engineering, Edmonton, Canada
2   University of Alberta, Radiology and Diagnostic Imaging, Edmonton, Canada

Introduction: When a pelvis is fractured and reconstruction is required, understanding pelvic symmetry and average shape is helpful. Symmetry allows for pelvic reconstruction of one half to be modelled after the other intact half [1]. Average pelvic shape helps to reconstruct pelvises with bilateral fractures [2]. Since the female pelvis must support both bipedal locomotion and childbirth, it faces more morphological constraints than the male pelvis [3]. This study investigates the differences in male and female symmetry and shape to test whether pelvic morphology is sex-based.

Objectives:
-   Evaluate pelvic symmetry of males and females
-   Categorize and compare male and female pelvic shape

Methods: Symmetry Analysis: CT scans of n=40 intact pelvises (20 male and 20 female) were converted to 3D models using Materialise-Mimics. Pelvic symmetry was determined by importing the models into Geomagic and using the 3D deviation analysis function, where the reference subject was the original pelvis, and the test subject was a reflected version of the same pelvis. Symmetry reports were created, including root mean squared (RMS) error, percentage of points between ±2mm deviation, and deviation colour maps (figures a and b).

Shape Classification: The models were oriented by creating a plane in each pelvis using common anatomical landmarks and aligning it with the global XY plane. The transverse diameter (TD) and anteroposterior diameter (APD) were determined by setting landmarks and measuring the distances between them. Classifications were made using Relationship Value and Pelvic Brim Index methods. The shape categories were anthropoid, gynecoid, android, and platypelloid [3, 4].

Results: The average RMS value for the female and male pelvises was 2.03 and 1.94, respectively. The average percentage of points between ±2mm deviation for females and males was 72.1 and 74.2, respectively. Females were categorized as 85% android, 10% gynecoid, and 5% platypelloid. Males were categorized as 45% android, 30% gynecoid, 20% platypelloid, and 5% anthropoid. Males showed more variability in PBI, ReV, and overall shape.

Conclusion: Symmetry was good overall and was similar between males and females. Both genders had the most pelvises in the android category, but males had more shape variability. Results suggest that both genders are likely to have a similar pelvic shape, but females have less variability, which is possibly related to the added morphological constraints of the female pelvis.
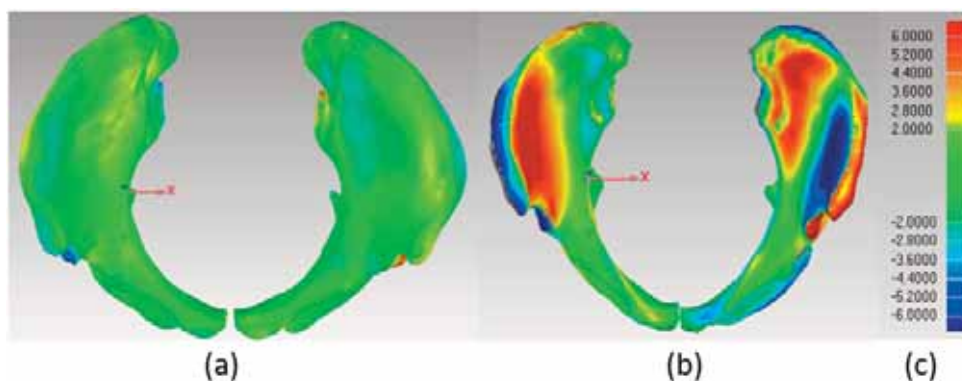
Figure caption: DCM of good symmetry (a), bad symmetry (b), and symmetry deviation range (mm) (c)

References:
[1]   M.S. Ead et al, 2020, MBEC, vol.58, no.1.
[2]   M.S. Ead et al, 2021, MRCAS, vol.17, iss.2.
[3]   H. Delprete, 2017, The Anatomical Record, vol.300, no.4.
[4]   W.E. Caldwell and H.C. Moloy, 1938, PRSM, vol.33, no.1.

PS1.1

Deep-learning for reconstructing automatically the 3D vertebral anatomy of scoliosis patients and healthy volunteers from MRI

Maria Antico[1], Amirebrahim Rezaeian[1], Paige J. Little[1], Hardy Jennings[1], Geoff Askin[1], Robert Labrom[1], Davide Fontanarosa[1], Peter Pivonka[1]

1   Queensland University of Technology, Australia

Adolescent Idiopathic Scoliosis (AIS) is a multi-dimensional deformity of the spine found in 2-3% of adolescents. 3D morphologically accurate reconstructions (i.e. segmentation) of the pathological spine are valuable both clinically for patient treatment planning and for biomechanical investigations to simulate patient-specific mechanical function. However, this pathology is typically assessed using X-ray-based methods limited to either a 2D visualization or a 3D model of the spine based on generic shape-fitting[1] and hence not fully representative of the patient-specific anatomy. MRI imaging can be considered a safe (radiation-free) and accurate modality for reconstructing 3-dimensionally the spinal anatomy, but it is presently unused for this purpose since it requires generating time-intensive manual segmentations.

Herein, we propose to solve this drawback by implementing a fully automatic method for segmenting both the vertebral body and posterior elements of AIS and healthy volunteers from MRI. A state-of-the-art deep learning network[2] was trained using a data-efficient method requiring limited labelled examples of the vertebral anatomy, including the apical vertebra (i.e. most deviated laterally from the central sacral line) and/or a lower thoracic level vertebra (e.g. T11 or T12) and adopting ad-hoc data augmentation to represent the unlabeled vertebral levels in the dataset. The major thoracic curve (T5-T12) was then reconstructed (Figure 1) at test-time by feeding to the network the image patches generated by translating a window of fixed size and stride onto the MRI volume and combining the resulting segmentations. The method implemented was tested on 63 MRI scans acquired at different time points from 25 AIS and 3 healthy volunteers using a 5-fold cross-validation and achieved a mean Dice Similarity Coefficient (DSC) comparable to the manual segmentations generated by 2 experts ($87.0\% \pm 0.9\%$ DSC).

This result indicates that the proposed algorithm can generate clinically accurate 3D reconstructions of the healthy and pathological spine, possibly leading to enhanced pathology analysis and patient-specific biomechanical simulations.
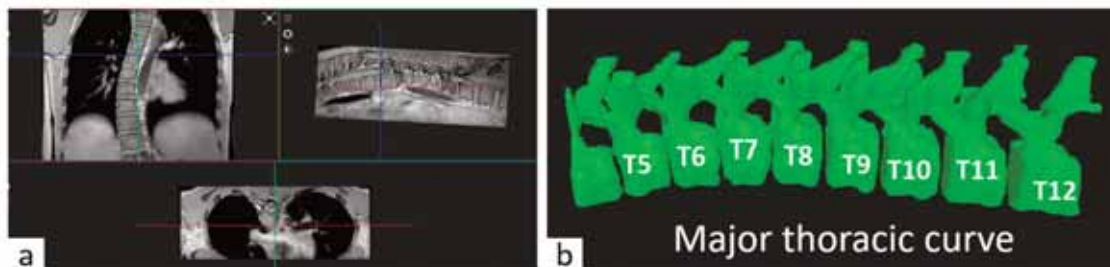
Figure 1: Example of automatic 3D image segmentation of the spine: (a) MRI image of AIS patient and (b) 3D reconstruction of major thoracic curve of the spine generated by the proposed deep-learning algorithm.

References:
[1]   E. Melhem, A. Assi, R. El Rachkidi, and I. Ghanem, "EOS® biplanar X-ray imaging: concept, developments, benefits, and limitations," Journal of Children's Orthopaedics. 2016.
[2]   O. Ronneberger, P. Fischer, and T. Brox, "U-Net: Convolutional Networks for Biomedical Image Segmentation," vol. arXiv:1505, pp. 1–8, 2015.

PS1.2
Development of a silent speech interface for augmented reality applications

Christine Walck[1], Riley Flanagan[1], Michael Fornito[2], **Tania Rivas**[1] [1]

1   Embry–Riddle Aeronautical University, Mechanical Engineering, Daytona Beach, United States
2   Embry–Riddle Aeronautical University, Department of Computer Science, Daytona Beach, United States

Silent speech interfaces using non-invasive surface electromyography (EMG) sensors have been utilized to control internet-of-things devices and provide communications in acoustically challenging environments [1, 2]. However, they have yet to be implemented into Augmented Reality (AR) displays; an area they could potentially revolutionize as a human-machine interface by offering low profile and fluid input. Current AR displays use explicit input such as hand gestures or buttons making them susceptible to privacy issues, movement restrictions, and unintentional input. For these reasons, our study focuses on the development of a silent speech interface using subvocalizations to control the AR display. Subvocalizations allow a convolution neural network to control the AR display within a multitude of environments where speech is masked from background noise or military operations requiring silence. To build the neutral network, pilot subvocalization data (i.e. muscle activations from the anterior cervical region) on a 22-year-old Caucasian male subject with no speech impairments was collected. The subject underwent 50 trials, each requiring him to subvocalize the words up, down, left, and right, in a serial sequence. To remove low and high frequency environmental noise, the data was filtered with a 2dB band pass filter at a frequency of 400Hz. Then, each word within a trial was parsed for individual subvocalizations. For example, the word right was parsed into 50 individual subvocalizations, creating a 1-D array database used to train a model for that specific word. Each database serves as an input into the convolution neural network. Preliminary results show the models are learning or being trained, to successfully recognize each word with an average classification accuracy of 82.5%. Each model is shown in Table 1. This number has the potential to be greater once the databases are further developed. Future research will provide an expansion of the training datasets to over 400 trials from a larger and more diverse subject pool (IRB 21- 117). Acquisition of additional training data through trials will reduce the variance in results, while improving classification accuracy and diversification.

Figure 1 shows the first three parses of the subvocalized word right.

Table 1 Lists accuracies for trained models.

Trained Model	Accuracy
1	66.66%
2	83.33%
3	91.66%
4	83.33%
5	91.66%
6	83.33%
7	83.33%
8	100.0%
9	66.66%
10	75.0%
MEAN	82.5%

Butter Filter - First Order (Digital Filter)
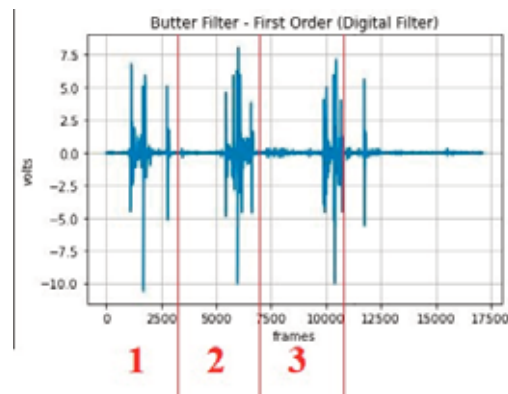
References:
[1]   E. Wadkins, "A Continuous Silent Speech Recognition System for AlterEgo, a Silent Speech Interface," 24 May 2019.
      [Online].Available:https://dspace.mit.edu/bitstream/handle/1721.1/123121/1128187233-MIT.pdf?sequence=1&isAllowed=y.
[2]   G. S. Meltzner, J. T. Heaton and Y. Deng, "The MUTE Silent Speech Recognition System," in INTERSPEECH, Burlington, 2013.

PS1.3

Effects of sampling rate and window length on hand posture recognition using an armband sensor

Jongman Kim[1], Bummo Koo[1], Yejin Nam[1], Youngho Kim[1]

1   Yonsei University, Biomedical Engineering, Wonju, Korea, Rep. of South

The pattern-recognition-based myoelectric prostheses offers amputees a natural, intuitive approach to more finely control the prostheses [1]. The purpose of the study was to investigate the effects of the sEMG-signal sampling rate and the feature extraction window length on the classification accuracy in hand-motion recognition.

Ten normal subjects and one forearm amputee were participated in this study, and a pre-developed armband sensor [2] was used to measure the sEMG signal of the right lower arm. Seven and four hand postures were performed by normal subjects and amputee, respectively. The EMG signal was measured at 500 Hz and down-sampled to 250, 100, and 50Hz. Four time-domain features (MAV, WL, ZC, SSC) were calculated as the sEMG feature vectors with six selected window lengths, which were increased in 50msec intervals (50~300msec). The feature vectors were applied to the classifiers as the single feature (MAV only) and all features (using four features; 4TD). ANN, SVM, DT and KNN were used to recognize the hand postures. In all classifier, the classification accuracy (CA) of amputee was lower than that of normal subject. As the sampling rate and the window length increased, the CA increased. ANN(4TD/500Hz/300msec) and KNN(MAV/500Hz/300msec) showed the highest CA of 96.6±5.5% and 84.2±25.7% in normal subject and amputee, respectively. However, there were no significant difference between 250~500Hz in sampling rate and 150~300msec in window length.

In this study, we attempted to confirm the effect of the sampling rate and the window length on the classification accuracy. The results for the two variables (sampling rate and window length) were similar for all classifiers considered here, and we expect similar results with other types of classifiers as well. Our results showed that for all classifiers and all subjects, the hand-motion classification accuracy increased with an increase in the sampling rate and the window length. Our findings would be helpful in selecting the appropriate sampling rate and window length for the prosthetics for daily use.

Figure caption: Classification accuracy for the normal subjects and an amputee subject

References:
[1]   Daley et al. (2012). J. Electromyogr. Kinesiol., 22(3): 478-484.
[2]   Kim et al. (2019). Int. J. Precis. Eng. Manuf., 20(11): 1997-2006.

PS1.4
Fall detection with ANN and SVM using different segmentation approaches

Bummo Koo[1], *Jongman Kim*[1], *Yejin Nam*[1], *Youngho Kim*[1]

1   Yonsei University Mirae Campus, Biomedical engineering, Weonju, Korea, Rep. of South

Falls become significant health risks of death or injury for the elderly. Fall detection algorithms were needed for minimizing the damage of falls and segmentation techniques are important to develop the fall detection algorithms. There are two segmentation techniques for the fall detection algorithms: sliding window [1] and impact-defined window [2] (Figure 1). Özdemir et al. [3] used impact-defined window to distinguish 16 ADLs and 20 falls. They showed that SVM (99.48%) was more accurate than ANN (95.68%). However, Kerdegari et al. [4] used sliding window to distinguish 9 ADLs and 11 falls. They showed ANN (90.15%) was more accurate than SVM (86.68%). The performance of algorithm depended on the subjects, motions, and classifiers, and therefore the direct comparison among studies were relatively difficult. In this study, we hypothesized and confirmed that suitable segmentation technique differs according to the classifiers (ANN and SVM).

Thirty healthy volunteers performed 9 simulated falls and 14 ADL movements. 3-axis accelerations and 3-axis angular velocities were measured using an IMU sensor attached to the middle of LASI and RASI. The commonly used feature vectors [5] with short computational times were selected (Figure 2). Data from 10 subjects were used to train the ANN and SVM classifier and data from the remaining 20 subjects were used to test the classifier. Also, SisFall dataset [6] consisting of 15 ADLs and 19 Falls from 30 subjects was used for additional test.

Table 1 showed the classification performance according to classifiers and segmentation techniques. Regarding the internal test, ANN (99.86% and 99.71%) was more accurate than SVM (99.71% and 99.42%) for all segmentation techniques. Regarding the external test, ANN (83.74%) was more accurate than SVM (81.39%) for sliding window, but SVM (96.39%) was more accurate than ANN (96.39%) for impact-defined window. For the internal test, the sliding window was more suitable with both classifiers. When the feature vector was extracted with the sliding window, more feature vectors were obtained than when the feature vector was extracted with the impact-defined window, and there were more grounds for judgment, so it was possible to detect falls more accurately. For the external test, the impact-defined window was more suitable with both classifiers, because the pattern of the data changes, but the feature points overlap.

Table 1: Classification performance

Test	Performance	Sliding window		Impact-defined window	
		ANN	SVM	ANN	SVM
Internal test	Sensitivity (%)	100.00	100.00	100.00	100.00
	Specificity (%)	99.76	99.52	99.52	99.05
	Accuracy (%)	99.86	99.71	99.71	99.42
External test	Sensitivity (%)	74.96	70.55	75.07	93.33
	Specificity (%)	92.07	91.69	95.05	99.28
	Accuracy (%)	83.74	81.39	85.32	96.39

References:
[1]   Putra et al. (2018). Sensors, 18(1): 20.
[2]   Liu et al. (2019). IEEE Sens. J., 20(6): 3303–3313.
[3]   Özdemir et al. (2016). Sensors, 16(8): 1161.
[4]   Kerdegari et al. (2012). ICIAS.
[5]   Vallabh et al. (2016). SoftCOM: 1–9.
[6]   Sucerquia et al. (2017). Sensors, 17(1): 198.

PS1.5

Hand gesture recognition for sign languages using 3DCNN for efficient detection

Taranya Elangovan[1], Arockia Xavier Annie R[1], Keerthana Sundaresan[1], **Pradhakshya JD[1]**

1   College of Engineering, Guindy, Anna University, Computer Science and Engineering, Chennai, India

Sign Language Recognition aims at providing an efficient and accurate mechanism for the recognition of hand gestures made in sign languages and converting them into text and speech. Sign language is a means of communication using bodily movements, especially using the hands and arms. With sign language recognition methods, dialog communication between the deaf and hearing society can become a reality. In this work, we carry out sign language recognition by building 3D convolutional neural network (3DCNN) models that can perform multi-class prediction on input videos containing hand gestures. On detection of the input, both text and speech are generated and presented as output to the user. In addition to this, we also implement real-time video recognition and continuous sign language recognition for multi-word videos. We present a method for recognition of words in three languages – Tamil Sign Language (TSL), Indian Sign Language (ISL), and American Sign Language (ASL), and outperform state-of-the-art alternatives with accuracies of 97.5%, 99.75% and 98% respectively.

References:
1.   Al-Hammadi, M., Muhammad, G., Abdul, W., Alsulaiman, M., Bencherif, M. A., & Mekhtiche, M. A. (2020). Hand Gesture Recognition for Sign Language Using 3DCNN. IEEE Access, 8, 79491-79509.
2.   Cui, R., Liu, H., & Zhang, C. (2019). A deep neural framework for continuous sign language recognition by iterative training. IEEE Transactions on Multimedia, 21(7), 1880-1891.
3.   Huang, J., Zhou, W., Li, H., & Li, W. (2018). Attention-based 3D-CNNs for large-vocabulary sign language recognition. IEEE Transactions on Circuits and Systems for Video Technology, 29(9), 2822-2832.
4.   Kishore, P. V. V., Prasad, M. V. D., Kumar, D. A., & Sastry, A. S. C. S. (2016, February). Optical flow hand tracking and active contour hand shape features for continuous sign language recognition with artificial neural networks. In 2016 IEEE 6th international conference on advanced computing (IACC) (pp. 346-351). IEEE.

PS1.7

Agent-based control of multiphysics systems

Paola Lecca[1], Angela Re[2]

1   Free University of Bozen-Bolzano, Faculty of Computer Science, Bolzano, Italy
2   Fondazione Istituto Italiano di Tecnologia, Centre for Sustainable Future Technologies, Turin, Italy

Agent-based computing aims at building autonomous software of hardware entities. Multi-agent systems comprise a process knowledge base and a group of functional agents. Agents in the system can communicate to each other to exchange information and can cooperate to share information. The autonomous computing power combined with the implementation of a many-to-many communication protocol can make these multi-agent systems intelligent. Such systems can monitor, analyze and respond to environmental cues [1, 2, 3]. By virtue of this ability, they can achieve timely decisions in dealing with various scenarios in process operations and manufacturing management. The development of intelligent agent-based systems is a very active research fields, whose main outcomes are artificial intelligence techniques of process simulation and rule-based decisions. Of great interest, but still scarcely explored today, is the design of agent-based control systems composed of simple locally interacting controller agents with demonstrated complex group behaviour. The difficulty relies in determining whether simple controller agent strategies will lead to desirable collective behaviour in a large system. System controllability is indeed the main problem in the design of multi-agent control systems. In this study we present mathematical methods for controllability analysis of multi-physics modelling of physical systems. Group of agents can be modelled as a network of modularized uni-physics components (Figure 1), where each component incorporates a mathematical model for the dynamical behavior and for the uncertainties due to modeling, discretization, finite precision computation errors, experimental uncertainty. Based on the multi-physics modeling concept, a new mathematical framework to perform controllability analysis can be developed and incorporated in the agent-based model itself to allow the adaptive control for the components as well as for the whole multi-physics model. We show a use case of the agent-based control of multi-physics systems in biochemical process industry and discuss the challenges not yet overcome with respect to the state of the art and previous studies of the authors [2, 3, 5].
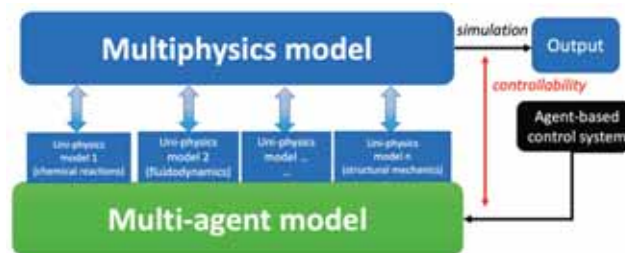
Figure 1: a multi-agent model controlled by a agent-based control system is proposed as a computational framework for a multi-physics model.

References:
[1]   Y. Yang, Research on Modeling and Simulation of Agent-based Intelligent Teaching System, Science Journal of Education. 8(1): 27-31, 2020.
[2]   L. Bao, J.C. Fritchman, Information of Complex Systems and Applications in Agent Based Modeling. Sci Rep 8, 617, 2018.
[3]   Murat Peksen, Multiphysics Modelling, Materials, Components, and Systems, Elsevier 2019.
[4]   Ying Gao, Zhigang Shang, Antonis Kokossis, Agent-based intelligent system development for decision support in chemical process industry, Expert Systems with Applications, Volume 36, Issue 8, Pages 11099-11107, 2009.
[5]   P. Lecca, A. Re, Observability of Bacterial Growth Models in Bubble Column Bioreactors, Computational Intelligence Methods for Bioinformatics and Biostatistics, Springer International Publishing pp. 309-322, Springer International Publishing, 2020.

PS1.8
Temporal change of brain mechanics after slicing

Jinju Chen[1], **John Exton[2]** *.Jonathan Higgins[3]*

1   Newcastle University, Engineering , Newcastle Upon Tyne, United Kingdom, UK
2   Newcastle University, Engineering , Newcastle Upon Tyne, UK
3   Newcastle University, Biosciences Institute, Faculty of Medical Sciences, UK

It is a common benchmark in the brain tissue mechanics literature that acute brain slices should be measured within <8 hours of the experimental animal being sacrificed1-3. The core assumption is that since there is no substantial protein degradation during this time, there will be no change to elastic modulus4,5. This assumption overlooks the effects of osmotic swelling of tissue on mechanical behaviour. To achieve consistent and accurate analysis of brain tissue mechanics, it is important to account for this softening or mitigate it via modifications to standard treatments.
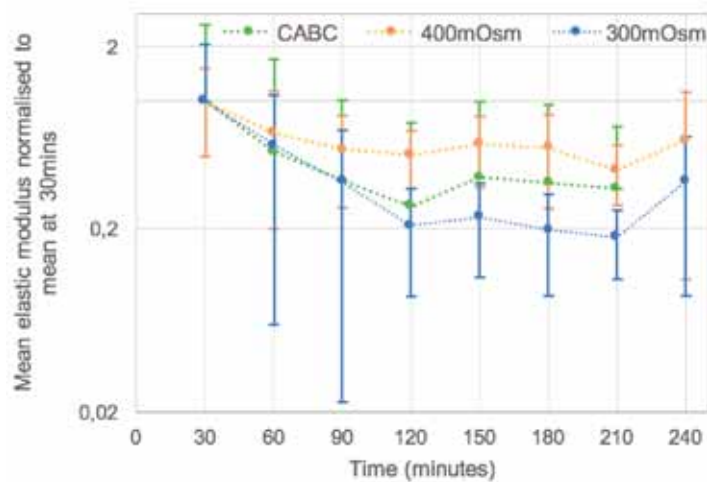
Therefore, the temporal change of brain tissue mechanics was investigated in the first 4hrs after the animal was sacrificed and the sample sliced. Brains from five female CD1 mice were sliced and their stiffness was measured using atomic force microscopy indentation tests at 30-minute timepoints, during which substantial reduction in tissue elastic modulus was found (see Fig. 1).

Two methods for counteracting this softening effect were also tested. This included immersing sliced tissues in an artificial cerebrospinal fluid (aCSF) with a molarity of 400mOsm (higher than the ~300mOsm for standard aCSF) and treating sliced tissues with 0.1units/ml of chondroitinase ABC enzyme (CABC). The high osmolarity samples showed a substantially smaller decrease of elastic modulus during the timepoints measured, whilst the CABC-treated samples softened similarly to the untreated samples until 90mins before stabilizing and showing a modest recovery (see Fig.1).

*Correspondence to: Jinju.chen@ncl.ac.uk

References:
1. MacManus, DB et al. Acta Biomater. 48, 309–318 (2017).
2. Pogoda, K. et al. New J. Phys. 16, 075002 (2014).
3. MacManus, DB et al. J. Biomech. 48, 3213–3218 (2015).
4. Fountoulakis, M et al. Exp. Neurol. 167, 86–94 (2001).
5. Ferrer, I. et al. J. Neuropathol. Exp. Neurol. 66, 35–46 (2007).

PS1.9
Biomechanical sex differences in concussion in an axonal injury model

Chaokai Zhang[1], *Wei Zhao*[1], *Songbai Ji*[1]

1   Worcester Polytechnic Institute, Department of Biomedical Engineering, Worcester, United States

Biological sex is a critical concussion risk factor. Most studies report that females sustain concussions more often than males, have worse outcomes, a different symptom constellation and delayed resolution of symptoms (albeit, others find no differences or the opposite) [1]. Nevertheless, the biomechanical basis for sex differences in concussion remains unknown. Ultrastructural analysis on rat and human axons reveals that female axons are consistently smaller with fewer microtubules than male axons [2]. Thus, we hypothesize that morphological differences in axon substructures are important to sex differences in concussion. In this study, we develop a male and a female axon model that include major substructures such as microtubules (MTs), microtubule associated protein (MAP) tau, neurofilament (NF) network, Axolemma, myelin sheath, and Ranvier node, with MT gap locations randomly generated (Figure 1). The sex-specific geometrical parameters were determined based on the literature, with values chosen to represent the two extreme ends (Table 1). This would yield the maximum difference in axon substructures between male and female.

Table 1 | Geometrical features of axon substructures

	Axolemma radius	# of MTs	MT. neighboring space	MT inner radius	MT outer radius	Axolemma thickness	g-ratio*
Male	300 nm [2]	19 [2]	30 nm [3]	9 nm [4]	15 nm [4]	7 nm [5]	0.5 [5]
Female	200 nm [2]	7 [2]	20 nm [6]	7 nm [3]	12.5 nm [3]		

g-Ratio: The ratio of the inner axonal diameter to the total outer (myelin sheath) diameter

To investigate the difference in mechanical responses of the male and female axons, a uniaxial elongation along the axonal direction with a strain of 30% at a rate of 1 s-1 was applied to the two ends of the axon through the axolemma and myelin sheath. Deformation of the MTs were driven by their connections with MAPs and NFs.

Concentrations of peak maximum principal strain (MPS) occurred around the Ranvier node in both models (not shown). Peak MPS along the MT bundle in the female axon model was ~90% higher than that of the male (Figure 1). These results agree with the general notion that females are more vulnerable to concussion than males and highlight the importance to use sex-specific axonal models to study the biomechanical basis of concussion.
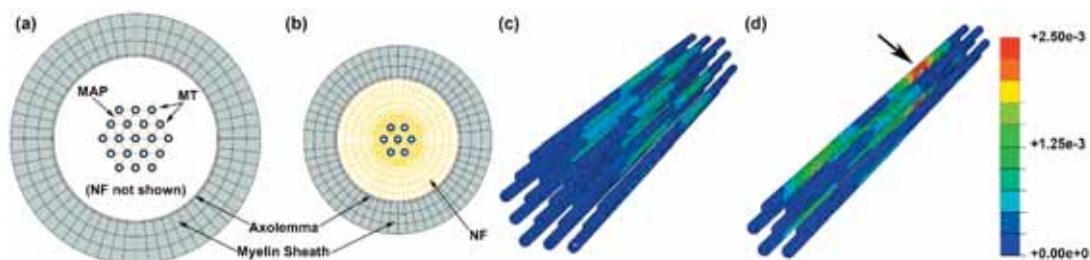
Figure 1 Cross-sections of the male (a) and female (b) axon models, showing 19 and 7 staggered MTs, respectively. They represent the two extreme ends of male and female axons (largest and densest MTs vs. smallest and least dense). Peak MPS along MTs in the female model (d; arrow) is ~90% higher than that in the male model (c).

References:
[1] Merritt et al., Clin. Neuropsychol, 2019.
[2] Dollé et al., Exp. Neurol, 2018.
[3] Montanino et al., Front. Neurol., 2018.
[4] Gittes et al., J. Cell Biol., 1993.
[5] Zhu et al., J. Neurotrauma, 2016.
[6] Rosenberg et al., Proc. Natl. Acad. Sci., 2008.

PS1.10

Comparison of patient-specific brain development models with neonatal data of controls and ventriculomegaly cases

Mireia Alenyà[1], *Maria Inmaculada Villanueva*[1], *Elisenda Eixarch*[2], *François Rousseau*[3], *Oscar Cámara*[1]

1   Pompeu Fabra University. Poblenou Campus, BCN-MedTech, Department of Information and Communications Technologies, Barcelona, Spain
2   BCNatal, IDIBAPS, Universitat de Barcelona, Barcelona, Spain
3   Institut Mines Télécom Atlantique, LaTIM - INSERM, Brest, France

The processes involved in the cortical folding generation during brain development are still not fully understood, but seemingly, differential growth between white and grey matter plays a key role. Computational modelling emerged as a powerful tool to study brain development, but the proposed models have been tested on unrealistic brain geometries or on few brains without validation with longitudinal data.

Here, the finite-element model (FEM) of brain growth, proposed by Tallinen et al. [1], was applied to 12 patient-specific fetal brain geometries (7 controls; 5 ventriculomegaly, VM, cases), extracted from magnetic resonance images (MRI) [2]. Grey matter was manually segmented by experts in each fetal MRI, while neonatal scans of the same subjects were segmented with the dHCP pipeline [3]. From each fetal segmentation, FEM meshes were built and six simulations were performed until neonatal stage, applying initial cortical thicknesses (Hi) within 0.76-5.96 mm.

Besides global measurements, the following local metrics were calculated aiming to evaluate the model performance: curvature; sulcal depth [4]; and folding power, computed with SpAnGy [5]. Anatomical multimodal surface matching [6] was used to register and compare simulated and real meshes.

Results showed that Hi had an impact on folding patterns, such that bigger Hi values entailed wider and deeper folds (Fig.a,b). Globally, the model underestimated the simulation's volume (Fig.d); while largest discrepancies appeared in the parietal-occipital area (Fig.e), no significant differences were observed between simulations of control and VM subjects.

A patient-specific modelling pipeline has been established to simulate brain development from fetal segmentations, later compared with neonatal data. Future work will focus on increasing the cohort and improving the model considering regional growth, local cortical thickness and the effect of axonal tension.
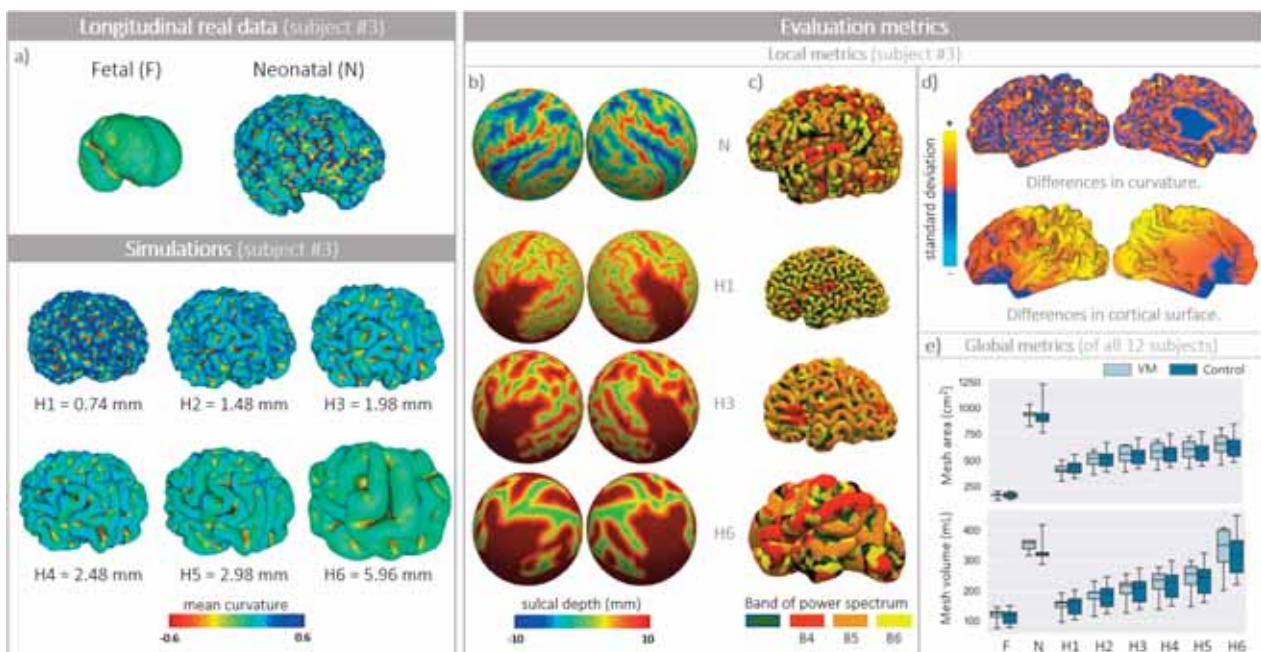
Figure: Comparison of simulated brain development with neonatal data. (a) Example of cortical morphology and curvature maps of real data and simulations with different cortical thicknesses (H1-H6). (b) Sulcal depth projected onto spheres and (c) power spectrum of curvature of the neonatal mesh and simulations H1, H3, H6. (d) Differences in curvature and cortical surface between simulations and real data. (e) Boxplots of global metrics.

References:
[1] Tallinen et al. (2016). On the growth and form of cortical convolutions. Nature Physics.
[2] Benkarim et al. (2018). Cortical folding alterations in fetuses with isolated non-severe ventriculomegaly. NeuroImage.
[3] Makropoulos et al. (2018). The developing human connectome project: A minimal processing pipeline for neonatal cortical surface reconstruction. NeuroImage.
[4] Wang et al. (2021). The influence of biophysical parameters in a biomechanical model of cortical folding patterns. Scientific Reports.
[5] Germanaud et al. (2012). Larger is twistier: spectral analysis of gyrification (SPANGY) applied to adult brain size polymorphism. NeuroImage.
[6] Robinson et al. (2014). MSM: a new flexible framework for Multimodal Surface Matching. NeuroImage.

PS1.11

FE reconstruction of controlled cortical impacts on rat brain

Daniel Baumgartner[1], Michael Lamy[2], Michael Gilchrist[3]

1   University of Strasbourg, ICUBE, Strasbourg, France
2   Alstom Transport, Reichshoffen, France
3   University College Dublin, School of Mechanical and Materials Engineering, Dublin, Ireland

The goal of this study is to establish sequelae of traumatic brain injuries following lower and higher levels of impact to the frontal lobe using a biomechanical finite element (FE) model of penetrating impact injury. Therefore, an animal model – a Sprague-Dawley rat – was used as a surrogate to a human model. A FE reconstruction of experimental indentation tests from Colgan et al. (2010) was done. The correlation between the observed injuries, on the one hand, and mechanical loadings of the brain, on the other hand, was established.

The FE model of a rat's head was obtained from medical images, and composed of three main features: a brain (cerebrum, cerebellum, olfactory bulbs and stem), a rigid skull and a layer of solid elements figuring the interface between the former two features. The brain was considered as a linear viscous elastic material, while the skull and the interface were given elastic material properties. The whole brain was composed of 118,016 hexahedral solid elements, and its viscosity was represented through a Boltzman mechanical behavior where, in particular, $K = 2.19$ GPa, $G_0 = 10$ kPa, $G_\infty = 2$ kPa, and $\tau = 8$ s.

In order to simulate indentation, a cylinder was meshed and added to the original model, so as to match the position of the indentor in the experimental setup. Dimensions and mass of the cylinder were adjusted to those of the real impactor. On the external surface of the head mesh, elements from the skull components were removed in order to represent the craniotomy act and exposed the underlying cerebral matter.

Two cases were modeled and simulated: a mild level of indentation (penetration depth = 0.87 mm) and a severe level of indentation (penetration depth = 2.62 mm). In both of them, a displacement was imposed to the rigid cylinder in the direction of its revolution axis. When the maximum depth of penetration was reached, the position was maintained by the locking of the imposed displacement. In order to make the indentation possible, the rigid skull was depicted to have no degree of freedom, in translation as well as rotation. The cylinder itself was allowed to move only in translation along its revolution axis, to ensure the displacement would not be altered by the contact between cylinder and cerebral matter. Once these boundary conditions and loading cases were defined, the model was able to simulate the penetration of the indenter in the cerebral matter.

In both cases, observed injuries – mainly cerebral spinal fluid drop and brain volume increase – were compared to calculated mechanical parameters such as brain pressure, brain shearing stress, and brain strain. That correlation attempt led to explain in time delayed brain injuries such as physiological evolutions.

PS1.12

Modeling of nonlinear ultrasound propagation in trans-cranial MRgFUS technique: a 2D-FEM analysis

Fabiano Bini[1], **Andrada Pica**[1], Maurizio Marrale[2], Cesare Gagliardo[3], Franco Marinozzi[1]

1 S apienza University of Rome, Department of Mechanical and Aerospace Engineering, Rome, Italy
2 University of Palermo, Department of Physics and Chemistry, Palermo, Italy
3 University of Palermo, Section of Radiological Sciences, Department of Biomedicine, Neuroscience and Advanced Diagnostics, Palermo, Italy

Introduction: Magnetic Resonance guided Focused Ultrasound (MRgFUS) is a promising non-invasive technique that can be used for the treatment of tumours in different anatomical areas, e.g. prostate, liver, breast or brain. Its working principle is based on the concentration of acoustic energy in a target area causing a locally increase of the temperature with consequent ablation of the tissue. A major concern for the MRgFUS application to brain is the skull presence that represents the main barrier to deliver ultrasound energy to the targeted area. The characteristics of bone tissue attenuate the ultrasound waves leading to noticeable heating effects at the skull level. The aim of this study is to simulate, by means of the finite element (FE) method, the transcranial nonlinear ultrasound propagation taking into account the detailed structure of bone tissue.

Methods: We developed a 2D axisymmetric FE model that mimics the propagation of focused ultrasound beams through skin, skull and brain tissue. The skull is represented as a three-layered system with two cortical plates packing a thin layer of trabecular bone. Information concerning the porosity of the trabecular region has been reconstructed from Computer Tomography images. The acoustic and thermal properties of the tissues were obtained from the available literature. A concave transducer that works at a frequency of 650 kHz is considered in the simulation. We assume that the space between transducer and tissue is filled by water.

Ultrasound propagation is determined through the Westervelt equation which accounts for the nonlinear interaction between the acoustic field and the tissues. The input signal, i.e. the pressure at the transducer interface, is modelled by means of a Dirichlet condition. In order to control reflection, absorbing layers have been implemented on the boundaries of the domains. The solution of the Westervelt equation is achieved applying the discontinuous Galerkin method that uses a time-explicit solver.

The solution of the pressure equation is subsequently coupled with Pennes bioheat equation to determine the temperature distribution in the tissue region. Dirichlet conditions are set to model boundary temperature conditions.

Results: The acoustic pressure distribution, acoustic intensity and temperature distribution were achieved from the FE simulation. Highest values of acoustic pressure occur in the focal area and in the cortical and trabecular regions. Ablative temperatures, i.e. superior to 55 Celsius degrees, are achieved in the target area and at the cortical-trabecular interface.

The thermal response in the focal region after the sonication time, i.e. 10 s, is in good agreement with clinical studies and allows to validate the effectiveness of the model.

Conclusion: The present FE model offers new insights to predict secondary heating effects of the MRgFUS technique in the skull region and to improve treatment planning.

PS1.13

Predicting neurological effects associated with traumatic brain injuries using video analysis and finite element modeling

Bianca Acot[1], Branko Glisic[1], Annegret Dettwiler[2], Michael Gilchrist[3]

1   Princeton University, Civil and Environmental Engineering, Princeton, United States
2   Princeton Neuroscience Institute, Princeton, United States
3   University College Dublin, Mechanical & Materials Engineering, Dublin, Ireland

Traumatic brain injuries are prevalent in contact sports like American football. However, little is known about how concussive head impacts trigger structural alterations in white matter fiber tracts and a particular neurochemical cascade, which may lead to long-term neurological impairment. Finite element model (FEM) simulations enable researchers to study the relation between predicted injury in the brain and head impact mechanics. To improve the accuracy of these simulations, this paper created a methodology to cyclically analyze and improve the process of finite element simulation of head impacts. Case studies of two college football players were analyzed through the following steps.

In the first step, footage of the game in which concussion occurred was analyzed in order to find the velocities of the concussive head impact. A mechanism of an accumulation of subconcussive, repetitive head impacts resulting in concussion was found for both subjects. Thus, a representative 'hard hit' was chosen as the case study. The head was tracked using Kinovea software and the head impact velocities were found. In the second step, the case study head impacts were simulated using the University College Dublin Brain Trauma Model (UCDBTM), a FEM of the head. A FEM of a football helmet was created and fitted to the UCDBTM and the velocities found in the first step were applied to the UCDBTM. The simulation output was Von Mises Stress (VMS) and Maximum Principal Strain (MPS). Areas of relatively high VMS and MPS, which indicate potential injury, within the white matter tract part, were identified as Regions of Interest (ROI). In the third step, diffusion tensor imaging (DTI) scans of each individual subject, showing the difference in radial diffusivity (RD) between pre- and post-concussion within the white matter tracts [3], were analyzed to find a qualitative relationship between the FEM results from Step 2 and neuroimaging results. Clusters of increased diffusivity, which are predicted to be areas of injury, were found in 6/7 of the ROIs found in Step 2; an example of this qualitative relationship for the corpus callosum, one of the ROIs, is shown in the figure. By analyzing a larger set of similar real-world head impact events and improving simulation accuracy, FEM simulations can be used as a sideline diagnostic tool identifying the amount of concussive hits over time and hence the potential long-term consequences of concussion.
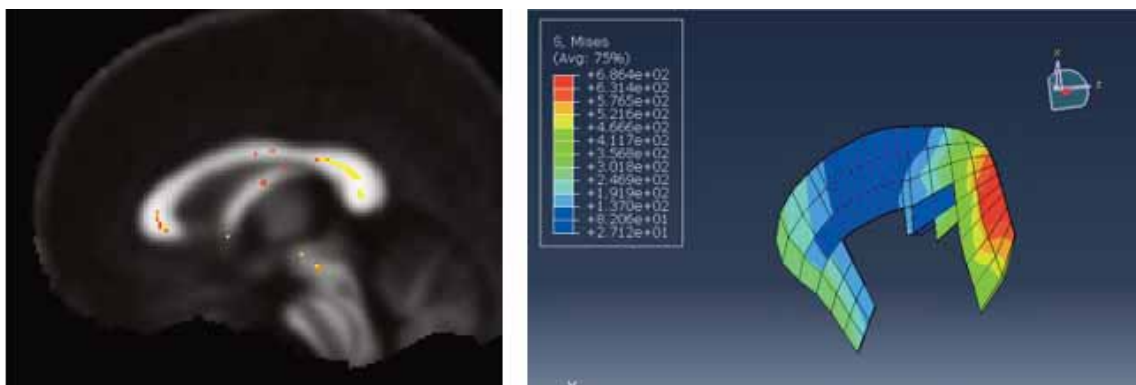
Figure caption: On the left, the DTI slice of the corpus callosum shows increased RD clusters. On the right, the FEM of the corpus callosum shows VMS. This is the corpus callosum of Subject A.

References:
[1]   Cubon et al., Brain Behav, 8(12):e01165, 2018

PS1.15
Unfolding the cortex via a mechanics-informed graph neural network

Shuolun Wang[1], Nagehan Demirci[2], Vicente Castro Solar[3 4 5], Francisco Sahli Costabal[3 4 5], Maria Holland[1 2]

1   University of Notre Dame, Department of Aerospace and Mechanical Engineering, Notre Dame, United States
2   University of Notre Dame, Bioengineering Graduate Program, Notre Dame, United States
3   Pontificia Universidad Católica de Chile, Department of Mechanical and Metallurgical Engineering, Chile
4   Pontificia Universidad Católica de Chile, Institute for Biological and Medical Engineering, Chile
5   Pontificia Universidad Católica de Chile, Medicine and Biological Sciences, Chile

Cortical thickness serves as an essential biomarker for many neurological disorders such as Autism Spectrum Disorder, schizophrenia, and epilepsy. Our recent work has suggested that the interactions between mechanics and biology plays a vital role in shaping the thickness variations [1]. In the current work, we aim to distinguish between cortical thickness variations that are artifacts of brain folding and those that are due to biological phenomena. To that end, we introduce the modified cortical thickness -- or the thickness the cortex would have if it were unfolded and free of the mechanical forces involved in brain folding. From our simulations of cortical folding (Figure 1a and b), we use the physics-based data to train a graph neural network [2]. Thus, our investigation is based on the underlying physics of the problem in the form of large deformation mechanics. After training, we can apply the neural network to MRI scans (Figure 1c) to "unfold" the cortex and calculate its corresponding thickness. This work opens the door for precise cortical thickness analysis in neurological disorders, leading to new early diagnosis pathways and effective treatment.

a)   b)   c)
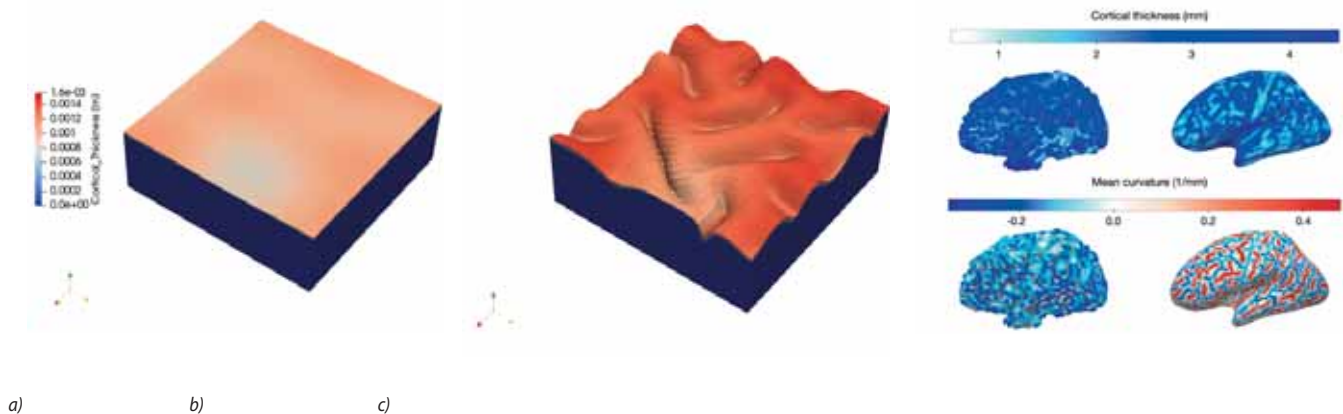
Figure 1: a) and b), the simulated contour of cortical thickness at the pial surface. c) Patterns of cortical thickness and mean curvature in one of N=564 human brains studied.

References:
[1]   Wang, Shuolun, Nagehan Demirci, and Maria A. Holland. "Numerical investigation of biomechanically coupled growth in cortical folding." Biomechanics and Modeling in Mechanobiology 20.2 (2021): 555-567.
[2]   Li, Guohao, et al. "Deepergcn: All you need to train deeper gcns." arXiv preprint arXiv:2006.07739 (2020).

PS2.3
Continuum bone remodelling considering cancellous and cortical bone

Ina Schmidt[1], *Areti Papastavrou*[2]*, Paul Steinmann*[2]

1   Nuremberg Tech, Faculty of Mechanical Engineering, Nürnberg, Germany
2   FAU Erlangen-Nürnberg, Faculty of Mechanical Engineering, Erlangen, Germany

The importance of bone in the body of mammals is obvious when considering their numerous vital functions. Understanding the remodelling processes of human bone resulting from the adaptability to loading habits and predicting bone strength and fracture risk are still important research topics nowadays.

One approach to solve this issue is based on a continuum bone model. Inspired by the theory of open system thermodynamics [1], this model focuses on the isotropic evolution of bone density in response to mechanical loading. The fully nonlinear theory is approximately solved using the finite element method.

This concept has already been investigated in several studies, however, most of them addressing exclusively cancellous bone. A novel approach not only incorporates the remodelling behaviour of cortical bone but also allows for an interaction of both structure types. Therefore, an initial volume fraction is introduced to distinguish between both [2].

A series of benchmark problems is used to illustrate and compare the novel perspective against previous numerical computations. Qualitatively, the new approaches show a plausible possibility of how implementation can be realised in a continuum model.

References:
[1]   E. Kuhl, P. Steinmann, Theory and numerics of geometrically non-linear open system mechanics. Int J Numer Meth Engng. 58(11):1593-1615, 2003
[2]   I. Schmidt, A. Papastavrou, P. Steinmann, Concurrent consideration of cortical and cancellous bone within continuum bone. Computer Methods in Biomechanics and Biomedical Engineering, DOI 10.1080/10255842.2021.1880573

PS2.5

Digital images correlation of two internal fixation implants during treatment of femur neck fractures

Maria Augusta Neto[1], Vítor Maranha Lopes[1], Luís Manuel Roseiro[2], Maria Fatima Paulino[1], Ana Martins Amaro[1]

1   University of Coimbra, Mechanical Department, Coimbra, Portugal
2   Polytechnic Institute of Coimbra, Mechanical Department, Coimbra, Portugal

Hip fracture is one of the primary concerns of the elderly, most of whom suffer from osteoporosis and various medical and mental diseases that result in their being a high-risk population. This study correlates the experimental results of a new Trochanteric Plate of Contention (TPC), which may improve the resistance to the cut-out failure of internal fixation devices, and the well-known Dynamic Hip Screw (DHS) system. Generally, it is well accepted that the DHS is the implant of choice in treating stable femur fractures (Kokoroghiannis et al., 2012) and it is also considered the implant of choice for implants comparisons purpose (Kouvidis et al., 2009). Hence, this study compares the strains, stresses, and displacements on these implants under compression tests. Data acquisitions were carried out using electrical and optical sensors. Two synthetic femurs produced using the fourth generation of composite bones were fractured and, posteriorly, fixed with the two fixation implants, i.e, TPC and DHS. Both devices were instrumented with strain gauges and rosettes, while spray-painted speckle patterns were experimentally created over the proximal zone of the two femurs. The experimental setups were tested under the same conditions. The experimental results showed that strain values are higher in the DHS than in the TPC device, particularly in the neighborhood of the cephalic screw. The experimental displacement field also showed that the TPC device has a stiffer behavior than the DHS. So, it is expected that this device will significantly enhance the medical device's behavior in osteoporotic femurs.

References:
Kokoroghiannis, C. et al. (2012) 'Evolving concepts of stability and intramedullary fixation of intertrochanteric fractures—A review', Injury. Elsevier, 43(6), pp. 686–693. doi: 10.1016/J.INJURY.2011.05.031.
Kouvidis, G. K. et al. (2009) 'Comparison of migration behavior between single and dual lag screw implants for intertrochanteric fracture fixation.', Journal of orthopaedic surgery and research. BioMed Central, 4, p. 16. doi: 10.1186/1749-799X-4-16.

PS2.6

Finite element screw-bone interface modelling in locking plate fixated femoral fractures for use in fracture healing algorithms

George Morgan[1], Hana Fox[1], Lucas Low[1], Spyros Masouros[1]

1   Imperial College London, Department of Bioengineering, London, United Kingdom

Bone fractures are often treated using internal fixation devices. The plate type; type and configuration of screws; and bone-plate offset all affect fracture stability and healing [1]. Here, we postulate the combination of finite element (FE) modelling with a fracture healing algorithm to better predict surgical outcomes for use in pre-operative planning and device development.

Computational models have been developed that quantify fracture healing based on the surrounding mechanical environment [2, 3]. They combine an algorithm that simulates callus and bone development with FE modelling of the mechanical environment at the fracture site. The addition of 3D fracture fixation devices into these models increases complexity and simulation time, which is detrimental to their utility. Specifically, screw-bone contact simulation is usually the most computationally expensive aspect. Different contact simulation methods have been compared in literature [4], but contact has never been removed entirely. This study compares five methods for modelling screw-bone contact interaction in an FE model of a simple femoral fracture secured with a locking plate.

An FE model of a simple transverse mid-diaphyseal femoral fracture, secured with a locking plate and locking screws of customised geometries with a bone-plate offset of 2 mm, was developed in MSC.Marc (v2020, MSC.Software). The femur was represented as a 400-mm-long hollow cylinder, with outer diameter, thickness, and fracture gap of 30, 7, and 10 mm, respectively. Screw-bone interfaces were modelled as: (a) suppressed screw-shaft threads and 'glued' contact, (b) suppressed threads and frictional contact with spring elements resisting screw pull-out [5], (c) active threads and 'glued' contact, (d) active threads and frictional contact, and (e) rigid-body elements with beam elements representing screw bending. Screw-plate interfaces were modelled with suppressed threads and 'glued' contact. An axial compressive force of 1 kN was applied. Inter-fragmentary strain (IFS) - an indicator of fracture healing defined as the ratio of change in fracture gap width to initial fracture gap width - was measured.

IFS for each model ((a)-(e)) was found to be: 23.2%; 31.0%; 26.6%; 17.4%; and 17.0%, respectively, and computational times were 423 s; 444 s; 60,541 s; 168,419 s; and 241 s, respectively.

These initial findings suggest that the models with active threads can be represented accurately with more computationally efficient alternatives. Experimental testing is needed to assess which model presents the best combination of computational efficiency and accuracy.

References:
1.   Beltran M.J. et al. J Am Acad Orthop Surg, 2016; 24(10):711-719
2.   Isaksson H. et al. J Biomech, 2006; 39(8):1507-1516.
3.   Simon U. et al. Comp Methods in Biomech and Biomed Eng, 2011; 14:79-93.
4.   MacLeod A.R. et al. J Biomech, 2012; 45:1712-1716.
5.   Moazen M. et al. J Eng in Medicine, 2013; 227(7):746-756.

PS2.9

Computational modeling of ligand binding competition at the cell–extracellular matrix interface

Zeynep Karagöz[1], Thomas Geuens[1], Vanessa LaPointe[1], Martijn van Griensven[1], Aurélie Carlier[1]

1   Institute for Technology-Inspired Regenerative Medicine (MERLN), Maastricht, Netherlands

Integrin transmembrane proteins play a central role in mechanotransduction at the cell–extracellular matrix interface. This process is central to cellular homeostasis and therefore particularly important when designing instructive biomaterials and organoid culture systems. Previous studies suggest that fine-tuning the extracellular matrix (ECM) composition and mechanical properties can improve organoid development [1]–[3]. Although experimentally very complex, computational models provide novel avenues to testing the effect of numerous different ECM ligands and mechanical properties on cell decision-making mechanisms.

We developed an ordinary differential equation–based model that enabled us to simulate three main interactions, namely integrin activation, competitive ligand binding and integrin clustering (Figure 1A). Our results clearly indicate that this competition between ligands defines the fate of the system. By simulating the model with different initial conditions for competing ligands and testing different sets of binding rates, we demonstrated that the ligand with the higher binding rate (L1) occupies more integrins at the steady state than does the competing ligand (L2) (Figure 1B). We have also demonstrated that an increase in the initial concentration of ligands does not ensure an increase in the steady state concentration of ligand-bound integrins (Figure 1B). Local parameter sensitivity analysis was in accordance with these observations. The L2-bound integrin concentration (IL2) was most sensitive to changes in binding and unbinding rates of the two competing ligands (k3, k4, k5, k6). Furthermore, the IL2 concentration was sensitive to the decrease in L1 initial concentration but not to changes in L2 initial concentration (Figure 1C).

In summary, with cell type specific, quantitative input on integrin-ligand binding rates, this computational model can be used to develop instructive cell culture systems
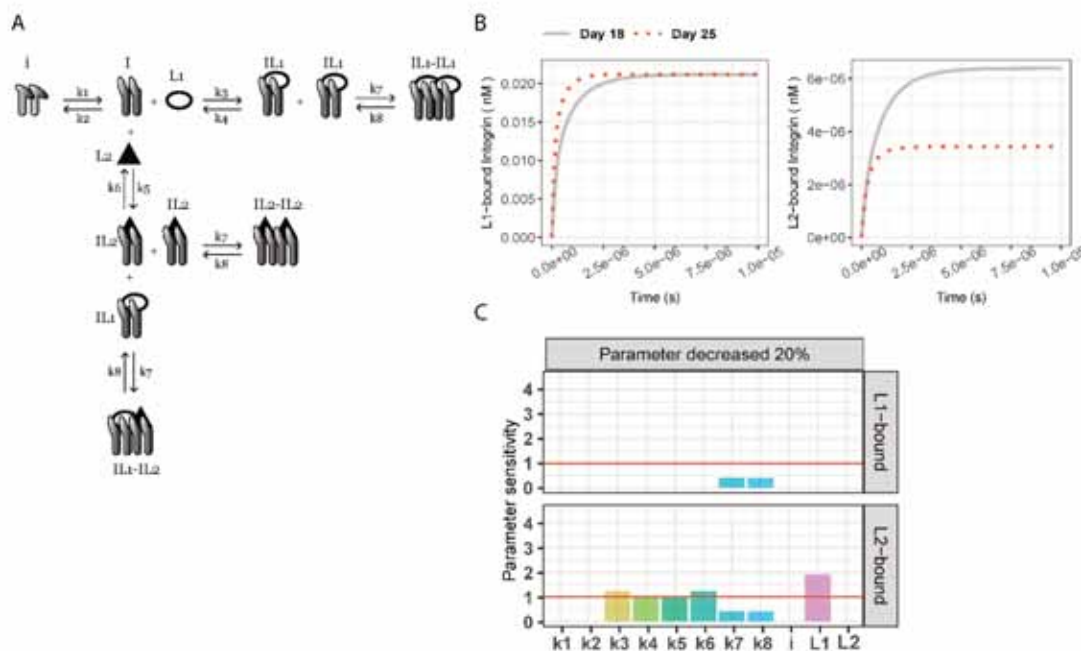
Figure 1: Figure caption: A) Schematic overview of the ligand competition model. B) L1- and L2-bound integrin concentration over time. C) Sensitivity of IL1 and IL2, ligand bound integrin molecular species to the 20% decrease in the model parameters.

References:
 [1]   T. Geuens et al., npj Regenerative Medicine, vol. 5, no. 1. pp. 1–6, 2020.
 [2]   N. Gjorevski et al., Nature, vol. 539, no. 7630, pp. 560–564, 2016.
 [3]   E. Garreta et al., Nat. Mater., vol. 18, no. 4, pp. 397–405, 2019.

PS2.11
Soft walls and soft body migration

Carles Bona Casas[1], Antonio Cerrato[1], Hugo Casquero[2], Joan Josep Cerda[3]

1   University of the Balearic Islands, Physics, Palma, Spain
2   University of Michigan-Dearborn, Dearborn, United States
3   University of the Balearic Islands, Palma, Spain

The study of soft-body motion in shear and Poiseuille flows is of particular interest when studying blood flow in narrow microvessels (diameter below 100 microns). At this scale, the layer of glycocalyx covering the vessel wall plays a crucial role to explain the Faharæus effect. The glycocalyx is a highly-hydrated fibrous meshwork of carbohydrates located at the surface of endothelial cells and therefore is the outermost part of the endothelium. Its malfunction is related to several diseases such as atherosclerosis, stroke, hypertension, kidney disease, sepsis and cancer.

Our work studies the mechanical role of this soft and thin layer in cell-scale blood flow by means of the divergence-conforming immersed boundary (DCIB) formulation proposed in [1,2]. The DCIB method follows up on previous works [3-5] where discretizations of the mathematical model proposed by the IB method based on non-uniform rational B-splines (NURBS) and T-splines were developed. In the DCIB method, the Eulerian velocity-pressure pair is discretized using divergence-conforming B-splines, which leads to inf-sup stable, H1-conforming, and pointwise divergence-free Eulerian solutions. The Lagrangian displacement is discretized using NURBS, which enables to robustly handle large mesh distortions. By combining the generalized-α method and a block-iterative solution strategy, the DCIB method results in a fully-implicit discretization, which is key to impose accurately the no-penetration and no-slip conditions at the fluid-solid interface.

The mechanical effect of a soft, deformable coating such as the glycocalyx or even the vessel wall itself is usually neglected in both in vitro and in silico setups. Our results show the presence of forces that are likely to have a significant influence on the behaviour of red blood cells and other bodies in blood circulation and are in line with previously reported experiments [6]. Therefore, the present contribution underlines the important, yet often overlooked, mechanical role that soft walls are likely to play in regulating cell/wall interactions in blood flow.

References:
1.   Casquero H, et al. J. of Comp. Phys., 2018; 374:625-653.
2.   Casquero H, et al. Comput. Method. Appl. M., 2015; 284: 943-970.
3.   Casquero H, et al. Int. J. Numer. Meth. Eng., 2016; 105: 855-888.
4.   Casquero H, et al. Comput. Method. Appl. M., 2017; 316: 646-667.
5.   Casquero H, et al. J. of Comp. Phys., 2021;425, 109872.
6.   Wang, Y., et al. Phys. Rev. Lett. 115, 248302 (2015).

PS2.13
Evaluation of enamel wear against different monolithic CAD/CAM ceramic materials

Ahmed Fouda[1 2], *Osama Atta*[2], *Christoph Bourauel*[1]

1   University Hospital Bonn, Oral Technology, Bonn, Germany
2   Suez Canal University, Department of Fixed Prosthodontics, Ismailia, Egypt

Wear of tooth substrates and dental restorative materials is considered a critical factor and can adversely affect the long-term outcome of the treatment [1]. Abrasive restorative materials can cause loss of tooth structure in the opposing dentition with subsequent increase in tooth hypersensitivity and/or caries susceptibility [2]

The aim of this in-vitro study was to determine the wear of natural human teeth caused by opposing glass ceramics, zirconia reinforced glass ceramics and monolithic zirconia.

Methods: Fifty ceramic discs were cut from five different ceramic materials: partially crystallised lithium disilicate (Emax CAD), fully crystallised lithium disilicate (Lisi CAD), zirconia reinforced lithium silicate (Celtra Duo), super translucent zirconia (Katana STML), ultra-translucent zirconia (Katana UTML). All the samples were finished according to the manufacturers' recommendations. All discs were subjected to 200.000 wear cycles against the buccal cusp of a natural premolar at a 20 N vertical force using a self-developed wear testing device. The teeth were scanned using a µCT scanner (Skyscan 1174) before and after the wear tests. Images were overlapped to determine the volumetric tooth loss (mm3) (Figures 1,2).

Results: The Celtra Duo resulted in the highest volumetric enamel loss mean value (0.45±0.13 mm3), while both monolithic zirconia groups UTML & STML showed the least volumetric enamel loss mean values (0.16±0.05 mm3) and (0.17±0.08 mm3) respectively. The mean value of the volumetric enamel loss associated with Emax CAD was (0.37±0.17 mm3), while the new Lisi CAD was more tooth friendly and showed less enamel loss with a mean value of (0.27±0.08 mm3).

Discussion: The wear behavior of glass ceramics has always been discussed controversially. Some in vitro studies revealed that glass ceramic material may provide wear characteristics similar to those for enamel, while other clinical investigations of inlays showed significantly higher values for enamel wear in the antagonists [3]. Currently, the results of this study showed that monolithic zirconia caused minimal wear to the opposing dentition and is preferred to glass ceramics when excessive wear is expected. The study also revealed that the new fully crystallized lithium disilicate materials can cause less wear to the opposing natural dentition than the two-stage partially crystallized lithium disilicate.
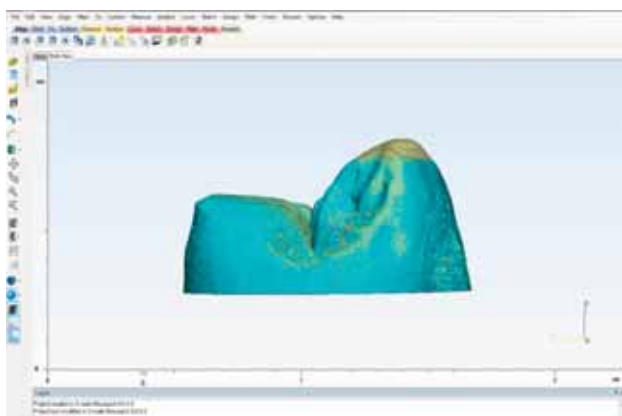
Figure 1: Matching and overlapping of the two µCT-scanned tooth crown 3D images (before and after the wear cycles) using 3-matic software.
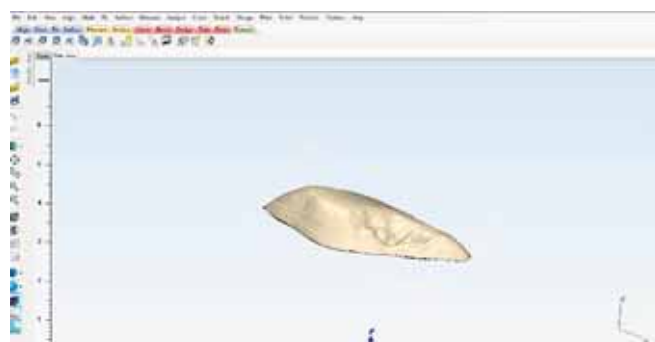
Figure 2: Visualisation of the subtraction of the worn enamel for calculation of the volumetric enamel loss.

References:
1. Oh WS et al. J Prosthet Dent. 2002;87:451-9.
2. Jacobi R et al. J Prosthet Dent. 1991;66:303-9.
3. Krämer N et al, J. Dent. Res, 85:1097–100, 2006.

PS2.14
Influence of periodontium morphology on initial tooth movement

Susanne Reimann[1][2], *Julia Ebner*[2], *Martin Hartmann*[2], *Ludger Keilig*[2], *Christoph Bourauel*[2]

1   University of Applied Science Bremerhaven, Medical Engeneering, Bremerhaven, Germany
2   University of Bonn, Germany, Oral Technology, Bonn, Germany

Aim: To examine the influence of the periodontal morphology on initial tooth mobility with finite element (FE) methods. Anatomically, the width of the periodontal gap is inconstant along the root. Nevertheless, most studies work with a constant width periodontium (PDL). Different PDL widths and different hourglass shapes of the PDL were examined. Our work also provides information about the influence of PDL material parameters on a movement simulation.

Method: Digital X-ray images of 21 single-root teeth from 13 orthodontically treated patients were measured by ten dentists. Based on an existing idealized FE model, consisting of a tooth with constant geometry, bone and PDL, eight models with PDL widths from 0.2mm to 0.8mm were created. By adjusting the PDL material parameters of all models so that the tooth movement was identical to the model with 0.2mm periodontal width, the influence of the PDL width on the material parameters was determined.

To create FE-models to examine the influence of the percentage reduction in the PDL width towards the center of the root (hourglass shape) on the initial tooth movement, further X-ray images of 43 patients were evaluated. The resulting further 18 models contained different versions of the hourglass shape in addition to different PDL widths.

Corresponding to force application of an orthodontic bracket, 1N was applied. Material parameters for tooth (20GPa), cortical (20GPa) and cancellous bone (500MPa) were calculated with $\varepsilon=0.3$. The material parameters for the PDL (E1=0.05, E2=0.28, $\varepsilon=0.075$) were taken from the literature. Models were generated and discretized with tetrahedrons.

Results and discussion: The width of the PDL has a significant influence on tooth movement. A tooth with a 0.8mm wide PDL showed 3.6 times the displacement compared to 0.2mm wide PDL.

Adjustment of the PDL material parameters to the tooth displacement in the 0.2mm gap width model showed a 240% increase for E1 and approximately 170% for E2 for the model with a PDL width of 0.8 mm. ε had to be reduced by 0.058.

Mean measured reduction in the width of the PDL (hourglass shape) was 33±7% (SD). Models were therefore generated with a stepwise reduction of 20% to 40%. This change in the PDL geometry resulted in only small changes in the tooth movement. The 40% hourglass shape of a 0.8mm wide PDL had the greatest impact compared to the constant width PDL with a reduction in tooth displacement of 5.7%.

Conclusion: This confirms an increase in tooth displacement with widening PDL. However, the anatomical hourglass shape has no great influence on the initial tooth movement. These findings are relevant for further investigations in this field.
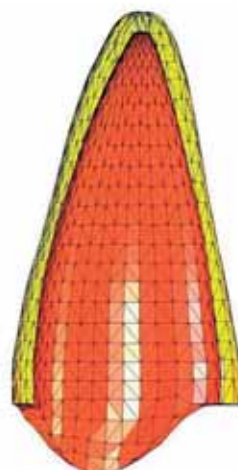
Figure caption: Longitudinal section through a 0.8mm wide PDL with a 40% reduction to the center of the root (arrows).

PS3.1

Evaluation of an optimization method for measuring treadmill walking motion using IMUs

Anirudh Bhateja[1], Ted Yeung[2], Thor Besier[2], Benjamin Fregly[1]

1 Rice University, Mechanical Engineering, Houston, United States
2 The University of Auckland, Auckland, New Zealand

Inertial measurement units (IMUs) could provide an attractive alternative to video motion capture systems for measuring walking in a non-laboratory setting. This study applied an optimization method to an 18-DOF lower body model to convert synthetic IMU data into corresponding joint angles.

Experimental video motion capture and IMU data were collected from a single subject who performed treadmill walking at a self-selected speed. OpenSim model scaling [1,2] was performed to scale a generic 3D OpenSim model [3] and attach dynamic markers and IMUs to the pelvis (6 DOFs) and lower body segments (6 DOFs per leg). Next, OpenSim inverse kinematics was performed to calculate pelvis and lower body joint angles as well as corresponding synthetic IMU measurements. Finally, synthetic noise was added to the synthetic IMU data to emulate actual IMU data. For the treadmill walking trial lasting over 30 seconds, pelvis and lower body joint angles were recovered from the noisy synthetic IMU data using a nonlinear least squares optimization method implemented in MATLAB. For each time frame, the optimization adjusted the kinematic model's joint positions, velocities, and accelerations to minimize errors between model and synthetic IMU data and between model and implicitly integrated joint positions and velocities. The actual values of the joint angles and its derivatives were used to set the initial states of the model.

The optimization method tracked the joint positions well for the duration of the treadmill walking trial (average RMS errors of < 2 mm for translations and < 0.1 deg for rotations). Thus, the optimization method could entrain the kinematic model to the natural system dynamics. The rotations were tracked better than were the translations since the noisy synthetic accelerometer data led to greater errors that could be corrected by the noisy synthetic gyroscope measurements. The optimization method was relatively insensitive to the selected cost function weights for position, velocity, and acceleration errors and produced fairly accurate and robust joint angle estimates but at the cost of high computation time. Work is under way to repeat the evaluation using actual IMU data synchronized with motion capture data.
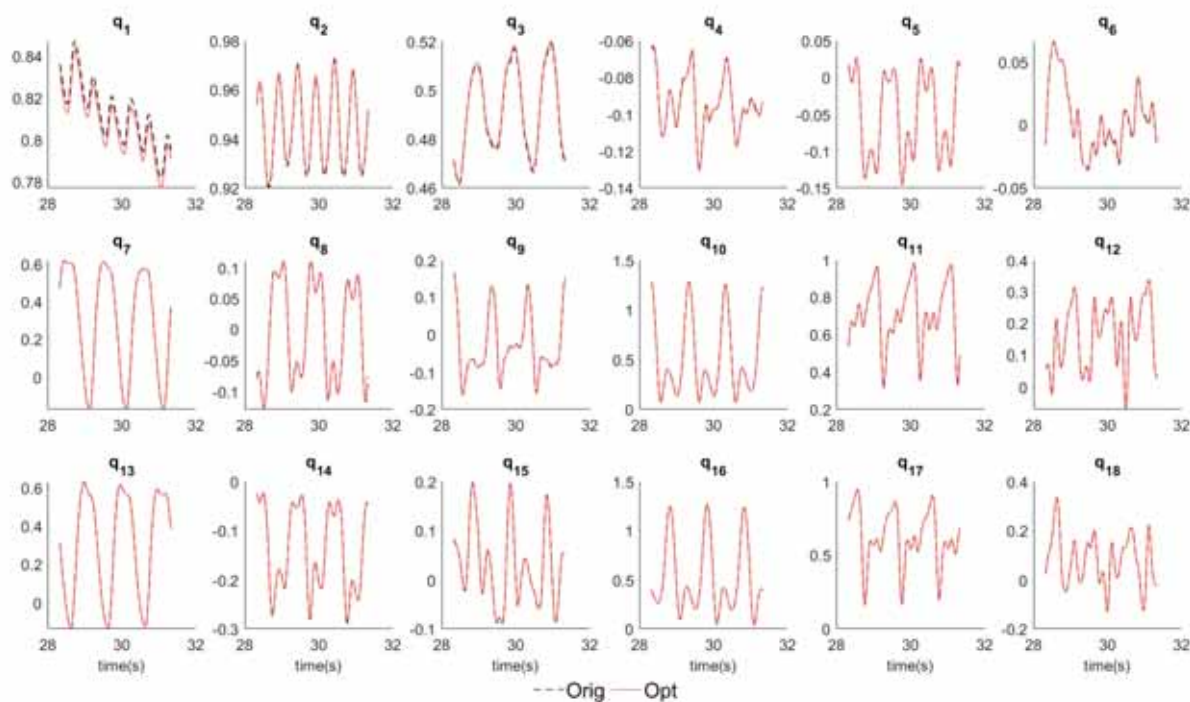
Figure caption: Optimization estimates for generalized coordinates during the last 3 seconds of treadmill walking. q_1-q_3 are pelvis translations (in meters), q_4-q_6 are pelvis rotations (in radians), q_7-q_{12} are right leg joint angles (in radians), q_{13}-q_{18} are left leg joint angles (in radians).

References:
Delp, S.L., et al. IEEE Transactions on Biomedical Engineering, vol 55, pp 1940-1950. (2007)
Seth, A, et al. PLoS Computational Biology, 14(7). (2018)
Rajagopal, Apoorva, et al. IEEE Transactions on Biomedical Engineering 63.10 (2016): 2068-2079. (2016)

PS3.3

Dominant and non-dominant subject-specific kinematic synergies used in collaborative activities of daily living

Verónica Gracia-Ibáñez[1], *Joaquín L Sancho-Bru*[1], *Margarita Vergara*[1], *Néstor J. Jarque-Bou*[1], *Pablo J. Rodríguez-Cervantes*[1]

1   Universitat Jaume I, Castellón de la Plana, Spain

Human hand kinematic synergies are widely used in robotics and hand prosthesis, and have been proposed for hand function assessment in clinics and rehabilitation. During reach-to-grasp, subjects use sparse combinations of synergies [1], each using a limited set of degrees of freedom. In [2], we obtained sparse kinematic synergies across subjects in 24 representative activities of daily living (ADL) for the dominant hand. Now, we compare the sparse synergies used by the right (dominant) and left (non-dominant) hands of eighteen healthy subjects while performing 21 collaborative ADL. Sixteen joint angles from each hand were recorded (CyberGlove, 100 Hz, validated calibration protocol [3]) and filtered, and each task resampled to 1000 frames. The process to obtain the synergies is the same as in [2], but applying principal component analysis (PCA) to the correlation matrix instead to the covariance matrix: (i) same data scaling to all subjects (based on active range of motion data) to make subjects-specific synergies comparable; (ii) for each hand and subject, four principal components (PCs) were obtained applying PCA (eigenvalue>1, Varimax rotation). For each hand, a hierarchical cluster analysis was applied to all PCs (grouping metric: absolute value of cosine; method: complete linkage), checking similarity of subject-specific synergies through the angle between them. The number of clusters was selected as the minimum ensuring that no cluster contains more than one synergy from the same subject. The mean synergy within each cluster was considered as representative synergy, core synergy (CS). Seven CSs and ten CSs were obtained for the right and left hand respectively. First three CSs are similar in both hands (mean angle between CSs of both hands < 20º) and represent digit arching and digit abduction. Higher order synergies in right hand represent palmar arching with index flexion (CS5), and thumb-index coordination (CS6), thumb opposition (CS4), or thumb carpometacarpal flexion (CS7), these three last CSs being mutually exclusive (each subject use only one of them). Conversely, in left hand, higher order synergies represent mixed and spurious movements, being less shared among subjects (Figure), except for CS5 that in left hand represent a different coordination of thumb and index finger. The results give us a better understanding of the synergies used by humans with their dominant hand, but also show how the non-dominant hand behaves in collaborative activities.
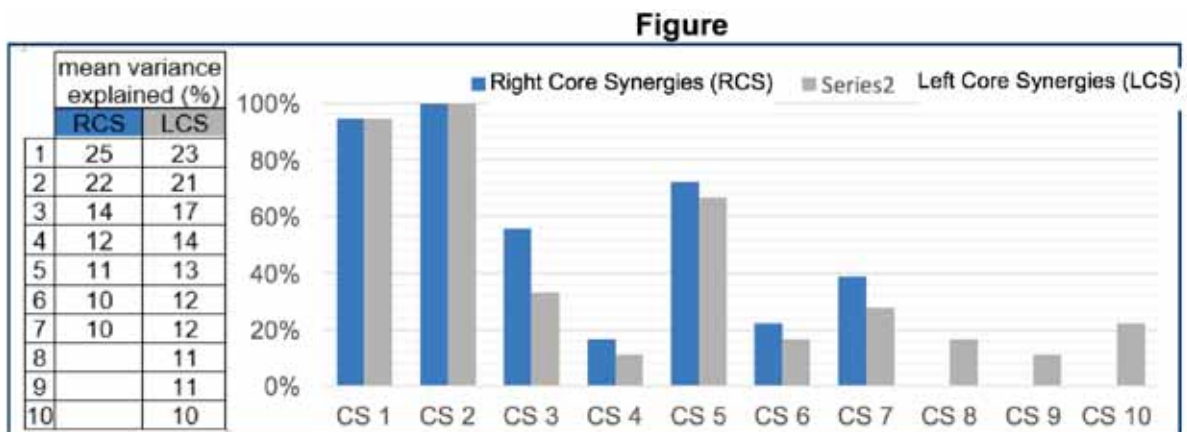
Figure caption: Percentage of people using CSs (right side) and mean variance explained by each CS (left side).

References:
[1]   R. Prevete, et al. Sci. Rep., vol. 8, no. 1, p. 616, Dec. 2018.
[2]   V. Gracia-Ibáñez et al. Sci. Rep., 2020.
[3]   V. Gracia-Ibáñez et al. Comput. Methods Biomech. Biomed. Eng., vol. 20, no. 6, pp. 587–597, 2017.

PS3.4

Novel knee arthrometer use in clinical settings for assessing tibiofemoral motion

Rose Schauffler[1], Jamie Hall[1], Trent Guess[1], Kylee Rucinski[1]

1   University of Missouri, Columbia, United States

Approximately 1 in 3 people globally live with a painful musculoskeletal condition with 1 in 5 of these occurring in the lower extremity1. Knee disorders account for over half of all lower extremity disorders or around 5% of all musculoskeletal disorders2. Anterior cruciate ligament (ACL) injuries are one of the most common musculoskeletal diagnoses affecting the knee3. The frequency of such disorders highlights a need for a device that can accurately measure quantitative three-dimensional motion of the tibia relative to the femur during functional knee movement. Motion capture methods do not accurately measure non-sagittal knee motion due to skin artifact and dual fluoroscopy methods are expensive and require a laboratory setting. Inexpensive methods used in the clinic such as goniometers are limited to sagittal plane static measurements. Limitations of these methods led to the development of the Mizzou Knee Arthrometer Testing System (MKATS) which can efficiently and accurately measure dynamic knee motion in clinics and sports training facilities. The MKATS consists of two electromagnetic sensors which measure relative motion between the femur and the tibia in six degrees of freedom. The sensors are connected to bones through a femoral clamp that is secured to the distal femur and a tibial clamp attached to the proximal tibia. Through a series of calibration steps and computational algorithms, sensor coordinate systems are transferred to an anatomical frame to acquire angles of rotation about the flexion-extension, internal-external, and varus-valgus axes. Following Institutional Review Board approval, MKATS was used to evaluate knee motion during functional tasks for healthy control subjects (n=20, 14 female, 25.6 ± 5.0 years) and ACL deficient populations (n=11, 4 female, 31.6 ± 9.3 years). Three cycles of each task were isolated, ensemble averages calculated, and cycle normalized for each subject (Figures 1 and 2). Paired t-tests revealed statistically significant differences between the internal-external rotation angles for those with ACL deficiencies compared to healthy subjects during more than 90% of the cycle during step-up and over tasks and during more than 60% of the cycle during lateral step-down tasks as shown in the shaded regions of Figures 1 and 2. ACL deficient subjects showed more external rotation in the involved limb than the controls which aligns with previous observations in literature4. Efficient and accurate tibiofemoral motion was obtained using a non-invasive device for 31 subjects during dynamic tasks. Such real time information may be useful as an early screening and diagnostic tool for clinicians including physical therapists, athletic trainers, and orthopedic specialists when treating associated disorders and when determining appropriateness for return to sport.
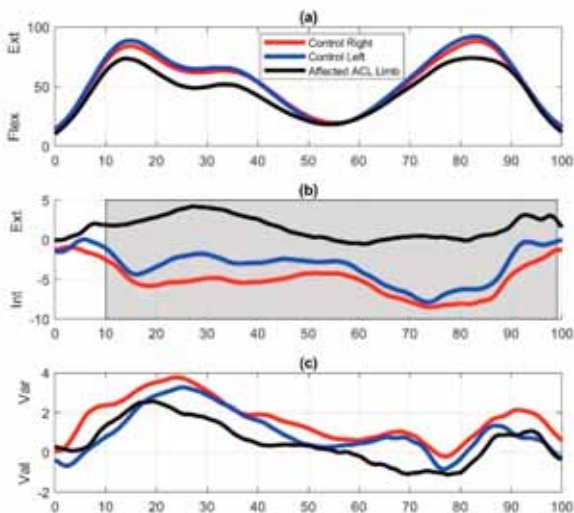
Figure 1: Rotation angles during step-up and over. (a) Flexion-extension. (b) Internal-external. Significantly different values between 10-99% of the cycle. (c) Varus-valgus.
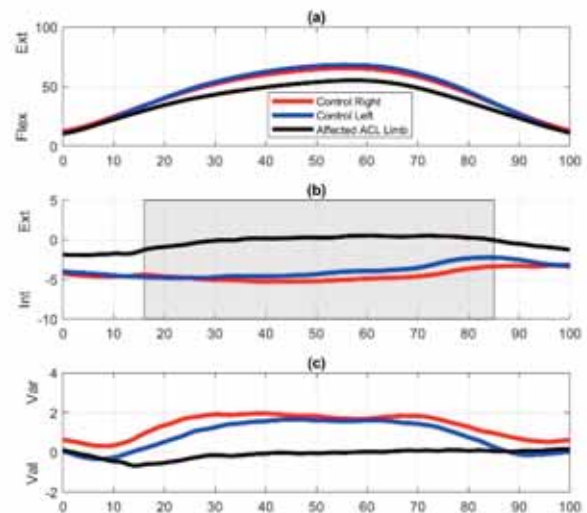
Figure 2: Rotation angles during lateral step-down. (a) Flexion-extension. (b) Internal-external. Significantly different values between 16-85% of the cycle. (c) Varus-valgus.

References:
1. James SL et al (2017), Lancet, 2. Reid CR, et al (2010) J Occupational Rehabilitation, 3. Moulton SG et al (2018), The Anterior Cruciate Ligament (Second Edition), 4. Bates NA, et al (2018), Clin Biomech.

PS3.5

Pipeline for real-time muscle force estimation based on Markers-EMG tracking algorithm: a proof-of-concept

Amedeo Ceglia[1], François Bailly[2], Mickael Begon[2]

1   Université de Montréal, Génie biomédicale, Montreal, Canada
2   Université de Montréal, École de kinésiologie et des Sciences de l'Activité Physique, Montréal, Canada

Introduction: Muscle force estimation will help clinicians to advise their patients in a rehabilitation context. Since they cannot be measured, numerical solutions have been developed to provide real-time feedback. Inverse methods are widely used for this purpose but suffer from a lack of reliability, even when combined with forward methods. In a previous study, we proposed a Markers-EMG tracking algorithm, a forward method based on Bioptim [1], using a moving horizon estimation. This algorithm was able to estimate muscle force with consistent dynamics at 24 Hz on simulated data [2]. The present study aims at providing a proof-of-concept of a pipeline for real-time muscle force estimation under experimental conditions. This method combines model scaling, EMG processing and our real-time muscle force estimation algorithm.

Method: One subject was selected and was asked to perform five free-velocity elbow flexions. Three surface EMG sensors were positioned over his biceps brachii long head and the triceps brachii (long head and lateral head). EMG signals were collected at 2000 Hz. In addition, six skin markers were placed on the shoulder, elbow and forearm. Marker trajectories were collected at 100 Hz using an optoelectronic system. A one degree of freedom musculoskeletal model actuated by five hill-type muscles was used to reconstruct the subject. The pipeline was divided into three parts. (i) Three maximal voluntary isometric contractions were performed to obtain the maximum voluntary activations of the three recorded muscles. We developed a python tool capable of computing maximal contraction using live data. (ii) A model scaling was performed using markers' position. (iii) Our algorithm was used to estimate muscle force. Markers and EMG data were provided to the estimator whenever they were needed until the user stopped the program. To improve performance, two computers were used with TCP/IP connection, one for data acquisition and the other for running the estimator. Also, multiprocessing algorithms were used for code efficiency. Finally, live graphs were displayed.

Results: After the model scaling and the MVC processing, preliminary results show that the algorithm was able to estimate muscle force with consistent dynamics. The estimator frequency was higher than 13 Hz (standard biofeedback), four times faster than offline estimation.

Discussion: These preliminary results are promising for real-time muscle force estimation using our markers-EMG tracking algorithm. In a future work we will apply the pipeline on a more complex model and movement. Also, a calibration of muscle parameters will be needed to accurately estimate muscle force.

References:
[1]   Michaud, B., et al. (2021). Bioptim, a Python framework for Musculoskeletal Optimal Control in Biomechanics. bioRxiv.
[2]   Bailly, F., et al. (2021). Real-time and dynamically consistent estimation of muscle forces using a moving horizon emg-marker tracking algorithm. Frontiers in bioengineering and biotechnology, 9, 112.

PS3.6

Towards robust step length estimation model for smartphones based on the motion of human body during walking

Melanija Vezočnik[1], Roman Kamnik[2], Matjaz B. Juric[1]

1   Faculty of Computer and Information Science, University of Ljubljana, Laboratory for Integration of Information Systems, Ljubljana, Slovenia
2   Faculty of Electrical Engineering, University of Ljubljana, Laboratory of Robotics, Ljubljana, Slovenia

Microelectromechanical-systems-based inertial sensors integrated into Internet-of-Things wearables and smartphones enable a vast number of applications including step length estimation related to healthcare as well as indoor navigation. Herein, we present our research towards a new step length estimation model stimulated by our previous work [1] that set the basis to combine biomechanics of human walking, sensor technology, and mathematics in this study.

We investigated the motion of the human body during long-term walking on a treadmill for several walking speeds and its impact on distance walked using a highly accurate optical measurement system. Data were acquired from a group of 10 healthy adults and include more than 10 hours of walking measurements altogether. The positions of anatomical landmarks on one side of the human body for slow, normal, and fast walking speeds were utilized for the derivation of the model as shown in Figure 1. They were analyzed by employing exploratory data analysis to identify relevant parameters common to all monitored anatomical landmarks that had the greatest impact on the motion of the human body during walking and could be used as a basis for an inertial-sensor-based solution for step length estimation, also suitable for smartphones. Thereafter, a new acceleration-based step length estimation model was obtained. It was evaluated in two types of environment—treadmill and rectangular-shaped test path—for long-term walking using four off-the-shelf smartphones testing different walking speeds as shown in Figure 1.

Initial results indicate that the proposed model outperformed related models in terms of accuracy of estimated walked distance under different circumstances. All the evaluation data are publicly available in our benchmark repository for evaluation of step length estimation models [2].
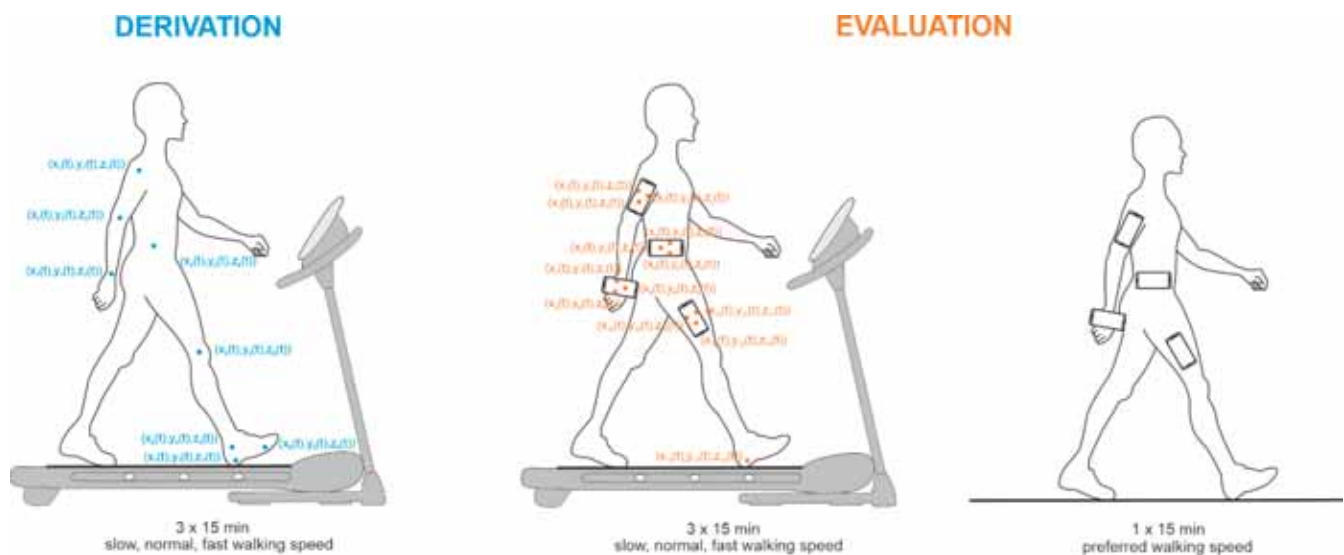
Figure 1: Design of the data acquisition for the derivation and evaluation of step length estimation model.

References:
[1]   M. Vezočnik and M. B. Juric, 'Average Step Length Estimation Models' Evaluation Using Inertial Sensors: A Review', IEEE Sensors Journal, vol. 19, no. 2, pp. 396–403, Jan. 2019, doi: 10.1109/JSEN.2018.2878646.
[2]   M. Vezočnik and M. B. Juric, 'Open repository for evaluation', Available online: https://github.com/repositoryadmin/SLERepository (accessed on Apr. 29, 2021).

PS3.7

On the use of mesh-based joint contact models within simulations using automatic differentiation

Gil Serrancoli[1], Jordi Torner[1], Simone Perelli[2 3], Joan Carles Monllau[2 3]

1   Multimedia Applications Lab, Universitat Politècnica de Catalunya, Barcelona, Spain
2   Institut Català de Traumatologia i Medicina de l'Esport (ICATME), Hospital Dexeus, Barcelona, Spain
3   Hospital del Mar, Department of Orthopaedic Surgery, Barcelona, Spain

Musculoskeletal simulations can be used to estimate or predict biomechanical variables in silico. Recent advances integrating automatic differentiation (AD) tools into OpenSim software [1] improve the efficiency of those simulations, usually obtained by solving an optimal control problem. This is because AD allows calculating the derivatives much faster than using traditional methods (up to 20 times for complex musculoskeletal methods), such as finite differences (FD). AD tools create an expression graph of the mathematical expressions and compute the derivatives. One of the main drawbacks is that conditionals (if-statements) are not easy to handle when building the expression graph, as in collision-detection algorithms.

We present a mesh-based elastic foundation contact model, which can be used within optimal control problems and solved using AD tools. At each optimization iteration, the minimum distance (maximum penetration) among mesh faces between two bodies are calculated based on a smoothed function (Figure 1A). We used the mesh-based contact model within a knee-prosthesis (Figure 1B) pose estimation analysis. The contact forces and the motion corresponding to a gait cycle of a femoral component and tibial tray of an instrumented knee prosthesis [2] were tracked so that the kinematics and dynamics were consistent. The optimal control problem was formulated using a direct collocation method and an implicit dynamics formulation. Six degrees of freedom (dofs) were considered between the femoral component and the tibial tray. Reserve actuators (three forces and three moments) were introduced to facilitate the tracking. The problem was solved computing the derivatives from the expression graph using AD and FD to compare the performance.

The results obtained both in AD and FD tracked the kinematics accurately (mean and standard deviation of RMSE values of 4.1 ± 2.4 mm for AD, and 4.5 ± 1.8 mm for FD) and contact forces (mean and standard deviation of RMS values of reserve actuators 51.4 ± 40.2 N for AD and 38.8 ± 28.0 N for FD). In both cases (AD and FD), the correlation coefficients between the modeled and the experimental inferior-superior contact force were 0.99. The main differences were in the convergence performance. Both computational time and number of iterations were lower using AD (541 s and 2077 iterations) than FD (1316 s and 3494 s). This type of contact model could also be integrated within an optimal control problem dealing with a full-body musculoskeletal system.
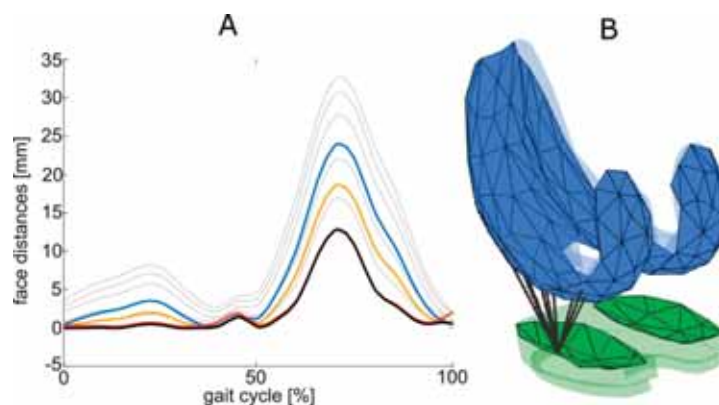
Figure 1: A. Example of the smooth calculation of minimum distance between faces of two bodies. B. Map of potential contact pairs.

References:
1.   Falisse et al., PLoS One 14 (10): 1–19, 2019.
2.   Fregly et al., J. Orthop. Res. 30 (4): 503–513, 2012.

PS3.8

Optimal synthesis of complex repetitive upper-limb movements using fatigable muscles

Benjamin Michaud[1], Mickael Begon[1]

1   École de Kinésiologie et des Sciences de l'Activité Physique, Montréal, Canada

Fatigue-related tasks are notably hard to study, but can be investigated using predictive simulations. For instance, by varying the penalties and parameters, the emergence of coping strategies for fatigue mitigation can be assessed. Muscle fatigue dynamics combined with static motion analysis have been used to track a fatigue score from a captured movement (Sharif Razavian & McPhee 2016). Optimal control synthesis in the form of Nonlinear Model Predictive Control (NMPC) has been successfully used to predict movement (Mehrabi et al. 2017), but was limited to planar motion and did not include a fatigue model. Our objective is to predict a complex upper-limb cyclic movement that includes a model of fatigue to assess coping strategies over a long period of time.

The optimal control programming (OCP) framework bioptim (Michaud et al. 2021) was used to formulate an NMPC program using an upper-limb musculoskeletal model augmented with a violin and a bow. The objective and constraints were designed to produce a violin-like movement. The dynamics of muscle fatigue of Xia & Frey Law (2008) was added to reduce the capability of the muscles to produce force as their fatigue builds up. Preliminary results were obtained by defining a single long window—i.e., 15 back-and-forth of the bow of 1 second each—of the NMPC solved all at once, effectively solving a regular OCP. Moreover, the fatigue parameters were uplifted to ensure that fatigue would appear during the duration of the movement.

As expected, the OCP algorithm produced a violin-like movement with muscle fatigue accumulating in the muscles. No coping strategy was found to reduce muscle fatigue over 15 seconds. That is because none of the muscle had their force sufficiently impaired to prevent the avatar from achieving the task. We expect longer simulation ran using NMPC will sufficiently impair the muscular capabilities to force the algorithm to find coping strategies.

This research may be used in the future to predict a personalized set of good variability and thereafter to provide real-time feedback for complex repetitive movements.

References:

Mehrabi N, Razavian RS, Ghannadi B, McPhee J. 2017. Predictive Simulation of Reaching Moving Targets Using Nonlinear Model Predictive Control. Frontiers in Computational Neuroscience. 10:143.

Michaud B, Bailly F, Charbonneau E, Ceglia A, Sanchez L, Begon M. 2021. Bioptim, a Python framework for Musculoskeletal Optimal Control in Biomechanics. bioRxiv.:2021.02.27.432868.

Sharif Razavian R, McPhee J. 2016. Minimization of Muscle Fatigue as the Criterion to Solve Muscle Forces-Sharing Problem [Internet]. In: [place unknown]: American Society of Mechanical Engineers Digital Collection; [accessed 2021 Apr 29].

Xia T, Frey Law LA. 2008. A theoretical approach for modeling peripheral muscle fatigue and recovery. Journal of Biomechanics. 41(14):3046–3052.

PS3.9

Characterizing the spectrum of hip morphology via statistical shape modeling and linear discriminant analysis

Joseph Mozingo[1], Penny Atkins[1], Travis Maak[1], Stephen Aoki[1], **Andrew Anderson**[1]

1   The University of Utah, United States

Femoroacetabular impingement syndrome (FAIS) is a painful motion-related structural hip disorder characterized by loss of sphericity of the femoral head, reduction in femoral-neck offset, and/or an overly-prominent acetabular rim. Radiographic findings indicate FAIS morphology is very prevalent among asymptomatic collegiate and senior-aged (>65y/o) competitive athletes, yet most of these athletes did not have a history of hip pain or radiographic evidence of osteoarthritis [1-2].These findings suggest current radiographic techniques are ineffective for identifying aspects of the deformity that are predictive of symptoms. Further, though radiographic measurements are a standard for diagnosis, they describe no more than 50% of the true, 3D shape of the femoral deformity in patients with FAIS [3]. Herein, statistical shape modeling (SSM) was leveraged to objectively quantify and compare variation in 3D femur morphology in asymptomatic collegiate athletes, FAIS patients, and healthy controls.

A CT/MRI scan of the femur was obtained in 5 collegiate athletes with no hip pain, 28 patients, and 26 controls having typically-developed hips (all male). Proximal femurs were segmented and converted to 3D surfaces using Amira v.6.0.1. Prior to input to the SSM pipeline, surfaces were smoothed, reflected if right-sided, and aligned via the iterative closest point algorithm. Correspondence particles (n=2,048) were placed at consistent anatomic sites across femurs using ShapeWorks 6.0. Procrustes analysis removed the effect of pose and scale from the optimization. Principal component analysis determined modes of variation from particle locations; modes containing significant variations were identified via parallel analysis. Particle locations were used to quantify mean shapes for FAIS and control groups. To evaluate the spectrum of morphology, a linear discriminant analysis (detailed in [4]) based on 3D shape (2,048[particles]*3[x/y/z coordinates]=6,144 scalar data vector) of the mean FAIS and control femurs (normalized to scores of -1 and 1, respectively) determined shape scores for athlete femurs.

The first 6 modes described significant variations, accounting for 80.5% of the total variation. Variation in the femoral head (mode 1), head-neck junction (modes 1, 2), and greater and lesser trochanters (mode 3) was observed (Figure). Shape scores for athletes were -1.5, -1.0, -0.9, 1.5, 3.1. Though asymptomatic, three athletes had negative scores, indicating 3D shape resembling FAIS. Expansion of the athlete cohort in the future could reveal whether SSM-based biomarkers can distinguish symptomatic morphology.
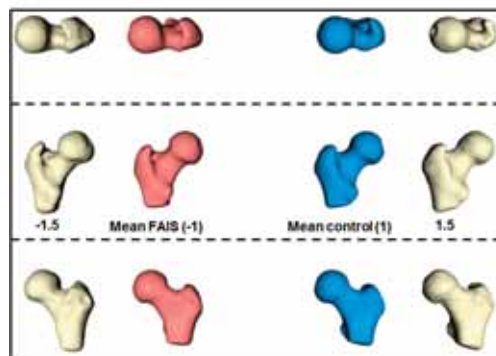
Figure caption: Shape scores of 2 athlete femurs (±1.5; white) relative to mean FAIS (red) and control (blue). Superior (top), posterior (middle), and anterior (bottom) views.

References:
[1] Kapron et al. (2011). J Bone Joint Surg Am, 93(19):e111.
[2] Anderson et al. (2016). Clin Orthop Relat Res, 474(2):342-52.
[3] Atkins et al. (2019). Clin Orthop Relat Res, 477(1):242-53.
[4] Atkins et al. (2017). J Orthop Res, 35(8):1743-53.

PS3.10

Influence of anatomical and implant factors on bone strain behaviour in total ankle replacement

Bryony Halcrow[1], Ruth Wilcox[1], Claire Brockett[1]

1   University of Leeds, Institute of Medical and Biological Engineering, Leeds, United Kingdom

Ankle arthritis affects between 1-4% of the population; arthroplasty is one of the late-stage surgical treatment options. Size of the implants can vary depending on patient anatomy. Undersized implants risk bone resorption or subsidence if they are not adequately seated on the cortical outer region of the tibia. Correct implant sizing can therefore be difficult to achieve. The aim of this study was to use subject specific finite element (FE) models to examine the effect of implant size in stemmed tibial ankle replacement designs and how this varies between subjects.

Specimen specific FE models were created from five cadaveric ankles (Abaqus/CAE 2017), scanned at 82μm in a microCT scanner (Scanco XtremeCT). The tibia and talus were segmented (ScanIP, 2019, Synopsys-Simpleware). Virtual implantation of four different sized stemmed ankle replacements was performed on each model (20 in total), following published surgical procedure. Implantation was performed with the ankle bones held in a neutral position to ensure correct alignment. All parts were meshed with linear tetrahedral elements (~ 115,000 total).

Load and flexion corresponding to peak axial load during the gait cycle was applied [1], with the inferior talus fixed at the subtalar joint surface. Implant-bone interface was fixed with sliding contact (Penalty, μ=0.05) between implant components. Image-based bone material properties were derived in a separate calibration study: 8 specimens were cut from distal human tibia, microCT-imaged and tested under axial compression. Image based FE models were then used to identify an optimum greyscale-to-modulus relationship and applied to the 20 ankle models.

Minimum principal strain distributions around the implant were measured. Inter-specimen strain variation was more pronounced than variation relating to implant size (Figure 1). Strains in bone around the stem and tip of the implant did not change significantly between implant sizes. Some specimens exhibited lower strains at the distal tibia for larger implants.

This study showed that variations seen between patients is likely to have a larger effect on bone strain around the implant than the size of the implant itself. Bone quality is thought to play a larger role in the success of implants, with bones exhibiting poorer bone quality showing higher strains. Increased strain around the implant tip region, above bone yield strains, could lead to alteration of bone material properties [2], with bone cysts and regions of osteolysis reported clinically, close to the tibial implant. Soft tissue effects were not considered here but visual inspection showed some implants would be unsuitable due to the large overhang of implant into surrounding joint space. Patient selection is thought to be more important than implant size for successful joint replacements.
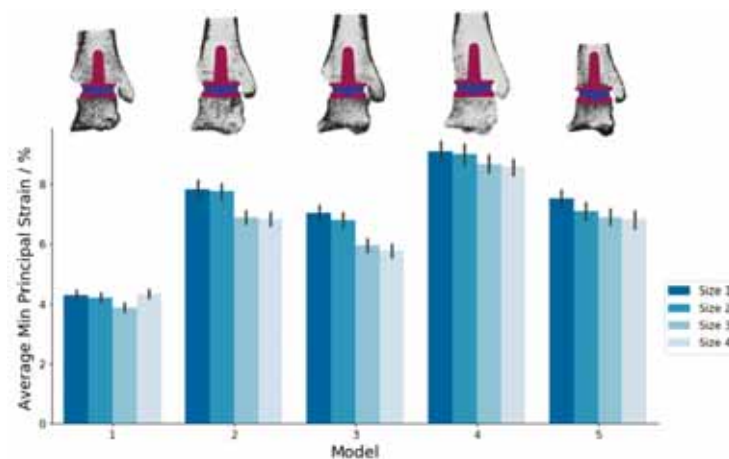
Figure 1: Minimum principal strains through bone around tip region of implant for all implant sizes. Schematic of ankle models showing greyscale distributions, with more dense bones appearing darker.

References:
[31] Smyth et al, Journal of Biomechanics, 53:105-110, 2017
[32] Morgan et al, Journal of Biomechanics, 34:569-577, 2001

PS3.11

Investigating the influence of personalized musculoskeletal models on the calculated stresses in the pelvic ring

Ahmed Soliman[1], Slawomir Kedziora[1], Jens Kelm[2], Torsten Gerich[3], Stefan Maas[1]

1   University of Luxembourg, Department of Engineering, Luxembourg, Luxembourg
2   Chirurgisch-Orthopädisches Zentrum, Illingen/Saar, Germany
3   Centre Hospitalier de Luxembourg, Luxembourg, Luxembourg

This study investigates the influence of personalizing musculoskeletal models on muscles-and contact-joints forces and on stresses in the pelvic ring during normal gait cycle. Customized MusculoSkeletal model (MS) provides more precise muscle and contact forces. Additionally, it enables more automatic coupling between MS and Finite Element (FE) environments by data transfer. All calculated forces are utilized to predict stress states in pelvis bones using FE software. In this study the generic MS model of AnyBody [AnyBody.7.1] software is adopted or personalized by morphing the pelvis in order to match exactly a 3D CT-scanned model of Sawbones artificial pelvis 4th generation. As a result of morphing, muscles attachment points and joints centers are more or less shifted. For the normal slow gait movement, the inverse dynamics analysis is run twice: first run for the generic MS then another time for the personalized MS. Comparison of both results is performed to highlight the difference in forces and stresses. Two moments of the gait-cycle are investigated, named Left Heel Strike (LHS), and Right Toe Off (RTO), respectively. Concerning joint contact forces, both models showed similar order of magnitude with notable deviations. During LHS, the right leg shows 5% lower hip joint contact force (HJC), while during RTO this deviation increases to 16%. Of course, muscles forces show similar pattern but with deviation up to 24% for right Gluteus Medius muscle during LHS and for the right Erector Spinae during RTO. The Lumbosacral Joint (LSJ) contact force shows deviation of 6.5% for LHS and almost no deviation for RTO. These deviations alter the peak stress and the stress history and the distribution within the pelvic ring. For LHS, the lower HJC lowers the equivalent stress up to 12% in the right superior ramus. This deviation drops to 10% in case of RTO. The personalized MS model shows similar trend with notable deviation at distinct gait positions. Hence, personalizing MS models provides more precise results. Another interesting outcome is enabling automatic or semi-automatic transfer of forces between the inverse dynamics and FE-software packages due to the fact that the geometry is now exactly the same.

PS3.12

Lower limb joint load comparison from subject specific musculoskeletal model simulation and direct measurements on different subject with instrumented implant during normal and abnormal gait

Carlos Rodrigues[1 2], Miguel Correia[1 2], João Abrantes[3], Marco Rodrigues[4], Jurandir Nadal[5]

1 University of Porto, Faculty of Engineering , Porto, Portugal
2 INESC TEC - Institute for Systems and Computer Engineering, Technology and Science, C-BER - Centre for Biomedical Engineering Research, Porto, Portugal
3 Lusófona University, CICANT (Centre for Research in Applied Communication, Culture, and New Technologies), Lisbon, Portugal
4 Federal University of Pernambuco, Department of Electronic and Systems, Recife, Brazil
5 Federal University of Rio de Janeiro, Biomedical Engineering Program, Rio de Janeiro, Brazil

Knowledge of joint internal loadings are essential for gait impairment diagnosis, intervention planning and post-operative rehabilitation. Nevertheless, direct measurement of joint internal loads can only be performed invasively, pointing for the need of subject specific musculoskeletal models and input data for estimation of specific subject joint internal loads at different gait conditions. Despite main reason for gait study is related with gait disorders, dominant information is available on normal gait with the need of subject specific model and simulation for abnormal gait due to specific condition of each subject disability. For this reason, there is an increasing need to validate model estimated joint internal loads, comparing computed values with direct measured loads of different subjects and gait conditions, contributing to improve musculoskeletal model predictions. Subject specific selected model corresponds to a 40-year-old healthy male voluntary with 70 kg and 1.86 m height. Ground reaction forces were acquired with two force plates at 2000 Hz and kinematic coordinates of reflective markers at lower limb selected anatomical points acquired with eight camera system at 100 Hz during normal gait (NG), stiff knee gait (SKG), and slow running (SR). Musculoskeletal analysis was performed based on stick-figure model of static trial and over-determinate kinematic analysis over dynamic trial, morphing Twente Lower Extremity Model (TLEM) matching the size and joint morphology of the stick-figure model and inverse dynamic analysis based on joint angles and kinetic boundary conditions, obtaining joint contact forces and force moments. Normalized joint contact forces to body weight from subject specific musculoskeletal simulation were compared as regards to NG, SKG and SR, as well as at the right, left and both sides lower limb joints with post-operative (PO) direct measurements from four patients, ages 61-83 years, average mass 82 kg and 1.71 m height, with hip and knee instrumented implants at different comparable gait conditions with NG, SKG and SR. Results pointed for lateral asymmetry at the comparison of the computed hip and knee joint forces on NG and SKG, whereas the ankle presented no asymmetry at the left and right sides. Differences were also detected at SR with higher peak joint forces in relation to NG and SKG. On direct measurement of instrumented implants, hip and knee forces presented lower values at SKG than NG and SR, pointing for SKG as a protection mechanism to reduce peak forces. Direct measurements presented lower values of peak forces at the hip and knee comparatively to musculoskeletal model simulation, possible linked with different subjects assessment, intervened/healthy conditions and the need on additional input data for more realistic subject specific model to increase noninvasive accuracy prediction of joint contact forces during human impaired gait.

PS3.13

Morphological variation and statistical shape model prediction in paediatric lower limb bones

Laura Carman[1], Julie Choisne[1], Thor Besier[1]

1   Auckland Bioengineering Institute, Auckland, New Zealand

The skeletal anatomy of children differs significantly from adults, yet we often scale down generic musculoskeletal models based on the adult skeleton¬¬ to represent children. ¬Subject-specific models can be built using medical imaging [1], but this is costly and time-consuming. Statistical shape models (SSM) have been used to predict bone shape in adult populations [2]. Developing a similar tool for a paediatric population would help to characterise the growing skeleton and predict unknown bone shapes. The aims of this study were to: 1) characterise bone shape variation in a typically developed paediatric population and 2) evaluate bone shape prediction error using a SSM.

Post-mortem CT scans of 333 children (137 F, Age: 12 ± 5Y, H: 148 ± 24cm, M: 49 ± 22kg) were obtained from the Victorian Institute of Forensic Medicine (VIFM, Melbourne, Australia). The pelvis (P), femurs (F), and tibia/fibulas (TF) were segmented. Each bone was non-rigidly registered and fitted to a template mesh, using radial basis functions to achieve nodal correspondence, and then rigidly aligned. A principal component analysis (PCA) [2] and subsequently a Procrustes analysis were performed to characterize the shape variation within the dataset. Accuracy was assessed using fitting error, compactness, specificity, and generality. The generality was assessed with a leave one out (LOO) analysis by performing a regression analysis between PCA outputs and demographic (age, height, mass, sex) and linear bone measurements (thigh and shank length, hip, knee, and ankle width).

The first principal component captured most of the variation in the dataset (P: 92%, F: 98%, TF: 97%). This was reduced in the Procrustes analysis (P: 28%, F: 17%, TF: 25%), where the first principal component shows the changes in bone shape within the dataset (Figure 1). The results from the LOO analysis gave an average RMSE of: (P: 5.31 ± 2.09mm, F: 5.21 ± 2.25mm, TF: 4.93 ± 2.19) using demographic measurements, which was reduced to: (P: 4.78 ± 1.75mm, F: 3.55 ± 1.16mm, TF: 3.89 ± 1.33mm) when linear bone measurements were included.

This unique dataset characterises morphological variation in paediatric bone and allows for prediction of new bone shapes with low errors using demographic and linear bone measurements for use in clinical settings and musculoskeletal modelling.
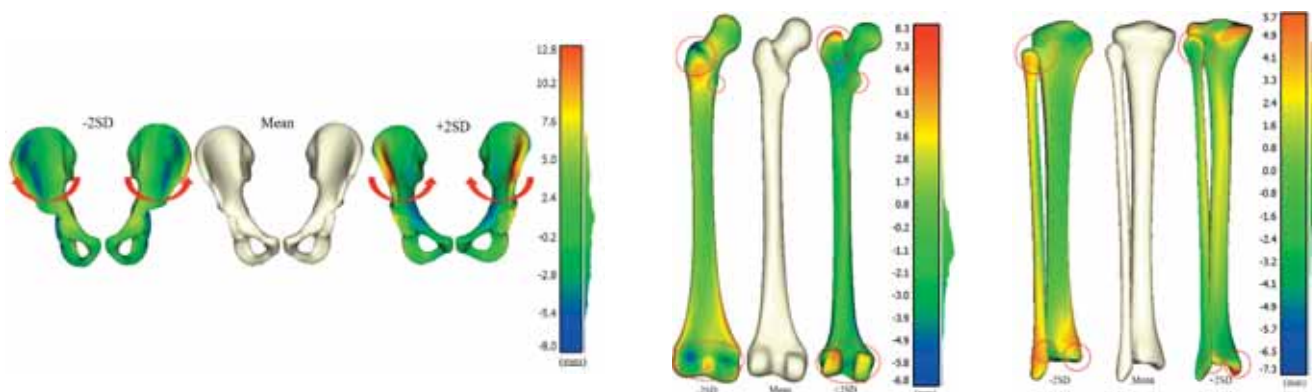
Figure caption: First principal component of the Procrustes analysis. From left to right: pelvis, femur, and tibia/fibula. Represented as the mean shape in cream and point distances at -2SD/+2SD to the left and right displayed on the colour bars.

References:
[1]   Scheys L et al. (2011).Gait&Posture,33:158-164
[2]   Zhang J et al. (2016).Med. Eng. Phys.,38:450–457

PS3.14

Pulmonary valve replacement surgery strategy using contracting band for patients with repaired tetralogy of fallot simulations using MRI-based biomechanical models: a multi-patient study

Han Yu[1], Pedro J. del Nido[2 3], Tal Geva[4 5], Zheyang Wu[6], Xueying Huang[7], Rahul H Rathod[4 5], Kristen L. Billiar[8], Dalin Tang[1 6]

1   Southeast University, School of Biological Science & Medical Engineering, Nanjing, China
2   Boston Children's Hospital, Dept. of Cardiac Surgery, Boston, United States
3   Harvard Medical School, Dept of Surgery, Boston, United States
4   Boston Children's Hospital, Dept. of Cardiology, Boston, United States
5   Harvard Medical School, Department of Pediatrics, Boston, United States
6   Worcester Polytechnic Institute, Mathematical Sciences Department, Worcester, United States
7   Xiamen University, School of Mathematical Sciences, Xiamen, China
8   Worcester Polytechnic Institute, Department of Biomedical Engineering, Worcester, United States

Tetralogy of Fallot (ToF) is a congenital heart defect and a main cause for late onset right ventricle (RV) failure. Current surgery procedures, including pulmonary valve replacement (PVR) with right ventricle remodeling, yield mixed results. Computational biomechanical modelling technique is widely used in cardiovascular study for investigation of mechanisms governing disease development, quantitative diagnostic and treatment strategies and improving surgical designs for better outcome. PVR with active band insertion was hypothesized to be of clinical usage to improve right ventricle function measured by ejection fraction. In lieu of risky open-heart surgery and experiments on animal and human, computational mechanical models were adapted to study the impact of PVR with different band insertion options.

Cardiac magnetic resonance (CMR) images were acquired from 7 TOF patients before and 6 months after PVR with patient consent obtained. Pre-PVR data were used for model construction. For each patient, 5 different surgery plans combined with passive and active contraction band with band active contraction ratio of 20%, 15% and 10% were studied. Those 5 plans include plans (a), (b) and (d) corresponding to one inserted band connecting ventricular septum and anterior to the middle of papillary muscle (PM), posterior to the middle of PM and the base of PM. Plan (c) is the combination of plan (a) and (b). Plan (e) is the combination of plan (c) and (d). Including the 7 no-band models, 147 computational bi-ventricle models were constructed to simulate RV cardiac functions and identify optimal band plans.

Surgery plan with 3 active contraction bands and band active contraction ratio of 20% had the best performance on improving RV function. The Mean±SD RV ejection fraction value from the 7 patients was 42.90%±5.68%, presenting a 4.19% absolute improvement or a 10.82% relative improvement over the mean value of baseline models (38.71%±5.73%, p=0.016). The EF improvements from the 7 patients varied from 2.87% to 6.01%. Mean±SD ΔEF values of the 7 patients for band options A-D and 20% band active contraction ratio were 2.51% ±0.80%, 2.13%±0.53%, 3.36% ±1.07%, 1.90%±0.40%, respectively.

This pilot work demonstrated that surgical procedures using active contraction bands have great potential to improve RV function measured by ejection fraction for patients with repaired ToF. It is possible to have higher right ventricle ejection fraction improvement with more bands and higher band active contraction ratio. Our findings with computational models need to be further validated by animal experiments before clinical trial could become possible.
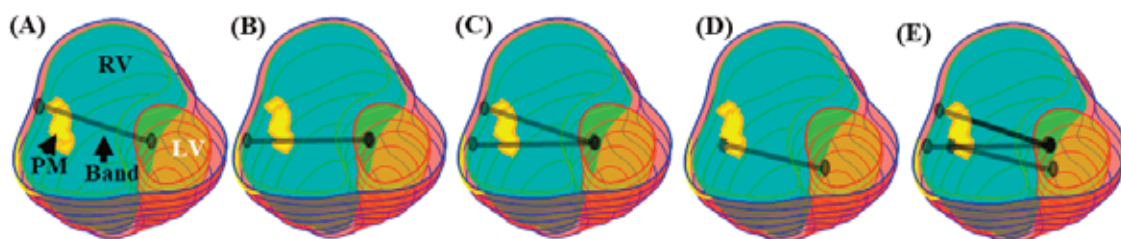
Figure caption: Figure 1. Five band insertion surgical plans.

PS3.15

Smart surgical planning for anatomical ACL reconstruction

Maria Sale[1], Alan Wang[1 2], Paul Monk[1], Marco TY Schneider[1]

1   Auckland Bioengineering Institute, The University Of Auckland, Auckland, New Zealand
2   Faculty of Medical and Health Sciences, University of Auckland, Auckland, New Zealand

Anterior Cruciate Ligament (ACL) ruptures are one of the most common knee injuries seen in sports medicine [1]. For most patients, reconstructive surgery is the standard treatment pathway to restore knee stability. The clinical outcome and risk of reinjury after surgery are heavily dependent on the graft placement [2]. This task can be challenging for low-volume surgeons, especially given the limited toolset available to identify the ideal graft fixation points within the knee. In this study, we present a computational workflow for planning ACL tunnels from standard clinical imaging data.

A deep convolutional neural network was developed using PyTorch [3] and trained on a dataset of clinical MRI (n=200) using a patch-based approach to segment the femur and tibia (Figure 1). The network is based on the 3D U-Net [4] architecture. A femoral statistical shape model (SSM) and tibial SSM were trained on a dataset of intact ACLs to predict where the anatomical attachment sites were. These were subsequently fitted to the knee to obtain a location for the ACL tunnels. A GUI was constructed to visualize the tunnel placement in a 3D knee model.

The results for a set of knees (n=51) were then compared to the ground truth and the attachment sites selected by an orthopaedic surgeon. The test set demonstrated that the predictive model had a 54% reduction in the Euclidian distance to the anatomical ACL attachment site compared to that of the clinically selected point.

The reduced error in the model's results (Table 1) indicates that further development and refinement of the workflow using image processing techniques and larger datasets are worth pursuing. The eventual integration of the model into a surgical pre-planning workflow has the potential to have a positive impact on patient outcomes.

Table 1: Summary of test data comparing model and surgeon's tunnel placements. Distances in mm.

Predictor	Femoral Tunnels					Tibial Tunnels				
	Mean Err	Std.	Max Err	Min Error	RMS	Mean Err	Std.	Max Err	Min Error	RMS
LOO Model (n=51)	1.89	1.41	8.56	0.23	2.35	2.21	1.32	6.05	0.4846	2.57
Surgeon (n=10)	6.69	1.38	8.72	4.31	6.83	4.96	2.74	9.83	1.38	5.67
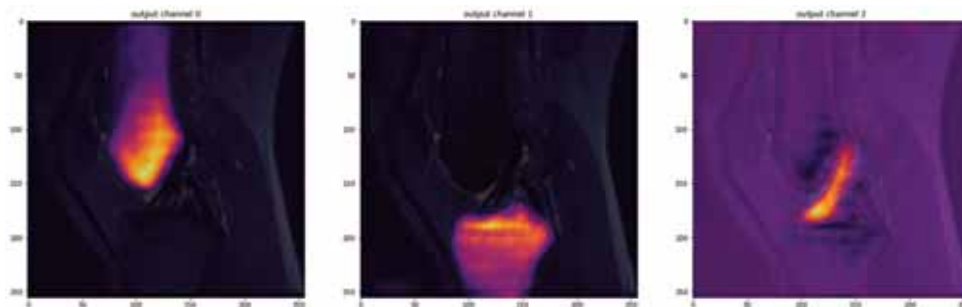
Figure 1: d-CNN segmentation results showing probability clouds for each target region.

References:
[1]   Majewski M. et al. (2006),The Knee, 13(3), 184-188
[2]   Behrend H. et al. (2006), Knee surgery, sports traumatology, arthroscopy: official journal of the ESSKA, 14(11), 1159–1165
[3]   Paszke, Adam, et al. "Pytorch: An imperative style, high-performance deep learning library." arXiv preprint arXiv:1912.01703 (2019).
[4]   Ronneberger O. et al. (2015), MICCAI, 234-241

PS4.1

Design-based models of heart valves and flow through bicuspid aortic valves

Alexander Kaiser[1], Rohan Shad[2], Nicole Schiavone[3], William Hiesinger[2], Alison Marsden[4]

1   Stanford University, Institute for Computational and Mathematical Engineering, Stanford, United States
2   Stanford University, Cardiothoracic Surgery, Stanford, United States
3   Stanford University, Mechanical Engineering, Stanford, United States
4   Stanford University, Bioengineering, Stanford, United States

In this work, we present a technique called design-based elasticity for fluid-structure interaction simulations of heart valves. To construct models, we require that tension in the valve leaflets supports a pressure and derive a resulting system of differential equations. The solution of this system represents the predicted closed, loaded configuration of the valve. From this loaded state, a reference configuration and material properties are derived. By tuning free parameters such as the maximum tension the leaflets may achieve, the resultant model geometry and constitutive law was designed to be consistent with experimental observations. The resultant model possesses material heterogeneity and anisotropy, properties that are challenging to measure experimentally. When simulated in fluid via the immersed boundary method, these models are highly effective, producing realistic flow rates during forward flow and closing reliably under back pressure over multiple beats. We then apply these models to study flows through bicuspid aortic valves. Simulations reveal dramatically different flow patterns through tricuspid and multiple phenotypes of bicuspid aortic valves depending on the location of cusp fusion. Hypotheses based on these results on the development and progression of ascending aortic dilation will be discussed.

PS4.2
Flow of a blood analogue in a microchannel bifurcation for microcirculation studies

Ines Gonçalves[1], João Varelas[2], Rui Lima[1], **Ana Moita**[3], Antonio Moreira[2]

1   Metrics, Mechanical Engineering Department, University of Minho, Guimarães, Portugal
2   IN+ - Center for Innovation, Technology and Policy Research, Instituto Superior Técnico, Universidade de Lisboa, Lisbon, Portugal
3   Military Academy, CINAMIL Departement of Exact Sciences and Engineering, Portugal

Microcirculation blood flow has been a topic of interest to prevent severe pathological conditions. It has been studied both in vivo [1] and in vitro [2]. However, and despite of the significant advances in this field, understanding of blood flow phenomena at the microcirculation level is still not yet completely understood nor described. An important obstacle against the further development of these studies is due to several difficulties such as sanitary, bureaucratic and technical problems, which have limited the use of real blood in long term flow experiments. Hence, it is crucial to develop a simple and stable blood analogue with flow properties close to real blood.

In this context, this work addresses a simple, cost-effective stable particulate blood analogue, which can mimic multiphase phenomena of real blood in microcirculation. The proposed fluid is based on a water and Brij L4 surfactant solution. The surfactant creates a precipitate of deformable particles. Our previous work addressed deformability behaviour in microchannels with a sudden contraction, which shows a good mimic of the deformable behaviour when compared to real blood cells. The work presented here, provides detailed additional information on the effect of the surfactant in the fluid viscosity and on the consequent Cell Free Layer formation and on the fluid flow in a microchannel bifurcation.

Results show that thermophysical properties of the developed analogue flow are in good agreement with those of real blood, particularly the shear thinning behaviour, which only differs significantly from that of real healthy blood for very high surfactant concentrations (>10wt%). On the other hand, surfactant concentrations of the order of 1-2% promote a clearer Cell Free Layer formation, but also endorses agglomeration and clogging.

References:
[1]   Namgung, B, Liang, L. H., Kim, S., 2014. Physiological significance of cell-free layer and experimental determination of its width in microcirculatory vessels. In: Lima et al. editors. Visualization and simulation of complex flows in biomedical engineering. Dordrecht: Springer; p. 75–87.
[2]   Catarino, S. O., Rodrigues, R. O., Pinho, D., Miranda, J. M., Minas, G., Lima, R., 2019. Blood Cells Separation and Sorting Techniques of Passive Microfluidic Devices: From Fabrication to Applications. Micromachines. 10:593.

PS4.4

Implication of 3D to 1D simulation to detect the severity of cardiovascular diseases based on CTA imaging

*Mohammad Ferdows[1], **Kazi Ekramul Hoque**[1], Sabrina R[1]*

1   *University of Dhaka, Applied Mathematics, Dhaka, Bangladesh*

Computed tomography angiography (CTA) based three-dimensional (3D) computational blood simulation is used for detecting coronary arteries' abnormality in developed countries. However, the 3D simulation needs a huge computational and economic burden. The supercomputer has engaged for the 3D simulation for solving Navier-Stokes nonlinear equations. One-dimensional (1D) image-based non-invasive virtual FFR (vFFR) is an emergent method to determine the functional assessment of coronary stenosis [1]. In 1D computation has received more attention because of this reduced order models are derived from the axisymmetric Navier-Stokes equations with Olufsen vessel walls. We have employed a robust and stabilized discontinuous upwind Petrov Galerkin finite element method for incompressible flow simulation.
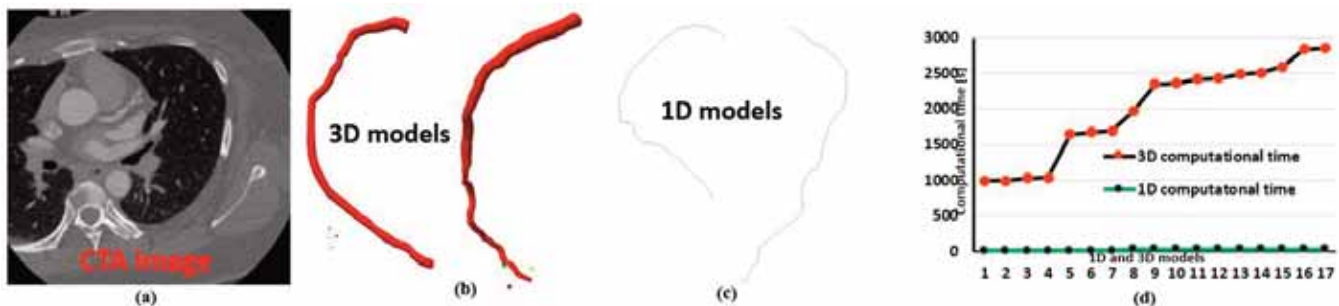
Figure 1: Presents (a) CTA image, (b) 3D models, (c) 1D models and (d) shows computational cost comparison between 3D and 1D models.

Accurate 3D geometry generation is one of the major challenging tasks for 3D computational heart flow simulations. The patient-based 17 coronary arterial segments have generated from patients' data. We have set different size (0%, 70%, 80% & 90%), locations (proximal, distal, bending and bifurcation) and types (concentric and eccentric) stenosis in 3D models. We have used exactly the same model for 1D models generation. An explicit velocity waveform at the inlet and pressure waveform was employed at the outlet [2]. We have obtained Pearson's correlation coefficient (r✗ =0.9747 and p<0.0001) presents a strong correlation between vFFR in 3D (vFFR3D) and vFFR1D values (vFFR3D is standard). We have observed the vFFR values remain invariant for two modalities (1D & 3D). Fig. 1(d) presents a comprehensive comparison between 1D and 3D computational time [s]. The lowest amount of mesh in 1D models' is 1100 and the highest is 2600. However, the number of volumetric mesh varies from 110000 to 400000. We observe from Fig. 1(d) that the 3D patient-based models' computational cost approximately 1000 times more than 1D. The statistical measurements demonstrate that both modalities have strongly correlated. There are some limitations to this procedure, which require additional studies. This non-invasive, low-risk and less computational expensive 1D technique could be employed to envisage the severity of cardiovascular diseases.

References:
[1]. P.J. Blanco et al.; Scientific Reports; DOI:10.1038/s41598-018-35344-0.
[2]. K. E. Hoque et al.; Physics of Fluids, https://doi.org/10.1063/5.0041335

Corresponding author email: ferdows@du.ac.bd

PS4.5

Numerical implementation and experimental validation of the constrained mixture model applied to arteries.

Alvaro Navarrete[1], *Andrés Utrera*[1], *Claudio García-Herrera*[1], *Diego Celentano*[2], *Emilio Hererra*[3], *Bernardo Krause*[4]

1   USACH, Mechanical Engineering, Estación Central, Chile
2   Campus San Joaquín, Pontificia Universidad Catolica de Chile, Department of Mechanical and Metallurgical Engineering, Macul, Chile
3   Institute of Biomedical Sciences ICBM, Faculty of Medicine, Chile
4   O'Higgins University, Institute of Health Sciences, Rancagua, Chile

Constrained Mixture Model (CMM) is used to describe cellular behaviors driven by mechano-chemical processes, determining its effect in a variety of analyses on arterial wall. According to the general principles of its formulation, it establishes the presence of a mixture formed by constituents that are deposited in it, and that are constrained to deform together in a stressed configuration, each with its characteristic mass fractions (Figure 1). In particular, for arterial tissue the mechanically relevant elements considered to be part of the mixture correspond to collagen and elastin fibers, along with smooth muscle cells. The application of the CMM approach is closely related to the existence of residual stresses in the arterial wall, which is consistent with the idea that each constituent element of the arterial wall is deposited in it, with different stretching directions and values, a phenomenon that should precisely be incorporated in the model described 1. In this work, the implementation of CMM in the context of the finite element method, and its respective experimental validation is presented. For this purpose, it is necessary to define adequate constitutive models (expressed through strain energy functions), deposition stretch tensors and mass fractions, according to the nature of each constituent of the arterial wall. By applying the CMM under in-vivo conditions of the pressurized artery, the stress field of the tissue is determined, while eliminating the effects of pressure, the residual stress field is obtained, which will be validated with a numerical-experimental procedure performed from experimental tests of residual strain (ring opening and pre-stretching), and subsequently numerical implementation of the process of artery closure and stretching of the arterial duct in order to obtain residual stress field.
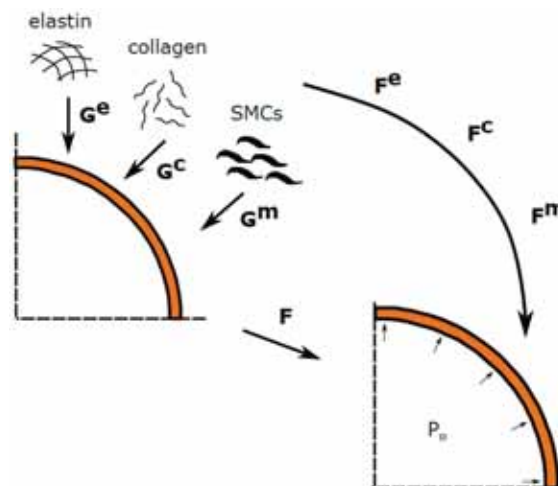
Figure 1: General framework of CMM, applied in a pressurized artery (in-vivo condition)

References:
1.   Bellini C, Ferruzzi J, Roccabianca S, Di Martino ES, Humphrey JD. A microstructurally motivated model of arterial wall mechanics with mechanobiological implications. Ann Biomed Eng. 2014;42(3):488-502. doi:10.1007/s10439-013-0928-x

PS4.6

A workflow for 3D(+t)-US-based wall stress analysis of AAAs including the intraluminal thrombus

Arjet Nievergeld[1 2], *Judith Fonken*[1 2], *Esther Maas*[1 2], *Frans van de Vosse*[1], *Marc van Sambeek*[1 2], *Richard Lopata*[1]

1   Eindhoven University of Technology, Biomedical Engineering, Eindhoven, Netherlands
2   Catharina Ziekenhuis, Eindhoven, Netherlands

Introduction: An abdominal aortic aneurysm (AAA) is a localized dilatation of the aorta, which in case of rupture has a mortality rate of 80%. Current clinical guidelines of intervention are based on AAA diameter, which has been proven to be an inadequate criterion. Biomechanical models can improve the prediction of rupture risk in a more patient-specific way, using e.g. CT, MRI or ultrasound (US) imaging [1, 2]. CT requires the use of X-ray and nephrotoxic contrast agents and MRI involves long scan times and high costs. US is safe, cheap, and adds temporal information for mechanical characterization of the AAA. However US has a low contrast, and limited field of view making it challenging to determine the entire geometry of the AAA. It is hypothesized that the intraluminal thrombus (ILT) lowers the wall stress and therefore should be included in rupture risk assessment [3]. To our best knowledge no Finite Element Analysis (FEA) of AAAs including ILT has been reported, based on 3D US. The objective of this study is to demonstrate the feasibility of using patient-specific US-based geometries in FEA to determine the effect of ILT on the stress in the vessel wall.

Methods: An in-house automatic segmentation algorithm was used to segment the ILT and vessel wall out of (3D+t)-US images. To approximate physiological boundary conditions, the meshes of the ILT and vessel wall were elongated by 3 cm using Bezier curves growing towards proximal and distal diameters of 2 cm. The vessel wall was meshed assuming a uniform wall thickness of 2 mm. For both vessel wall and ILT a Neo-Hookean model was used with a shear modulus of 1 MPa and 20 kPa respectively.

Results/Discussion: As shown in the figure below the 99th percentile stress for the model with ILT (118 kPa) was lower compared to the model without ILT (142 kPa), which was also hypothesized. First results show the feasibility of the fully automatic workflow. The workflow also provides means to perform a local stiffness estimation based on US speckle tracking and blood pressure estimations. Eventually this fully automatic workflow can be used in a longitudinal study to estimate the patient-specific AAA rupture risk in a more accurate way.
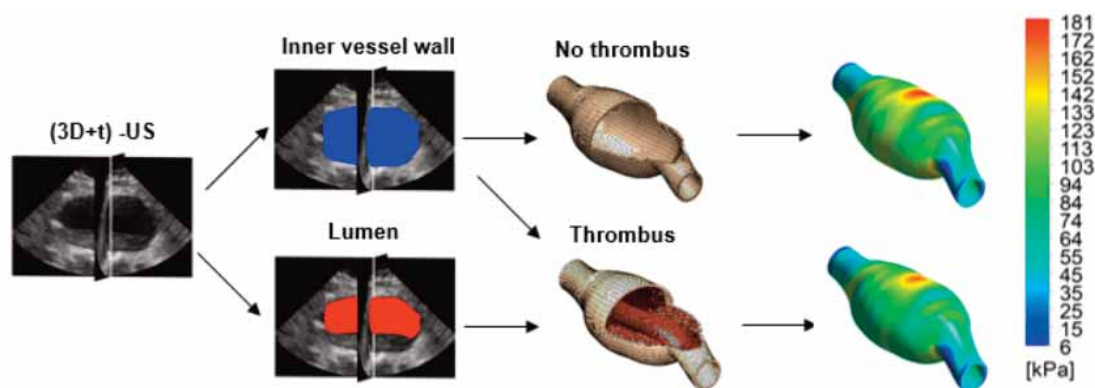
Figure caption: Workflow of (3D+t)-US-based wall stress analysis for a mesh only containing the vessel wall and a mesh including both vessel wall and thrombus.

References:
[33] Van Disseldorp et al, Eur J Vasc Endovasc Surg, 59: 81-91, 2020
[34] Kok et al, J Vasc Surg 61: 1175-1185, 2015
[35] Domonkos et al. , Int. Angiol.38: 39-45, 2019

PS4.7
Numerical flow simulations in a liver-on-a-chip

Violeta Carvalho[1], Nelson Rodrigues[1], José Carlos Teixeira[1], Raquel Rodrigues[2], Rui A. Lima[1], Senhorinha FCF Teixeira[3]

1,   Department of Mechanical Engineering, Guimarães, Portugal
2,   Department of Industrial Electronics, Guimarães, Portugal
3,   Production and Systems Department , Guimarães, Portugal

Organ-on-a-chip (OoC) platforms are engineered microscale in vitro tissues that recapitulate typical functions of human organs [1]. By providing a physiologically relevant tissue microenvironment, these in vitro models have revolutionized the development of innovative drugs, turning this process more effective, efficient, and cost-effective, and have helped the understanding of several diseases. Amongst the various pathologies recapitulated in OoC, cancer is one of the most studied since it remains the second leading cause of death worldwide according to the World Health Organization data, and the conventional treatments often used present low targeting and undesirable toxicity. Hence, more effective treatments have been investigated. Despite the OoC models are vital to predict and study several phenomena of cancer development and treatment, the ability of numerical approaches to study multiphysics problems makes them powerful to rapidly analyze and understand biological processes that encompass physical phenomena at a lower cost and faster. Furthermore, numerical studies allow determining critical parameters which are difficult to be measured empirically and present great potential to optimize device parameters. Accordingly, numerical simulations are getting increasing recognition by regulatory authorities and should be used as a complementary tool for in vitro testing.

Given the importance of numerical simulations as an auxiliary tool for experimental tests, in the present work, a numerical and experimental study was carried out in a liver-on-a-chip platform. The numerical simulations were conducted in Ansys® software, and the flow visualization tests were performed by using a high-speed video microscopy system. The numerical model allowed to estimate the oxygen diffusion along the OoC model (Figure 1 A) and the velocity fields in the OoC (Figure 1 B) which complemented the experimental tests that have been performed. In general, it was observed that the oxygen tends to diffuse where the flow velocity is lower, and the fluid flow results obtained experimentally and numerically showed to be in good agreement both in the inlet (Figure 2 A) and outlet (Figure 2 B).
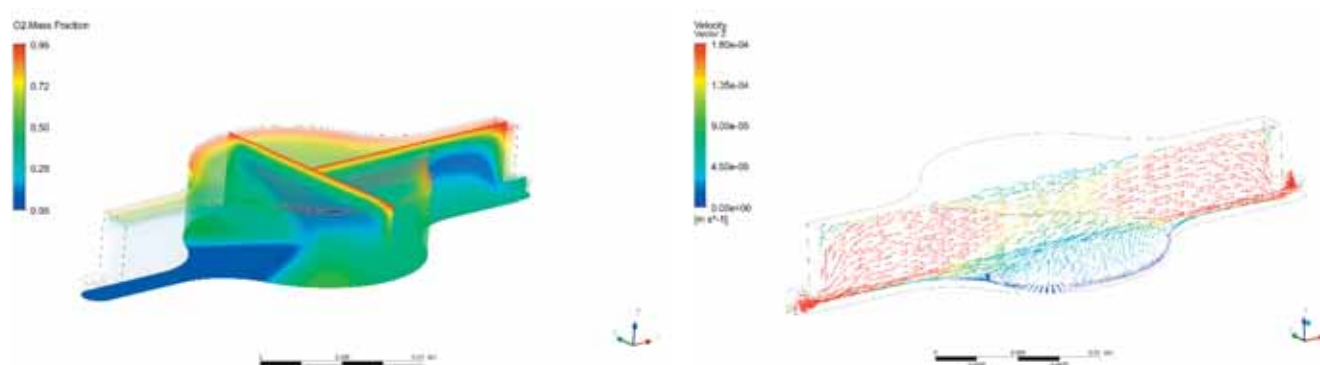
Figure 1: Numerical results of A) oxygen mass fraction inside the OoC, and B) velocity fields (m/s) along the OoC.
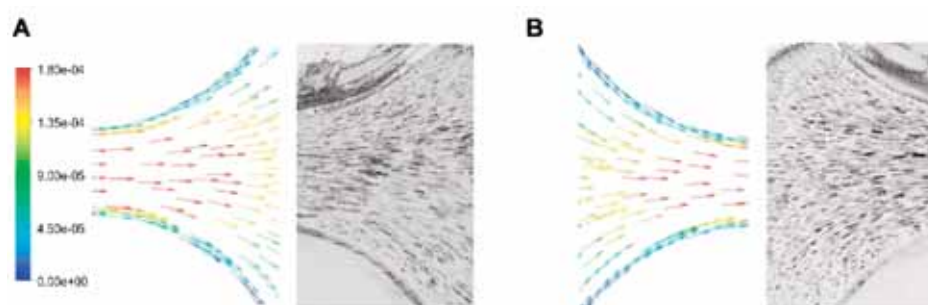
Figure 2: Experimental and numerical results (m/s) of A) fluid flowing from the inlet and B) fluid reaching the outlet.

References:
[1]   V. Carvalho, et al, 3D Printing Techniques and Their Applications to Organ-on-a-Chip Platforms : A Systematic Review, Sensors. 21 (2021) 3304. https://doi.org/https://doi.org/10.3390/s21093304.

PS4.9

Aortic root fluid-structure interaction modeling to guide porcine and bovine valve selection in aortic valve replacement surgery

Caili Li[1], Dalin Tang[2 3], Jing Yao[4], Yongfeng Shao[5], Haoliang Sun[5], Peter Hammer[6], Chanjuan Gong[7], Christopher Baird[6]

1   Southeast University, School of Mathematics, Nanjing, China
2   Southeast University, School of Biological Science & Medical Engineering, Nanjing, China
3   Worcester Polytechnic Institute, Mathematical Sciences Department, Worcester, United States
4   First Affiliated Hospital of Nanjing Medical University, Department of Cardiology, Nanjing, China
5   First Affiliated Hospital of Nanjing Medical University, Department of Cardiovascular surgery, Nanjing, China
6   Boston Children's Hospital, Harvard Medical School, Department of Cardiac Surgery, Boston, United States
7   First Affiliated Hospital of Nanjing Medical University, Department of Anesthesiology, Nanjing, China

Aortic valve replacement (AVR) outcome may be influenced by the choice of bioprosthesis. Porcine aortic valve (PAV) and bovine aortic valve (BAV) are commonly used in AVR surgery, but their specific choice has not been recommended. A detailed comparison between PAV and BAV based on their hemodynamic and stress/strain performances would help to better understand valve cardiac function and select valve type for AVR outcome optimizations.

Eight fluid-structure interaction (FSI) models with 4 sizes (19, 21, 23, and 25 mm) of PAV and BAV were constructed to simulate and compare the blood flow velocity, systolic cross-valve pressure gradient (SCVPG), geometric orifice area (GOA), flow shear stresses (FSS) and stress/strain. Anisotropic Mooney-Rivlin model was used to describe mechanical properties of PAV and BAV leaflets. The arterial pressure and left ventricle outflow track flow data were obtained from a patient undergoing AVR surgery to provide realistic boundary conditions for FSI model.

Our results showed that compared with PAV, BAV has better overall hemodynamic performance, with lower maximum flow velocity (7.17%) and pressure (9.82%), smaller mean SCVPG (8.92%), larger GOA (9.56%) and lower FSS (6.61%). During the peak systolic phase, the average stress on the leaflets of the BAV were lower than that on PAV, and the average stress values from the 4 bovine valve models was 93.25±8.72 kPa, 5.76% lower than that from porcine valve models. We also observed that larger valves of both PAV and BAV had significantly superior hemodynamic results and lower mean leaflet stress. The maximum velocity, peak pressure, mean SCVPG, maximum FSS and average stress values from Size 25 bovine model were 36.98%, 15.81%, 39.05%, 38.83% and 18.90% lower than Size 19, respectively.

Our preliminary modeling results suggested that bovine valve has better hemodynamics and lower leaflets average stress. More patient studies are needed to validate our findings.

PS4.11
Personalized pulmonary poromechanics in health and idiopathic pulmonary fibrosis

Martin Genet[1 2], Cécile Patte[1 2], Catalin Fetita[3], Pierre-Yves Brillet[4 5], Dominique Chapelle[1 2]

1   École Polytechnique, Laboratoire de Mécanique des Solides (LMS), Palaiseau, France
2   Inria Saclay Île-De-France, MΞDISIM, Palaiseau, France
3   Telecom SudParis, SAMOVAR, Évry-Courcouronnes, France
4   Université Sorbonne Paris Nord, Hypoxie et Poumon, Villetaneuse, France
5   Avicenne Hospital (AP-HP), Radiology, Bobigny, France

Introduction: Lung biomechanics has been extensively studied by physiologists, experimentally as well as theoretically, laying the ground for our current fundamental understanding of the relationship between function and mechanical behavior. However, many questions remain, notably in the intricate coupling between the multiple parenchymal constituents. These fundamental questions represent real clinical challenges, as pulmonary diseases are an important health burden. Interstitial lung diseases, for instance, affect several million people globally. Idiopathic Pulmonary Fibrosis (IPF), notably, a progressive form of interstitial lung disease where some alveolar septa get thicker and stiffer while others get completely damaged, remains poorly understood, poorly diagnosed, and poorly treated [Nunes et al., 2015].

Methods: We recently developed a model of the lungs at the breathing time scale and the organ space scale [Patte et al., 2019], based on a general poromechanical formulation [Chapelle & Moireau, 2014], where the "solid" phase is composed of both tissue and blood while the fluid phase is the air. Several pulmonary-specific hypotheses have been formulated, notably that the end-inhalation and end-exhalation states are in static equilibrium. Moreover, specific boundary conditions are imposed on the lungs themselves, modeling the effect of diaphragm-induced loading and rib cage: a pressure applied on lung surface representing pleural pressure, and a frictionless contact with the moving thorax. Moreover, the constitutive behavior allows to reproduce the volumetric response of lungs to a change of pressure as observed in experimental data.

The proposed model can be personalized using clinical data [Patte et al., 2019]. From two 3D CT-scans, acquired at end-exhalation and at end-inhalation, we obtain a personalized geometry through image segmentation [Fetita et al., 2019]), a personalized porosity, personalized motion & boundary conditions through image registration [Genet et al., 2018]. Such data allow also to personalize regional mechanical parameters by minimizing the discrepancy between measured and computed motion.

Results: We will present results based on control and patient data. Notably, we will show that the model and estimation procedure can quantify the regional tissue stiffening induced by idiopathic pulmonary fibrosis.

Conclusion: Our results illustrate how our pulmonary poromechanical model can be used as a diagnosis tool in the clinic when it is personalized to a patient using clinical data acquired in standard protocols.
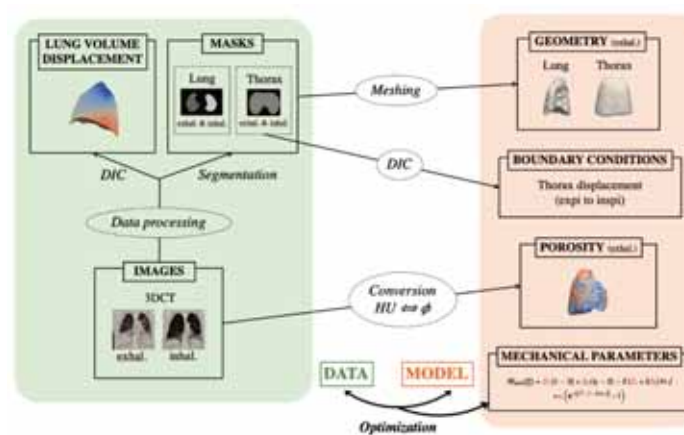
Figure caption: Schematic of the proposed clinical image-based model personalization procedure.

References:
Chapelle & Moireau. (2014). European Journal of Mechanics Part B: Fluids, 46.
Fetita et al. (2019). Medical Imaging 2019: Computer-Aided Diagnosis.
Genet et al. (2018). Medical Image Analysis, 50.
Nunes et al. (2015). European Respiratory Journal, 45(3).
Patte et al. (2019). 15ème Colloque National en Calcul de Structures (CSMA2019).

PS5.1

New insights on wave propagation through a visco – elatic semi-infinite solid equivalent to human skin

Amaury Guillermin[1], *Meriem Ayadh*[1], *Robin Chatelin*[2], *Eric Feulvarch*[2], *Hassan Zahouani*[1]

1   École Centrale de Lyon / LTDS, Écully, France
2   National School of Engineers of Saint-Etienne (ENISE) / LTDS, Saint-Étienne, France

Biological tissues are known for years through medicine, more especially dermatology. However, in term of mechanical behavior, insights are, usually, based on pure elastic model … not considering the viscosity, an important effect linked to ageing. To address this issue, the method we propose offers new insights characterizing some typical information of wave propagation in a visco – elastic semi – infinite solid.

Initially, to taking in account the viscous behavior of the skin, a creep recovery testing method has been developed. The experimental tests are carried out in vivo and reveal the mechanical behavior of the skin tested, in its elastic and viscous parts. The mechanical behavior is expressed in terms of Prony serie, allowing us the conversion between different constitutive equations, such as generalized Maxwell model or generalized Kelvin Voigt model.

This first result gives us the possibility to use a visco – elastic behavior, in a simulation framework. In our case, due to the limitations of in vivo testing, the use of numerical methods is truly handy. To investigate wave propagation, one of the suitable ways is to apply a harmonic force, long enough and strong enough to spread in the entire medium a wave: here, finite elements method supports the achievement of this kind of testing. Coupled with the visco – elastic behavior (previously) computed, the presented numerical method guarantees the modeling included the elastic and viscous parts of the skin behavior.

Thanks to numerical methods, a wave field can be retrieved and analyzed using spectral analysis. This analysis highlights phase velocities and attenuations of the wave propagating due to the harmonic solicitations.

These two parameters permit a lot more insights on what happened on the inside of this medium: phase velocities are linked to wave's speed propagation in depth, attenuation is linked to the medium damping, …

All these information ca be monitored and gathering to understand, mechanically, the skin tissue ageing process; to diagnose some illness of this tissue, and so on …

PS5.2
Subcutaneous skin viscoelasticity imaging: UNDERSKIN®

Alexandre Bergheau[1], *Vargiolu Roberto*[1], *Ouillon Lucas*[1], *Zahouani Hassan*[1]

1   University of Lyon Ecole Centrale de Lyon , Laboratory of Tribology and System Dynamics (LTDS) - UMR 5513 CNRS, ECL-ENISE, ECULLY, France

The analysis of the mechanical behavior of human skin is of paramount importance on the grounds of the multiple applications in plastic surgery, dermatology, and cosmetics. The focus of this study is the development of UNDERSKIN® [1] which measures skin's elasticity in vivo and reconstructed skin both subcutaneously. The principles of the propagation of surface waves are utilized to observe the elastic properties of the skin beneath the surface. UNDERSKIN® records and measures these ripples with an optical displacement sensor which consists of 400 receivers spaced of 17.5µm with a total length of 7mm. This, going from the skin ripple to the subcutaneous skin elasticity via the dispersion analysis of the Rayleigh velocity, is the core of UNDERSKIN®'s signal processing. Indeed, besides being a cornerstone, the dispersion analysis, in which the ratio of the phase velocity and the frequency, will result in the corresponding wavelength, hence the penetration depth of the shear wave. Consequently, for a given phase velocity and wavelength, we obtain the shear velocity with its penetration depth and so the Elastic Modulus. We then produce a detailed visual of what is happening in the elastic behavior across the epidermis, the dermis, and the hypodermis. Apart from that, the process expands including a viscoelastic approach giving then crucial information such as the damping as a function of the frequency.

UNDERSKIN® is a device comprised of a multi-jointed robotic arm, an airflow source of the surface waves (contact-free indenter), and an optical displacement sensor to record the displacement of the surface waves. Therefore, not only will it provide essential skin information such as the anisotropy of the skin tension lines, tension forces, and the density of the collagen fibers but it will also reveal the effectiveness of a cosmetic product, the healing of a wound, the reading of cellulite and have the potential of early foreign body detection. The result is a 1D-3D internal visual shown in figure 1 and 2.
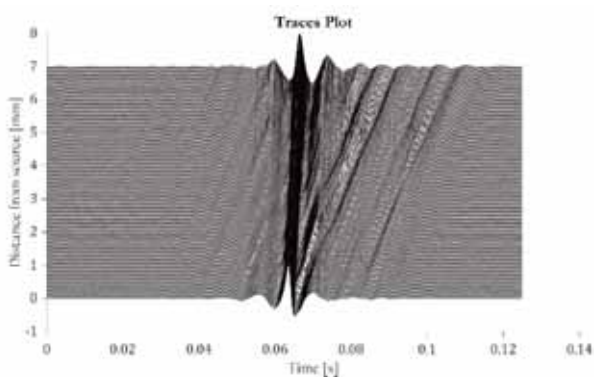
Figure 1: Surface wave recorded at the skin's surface with UNDERSKIN®: displacement image at each receiver location
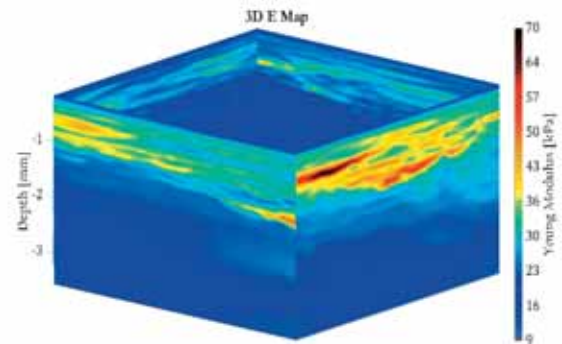
Figure 2: 3D Elastic Modulus map resulted from UNDERSKIN®'s signal processing

References:
[1]:   Patent filed in November 2020 with PULSALYS

PS5.3
Development of a continuum damage model to predict accumulation of sub-failure damage in tendons

Alexandra Allan[1 2], *Jared Zitnay*[1 2], *Jeffrey Weiss*[1 2], *Steve Maas*[2]

1   The University of Utah, Biomedical Engineering, Salt Lake City, United States
2   Scientific Computing and Imaging Institute (SCI Institute), Salt Lake City, United States

Introduction: Many physically debilitating conditions involve sub-failure mechanical damage to tissues such as tendons. Our lab found that the amount of denatured collagen in rat tail tendon (RTT) fascicles increased over cyclic loading to a constant load level (creep cyclic fatigue) (Fig.1a) [1] with fluorescently tagged collagen hybridizing peptides (CHPs) that bind to denatured collagen. To better understand tendon sub-failure damage progression, computational modeling of tendons via finite element analysis in FEBio has been conducted. The project objective was to develop, implement, and test the ability of a new continuum damage mechanics (CDM) model in FEBio [3] to represent the sub-failure damage behavior seen in our RTT fascicle creep cyclic fatigue data.
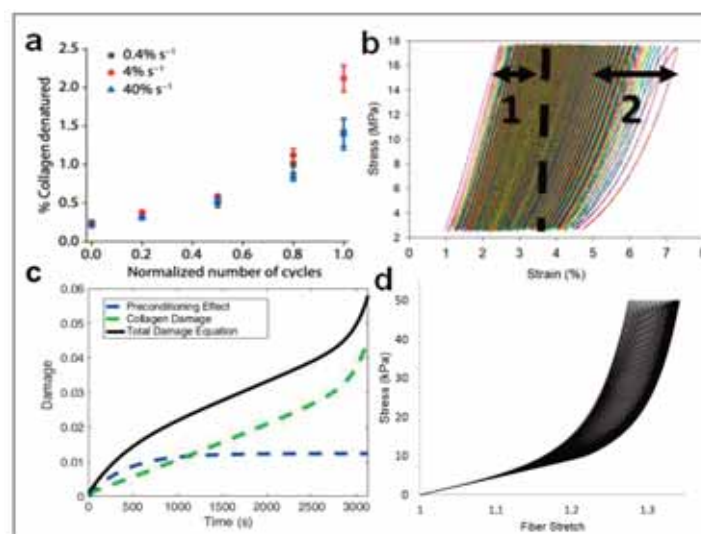
Materials and methods: There appear to be two mechanisms responsible for the creep cyclic fatigue softening behavior of RTT fascicles over the number of cycles: the preconditioning effect and collagen damage (denoted by 1 & 2 in Fig. 1b). In FEBio, the RTT fascicle was described by an undamaged elastic constitutive model made up of the Transversely Isotropic Veronda Westmann material convolved with a modified CDM model initially presented by Balzani [4].

Results and discussion: Within the modified CDM model, exponential and sigmoidal functions describe the preconditioning and collagen damage (Fig. 1c), characterized with continuous and discontinuous damage mechanisms. The modified damage model was tested on an arterial tissue model from Balzani [4] and subjected to creep cyclic fatigue, producing a similar softening effect as seen with our RTT fascicles (Fig. 1d).

Conclusions: The continuous damage formulation provided a means for damage accumulation during cyclic loading and unloading [5], while discontinuous damage accumulates damage with increasing maximum strain over time [6]. Therefore, the combination of the continuous and discontinuous damage functions provides the ability to predict sub-failure damage in tendons from constant and increasing cyclic fatigue.

Figure caption: Figure 1: a) CHP fluorescence imaging provides the % collagen denatured over the number of cycles to failure in creep cyclic fatigue [1] b) The stress-strain curve of a RTT fascicle subjected to creep cyclic fatigue with the 1. preconditioning effect and 2. collagen damage mechanisms indicated c) The total damage equation over time made from the addition of the exponential and sigmoidal equations d) Stress-stretch curve modeled in FEBio showing softening of arterial tissue [4] subjected to creep cyclic fatigue.

References:
[1] Zitnay JL, et al., Science Advances, 6(35): eaba2795, 2020.
[2] Zitnay JL, et al., Nature Communications, 8:14913, 2017.
[3] Maas SA, et al., Journal of Biomechanical Engineering, 134(1), 2012.
[4] Balzani D, et al. Computer Methods in Applied Mechanics and Engineering, 213-216:139-151, 2012.
[5] Miehe C, European Journal of Mechanics and Solids, 14(5):697–720, 1995.
[6] Simo JC, Computer Methods in Applied Mechanics and Engineering. 60(2):153-173, 1987.

PS5.4

Sources of inconsistency in mean mechanical response of abdominal aortic aneurysm tissue

Radek Vitásek[1], Didier Gossiho[2], Stanislav Polzer[1]

1   Technical University of Ostrava, Department of Applied Mechanics, Ostrava-Poruba, Czech Republic
2   The University of Iowa, Department of Biomedical Engineering, Iowa City, United States

Introduction: There is a striking difference in the reported mean response of abdominal aortic aneurysm tissue in academic literature depending on the type of tests (uniaxial vs biaxial) performed. That can be caused either by difference in tested populations or by differences in experimental protocols. We explored the second hypothesis in this study by trying to reproduce observed differences using porcine aortic tissue as a substitute for aneurysmal tissue.

Methods: Nine samples of porcine aorta were created and both uniaxial and biaxial tests were performed. Three effects were investigated. (i) Effect of sample (non) preconditioning, (ii) effect of objective function used (normalised vs non-normalised), and (iii) effect of chosen procedure used for mean response calculation: constant averaging (CA) vs fit to averaged response (FAR) vs fit to all data (FAD). Both the overall shape of mean curve and mean initial stiffness were compared

Results: (i) Non-preconditioning led to a much stiffer response, and initial stiffness was about three times higher for a non-preconditioned response based on uniaxial data compared to a preconditioned biaxial response. (ii) Our data showed a disadvantage of the CA approach in estimating mean response because this approach is sensitive to starting points. CA led to a much stiffer response compared to FAR and FAD procedures which gave similar results, with FAD also being applicable to biaxial data. Application of the FAR approach to a biaxial response is constrained by the necessity to perform a strain-controlled protocol in which the strain ratio can be controlled. (iii) Normalised objective function produced a mean response with six times lower initial stiffness and more pronounced nonlinearity compared to non-normalised objective function.

Discussion: We demonstrated it is possible to reproduce a mechanically inconsistent response purely by using the chosen experimental protocol which suggest it is unlikely there are major differences among AAA patients in different countries. Data from non-preconditioned failure tests should not be used for FE simulation of the elastic response of aneurysms as they do not represent its elastic response and are unrealistically stiff. CA should not be used to obtain a mean response since it produce artificially stiff response especially in case of biaxial response.

References:
1.   Vitásek, R., Gossiho, D., & Polzer, S. (2021). Sources of inconsistency in mean mechanical response of abdominal aortic aneurysm tissue. Journal of the Mechanical Behavior of Biomedical Materials. https://doi.org/10.1016/j.jmbbm.2020.104274

PS5.5

Bioinspired composites based on unique coral collagen fibers: towards engineered vascular grafts

Shir Wertheimer[1], *Mirit Sharabi*[2], *Rami Haj-Ali*[1]

1   Tel Aviv University, School of Mechanical Engineering, Tel Aviv-Yafo, Israel
2   Ariel University, The Department of Mechanical Engineering & Mechatronics, Ari'el, Israel

Cardiovascular Diseases (CVDs) are the leading cause of death worldwide. Coronary artery disease (CAD) is 42% among CVDs. CAD is characterized by a narrowing of arteries that restricts normal blood flow. In severe cases, surgical interventions are conducted to implant either autologous vessels or synthetic grafts that are used successfully as replacements for larger diameter (>6mm) blood vessels. However, these replacements are not compatible in the case of small-diameter blood vessels.

This study introduces a new biocomposite material system consisting of unique and long (cm-scale) collagen fibers derived from soft corals embedded within an alginate hydrogel matrix. These constructs were designed as a new class of tissue-engineered small-diameter blood vessels. Tubular constructs consisting of both circumferentially and longitudinally oriented collagen fibers were fabricated and characterized. A new mechanical testing setup has been designed to test the mechanical properties of the grafts. The setup is capable of applying internal pressure levels of 0-300 mmHg. The biocomposite tubes demonstrated compliance of 4.88±0.99 %/100 mmHg for a physiologic pressure range of 80-120 mmHg, similar to native coronary arteries. In addition, a 3D structural finite element (FE) model was generated to simulate the mechanical response of the construct. The FE model is composed of axial and circumferential fibers embedded within continuum alginate 3D-elements. The model was able to predict the measured pressure-strain response of the biocomposite construct [1].

Furthermore, In-vitro biocompatibility tests and cell growth on the collagen fibers were also conducted. Seeded fibroblasts demonstrated good viability, and cell configurations were highly aligned with the collagen fiber orientation during the entire experiment, which lasted 32 days [2].

The proposed novel biocomposite graft demonstrated physiological mechanical compliance with the native vessels together with biological compatibility. These novel constructs can be the basis for developing novel biomimetic small-diameter blood-vessel grafts.
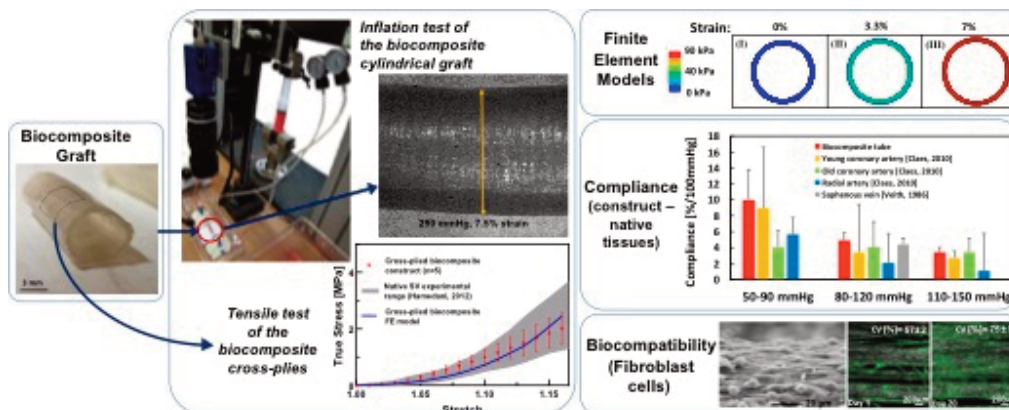
Figure caption: Vascular graft mechanical characterization and biocompatibility test

References:
[1]   Wertheimer, S.,* Sharabi, M.,* Shelah, O., Lesman, A., & Haj-Ali, R. (2021). Bio-composites reinforced with unique coral collagen fibers: Towards biomimetic-based small diameter vascular grafts. Journal of the Mechanical Behavior of Biomedical Materials.
[2]   Shelah, O.,* Wertheimer, S.,* Haj-Ali, R., & Lesman, A. (2021). Coral-Derived Collagen Fibers for Engineering Aligned Tissues. Tissue Engineering Part A.

*Both these authors contributed equally to this work.

PS5.6

Computational modeling and evaluation of TPMS scaffolds for tissue engineering

Andre Castro[1], *Tiago Pires*[1], *Jorge Santos*[1], *Paulo Fernandes*[1]

1   IDMEC, Instituto Superior Técnico, Universidade de Lisboa, Lisbon, Portugal

Scaffolds for Tissue Engineering (TE) can be defined as porous structures that provide support for the growth of new tissue, by ensuring adequate cellular differentiation and proliferation [1]. This study is focused on estimating the mechanobiological behavior of the cell adhesion substrate within triply periodic minimal surfaces (TPMS) scaffolds (3 types, SD, SP and SG, with 60, 70 and 80% porosity): the fluid flux and deformation occurring within an integrated soft tissue substrate (collagen hydrogel) are calculated while varying geometry and porosity, assuming that this collagen substrate will host cell seeding, differentiation and proliferation [2]. The tortuosity of each scaffold was analytically evaluated based on the location of each pore and its interconnectivity with the adjacent pores, using a custom Matlab® (Mathworks, USA) script. The finite element (FE) models of the 9 scaffold-substrate constructs were built in ABAQUS® (Dassault Systèmes Simulia Corp., USA), being tested under different compression magnitudes (6, 8 and 10%) and compression periods (10, 20 and 30s). This allowed for the evaluation of the mechanobiological output (MBO), i.e., the mechanobiological response of the scaffold-substrate construct [2].

The fluid permeation paths were significantly different: only paths corresponding to straight lines were obtained for SP, while the streamlines for SG and SD structures were more intricate. The FE simulations showed that the probabilities for bone formation increased from 23.18% (SD) to 29.81% (SP) when increasing the compression period from 10 to 30s. The major probability for cell death (43.55%) occurred with the SD70 model under 10% compression for 10s. It was also shown that the increase of porosity allows for an increase of bone and cartilage formation near the scaffold, particularly with SD and SG scaffolds.

The MBO method showed that strain rate is the most influential factor to achieve bone and cartilage formation, and longer consolidation times contribute low levels of scaffold-induced cell death. The TPMS geometry with lowest MBO variability was the SG, probably indicating that this geometry would be the best fit for bone and cartilage TE applications. The SP models may only suitable for larger scale applications where no tortuosity is required for cell seeding.

Figure caption: Section cut of 70% porosity scaffold-substrate FE models, considering the MBO for 20s compression time and 6% compression magnitude. Left to right: SD70-SG70-SP70.

References:
[1]   Ali, D. (2019). Effect of scaffold architecture on cell seeding efficiency: A discrete phase model CFD analysis. Comput Biol Med, 109(February), 62–69.
[2]   Castro, A. P. G., & Lacroix, D. (2018). Micromechanical study of the load transfer in a polycaprolactone–collagen hybrid scaffold when subjected to unconfined and confined compression. Biomech Model Mechanobiol, 17(2), 531–541.

PS5.7

Implementation and accuracy evaluation of nonlinear effects within the framework of a physics-based inverse method in Traction Force Microscopy

Alejandro Apolinar-Fernández[1], *Mar Cóndor*[2], *Jorge Barrasa Fano*[2], *Hans van Oosterwyck*[2], *Jose Antonio Sanz-Herrera*[1]

1   Universidad de Sevilla, Escuela Técnica Superior de Ingeniería, Seville, Spain
2   KU Leuven, Department of Mechanical Engineering, Biomechanics section, Leuven, Belgium

Traction Force Microscopy (TFM) is an experimental method applied to estimate the forces exerted by cells on the surrounding extracellular matrix (ECM) during migration. Provided one can measure the displacement field within a hydrogel that mimics the extracellular matrix, as well as the mechanical behaviour of the hydrogel, cell tractions and forces can be recovered. The forward method computes the cellular tractions and hydrogel stresses directly from the measured displacements through the constitutive relation considered for the hydrogel. The inverse method uses the measured displacement field as input data within a minimization problem based on a regularized strategy. Recently, we developed a novel inverse method which searches for a new displacement field that approximates the measured one, ensuring that force equilibrium within the ECM is satisfied [1]. This inverse method significantly outperforms the forward one for both linear and nonlinear elastic hydrogels [1, 2]. However, a linear approach to traction field reconstruction would be less complex and less computationally demanding than a nonlinear one, especially with regard to the numerical implementation of elaborate constitutive hyperelastic laws. It is thus interesting to study how much the linear reconstruction deviates from a nonlinear one, as well as to investigate the role of nonlinearities in TFM performance. The aim of this work is then twofold. First, to calibrate experimentally measured hydrogel mechanical behaviour through both linear and hyperelastic models. The assumed hyperelastic model takes into consideration the fibrous microstructure of the hydrogels [3]. Second, to use these models to synthetically reproduce TFM experiments for different geometries of real cells embedded in the considered hydrogels, assessing the accuracy of estimated cellular tractions. The in-silico models include the generation of ground-truth cases which assume the fitted hyperelastic model [3] as the real behaviour of the hydrogel for comparison purposes. Simulations are then carried out with corrupted displacement fields for different levels of hydrogel deformability. The uncertainty of the hydrogel's mechanical behaviour is considered by adding noise to the fitted model parameters. The performance of our TFM algorithms for traction recovery is evaluated for these different conditions. In addition, the tractions error quantification is compared with the linear case, in order to establish the availability of this approach in TFM.
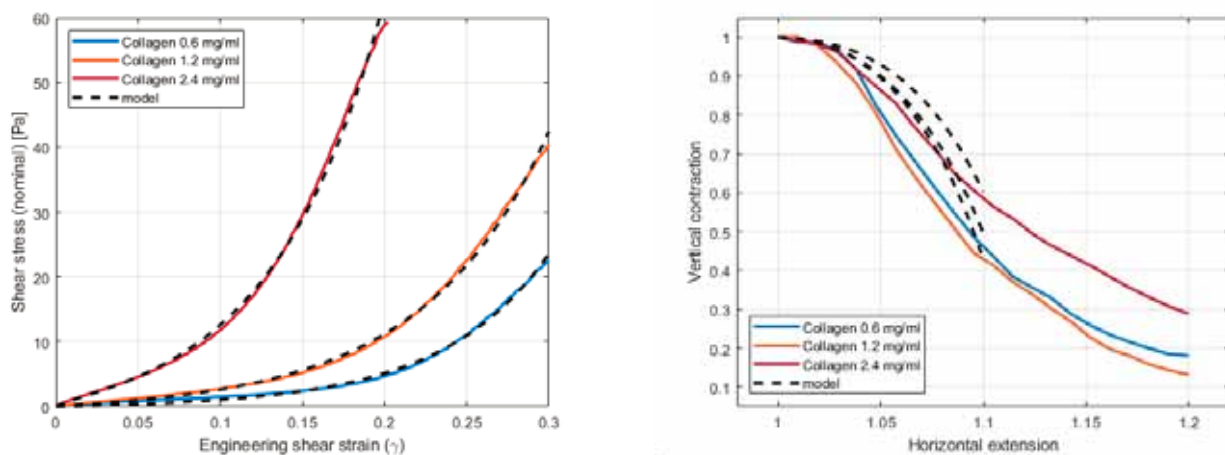
Figure caption: Fitting of experimental curves (solid) carried out with the SAEN model (dashed) [3] for simple shear (left) and vertical contraction (right) experiments.

References:
[1]   J.A. Sanz-Herrera et al. Soft Matter (2021)
[2]   J. Barrasa-Fano et al. bioRxiv 2020.12.08.411603 (2020)
[3]   J. Steinwachs et al. Nat Methods 13, 171–176 (2015)

PS5.8

Assessing the mechanics of molar teeth with different designs of indirect restorations using finite element models.

Rosti Readioff[1], Emad Moawad[2], Brendan Geraghty[3], Fadi Jarad[2]

1   University of Leeds, Institute of Medical and Biological Engineering, School of Mechanical Engineering, Leeds, United Kingdom
2   University of Liverpool, Department of Restorative Dentistry, School of Dentistry, Liverpool, United Kingdom
3   University of Liverpool, Department of Musculoskeletal and Ageing Science, Institute of Life Course and Medical Sciences, Liverpool, United Kingdom

It has been reported that posterior teeth have a high incidence of fracture. One of the main risk factors is preparing them for restoration; however, it is unclear how different designs of restoration can contribute to failure mode of the teeth [1]. This study aimed to develop subject-specific finite element (FE) models of decayed human molar teeth with three indirect restoration designs. Inlay, onlay and crown restorations were investigated for their impact on the structural mechanics of the restored teeth during simulated masticatory forces.

Extracted human molar teeth were imaged using micro-CT machine (SKYSCAN 1272, Bruker, USA) at 20 microns resolution. Enamel and dentine layers from each tooth were segmented from the micro-CT images using Simpleware ScanIP (V2019, Synopsys, CA, USA). To build three-dimensional (3D) geometries, the molar teeth were segmented using thresholding followed by manual smoothing for noise removal. For each tooth, six 3D geometries were generated to represent before and after using inlay, onlay and crown restorations (Figure). The 3D geometries were meshed with linear tetrahedral elements, with a minimum and maximum element edge length of 0.1 and 1mm, respectively which were exported into Abaqus FE software. The FE models were quasi-static analyses, with geometric non-linearity and unsymmetric matrix storage. Linear elastic material properties were defined for enamel (E=84100MPa, v=0.33) and dentine (E=18600MPa, v=0.31) [2]. Inlay, onlay and crown sections were modelled with porcelain material properties (E=69000MPa, v=0.25) [3]. The distal end of the dentine was constrained in all directions.

All FE models were analysed for two loading scenarios. The first was applying a vertical masticatory load of 250N to the central fossa of the teeth. The second scenario was applying lateral load of 250N to the lingual plane of the buccal cusp at 45° to the longitudinal axis of the tooth [4]. Stress-distribution and deformation maps after the application of the loading scenarios were assessed on the occlusal surface of the FE models.

We developed FE models representing different stages of inlay, onlay and crown restorative procedures. The FE simulations showed that oblique load causes higher deformation compared to applying vertical loads (Figure). During vertical loading, the crown tooth deformed more uniformly compared to the inlay and onlay restored teeth. Future study will simulate varying scenarios of restored posterior teeth with different types of restoration designs and materials.
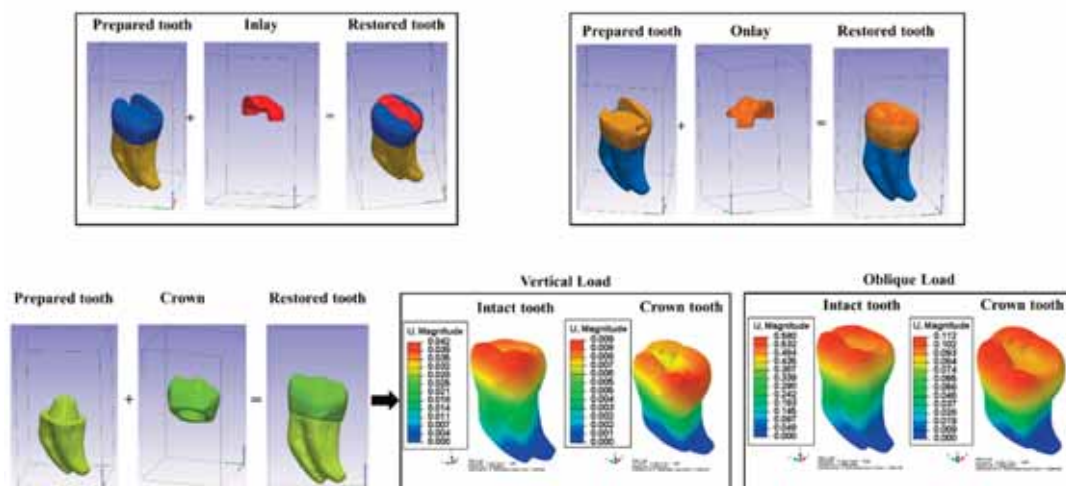
Figure caption: 3D models of crown, inlay and onlay teeth developed and utilised for mechanical comparison with an intact tooth during vertical and oblique masticatory forces.

References:
[1] Lubisich et al., Journal of Esthetic and Restorative Dentistry, 2010.
[2] Rees et al., Clinical Materials, 1993.
[3] Couegnat et al., Dental Material, 2006.
[4] Hernández-Vázquez et al., Applied Bionics and Biomechanics, 2018.

PS5.9
Visualization and quantification of cell flow by bubbly cell tracking

Masayuki Kashiwa[1], Takuya Toyoshima[1], Yukitaka Ishimoto[1]

1   Akita Prefectural University, Mechanical engineering, Yurihonjo, Japan

For clinical applications, researchers have paid attention to biological tissues and their multicellular mechanical structures. However, most of the mechanical aspect of morphological mechanisms remain unclear. So far, mathematical models have been developed to elucidate the mechanism: the vertex model (VM) [1, 2] by polygonal approximation of cells, and the bubbly vertex model (BVM) [3] with the curvature of cell boundaries, and so on. None of them led to the basic equations for migration and deformation of cell populations yet. The main reasons are that physical properties of tissues differ among morphogenetic stages or organs, the cell boundary tensions are non-uniform, and the stress-strain relationship of a tissue or of a cell has not been clarified.

In order to perform non-invasive measurements of cellular properties, cell boundary tensions or cell pressures, etc., one needs to develop quantification methods of cell flow from confocal images as precisely as possible. However, conventional methods, such as particle image velocimetry (PIV) and particle tracking velocimetry (PTV), do not fit naively to various cellular events: deformation, division, apoptosis, rearrangement, etc. Live-imaging techniques, autonomous cell motion and cell-cell interaction also limit the quality of experimental data. Therefore, automatic detection of cell nuclei or cell boundaries in live imaging data is difficult. In addition, compared to the linearly stretched cell membranes of mechanically stable tissues, it is rather difficult to detect automatically the non-linearly bent cell membranes often found in the early morphogenetic stages.

In this paper, we extract cell boundaries from the live imaging data, fit them to the tissue shape defined by BVM (Fig. 1), and perform vertex and edge (cell boundary) tracking similar to PTV, because the tissue at the time of the experiment showed many non-linear cell boundaries, and cellular rearrangement occurred frequently. We also attempt to visualize and evaluate the cell flow quantified from the real data.
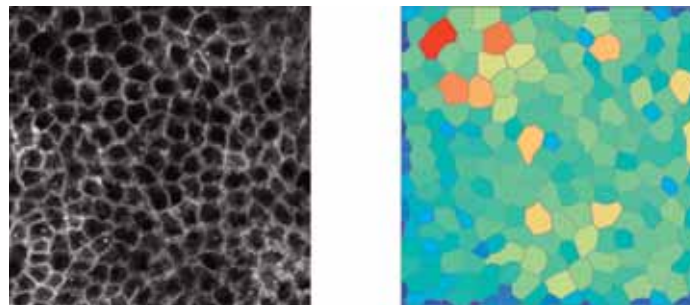
Figure caption: (Left) Drosophila tissue of a pupal wing (by the courtesy of Prof. O. Shimmi). (Right) Quantified configuration of the tissue in the left image.

Fig. 1. Fitting the extracted cell boundaries to the cell shape defined by BVM.

References:
[1]   H. Honda, Int. Rev. Cytol. 81, 191 (1983).
[2]   D. B. Staple, et al., Eur. Phys. J. E 33, 117 (2010).
[3]   Y. Ishimoto and Y. Morishita, Phys. Rev. E 90, 052711 (2014).
[4]   G. W. Brodland, et al., PLoS ONE 9, e99116 (2014).
[5]   B. Guirao, et al., eLife. 4, e08519 (2015).

PS5.11
Simulation of cell proliferation using a meshless tool

Maria Inês Barbosa[1], Jorge Belinha[2], Renato Natal Jorge[3], Ana Carvalho[4]

1   Institute of Science and Innovation in Mechanical and Industrial Engineering (INEGI), Porto, Portugal
2   School of Engineering Polytechnic of Porto (ISEP), Mechanical Engineering Department, Porto, Portugal
3   Faculty of Engineering of the University of Porto (FEUP), Mechanical Engineering Department, Porto, Portugal
4   Institute for Research and Innovation in Health (I3S), Cytoskeletal Dynamics Department, Porto, Portugal

In order to maintain the haemostasis of the body, a natural balance between cell proliferation and cell death has to be maintained. Thus, when necessary, cells divide into two new ones through a controlled process that is mainly dependent on the availability of oxygen and glucose [1]. However, this process has yet to be fully understood due to its high degree of complexity. Numerical methods have emerged and have been used to solve several problems in many fields. Regarding the study of cells, these methods are already used to solve different types of approaches, and used as an alternative to conventional analyses, allowing to save time and money [2]. Within these methods, it is possible to highlight the meshless methods, which are an efficient approach that emerged as an alternative to traditional methods, since they are able to overcome some disadvantages that are related to these last ones. However, the available literature is not yet as extensive as in other methods [3]. The aim of this work was to simulate the process of cell proliferation resorting to a new algorithm that is solved by the meshless method called Radial Point Interpolation Method (RPIM). In this algorithm, the cell is allowed to grow to the double of its volume and divide when this value is achieved, following the created phenomenological law. Moreover, the whole process is also dependent on the concentrations of oxygen and glucose and their influence on the cell proliferation was studied. The viability of the method to solve this problem was also taken into account since, to the knowledge of the authors, it was never used in the study of this type of problems. In the end, the algorithm leads to satisfactory and coherent results. It was capable of simulating cell proliferation, under different concentration of oxygen and glucose, as expected (Figure). Furthermore, the RPIM proved to be a viable option to solve this problem. In spite of this, several improvements should be done in future work in order to obtain a more complex algorithm.

Figure caption: Cell proliferation generated by the algorithm.

References:
[1]   King, KL, and JA Cidlowski. 1998. "Cell cycle regulation and apoptosis." Annual review of physiology no. 60 (1):601-617.
[2]   Bathe, Klaus-Jürgen, Hou Zhang. 2004. "Finite element developments for general fluid flows with structural interactions." International Journal for Numerical Methods in Engineering no. 60 (1):213-232.
[3]   Belinha, Jorge. 2016. "Meshless Methods: The Future of Computational Biomechanical Simulation." Journal of Biometrics & Biostatistics no. 07. doi: 10.4172/2155-6180.1000325.

PS5.12

A new tool for quantifying cell mechanics and cell-to-surface adhesion

*Jinju Chen[1], **Ma Luo**[1] Jonathan M.G. Higgins[2], Wenjian Yang[1]*

1   Newcastle University, Engineering , Newcastle Upon Tyne, UK
2   Newcastle University, Biosciences Institute, Faculty of Medical Sciences, UK

Cell mechanics of living cells are vital for many cell functions, including mechanotransduction[1-3], migration, and differentiation[4]. It is known that changes in cell mechanics are often correlated with disease progression [5, 6]. Cell-matrix adhesion is important for the patterning, integrity and homeostasis of tissues and may provide a target for therapy, for example in cancer metastasis [7]. Cell mechanics and adhesion between cells and the matrix are also important for tissue engineering. Therefore, it is important to study cell mechanics and cell-to-material adhesion. However, simultaneous characterization of the cell-to-material adhesion and viscoelastic properties of the same cell is challenging. In this study, we present a new approach to simultaneously determine these properties for single cells, using Microfluidics-based Atomic Force Microscopy. MCF-7 cells were cultured on in tissue culture treated polystyrene petri dishes for 1 day at 37°C, 5% CO_2 95% relative humidity. A total of 95 measurements were performed.

It is found that well-spread cells tended to have stronger adhesion (see Fig.1), which may be due to the greater area of contact between cellular adhesion receptors and the surface, as confirmed with our confocal images. By contrast, equilibrium and instantaneous moduli of MCF-7 cells were about 0.4kPa and 4kPa, which have little dependence on cell shape. This experimental method could be a powerful tool for establishing quantitative correlations among different physical characteristics of numerous cell types in normal or diseased states, as well as elucidating the underpinning biological and pathological implications.
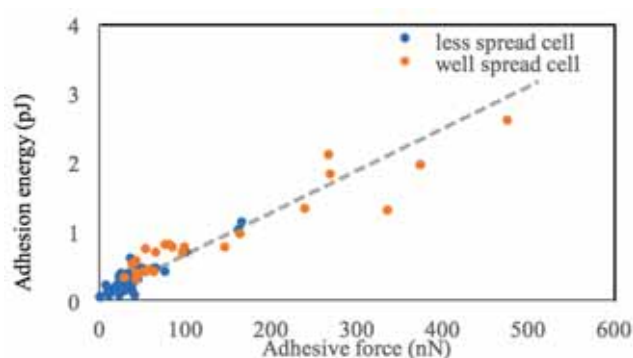
Figure 1. Comparison of adhesion energy against adhesive force for well spread and less spread cells.

References:
1.   Dey, K., et al., Biomaterials Science, 2020. 8(24): p. 7033-7081.
2.   Kothapalli, C., et al., Biomaterials Science, 2020. 8(19): p. 5452-5464.
3.   Chen, J., et al., Biophysical Journal, 2012. 103(6): p. 1188-1197.
4.   Diz-Munoz, A., et al. Trends in Cell Biology, 2013. 23(2): p. 47-53.
5.   Haugh, M.G., et al., Tissue Engineering Part A, 2011. 17(9-10): p. 1201-1208.
6.   Lekka, M., et al., European Biophysics Journal with Biophysics Letters, 1999. 28(4): p. 312-316.
7.   Janiszewska, M., et al., Journal of Biological Chemistry, 2020. 295(8): p. 2495-2505.

Correspondence and requests for materials should be addressed to J.C. (email: jinju.chen@ncl.ac.uk)

PS6.1

A systematic review of the uses and benefits of three dimensional printing in orthopaedic surgery

Firas Nasr[1], *Caroline Hing*[1]

1   St George's, University of London, United Kingdom

Introduction: Three-Dimensional (3-D) printing was first used in the medical field in the early 1990s to create a model of the cranial anatomy and has seen a rapid increase in use over the last decade. The objective of this systematic review was to analyse the uses and benefits of 3-D printing in orthopaedic surgery. Key areas of focus were highlighted such as pre-operative planning, patient specific implants, instruments, and orthoses.

Method: The PRISMA methodology was followed and literature searches were conducted on Medline, Embase and the Cochrane library. MeSH search terms and Boolean operators included '3-D printing', 'orthopaedic', 'pre-operative plan', 'implants', 'patient specific instruments' AND 'orthosis'. Duplicate studies, literature from before 2015 and non-human subjects were all excluded from the review.

Results: The searches resulted in 36 studies included in the final review for analysis (8 case reports, 7 case series, 9 case-control studies and 12 randomised control studies). The increasing interest in the use of 3-D printing in orthopaedics is reflected in the rise in the number of publications between 2015 (1 study) and 2020 (11 studies). The most common application of 3-D printing reported by 75% of the studies was the use of 3-D printed anatomical models to aid in pre-operative planning. The 3-D printed anatomical models were also utilized for surgical simulation (31%), intraoperative navigation (8%), and patient/family and surgical education (8%). The use of 3-D printing to manufacture patient specific orthoses, implants and instruments was reported in 14%, 11% and 8% of the studies respectively. The advantage of 3-D printing reported most (56% of studies) was the educational and training opportunities the 3-D printed models provided for junior surgeons. Doctor-patient communication and improved consenting was a reported benefit in 28% of the studies. Objective benefits of using 3-D printing such as significantly reduced operating time (42%), instrumentation time (11%), fluoroscopy time (31%) and intraoperative blood loss (33%) were also reported.

Conclusion: Orthopaedic surgery can be complex and technically challenging. The literature shows 3-D printing of anatomical models has improved pre-operative planning, allowed for surgical simulation, training and education. These benefits have led to improved operating metrics in patient where 3-D printed models were used. There are currently no studies which demonstrate these reported benefits have led to improved patient outcomes.

Figure 1 - PRISMA flow chart of included studies

Identification

References identified in database search
n = 519
EMBASE n = 416
MEDLINE n = 139
Cochrane Library n = 34

Screening

References after exclusions due to:
duplications (n = 266)
published before 2015 (n = 15)
n = 281

Eligibility

References after exclusions due to:
Not orthopaedic related (n = 76)
Not 3-D printing related((n = 66)
Not in english language (n = 15)
Related to vetinary medicine (n = 12)
n = 112

Included

References included in systematic review following exlusions due to:
Literature review (n = 34)
Conference presentations (n = 27)
No full text available (n = 15)
n = 36
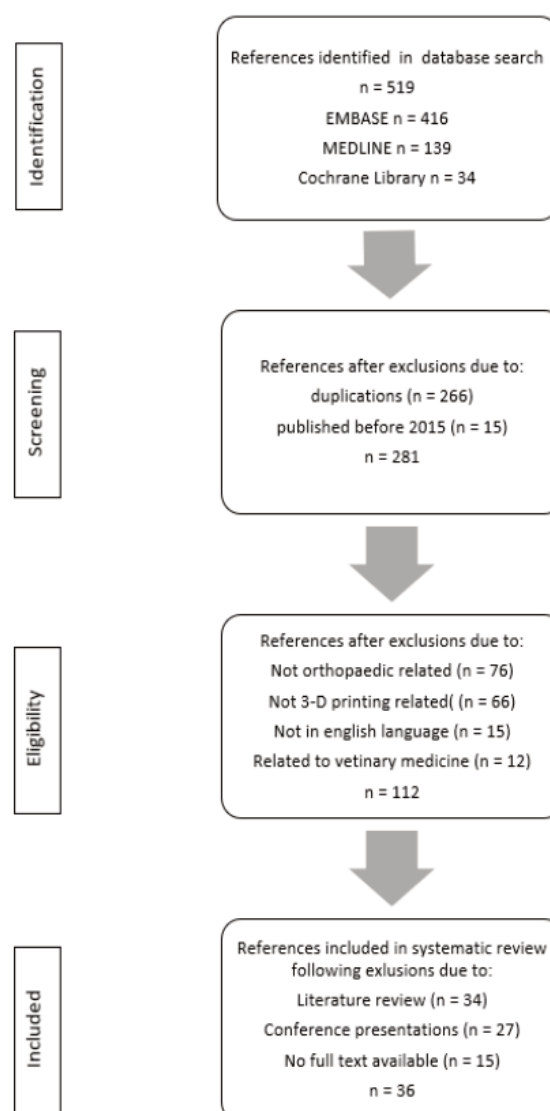
PS6.2

Automatic registration of dental cast on non-segmented CTscan

Marco Arbotto[1], Alexandre Barbas[2], Guillaume Dubois[1], Laurent Gajny[1], Philippe Rouch[1], Thomas Schouman[1][3]

1   Institut de Biomecanique Humaine Georges Charpak (IBHGC), Arts et Metiers Institute of Technology, Paris, France, France
2   Materialise NV
3   Sorbonne Universite, AP-HP, Hopital Pitie-Salpetriere, Service de Chirurgie Maxillo-Faciale, Paris, France

Orthognathic surgery is a type of surgery whose aim is to correct conditions related to structure, skeletal disharmonies and malocclusion of the jaw and the lower face. Key step in the planning of the orthognathic surgery is the manual dental cast registration to the medical image[1]. Computerized tomography (CT-Scan) is one of the most commonly used imaging technique, although it requires segmentation for it to be employed in the registration phase. The segmentation step is a manual and time consuming task normally performed by a trained operator. In this work, a novel technique of automatic dental cast registration is presented, based on non-segmented CT-scan.

The registration is performed on bi-planar digitally reconstructed radiographs (DRR) generated from the CT-Scans, using a parallel generalized simulated annealing optimization framework[2][3]. The optimization technique proposed is able to perform the automatic registration of the dental casts independently and in parallel. A collision detection function is also embedded, which allows to limit the interpenetrations between the meshes.

The presented algorithm has been tested on 50 orthognathic cases, which include clinically validated segmentation of the hard tissue and aligned dental cast meshes. Each mesh has been pre-processed to maintain only the teeth crowns and then randomly displaced to simulate an initial coarse manual repositioning in the range of [-2, +2] mm for translation and [-5, +5] degrees for rotation. The DRRs have been processed using a wavelet denoising filter and contrast limited adaptive histogram equalization (CLAHE). The accuracy of the registration has been measured as the average point-to-point distance between the dental casts registered with the proposed algorithm and the dental casts in their validated positions.

Results showed an average point-to-point deviation of 0.8mm (SD 0.33mm) for the maxillary cast and 0.68mm (SD 0.39mm) for the mandibular cast. Results have shown the ability of the proposed method to register a dental cast to a non-segmented CT-scan with an average deviation below 1mm, demonstrating its robustness to casts and image artefacts.

The novel automatic technique of dental cast registration based on non-segmented CT-scan presented in this work, allows to overcome manual thus time-consuming steps such as segmentation of CT-Scan and dental cast registration. Ideally, the proposed method could be extended to radiographic images. The promising results suggest further investigations, with a perspective of implementation in orthognathic surgery planning routine.

References:
[1]   B. B. Farrell, P.B. Franco, M.R. Tucker, "Virtual Surgical Planning in Orthognathic Surgery", Oral and Maxillofacial Surgery Clinics of North America, 2014
[2]   C. Tsallis and D. A. Stariolo, "Generalized simulated annealing," Phys. A, Elsevier, 1996.
[3]   Penney GP, Weese J, Little JA, Desmedt P, Hill DL, Hawkes DJ. "A comparison of similarity measures for use in 2D-3D medical image registration". IEEE Trans Med Imaging. 1998

PS6.3

Using optical coherence tomography and intravascular ultrasound imaging to quantify coronary plaque cap thickness and stress/strain using 3D thin-layer models

Rui Lv[1], Akiko Maehara[2], Mitsuaki Matsumura[2], Liang Wang[1], Xiaoya Guo[4], Qingyu Wang[1], Gary Mintz[2], Dalin Tang[5]

1   Southeast University, Nanjing, China
2   Columbia University, New York, United States
4   Nanjing University of Posts and Telecommunications, Nanjing Shi, China
5   Worcester Polytechnic Institute, Worcester, United States

Background: Accurate quantification of vulnerable plaque cap thickness and cap stress/strain is of great importance for plaque vulnerability assessment and many clinical applications. Intravascular ultrasound (IVUS) is commonly used in clinical practice for diagnosis and treatment decisions. However, due to IVUS limited resolution (about 150-200 μm), it is not sufficient to detect vulnerable plaques with a threshold cap thickness of 65 μm. Optical Coherence Tomography (OCT) has a resolution of 15-20 μm and can measure fibrous cap thickness more accurately. The aim of this study was to use OCT as the benchmark to obtain patient-specific coronary plaque cap thickness and evaluate the differences between OCT and IVUS fibrous cap quantifications. A 3D thin-wall model was also used to demonstrate the impact of accurate cap thickness quantification on plaque cap stress/strain calculations.

Methods: Data from 10 patients (mean age: 70.4; m: 6; f: 4) with coronary heart disease who underwent IVUS, OCT and angiography were collected at Cardiovascular Research Foundation (CRF) using approved protocol with informed consent obtained. 348 slices with lipid core and fibrous caps were selected for study. Convolutional Neural Network (CNN)-based and expert-based data segmentation were performed using established methods previously published. Cap thickness data were extracted to quantify differences between IVUS and OCT measurements.

Results: For the 348 slices analyzed, the mean value difference between OCT and IVUS cap thickness measurements was 1.83% (p=0.031). However, mean value of point-to-point differences was 35.76%. Comparing minimum cap thickness for each plaque, the mean value of the 20 plaque IVUS-OCT differences was 44.46%, ranging from 2.36% to 91.15%. For a sample slice from Patient 5 (see Figure 1), the maximum cap stress from IVUS model was 181.67 kPa, which was 47.42% higher than that (123.23 kPa) from the OCT model. Maximum cap strain from the IVUS model was 0.248, which was 8.3% higher than that (0.229) from OCT model.

Conclusions: These preliminary results demonstrated that there were significant differences between IVUS and OCT plaque cap thickness measurements. Large scale patient studies are needed to confirm our findings.
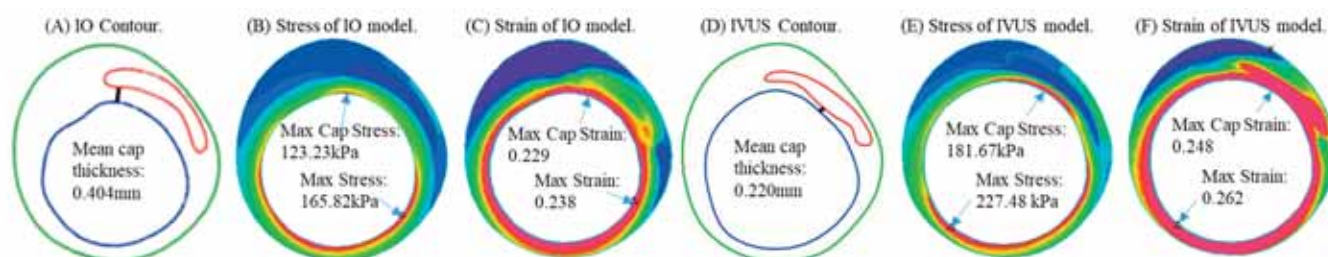
Figure caption: Figure 1. A sample to show the differences of mean cap thickness, maximum fibrous cap stress and strain and maximum stress and strain on lumen contour for IVUS+OCT(IO) and IVUS.

PS6.4

Model comparisons for coronary stable and unstable plaque: 2D and 3D fluid-structure interaction simulations

Wang Qingyu[1], *Wang Liang[1]*, *Akiko Meahara[2]*, *Habib Samady[3]*, *Zheng Jie[4]*, *Gary S. Mintz[2]*, *Gregg W. Stone[2 5]*, *Tang Dalin[1 6]*

1   Southeast University, School of Biological Science and Medical Engineering, Nanjing, China
2   Columbia University, The Cardiovascular Research Foundation, New York, United States
3   mory University School of Medicine, Department of Medicine, Atlanta, United States
4   Washington University, Mallinckrodt Institute of Radiology, St. Louis, United States
5   Icahn School of Medicine at Mount Sinai, The Zena and Michael A. Wiener Cardiovascular Institute, New York, United States
6   Worcester Polytechnic Institute, Mathematical Sciences Department, Worcester, United States

Introduction: Various modeling strategies, including 2D structure-only model, 3D structure-only model and 3D fluid-structure interaction (FSI) model have been used to investigate coronary plaque progression and vulnerability assessment [1]. However, previously comparison publications mostly analyzed model differences using single patient data or idealized geometries. Model differences between stable and unstable plaques have not been considered. The differences among 2D and 3D FSI models of different patients and vulnerable plaques are of great significance for the clinical application of simulation models.

Methods: In vivo intravascular ultrasound (IVUS) coronary plaque data were acquired from seven patients at Cardiovascular Research Foundation (CRF) using protocol approved by the local institute and informed consents were obtained. 2D and 3D FSI models were constructed for seven patients to perform model comparisons and quantify impact of plaque vulnerability on plaque wall stress/strain (PWS/PWSn) calculations. Three hundred and eighty-eight (388) high-quality slices from seven patients were selected for our study. The 388 plaque samples were classified into stable (n=251) and unstable (n=137) groups according to morphological index values (integers 0-4) defined in [2]. Slices with Index ≥2 were defined as unstable. Slices with Index<2 were considered as stable. For each slice, PWS and PWSn values from 100 evenly-spaced points at the lumen were obtained for analysis.

Results: Figure 1 gave PWS and PWSn plots on sample stable and unstable slices from 3D FSI models showing their differences. PWS and PWSn values of 137 unstable plaque slices from 2D model were 40.40% and 39.57% higher than those of 3D FSI model, respectively. PWS relative error patient variation range was 8.78%-129.50%, while PWSn relative error variation range was 8.84%-79.62%. For the stable plaque group (251 slices), PWS and PWSn values from 2D model were 24.61% and 33.59% higher than those of 3D FSI model, respectively. PWS relative error variation range was 4.98% to 73.97%, while PWSn relative error variation range was 11.29%-64.80%. Overall, comparing 2D and 3D FSI model differences for stress/strain calculations, the unstable group had greater model differences than those from the stable group.

Conclusion: PWS and PWSn errors using 2D models for stable and unstable plaques had noticeable differences. The present multiple patient study is a step in emphasizing the importance of considering plaque vulnerability variations in model differences.
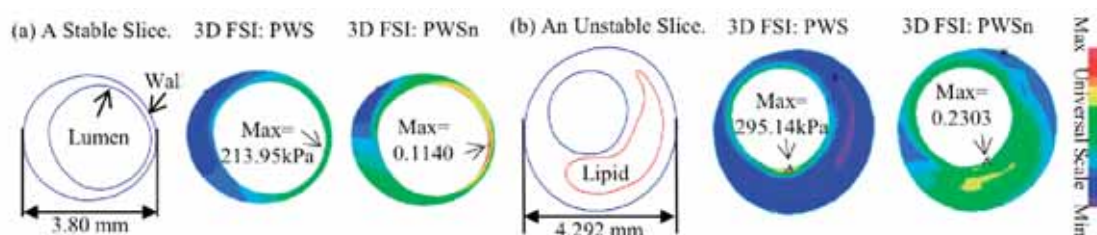
Figure 1. PWS and PWSn plots on sample stable and unstable slices from 3D FSI models showing their differences. Maximum PWS and PWSn occurred on thin cap of the unstable slice.

References:
1.   Huang Y, et al., J Biomech 2014; 47:1465-71.
2.   Wang L, et al., PLoS Comput Biol 2015; 11: e1004652.

PS6.6

Assessing methodological uncertainty of in-vitro digital volume correlation bone strain measurements in total shoulder arthroplasties

Jakub Targosinski[1], Jonathan Kusins[1], Nicole Martensson[1], Andrew Nelson[1], Nikolas Knowles[2], Louis Ferreira[1]

1   Western University, London, Canada
2   University of Calgary, Calgary, Canada

Digital volume correlation (DVC) performed on micro-computed tomography (CT) imagery provides a measurement technique which can measure full-field deformations of loaded osseous tissues. This experimental approach is of interest in the investigation of the failure mechanisms of glenoid implants in total shoulder arthroplasties, as it allows for direct experimental measurement of strains at the bone-cement-implant interface [1–4]. It is therefore important to understand the methodological limitations of the bone strain measurements made and the inherent uncertainty present in this approach. Micro-CT scans of two cadaveric scapulae, from donors who had been treated with shoulder replacement in life, were captured with differing numbers of CT projections under loaded and unloaded conditions. DVC strain measurements were quantified from the unloaded and loaded volumetric images with five distinct sub-volume sizes. The mean absolute error and measurement sensitivity were quantified in the DVC strains as a function of projection count and sub-volume size, establishing relationships between measurement spatial resolution, image quality, and strain measurement error. Observations revealed that with careful selection of DVC spatial resolution and CT projection count, scan times can be halved with no impact on DVC strain accuracy. DVC can potentially be a useful preclinical evaluation tool to quantify the internal strain within bone-implant constructs.
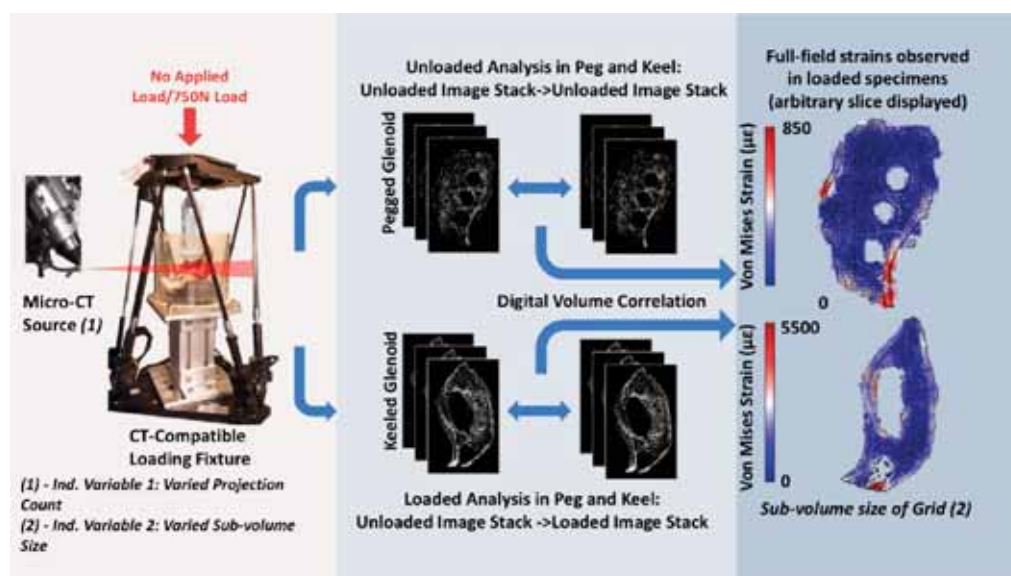
Figure 1: Simplified workflow of the unloaded and loaded DVC analyses performed. For the unloaded analysis, every combination of the two independent variables was investigated. For the loaded analysis, the spatial resolution of the DVC measurement was fixed based on the findings of the unloaded analysis at a value of 1072 µm (32 voxels).

References:

1. Liu, L., Morgan, E.F.: Accuracy and precision of digital volume correlation in quantifying displacements and strains in trabecular bone. J. Biomech. 40, 3516–3520 (2007). https://doi.org/10.1016/j.jbiomech.2007.04.019.
2. Palanca, M., Tozzi, G., Cristofolini, L., Viceconti, M., Dall'Ara, E.: Three-Dimensional Local Measurements of Bone Strain and Displacement: Comparison of Three Digital Volume Correlation Approaches. J. Biomech. Eng. 137, (2015). https://doi.org/10.1115/1.4030174.
3. Dall'Ara, E., Peña-Fernández, M., Palanca, M., Giorgi, M., Cristofolini, L., Tozzi, G.: Precision of digital volume correlation approaches for strain analysis in bone imaged with micro-computed tomography at different dimensional levels. Front. Mater. 4, 31 (2017). https://doi.org/10.3389/fmats.2017.00031.
4. Comini, F., Palanca, M., Cristofolini, L., Dall'Ara, E.: Uncertainties of synchrotron microCT-based digital volume correlation bone strain measurements under simulated deformation. J. Biomech. 86, 232–237 (2019). https://doi.org/10.1016/j.jbiomech.2019.01.041.

PS6.7

Repair of coronary plaque optical coherence tomography image using an automatic vessel wall delineation approach and its impact on plaque stress/strain calculations

Mengde Huang[1], *Jian Zhu*[2], *Liang Wang*[1], *Yangyang Qu*[2], *Xiaoguo Zhang*[2], *Lijuan Chen*[2], *Genshan Ma*[2], *Dalin Tang*[1 3]

1   School of Biological Science and Medical Engineering, Southeast University, Nanjing, China., NanJing, China
2   Zhongda Hospital, Southeast University, Nanjing Shi, China
3   Worcester Polytechnic Institute, Worcester, United States

Background: Intravascular optical coherence tomography (OCT) is a new imaging modality which is rapidly developing in recent years. It provides unprecedented resolution to about 10 μm, which allows for detection of vulnerable coronary plaques, accurate cap thickness quantification, and construction of OCT-based patient-specific plaque models for more accurate stress/strain calculations. However, its merit comes at the expense of low penetration depth, which means vessel wall can be obscured by lipid or calcium in diseased regions. It is a great challenge to repair these fragmentary OCT image slices to re-construct complete 3D vessel geometries and make biomechanical models.

Method: This study aims to identify the location of unknown vessel wall segments and delineate the entire vessel wall based on an automatic image processing approach. An OCT pullback of one patient (female, age 67) was acquired at ZhongDa Hospital, Southeast University, Nanjing, China, with informed consent obtained. An automatic delineation method to repair the fragmentary OCT image slices is described as follows. Lumen was segmented by Otsu's thresholding method. A modified Canny method was then performed to detect the visible vessel wall. Simple ellipse fitting was used to fit the known data points, and obtaining the entire vessel boundary. Manual delineation was performed by a trained expert and the manually-repaired slices were used as the gold standard. 3D thin-slice models were constructed using the slices repaired by the two methods to study the impact of the automatic delineation method on plaque stress and strain calculations.

Results: Comparison of contours, stress and strain plots of two methods from a sample slice is shown in Fig.1. The average distance (100 data points taken on the out-wall) between two contours is 0.035mm (relative error 2.68%). Maximum cap stress and strain of the model using automatic delineated contour were 126.60kPa and 0.2230, compared to 125.49kPa and 0.2056 from the model using manual annotated contour, respectively. The impact on cap stress was only 0.88%, fairly impressive.

Conclusion: The similarities of stress and strain distribution and small value differences between two models demonstrated the feasibility of the automatic vessel wall delineation approach. More patient data and 3D delineation and model constructions are needed to further develop the method and validate the initial findings.
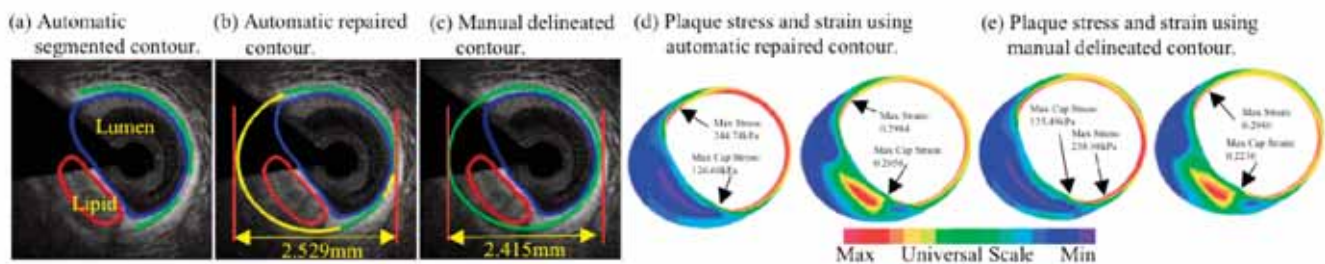
Figure caption: Figure 1. Comparison of automatic and manual delineation approaches: contours and stress and strain plots.

PS6.8

Improving coactivation estimation of inverse hand models using muscle synergies

Joaquín L Sancho-Bru[1], Néstor J. Jarque-Bou[1], **Verónica Gracia-Ibáñez**[1], Margarita Vergara[1]

1   Universitat Jaume I, Spain

Hand biomechanical models can help to study the muscles role in daily activities. Inverse models lead to an indeterminate problem, with more unknowns (muscle and tendon forces) than available equations, solved by minimizing a cost function, such as the sum of the squared muscle stresses [1]. However, such models do not reproduce the experimentally observed muscle coactivation [2]. Here, we propose to improve a previous biomechanical hand model [3] by using muscle synergies, which have been experimentally confirmed [4], i.e., groups of co-activating muscles are coordinated by time-varying activation commands. However, representative synergies of all hand muscles have not been identified yet because previous studies are limited to few muscles and simple tasks. To cope for this, we have used surface-EMG data of a previous study [5], with measurements from 30 forearm spots (six subjects, 21 daily activities) and assigned each extrinsic muscle to one spot, based on muscle locations under the forearm skin. Then, synergies were obtained through principal component analysis (standardized data, Varimax rotation) using all the data (subjects and tasks), finding that four synergies explained 78.5 % of variance.

The original model was modified, forcing the activation levels of the extrinsic muscles to be a combination of the synergies found. The original model and the synergy approach were used to estimate the muscle activations required to hold a cylinder (0.405 kg, ⌀64 mm) with the fingertips, by inputting the posture and fingertip forces measured with a Cyberglove and a Finger-TPS. No solution satisfied the constraints with the synergistic model, as the coactivation forced some extrinsic muscles to increase their activations, and the intrinsic muscles were unable to counteract them. A modified synergy approach was considered: only a given activation percentage of each extrinsic muscle was driven by the synergies (the same percentage for all muscles), to simulate that not all variance was explained with the four synergies considered. The maximum percentage of contribution of the synergies yielding a feasible solution was 50%, the resulting estimation showing a more realistic simultaneity than the original model (Figure).

The proposed synergistic model seems to provide more realistic estimations, although identify more reliable synergies of all hand muscles requires more effort, as implies the simultaneous measurement of intramuscular EMG from all muscles during representative tasks.

FP – Flexor digitorum profundus
FS – Flexor digitorum superficiales
DI – First dorsal interosseous
LU – First Lumbrical
EDC – Extensor digitorum comunis
EI – Extensor indicis propius
VI – First volar interosseous
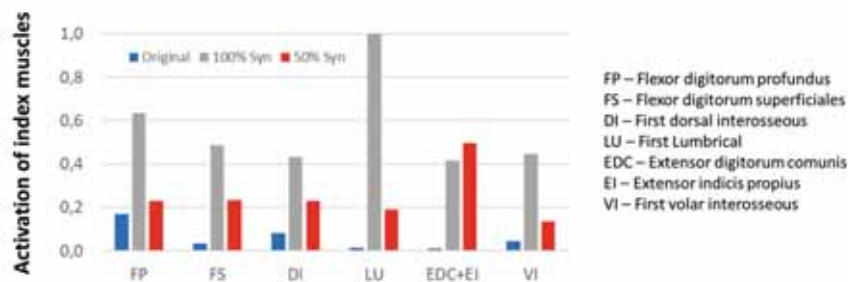
Figure caption: Estimated activation of index muscles with the different approaches

References:
[1] Crowninshield R, Brand R. 1981. J Biomech. 14(11):793–801.
[2] Valero-Cuevas F. 2005. J Biomech. 38(4):673-84.
[3] Sancho-Bru J L, et al. 2008. Ann Biomed Eng, 36(1):102-107.
[4] Weiss E J, Flanders M. 2004. J Neurophysiol, 92(1): 523-535.
[5] Jarque-Bou N J, et al. 2018. J Neuroeng Rehab, 15, 91.

PS6.9

Reconstruct CT images using historical images for metal artifact reduction

Ziheng Deng[1], **Jun Zhao[1]**

1   Shanghai Jiao Tong University, School of Biomedical Engineering, Shanghai, China

Metal artifact reduction (MAR) is an important issue for commercial CT systems. During the CT scan, metal objects of high density strongly attenuate the X-rays and result in unreliable projection data. To reduce the metal artifacts, one approach is to remove the projections that pass through the metal objects. For incomplete projection data, Compressed sensing (CS) based algorithms are proposed to reconstruct CT images. However, the CS methods achieve limited success in the MAR problem. Most of the algorithms fail to restore the fine details around the metal objects. Instead, these regions are over-smoothed by improper regularization. In this paper, we propose to utilize the historical CT images of the same patients to compensate for the missing data. The prior knowledge of the bone structures plays an important role in this method.

In clinical cases, previous CT scans might be taken years ago. Therefore, differences in structures are inevitable and it is impractical to use the historical image directly. To deal with this problem, we first derive a fused image by incorporating the information of the historical image and a linear interpolation MAR (LI-MAR) pre-corrected image. The LI-MAR algorithm can partly remove the metal artifacts and serve as a background image, while the prior knowledge of the bone tissues is provided by the historical image. An optimization-based algorithm is used to register the two images. In this way, the fused image can involve the prior information from the historical images and avoid introducing extra errors. After that, a fused image initialized model-based iterative reconstruction algorithm is adopted to obtain the final result.

The proposed method is evaluated on simulated data. We collect clinical images from two CT scans of the same patient [1] and simulate metal artifacts on the second set. Though obvious differences exist between the historical images and the target images, our algorithm removes most of the metal artifacts and restores the bone tissues well.
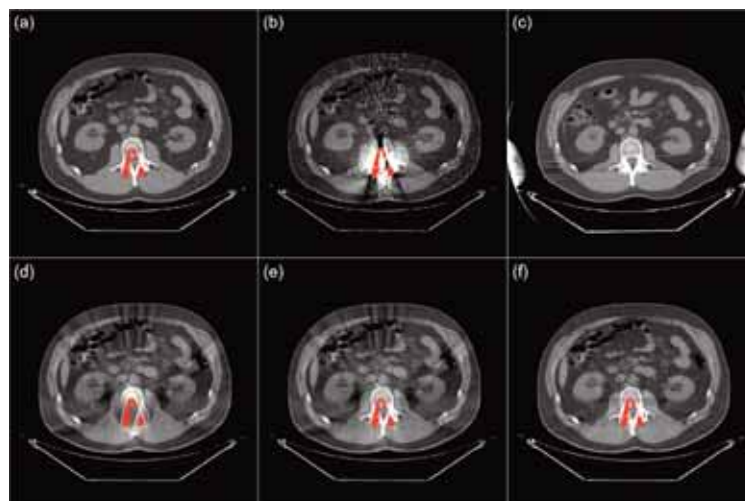
Figure caption: Figure 1. Reconstruction images. (a) the ground truth, (b) the uncorrected image, (c) the historical image, (d) the result of the LI-MAR method, (e) the fused image, (f) the result of the proposed method. Red pixels stand for the inserted metal implants.

References:
[1]   Kinahan, P., Muzi, M., Bialecki, B., & Coombs, L. (2019). Data from the ACRIN 6685 Trial HNSCC-FDG-PET/CT [Data set]. The Cancer Imaging Archive. https://doi.org/10.7937/K9/TCIA.2016.JQEJZZNG.

PS6.10

Multiphysics model of a 3D bioengineered haematopoietic niche mimicking the physiological environment for the production of functional platelets.

Alberto Bocconi[1 2], Christian A. Di Buduo[2], Roberto Fedele[3], Alessandra Balduini[2], Manuela T. Raimondi[1]

1   Politecnico di Milano, Dipartimento di Chimica, Materiali e Ingegneria Chimica "Giulio Natta", Milano, Italy
2   Università di Pavia, Dipartimento di Medicina Molecolare, Pavia, Italy
3   Politecnico di Milano, Dipartimento di Ingegneria Civile e Ambientale (DICA), Milano, Italy

The development of a viable strategy to produce platelets in vitro exhibits a growing interest. Platelets are blood cells highly specialized in ensuring bleeding arrest and tissue repair. In nature, platelets are produced in the bone marrow haematopoietic niche by megakaryocytes, cells that protrude cytoplasmatic extensions into the lumen of bone marrow sinusoid capillaries. Here, shear forces generated by the blood flow mechanically detach platelets and drive them into circulation [1].

On this ground, a bioengineered bone marrow culture model needs to mimic the 3D architecture, composition and hydrodynamic environment of the native tissue. Recently, our group successfully used silk fibroin to fabricate a biocompatible 3D porous scaffold that promote platelet production by in vitro differentiated megakaryocytes [2]. The silk scaffold was implemented into the perfusion chamber of a milli-fluidic optically accessible bioreactor (MOAB) [3]. Such innovative bioreactor, thanks to the combination of interstitial perfusion and confocal optical accessibility, allows a complete control on the local conditions imposed to cells, in terms of fluid dynamics and mass transport.

In this contribution the optimal perfusion rate of the MOAB bioreactor was estimated via a computational finite element (FE) multi-physics model, that guarantees to mimic physiological fluid dynamics and oxygen transport inside this engineered haematopoietic niche. To this purpose, high resolution images of the 3D porous silk scaffold (3x6x0.5mm) were acquired by means of X-ray micro-tomography scanner (X-25, NorthStarImaging). Then, image segmentation and 3D geometry reconstruction were developed by an image processing software for 3D design and modeling. The multiphysics analyses were carried out in a COMSOL♣ multiphysics platform, apt to couple computational fluid dynamics with transport phenomena. In particular, flow rates lower than 600 µL/min guarantee a shear stress distribution inside the culture chamber within the physiological range of 0-410 mPa [4][5]. Further, the pO_2 predicted assuming 50,000 seeded cells ranges from 14 to 20% consistently with blood oxygenation in capillaries.

Thus, the finite element model predicted successfully the distribution of oxygen gradient inside the bioreactor guaranteeing normoxic culture conditions, and the shear stress at the fluid-cells interface, for several values of perfusion flow rates. Although the above results are still preliminary, our bioengineered haematopoietic niche coupled to the computational model for prediction/monitoring/control, represents a promising candidate for producing platelets, since the main physical and biochemical features of the human bone marrow can be reproduced.

References:
1.   Dolgin E. Nature. 2017;549(7673):S12-S15.
2.   Di Buduo CA et al. Biomaterials. 2017;146:60-71.
3.   Izzo L et al. Biomed Microdevices. 2019;21(1):29.
4.   Junt T et al. Science. 2007;317(5845):1767-70
5.   Bixel MG et al. Cell Rep. 2017;18(7):1804-1816

PS6.11

Agent-based multiscale modeling to simulate inflammatory stage of bone fracture healing

Edoardo Borgiani[1 2], Liesbet Geris[1 2]

1   U Liege, Biomechanics Research Unit, GIGA in silico medicine, Liege, Belgium
2   KU Leuven, Biomechanics Section, Department of Mechanical Engineering, Heverlee, Belgium

Bone fracture regeneration is characterized by the cooperation of numerous biological and mechanical factors regulating the process to successfully repair the injury without leaving scars. Following bone injury, inflammatory cells are the first responders and it is therefore described that their dysfunction or suppression could affect the whole regenerative process, leading to delays or non-unions [1]. In vivo studies of the inflammatory response to bone injury remain particularly challenging due to the numerous factors interacting at multiple time- and length-scales. We propose a novel multiscale computational approach to capture the stochastic nature of the events during the early stages of bone healing. A finite element model, based on an existing study [2], is included to simulate the mechanical environment of bone fracture. However, the innovative aspect of this model regards the introduction of an agent-based model to investigate the cell dynamics during the inflammatory response. This discrete in silico model will reproduce the hidden mechano-biological processes at the cellular level, which are challenging to study experimentally but whose understanding could provide interesting clinical insights. It simulates the behavior of immune and repair cells by reproducing their spatio-temporal dynamics within the fracture domain. Besides, at the sub-cellular level, the model simulates the concentration dynamics of inflammatory cytokines and growth factors. The iterative nature of the simulation allows to follow how the mechano-biological environment evolves during the inflammatory phases of bone fracture regeneration at the different scales. To date, the model simulates the biological activities of the macrophages at cellular level (e.g. migration, proliferation, polarization). In addition, these in silico macrophages are programmed to remove debris from the injury site and release specialized inflammatory cytokines (Figure). The analysis of the simulation outcomes at different scales nicely highlights the spatial distribution of tissues, cell populations, and sub-cellular signals through the development of the healing process. The principal aim of this model is to extend the vast collection of bone fracture regeneration computer models with a brand new one that explores the fracture healing process since its initial inflammatory stage. More inflammatory cells (e.g. neutrophils, T cells), repair cells and additional subcellular elements will be added in the future to improve the accuracy and the validity of the current model. The platform has the potentialities to become a clinical tool to explore critical healing case scenarios and provide insights about the effectiveness of treatments and therapeutics since the first instants post-injury.
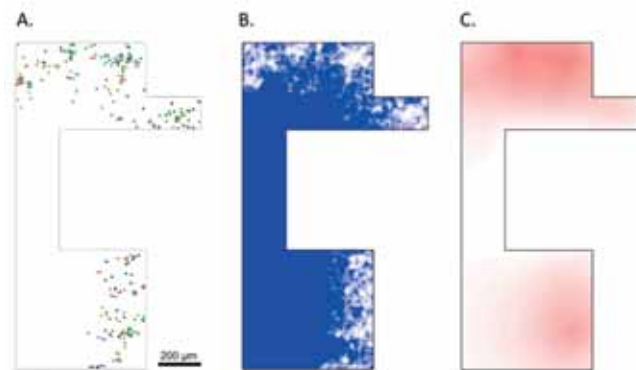
Figure caption: "Model outcome after 24 hours post-injury. (A) Macrophages distribution (different colors to identify macrophage polarization); (B) debris presence (white is cleaned area); (C) TNFα cytokine density (higher concentration in red)."

References:
[1]   Maruyama et al., Front Endocrinol (Lausanne). 2020; 11:386.
[2]   Geris et al., Biomech Model Mechanobiol. 2010; 9:713.

PS6.12

Predicting the shape and mechanical properties of early limb bud using individual cell based modeling

Yvenn Sermeus[1 2], Maxim Cuvelier[1 2], Liesbet Geris[2 3], Tylzanowski Przemko[4 5], Bart Smeets[1 2]

1   KU Leuven, MeBioS, Leuven, Belgium
2   KU Leuven, Prometheus, Belgium
3   U Liège, GIGA In silico medicine, Belgium
4   KU Leuven, SBERC, Belgium
5   Medical University of Lublin, Department of Biochemistry and Molecular Biology, Poland

The initial stages of bone tissue development are marked by condensation of mesenchymal cells, a critical step for the resulting biological structure. Micro-aggregate experiments have revealed that mimicking both the chemical and mechanical environment of in vivo development typically increases in vitro engineered tissue quality [1]. Despite progress in defining underlying biochemical signaling pathways driving condensation, the effect and origin of mechanical cues are poorly understood. Thus, to accurately replicate the mechanical environment a better understanding of in vivo mechanical condensation is needed.

In this work, the developing chick limb is studied as a model-system for mesenchymal condensation. Here, condensation occurs simultaneously with the outgrowth and widening that shapes the limb bud. A distinct paddle shape results from the interplay between active developmental processes, individual cellular mechanical properties, cellular interactions and ectodermal molding [2]. These four factors are hypothesized to influence the cells mechanical state thereby controlling the condensation process, particularly through mechanical stress. We propose an individual cell-based model where mesenchymal cells are represented as individual agents. Interactions between the cells are modeled using two types of forces. Passive attraction-repulsion forces are used to represent cell-cell adhesion and cortical tension. The effect of active cell protrusions is represented as a directed migratory force. The direction is based on the cell polarization which can either be randomly diffusing or directed by a chemical gradient. The ectoderm surrounding the mesenchyme functions as a boundary condition, and is modeled as a visco-elastic material. Our simulations indicate that graded proliferation mediated by FGF and directed intercalations directed by a WNT3a gradient are needed to ensure limb bud elongation.

References:
[1]   N. Mahmoudifar (2012) Trends Biotechnol, 30(3): 166-176
[2]   S. Hopyan (2017) Dev Biol, 429(2): 429-433.

PS6.13
A finite element model of the triceps surae in infant humans

Mousa Kazemi[1], Ali Mirjalili[2], Anne Agur[3], Justin Fernandez[1 4], Thor Besier[1 4], Geoffrey Handsfield[1]

1   Auckland Bioengineering Institute, Auckland, New Zealand
2   University of Auckland, Anatomy and Medical Imaging, Auckland, New Zealand
3   University of Toronto, Department of Surgery, Toronto, Canada
4   University of Auckland, Engineering Science, Auckland, New Zealand

The Triceps Surae (TS) muscle group plays a vital role in bipedal standing and walking, but it is unclear how the TS muscles change from infancy, when human mobility is distinctly non-bipedal. An interesting question exists: how do the TS muscles change from infancy to accommodate weight-bearing and walking? For instance, it has been observed the that medial and lateral gastrocnemius are similar in size prior to walking, and the medial gastrocnemius (MG) shows remarkable growth during the 1st year of independent walking [1], but it is unclear if MG growth precedes the shift to walking or if walking mechanically stimulates the muscle to grow. Muscle strength impairments in the very young are also implicated in the development of pathological gaits; yet very little is known about infant muscle architecture and function, and walking disabilities are typically not clearly identified by parents before 5-10 years of age [2]. It is clear that calf muscle anatomy is starkly different in infants compared to children [1]. Our understanding of paediatric muscle architecture and mechanics will benefit tremendously from a pipeline incorporating detailed anatomical assessment and the development of biomechanical models. We present here a novel finite element (FE) model developed from digitized cadaver data from a rare data set [1] that will be used to evaluate the relationship between muscle activation, plantarflexion, and local muscle mechanics. Using convex hulls, muscles were built around fascicle tracts and concentric plantar flexion was simulated in FEBio (Figure 1). We observed high Cauchy stresses and along-fiber strains in the origin and insertion regions of the infant TS muscles, suggesting rapid muscle remodelling in these regions. This modelling pipeline will be used to explore the hypothesis that infant musculature responds to the mechanical demands of walking, and exploring the relationship between mechanical loads and changes to local muscle architecture in infants.
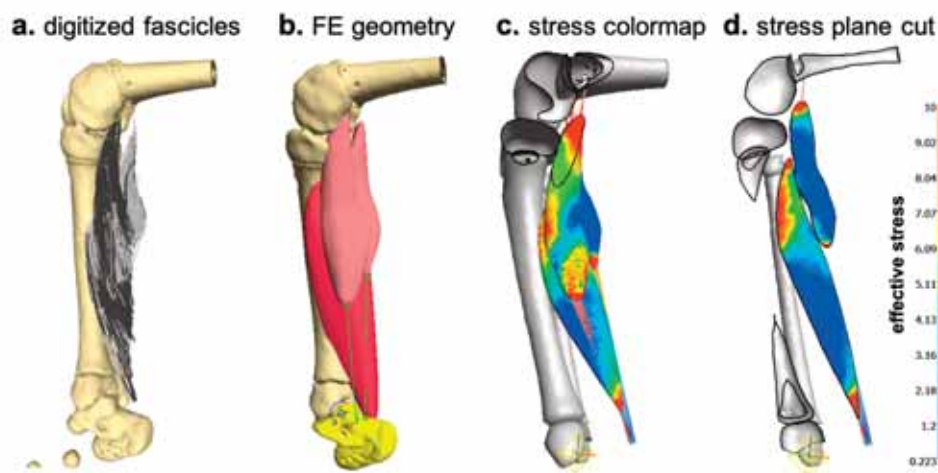
Figure 1. a) muscle fascicles digitized from infant cadaver. b) finite element geometry generated from digitized data, using fascicle tracts as fibre directions for the FE model. c) effective stress in the 3 triceps surae muscles during plantarflexion. d) plane cut reveals high stress in origins/ insertions of infant muscles.

References:
[1]   Bradshaw LR, Breinhorst EM, Stott NS, Agur AM, Mirjalili SA. 2020. The architecture of the 6-month-old gastrocnemius: A 3D volumetric study. European Journal of Anatomy 24(6):491-9.
[2]   Burns J, Ryan MM, Ouvrier RA. 2009. Evolution of foot and ankle manifestations in children with CMT1A. Muscle & Nerve: Official Journal of the American Association of Electrodiagnostic Medicine 39(2):158-66.

PS6.14

A novel method to estimate angular stiffness of prosthetic feet designs from FEA simulations

Marlon Rodriguez[1], *Christian Javier Cifuentes De la Portilla*[2], *Carlos Francisco Rodriguez Herrera*[1]

1   Universidad de los Andes, Department of Mechanical Engineering, Bogotá, Colombia
2   Universidad de los Andes, Department of Biomedical Engineering, Bogotá, Colombia

An important kinetic and kinematic relationship between joint angle and torque is the angular stiffness, defined as the local tangent to the moment-angle curve exhibited for a given joint [1]. When this concept is applied to the ankle, it describes the relation between ankle torque and the progression of the shank over the foot during stance phase [2]. There is little data on how to estimate the ankle angular stiffness (AAS) in prosthetic feet and no method to directly measure it has been described. The objective of this study was to design and evaluate a computational method to estimate the AAS of prosthetic feet using published data of a nominal gait analysis. The finite element model was created from a CAD geometry whose shape and dimensions were defined from anthropometric data. The model includes entry values such as ground reaction forces (GRF), the path of the center of pressure (COP) and an anatomical marker-based position system to identify the virtual joints (fig. 1A). The simulations were carried out emulating the stance phase of the gait cycle and generating perturbations by applying the GRF at the different positions of the COP. The displacement of the markers was obtained to calculate the ankle angle and to construct the moment-angle curve. Results show that the behavior of the curve is not consistent with the human ankle joint biomechanics properties (fig. 1C). It is necessary to make modifications to the method and assess the need to include more variables, so it resembles more the desired biomechanical behavior. The approach followed shows that there are possibilities to create computational models to estimate kinetic and kinematic parameters such as the angular stiffness of the lower limb joints. Including this procedure in the design stage can be very useful for improving the performance of prosthetic feet designs.
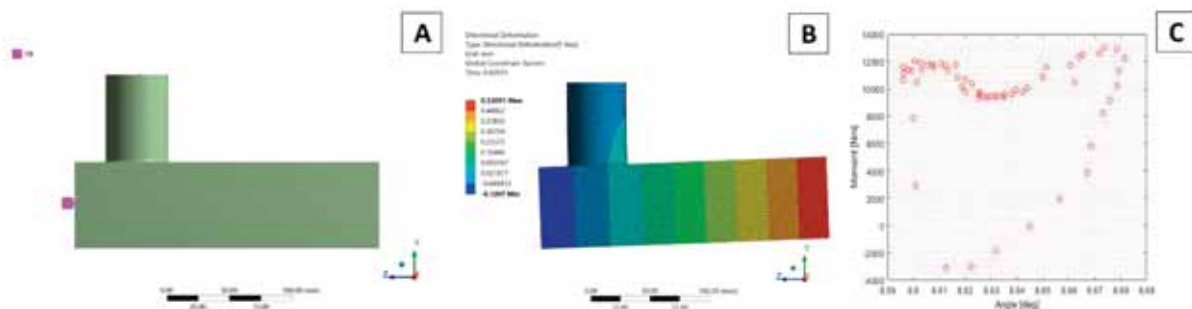
Figure 1. (A) Anatomical marker-based position system. (B) Deformation in the Y axis for a time of 0.42 s. (C) Moment-angle curve of the ankle joint.

References:
[1]   K. Shamaei, G. S. Sawicki, and A. M. Dollar, "Estimation of Quasi-Stiffness and Propulsive Work of the Human Ankle in the Stance Phase of Walking," PLoS One, vol. 8, no. 3, 2013.
[2]   P. G. Adamczyk, M. Roland, and M. E. Hahn, "Novel method to evaluate angular stiffness of prosthetic feet from linear compression tests," J. Biomech. Eng., vol. 135, no. 10, pp. 2–6, 2013.

PS6.15

Biomechanical study, by finite element analysis, of the material influence for lateral plates in the treatment of distal femoral fractures

Jorge Rosell[1], Marta Sarasa[2], José Manuel Naveiro[1], Beatriz Redondo[2]

1   EINA, University of Zaragoza, Mechanical Engineering, Zaragoza, Spain
2   Lozano Blesa" University Clinical Hospital of Zaragoza, Traumatology, Zaragoza, Spain

Femur fractures account for around 13% of those that occur in humans, the most serious being in long bones [1]. One of the most common treatments is lateral plates. However, there are several debates currently regarding this treatment: material (steel or titanium), length, number, and distance between screws to the fracture site. The aim is to achieve correct fracture stability but creating a balance between stiffness and mobility at the fracture focus [2-3].

This study proposes the biomechanical analysis of a distal fracture in Wiss zone 4, with fracture gaps of 0.5, 3 and 20 mm, analysing the effect that different materials have on the most critical parameters for adequate consolidation: global stability of the osteosynthesis, axial and rotational displacement and stresses in the lateral plate and in the cortical bone.

Three Finite Element models were implemented, varying the fracture gap. The plate length, 243 mm, and the screws configuration remain unchanged. Each model is analysed with stainless steel and titanium alloy as materials for the lateral plate.

Comparing titanium alloy versus stainless steel, for the models with gaps of 3 and 20 mm, respectively, the global displacement is increased by 80.43% and 80.56%, the axial displacement in the anatomical axis of the femur is increased by 102.65% and 104.51%, the plate rotation is increased by 90.47% and 90.40%. The von Mises stress in the plate is increased by 12.54% and 12.52% and the maximum stress in the cortical bone is increased by 38.82% and 37.06%.

In the case of 0.5 mm gap, contact between fracture surfaces occurs in the model with titanium alloy. The global displacement is increased by 10.35%, the axial displacement is increased by 5.55%, the plate rotation is increased by 2.65%. The von Mises stress in the plate is decreased by 28.81% and the maximum stress in the cortical bone is increased by 12.67%.

As conclusion, the use of titanium alloy in lateral plates leads to an increase of the global displacement and the micro-movements at the fracture focus. Greater mobility at the fracture focus, within a certain threshold, can be beneficial and stimulate bone regeneration. Titanium alloy leads to an increase in the stresses measured on the cortical bone, always below the limit in which the bone can break or splinter. If the fracture surfaces contact, the behaviour of the plate changes and the results are closer for both materials.

Figure 1: Finite element models with 0.5, 3 and 20 mm fracture gaps.
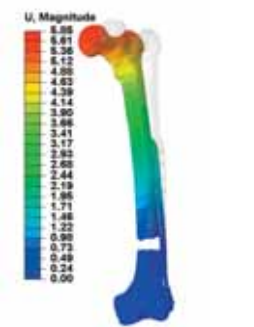
Figure 2: Global displacement (mm). Scale factor of 5. Model with 20 mm gap and steel.
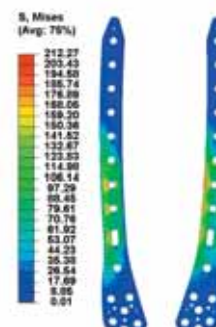
Figure 3: Lateral Plate von Mises stress (MPa). Model with 20 mm gap and steel.
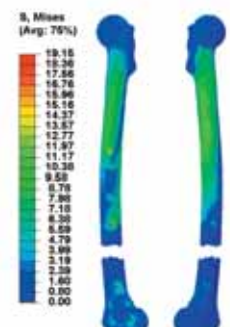
Figure 4: Cortical bone von Mises stress (MPa). Model with 20 mm gap and steel.

References:
[1]   Court-Brown CM, Caesar B. Epidemiology of adult fractures: a review. Injury 2006, 37: 691-697.
[2]   Frigg R et al. The development of the distal femur Less Invasive Stabilization System (LISS). Injury 2001, 32: SC24-31.
[3]   Schandelmaier P et al. Distal femoral fractures and L.I.S.S. stabilization. Injury 2001, 32: SC55- 63.

PS6.16
Can a numerical model predict the risk of blood clot embolism in stroke?

Mahdi Daei Daei[1], Abdul Barakat[1]

1   École Polytechnique, Palaiseau, France

Strokes are among the most debilitating pathologies worldwide. The development of a stroke involves the blockage of a cerebral blood vessel by a thrombus (a blood clot). A common technique for stroke treatment is stentriever thrombectomy, which involves clot removal using a stent-like device. A principal concern with stentrievers is the possibility of clot rupture (embolism) which can lead to secondary strokes. The goal of this project is to develop a computational framework that provides a map of the risk of clot rupture for different clot types. A computational model of the blood clot, the stentriever (with its deployment system), and the complex cerebral vascular geometry was reconstructed and input into ABAQUS. The computational results provide the stresses in both the stentriever and the blood clot at various points during the retrieval process. A "damage model" links the stresses within the clot to the likelihood of clot rupture. The forces required for successful retrieval of different types of thrombi are also computed. Different clot types with different mechanical properties and different friction coefficients were tested with the numerical model and a risk map of elastic modulus vs friction coefficient was provided. (red: failed to retrieve, green: successfully retrieved) .
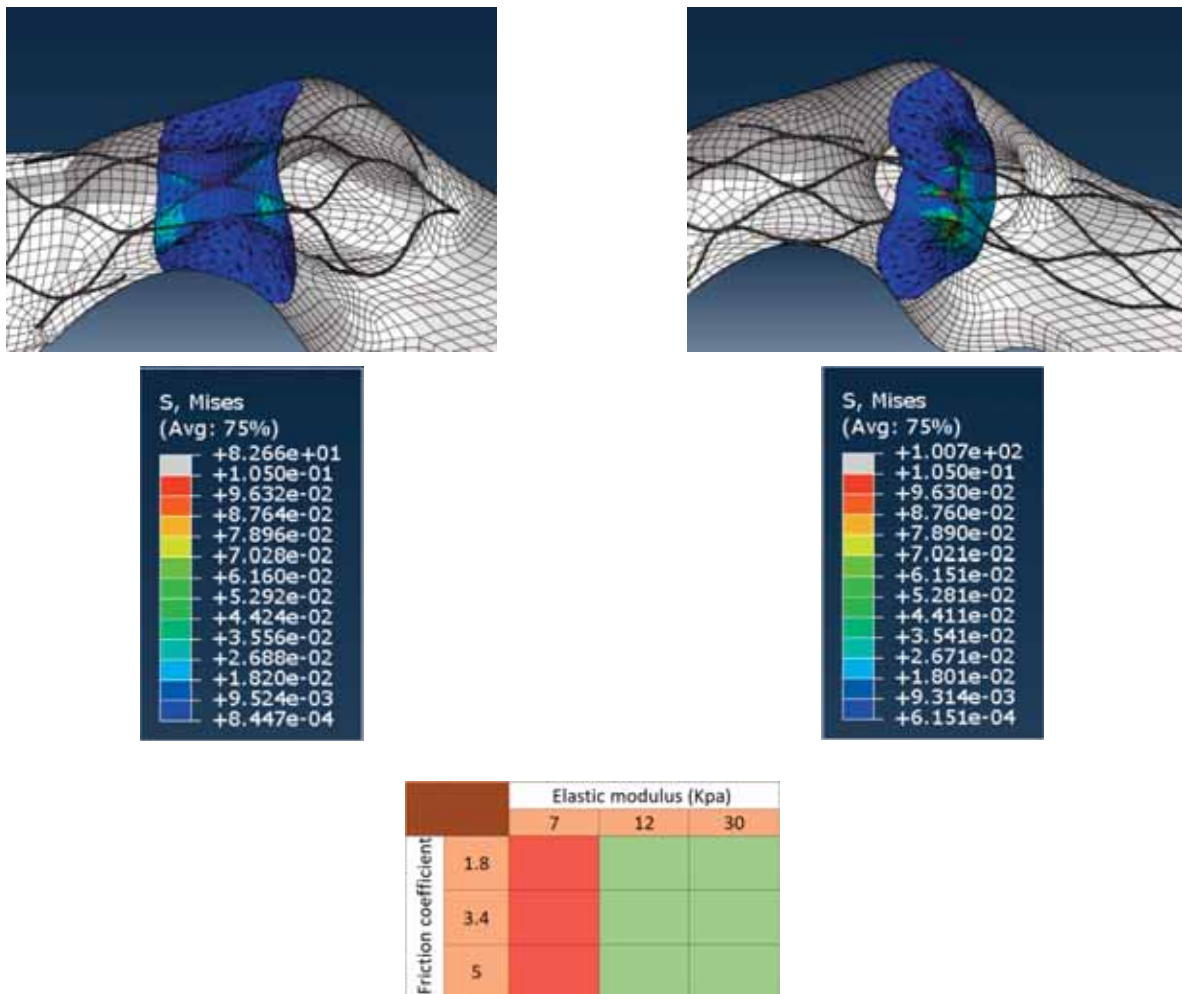
Figure caption: Top left: stress contour of the clot after stnentriever deployment. Top right: stress contour of the clot after stentriever retrieval. Bottom: risk map of clot rupture. (red: failed to retrieve, green: successfully retrieved)

PS6.17

Finite element model of human rotator cuff: a study of the shoulder's rotation modelling main glenohumeral muscles and ligaments

Luis Eduardo Ortega-Ortiz[1], Juan Salgado[1], Gustavo Gil-Noriega[2], Jairo Villa-Bandera[2], Christian Javier Cifuentes De la Portilla[1]

1   Universidad de los Andes, Bogotá, Colombia
2   Hospital Militar Central, Bogotá, Colombia

Glenohumeral joint arthrosis development is jet to be fully understood, this is mainly because arthrosis origin is not known yet. Only some factors such as age, gender or past joint fractures has been associated with its development. Although glenohumeral joint complexity and the challenges an in-vivo study entail, computer-based analysis has proven to be useful and a viable way to understand joint failure and fatigue. Taking this into account, a finite element model of the glenohumeral joint could allow professionals to understand how rotator cuff injury induces glenohumeral arthrosis development and how the joint anatomy changes. This analysis could help doctors decide the best treatment and whether a surgical approach is possible.

Firstly, based on an CT scan a 3D segmentation of the glenohumeral joint was created (including humerus, clavicle and scapula). Afterwards, rotator cuff muscles (Supraspinatus, Infraspinatus, teres minor and subscapularis) were segmented with the coracohumeral ligament and glenohumeral ligaments (Figure 1).

Moreover, the model will help identify what muscle or group of muscles contributes more to the development of glenohumeral joint arthrosis. The inclusion of the rotator cuff muscles and glenohumeral ligaments geometry allows the study of the movements of the shoulder often conducted by doctors for the assessment of shoulder injuries. The figure 2 include the first approaches to the modelling of rotation of the rotator cuff."
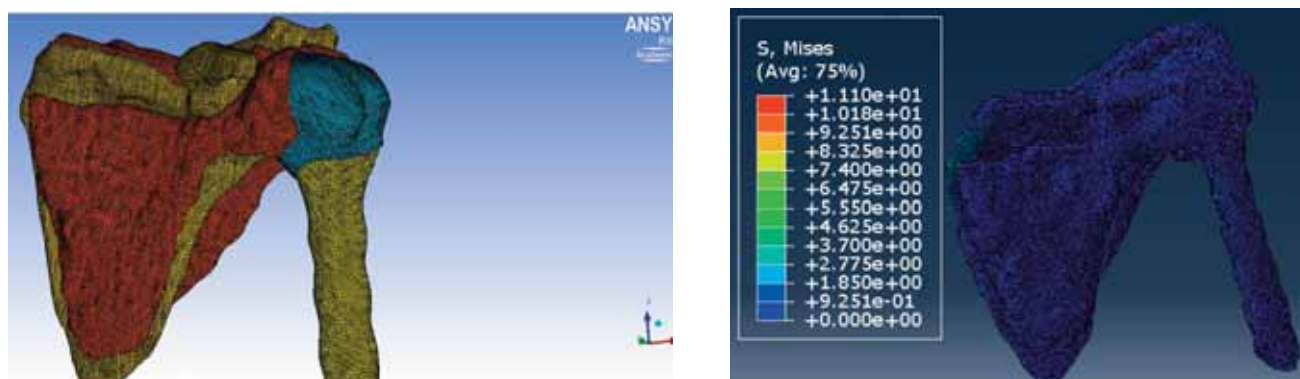
Figure caption: Figure 1: Complete Glenohumeral model Figure 2: Partial rotation stress

PS6.18

Three-dimensional model of the upper limb focused on the study of alternative treatments for osteoarthritis of the distal radioulnar joint

Cristian Jair Verjel Torrado[1], Tatiana Herrera[1], Christian Javier Cifuentes De la Portilla[1], Camilo Romero[2]

1   Universidad de los Andes, Biomedical engineering, Bogotá, Colombia
2   Instituto Roosvelt, Bogotá, Colombia

Osteoarthritis of the radioulnar joint is characterized by incongruence and/or instability of the area as a result of direct or indirect attacks [1]. Currently, there is no objective evaluation of treatments and their effect on patients. These can leave a forearm at risk of instability, pain and clicking at the remaining end of the ulna, also known as impingement syndrome [2][3]. The aim of this project is to develop a three-dimensional finite element model of the upper limb and relevant muscles in impingement syndrome, for the study of alternative treatments for osteoarthritis of the distal radioulnar joint. To achieve this, two three-dimensional reconstructions were performed from magnetic resonance imaging and computed tomography of the upper limb of a healthy patient. The first reconstruction includes the dense and soft tissues of the upper limb of a healthy patient (Fig. 1A). These tissues include the brachialis muscle, abductor pollicis longus, extensor pollicis brevis, pronator teres, and pronator quadratus, which promote impingement syndrome [3]. The second reconstruction includes the same tissues as above, adapting the Darrach procedure (fig.2A) which involves creating complete instability at the distal radioulnar joint by resecting the distal third of the ulna [3][4]. The dense and soft tissue reconstructions for both cases respect the anatomical distribution, original geometry and biomechanical properties of the tissues. Subsequently, both reconstructions were placed at a 90° angle as this is one of the methods to evaluate impingement syndrome in the patient (Fig. 1B; Fig. 2B). Finally, a mesh was made in each of the new reconstructions that, together with the force vectors of each reconstructed muscle, will be useful when assessing the feasibility of different treatments for radio-ulnar joint osteoarthritis (fig. 1C; fig. 2C). The detailed use of reconstructions and meshes of this type will allow accurate simulations of the model, providing information that would be lost with simpler models.
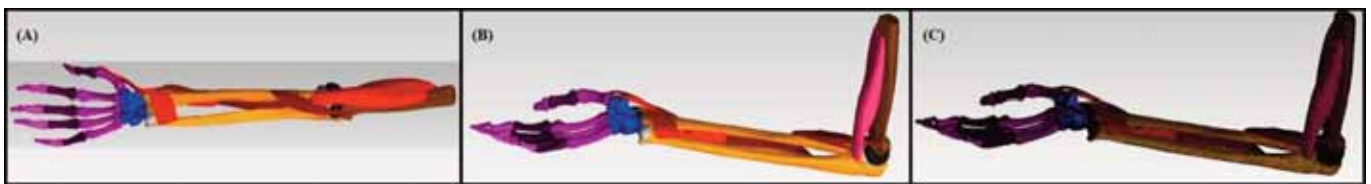
Figure 1: A) Upper limp reconstruction of the upper limb of a healthy patient. B) Positioning of the reconstruction at 90°. C) Mesh of the reconstruction.
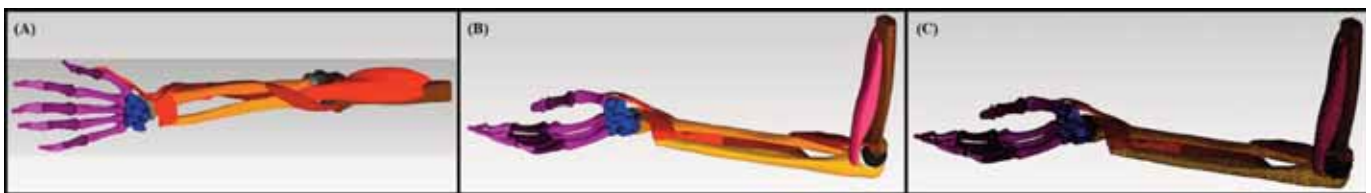
Figure 2: A) Upper limp reconstruction of the upper limb of a patient with Darrach procedure. B) Positioning of the reconstruction at 90°. C) Mesh of the reconstruction.

References:
[36] F. Polo Simón, E.P. Zancolli, L. Vicentela Iturrieta, P.S. Rotella, L.R. Scheker, "Artrosis de la articulación radiocubital distal", Revista Iberoamericana de Cirugía de la Mano, vol. 44, pp 59-65, 2016.
[37] Daniel, Hinzpeter. "Diagnóstico y tratamiento del dolor cubital de muñeca en el deportista". Revista Médica Clínica Las Condes. 23. 299-312. (2012). doi: 10.1016/S0716-8640(12)70314-0.
[38] Romero. C (private communication), 2020.
[39] Cerveró, Rafael. "Inestabilidad longitudinal del antebrazo. Fracturas de Essex-Lopresti. Clasificación y tratamiento". Trauma Fundacion Mapfre. vol. 21. pp 207-218.

AUTHOR INDEX

Bold = Presenting author